

# The reactivity of iron NHC complexes, their application in epoxidation catalysis and the development of new NHC ligand systems

Tim Pascal Schlachta

Vollständiger Abdruck der von der TUM School of Natural Sciences der Technischen Universität München zur Erlangung eines

**Doktors der Naturwissenschaften (Dr. rer. nat.)**

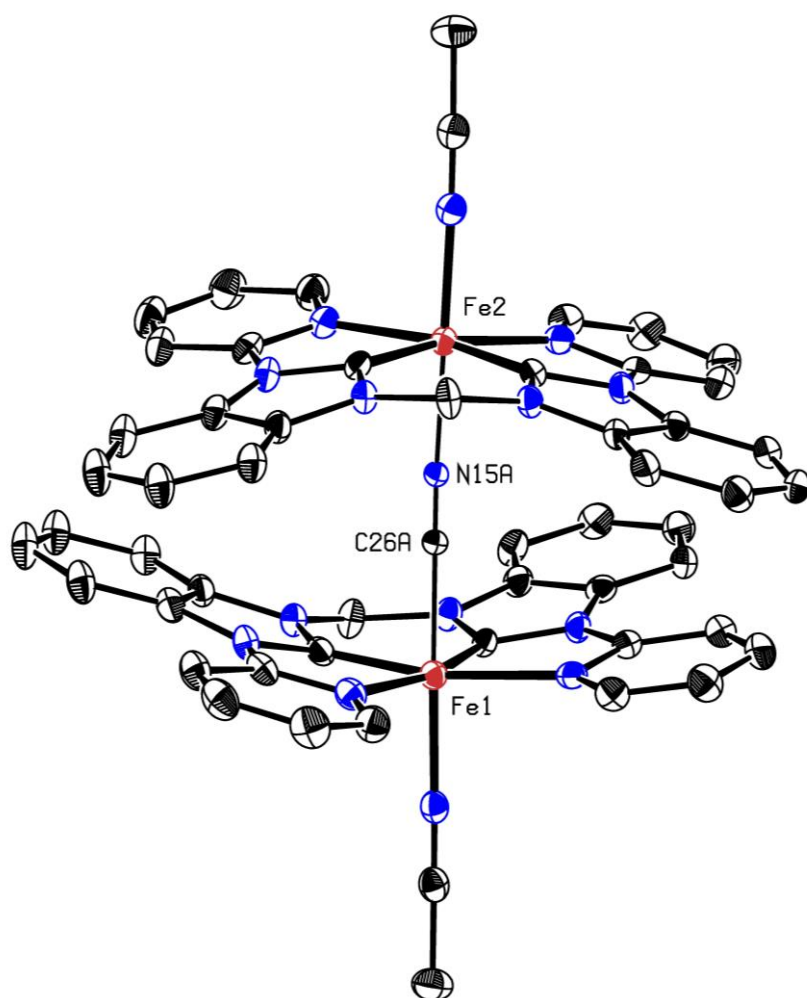
genehmigten Dissertation.

Vorsitz: Prof. Dr. Lukas Hintermann

Prüfer der Dissertation:

1. Prof. Dr. Fritz E. Kühn
2. Prof. Dr. Klaus Köhler
3. Prof. Dr. João D. G. Correia

Die Dissertation wurde am 27.05.2024 bei der Technischen Universität München eingereicht und durch die TUM School of Natural Sciences am 24.06.2024 angenommen.



ORTEP-style representation of diiron end-on  $\mu_2$ - $\eta^1$ : $\eta^1$ -CN bridged complex  $[(\text{MeCN})(\text{NHC})\text{Fe}]_2(\mu_2$ - $\eta^1$ : $\eta^1$ -CN)(PF<sub>6</sub>)<sub>3</sub> (**31**). Hydrogen atoms and hexafluorophosphate anions are omitted for clarity. Thermal ellipsoids are shown at a 50% probability level.

*Für meine Eltern*

Die vorliegende Arbeit wurde im Zeitraum von Februar 2021 bis Mai 2024 im Fachgebiet Molekulare Katalyse der Technischen Universität München angefertigt.

# Danksagung

Ganz besonders und herzlich möchte ich mich bei meinem Doktorvater, Herrn Professor Dr. Fritz E. Kühn, für die freundliche Aufnahme in seinem Arbeitskreis und für die Ermöglichung der Doktorarbeit bedanken. Er gab mir die für die Entwicklung einer Forscherpersönlichkeit erforderliche wissenschaftliche Freiheit und unterstützte mich durch zahlreiche fachlich herausfordernde, konstruktive Gespräche. Dies trug zur Motivation meiner Forschungsarbeiten bei und es gelang ihm dadurch stets, mich für die wissenschaftliche Arbeit zu begeistern und neue Ideen zu entwickeln. Sein kooperativer Führungsstil sowie seine Menschlichkeit haben mir maßgeblich für das Gelingen der Arbeit geholfen. Ich werde diese von ihm begleitete wissenschaftliche Entwicklungsphase dauerhaft in bester Erinnerung behalten. Hervorzuheben ist auch seine ständige Erreichbarkeit für alle Anliegen. Er hat diese sehr ernst genommen und Rückmeldung bzw. ein Feedback immer sehr zeitnah erteilt (auch außerhalb regulärer Arbeitszeiten). Die Unterstützung, auch über die Interessen des Arbeitskreises hinaus, ist nicht selbstverständlich und das weiß ich sehr zu schätzen.

Herauszuheben ist der ausgesprochene Teamgeist der ganzen Arbeitsgruppe und die große Hilfsbereitschaft im Laboralltag. Die damit verbundene ausgezeichnete Arbeitsatmosphäre sowie die sehr netten Gespräche zwischendurch und die gemeinsame Zeit auch außerhalb der Uni trugen zu einem angenehmen Arbeitsalltag bei. Ich werde die geselligen Abende, gemeinsame Unternehmungen und Hüttenaufenthalte in bester Erinnerung behalten. Ich bedanke mich insbesondere bei Nicole Dietl für die Versorgung mit Nervennahrung und zusammen mit Leon Richter für das Messen der zahlreichen ESI-MS Proben; Yogi Büchele für die konstruktive und sehr angenehme Zusammenarbeit bei der Erarbeitung unserer gemeinsamen Publikation und zusammen mit Michael Sauer für die technische Unterstützung bei der Betreuung der Gloveboxen; Alberto Piccoli für die „late night sessions and talks“; und Greta Zábó für die umfangreichen Katalysetests. Auch möchte ich allen Koautoren der entstandenen Publikationen für die sehr fruchtbare Kooperation danken.

Außerdem leisteten im Rahmen ihrer Forschungspraktika und Abschlussarbeiten sehr wertvolle (synthetische) Unterstützung Rosalie Baus, Christian Jung, Maximilian Schick, Marina Speckbacher und Johannes Voigtland.

Zusätzlich möchte ich meinen persönlichen Dank noch aussprechen bei Robert Reich und Markus Drees für die außerfachliche Unterstützung und bei Frau Hifinger vom Sekretariat für die Hilfe bei allem Bürokratischen.

Abschließend möchte ich mich bei all jenen ganz herzlich bedanken, die durch ihre fachliche, persönliche und moralische Unterstützung zum Gelingen meiner Doktorarbeit beigetragen haben.

## Abstract

The development of sustainable catalysts is essential in order to successfully meet today's climate and environmental protection challenges. Iron stands out as a particularly suitable metal due to its good availability, low price and its use in many enzymes in nature, which has been perfected over millions of years. Epoxidation is an important reaction in the chemical industry and research. Heterogeneous catalyst systems are widely used, but homogeneous catalysts can also be a very good alternative, especially for highly selective or asymmetric epoxidation to produce fine chemicals. *N*-heterocyclic carbenes (NHC) are an exceptionally promising class of ligands for homogeneous systems, and their use in iron epoxidation catalysts has been shown to result in very high activities in research work.

The first part of this dissertation is the continuation of research on bio-inspired iron NHC complexes in homogeneous catalytic epoxidation and the closely related development of new NHC ligand systems. Several novel iron NHC complexes with different electronic properties are developed and tested in catalysis. This work contributes to a better understanding of the extent to which the catalytic properties of the iron NHC complexes, e.g. their activity and stability, can be optimized by the electronic modifications. In addition, the degradation mechanism of the most catalytically active iron NHC complex can be identified and comprehensively characterized. Furthermore, chiral NHC ligand precursors can be successfully synthesized. These represent a promising platform for enantioselective epoxidation catalysts.

Further investigations of this dissertation deal with the reactivity of iron NHC complexes. A rare example of an oxygen-bridged diiron tetracarbene complex in high oxidation states can be isolated and its degradation is investigated. Structurally similar to highly reactive intermediates in enzymes, it is suitable for future reactivity studies, such as C–H activation. An unexpected CN-bridged diiron complex from acetonitrile is also isolated and characterized. Current research in the field of cyclic iron tetracarbene complexes is comprehensively presented and evaluated in a review article.

In the third part of this work, new multidentate NHC ligand systems are developed and palladium, platinum and gold tetracarbene complexes are synthesized for potential medical application. Here, one gold complex can induce cell death in cancer cells, even in cells that are resistant to cisplatin, a common cytostatic drug.

# Kurzzusammenfassung

Um die heutigen Herausforderungen des Klima- und Umweltschutzes erfolgreich bewältigen zu können, ist die Entwicklung nachhaltiger Katalysatoren von essenzieller Bedeutung. Eisen sticht hierbei als ein besonders geeignetes Metall hervor aufgrund seiner guten Verfügbarkeit, des niedrigen Preises und seiner über Millionen von Jahren perfektionierten Verwendung in vielen Enzymen in der Natur. Die Epoxidierung stellt eine wichtige Reaktion in der chemischen Industrie und Forschung dar. Weit verbreitet sind dabei heterogene Katalysatorsysteme, aber auch homogene Katalysatoren können hier eine sehr gute Alternative sein, insbesondere für die hochselektive oder asymmetrische Epoxidierung zur Herstellung von Feinchemikalien. *N*-heterocyclische Carbene (NHC) stellen bei den homogenen Systemen eine äußerst vielversprechende Ligandenklasse dar, bei deren Einsatz in Eisen-Epoxidationskatalysatoren sehr hohe Aktivitäten in Forschungsarbeiten nachgewiesen werden konnten.

Der erste Teil dieser Dissertation ist die Fortführung der Forschung zu bio-inspirierten Eisen-NHC-Komplexen in der homogenen katalytischen Epoxidierung und die damit eng verbundene Entwicklung neuer NHC-Ligandensysteme. Es werden mehrere neuartige Eisen-NHC-Komplexe mit unterschiedlichen elektronischen Eigenschaften entwickelt und in der Katalyse getestet. Hier trägt diese Arbeit zu einem besseren Verständnis bei, inwiefern die katalytischen Eigenschaften der Eisen-NHC-Komplexe, z.B. deren Aktivität und Stabilität, durch die elektronischen Modifikationen optimiert werden können. Darüber hinaus gelingt es, den Abbaumechanismus des katalytisch aktivsten Eisen-NHC-Komplexes zu identifizieren und umfassend zu charakterisieren. Des Weiteren können chirale NHC-Ligandenvorstufen erfolgreich synthetisiert werden. Diese stellen eine aussichtsreiche Plattform für enantioselektive Epoxidationskatalysatoren dar.

Weitere Untersuchungen dieser Dissertation befassen sich mit der Reaktivität von Eisen-NHC-Komplexen. Ein seltenes Exemplar eines sauerstoffverbrückten Dieisentetracarbenkomplexes in hohen Oxidationsstufen kann isoliert werden und sein Abbau wird untersucht. Strukturell ähnlich zu hochreaktiven Zwischenstufen in Enzymen eignet es sich für zukünftige Reaktivitätsstudien, wie z.B. der C–H Aktivierung. Auch wird ein unerwarteter CN-verbrückter Dieisenkomplex aus Acetonitril isoliert und charakterisiert. Die aktuelle Forschung auf dem Gebiet zyklischer Eisentetracarbenkomplexe wird in einem Übersichtsartikel umfassend dargestellt und bewertet.

Im dritten Teil dieser Arbeit werden neue mehrzählige NHC-Ligandensysteme entwickelt und damit Palladium-, Platin- und Goldtetracarbenkomplexe für eine potenzielle medizinische Anwendung synthetisiert. Hier kann ein Goldkomplex den Zelltod in Krebszellen einleiten; auch in Zellen, die eine Resistenz zu Cisplatin, einem gängigen Zytostatikum, aufweisen.

# Abbreviations

$^{13}\text{C}_{\text{NHC}}$	$^{13}\text{C}$ carbene carbon signal
a.u.	arbitrary unit
Bn	benzyl
CAAC	cyclic (alkyl)(amino)carbene
CAArC	cyclic (aryl)(amino)carbene
CN <sup>t</sup> Bu	<i>tert</i> -butyl isocyanide
COD	1,5-cyclooctadiene
CV	cyclic voltammetry
Cys	cysteine
DFT	density-functional theory
Dipp	1,5-diisopropylphenyl
DMAP	4-(dimethylamino)pyridine
EPR	electron paramagnetic resonance
eq.	equivalents
ESI-MS	electrospray ionization mass spectrometry
Fc	ferrocene
Fc <sup>+</sup>	ferrocenium cation
FT-IR	Fourier-transform infrared spectroscopy
HEP	Huynh's electronic parameter
HOMO	highest occupied molecular orbital
<sup>i</sup> Pr	isopropyl
<sup>i</sup> Pr <sub>2</sub> -bimy	1,3-diisopropylbenzimidazol-2-ylidene
IR	infrared
L	ligand
LEP	Lever electronic parameter
LUMO	lowest unoccupied molecular orbital
MCA	methyl cation affinity
Me	methyl
Mes	mesityl
MIC	mesoionic carbene
MTO	methyltrioxorhenium
Nalm-6 cells	human B cell precursor leukemia cell line

NHC	<i>N</i> -heterocyclic carbene
NHE	E = Si, Ge, Sn, Pb
NHGe	<i>N</i> -heterocyclic germylene
NHPb	<i>N</i> -heterocyclic plumbylene
NHSi	<i>N</i> -heterocyclic silylene
NHSn	<i>N</i> -heterocyclic stannylene
NMR	nuclear magnetic resonance
No.	number
Nuc	generic nucleophile
OTf	triflate anion, CF <sub>3</sub> SO <sub>3</sub> <sup>-</sup>
PEG	polyethylene glycol
Ph	phenyl
PHC	phosphorus containing heterocyclic carbene, <i>P</i> -heterocyclic carbene
ppm	parts per million
<i>p</i> -Tol	<i>para</i> -toluene
R	placeholder for a (organic) chemical rest
r.t.	room temperature
Ref.	reference
ROS	reactive oxygen species
S	selectivity
salen	tetradentate symmetrical ligand obtained by reaction of salicylaldehyde (sal) and ethylenediamine (en)
SC-XRD	single crystal X-ray diffraction
SK-N-AS cells	human neuroblastoma cell line
<sup>t</sup> Bu	<i>tert</i> -butyl
TEP	Tolman electronic parameter
Th	thianthrene
TIPS	triisopropylsilyl
TMS	trimethylsilyl group, [-Si(CH <sub>3</sub> ) <sub>3</sub> ]
TOF	turnover frequency (TON per hour [h <sup>-1</sup> ])
TON	turnover number (dimensionless number: mol <sub>product</sub> /mol <sub>catalyst</sub> )
X	conversion

# Table of Contents

1.	Introduction.....	1
1.1.	<i>N</i> -heterocyclic carbenes (NHCs).....	1
1.1.1.	Structural features of NHCs .....	2
1.1.2.	Classes of NHCs.....	3
1.1.3.	General considerations about the properties of NHCs.....	8
1.1.4.	Quantification of the electronic properties of NHCs .....	8
1.1.4.1.	$pK_a$ value of azolium salts .....	8
1.1.4.2.	Nucleophilicity and Lewis basicity of NHCs .....	9
1.1.4.3.	NMR measurements .....	10
1.1.4.4.	Infrared (IR) spectroscopy: Tolman electronic parameter (TEP).....	13
1.1.4.5.	Electrochemical measurements .....	14
1.1.4.6.	Computational methods .....	14
1.1.5.	Quantification of the steric properties of NHCs.....	15
1.1.6.	Synthesis of NHCs.....	16
1.1.7.	Applications of NHCs .....	16
1.2.	Iron NHC complexes.....	17
1.2.1.	Synthesis and applications of iron NHC complexes.....	18
1.2.2.	Design of iron NHC complexes .....	19
1.3.	Homogeneous olefin epoxidation catalysis.....	21
1.3.1.	Bio-inspired iron epoxidation catalysis.....	22
1.3.2.	Iron NHC complexes in epoxidation catalysis.....	23
1.3.3.	Enantioselective epoxidation .....	28
2.	Objective .....	30
3.	Results and discussion – publication summaries .....	31
3.1.	Degradation pathways of a highly active iron(III) tetra-NHC epoxidation catalyst ..	32
3.2.	Mimicking reactive high-valent diiron- $\mu_2$ -oxo intermediates of nonheme enzymes by an iron tetracarbene complex.....	34

3.3.	The first macrocyclic abnormally coordinating tetra-1,2,3-triazole-5-ylidene iron complex: a promising candidate for olefin epoxidation .....	36
3.4.	Cyclic iron tetra N-heterocyclic carbenes: synthesis, properties, reactivity, and catalysis.....	37
3.5.	Tailoring activity and stability: Effects of electronic variations on iron-NHC epoxidation catalysts.....	38
3.6.	Chiral imidazolium and triazolium salts as NHC and aNHC ligand precursors: A promising framework for asymmetric epoxidation catalysis .....	40
3.7.	Synthesis, characterization, and biomedical evaluation of ethylene-bridged tetra-NHC Pd(II), Pt(II) and Au(III) complexes, with apoptosis-inducing properties in cisplatin-resistant neuroblastoma cells.....	41
4.	Unpublished results .....	43
4.1.	Impact of ligand design on an iron NHC epoxidation catalyst.....	43
4.2.	Formation of a diiron-( $\mu_2$ - $\eta^1$ : $\eta^1$ -CN) complex from acetonitrile solution .....	45
5.	Conclusion and outlook .....	47
6.	Reprint permissions .....	49
6.1.	Degradation pathways of a highly active iron(III) tetra-NHC epoxidation catalyst ..	49
6.2.	Mimicking reactive high-valent diiron- $\mu_2$ -oxo intermediates of nonheme enzymes by an iron tetracarbene complex.....	50
6.3.	The first macrocyclic abnormally coordinating tetra-1,2,3-triazole-5-ylidene iron complex: a promising candidate for olefin epoxidation .....	51
6.4.	Cyclic iron tetra N-heterocyclic carbenes: synthesis, properties, reactivity, and catalysis.....	52
6.5.	Tailoring activity and stability: Effects of electronic variations on iron-NHC epoxidation catalysts.....	53
6.6.	Chiral imidazolium and triazolium salts as NHC and aNHC ligand precursors: A promising framework for asymmetric epoxidation catalysis .....	54
6.7.	Synthesis, characterization, and biomedical evaluation of ethylene-bridged tetra-NHC Pd(II), Pt(II) and Au(III) complexes, with apoptosis-inducing properties in cisplatin-resistant neuroblastoma cells.....	55
7.	Complete list of publications .....	56
8.	Bibliographic data of complete list of publications .....	60

9. References.....	70
10. Appendix.....	90
10.1. Formation of a diiron- $(\mu_2-\eta^1:\eta^1\text{-CN})$ complex from acetonitrile solution – supporting data	90

# 1. Introduction

## 1.1. *N*-heterocyclic carbenes (NHCs)

*N*-heterocyclic carbenes (NHCs) are a group of organic compounds containing a heterocycle with at least one nitrogen atom and a carbene carbon.<sup>[1-3]</sup> Carbenes are neutral molecules having a divalent carbon atom with an electron sextet resulting in two unbound electrons.<sup>[1]</sup> Due to the incomplete electron octet and the free electrons, carbenes are usually highly reactive and unstable.<sup>[1, 4]</sup> However, in 1988, the first isolable carbene was reported by Bertrand *et al.*, recognizing the stability-enhancing effect of heteroatoms (P or Si) next to the carbene carbon atom (Figure 1).<sup>[1, 4-5]</sup> This resembles a groundbreaking discovery due to the till then considered transient nature of free carbenes. While the first NHC metal complexes were obtained by Wanzlick, Schönherr and Öfele in 1968,<sup>[6-7]</sup> it took until 1991 for the first isolable NHC to be reported by Arduengo *et al.* (Figure 1).<sup>[8]</sup> The remarkable stability and comparatively simple synthesis of the first isolable NHC enabled the targeted use of NHCs in the laboratory and thus established a completely new field of research.<sup>[1]</sup>

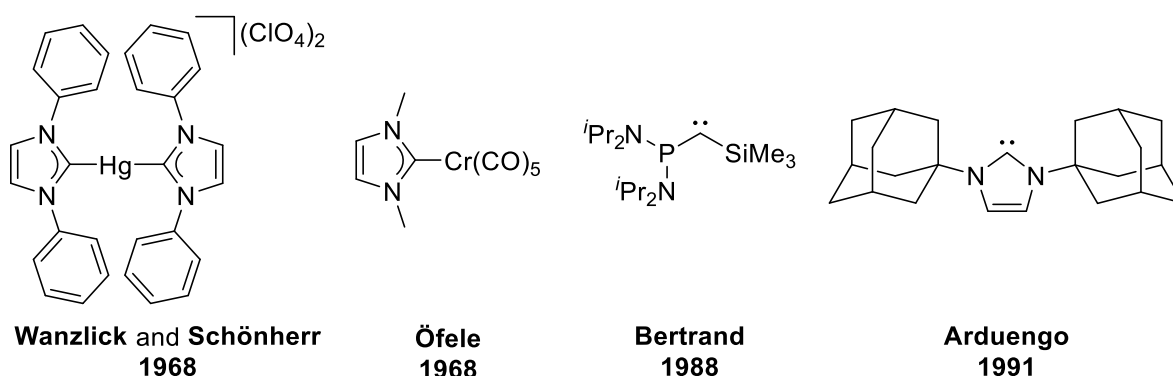


Figure 1. First NHC metal complexes reported by Wanzlick, Schönherr and Öfele, the first isolable carbene by Bertrand *et al.* and the first isolable NHC published by Arduengo *et al.*<sup>[5-8]</sup>

Classical carbenes often possess a triplet electronic ground state (Figure 2), energetically favored by the Hund's rule (especially for linear carbenes).<sup>[9-10]</sup> In contrast, NHCs have a singlet ground state electronic configuration, stabilized mesomerically by the  $\pi$ -electron donation of the adjacent nitrogen atoms into the empty  $p_z$  orbital of the carbene atom.<sup>[1, 10]</sup> The singlet state is additionally stabilized inductively by the  $\sigma$ -electron withdrawal of the electronically more negative neighboring nitrogen atoms, lowering the energy of the occupied  $\sigma$  orbital of the carbene carbon.<sup>[1, 10]</sup> Both interactions combined can be described as +M/-I push-pull effect.<sup>[2, 11]</sup> The bent geometry of the carbene induced by the cyclic nature of NHCs further promotes the singlet state.<sup>[1]</sup>

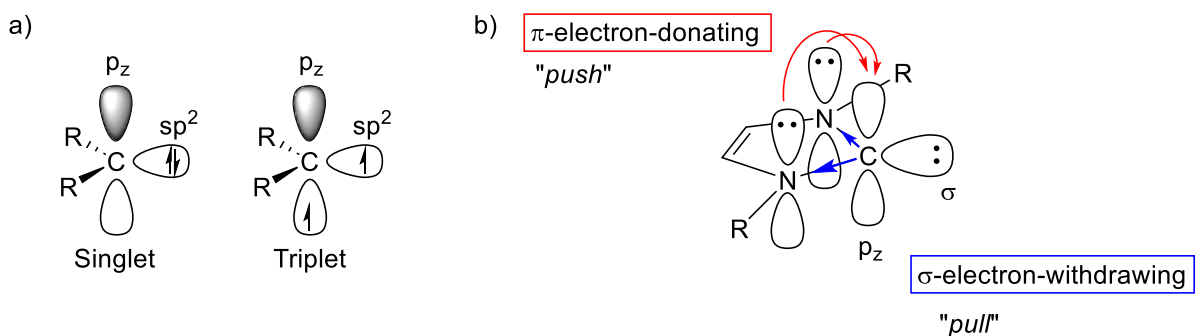


Figure 2. a) Schematic representation of singlet and triplet electronic ground state for carbenes (adapted from<sup>[10, 12]</sup>). b) Schematic representation of the electronic stabilization of the singlet carbene by the adjacent nitrogen atoms (adapted from<sup>[1-2]</sup>).

The lone pair at the carbene carbon in plane of the heterocycle makes NHCs nucleophilic, in contrast to classical transient carbenes, which are mostly electrophilic.<sup>[1]</sup> This results in NHCs being (usually) strong two-electron- $\sigma$ -donors with a weak  $\pi$ -acceptor character that can bind to various metallic and non-metallic compounds.<sup>[1]</sup> Their use as ligands in coordination chemistry and other applications are described below. However, the properties of NHCs can be affected to a high extent and vary between the classes of NHCs (see below).

### 1.1.1. Structural features of NHCs

NHCs contain several structural features that allow an easy modification to a high degree. This enables the NHC's properties to be tailored to the respective purpose, which has contributed significantly to the fact that NHCs are so widely used scientifically.

The backbone of the NHC can be saturated or unsaturated (Figure 3). An unsaturated backbone from a heteroaromatic precursor enhances the stability of the formed NHC by ca. 100 kJ/mol due to partial aromaticity, reducing the need for stabilization by steric bulky wing-tips.<sup>[1, 13-14]</sup> On the other hand, in a NHC with a saturated backbone, the electron density is more concentrated on the C2 carbene carbon atom because of the lack of  $\pi$  interactions, increasing the basicity of the carbene.<sup>[10, 15]</sup> As a result, NHCs with a saturated backbone are considered to be slightly stronger  $\sigma$ -donor ligands than their unsaturated counterparts (see below). Substituents can be added to the backbone influencing the electronic properties of the NHC. For example, the addition of methyl groups at the 4,5 position increases the electron density at the carbene carbon due to the +I effect of the substituents, enhancing the  $\sigma$ -donor strength of the modified NHC.<sup>[11]</sup>

The substituents at the nitrogen atoms, also called wingtips, protect the NHC from potential dimerization forming C=C double bonds or other decomposition pathways.<sup>[4, 16]</sup> Similar to substituents at the backbone, they influence the electronic properties of the NHC.<sup>[11]</sup> This position is also often used to connect multiple NHCs together.

The structural features and their effects are summarized in Figure 3. The targeted design of NHCs can be illustrated using the example of ruthenium-catalyzed homogeneous olefin metathesis, where NHCs are applied as ligands (Figure 4).<sup>[17-20]</sup> By introduction of a polyethylene glycol (PEG) group to the backbone, the catalyst becomes water-soluble, allowing olefin metathesis in water.<sup>[17, 21]</sup> Enantioselective olefin metathesis is achieved by employment of a chiral backbone.<sup>[17, 22-25]</sup> Z-selective olefin metathesis of the thermodynamically less favored Z-olefin was reported with a bidentate binding adamantyl wingtip.<sup>[17, 26-27]</sup>

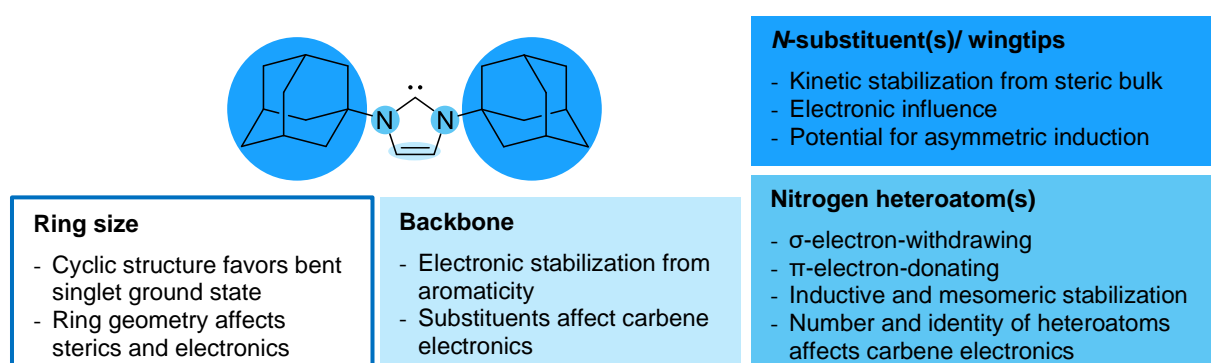


Figure 3. Structural features of NHCs and their effects displayed on the first stable, isolated NHC by Arduengo *et al.*<sup>[8]</sup> (adapted from<sup>[1, 10]</sup>).

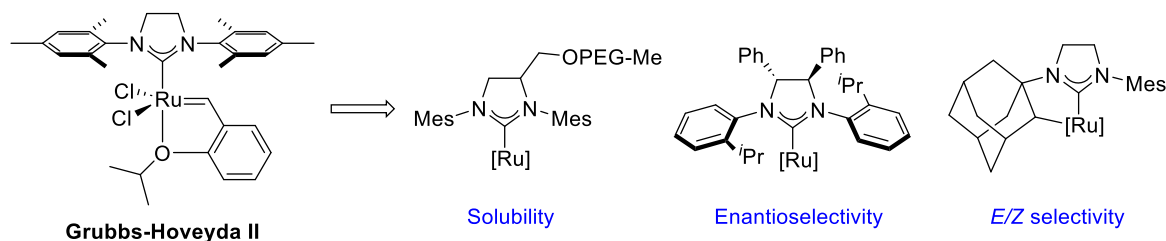


Figure 4. Targeted design of NHC ligands illustrated using the example of ruthenium-catalyzed homogeneous olefin metathesis (adapted from<sup>[17]</sup>). Mes = mesityl, PEG = polyethylene glycol, Me = methyl, Ph = phenyl, *i*Pr = isopropyl.

### 1.1.2. Classes of NHCs

Since the report of the first isolable NHC by Arduengo *et al.*,<sup>[8]</sup> the research field has evolved considerably and nowadays a whole library of NHCs exists. Some of the most relevant groups of NHCs are shown in Figure 5.<sup>[4]</sup> The classical Arduengo-type carbenes possess a saturated or unsaturated backbone and varying *N*- and backbone substituents. There is no prerequisite for a stable carbene to possess two nitrogen atoms next to the carbene carbon.<sup>[28]</sup> Thus, NHCs

with one different heteroatom have been developed, such as thiazol-2-ylidene, containing sulfur, or oxazol-2-ylidene, containing oxygen. Both are expected to have rather weaker  $\sigma$ -donating properties than imidazol-2-ylidenes (oxazol-2-ylidenes slightly weaker than thiazol-2-ylidenes), but to be significantly better  $\pi$ -acceptors (thiazol-2-ylidenes slightly better than oxazol-2-ylidenes), due to reduced  $\pi$ -donation of the O/S atom into the  $p_z$  orbital of the carbene carbon.<sup>[29-31]</sup> The incorporation of additional heteroatoms in the ring structure is possible as well, for example nitrogen in the case of 1,2,4-triazol-5-ylidenes. 1,2,4-Triazol-5-ylidenes are weaker  $\sigma$ -donors than imidazol-2-ylidenes but slightly better  $\pi$ -acceptors.<sup>[31-32]</sup>

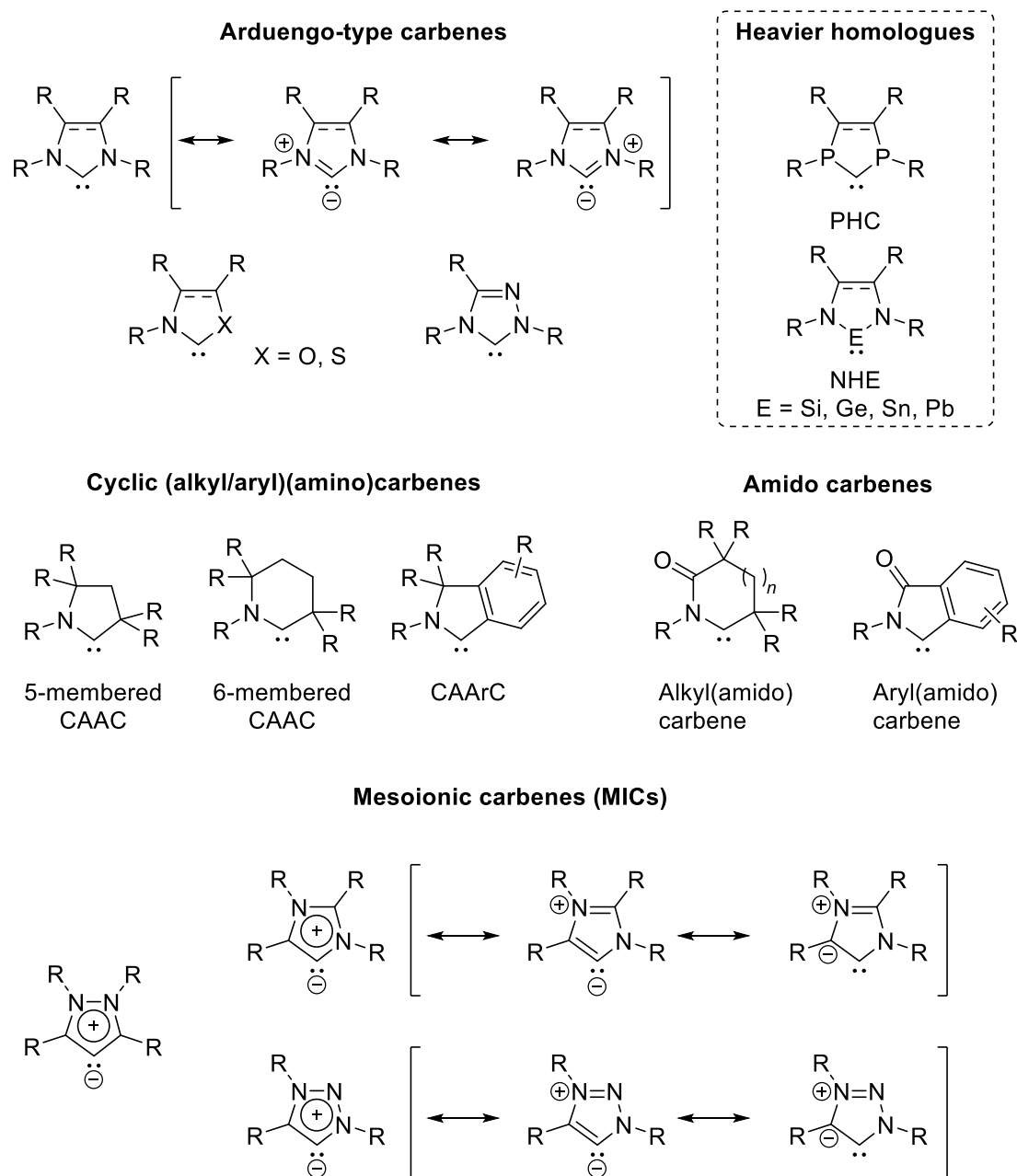


Figure 5. Selected most relevant groups of NHCs and exemplary resonance structures (adapted from<sup>[4, 28, 32-34]</sup>). Heavier NHC homologues are shown for completeness.

Several classes of heavier homologues of NHCs exist, which are structurally similar to Arduengo-type carbenes and are listed here for completeness. One rather new class are phosphorus containing heterocyclic carbenes (PHCs). The first stable isolated PHC was reported in 2005 by Bertrand *et al.*<sup>[35-36]</sup>, albeit first PHC metal complexes have been already published a few years earlier (Figure 6).<sup>[35, 37-40]</sup> Heavier elements of the group 15 have been calculated to be in principle suitable for stabilization of the carbene carbon due to similar  $\pi$ -donor properties compared to nitrogen.<sup>[41-42]</sup> However, while a theoretical NHC with hydrogen atoms as *N*-substituents is calculated to be perfectly planar, the structurally analog calculated PHC contains strongly pyramidalized phosphorus centers, which hinders an efficient stabilization of the carbene (Figure 6).<sup>[42-46]</sup> The pyramidity can be reduced by application of steric demanding *P*-substituents,<sup>[42, 47]</sup> allowing the isolation of the stable PHC by Bertrand *et al.*<sup>[35-36]</sup>. PHCs are stronger  $\sigma$ -donors than Arduengo-type NHCs, even around as strong as MICs (see below), but are very weak  $\pi$ -acceptors.<sup>[28, 35-36]</sup>

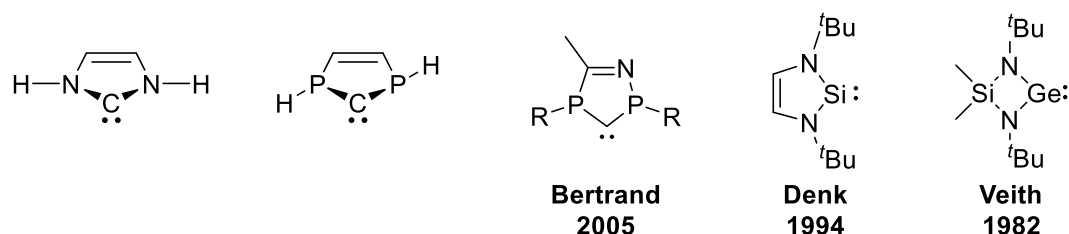


Figure 6. From left to right: Schematic representation of the planar nitrogen atoms in a calculated NHC (left) and pyramidalized phosphorus atoms in a calculated PHC (second from left, adapted from<sup>[42]</sup>). Middle: first stable isolated PHC by Bertrand *et al.*<sup>[35]</sup> R = 2,4,6-tri-*tert*-butylphenyl. Second from right: first stable isolated NHSi by Denk *et al.*<sup>[48]</sup> Right: first stable isolated NHGe by Veith *et al.*<sup>[49]</sup>

The substitution of the carbene carbon in a NHC with other group 14 elements like silicon and germanium leads to the respective heavier NHC homologues *N*-heterocyclic silylene (NHSi) and *N*-heterocyclic germylene (NHGe). The first stable isolated NHSi has been published 1994 by Denk *et al.* (Figure 6).<sup>[48]</sup> Interestingly, stable NHGes have been developed independently of the Arduengo NHC and the first example has been reported as early as 1982 by Veith *et al.* (Figure 6).<sup>[49-52]</sup> The heavier NHC homologues have been determined to be weaker  $\sigma$ -donors than NHCs but stronger  $\pi$ -acceptors. The  $\sigma$ -donor strength is decreasing in the order NHC > phosphanes > NHSi > NHGe, while the  $\pi$ -accepting properties are increasing in the order phosphanes < NHC < NHSi < NHGe.<sup>[52-57]</sup> However, as for NHCs, the properties are heavily dependent on the chemical environment around the divalent center in general. There are also *N*-heterocyclic stannylenes (NHSn) and plumbynes (NHPb) and the  $\sigma$ -donor strength is expected to decrease towards the heavier elements of the group 14.<sup>[54, 56, 58-62]</sup> Furthermore, there is a rich chemistry of isoelectronic main-group NHC analogues with group 13 – 16 elements.<sup>[12, 63]</sup>

As stated above, two nitrogen atoms are not necessarily required for the stabilization of the carbene.<sup>[28]</sup> There are several classes of stable NHCs with only one nitrogen atom next to the carbene and the other neighboring atom being carbon. The group of cyclic (alkyl)(amino)carbenes (CAACs) has been developed in 2005 by Bertrand *et al.* (Figure 5).<sup>[64]</sup> One of the nitrogen atoms is replaced with a carbon atom containing alkyl substituents. With the replacement of the more electronegative nitrogen atom and the +I inductive effect of the new alkyl neighbor, the electron density of the carbene carbon is increased. Having a more electron-rich carbene carbon, CAACs are somewhat stronger  $\sigma$ -donors than Arduengo-type NHCs.<sup>[4, 42]</sup> Simultaneously, the absence of the  $\pi$ -donation into the  $p_z$  orbital of one nitrogen atom makes the carbene more electrophilic, resulting in CAACs being by trend stronger  $\sigma$ -donors and  $\pi$ -acceptors than Arduengo NHCs.<sup>[4, 65-66]</sup> Aryl substituents can be added instead of alkyl groups, yielding cyclic (amino)(aryl)carbenes (CAArCs), which keep the strong  $\sigma$ -donating properties of CAACs, but exhibit better  $\pi$ -accepting properties.<sup>[4, 67]</sup> Increasing the ring size of CAACs from 5-membered to a 6-membered ring further improves both the nucleophilicity and electrophilicity, making the 6-membered CAACs the strongest  $\sigma$ -donors and  $\pi$ -acceptors among the series of CAA(r)Cs, and stronger  $\sigma$ -donors and  $\pi$ -acceptors than Arduengo-type carbenes.<sup>[4, 68]</sup>

Another class of NHCs with one adjacent nitrogen atom are (cyclic) amido carbenes (Figure 5). Amido carbenes are built similar to CAACs and can be divided into alkyl(amido)carbenes, diamidocarbenes and aryl(amido)carbenes.<sup>[4, 69-70]</sup> The electron-withdrawing carbonyl group increases the electrophilicity, making amido carbenes even stronger  $\pi$ -acceptors than CAA(r)Cs.<sup>[4, 67]</sup> However, this comes at the cost of the  $\sigma$ -donor strength, which leads amido carbenes to be weak  $\sigma$ -donors, significantly weaker than Arduengo NHCs.<sup>[67]</sup> The  $\pi$ -accepting properties are increasing in amido carbenes from alkyl(amido)carbenes, over diamidocarbenes (incorporation of a second electron-withdrawing carbonyl group) to peak in aryl(amido)carbenes, which are the strongest  $\pi$ -acceptors.<sup>[4]</sup> Diamidocarbenes and aryl(amido)carbenes are similar poor  $\sigma$ -donors, but both are even weaker  $\sigma$ -donors than alkyl(amido)carbenes.<sup>[71]</sup> However, the  $\sigma$ -donor properties of diamidocarbenes and aryl(amido)carbenes are still in the same order of magnitude of phosphanes and are particularly similar to arylphosphanes (e.g. PPh<sub>3</sub>).<sup>[4, 72]</sup>

Mesoionic carbenes (MICs) are the last large class of NHCs to be discussed here (Figure 5).<sup>[73-74]</sup> They are also called abnormal carbenes. Historically, the “normal” coordination mode of Arduengo NHCs was *via* the C2 ring carbon atom and imidazolylidenes instead bound *via* the C4/5 position were thus labelled as abnormal carbenes.<sup>[42, 75-78]</sup> The usual C2 coordination for 1,3-imidazolium salts can be explained by the lower acidity of the backbone (C4–H  $pK_a > 30$ ) compared to the C2–H position ( $pK_a \approx 18$ ).<sup>[79-84]</sup> Making the C2 position inaccessible, for example by methylation, allows for a targeted synthesis of abnormal carbenes. Mesoionic is however the preferred, correct term for abnormal carbenes.<sup>[75]</sup> This term originates from the fact

that these carbenes are mesoionic compounds, *i.e.* no reasonable resonance structure without additional charges can be drawn for the free carbene, as demonstrated in Figure 5.<sup>[34]</sup> MICs are in general stronger  $\sigma$ -donors than Arduengo-type NHCs and even stronger than CAA(r)Cs.<sup>[31, 34, 85]</sup> Selected subgroups of MICs are 1,2,3-triazol-5-ylidenes, imidazol-5-ylidenes (or also -4-ylidenes)<sup>[79]</sup> and pyrazolin-4-ylidenes. Pyrazolin-4-ylidenes can also be called remote carbenes, as they do not have stabilizing heteroatoms next to the carbene carbon.<sup>[75]</sup> The  $\sigma$ -donation strength increases in the following order; 1,2,3-triazol-5-ylidenes are strong  $\sigma$ -donors but are surpassed by imidazol-5-ylidenes, whereas pyrazolin-4-ylidenes are the strongest in this series.<sup>[31, 34]</sup> MICs are even weaker  $\pi$ -acceptors than Arduengo-type NHCs and thus effectively act as “pure  $\sigma$ -donors”. Imidazol-5-ylidenes and 1,2,3-triazol-5-ylidenes have similar weak  $\pi$ -accepting properties, and pyrazolin-4-ylidenes are the weakest  $\pi$ -acceptors.<sup>[31]</sup>

To summarize, the  $\sigma$ -donor and  $\pi$ -accepting properties of all discussed classes of NHCs are ranked in Figure 7 relative to each other. It needs to be noted, that Figure 7 only shows general trends and the properties of each NHC are highly dependent on the chemical environment of the carbene. In addition, the properties can vary even within a group between its subgroups, as can be observed with CAA(r)s, for example.

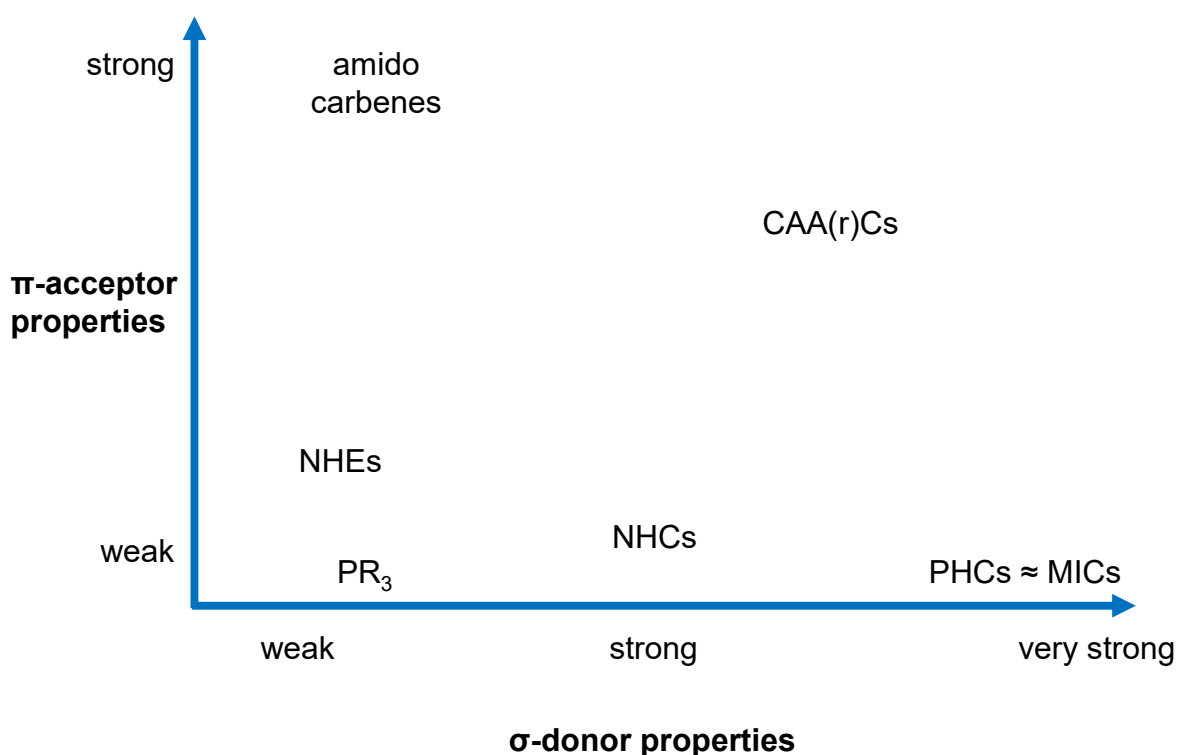


Figure 7. Visualization of the  $\sigma$ -donor and  $\pi$ -accepting properties of the discussed classes of NHCs.

### 1.1.3. General considerations about the properties of NHCs

With the variety of NHCs described, it is important to know their properties in order to select the most suitable NHC for the respective application. The steric and electronic properties are dependent on the chemical structure of the NHC. However, one should also consider the context where the NHC is applied, e.g. as ligand in a metal complex. Here, the electronic contributions of the NHC ligand –  $\sigma$ -donation,  $\pi$ -donation and  $\pi$ -acceptance – will depend on the electron density of the metal center, which is in turn influenced by coligands, the oxidation state and the element itself.<sup>[86-88]</sup> A weak  $\pi$ -acceptor NHC might experience a larger  $\pi$ -backbonding in the case of an electron-rich transition metal (e.g. Ni<sup>0</sup>)<sup>[89-90]</sup> than a strong  $\pi$ -acceptor NHC from a more Lewis-acidic transition metal.<sup>[86-88]</sup> In fact, a strong  $\sigma$ -donor NHC increases the electron density of the metal center and thus can promote  $\pi$ -backbonding to the NHC ligand from the metal.<sup>[87]</sup> NHCs have been found to act as  $\pi$ -donors as well, which contributes to the total orbital interactions between the ligand and the metal (e.g. 6% in the case of [ZrCl<sub>4</sub>(NHC)], NHC = imidazol-2-ylidene).<sup>[91]</sup> This contribution is especially important for coordinatively unsaturated complexes.<sup>[89, 92]</sup> But also the steric properties of the NHC are to be considered. For example, a steric demanding NHC might limit the orbital overlap with the metal center due to interligand repulsion, thus not offering the theoretically and experimentally determined electronic properties of the free NHC.<sup>[88-89]</sup>

### 1.1.4. Quantification of the electronic properties of NHCs

The electronic properties of NHCs have so far only been qualitatively discussed (see above). Selected methods to quantify the electronic properties of NHCs are presented in the following section.

#### 1.1.4.1. pK<sub>a</sub> value of azolium salts

The deprotonation of the respective azolium salt is one of the most frequently used methods to generate free NHCs (Scheme 1). For that reason, it is helpful to know the pK<sub>a</sub> value of the azolium salt for the choice of base. Imidazolium salts possess a pK<sub>a</sub> value between 16 to 23 at the 2 position.<sup>[93]</sup> The pK<sub>a</sub> value gives insight into the basicity of the free NHC but that can only be roughly translated to  $\sigma$ -donor strength and has to be interpreted with caution as other factors like the *N*-substituents and class of heterocycle also have to be taken into account. While NHC classes with stronger  $\sigma$ -donor properties appear to be by trend less acidic (*i.e.* the corresponding free NHC more basic), the 1,2,3-triazolium salt with mesityl wings is more acidic

( $22.3 \pm 0.1$ )<sup>[94]</sup> than its structurally analog imidazolium salt ( $22.8 \pm 0.1$ )<sup>[95]</sup>, even though the corresponding free MIC is a stronger  $\sigma$ -donor than the Arduengo-type NHC (Figure 8).<sup>[85]</sup> The anion of azolium salts has been found to have a negligible effect on the  $pK_a$  value, allowing the comparison solely based on the azolium cation.<sup>[85, 95-97]</sup>

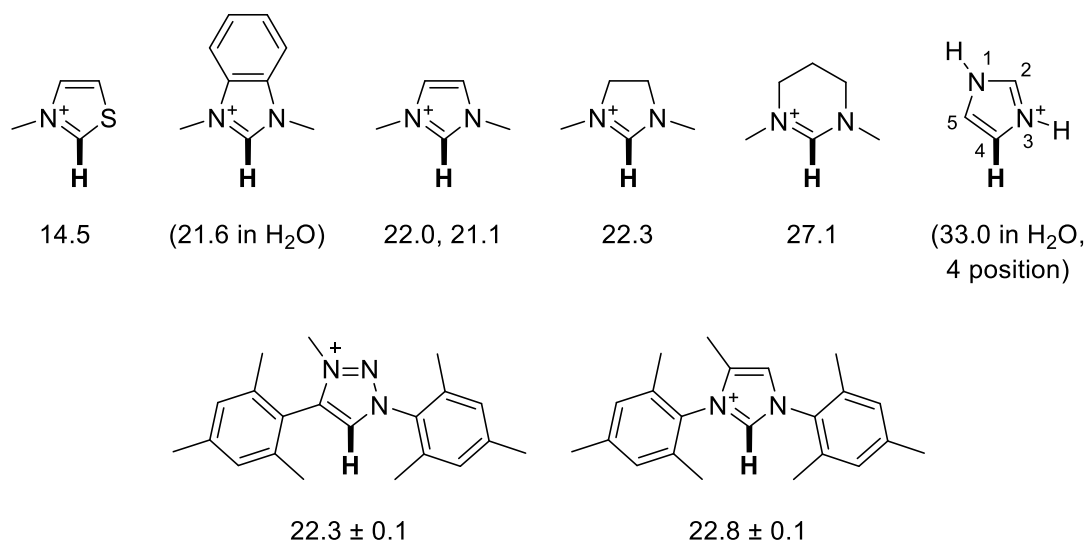


Figure 8.  $pK_a$  values of a few azolium salts, measured in DMSO if not stated else.<sup>[93-95, 97-100]</sup>

#### 1.1.4.2. Nucleophilicity and Lewis basicity of NHCs

The nucleophilicity of an NHC is important in organocatalytic reactions of NHCs (see below) and can be determined by reaction of the NHC with a series of electrophiles.<sup>[86]</sup> The nucleophilicity parameter  $N$  of the imidazolinyliidene and imidazolylidene is very high, whereas the triazolylidene is significantly less nucleophilic and on the same level as  $PPh_3$  and DMAP, the latter being used as nucleophilic catalyst (Figure 9).<sup>[86, 101]</sup> However, the Lewis basicity of all three NHCs is significantly higher than that of  $PPh_3$  and DMAP, as revealed by DFT calculations of the methyl cation affinity (MCA).<sup>[86, 102]</sup>

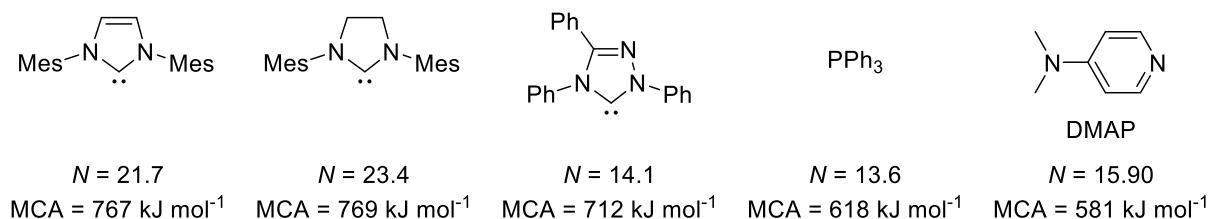


Figure 9. Nucleophilicity parameter  $N$  and Lewis basicity (MCA) of several NHCs and reference examples.<sup>[86, 102-104]</sup>

### 1.1.4.3. NMR measurements

There are several quantization methods that are based on NMR spectroscopy.

One method to assess the electron-donating ability of NHCs (and other ligands in general) was developed by Huynh *et al.*<sup>[105]</sup> Here, a Pd<sup>II</sup> complex is employed containing a benzimidazolyli-dene spectator ligand (<sup>i</sup>Pr<sub>2</sub>-bimy, Figure 10). The ligand of interest is added to the Pd<sup>II</sup> complex in *trans* position to the benzimidazolylidene and the resulting chemical shift of the <sup>13</sup>C carbene carbon signal (<sup>13</sup>C<sub>NHC</sub>) of the benzimidazolylidene spectator ligand is measured.<sup>[105]</sup> A strong electron donating ligand increases the “free carbene” character of the benzimidazolylidene spectator ligand and thus leads to a downfield shift of its <sup>13</sup>C<sub>NHC</sub> signal.<sup>[88]</sup> Free NHCs are highly deshielded and in addition have a higher probability of a singlet-triplet transition (Figure 2), contributing to the paramagnetic shielding term and resulting in downfield shifted <sup>13</sup>C<sub>NHC</sub> signals between ca. 200-330 ppm.<sup>[11, 88, 102]</sup> Upon complexation, the probability of a singlet-triplet transition is decreased and the carbene strongly shielded, resulting in an upfield shift of the <sup>13</sup>C<sub>NHC</sub> signal.<sup>[11, 88, 102]</sup> Thus, when only a weak electron donating ligand is applied, the <sup>13</sup>C<sub>NHC</sub> signal of the benzimidazolylidene spectator ligand will stay rather upfield shifted. This chemical shift is also called Huynh’s electronic parameter (HEP).<sup>[88]</sup> Selected examples and their corresponding HEP values are shown in Figure 11. HEP primarily measures the σ-donation of a ligand.<sup>[88, 106]</sup> The principle of HEP could be expanded on similar linear Au<sup>I</sup> complexes, too, with good correlation to the obtained HEP values from the Pd<sup>II</sup> complex.<sup>[102, 107-108]</sup> When comparing HEP values, a difference of >0.4 ppm (3σ) is considered to be significant by means of statistic uncertainty.<sup>[11, 105]</sup>

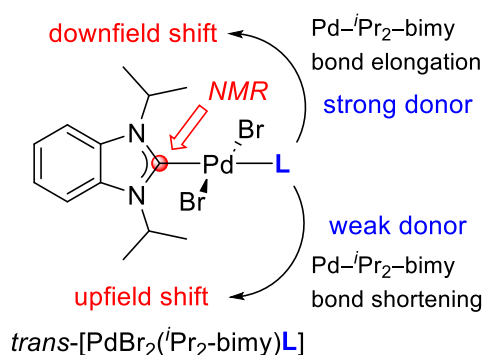


Figure 10. Working principle of HEP (adapted from<sup>[11, 109]</sup>). <sup>i</sup>Pr<sub>2</sub>-bimy = 1,3-diisopropylbenzimidazol-2-ylidene, L = ligand to be measured.

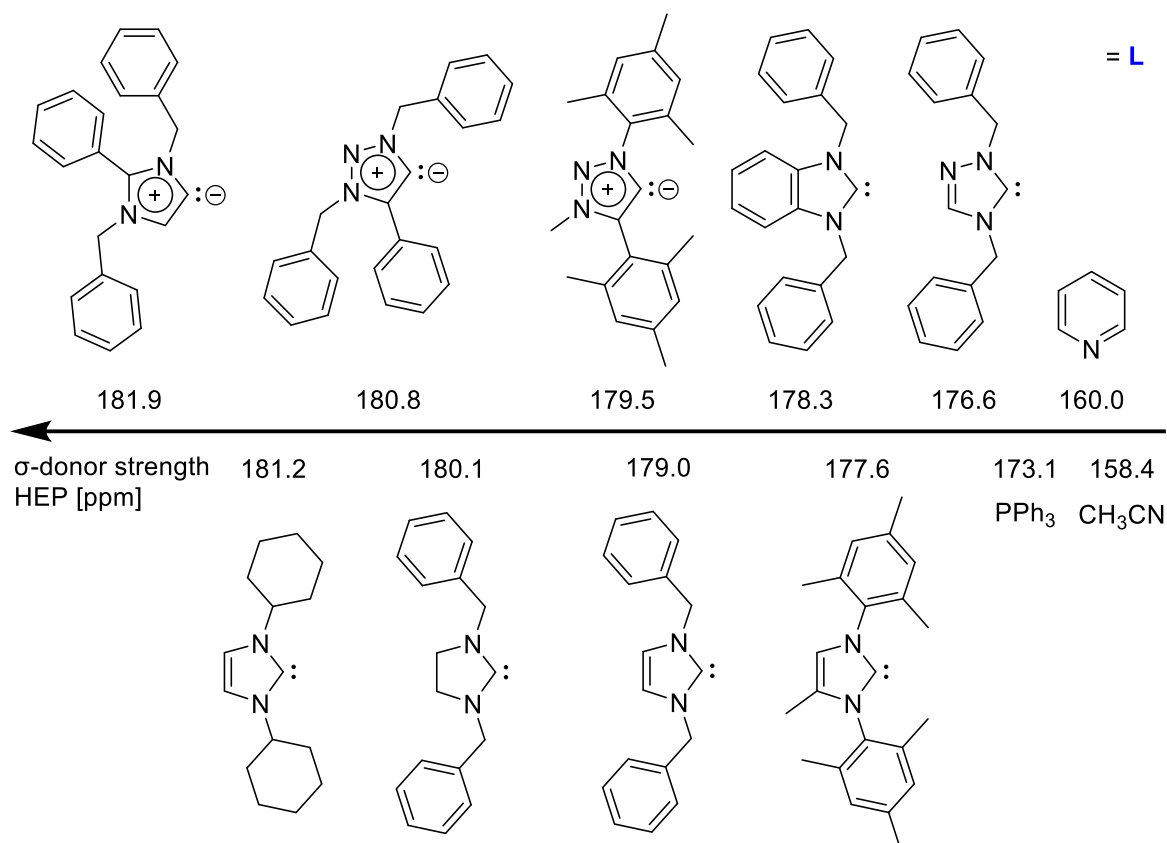


Figure 11. HEP values of some ligands. The  $\sigma$ -donor strength increases to higher HEP values.<sup>[85, 88, 105, 108, 110-113]</sup>

Methods to determine the  $\pi$ -acceptor strength of NHCs have been developed by Bertrand *et al.* and Ganter *et al.*<sup>[114-115]</sup> The NHCs are converted to carbene-phosphinidene adducts and selenoureas. Both NHC-derived compounds can exist in two extreme resonance structures (Figure 12).<sup>[102]</sup> The chemical shift of the  $^{31}\text{P}$  NMR or  $^{77}\text{Se}$  NMR signal is measured. NHCs being primarily  $\sigma$ -donors will adopt form **A**, where the P/Se atom is highly shielded resulting in an upfield NMR signal.<sup>[115]</sup> Strong  $\pi$ -acceptor NHCs will lead to form **B**, with a deshielded P/Se atom and thus a downfield shifted NMR signal.<sup>[115]</sup> The scale for NHCs ranges from ca. -60 to 80 ppm for the  $^{31}\text{P}$  NMR signal and from ca. -60 to 1200 ppm for the  $^{77}\text{Se}$  NMR signal, depending on the deuterated solvent.<sup>[88, 116]</sup> Selected examples are shown in Figure 12. However, care must be taken when interpreting these values. The values do not purely give information about the  $\pi$ -acceptor strength but rather the overall  $\pi$ -backbonding, that the NHC is experiencing. Stronger  $\sigma$ -donor NHCs will make the P/Se atom more electron-rich, thus promoting the  $\pi$ -backdonation.<sup>[88]</sup> In the case of two NHCs with a similar  $\pi$ -acceptor strength, the overall  $\pi$ -backdonation will be higher for the one NHC with better  $\sigma$ -donation to the P/Se atom, resulting in a more downfield shifted NMR signal. For that reason, parameters like HEP or TEP (see below) should be consulted to determine the relative contribution of  $\sigma$ -donation.<sup>[102]</sup> Furthermore, the steric bulk of NHCs has to be considered, especially when comparing NHCs with different *N*-substituents.<sup>[117]</sup>

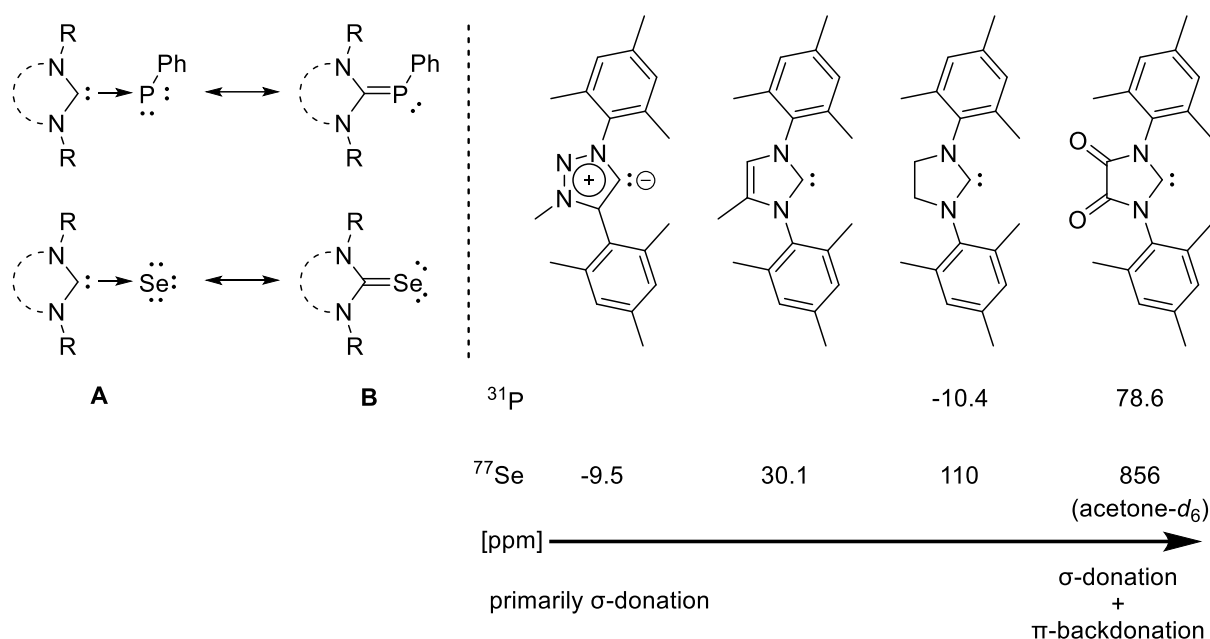


Figure 12. Left: Resonance forms of carbene-phosphinidene adducts and selenoureas (adapted from<sup>[115]</sup>). Right:  $^{31}\text{P}$  and  $^{77}\text{Se}$  chemical shift of some ligands.  $^{31}\text{P}$  NMR measured in  $\text{C}_6\text{D}_6$ ,  $^{77}\text{Se}$  NMR measured in  $\text{CDCl}_3$ , if not stated otherwise.<sup>[85, 88, 114-115, 118-120]</sup> Lewis structures of the NHCs only, without P-Ph/Se rest.

The  $^1J_{\text{CH}}$  coupling constant in azolium salts, *i.e.* NHC ligand precursors, can indicate the  $\sigma$ -donor strength of the respective free NHCs (Figure 13).<sup>[121-122]</sup> The coupling constant ranges over ca. 180 to 230 Hz and a weaker  $\sigma$ -donor corresponds to a higher  $^1J_{\text{CH}}$  coupling constant.<sup>[88, 122]</sup> The  $^1J_{\text{CSe}}$  coupling constant shows the same trend and can also be used as indicator for the  $\sigma$ -donor strength of the corresponding free NHC, showing a good correlation to HEP (Figure 13).<sup>[85, 118, 121]</sup>

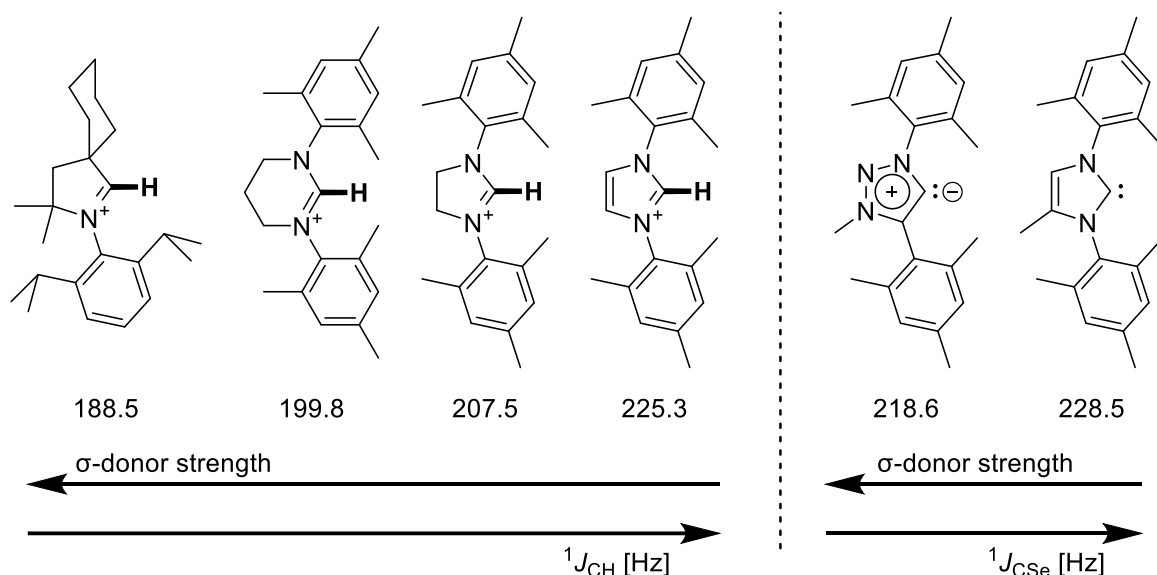


Figure 13. Left: Selected azolium salts with their corresponding  $^1J_{\text{CH}}$  coupling constant.  $^1\text{H}$  and  $^{13}\text{C}$  NMR measured in  $\text{DMSO}-d_6$  ( $^1J_{\text{CH}}$ ).<sup>[122]</sup> Right: Selected NHCs and the  $^1J_{\text{CSe}}$  coupling constant of the corresponding selenoureas.  $^{13}\text{C}$  NMR measured in  $\text{CDCl}_3$  ( $^1J_{\text{CSe}}$ ).<sup>[85, 118]</sup>

#### 1.1.4.4. Infrared (IR) spectroscopy: Tolman electronic parameter (TEP)

The Tolman electronic parameter (TEP) is one of the most frequently used methods for quantification of the electronic properties of NHCs.<sup>[102]</sup> It was originally developed for phosphanes and can be used to determine the electron donation of a ligand in transition metal carbonyl complexes.<sup>[102, 123]</sup> A strong electron donating NHC will make the metal center more electron rich, which leads to a stronger backdonation from the metal into the  $\pi^*$  antibonding orbital of the carbonyl ligand. As a result, the initial  $\text{C}\equiv\text{O}$  triple bond is weakened, which can be quantified in the infrared (IR) spectrum of the complex, represented in a lower wavenumber of the CO vibration.<sup>[88, 102]</sup> In case of tetrahedral  $[\text{Ni}(\text{CO})_3\text{NHC}]$  complexes, the  $A_1$  CO stretching frequency is measured.<sup>[88]</sup> Due to the high toxicity of the precursor,  $\text{Ni}(\text{CO})_4$ , *cis*- $[\text{MX}(\text{CO})_2(\text{NHC})]$  ( $\text{M} = \text{Rh}$  or  $\text{Ir}$ ,  $\text{X} = \text{halide}$ ) complexes have been used later, where the averaged wavenumber ( $\tilde{\nu}_{\text{av}}$ ) of both CO vibrational frequencies is used.<sup>[88]</sup> Some examples of NHCs with their TEP values are presented in Figure 14. However, there are some limitations regarding TEP. For example, TEP only gives information about the net electron density at the metal center, without separating  $\sigma$ -donation from  $\pi$ -backbonding.<sup>[85, 122]</sup> In addition, the TEP scale is rather small, e.g. classical Arduengo NHCs differ by ca.  $4 \text{ cm}^{-1}$ .<sup>[88]</sup> Considering a statistical error of  $3\sigma$  ( $>99\%$ ) =  $\pm 1.5 \text{ cm}^{-1}$ , a differentiation between these NHCs becomes difficult.<sup>[88]</sup> Furthermore, the halide in the complex and the solvent used influence the TEP, and the steric bulk of the NHC has to be considered.<sup>[88]</sup> The interconversion of the wavenumbers from the Rh and Ir complexes to TEP values is possible, albeit at additional uncertainty.<sup>[88]</sup>

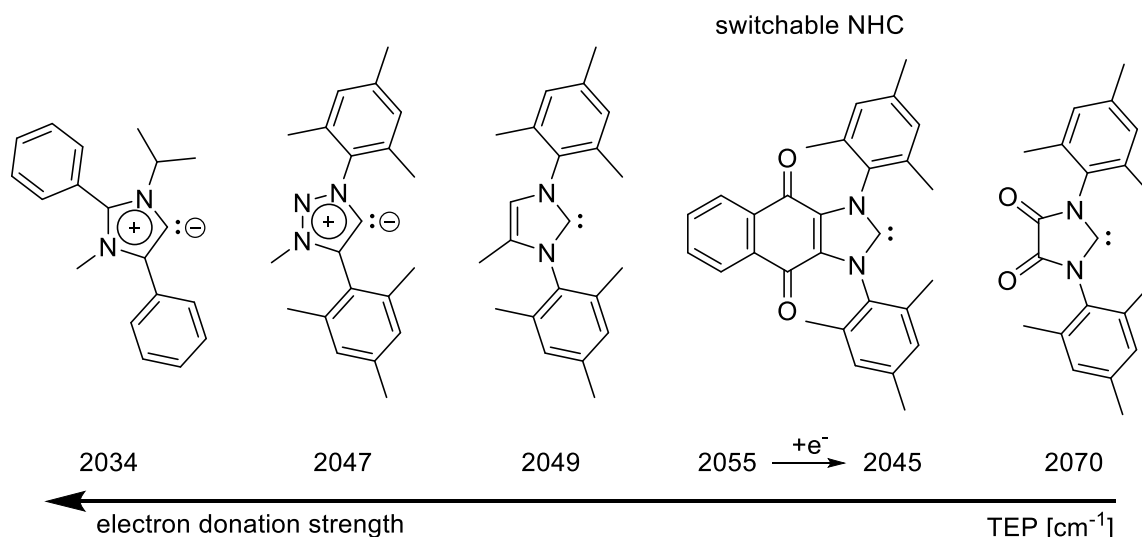


Figure 14. TEP values (calculated based on interconversion equations) of some NHCs.<sup>[85, 88, 102, 124-126]</sup>

### 1.1.4.5. Electrochemical measurements

The redox potential of a metal complex can be influenced by its surrounding ligands. Strong electron donating ligands facilitate the oxidation of the metal, lowering the redox potential. A weak electron donating, or strong accepting ligand, rises the redox potential. Using this principle, NHCs can be ranked according to the resulting redox potential, indicating their electronic properties. Additionally, an electrochemical parameter (often called Lever electronic parameter (LEP))<sup>[127]</sup> can be determined for the measured ligand and be used to predict the redox potential for another metal complex.<sup>[88]</sup> A systematic measurement of various NHCs has been performed for *cis*-[MCl(COD)(NHC)] (M = Rh or Ir, COD = 1,5-cyclooctadiene) complexes (Figure 15).<sup>[88]</sup> The measured redox potentials range from ca. +0.6 to +1.1 V.<sup>[88]</sup> Important for this method are reversible or quasi-reversible redox processes and innocent ligands (*i.e.* not redox active).<sup>[88, 128]</sup>

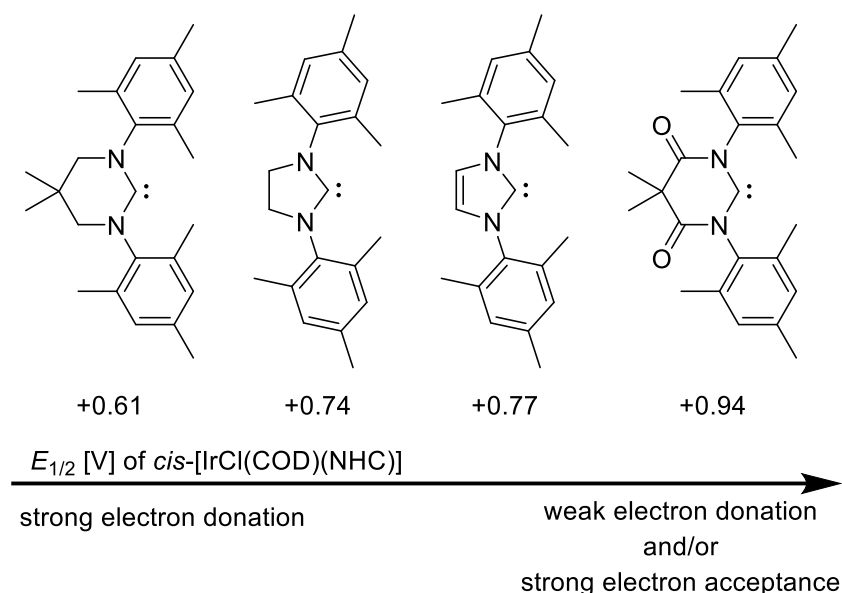


Figure 15. Redox potentials for some NHC ligands.<sup>[88, 129-130]</sup>

### 1.1.4.6. Computational methods

Using computational methods, the experimentally obtainable parameters (see above) can be calculated with good correlation, e.g. TEP,<sup>[131-133]</sup> but also other, new metrics can be determined.<sup>[89, 102, 134-136]</sup> Frontier orbital analysis of free NHCs can give valuable insight into the electronic properties of NHCs.<sup>[28, 89]</sup> An energetically higher-lying HOMO is indicative of a stronger  $\sigma$ -donation and higher nucleophilicity – a lower LUMO corresponds to better  $\pi$ -acceptance and electrophilicity (Figure 16).<sup>[68, 89]</sup> The energy of the HOMO has been found to indicate the NHC–metal bond energy in the absence of steric relevant bulk at the NHC and without significant  $\pi$ -backbonding from the metal (e.g. metal carbonyl complex), with a higher

HOMO related to a larger bond energy.<sup>[89]</sup> The singlet-triplet gap is the “energy difference between the relaxed structures of the singlet and the triplet states”.<sup>[89]</sup> The HOMO-LUMO gap and the singlet-triplet gap correlate with each other and a transition from singlet to triplet is roughly similar to a transition from HOMO to LUMO (Figure 16).<sup>[89, 137]</sup> The singlet-triplet gap can be used as metric for the reactivity of the NHC and probability to dimerize, with a larger gap indicating a more stable, monomeric carbene.<sup>[68, 78, 89, 138]</sup>

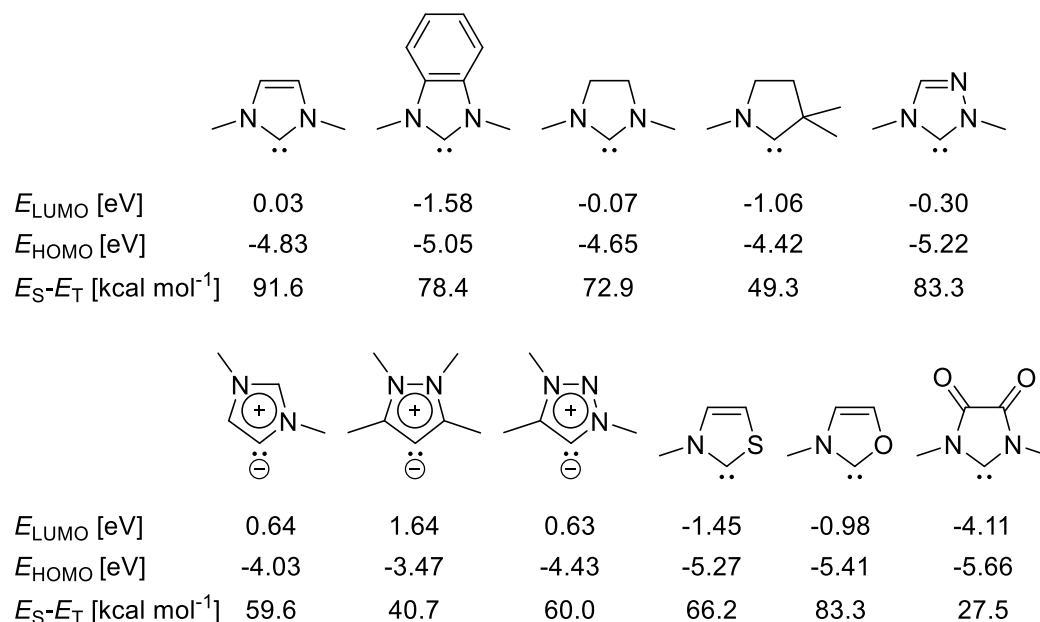


Figure 16. Calculated energy of the HOMO, LUMO and singlet-triplet gap ( $E_{\text{S}}-E_{\text{T}}$ ) of selected calculated NHCs.<sup>[31]</sup>

### 1.1.5. Quantification of the steric properties of NHCs

The steric properties of NHCs can be evaluated using the percent buried volume, which produces a single parameter and describes the buried volume of a NHC upon coordination to a metal in a virtual sphere with fixed properties ( $d = 2.00$  or  $2.28$  Å,  $r = 3.5$  Å, Figure 17).<sup>[112, 139]</sup>

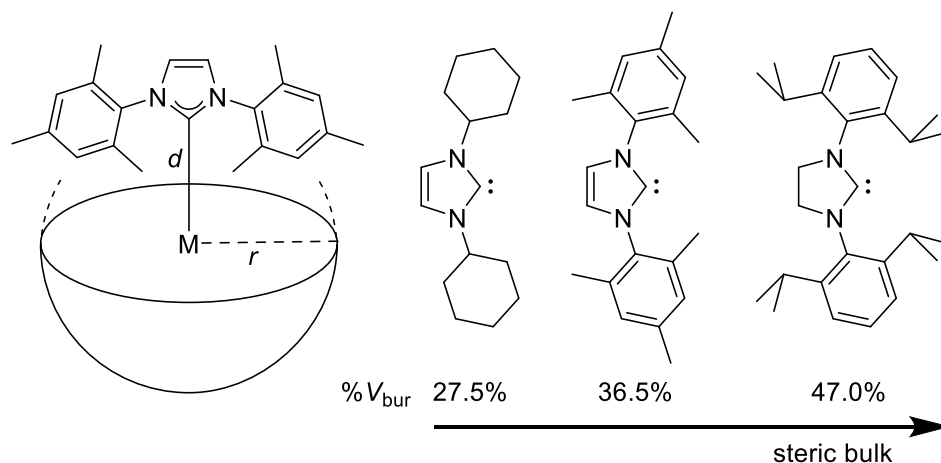
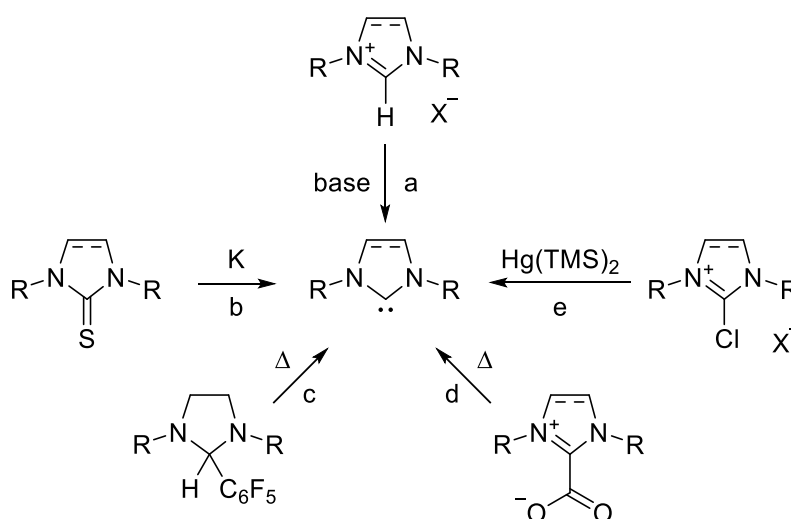


Figure 17. Principle of percent buried volume ( $\% V_{\text{bur}}$ , adapted from<sup>[1]</sup>).  $\% V_{\text{bur}}$  of some NHCs.<sup>[139-140]</sup>

Steric maps are another method and provide a visualization of the steric profile.<sup>[139]</sup>

### 1.1.6. Synthesis of NHCs

Azolium salts are common precursors for NHCs. An easy route to obtain azolium salts is the quaternization of the nitrogen atom of a neutral heterocycle, for example *N*-substituted imidazole.<sup>[33, 80, 141-142]</sup> An alternative is to directly obtain the azolium salt through cyclization, by final introduction of the precarbenic unit, the backbone, or the amino moiety.<sup>[80]</sup> The deprotonation of the azolium salt with a base is one of the most common routes to free NHCs (a, Scheme 1).<sup>[93]</sup> Another method is the reduction of thiourea with molten potassium in boiling THF (b), with the advantage of the insoluble by-product  $K_2S$ , thus readily removable.<sup>[80, 93, 143-144]</sup> A third route (c) involves the vacuum pyrolysis of the NHC precursor to release volatile by-products such as  $C_6F_5H$ , MeOH,  $CHCl_3$ ,  $CHF_3$ .<sup>[80, 93, 145-146]</sup> Similarly, NHC-CO<sub>2</sub> and NHC-metal (Sn<sup>II</sup>, Mg<sup>II</sup>, Zn<sup>II</sup>) adducts can be used to form NHCs *in situ* (d).<sup>[80, 93, 147-148]</sup> Finally, chloro amidinium and azolium salts can be reduced with  $Hg(TMS)_2$  (e).<sup>[80, 93, 149]</sup>



Scheme 1. Common routes to NHCs (adapted from<sup>[93]</sup>). TMS = trimethylsilyl.

### 1.1.7. Applications of NHCs

Despite being developed three decades ago, NHCs are still highly relevant in various fields of chemistry.<sup>[4]</sup> With their strong electron donating properties, the most obvious application is the use of NHCs in coordination chemistry as ligands bound to transition metals.<sup>[1]</sup> NHCs appeared to be both better  $\sigma$ -donors and  $\pi$ -acceptors than the frequently used phosphanes, therefore replacing phosphanes on several occasions in transition metal complexes, with the Grubbs catalyst for olefin metathesis being the most prominent example (Figure 4). In addition, NHCs

tend to form thermodynamically stronger NHC–metal bonds in complexes than their phosphane analogs, making NHC complexes more thermally and oxidatively stable compared to the phosphane counterparts.<sup>[1, 150]</sup> NHC complexes of 5d metals usually are more stable than those of 3d or 4d elements.<sup>[72, 91]</sup> However, NHC–metal bonds can be quite kinetically labile, as recently reported.<sup>[151]</sup> In general, the choice of ligand depends strongly on the task at hand, and the electronic properties of NHCs are not always desirable.<sup>[72, 152]</sup>

The most important application of NHC transition metal complexes is homogeneous catalysis (e.g. Figure 4).<sup>[1, 153-157]</sup> Transition metal NHC complexes have also become interesting for medicinal chemistry, with especially Ag and Au, but also Pd, Pt, Rh, Ru and Ir NHC complexes being promising candidates for antibacterial and anticancer agents.<sup>[1, 158-160]</sup> Other applications of NHCs coordinated to transition metals include heterogeneous catalysis and organometallic materials like metal-organic frameworks.<sup>[1, 17, 161-164]</sup>

The coordination of NHCs to main group elements is a second large field of research.<sup>[1, 4, 165-167]</sup> NHC main group adducts can act as new ligands, for example *N*-heterocyclic olefins or imines.<sup>[4, 168-170]</sup> NHCs are employed to stabilize highly reactive species, like a Al=Al dialumene.<sup>[4, 171]</sup> Furthermore, NHCs can activate small molecules, as part of frustrated Lewis pairs or by themselves.<sup>[1, 172-174]</sup> Here, the classes of NHCs show a different reactivity, for example, CAACs can activate CO, H<sub>2</sub> and NH<sub>3</sub>, while Arduengo-type NHCs are unreactive in this regard.<sup>[28, 175-177]</sup>

A third field of research is the application of NHCs as organocatalysts in a wide range of organic transformations.<sup>[1, 178-179]</sup> The reaction of the NHC with a carbonyl group is usually the initial step.<sup>[1]</sup>

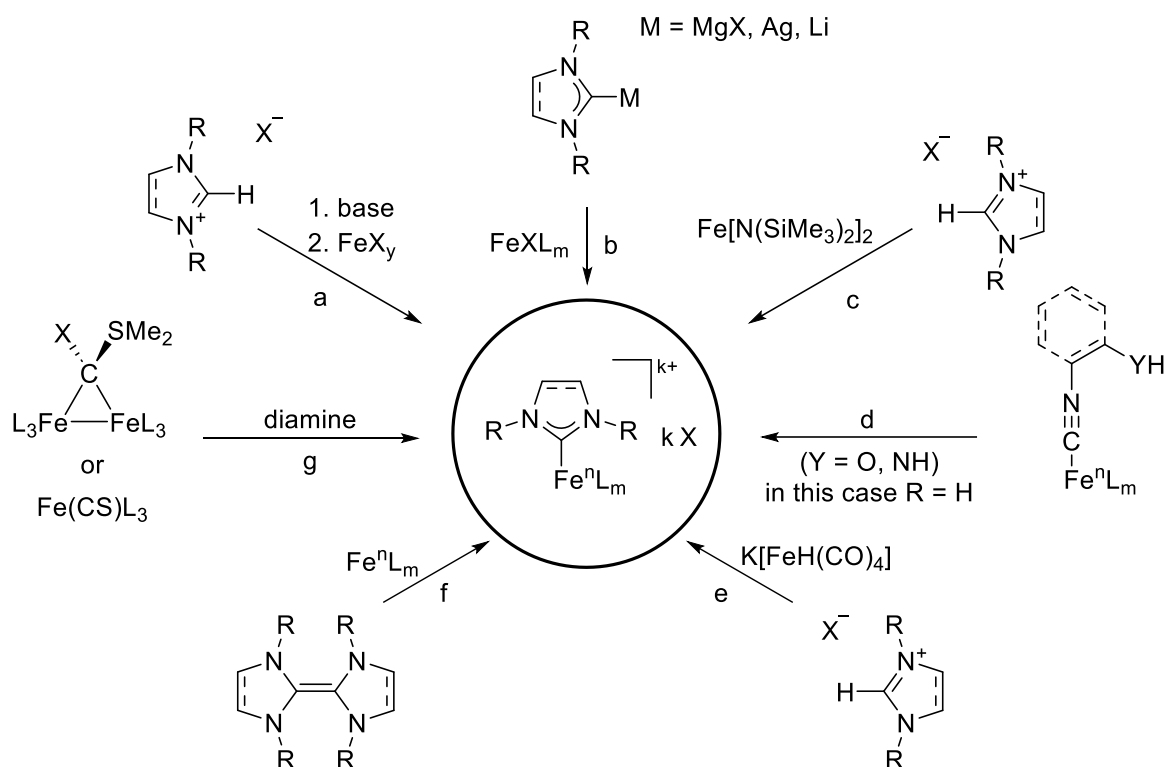
## 1.2. Iron NHC complexes

Iron is one of the most abundant elements in the Earth's crust, making it readily available and relatively cheap compared to noble metals.<sup>[180-181]</sup> It can be present in formal oxidation states ranging from -2 to +6.<sup>[181-184]</sup> Iron is an essential trace element and iron, iron oxides and most of iron salts are relatively nontoxic.<sup>[181, 185]</sup> Around 1.300 ppm of residual iron is considered acceptable in drug substances, whereas ≤10 ppm is mandated for the majority of other transition metals.<sup>[181, 186]</sup> Iron plays an important role in biology and is involved in many transformations driven by iron containing enzymes.<sup>[187]</sup> The above mentioned facts make iron an interesting element to use in chemistry, especially in catalysis, considering the potential economic benefits. The social demand for environmental benign and sustainable chemical solutions

(“green chemistry”) further contributes. Iron is already an important transition metal in heterogeneous catalysis, with the two most prominent examples being the Haber-Bosch and the Fischer-Tropsch processes.<sup>[187]</sup> Instead, the field of homogeneous catalysis has been rather dominated by noble metals, and research on iron catalysis has only started to emerge and gain momentum in the last 15-20 years.<sup>[181, 188-190]</sup> Still in 2011, Beller and coworkers wondered, why iron catalysis was underdeveloped compared to other transition metals, while it “should be one of the most used metals in homogeneous catalysis”<sup>[190]</sup> in their opinion, due to the combination of the above mentioned arguments.<sup>[190]</sup> Nowadays, iron is described as “multitasking champion”<sup>[181]</sup> due to the fact that “iron catalysis is potentially capable of covering almost the entire range of organic synthesis”<sup>[181]</sup> and backed by recent developments.<sup>[11, 181, 187-189, 191-192]</sup>

### 1.2.1. Synthesis and applications of iron NHC complexes

The first example of an iron NHC complex was reported by Öfele in 1969.<sup>[193]</sup> However, it took more than 30 years for the research field to come back into the focus of chemists, but it has been growing ever since.<sup>[187]</sup> The first three methods are the most common synthesis routes for iron NHC complexes (a-c, Scheme 2).<sup>[187]</sup> The first method (a) involves an external base to deprotonate the NHC precursor, followed by the addition of an iron precursor, usually an iron(II) or iron(III) halide salt.<sup>[187, 194]</sup> In theory, any isolable free NHC can be used in this way. The transmetalation route (b) is a useful alternative to the first route.<sup>[187, 195]</sup> Finally, the application of an internal base (c) is an effective method to directly obtain the respective iron(II) NHC complex from the azolium salt.<sup>[196]</sup> The iron precursor  $\text{Fe}[\text{N}(\text{SiMe}_3)_2]_2$  contains two equivalent (eq.) of internal base, therefore able to deprotonate two molecules of the NHC precursor at once. This is the most popular route for the synthesis of iron(II) NHCs.<sup>[187]</sup> Less frequently used methods are the cyclization of iron-bound isocyanides (d), also known as template synthesis and allowing post-complexation reactivity of the ligand (**A** in Figure 18),<sup>[197-200]</sup> the complexation of the azolium salt with the iron precursor  $\text{K}[\text{FeH}(\text{CO})_4]$  (e),<sup>[193, 201]</sup> the complexation of the NHC dimerization product with iron precursors like  $\text{Fe}(\text{CO})_5$  (f)<sup>[202-203]</sup> and formation of the NHC ligand from a precoordinated carbon atom<sup>[204-205]</sup> (g, Scheme 2).<sup>[187]</sup> The route of choice depends on the specific case and sometimes one method might give higher yields than the other or not be successful at all.<sup>[11, 206-207]</sup>



Scheme 2. Common pathways to Fe NHC complexes (adapted from<sup>[187, 208]</sup>).  $n = -2$  to  $+6$ ,  $m = 3-5$ .

Nowadays, iron NHC complexes have been applied in various catalytic reactions covering oxidation, reduction, cyclization, polymerization, C–C and C–X bond formation, up to transformations like the deuteration or tritiation of  $sp^2$  C–H bonds (**B**, Figure 18), being highly relevant for medicinal chemistry.<sup>[1, 4, 187, 191-192, 209-225]</sup> Other research focuses, for example, on the potential application of iron NHCs as photosensitizers in photovoltaics and artificial photosynthesis.<sup>[226-232]</sup> The reactivity of iron NHC complexes is also being studied and species with high oxidation states can be isolated, e.g.  $Fe^V \equiv N$  (**C**, Figure 18),<sup>[218, 233]</sup> enabled by the strong electron donation of the NHC ligands.<sup>[234]</sup>

## 1.2.2. Design of iron NHC complexes

There are many variables in the design of iron NHC complexes that can be changed in order to receive the respective complex tailored to the demand and application. Some of the variables are briefly discussed in the following. The type of NHC, any NHC modification and the used coligands significantly impact the electronic and steric properties of the iron complex. Also, the number of NHC moieties is decisive and can usually vary between one and six (Figure 18). The connectivity of the NHC and other coligands amongst each other is another variable to be determined. The chelating effect can be used with multidentate ligands, inducing greater stability in the complex formed. Simultaneously, the rigidity of the multidentate ligand is another important factor, for example, one catalytic application might benefit from a rigid ligand<sup>[235-237]</sup>

whereas another might need a more flexible ligand<sup>[11, 238-239]</sup>. The rigidity or flexibility of the ligand can also impact the structure of the iron complex.<sup>[240-242]</sup> The type of counterion can have an influence on the solubility of the complex, for example, the weakly coordinating  $\text{PF}_6^-$  anion can decrease the polarity of the complex, increasing its solubility towards less polar solvents. The oxidation state defines the Lewis acidity of the iron center. The complex synthesis in coordinating solvents like MeCN or DMSO can lead to coordinating solvent molecules to the iron atom. The coordination strength of the used ligands is important to consider for catalysis, where accessible coordination sites are required. Here, solvent molecules are helpful, as they are oftentimes labile coordinating ligands (see e.g.  $\sigma$ -donor strength of MeCN in Figure 11) and allow substrate binding to the iron center during catalysis. Non-coordinating functional groups at the ligands can allow for immobilization of the iron NHC complex or for post-complexation reactivity (see **A** in Figure 18). For some applications, having a complex with multiple iron centers might be desirable, for example for bio-inspired catalysts.

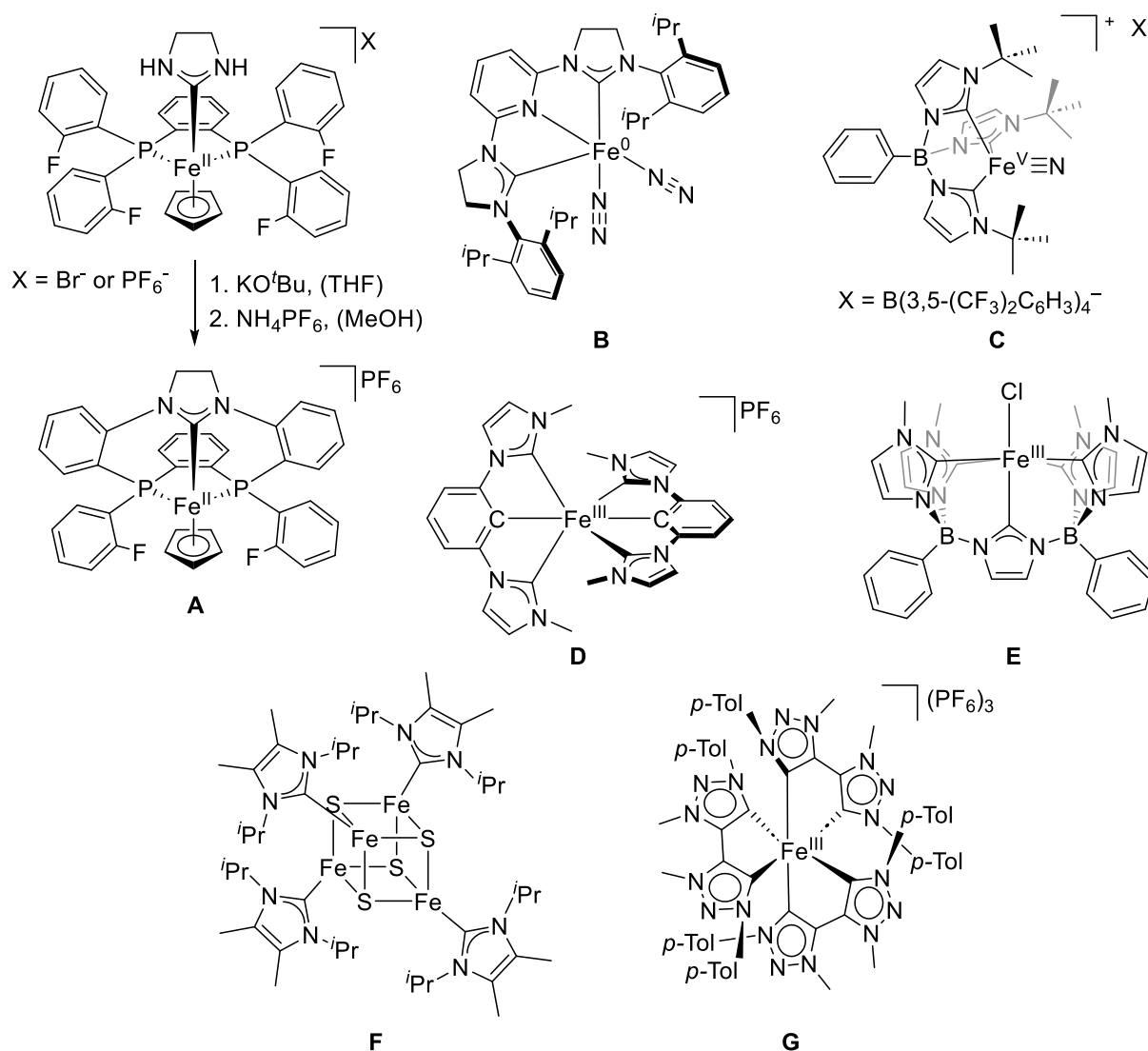
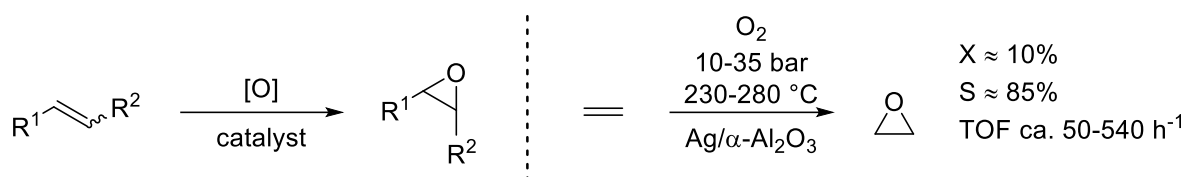


Figure 18. Selected iron NHC complexes with various characteristics (adapted from<sup>[192, 233-234, 243-248]</sup>). *p*-Tol = *para*-toluene. Formally  $\text{Fe}^{\text{II}}$  atoms in **F** ( $[\text{Fe}_4\text{S}_4]^0 \cong 4\text{Fe}^{2+} + 4\text{S}^{2-}$ ). <sup>t</sup>Bu = *tert*-butyl.

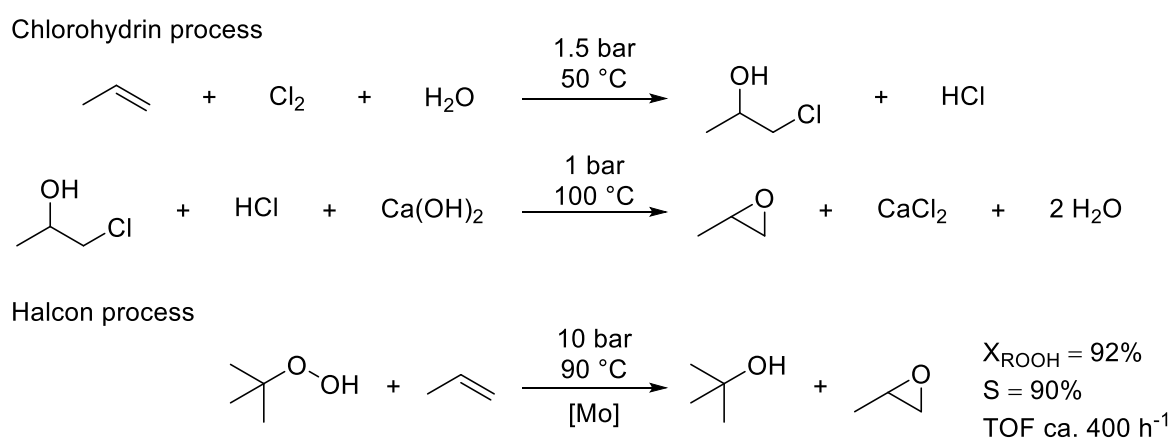
### 1.3. Homogeneous olefin epoxidation catalysis

The epoxidation of olefins (Scheme 3) is an important reaction for the production of commodity chemicals to fine chemicals.<sup>[249]</sup> The annual production volume can be up to millions of tons.<sup>[249]</sup> The production of commodity chemicals – and most other epoxides in industry – is usually performed with commercial, heterogeneous catalysts, because of their robustness and the possibility to easily separate the product as well as recycle the catalyst.<sup>[249-250]</sup> For example, ethylene is converted to ethylene oxide with a silver catalyst supported on  $\alpha$ - $\text{Al}_2\text{O}_3$  by direct oxidation with oxygen or air (Scheme 3).<sup>[249, 251]</sup> The worldwide production of ethylene oxide was around 31.6 million tons in 2022 and the majority is used to obtain ethylene glycol.<sup>[249, 252]</sup>



Scheme 3. Catalytic epoxidation of olefins (left). Heterogeneous oxidation of ethylene to ethylene oxide (right, adapted from<sup>[249, 251]</sup>). X = conversion, S = selectivity, TOF = turnover frequency.

Heterogeneous processes often require harsh conditions while giving rather low product yields (Scheme 3).<sup>[225, 253]</sup> In this regard, homogeneous catalysts can be an alternative. However, the possible drawbacks of homogeneous catalysts have to be considered, e.g. difficult separation of the catalyst from the product, loss of the catalyst/ligand(s) after separation and due to degradation during reaction, and cost of the ligand/catalyst synthesis.<sup>[253]</sup> The production of propylene oxide was historically performed uncatalyzed *via* the chlorohydrin process (Scheme 4).<sup>[249]</sup> The Halcon process offers a more economical alternative for the production of propylene oxide using a homogeneous Mo naphthenate catalyst with *tert*-butyl hydroperoxide or ethylbenzene hydroperoxide as oxidants and is therefore a prominent example of an industrial homogeneous epoxidation process (Scheme 4).<sup>[254]</sup>



Scheme 4. Chlorohydrin process (top) and Halcon process (bottom, adapted from<sup>[249, 253-254]</sup>).

Homogeneous catalysts are also applied in highly selective or asymmetric epoxidations in industry (see 1.3.3), but these tend to be niche applications on a rather small scale.<sup>[255-256]</sup> Most other homogeneous epoxidation catalysts have so far only been of interest to the scientific community due to the disadvantages mentioned above, although some catalysts achieve significantly higher TOFs than the heterogeneous processes.<sup>[249-250, 257]</sup> Biological systems are also being investigated and either extracted enzymes or living cells are used. Enzymes have similar drawbacks like homogeneous catalysts and living cell catalysis has to deal with the toxicity of the products, or used chemicals in general, and energy as well as mass transfer problems.<sup>[249]</sup>

### 1.3.1. Bio-inspired iron epoxidation catalysis

Epoxides are present in many natural products. The compounds can exhibit a variety of properties, for example antibiotic, antiviral, antifungal or antitumor activities.<sup>[258-260]</sup> In nature, the epoxides are mainly formed through formal dehydrogenation of neighboring C–H and CO–H groups or epoxidation, *i.e.* insertion of an oxygen atom into the C=C double bond of an alkene.<sup>[258-260]</sup> The epoxidation is catalyzed by various enzymes, for example flavin based enzymes, heme and nonheme mononuclear iron enzymes as well as nonheme diiron enzymes.<sup>[258-266]</sup> The most studied enzymes are cytochromes P450 containing a heme unit.<sup>[267-270]</sup> Originally to study their mechanism, biomimetic iron porphyrin complexes have been developed.<sup>[271-274]</sup> The epoxidation mechanism of cytochromes P450 begins with the low-spin iron(III) resting state, followed by the coordination of an oxygen molecule to the reduced high-spin iron(II) center, resulting in an iron(III)-hydroperoxo intermediate ( $\text{Fe}^{\text{III}}\text{--OOH}$ ), which undergoes O–O heterolysis to form  $\text{Fe}^{\text{IV}}\text{=O}(\text{por}\cdot)$ , a porphyrin  $\pi$  cation radical, as active species and oxidant in the reaction (Figure 19).<sup>[269, 275-276]</sup> Due to the ability of cytochromes P450 to oxidize non-activated substrates under mild conditions with high activity and selectivity,<sup>[249, 277]</sup> these enzymes also became interesting models for bio-inspired iron epoxidation (and C–H oxidation) catalysts, in addition to the above mentioned characteristics of iron (see 1.2).<sup>[271, 273, 278-279]</sup> The research has later been extended to bio-inspired nonheme iron complexes,<sup>[280]</sup> which can have accessible *cis* coordination sites allowing for *cis*-dihydroxylation of alkenes in addition to epoxidation and in contrast to the heme systems.<sup>[269]</sup> The ligand topology of the complex influences the selectivity towards epoxide or *cis*-diol, and labile ligands in *cis* coordination are proposed to be essential for *cis*-dihydroxylation.<sup>[10, 237, 281-283]</sup> Iron complexes with tetradentate ligands have been studied the most and have been shown to be the most efficient systems in oxidation catalysis compared to compounds with bidentate, tridentate or pentadentate ligands (Figure 19).<sup>[237]</sup> The most active bio-inspired, *N*-ligated iron complexes achieve TOFs up to 25 200 h<sup>-1</sup>

in epoxidation.<sup>[284]</sup> Turnover numbers (TON, a measure of the lifetime/stability of the catalyst)<sup>[250]</sup> of less than 100 are usually reported for *N*-ligated iron complexes in epoxidation<sup>[216]</sup> and the highest TONs are 180<sup>[284]</sup>, 715<sup>[285]</sup> and 252<sup>[286]</sup>. The proposed mechanism for epoxidation by nonheme iron complexes with tetradentate ligands and *trans* labile coordination sites is shown below (Scheme 6).<sup>[216]</sup>

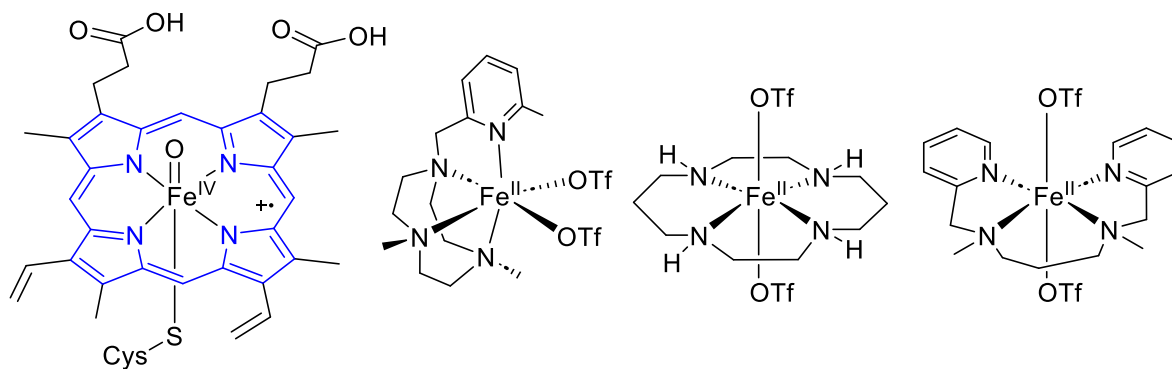


Figure 19. Active species of cytochromes P450,  $\text{Fe}^{\text{IV}}=\text{O}(\text{por}\cdot)$ , also called compound I (left). The porphyrin framework is marked blue. Selected examples of nonheme iron(II) complexes applied in epoxidation catalysis (right, adapted from<sup>[10, 237, 269-270, 277, 282, 286-288]</sup>). Cys = cysteine, OTf = triflate anion.

### 1.3.2. Iron NHC complexes in epoxidation catalysis

Organometallic Re and Mo complexes have been intensively studied in epoxidation catalysis.<sup>[214, 225, 250, 256]</sup> The two most active systems among them are methyltrioxorhenium (MTO, ca.  $39\,000\text{ h}^{-1}$ )<sup>[289]</sup> and a  $\eta^5$ -cyclopentadienyl Mo NHC complex (ca.  $53\,000\text{ h}^{-1}$ , Figure 20)<sup>[290]</sup>, being in the same range of extracted cytochrome P450 enzymes (ca.  $43\,000\text{ h}^{-1}$ )<sup>[249, 291]</sup> but beating *N*-ligated iron complexes in this regard (see 1.3.1).<sup>[214, 250]</sup>

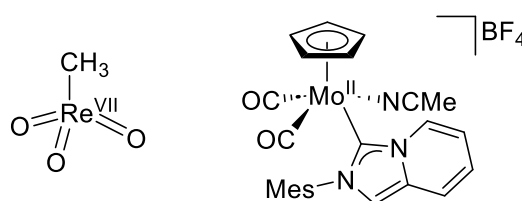


Figure 20. Two most active Re and Mo complexes in epoxidation catalysis (adapted from<sup>[289-290]</sup>).

With the growing research in the field of iron NHC complexes and the benefits of using iron in catalysis (1.2), the iron enzymes in nature as models for oxidation catalysis and the intensively investigated *N*-ligated biomimetic and bio-inspired iron complexes (1.3.1), as well as the good results obtained with other organometallic compounds (see above), it became interesting to study organometallic bio-inspired iron complexes in oxidation catalysis.<sup>[225]</sup> Iron(II) complex **1** (Figure 21) containing an open-chain bis(pyridine-NHC) ligand was the first iron NHC complex

to be employed in epoxidation catalysis.<sup>[292]</sup> H<sub>2</sub>O<sub>2</sub> proved to be the most efficient oxidant. Various substrates in moderate to high selectivity could be oxidized. An initial TOF of ca. 2 600 h<sup>-1</sup> could be determined in the epoxidation of *cis*-cyclooctene at 25 °C with 2 mol% of **1**, which is a slightly higher activity than the majority of *N*-ligated iron complexes under additive-free conditions show.<sup>[292]</sup> *cis*-Cyclooctene is a frequently used model and benchmark substrate in academic research.<sup>[250]</sup> Complex **1** was furthermore extensively studied in C–H hydroxylation of several substrates like cyclohexane or benzene.<sup>[223, 293-296]</sup> The stability/TON of **1** in C–H hydroxylation could be increased by up to 34% by axial ligand substitution of one MeCN moiety with strongly binding *tert*-butyl isocyanide (CN<sup>t</sup>Bu), resulting in only one accessible coordination site during catalysis with just one labile axial coordinating MeCN.<sup>[294]</sup>

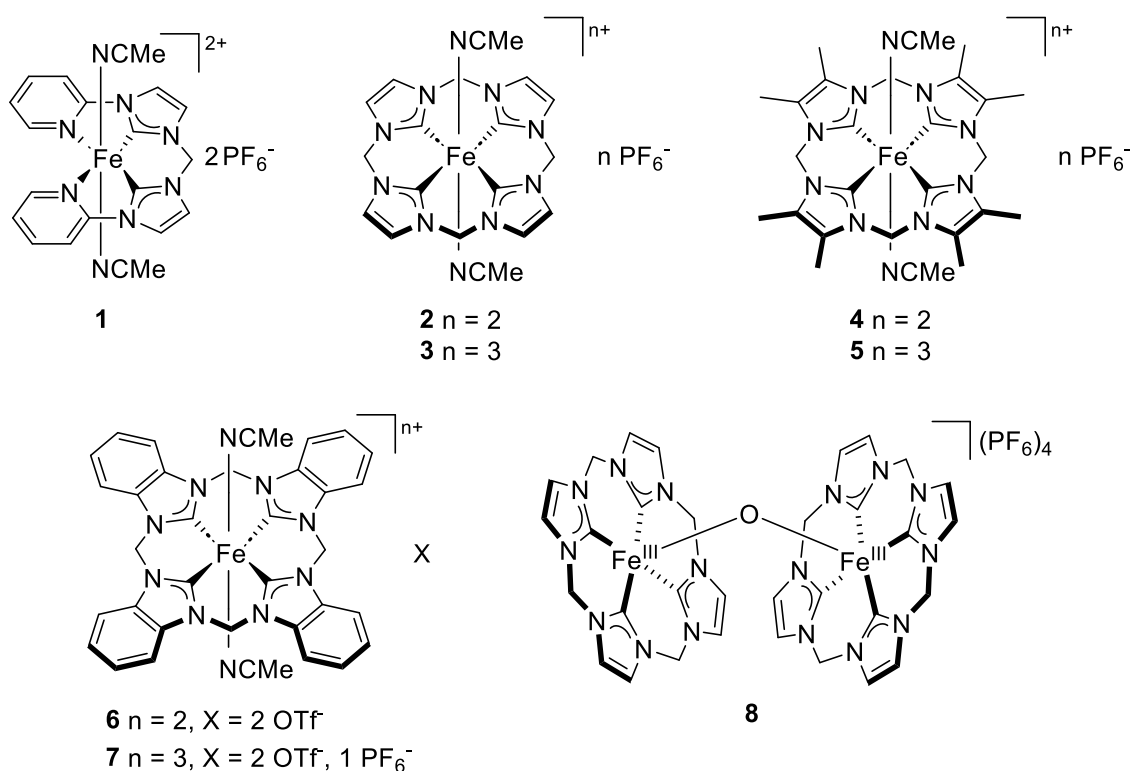


Figure 21. Iron(II) and iron(III) NHC complexes employed in epoxidation catalysis (adapted from<sup>[11, 240, 297-300]</sup>).

The developed cyclic iron tetracarbene complexes (**2-7**, Figure 21) structurally resemble the heme group as can be found in cytochromes P450 (Figure 19). They are however electronically distinct, mainly due to the strong  $\sigma$ -donation in equatorial plane to the iron center, resulting in a different reactivity compared to iron porphyrins.<sup>[11]</sup> The class of cyclic iron tetracarbene complexes has a rich chemistry, with diverse reactivity including isolable iron(IV) compounds stabilized by the strong electron donating tetracarbene ligand and, apart from epoxidation, iron tetracarbenes are applied in aziridination, CO<sub>2</sub> reduction and C–H activation.<sup>[11]</sup> Due to their structural similarity to heme, the shown iron tetracarbenes **2-7** (Figure 21) have been employed in epoxidation catalysis. Both **2** and **3** achieve very high TOFs (**2**: ca. 50 000 h<sup>-1</sup>, **3**: ca. 183 000 h<sup>-1</sup>, Table 1) in the epoxidation of *cis*-cyclooctene at 20 °C.<sup>[297]</sup> The activity is reduced

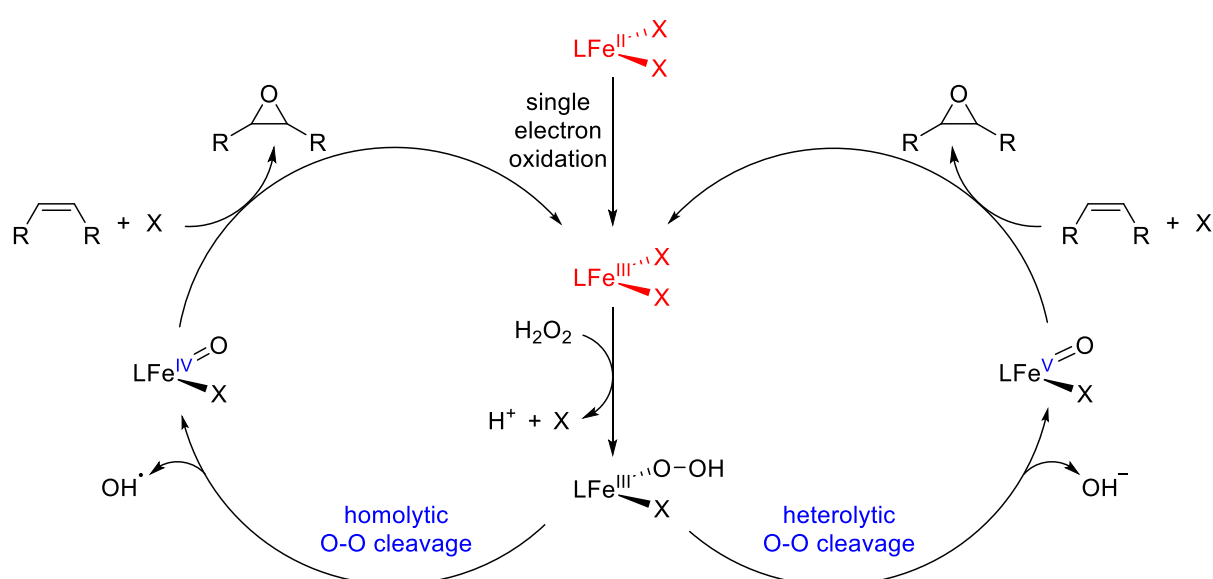
at lower temperatures, while a TON of 4 300 was determined at -30 °C for **3**. Various substrates are oxidized at very high selectivity and no diol formation is observed.<sup>[297]</sup>

Table 1. Selected catalytic performance of **2**, **3** and **8** in the epoxidation of *cis*-cyclooctene.<sup>[297, 301]</sup>

Cat.	Additive	X [%] <sup>a</sup>	S [%] <sup>a</sup>	TOF [h <sup>-1</sup> ] <sup>b</sup>	TON
<b>2</b>	–	24	94	50 000	480
<b>2</b>	Sc(OTf) <sub>3</sub>	59	>99	415 000	1180
<b>3</b>	–	51 <sup>c</sup>	>99	183 000	–
<b>3</b>	Sc(OTf) <sub>3</sub>	58	>99	413 000	1160
<b>8</b>	–	7	>99	23 000	140
<b>8</b>	Sc(OTf) <sub>3</sub>	58	>99	405 000	1160

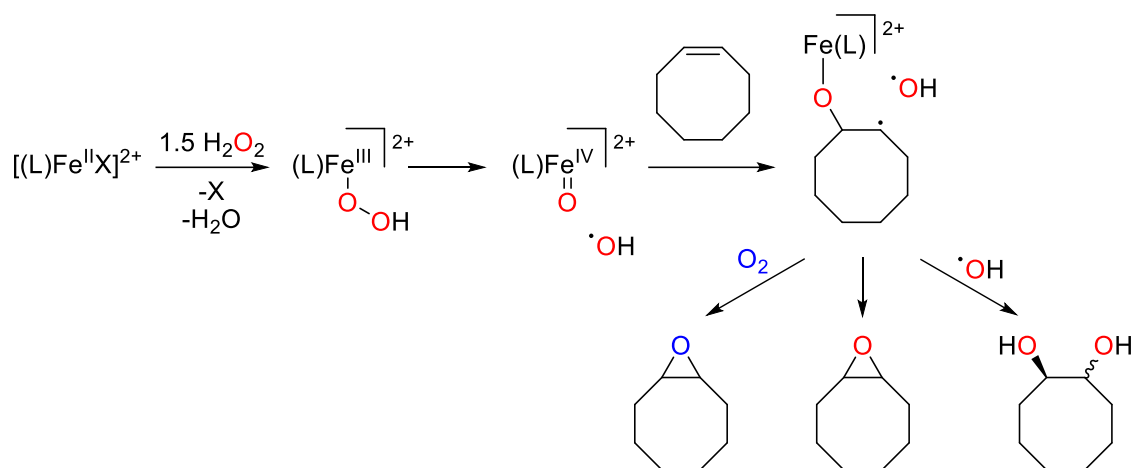
Reaction conditions: *cis*-cyclooctene (269 μmol, 100 mol%), H<sub>2</sub>O<sub>2</sub> (404 μmol, 150 mol%), catalyst (0.135 μmol, 0.05 mol% based on iron), additive (1.35 μmol, 0.5 mol%); solvent: acetonitrile; T = 20 °C. <sup>a</sup> All conversions (X) and selectivities (S) were determined by GC-FID after a reaction time of 5 min. <sup>b</sup> TOFs were determined after 10 s. <sup>c</sup> Catalyst concentration: 0.1 mol%, conversion was determined after 10 s.

The oxidation of iron(II) complex **2** to iron(III) analog **3** is proposed to be the first step in catalysis due to the observation of an induction period with **2** but not **3**.<sup>[297]</sup> Based on the mechanistic investigations with *N*-ligated iron complexes,<sup>[216]</sup> the following mechanism is suggested (Scheme 5): The iron(III) complex reacts with H<sub>2</sub>O<sub>2</sub> to result in an Fe<sup>III</sup>–OOH intermediate, followed by (presumably rate-determining) homolytic or heterolytic cleavage to form Fe<sup>IV</sup>=O or Fe<sup>V</sup>=O, respectively, as active species. After an electrophilic attack on the alkene, the epoxide is obtained.<sup>[111]</sup> It needs to be noted that no comprehensive mechanistic studies on iron NHC epoxidation catalysis have been performed yet, and no Fe<sup>III</sup>–OOH NHC complex and only a Fe<sup>IV</sup>=O complex with a larger tetracarbene ligand have been isolated – the latter complex has not yet been investigated in epoxidation catalysis.<sup>[225]</sup>



Scheme 5. Proposed mechanism for the epoxidation of olefins by iron NHCs, based on the mechanistic studies of *N*-ligated iron complexes (adapted from<sup>[216, 223, 225]</sup>). Compounds marked in red have been isolated.

Nonheme iron complexes with tetradentate ligands and *trans* labile coordination sites – thus structurally similar to the iron NHC complexes **1-7** – are expected to proceed *via* the Fe<sup>IV</sup>=O as active species (Scheme 6). The epoxide is either formed by transfer of the oxygen to the C=C double bond or by a radical mechanism with molecular oxygen. In one case, the diol was observed in inert atmosphere with MeCN as solvent.<sup>[10, 216, 302]</sup> On the other hand, the activation of the Fe<sup>III</sup>-OOH intermediate by Sc(OTf)<sub>3</sub> (see below) leads to the Fe<sup>V</sup>=O species after heterolytic cleavage in the case of nonheme iron complexes, however with *cis* labile coordination sites.<sup>[303]</sup>



Scheme 6. Proposed mechanism for the epoxidation of olefins by nonheme iron complexes without *cis*-labile sites (adapted from<sup>[10, 216, 302]</sup>).

One degradation pathway of **2/3** in catalysis was identified as the formation of a stable diiron(III)- $\mu_2$ -oxo complex (**8**, Figure 21) from **2** and **3** under oxidative conditions, having a comparatively low catalytic activity (Table 1).<sup>[301]</sup> Upon addition of a Lewis acid like Sc(OTf)<sub>3</sub>, both **2** and **8** form the same catalytically active complex **3**.<sup>[301]</sup> This means that by adding Sc(OTf)<sub>3</sub>, the less reactive decomposition product **8** can be reactivated and the necessary preoxidation of **2** to **3** is facilitated. This is reflected in the catalytic results: all three compounds **2**, **3** and **8** show effectively the same activity and stability in the presence of Sc(OTf)<sub>3</sub> (Table 1).<sup>[301]</sup> A remarkable TOF of  $>400\,000\ h^{-1}$  is determined,<sup>[301]</sup> making it the most active homogeneous epoxidation catalyst. It is over eight times more active than the most active iron *N*-ligated complexes, extracted enzymes and organometallic epoxidation catalysts (see above). Only in living cell catalysis a higher TOF of approximately  $500\,000\ h^{-1}$  was reported.<sup>[249, 304]</sup> The stability of **3** is also significantly increased by suppressing the deactivation path, resulting in a very high TON of ca. 1 100 at 20 °C.<sup>[301]</sup> However, reusable epoxidation catalysts with TONs up to 16 000 and higher have been reported.<sup>[305-306]</sup> The results of **2**, **3** and **8** are certainly also supported by the Lewis acid Sc(OTf)<sub>3</sub> activating the Fe<sup>III</sup>-OOH intermediate and facilitating the rate-determining  $OH^+/OH^-$  cleavage to faster generate the active Fe<sup>IV</sup>=O or Fe<sup>V</sup>=O oxidant.<sup>[284, 303, 307-308]</sup>

The backbone modification of the tetracarbene ligand with methyl groups results in a more electron donating ligand in **4/5**. The opposite is true in **6/7**. **4/5** are more active than **6/7**, but less active than **2/3** due to a low stability.<sup>[11, 299]</sup> **6/7** show a low activity at 20 °C in the presence of Sc(OTf)<sub>3</sub> (**7**: 11 000 h<sup>-1</sup>) but almost equally high TON of 1000 (**7**) compared to the benchmark system **2/3**.<sup>[299]</sup> The TOF of **7** increases with temperature and the opposite is the case with the TON, resulting in a TOF of 95 000 h<sup>-1</sup> and TON of 360 at 80 °C in the presence of Sc(OTf)<sub>3</sub>.<sup>[299]</sup>

Iron(II) NHC complexes **9/10** have *cis* labile coordination sites and an equilibrium between the *cis*-β and *cis*-α topology has been observed (Figure 22).<sup>[308-311]</sup> They were also applied in epoxidation catalysis and **10** had a better catalytic performance than **9**. In the case of iron complexes with *cis* labile coordination sites, not only Lewis acids but also coordinating (e.g. acetic acid) or non-coordinating (e.g. HClO<sub>4</sub>) Brønsted acids have a beneficial effect on the catalytic activity, with the same underlying principle of accelerating the heterolytic cleavage of Fe<sup>III</sup>-OOH (see above).<sup>[284, 307-308, 312]</sup> In addition, coordinating Brønsted acids can increase the selectivity towards epoxide formation, because they suppress the competing coordination of water, and the latter can lead to the ring-opening of the epoxide and subsequent *cis*-diol production.<sup>[284, 308]</sup> Indeed, both Lewis acids (Sc(OTf)<sub>3</sub>) and Brønsted acids (HClO<sub>4</sub>, acetic acid) could significantly increase the activity of **10**.<sup>[308]</sup> However, the selectivity was decreased in the case of Sc(OTf)<sub>3</sub> and HClO<sub>4</sub> due to ring opening of the formed epoxide induced by the Lewis/Brønsted acid.<sup>[308, 313]</sup> Under optimal conditions using 1.0 eq. of acetic acid at 20 °C and 0.1 mol% of **10**, a TON of 200 and a TOF of 76 000 h<sup>-1</sup> with 97% selectivity towards the epoxide could be determined.<sup>[308]</sup>

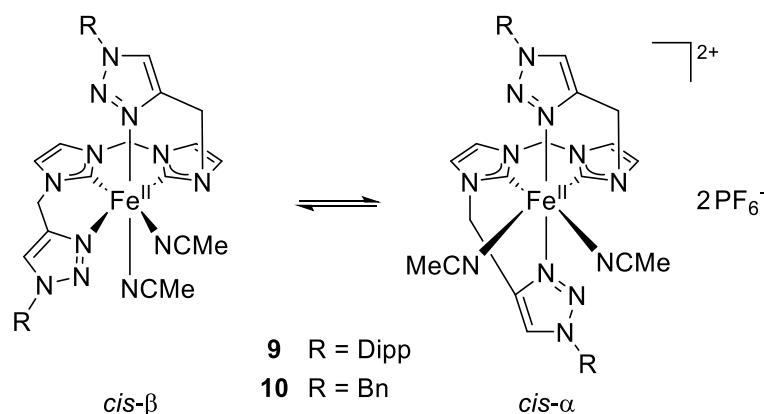
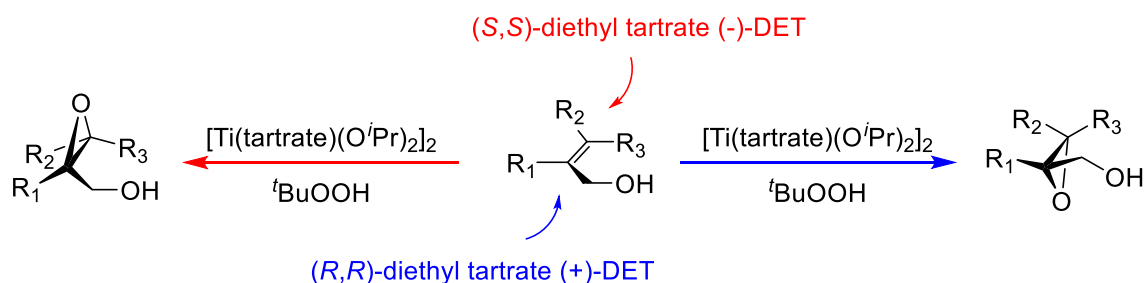


Figure 22. Iron(II) NHC complexes with *cis* labile coordination sites employed in epoxidation catalysis (adapted from<sup>[308]</sup>). Dipp = 1,5-diisopropylphenyl. Bn = benzyl.

### 1.3.3. Enantioselective epoxidation

The synthesis of chiral epoxides is important for the production of fine chemicals and pharmaceuticals.<sup>[249, 314-316]</sup> The two most prominent systems for asymmetric epoxidation were developed by Katsuki and Sharpless<sup>[317]</sup> for the enantioselective epoxidation of (exclusively) allylic alcohols as well as the groups of Katsuki<sup>[318-320]</sup> and Jacobsen<sup>[321-323]</sup> for the enantioselective epoxidation of general unfunctionalized alkenes. These systems have also found its way into industry on a small scale.<sup>[255]</sup> The Sharpless-Katsuki method uses a  $[\text{Ti}(\text{tartrate})(\text{O}^i\text{Pr})_2]_2$  catalyst, which is formed *in-situ* from the reaction of  $\text{Ti}(\text{O}^i\text{Pr})_4$  and a chiral diethyl tartrate. The used chiral diethyl tartrate conducts the addition of the epoxide oxygen (Scheme 7).<sup>[317]</sup> Sharpless was awarded with the 2001 Nobel Prize in Chemistry for his pioneering work in asymmetric epoxidation.<sup>[324]</sup>



Scheme 7. Sharpless-Katsuki asymmetric epoxidation of allylic alcohols, published in 1980 (adapted from<sup>[325]</sup>).

The Jacobsen-Katsuki epoxidation relies on Mn(III) salen catalysts with a chiral bridge (Figure 23).<sup>[326]</sup>

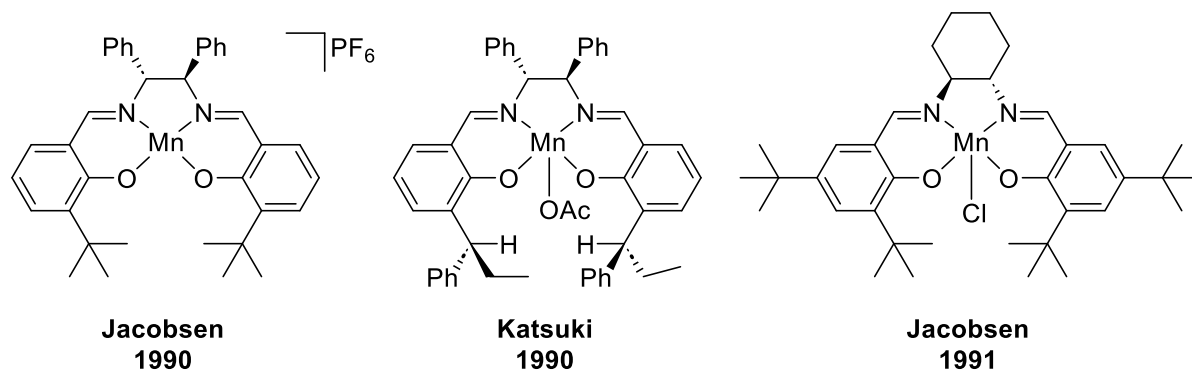


Figure 23. First chiral Mn(III) salen complexes developed by Jacobsen and Katsuki for the enantioselective epoxidation of general unfunctionalized alkenes (adapted from<sup>[318, 321-322]</sup>).

Nowadays, there is a plethora of chiral-directing catalytic systems with different approaches developed for the asymmetric epoxidation of various substrates.<sup>[256, 305, 315-316, 325, 327-332]</sup> The most notable mention is the metal-free organocatalytic epoxidation (Figure 24)<sup>[316]</sup> and the 2021 Nobel Prize in Chemistry was awarded to List and MacMillan “for the development of asymmetric organocatalysis”.<sup>[333]</sup>



## 2. Objective

One objective of this thesis is the continuation of the research regarding iron NHC epoxidation catalysis. In this regard, new ligand systems are developed and their influence on the catalytic performance of the respective iron NHC complexes is investigated. In addition, the degradation of the most active iron NHC catalyst is studied.

Furthermore, another subject of this work is the investigation of the reactivity of iron NHC complexes. Here, the oxidation of a diiron(III)- $\mu_2$ -oxo compound up to diiron(IV)- $\mu_2$ -oxo is studied and moreover a  $\mu_2$ - $\eta^1:\eta^1$ -CN bridged diiron complex is discovered. A critical review article about the chemistry of cyclic iron tetracarbene complexes is elaborated and their synthesis, properties, reactivity, and catalytic applications are discussed in-depth.

Finally, new NHC ligand systems are to be developed as framework for transition metal complexes with various applications. In this respect, the synthesis of chiral NHC and mesoionic carbene ligand precursors are first strides towards enantioselective epoxidation catalysts. In addition, several new multidentate NHC ligand systems are designed and open-chain as well as cyclic palladium, platinum, and gold tetracarbene complexes are obtained. Their apoptotic effect in cancer cells is investigated.

### **3. Results and discussion – publication summaries**

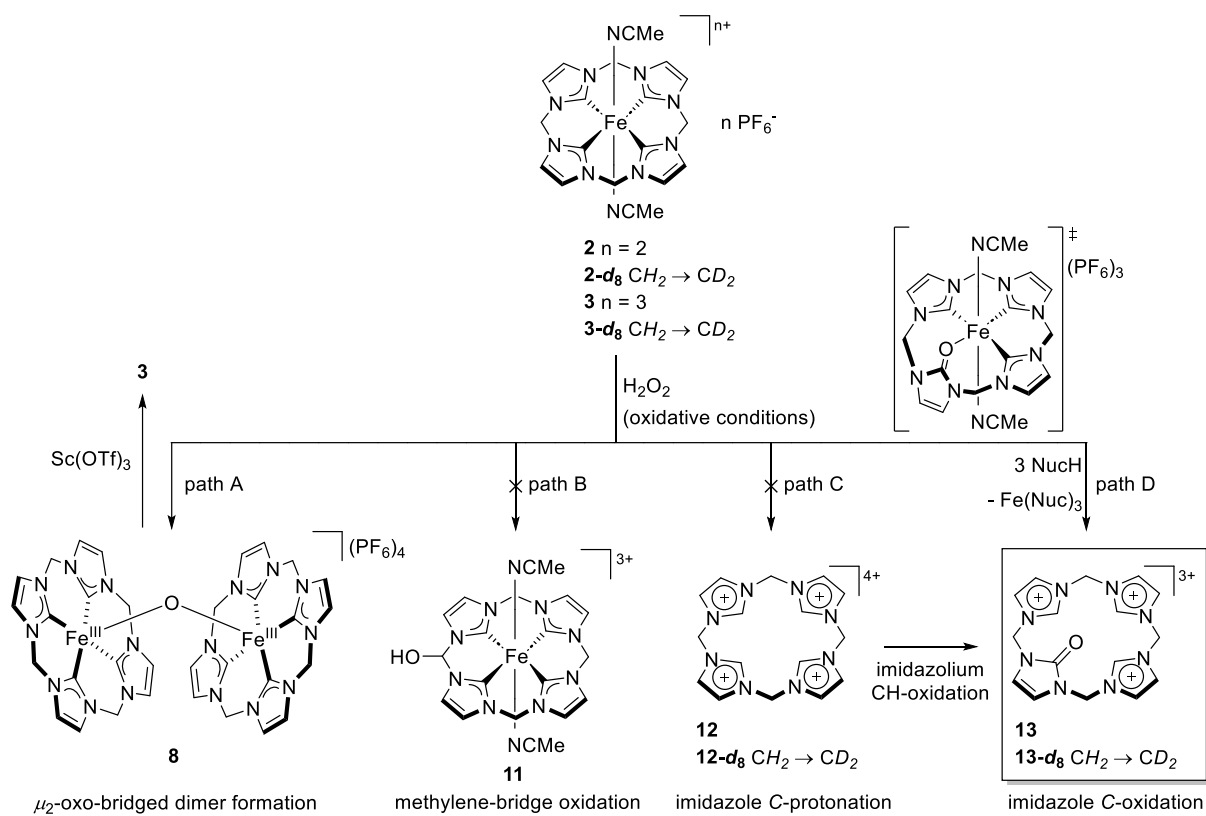
This chapter summarizes the published results of the doctoral thesis. The publications are ordered chronologically. A complete list of publications is given in chapter 7. The individual contributions of Tim P. Schlachta to the publications are given in Table 2, chapter 7. The full text of the publications is attached to this thesis, reprint permissions and bibliographic data are given in chapter 6 and 8, respectively.

### 3.1. Degradation pathways of a highly active iron(III) tetra-NHC epoxidation catalyst

Florian Dyckhoff, Jonas F. Schlagintweit, Marco A. Bernd, Christian H. G. Jakob, **Tim P. Schlachta**, Benjamin J. Hofmann, Robert M. Reich, Fritz E. Kühn

*Catal. Sci. Technol.* **2021**, *11*, 795-799, DOI: 10.1039/D0CY02433C <sup>[335]</sup>

Understanding the degradation of a catalyst is important to take measures to increase its stability during reaction and achieve an overall better catalytic performance. The aim of this study is to elucidate the degradation of the highly active iron tetracarbene complexes **2/3** during epoxidation catalysis. One already determined degradation pathway of **2/3** is the formation of a stable diiron(III)- $\mu_2$ -oxo complex **8** with rather low activity (Table 1).<sup>[301]</sup> However, **8** can be reactivated to the catalytically active complex **3** by Lewis acid Sc(OTf)<sub>3</sub> (Scheme 8, path A) and the stability in TON is more than doubled (Table 1).<sup>[301]</sup> As the lifetime of **2/3** is still rather low for real-life applications, further investigation is conducted to determine the ultimate degradation route of **2/3** during catalysis.<sup>[335]</sup> The formation of a dead-end  $\mu_2$ -oxo-bridged Fe–O–Fe complex and the C–H oxidation of the methylene bridges are the most frequently observed degradation paths for nonheme iron oxidation catalysts.<sup>[11, 335-343]</sup> A methylene-bridge oxidation can be excluded for **2/3** due to the absence of a kinetic isotope effect in catalytic studies between **3** and an analog complex with deuterated methylene bridges, **3-*d*<sub>8</sub>** (Scheme 8, path B). A threefold protonated and mono oxidized species derived from the tetracarbene ligand is found in NMR (**13**, Scheme 8). To avoid protonation of the ligand during catalysis, the addition of intercepting bases is considered. Upon addition of bases to a solution of **3** in MeCN, the immediate reduction of **3** to **2** is observed due to the oxidation of the axial MeCN ligands or MeCN solvent to glycolonitrile. Axial ligand substitution of **3** with <sup>t</sup>BuCN or PhCN is conducted,<sup>[344]</sup> both containing less activated C–H bonds to avoid undesired oxidation. Catalytic tests of these derivatives of **3** in different solvents in the presence of additive bases do not show a beneficial effect in catalysis. No fully protonated ligand (**12**) can be observed in mass spectroscopic experiments under oxidative conditions, but rather **13** and a species derived from **3** containing a mono oxidized NHC ligand still coordinated to the iron atom. Therefore, path C is finally excluded. To conclude, the oxidation of one carbene initiates decoordination of the NHC ligand from the iron center, followed by the protonation of the remaining three carbenes (Scheme 8, path D).



Scheme 8. Excluded (path B and path C) and determined degradation pathways (path A and path D) for iron tetra-carbene complexes **2/3** in epoxidation catalysis (adapted from<sup>[11, 335, 345]</sup>). Nuc = generic nucleophile.

### 3.2. Mimicking reactive high-valent diiron- $\mu_2$ -oxo intermediates of nonheme enzymes by an iron tetracarbene complex

Tim P. Schlachta,<sup>#</sup> Markus R. Anneser,<sup>#</sup> Jonas F. Schlagintweit, Christian H. G. Jakob, Carolin Hintermeier, Alexander D. Böth, Stefan Haslinger, Robert M. Reich, Fritz E. Kühn

<sup>#</sup> Tim P. Schlachta and Markus R. Anneser contributed equally to this work.

*Chem. Commun.* **2021**, 57, 6644-6647, DOI: 10.1039/D1CC02027G <sup>[346]</sup>

Nonheme diiron enzymes catalyze several reaction types through the activation of oxygen.<sup>[346-347]</sup> One prominent example is soluble methane monooxygenase, converting methane to methanol.<sup>[348]</sup> All of these enzymes involve highly reactive diiron-oxygen intermediates as active species, oftentimes with iron centers in high oxidation states (+3 or higher), for example a diiron(IV)- $\mu_2$ -oxo species (intermediate Q) for soluble methane monooxygenase<sup>[347, 349]</sup> or diiron(III,IV)- $\mu_2$ -oxo intermediate in ribonucleotide reductases.<sup>[346, 350]</sup> Biomimetic models to study the mechanisms of these enzymes are rare and usually rely on *N*-donor ligands.<sup>[347, 351-353]</sup>

In this article, the chemistry of **8** is further explored. Upon single-electron oxidation of **8**, a diiron(III,IV)- $\mu_2$ -oxo complex can be isolated and characterized (**14**, Figure 25, Scheme 9). **14** has a nearly linear axis intersecting the axial MeCN ligands and the FeOFe unit (Fe–O–Fe 176.34°), in contrast to **8**, which is more bent (**8**: Fe–O–Fe 162.7°)<sup>[300]</sup>. In addition, there are two coordinating axial MeCN ligands in **14**, possibly because of the more Lewis acidic iron centers.<sup>[11]</sup> EPR measurements reveal an overall spin *S* = 1/2 for the paramagnetic complex **14** while the diiron(III)- $\mu_2$ -oxo complex **8** is diamagnetic due to antiferromagnetic coupling.

The possibility of a diiron(IV)- $\mu_2$ -oxo species is indicated in CV. Furthermore, the formation of a new species can be monitored in UV/Vis upon addition of two equivalents of one-electron oxidant thianthrenyl hexafluorophosphate to a solution of **8**, proceeding *via* the interim generation of **14**. The decay of this species to **3** is observable in UV/Vis and NMR. The species could not be isolated but is very likely to be a diiron(IV)- $\mu_2$ -oxo complex (**15**, Scheme 9) based on the collected data from CV, UV/Vis and NMR. The decay of this species to **3** proceeds with an oxygen transfer to thianthrene forming thianthrene 5-oxide. Two-electron oxidation of **8** by two equivalents of thianthrenyl hexafluorophosphate at room temperature also directly yields two equivalents of **3** and one equivalent of thianthrene and thianthrene 5-oxide, respectively (Scheme 9).

**14** and **15** are the first examples of diiron(III/IV)- and diiron(IV)- $\mu_2$ -oxo complexes with NHC ligands. In addition, **14** is only the third reported crystallized example among the group of diiron(III/IV)- and diiron(IV)- $\mu_2$ -oxo complexes.

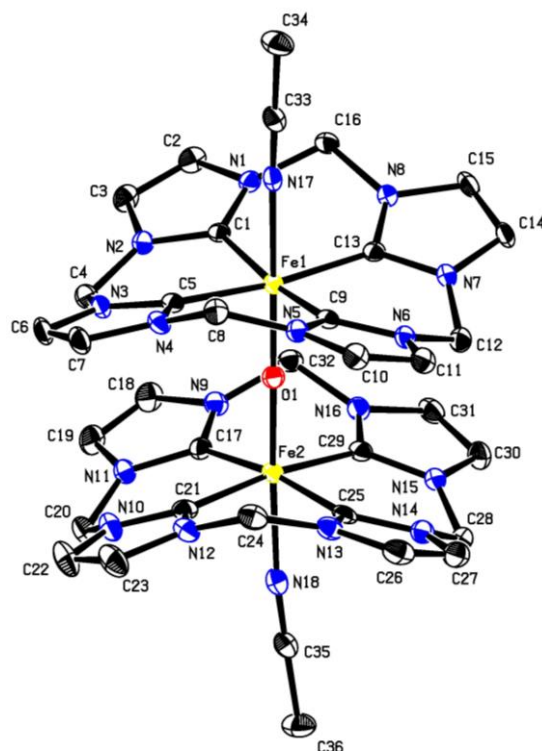
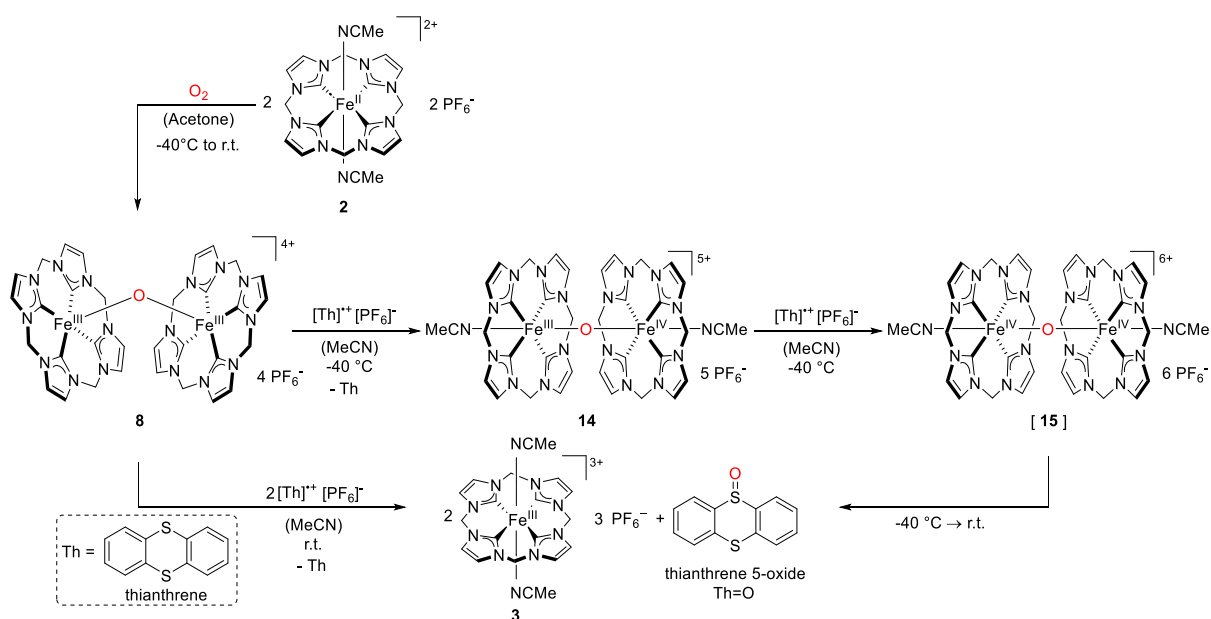


Figure 25. ORTEP-style representation of the cationic fragment of **14**.<sup>[346]</sup> Hydrogen atoms and  $\text{PF}_6^-$  anions are omitted for clarity and thermal ellipsoids are shown at a 50% probability level. Selected bond lengths ( $\text{\AA}$ ) and angles ( $^\circ$ ): Fe1–C1 1.929(2), Fe2–C17 1.931(3), Fe1–O1 1.7272(17), Fe2–O1 1.7298(17), Fe1–N17 1.984(2), Fe2–N18 1.987(2), Fe1–O1–Fe2 176.34(11), C1–Fe1–C5 89.43(10), C1–Fe1–O1 95.55(9), O1–Fe1–N17 178.09(8). Reproduced from Ref. <sup>[346]</sup> with permission from the Royal Society of Chemistry.



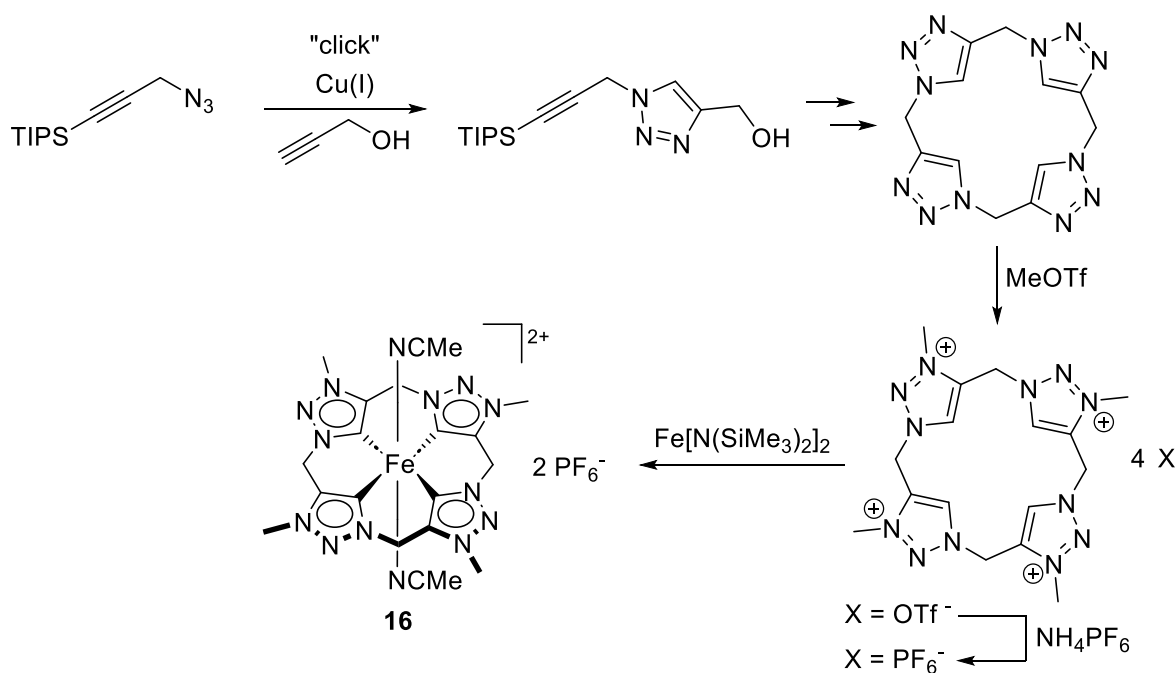
Scheme 9. Reactivity of **8** (adapted from<sup>[346]</sup>). Th = thianthrene, r.t. = room temperature.

### 3.3. The first macrocyclic abnormally coordinating tetra-1,2,3-triazole-5-ylidene iron complex: a promising candidate for olefin epoxidation

Greta G. Zámbo, Johannes Mayr, Michael J. Sauer, **Tim P. Schlachta**, Robert M. Reich, Fritz E. Kühn

*Dalton Trans.* **2022**, 51, 13591-13595, DOI: 10.1039/D2DT02561B [354]

As shown in the introduction, MICs are significantly stronger  $\sigma$ -donors than Arduengo-type NHCs, while having negligible  $\pi$ -acceptor properties. So far, all cyclic iron tetracarbenes have been based on Arduengo-type NHCs. In this article, the first synthesis of an iron(II) tetracarbene complex with 1,2,3-triazol-5-ylidene moieties is described (**16**, Scheme 10). The strong electron donation of the new tetracarbene ligand is showcased in the upfield shift of the  $^{13}\text{C}_{\text{NHC}}$  signal (**16**: 190.35 ppm vs. 205.05 ppm for **2**) and in a more negative redox potential (**16**: -0.34 V vs. 0.15 V for **2**).<sup>[11]</sup> **16** is applied in preliminary catalytic epoxidation studies. At 20 °C in the presence of  $\text{Sc}(\text{OTf})_3$ , a (initial) TOF of 41 000  $\text{h}^{-1}$  can be determined in the epoxidation of *cis*-cyclooctene using 0.5 mol% of **16**. A conversion of 97% is reached after 30 min. Without  $\text{Sc}(\text{OTf})_3$ , the catalyst's lifetime is significantly shortened, and the reaction is already finished after 30 s with a conversion of 37%. Lower temperatures benefit the catalyst's stability and at -10 °C, a conversion of 89% can be reached (still in the absence of  $\text{Sc}(\text{OTf})_3$ ).



Scheme 10. Simplified synthesis of **16** (adapted from<sup>[11, 354]</sup>). TIPS = triisopropylsilyl.

### 3.4. Cyclic iron tetra N-heterocyclic carbenes: synthesis, properties, reactivity, and catalysis

Tim P. Schlachta, Fritz E. Kühn

*Chem. Soc. Rev.* **2023**, *52*, 2238-2277, DOI: 10.1039/D2CS01064J <sup>[11]</sup>

This article provides a review about the field of cyclic iron tetracarbenes and all articles up to January 2023 are summarized. The synthesis, properties, reactivity, and catalytic applications of cyclic iron tetracarbenes are discussed in-depth.

The macrocyclic ligand precursor is prepared first in all cases, followed by the complexation to form the cyclic iron tetracarbene. Three methods are applied, namely the direct metalation with the internal base  $\text{Fe}[\text{N}(\text{SiMe}_3)_2]_2$ , combination of an external base and iron precursor, and the transmetalation from the respective Ag complex with an iron precursor.

It is discovered that the  $\sigma$ -donor strength of the tetracarbene ligands can be evaluated with the  $^{13}\text{C}_{\text{NHC}}$  signal (stronger = upfield shifted) and redox potential (stronger = more negative) of the iron complex. In addition, a correlation between the  $^{13}\text{C}_{\text{NHC}}$  signal and redox potential is found. More insights about the electronic properties can be obtained from Mössbauer spectroscopy. Structural properties can be derived from the crystal structures.

The chemistry of cyclic iron tetracarbenes is manifold. Simple axial ligand modifications can significantly impact the electronic properties and, for example, lead to a different spin state of the complex. Various diiron complexes in oxidation states up to +4 containing O, N, P or  $\text{S}_2$  as bridging atoms are described. An iron(IV)-oxo tetracarbene complex is capable of hydrogen atom transfer of various substrates with a C–H bond dissociation energy in the range of 75 to 80 kcal mol<sup>-1</sup> with a medium activity. The chelating, strong electron donating properties of tetracarbene ligands allow for the isolation of other iron(IV) complexes, like the first examples of five-coordinated iron(IV) imides.

Cyclic iron tetracarbenes are also used as catalysts and achieve a very high activity in electrochemical  $\text{CO}_2$  reduction without a proton source and are the most active systems in homogeneous epoxidation of alkenes. Furthermore, they are applied in aziridination catalysis. Several mechanistic studies have been performed in  $\text{CO}_2$  reduction and aziridination catalysis.

To conclude, cyclic iron tetracarbene complexes have a very strong electron donating carbene ligand, which can stabilize iron complexes in high oxidation states. Due to the resulting electronic properties and structure, a different reactivity is observed for cyclic iron tetracarbenes compared to e.g. heme and nonheme N-ligated iron complexes.

### 3.5. Tailoring activity and stability: Effects of electronic variations on iron-NHC epoxidation catalysts

Tim P. Schlachta, Greta G. Zámbo, Michael J. Sauer, Isabelle Rüter, Carla A. Hofer, Serhiy Demeshko, Franc Meyer, Fritz E. Kühn

*J. Catal.* **2023**, 426, 234-246, DOI: 10.1016/j.jcat.2023.07.018 <sup>[355]</sup>

In this article, the effect of electronic variations on iron NHC epoxidation catalysts is further explored. As described in the introduction, the tetracarbene ligand modifications of **2/3** to yield complexes **4-7** did not result in a better catalytic performance compared to **2/3**. Here, complex **1** is chosen as model system to obtain more information on the suitability of ligand modifications of iron NHC complexes for optimizing their catalytic performance in epoxidation.

The equatorial ligand is modified to give a more electron donating ligand (**17**, Figure 26) and a more electron accepting ligand (**18**). These electronic properties are verified by NMR and CV. The quadrupole splitting determined by Mössbauer spectroscopy also correlates with the donor strength of the NHC ligands and indicates the deformation of the electric field around the iron center due to the strong electron donation in equatorial plane. The three complexes are further characterized by DFT calculations and SQUID magnetometry, among others.

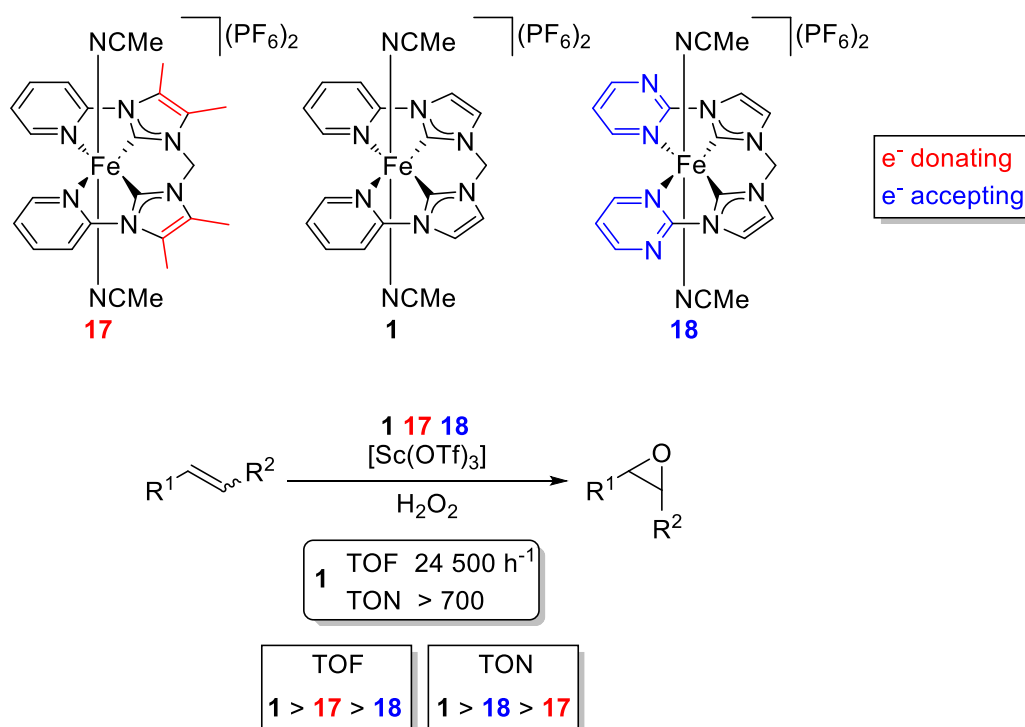


Figure 26. Modified iron NHC complexes employed in epoxidation catalysis (adapted from<sup>[355]</sup>).

The three complexes are applied in the epoxidation of *cis*-cyclooctene. The unmodified complex **1** achieves the highest TOF (24 500 h<sup>-1</sup>) and TON (>700) at 20 °C in the presence of Sc(OTf)<sub>3</sub>. **17** has the second highest TOF (7 600 h<sup>-1</sup>) but **18** has the second highest TON (49) due to its long lifetime under oxidative conditions. All complexes show a high selectivity. Various other alkene substrates are screened. A higher activity and conversion are achieved for the more nucleophilic alkenes.

### 3.6. Chiral imidazolium and triazolium salts as NHC and aNHC ligand precursors: A promising framework for asymmetric epoxidation catalysis

Tim P. Schlachta, Leon F. Richter, Fritz E. Kühn

*Results in Chemistry* **2024**, 7, 101421, DOI: 10.1016/j.rechem.2024.101421 <sup>[356]</sup>

The previously studied iron NHC complexes achieve a superior catalytic performance in epoxidation reaction compared to *N*-ligated iron complexes (see 1.3.2). Especially **2/3** are the most active homogeneous epoxidation catalysts. However, many pharmaceuticals and fine chemicals contain chiral epoxides or require them in intermediates for further transformations. A prominent system for catalytic enantioselective epoxidation is the Jacobsen-Katsuki method based on Mn(III) salen catalysts with a chiral bridge (see 1.3.3). The motivation for this study is to combine the benefits of NHC ligands with the chiral-directing salen ligand framework containing a chiral cyclohexane bridge.

Three systems are designed (Figure 27). One triazolium salt as MIC precursor (**19**) and two imidazolium salts as Arduengo-type NHC precursor (**20**, **21**). The phenol wings from the salen ligand model are kept in **19** and **21**, as they can stabilize the high oxidation state of iron during epoxidation catalysis through ionic interactions.<sup>[357]</sup> A pyridine wing is employed in **20** in analogy to complex **1** (Figure 21). The syntheses of the imidazolium salts are straightforward, while the synthesis of the triazolium salt requires several tests and optimization to finally obtain **19** through a multi-step synthesis route.

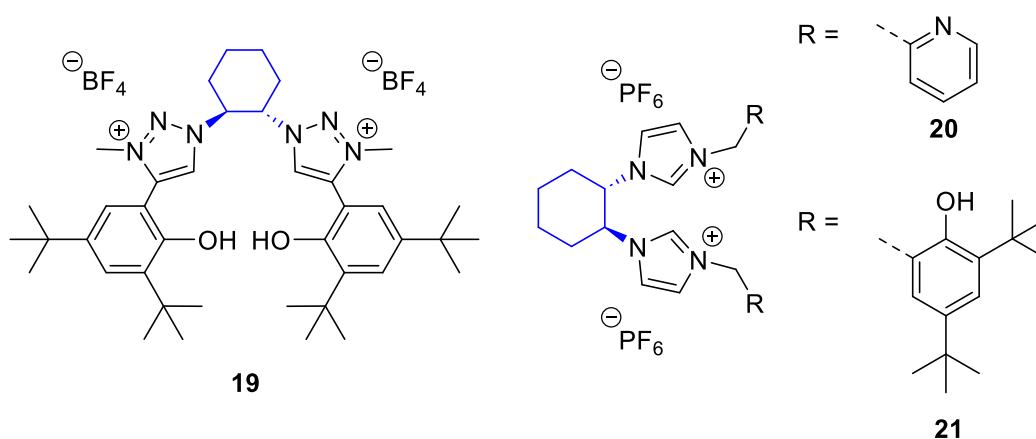


Figure 27. Synthesized chiral imidazolium and triazolium NHC ligand precursors (adapted from<sup>[356]</sup>).

### 3.7. Synthesis, characterization, and biomedical evaluation of ethylene-bridged tetra-NHC Pd(II), Pt(II) and Au(III) complexes, with apoptosis-inducing properties in cisplatin-resistant neuroblastoma cells

Wolfgang R. E. Büchele,<sup>#</sup> Tim P. Schlachta,<sup>#</sup> Andreas L. Gebendorfer, Jenny Pamperin, Leon F. Richter, Michael J. Sauer, Aram Prokop, Fritz E. Kühn

<sup>#</sup> Wolfgang R. E. Büchele and Tim P. Schlachta contributed equally to this work.

*RSC Adv.* **2024**, *14*, 10244-10254, DOI: 10.1039/D4RA01195C <sup>[358]</sup>

This article deals with the development of several new multidentate NHC ligand systems. One ligand contains two imidazolin-2-ylidene units connected with an ethylene bridge. This ligand forms open-chain tetracarbene Pd and Pt complexes with two coordinated NHC ligands (**22**, **23**, Figure 28). Furthermore, two cyclic tetracarbene ligands with saturated and unsaturated backbone are developed. These ligands are larger analogs to the tetracarbene employed in the iron complexes **2/3**, having ethylene instead of methylene bridges. In addition, the synthetic approach to a saturated analog of the tetracarbene ligand of **2/3**, calix[4]imidazolium, is described. The cyclic tetracarbenes form complexes with Pd, Pt and Au *via* transmetalation with Ag<sub>2</sub>O. The ethylene-bridges make the tetracarbenes more flexible than their methylene analogs, resulting in a strongly saddle-shaped structure as revealed by SC-XRD (Figure 29).

The tetracarbene complexes **22**, **26** and **29** and their ligand precursors are tested in Nalm-6 cells (human B cell precursor leukemia cell line) and SK-N-AS cells (human neuroblastoma cell line) regarding their ability to induce apoptosis. **29** shows an apoptotic effect on SK-N-AS cells, presumably *via* the mitochondrial and ROS (reactive oxygen species) pathway. However, a relatively high concentration of **29** is required. Furthermore, **29** is able to overcome cisplatin resistance *in vitro* in cisplatin resistant SK-N-AS cells.

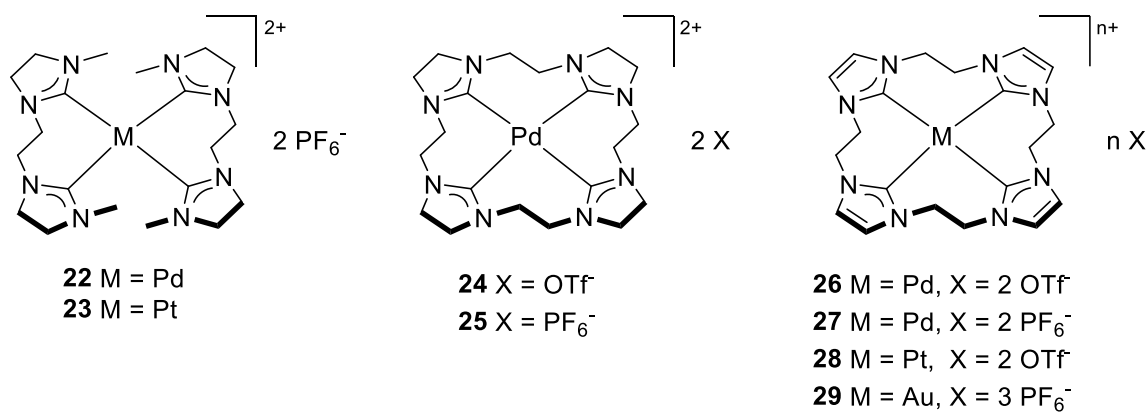


Figure 28. Synthesized transition metal complexes (Pd<sup>II</sup>, Pt<sup>II</sup>, Au<sup>III</sup>) with an open-chain tetracarbene ligand with saturated backbone (imidazolin-2-ylidene units, **22**, **23**), with a cyclic tetracarbene ligand with saturated backbone (imidazolin-2-ylidene units, **24**, **25**) and a cyclic tetracarbene ligand with unsaturated backbone (imidazol-2-ylidene units, **26-29**) (adapted from<sup>[358]</sup>).

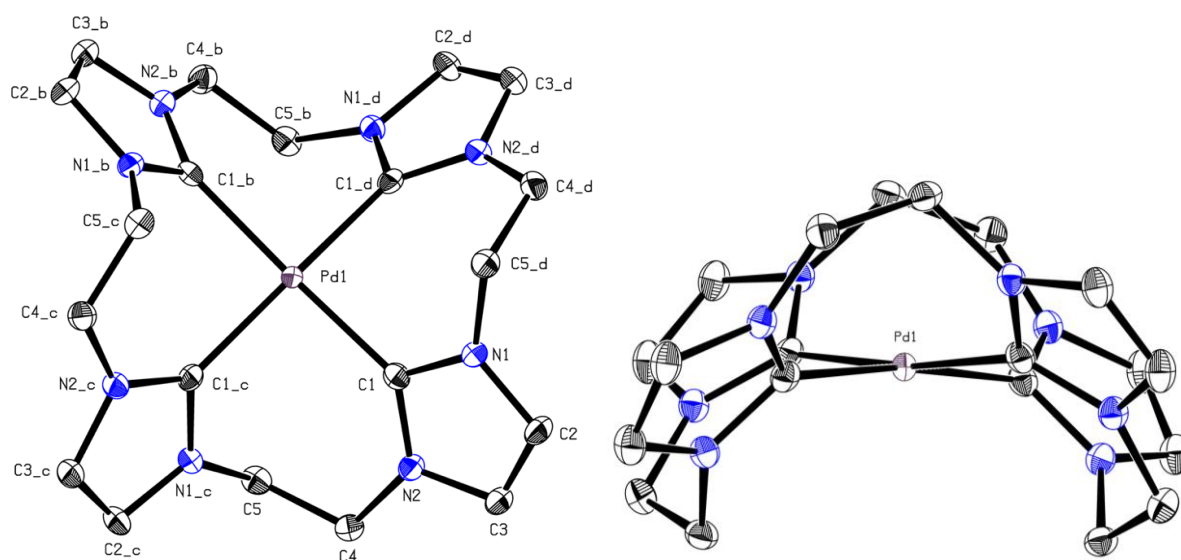


Figure 29. ORTEP-style representation of the cationic fragment of **27**. Hydrogen atoms and PF<sub>6</sub><sup>-</sup> anions are omitted for clarity and thermal ellipsoids are shown at a 50% probability level. Left: Top perspective, right: side perspective. Selected bond lengths (Å) and angles (°): C1–Pd 2.019(2), C1–Pd1–C1\_b 172.03(12), C1–Pd1–C1\_d–N2\_d 53.62, C5–Pd1–C5\_b 98.97°. Reproduced and modified from Ref. <sup>[358]</sup> with permission from the Royal Society of Chemistry.

## 4. Unpublished results

This chapter summarizes the unpublished results of the doctoral thesis. The individual contributions of Tim P. Schlachta to the results are given in Table 2, chapter 7.

### 4.1. Impact of ligand design on an iron NHC epoxidation catalyst

Tim P. Schlachta, Greta G. Zámbo, Michael J. Sauer, Isabelle Rüter, Fritz E. Kühn

*submitted 2024*

This article continues the study of the effect of electronic variations on the catalytic performance of iron NHC epoxidation catalysts (see 3.5). This time, the NHC backbone is modified with a benzene group (**30**, Figure 30) to resemble the ligand modification in iron tetracarbene complexes **6/7** to allow a more concrete comparison. Furthermore, a synthetic approach of a NHC ligand precursor with 2-imidazoline units instead imidazole, structurally similar to the ligand in **1**, is described. However, formylation as well as hydrolysis can be identified as potential problems.

Iron(II) NHC complex **30** is comprehensively characterized. It has the most positive redox potential ( $E_{1/2} = 0.625$  V vs. Fc/Fc<sup>+</sup>) compared to the series of NCCN complexes, **1** (0.423 V), **17** (0.337 V) and **18** (0.559 V).<sup>[240, 242, 355, 359-360]</sup> This demonstrates the weaker  $\sigma$ -donation and stronger  $\pi$ -acceptance of the NHC units, also reflected in the strongly downfield shifted <sup>13</sup>C<sub>NHC</sub> signal of **30** (230.31 ppm vs. **1**: 216.15, **17**: 215.49, **18**: 216.24 ppm).<sup>[240, 355]</sup> While the quadrupole splitting of the NCCN complexes is ranked with increasing electron donor strength of the NHC ligand (**18** < **1** < **17**),<sup>[355]</sup> the quadrupole splitting of **30** ( $\Delta E_Q = 2.23$  mm s<sup>-1</sup>) is effectively as high as **17**, possibly due to the  $\pi$ -accepting properties of the benzimidazol-2-ylidene moieties.

In catalytic epoxidation of *cis*-cyclooctene, **30** shows a pronounced induction phase – oxidation from Fe<sup>II</sup> to Fe<sup>III</sup> – even upon addition of Sc(OTf)<sub>3</sub> at 20 °C. Higher temperatures presumably facilitate the preoxidation to iron(III) as **30** is more active at these conditions. A TOF of 10 200 h<sup>-1</sup> and TON of 706 can be determined at 60 °C in the presence of Sc(OTf)<sub>3</sub>. Thus, even though **30** has a less electron donating NHC ligand, it displays equal stability as the unmodified complex **1**, but a lower activity. This is in contrast to the results obtained with the iron tetracarbene complexes **6/7** with benzimidazol-2-ylidene units, which could not achieve the same TON as the unmodified iron tetracarbene system **2/3** (see 1.3.2). In the epoxidation

of other substrates, **30** gives only modest conversions due to its low reactivity at 20 °C. In turn, the slow reaction rates in epoxidation catalysis make **30** a suitable candidate for mechanistic studies and especially low temperatures can produce optimal, controlled conditions.

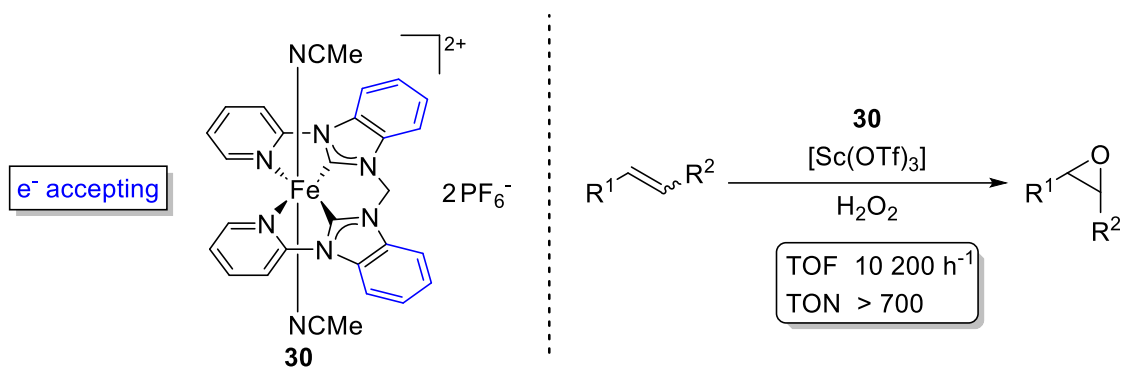


Figure 30. Modified iron NHC complex **30** containing benzimidazol-2-ylidene units applied in epoxidation catalysis.

## 4.2. Formation of a diiron-( $\mu_2\text{-}\eta^1\text{:}\eta^1\text{-CN}$ ) complex from acetonitrile solution

Tim P. Schlachta, (...), Fritz E. Kühn

to be submitted 2024

The activation of C–C bonds by transition metal complexes is of constant interest and MeCN has attracted attention as cyanide source with relatively low toxicity for organic cyanation reactions.<sup>[361-364]</sup> When a solution of **30** in CD<sub>3</sub>CN was slowly evaporated over the course of six months under ambient conditions, an unexpected diiron end-on  $\mu_2\text{-}\eta^1\text{:}\eta^1\text{-CN}$  bridged complex [(MeCN)(NHC)Fe]<sub>2</sub>( $\mu_2\text{-}\eta^1\text{:}\eta^1\text{-CN}$ )(PF<sub>6</sub>)<sub>3</sub> (**31**, Figure 31) was obtained as determined by X-ray diffraction. The two iron centers are bridged by a cyanide anion, hence three PF<sub>6</sub><sup>-</sup> anions are present in the crystal structure. Under similar conditions, *i.e.* MeCN solution, room temperature and air, a dinuclear Cu(II) cryptate has been found to form a  $\mu_2\text{-}\eta^1\text{:}\eta^1\text{-CN}$  bridged complex by C–C bond cleavage of MeCN.<sup>[362]</sup> A possible mechanism involves the activation of the sp-hybridized carbon of MeCN, bound to one Cu atom (MeCN-Cu), by the second Cu center. The increased electrophilicity of the methyl group allows cleavage by H<sub>2</sub>O to form MeOH and the cyanide bridged compound.<sup>[361-362]</sup> Another possible mechanism for the formation of **31** might be the C–H oxidation of MeCN by the iron complex **30** to form glycolonitrile, as observed with **3** (see 3.1), and subsequent release of cyanide upon decay of glycolonitrile.<sup>[335, 365-366]</sup> Due to the stronger Me–CN bond (122 kcal mol<sup>-1</sup>) compared to the H–CH<sub>2</sub>CN bond (93 kcal mol<sup>-1</sup>),<sup>[363, 367-369]</sup> the C–H oxidation of MeCN seems to be with a higher probability the origin of cyanide in this case. However, C–C bond cleavage of MeCN by UV irradiation is known<sup>[364]</sup> and given the fact that the crystallization setup with **30** was accessible for sunlight for six months, C–C bond cleavage of MeCN does not appear to be completely improbable.

Originally, the crystal structure was solved as diiron-( $\mu_2\text{-}\eta^1\text{:}\eta^1\text{-N}_2$ ) complex. However, there are several arguments against a diiron-( $\mu_2\text{-}\eta^1\text{:}\eta^1\text{-N}_2$ ) complex:

- 1) The main argument against a diiron-( $\mu_2\text{-}\eta^1\text{:}\eta^1\text{-N}_2$ ) complex is the fact that the crystal structure contains three counterions. As the crystallization was performed with **30** containing an iron(II) center, bridging two iron(II) atoms with a neutral N<sub>2</sub> ligand should give four counterions. Otherwise, three counterions would indicate that a redox process has occurred during formation of **31**, but the nature of a hypothetical reducing agent and the location of reduction are highly speculative. The main components of the crystallization experiment were **30** and CD<sub>3</sub>CN as well as unreacted ligand precursor as minor impurity (see 10.1). In cyclic voltammetry of **30**, the first reduction event occurred at -1.78 V (vs. Fc/Fc<sup>+</sup>). A preliminary experiment measuring

**30** in cyclic voltammetry under N<sub>2</sub> atmosphere (instead of Ar) did not show significant redox processes or electric current relating to a reduction of N<sub>2</sub> or formation of a diiron-( $\mu_2$ - $\eta^1$ : $\eta^1$ -N<sub>2</sub>) complex (see 4.1). Considering all facts, an occurred redox process is very implausible.

2) Dinitrogen is a weak  $\sigma$ -donor and weak  $\pi$ -acceptor, and substitution of the N<sub>2</sub> ligand with CO or nitriles like MeCN is often observed.<sup>[370-371]</sup> A diiron-( $\mu_2$ - $\eta^1$ : $\eta^1$ -N<sub>2</sub>) version of **31** would be very surprising in this context, since one axial MeCN ligand coordinates with one iron center each, the crystallization of **31** occurred from (deuterated) MeCN as solvent and the prior occupation of both axial coordination sites by MeCN in **30**. Interesting is also the stability of **31** under air, rather uncommon for diiron-( $\mu_2$ - $\eta^1$ : $\eta^1$ -N<sub>2</sub>) complexes,<sup>[370, 372-374]</sup> and an affinity to N<sub>2</sub> over O<sub>2</sub> would be very unusual considering other Fe compounds tending to form diiron- $\mu_2$ -oxo species<sup>[11, 346]</sup>.

3) A diiron-( $\mu_2$ - $\eta^1$ : $\eta^1$ -N<sub>2</sub>) complex should show a distinctive  $\nu_{\text{NN}}$  absorption band in Raman spectroscopy and be IR inactive due to centrosymmetric structure.<sup>[375-377]</sup> No  $\nu_{\text{NN}}$  was detected in crude material either by IR or Raman. However, no pronounced  $\nu_{\text{CN}}$  stretch could be observed as well and interestingly, complex **30** also does not show a characteristic  $\nu_{\text{CN}}$  band in IR, contrary to its similar complexes<sup>[240]</sup>, but signals attributable to axial MeCN are visible in the Raman spectrum (see 10.1).

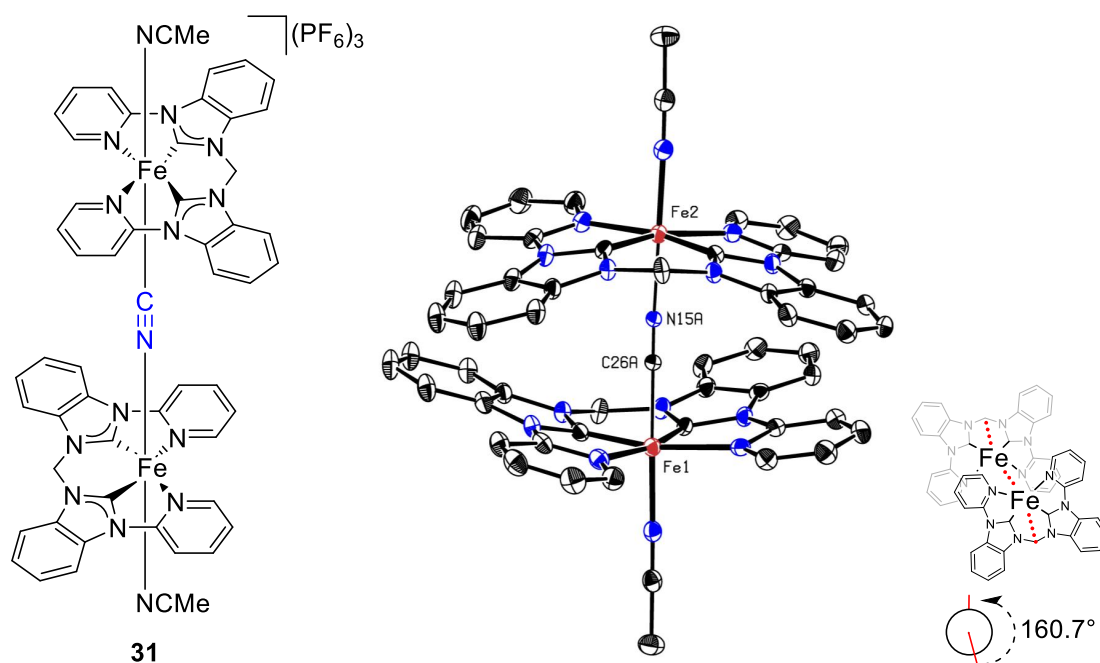


Figure 31. Left: Diiron end-on  $\mu_2$ - $\eta^1$ : $\eta^1$ -CN bridged complex [(MeCN)(NHC)Fe]<sub>2</sub>( $\mu_2$ - $\eta^1$ : $\eta^1$ -CN)(PF<sub>6</sub>)<sub>3</sub> (**31**). Right: ORTEP-style representation of **31**. Hydrogen atoms and hexafluorophosphate anions are omitted for clarity. Thermal ellipsoids are shown at a 50% probability level. Notable are the strongly bent NHC ligands, in contrast to **30**, and their rotation towards each other of 160.7°.

## 5. Conclusion and outlook

Several areas were investigated in this thesis:

- 1) Homogeneous epoxidation catalysis with iron NHC complexes and the closely related development of new NHC ligand systems
- 2) The reactivity of iron NHC complexes
- 3) The synthesis of transition metal tetracarbene complexes with a brief excursus on their application in medicinal chemistry

To 1)

Modification of an open-chain NHC ligand resulted in a series of iron NHC complexes with varying electronic properties. They have been employed in epoxidation catalysis to gain more information on the suitability of ligand modifications of iron NHC complexes for optimizing their catalytic performance in epoxidation (see 3.5, 4.1). Interestingly, the unmodified iron NHC complex achieves the best catalytic performance, both in activity and stability. One complex with a less electron donating NHC ligand is equally stable but less active. Complementary to the iron tetracarbene benchmark system, a MIC analog with 1,2,3-triazol-5-ylidene moieties was synthesized (see 3.3). However, this complex, having a stronger electron donating mesoionic tetracarbene ligand, also achieves a lower activity in epoxidation catalysis than the Arduengo-type unmodified benchmark. Therefore, no direct correlation can be established between the electron density of the iron center, which is controlled by the electron donating or accepting ligands, and the catalytic performance of the iron complex in epoxidation. Other parameters might have a considerable impact, such as the stability of the ligand under oxidative conditions or the ligand rigidity.

The ultimate degradation of the iron tetracarbene benchmark catalyst was identified to be the oxidation of one carbene, initiating decoordination of the NHC ligand from the iron center followed by the protonation of the remaining three carbenes (see 3.1). The degradation mechanism is thinkable to proceed *via* an inter- and/or intramolecular path, *i.e.* amongst neighboring iron tetracarbene complexes in solution or within one single iron tetracarbene complex, respectively. As long as not both inter- and intramolecular pathways are occurring parallel during catalysis, exclusion of an intermolecular route might be possible by immobilizing the iron tetracarbene so that the complexes are forced to keep a distance during catalysis. Immobilization of the catalyst or the use of ionic liquids, which allow the catalyst to be recycled, also increase its suitability for industrial applications.<sup>[255]</sup> In this context, however, the cost aspect of more

sophisticated ligand systems should be considered. A deeper understanding about the epoxidation mechanism is also helpful to develop strategies to improve the catalytic performance of the iron NHC complexes. Mechanistic studies can for example involve labelling experiments or quantitative formation and *in-situ* characterization – or even isolation – of potential intermediates under controlled conditions like low temperature by use of stoichiometric amounts of the catalyst.

Chiral NHC and MIC ligand precursors were developed having a chiral cyclohexane bridge (see 3.6). These offer a promising framework for organometallic complexes for asymmetric epoxidation catalysis.

To 2)

The reactivity of an  $\mu_2$ -oxo-bridged complex consisting of two iron(III) tetracarbenes was investigated (see 3.2). With single-electron oxidation, a diiron(III,IV)- $\mu_2$ -oxo complex could be isolated and characterized. Furthermore, the existence of a diiron(IV)- $\mu_2$ -oxo species is indicated, which is capable of an oxygen transfer to thianthrene. The versatile chemistry of cyclic iron tetracarbene complexes was also reviewed and their synthesis, properties, reactivity, and catalytic applications were discussed in-depth (see 3.4). An unexpected diiron end-on  $\mu_2$ - $\eta^1$ : $\eta^1$ -CN bridged complex was found in a crystallization experiment with an open-chain iron NHC complex (see 4.2). The cyanide is presumably originating from the solvent MeCN by C–C bond cleavage or through C–H oxidation.

To 3)

Several new multidentate NHC ligand systems were designed and various open-chain as well as cyclic palladium, platinum, and gold tetracarbene complexes were obtained (see 3.7). The gold tetracarbene complex induces apoptosis in SK-N-AS cells (human neuroblastoma cell line) and overcomes cisplatin resistance *in vitro* in cisplatin resistant SK-N-AS cells, although at a relatively high concentration.

## 6. Reprint permissions

### 6.1. Degradation pathways of a highly active iron(III) tetra-NHC epoxidation catalyst

Florian Dyckhoff, Jonas F. Schlagintweit, Marco A. Bernd, Christian H. G. Jakob, **Tim P. Schlachta**, Benjamin J. Hofmann, Robert M. Reich, Fritz E. Kühn

*Catal. Sci. Technol.* **2021**, *11*, 795-799, DOI: 10.1039/D0CY02433C <sup>[335]</sup>

Reproduced from Ref. <sup>[335]</sup> with permission from the Royal Society of Chemistry.

“If you are the author of this article, you do not need to request permission to reproduce figures and diagrams provided correct acknowledgement is given. **If you want to reproduce the whole article in a third-party publication (excluding your thesis/dissertation for which permission is not required)** please go to the Copyright Clearance Center request page.”

Obtained from <https://doi.org/10.1039/D0CY02433C>

The screenshot shows the article page for "Degradation pathways of a highly active iron(III) tetra-NHC epoxidation catalyst" from the journal Catalysis Science & Technology, Issue 3, 2021. The authors listed are Florian Dyckhoff, Jonas F. Schlagintweit, Marco A. Bernd, Christian H. G. Jakob, Tim P. Schlachta, Benjamin J. Hofmann, Robert M. Reich, and Fritz E. Kühn. The abstract discusses the investigation of pivotal degradation pathways for a highly active non-heme iron epoxidation catalyst. It mentions that in-depth HR-ESI-MS and NMR spectroscopy decomposition studies, along with comparative catalytic experiments, have excluded generally accepted literature paths such as  $\mu_2$ -oxo bridged  $\text{Fe}^{\text{III}}\text{-O-Fe}^{\text{III}}$  dimer formation and methylene bridge oxidation. Instead, the Fe-NHC bond is identified as the "weak spot", and direct oxidation of one of the carbenes (ImC=O) is shown to result in its de-coordination and induce protonation of the other NHC moieties, completely deactivating the catalyst. Evidence for protonation prior to carbene oxidation has not been found in this study.

The right-hand side of the screenshot shows a sidebar with navigation options: "About", "Cited by", and "Related". Under "About", the article title and authors are listed, along with the journal name and DOI. It also includes a "Check for updates" button and a "Copyright Clearance Center request page" link. A note states that if you are an author contributing to an RSC publication, you do not need to request permission provided correct acknowledgement is given. Another note states that if you are the author of this article, you do not need to request permission to reproduce figures and diagrams provided correct acknowledgement is given. A final note states that if you want to reproduce the whole article in a third-party publication (excluding your thesis/dissertation for which permission is not required), please go to the Copyright Clearance Center request page. A link to "how to correctly acknowledge RSC content" is also provided.

Obtained from <https://doi.org/10.1039/D0CY02433C>

## 6.2. Mimicking reactive high-valent diiron- $\mu_2$ -oxo intermediates of nonheme enzymes by an iron tetracarbene complex

Tim P. Schlachta,<sup>#</sup> Markus R. Anneser,<sup>#</sup> Jonas F. Schlagintweit, Christian H. G. Jakob, Carolin Hintermeier, Alexander D. Böth, Stefan Haslinger, Robert M. Reich, Fritz E. Kühn

<sup>#</sup> Tim P. Schlachta and Markus R. Anneser contributed equally to this work.

*Chem. Commun.* **2021**, 57, 6644-6647, DOI: 10.1039/D1CC02027G <sup>[346]</sup>

Reproduced from Ref. <sup>[346]</sup> with permission from the Royal Society of Chemistry.

“If you are the author of this article, you do not need to request permission to reproduce figures and diagrams provided correct acknowledgement is given. **If you want to reproduce the whole article in a third-party publication (excluding your thesis/dissertation for which permission is not required)** please go to the Copyright Clearance Center request page.”

Obtained from <https://doi.org/10.1039/D1CC02027G>

The screenshot shows the article page for "Mimicking reactive high-valent diiron- $\mu_2$ -oxo intermediates of nonheme enzymes by an iron tetracarbene complex" in the journal *Chemical Communications*, Issue 54, 2021. The authors listed are Tim P. Schlachta, Markus R. Anneser, Jonas F. Schlagintweit, Christian H. G. Jakob, Carolin Hintermeier, Alexander D. Böth, Stefan Haslinger, Robert M. Reich, and Fritz E. Kühn. The abstract states: "The first diiron(III,IV)- $\mu_2$ -oxo tetracarbene complex is isolated and characterized by SC-XRD, UV/Vis, EPR, Evans' NMR and elemental analysis. CV indicates the presence of a transient high-valent diiron(IV)- $\mu_2$ -oxo species. Its formation and decay is investigated via UV/Vis kinetics and NMR." On the right side, there is a sidebar with tabs for "About", "Cited by", and "Related". The "About" tab is active, showing the article title, authors, journal information, and a copyright notice: "To request permission to reproduce material from this article, please go to the Copyright Clearance Center request page. If you are an author contributing to an RSC publication, you do not need to request permission provided correct acknowledgement is given. If you are the author of this article, you do not need to request permission to reproduce figures and diagrams provided correct acknowledgement is given. If you want to reproduce the whole article in a third-party publication (excluding your thesis/dissertation for which permission is not required) please go to the Copyright Clearance Center request page. Read more about how to correctly acknowledge RSC content."

Obtained from <https://doi.org/10.1039/D1CC02027G>

### 6.3. The first macrocyclic abnormally coordinating tetra-1,2,3-triazole-5-ylidene iron complex: a promising candidate for olefin epoxidation

Greta G. Zámbo, Johannes Mayr, Michael J. Sauer, **Tim P. Schlachta**, Robert M. Reich, Fritz E. Kühn

*Dalton Trans.* **2022**, *51*, 13591-13595, DOI: 10.1039/D2DT02561B [354]

Reproduced from Ref. [354] with permission from the Royal Society of Chemistry.

“If you are the author of this article, you do not need to request permission to reproduce figures and diagrams provided correct acknowledgement is given. **If you want to reproduce the whole article in a third-party publication (excluding your thesis/dissertation for which permission is not required)** please go to the Copyright Clearance Center request page.”

Obtained from <https://doi.org/10.1039/D2DT02561B>

The screenshot shows the article page on Dalton Transactions. The article title is "The first macrocyclic abnormally coordinating tetra-1,2,3-triazole-5-ylidene iron complex: a promising candidate for olefin epoxidation". The authors listed are Greta G. Zámbo, Johannes Mayr, Michael J. Sauer, Tim P. Schlachta, Robert M. Reich, and Fritz E. Kühn. The abstract states: "The first macrocyclic and abnormally coordinating, mesoionic N-heterocyclic carbene iron complex has been synthesised and characterised via ESI-MS, EA, SC-XRD, CV, NMR and UV/Vis spectroscopy. <sup>13</sup>C-NMR spectroscopy and CV measurements indicate a strong  $\sigma$ -donor ability of the carbene moieties, suggesting an efficient catalytic activity of the iron complex in oxidation reactions. Initial tests in the epoxidation of *cis*-cyclooctene as a model substrate confirm this assumption." On the right side, there is a pop-up window with a close button (X) containing the following text: "The first macrocyclic abnormally coordinating tetra-1,2,3-triazole-5-ylidene iron complex: a promising candidate for olefin epoxidation. G. G. Zámbo, J. Mayr, M. J. Sauer, T. P. Schlachta, R. M. Reich and F. E. Kühn, *Dalton Trans.*, 2022, **51**, 13591 DOI: 10.1039/D2DT02561B. To request permission to reproduce material from this article, please go to the [Copyright Clearance Center request page](#). If you are an author contributing to an RSC publication, you do not need to request permission provided correct acknowledgement is given. If you are the author of this article, you do not need to request permission to reproduce figures and diagrams provided correct acknowledgement is given. If you want to reproduce the whole article in a third-party publication (excluding your thesis/dissertation for which permission is not required) please go to the [Copyright Clearance Center request page](#). Read more about [how to correctly acknowledge RSC content](#)." There are also navigation tabs for "About", "Cited by", and "Related".

Obtained from <https://doi.org/10.1039/D2DT02561B>

## 6.4. Cyclic iron tetra N-heterocyclic carbenes: synthesis, properties, reactivity, and catalysis

Tim P. Schlachta, Fritz E. Kühn

*Chem. Soc. Rev.* **2023**, *52*, 2238-2277, DOI: 10.1039/D2CS01064J <sup>[11]</sup>

Reproduced from Ref. <sup>[11]</sup> with permission from the Royal Society of Chemistry.

“If you are the author of this article, you do not need to request permission to reproduce figures and diagrams provided correct acknowledgement is given. **If you want to reproduce the whole article in a third-party publication (excluding your thesis/dissertation for which permission is not required)** please go to the Copyright Clearance Center request page.”

Obtained from <https://doi.org/10.1039/D2CS01064J>

The screenshot shows the article page for "Cyclic iron tetra N-heterocyclic carbenes: synthesis, properties, reactivity, and catalysis" by Tim P. Schlachta and Fritz E. Kühn. The page includes a header with "Issue 6, 2023" and "From the journal: Chemical Society Reviews". The article title is prominently displayed, along with a "Check for updates" button. Below the title, the authors' names are listed with ORCID iD icons. An "Abstract" section follows, providing a summary of the article's content. On the right side, there is a sidebar with navigation options: "About", "Cited by", and "Related". The "Cited by" section is active, showing the article title, authors, and journal information. It also contains a copyright notice and a link to the Copyright Clearance Center request page. The sidebar has a close button (X) in the top right corner.

Obtained from <https://doi.org/10.1039/D2CS01064J>

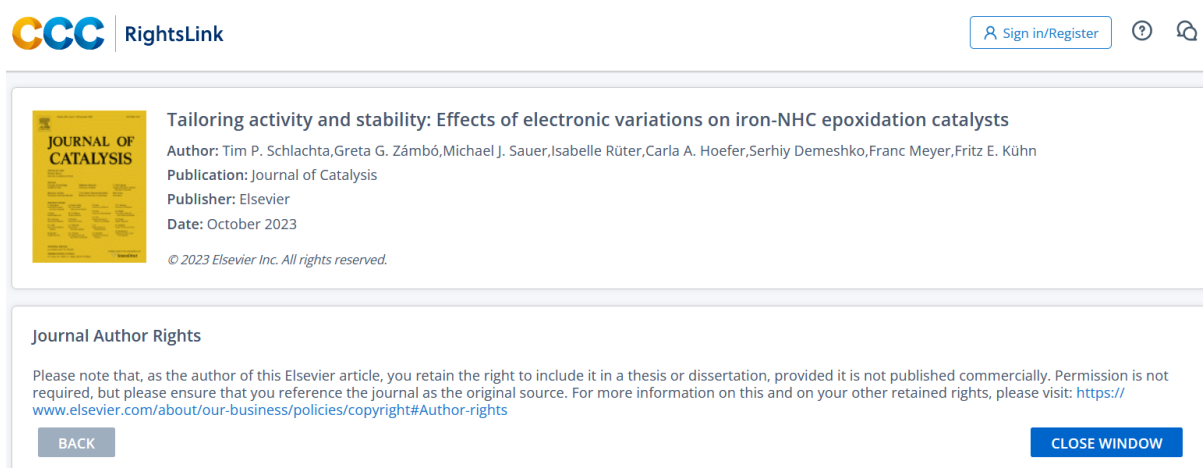
## 6.5. Tailoring activity and stability: Effects of electronic variations on iron-NHC epoxidation catalysts

Tim P. Schlachta, Greta G. Zámbo, Michael J. Sauer, Isabelle Rüter, Carla A. Hofer, Serhiy Demeshko, Franc Meyer, Fritz E. Kühn

*J. Catal.* **2023**, 426, 234-246, DOI: 10.1016/j.jcat.2023.07.018 <sup>[355]</sup>

**“Please note that, as the author of this Elsevier article, you retain the right to include it in a thesis or dissertation, provided it is not published commercially. Permission is not required, but please ensure that you reference the journal as the original source. For more information on this and on your other retained rights, please visit: <https://www.elsevier.com/about/our-business/policies/copyright#Author-rights>”**

Obtained from <https://s100.copyright.com/AppDispatchServlet?publisherName=ELS&contentID=S0021951723003159&orderBeanReset=true>



The screenshot displays the RightsLink interface. At the top left is the CCC RightsLink logo. On the top right, there are links for 'Sign in/Register', a help icon, and a share icon. The main content area is divided into two sections. The first section, titled 'Tailoring activity and stability: Effects of electronic variations on iron-NHC epoxidation catalysts', includes the author list (Tim P. Schlachta, Greta G. Zámbo, Michael J. Sauer, Isabelle Rüter, Carla A. Hofer, Serhiy Demeshko, Franc Meyer, Fritz E. Kühn), the publication (Journal of Catalysis), the publisher (Elsevier), and the date (October 2023). Below this is a copyright notice: '© 2023 Elsevier Inc. All rights reserved.' The second section, titled 'Journal Author Rights', contains the text: 'Please note that, as the author of this Elsevier article, you retain the right to include it in a thesis or dissertation, provided it is not published commercially. Permission is not required, but please ensure that you reference the journal as the original source. For more information on this and on your other retained rights, please visit: <https://www.elsevier.com/about/our-business/policies/copyright#Author-rights>'. At the bottom of this section are two buttons: 'BACK' and 'CLOSE WINDOW'.

Obtained from <https://s100.copyright.com/AppDispatchServlet?publisherName=ELS&contentID=S0021951723003159&orderBeanReset=true>

**“As an Elsevier journal author, you have the right to Include the article in a thesis or dissertation (provided that this is not to be published commercially) whether in full or in part, subject to proper acknowledgment; see the Copyright page for more information. No written permission from Elsevier is necessary. This right extends to the posting of your thesis to your university’s repository provided that if you include the published journal article, it is embedded in your thesis and not separately downloadable.”**

Obtained from <https://www.elsevier.com/about/policies-and-standards/copyright/permissions>

## 6.6. Chiral imidazolium and triazolium salts as NHC and aNHC ligand precursors: A promising framework for asymmetric epoxidation catalysis

Tim P. Schlachta, Leon F. Richter, Fritz E. Kühn

*Results in Chemistry* **2024**, 7, 101421, DOI: 10.1016/j.rechem.2024.101421 <sup>[356]</sup>

**“Please note that, as the author of this Elsevier article, you retain the right to include it in a thesis or dissertation, provided it is not published commercially. Permission is not required, but please ensure that you reference the journal as the original source. For more information on this and on your other retained rights, please visit: <https://www.elsevier.com/about/our-business/policies/copyright#Author-rights>”**

Obtained from <https://s100.copyright.com/AppDispatchServlet?publisherName=ELS&contentID=S2211715624001176&orderBeanReset=true>



Sign in/Register ?



Chiral imidazolium and triazolium salts as NHC and aNHC ligand precursors: A promising framework for asymmetric epoxidation catalysis  
Author: Tim P. Schlachta, Leon F. Richter, Fritz E. Kühn  
Publication: Results in Chemistry  
Publisher: Elsevier  
Date: January 2024  
© 2024 The Author(s). Published by Elsevier B.V.

Journal Author Rights

Please note that, as the author of this Elsevier article, you retain the right to include it in a thesis or dissertation, provided it is not published commercially. Permission is not required, but please ensure that you reference the journal as the original source. For more information on this and on your other retained rights, please visit: <https://www.elsevier.com/about/our-business/policies/copyright#Author-rights>

BACK CLOSE WINDOW

Obtained from <https://s100.copyright.com/AppDispatchServlet?publisherName=ELS&contentID=S2211715624001176&orderBeanReset=true>

**“As an Elsevier journal author, you have the right to Include the article in a thesis or dissertation (provided that this is not to be published commercially) whether in full or in part, subject to proper acknowledgment; see the Copyright page for more information. No written permission from Elsevier is necessary. This right extends to the posting of your thesis to your university’s repository provided that if you include the published journal article, it is embedded in your thesis and not separately downloadable.”**

Obtained from <https://www.elsevier.com/about/policies-and-standards/copyright/permissions>

## 6.7. Synthesis, characterization, and biomedical evaluation of ethylene-bridged tetra-NHC Pd(II), Pt(II) and Au(III) complexes, with apoptosis-inducing properties in cisplatin-resistant neuroblastoma cells

Wolfgang R. E. Büchele,<sup>#</sup> **Tim P. Schlachta**,<sup>#</sup> Andreas L. Gebendorfer, Jenny Pamperin, Leon F. Richter, Michael J. Sauer, Aram Prokop, Fritz E. Kühn

<sup>#</sup> Wolfgang R. E. Büchele and Tim P. Schlachta contributed equally to this work.

*RSC Adv.* **2024**, *14*, 10244-10254, DOI: 10.1039/D4RA01195C [358]

Reproduced from Ref. [358] with permission from the Royal Society of Chemistry.

“This article is licensed under a Creative Commons Attribution 3.0 Unported Licence. **You can use material from this article in other publications without requesting further permissions from the RSC, provided that the correct acknowledgement is given.**”

Obtained from <https://doi.org/10.1039/D4RA01195C>

The screenshot shows the article page on the RSC Advances website. At the top, it indicates 'Issue 15, 2024, Issue in Progress' and provides navigation links for 'Previous Article' and 'Next Article'. The article title is 'Synthesis, characterization, and biomedical evaluation of ethylene-bridged tetra-NHC Pd(II), Pt(II) and Au(III) complexes, with apoptosis-inducing properties in cisplatin-resistant neuroblastoma cells'. The authors listed are Wolfgang R. E. Büchele, Tim P. Schlachta, Andreas L. Gebendorfer, Jenny Pamperin, Leon F. Richter, Michael J. Sauer, Aram Prokop, and Fritz E. Kühn. An abstract is provided, describing the synthesis and characterization of cyclic ethylene-bridged tetradentate NHC ligands and their complexes with Pd(II), Pt(II), and Au(III). A Creative Commons Attribution 3.0 Unported Licence notice is also visible, along with a link to 'how to correctly acknowledge RSC content'.

Obtained from <https://doi.org/10.1039/D4RA01195C>

## 7. Complete list of publications

- [12] **T. P. Schlachta**, (...), Fritz E. Kühn, "Formation of a diiron-( $\mu_2$ - $\eta^1$ : $\eta^1$ -CN) complex from acetonitrile solution", *to be submitted* **2024**.
- [11] **T. P. Schlachta**, Greta G. Zámbo, Michael J. Sauer, Isabelle Rüter, Fritz E. Kühn, "Impact of ligand design on an iron NHC epoxidation catalyst", *submitted* **2024**.
- [10] W. R. E. Büchele,<sup>#</sup> **T. P. Schlachta**,<sup>#</sup> A. L. Gebendorfer, J. Pamperin, L. F. Richter, M. J. Sauer, A. Prokop, F. E. Kühn, "Synthesis, characterization, and biomedical evaluation of ethylene-bridged tetra-NHC Pd(II), Pt(II) and Au(III) complexes, with apoptosis-inducing properties in cisplatin-resistant neuroblastoma cells", *RSC Adv.* **2024**, *14*, 10244-10254, DOI: 10.1039/D4RA01195C.
- [9] **T. P. Schlachta**, L. F. Richter, F. E. Kühn, "Chiral imidazolium and triazolium salts as NHC and aNHC ligand precursors: A promising framework for asymmetric epoxidation catalysis", *Results in Chemistry* **2024**, *7*, 101421, DOI: 10.1016/j.rechem.2024.101421.
- [8] C. A. Hoefler, N. K. Dietl, G. G. Zámbo, **T. P. Schlachta**, R. M. Reich, F. E. Kühn, "Unraveling the potential of backbone modifications in iron(II) NHC complexes for olefin aziridination and imination", *J. Organomet. Chem.* **2024**, *1006*, 123018, DOI: 10.1016/j.jorganchem.2024.123018.
- [7] **T. P. Schlachta**, G. G. Zámbo, M. J. Sauer, I. Rüter, C. A. Hoefler, S. Demeshko, F. Meyer, F. E. Kühn, "Tailoring activity and stability: Effects of electronic variations on iron-NHC epoxidation catalysts", *J. Catal.* **2023**, *426*, 234-246, DOI: 10.1016/j.jcat.2023.07.018.
- [6] **T. P. Schlachta**, F. E. Kühn, "Cyclic iron tetra N-heterocyclic carbenes: synthesis, properties, reactivity, and catalysis", *Chem. Soc. Rev.* **2023**, *52*, 2238-2277, DOI: 10.1039/D2CS01064J.
- [5] G. G. Zámbo, J. Mayr, M. J. Sauer, **T. P. Schlachta**, R. M. Reich, F. E. Kühn, "The first macrocyclic abnormally coordinating tetra-1,2,3-triazole-5-ylidene iron complex: a promising candidate for olefin epoxidation", *Dalton Trans.* **2022**, *51*, 13591-13595, DOI: 10.1039/D2DT02561B.
- [4] A. Holas,<sup>§</sup> C. Y. Koch,<sup>§</sup> J. Leibold,<sup>§</sup> A. Prendi,<sup>§</sup> **T. P. Schlachta**,<sup>§,\*</sup> A. S. Schmid,<sup>§</sup> L. Schmitt,<sup>§</sup> "On the energy consumption of online and on-site lectures", *Environ. Res. Commun.* **2022**, *4*, 061002, DOI: 10.1088/2515-7620/ac77df.
- [3] **T. P. Schlachta**,<sup>#</sup> M. R. Anneser,<sup>#</sup> J. F. Schlagintweit, C. H. G. Jakob, C. Hintermeier, A. D. Böth, S. Haslinger, R. M. Reich, F. E. Kühn, "Mimicking reactive high-valent diiron- $\mu_2$ -oxo intermediates of nonheme enzymes by an iron tetracarbene complex", *Chem. Commun.* **2021**, *57*, 6644-6647, DOI: 10.1039/D1CC02027G.
- [2] F. Dyckhoff, J. F. Schlagintweit, M. A. Bernd, C. H. G. Jakob, **T. P. Schlachta**, B. J. Hofmann, R. M. Reich, F. E. Kühn, "Degradation pathways of a highly active iron(III) tetra-NHC epoxidation catalyst", *Catal. Sci. Technol.* **2021**, *11*, 795-799, DOI: 10.1039/D0CY02433C.
- [1] **T. P. Schlachta**,<sup>#</sup> J. F. Schlagintweit,<sup>#</sup> M. R. Anneser, E.-M. H. J. Esslinger, M. Muhr, S. Haslinger, F. E. Kühn, "Modification of bio-inspired tetra-NHC iron complexes with axial nitrile ligands", *Inorg. Chim. Acta* **2021**, *518*, 120228, DOI: 10.1016/j.ica.2020.120228.

# Equally contributing authors

\* Corresponding author

§ All authors contributed equally and are in alphabetical order.

ORCID iD: <https://orcid.org/0000-0002-6343-2818>

Table 2. Contributions of T. P. Schlachta to the publications. # Equally contributing first authors (referring to publications [1], [3], [10]). \* Corresponding author (referring to publication [4]). § All authors contributed equally and are in alphabetical order (referring to publication [4]).

No.	Bibliographic Data	Ref.	Chapter	Author	Contribution, CRediT roles
[12]	<i>to be submitted</i> <b>2024</b>	–	4.2	1 <sup>st</sup>	conceptual approach, experimental work and related data interpretation, project administration, conception and writing – original draft, writing – review & editing, data curation, formal analysis, investigation, methodology, visualization
[11]	<i>submitted</i> <b>2024</b>	–	4.1	1 <sup>st</sup>	conceptual approach, experimental work and related data interpretation, project administration, conception and writing – original draft, writing – review & editing, data curation, formal analysis, investigation, methodology, visualization
[10]	<i>RSC Adv.</i> <b>2024</b> , 14, 10244-10254	[358]	3.7	2 <sup>nd</sup> #	conceptual approach, experimental work and related data interpretation, project administration, conception and writing – original draft, writing – review & editing, data curation, formal analysis, investigation, methodology, visualization
[9]	<i>Results in Chemistry</i> <b>2024</b> , 7, 101421	[356]	3.6	1 <sup>st</sup>	conceptualization, data curation, formal analysis, investigation, methodology, project administration, visualization, writing – original draft, writing – review & editing, experimental work and related data interpretation
[8]	<i>J. Organomet. Chem.</i> <b>2024</b> , 1006, 123018	[378]	–	4 <sup>th</sup>	experimental work, writing – review & editing
[7]	<i>J. Catal.</i> <b>2023</b> , 426, 234-246	[355]	3.5	1 <sup>st</sup>	conceptual approach, experimental work and related data interpretation, project administration, conception and writing – original draft, writing – review & editing, data curation, formal analysis, investigation, methodology, visualization
[6]	<i>Chem. Soc. Rev.</i> <b>2023</b> , 52, 2238-2277	[11]	3.4	1 <sup>st</sup>	conceptualization, data curation, formal analysis, investigation, methodology, visualization, writing – original draft, writing – review & editing
[5]	<i>Dalton Trans.</i> <b>2022</b> , 51, 13591-13595	[354]	3.3	4 <sup>th</sup>	experimental work and related data interpretation, conception, writing – review & editing, data curation, formal analysis, investigation, methodology, visualization
[4]	<i>Environ. Res. Commun.</i> <b>2022</b> , 4, 061002	[379]	–	5 <sup>th</sup> *,§	conceptualization, data curation, investigation, methodology, visualization, writing – original draft, writing – review & editing
[3]	<i>Chem. Commun.</i> <b>2021</b> , 57, 6644-6647	[346]	3.2	1 <sup>st</sup> #	experimental work and related data interpretation, conception and writing – original draft, writing – review & editing, data curation, formal analysis, investigation, methodology, visualization

[2]	<i>Catal. Sci. Technol.</i> <b>2021</b> , 11, 795-799	[335]	3.1	5 <sup>th</sup>	experimental work and related data interpretation, writing – review & editing, data curation, investigation
[1]	<i>Inorg. Chim. Acta</i> <b>2021</b> , 518, 120228	[344]	–	1 <sup>st</sup> #	experimental work and related data interpretation, conception and writing – original draft, writing – review & editing, data curation, formal analysis, investigation, visualization

CRedit: <https://credit.niso.org/contributor-roles-defined/>

## 8. Bibliographic data of complete list of publications

### Modification of bio-inspired tetra-NHC iron complexes with axial nitrile ligands

Tim P. Schlachta,<sup>#,a</sup> Jonas F. Schlagintweit,<sup>#,a</sup> Markus R. Anneser,<sup>a</sup> Eva-Maria H.J. Esslinger,<sup>a</sup> Maximilian Muhr,<sup>b</sup> Stefan Haslinger,<sup>a</sup> Fritz E. Kühn<sup>a,\*</sup>

*Inorg. Chim. Acta* **2021**, 518, 120228, DOI: 10.1016/j.ica.2020.120228

<sup>a</sup> Department of Chemistry and Catalysis Research Center, Molecular Catalysis, Technische Universität München, Lichtenbergstr. 4, 85748 Garching bei München, Germany

<sup>b</sup> Department of Chemistry and Catalysis Research Center, Chair of Inorganic and Metal-Organic Chemistry, Technische Universität München, Lichtenbergstr. 4, 85747 Garching bei München, Germany

# Equally contributing authors

\* Corresponding author

Ref. <sup>[344]</sup>

Direct link: <https://doi.org/10.1016/j.ica.2020.120228>

## Degradation pathways of a highly active iron(III) tetra-NHC epoxidation catalyst

Florian Dyckhoff, Jonas F. Schlagintweit, Marco A. Bernd, Christian H. G. Jakob, **Tim P. Schlachta**, Benjamin J. Hofmann, Robert M. Reich, Fritz E. Kühn\*

*Catal. Sci. Technol.* **2021**, *11*, 795-799, DOI: 10.1039/D0CY02433C

Molecular Catalysis, Catalysis Research Center and Department of Chemistry, Technische Universität München, Lichtenbergstr. 4, 85748 Garching bei München, Germany

\* Corresponding author

Ref. <sup>[335]</sup>

Direct link: <https://doi.org/10.1039/D0CY02433C>

## Mimicking reactive high-valent diiron- $\mu_2$ -oxo intermediates of non-heme enzymes by an iron tetracarbene complex

Tim P. Schlachta,<sup>#</sup> Markus R. Anneser,<sup>#</sup> Jonas F. Schlagintweit, Christian H. G. Jakob, Carolin Hintermeier, Alexander D. Böth, Stefan Haslinger, Robert M. Reich, Fritz E. Kühn\*

*Chem. Commun.* **2021**, 57, 6644-6647, DOI: 10.1039/D1CC02027G

Molecular Catalysis, Catalysis Research Center and Department of Chemistry, Technische Universität München, Lichtenbergstr. 4, 85748 Garching bei München, Germany

<sup>#</sup> Equally contributing authors

\* Corresponding author

Ref. <sup>[346]</sup>

Direct link: <https://doi.org/10.1039/D1CC02027G>

## On the energy consumption of online and on-site lectures

Alexander Holas,<sup>§,a,b,c</sup> Catherine Y. Koch,<sup>§,a,d</sup> Joachim Leibold,<sup>§,a,e</sup> Alesia Prendi,<sup>§,a,f</sup> **Tim P. Schlachta**,<sup>§,a,g,\*</sup> Anna Sophia Schmid,<sup>§,a,h</sup> Leonard Schmitt<sup>§,a,i</sup>

*Environ. Res. Commun.* **2022**, *4*, 061002, DOI: 10.1088/2515-7620/ac77df

<sup>a</sup> Technical University of Munich, Junge Akademie, Arcisstr. 21, 80333 München, Germany

<sup>b</sup> Zentrum für Astronomie der Universität Heidelberg, Institut für Theoretische Astrophysik, Philosophenweg 12, 69120 Heidelberg, Germany

<sup>c</sup> Heidelberg Institute for Theoretical Studies, Schloss-Wolfsbrunnenweg 35, 69118 Heidelberg, Germany

<sup>d</sup> Technical University of Munich, School of Engineering and Design, Department of Mechanical Engineering, Boltzmannstr. 15, 85748 Garching, Germany

<sup>e</sup> Technical University of Munich, Department of Physics, James-Franck-Str. 1, 85748 Garching, Germany

<sup>f</sup> Technical University of Munich, School of Engineering and Design, Department of Architecture, Arcisstr. 21, 80333 München, Germany

<sup>g</sup> Technical University of Munich, Department of Chemistry, Lichtenbergstr. 4, 85748 Garching, Germany

<sup>h</sup> Technical University of Munich, School of Social Sciences and Technology, Richard-Wagner-Str. 1, 80333 München, Germany

<sup>i</sup> Technical University of Munich, School of Medicine, Ismaninger Str. 22, 81675 Munich, Germany

§ All authors contributed equally and are in alphabetical order.

\* Corresponding author

Ref. <sup>[379]</sup>

Direct link: <https://doi.org/10.1088/2515-7620/ac77df>

## The first macrocyclic abnormally coordinating tetra-1,2,3-triazole-5-ylidene iron complex: a promising candidate for olefin epoxidation

Greta G. Zámbo, Johannes Mayr, Michael J. Sauer, **Tim P. Schlachta**, Robert M. Reich, Fritz E. Kühn\*

*Dalton Trans.* **2022**, 51, 13591-13595, DOI: 10.1039/D2DT02561B

Molecular Catalysis, Department of Chemistry and Catalysis Research Centre, Technische Universität München, Lichtenbergstr. 4, 85784 Garching bei München, Germany

\* Corresponding author

Ref. <sup>[354]</sup>

Direct link: <https://doi.org/10.1039/D2DT02561B>

# Cyclic iron tetra N-heterocyclic carbenes: synthesis, properties, reactivity, and catalysis

Tim P. Schlachta, Fritz E. Kühn\*

*Chem. Soc. Rev.* **2023**, *52*, 2238-2277, DOI: 10.1039/D2CS01064J

Technical University of Munich, School of Natural Sciences, Department of Chemistry and Catalysis Research Center, Molecular Catalysis, Lichtenbergstraße 4, 85748 Garching, Germany

\* Corresponding author

Ref. <sup>[1]</sup>

Direct link: <https://doi.org/10.1039/D2CS01064J>

## Tailoring activity and stability: Effects of electronic variations on iron-NHC epoxidation catalysts

Tim P. Schlachta,<sup>a</sup> Greta G. Zámbo,<sup>a</sup> Michael J. Sauer,<sup>a</sup> Isabelle Rüter,<sup>b</sup> Carla A. Hofer,<sup>a</sup> Serhiy Demeshko,<sup>b</sup> Franc Meyer,<sup>b</sup> Fritz E. Kühn<sup>a,\*</sup>

*J. Catal.* **2023**, *426*, 234-246, DOI: 10.1016/j.jcat.2023.07.018

<sup>a</sup> Technical University of Munich, School of Natural Sciences, Department of Chemistry and Catalysis Research Center, Molecular Catalysis, Lichtenbergstraße 4, 85748 Garching, Germany

<sup>b</sup> Georg-August-Universität Göttingen, Institut für Anorganische Chemie, Tammannstraße 4, 37077 Göttingen, Germany

\* Corresponding author

Ref. <sup>[355]</sup>

Direct link: <https://doi.org/10.1016/j.jcat.2023.07.018>

# Unraveling the potential of backbone modifications in iron(II) NHC complexes for olefin aziridination and imination

Carla A. Hoefler,<sup>#</sup> Nicole K. Dietl,<sup>#</sup> Greta G. Zámbo, **Tim P. Schlachta**, Robert M. Reich, Fritz E. Kühn\*

*J. Organomet. Chem.* **2024**, 1006, 123018, DOI: 10.1016/j.jorganchem.2024.123018

Technical University of Munich, School of Natural Sciences, Department of Chemistry and Catalysis Research Center, Molecular Catalysis, Lichtenbergstraße 4, 85748 Garching, Germany

<sup>#</sup> Equally contributing authors

\* Corresponding author

Ref. <sup>[378]</sup>

Direct link: <https://doi.org/10.1016/j.jorganchem.2024.123018>

# Chiral imidazolium and triazolium salts as NHC and aNHC ligand precursors: A promising framework for asymmetric epoxidation catalysis

Tim P. Schlachta, Leon F. Richter, Fritz E. Kühn\*

*Results in Chemistry* **2024**, 7, 101421, DOI: 10.1016/j.rechem.2024.101421

Technical University of Munich, School of Natural Sciences, Department of Chemistry and Catalysis Research Center, Molecular Catalysis, Lichtenbergstraße 4, 85748 Garching, Germany

\* Corresponding author

Ref. <sup>[356]</sup>

Direct link: <https://doi.org/10.1016/j.rechem.2024.101421>

# Synthesis, characterization, and biomedical evaluation of ethylene-bridged tetra-NHC Pd(II), Pt(II) and Au(III) complexes, with apoptosis-inducing properties in cisplatin-resistant neuroblastoma cells

Wolfgang R. E. Büchele,<sup>#,a</sup> **Tim P. Schlachta**,<sup>#,a</sup> Andreas L. Gebendorfer,<sup>a</sup> Jenny Pamperin,<sup>c,d</sup> Leon F. Richter,<sup>a</sup> Michael J. Sauer,<sup>a</sup> Aram Prokop,<sup>b,c,d,\*</sup> Fritz E. Kühn<sup>a,\*</sup>

*RSC Adv.* **2024**, *14*, 10244-10254, DOI: 10.1039/D4RA01195C

<sup>a</sup> Technical University of Munich, School of Natural Sciences, Department of Chemistry and Catalysis Research Center, Molecular Catalysis, Lichtenbergstraße 4, 85748 Garching, Germany

<sup>b</sup> Department of Pediatric Hematology/Oncology, Children's Hospital Cologne, Amsterdamer Straße 59, 50735 Cologne, Germany

<sup>c</sup> Department of Pediatric Oncology/Hematology, Helios Clinics Schwerin, Wismarsche Straße 393-397, 19055 Schwerin, Germany.

<sup>d</sup> Department of Human Medicine, MSH Medical School Hamburg, Am Kaiserkai 1, 20457 Hamburg, Germany

# Equally contributing authors

\* Corresponding authors

Ref. <sup>[358]</sup>

Direct link: <https://doi.org/10.1039/D4RA01195C>

## 9. References

- [1] M. N. Hopkinson, C. Richter, M. Schedler, F. Glorius, *Nature* **2014**, *510*, 485-496, DOI: 10.1038/nature13384.
- [2] D. Bourissou, O. Guerret, F. P. Gabbaï, G. Bertrand, *Chem. Rev.* **2000**, *100*, 39-92, DOI: 10.1021/cr940472u.
- [3] P. de Frémont, N. Marion, S. P. Nolan, *Coord. Chem. Rev.* **2009**, *253*, 862-892, DOI: 10.1016/j.ccr.2008.05.018.
- [4] P. Bellotti, M. Koy, M. N. Hopkinson, F. Glorius, *Nat. Rev. Chem.* **2021**, *5*, 711-725, DOI: 10.1038/s41570-021-00321-1.
- [5] A. Igau, H. Grutzmacher, A. Baceiredo, G. Bertrand, *J. Am. Chem. Soc.* **1988**, *110*, 6463-6466, DOI: 10.1021/ja00227a028.
- [6] H.-W. Wanzlick, H.-J. Schönherr, *Angew. Chem. Int. Ed. Engl.* **1968**, *7*, 141-142, DOI: 10.1002/anie.196801412.
- [7] K. Öfele, *J. Organomet. Chem.* **1968**, *12*, P42-P43, DOI: 10.1016/S0022-328X(00)88691-X.
- [8] A. J. Arduengo, R. L. Harlow, M. Kline, *J. Am. Chem. Soc.* **1991**, *113*, 361-363, DOI: 10.1021/ja00001a054.
- [9] E. Riedel, *Allgemeine und Anorganische Chemie*, De Gruyter: **2010**, DOI: 10.1515/9783110227826.
- [10] T. P. Schlachta, master's thesis, Technical University of Munich (Garching, Germany), **2020**.
- [11] T. P. Schlachta, F. E. Kühn, *Chem. Soc. Rev.* **2023**, *52*, 2238-2277, DOI: 10.1039/D2CS01064J.
- [12] C. Janiak, H.-J. Meyer, D. Gudat, R. Alsfasser, E. Riedel, H.-J. Meyer, *Riedel Moderne Anorganische Chemie*, De Gruyter: Berlin, Boston, **2012**, DOI: 10.1515/9783110249019.
- [13] C. Heinemann, T. Müller, Y. Apeloig, H. Schwarz, *J. Am. Chem. Soc.* **1996**, *118*, 2023-2038, DOI: 10.1021/ja9523294.
- [14] A. J. Arduengo, H. V. R. Dias, R. L. Harlow, M. Kline, *J. Am. Chem. Soc.* **1992**, *114*, 5530-5534, DOI: 10.1021/ja00040a007.
- [15] M. Scholl, S. Ding, C. W. Lee, R. H. Grubbs, *Org. Lett.* **1999**, *1*, 953-956, DOI: 10.1021/ol990909q.
- [16] V. P. W. Böhm, W. A. Herrmann, *Angew. Chem. Int. Ed.* **2000**, *39*, 4036-4038, DOI: 10.1002/1521-3773(20001117)39:22<4036::AID-ANIE4036>3.0.CO;2-L.
- [17] M. Koy, P. Bellotti, M. Das, F. Glorius, *Nature Catalysis* **2021**, *4*, 352-363, DOI: 10.1038/s41929-021-00607-z.
- [18] O. M. Ogba, N. C. Warner, D. J. O'Leary, R. H. Grubbs, *Chem. Soc. Rev.* **2018**, *47*, 4510-4544, DOI: 10.1039/C8CS00027A.
- [19] C. Samojłowicz, M. Bieniek, K. Grela, *Chem. Rev.* **2009**, *109*, 3708-3742, DOI: 10.1021/cr800524f.
- [20] G. C. Vougioukalakis, R. H. Grubbs, *Chem. Rev.* **2010**, *110*, 1746-1787, DOI: 10.1021/cr9002424.
- [21] S. H. Hong, R. H. Grubbs, *J. Am. Chem. Soc.* **2006**, *128*, 3508-3509, DOI: 10.1021/ja058451c.
- [22] T. J. Seiders, D. W. Ward, R. H. Grubbs, *Org. Lett.* **2001**, *3*, 3225-3228, DOI: 10.1021/ol0165692.
- [23] T. W. Funk, J. M. Berlin, R. H. Grubbs, *J. Am. Chem. Soc.* **2006**, *128*, 1840-1846, DOI: 10.1021/ja055994d.
- [24] J. J. Van Veldhuizen, J. E. Campbell, R. E. Giudici, A. H. Hoveyda, *J. Am. Chem. Soc.* **2005**, *127*, 6877-6882, DOI: 10.1021/ja050179j.
- [25] J. J. Van Veldhuizen, S. B. Garber, J. S. Kingsbury, A. H. Hoveyda, *J. Am. Chem. Soc.* **2002**, *124*, 4954-4955, DOI: 10.1021/ja020259c.

- [26] K. Endo, R. H. Grubbs, *J. Am. Chem. Soc.* **2011**, *133*, 8525-8527, DOI: 10.1021/ja202818v.
- [27] R. K. M. Khan, S. Torker, A. H. Hoveyda, *J. Am. Chem. Soc.* **2013**, *135*, 10258-10261, DOI: 10.1021/ja404208a.
- [28] M. Melaimi, M. Soleilhavoup, G. Bertrand, *Angew. Chem. Int. Ed.* **2010**, *49*, 8810-8849, DOI: 10.1002/anie.201000165.
- [29] J. Zhang, T. Li, X. Li, A. Lv, X. Li, Z. Wang, R. Wang, Y. Ma, R. Fang, R. Szostak, M. Szostak, *Communications Chemistry* **2022**, *5*, 60, DOI: 10.1038/s42004-022-00675-7.
- [30] M. Joost, M. Nieger, M. Lutz, A. W. Ehlers, J. C. Slootweg, K. Lammertsma, *Organometallics* **2020**, *39*, 1762-1771, DOI: 10.1021/acs.organomet.0c00066.
- [31] D. M. Andrada, N. Holzmann, T. Hamadi, G. Frenking, *Beilstein J. Org. Chem.* **2015**, *11*, 2727-2736, DOI: 10.3762/bjoc.11.294.
- [32] G. Guisado-Barrios, M. Soleilhavoup, G. Bertrand, *Acc. Chem. Res.* **2018**, *51*, 3236-3244, DOI: 10.1021/acs.accounts.8b00480.
- [33] J. M. Aizpurua, M. Sagartzazu-Aizpurua, Z. Monasterio, in *Chemistry of 1,2,3-triazoles* (Eds.: W. Dehaen, V. A. Bakulev), Springer International Publishing: Cham, **2015**, pp. 211-267, DOI: 10.1007/7081\_2014\_120.
- [34] G. Guisado-Barrios, J. Bouffard, B. Donnadieu, G. Bertrand, *Angew. Chem. Int. Ed.* **2010**, *49*, 4759-4762, DOI: 10.1002/anie.201001864.
- [35] D. Martin, A. Baceiredo, H. Gornitzka, W. W. Schoeller, G. Bertrand, *Angew. Chem. Int. Ed.* **2005**, *44*, 1700-1703, DOI: 10.1002/anie.200462239.
- [36] J. D. Masuda, D. Martin, C. Lyon-Saunier, A. Baceiredo, H. Gornitzka, B. Donnadieu, G. Bertrand, *Chem Asian J.* **2007**, *2*, 178-187, DOI: 10.1002/asia.200600300.
- [37] T. Cantat, N. Mézailles, N. Maigrot, L. Ricard, P. Le Floch, *Chem. Commun.* **2004**, 1274-1275, DOI: 10.1039/B403436H.
- [38] E. Niecke, A. Fuchs, M. Nieger, O. Schmidt, W. W. Schoeller, *Angew. Chem. Int. Ed.* **1999**, *38*, 3031-3034, DOI: 10.1002/(SICI)1521-3773(19991018)38:20<3031::AID-ANIE3031>3.0.CO;2-G.
- [39] J. Ruiz, M. E. G. Mosquera, G. García, E. Patrón, V. Riera, S. García-Granda, F. Van der Maelen, *Angew. Chem. Int. Ed.* **2003**, *42*, 4767-4771, DOI: 10.1002/anie.200219604.
- [40] N. D. Jones, G. Lin, R. A. Gossage, R. McDonald, R. G. Cavell, *Organometallics* **2003**, *22*, 2832-2841, DOI: 10.1021/om030003v.
- [41] J. Kapp, C. Schade, A. M. El-Nahasa, P. von Ragué Schleyer, *Angew. Chem. Int. Ed. Engl.* **1996**, *35*, 2236-2238, DOI: 10.1002/anie.199622361.
- [42] F. E. Hahn, *Angew. Chem. Int. Ed.* **2006**, *45*, 1348-1352, DOI: 10.1002/anie.200503858.
- [43] C. Boehme, G. Frenking, *J. Am. Chem. Soc.* **1996**, *118*, 2039-2046, DOI: 10.1021/ja9527075.
- [44] D. A. Dixon, A. J. Arduengo, *J. Phys. Chem.* **1991**, *95*, 4180-4182, DOI: 10.1021/j100164a003.
- [45] Á. Fekete, L. Nyulászi, *J. Organomet. Chem.* **2002**, *643-644*, 278-284, DOI: 10.1016/S0022-328X(01)01222-0.
- [46] W. W. Schoeller, D. Eisner, *Inorg. Chem.* **2004**, *43*, 2585-2589, DOI: 10.1021/ic030234u.
- [47] L. Nyulászi, *Tetrahedron* **2000**, *56*, 79-84, DOI: 10.1016/S0040-4020(99)00775-9.
- [48] M. Denk, R. Lennon, R. Hayashi, R. West, A. V. Belyakov, H. P. Verne, A. Haaland, M. Wagner, N. Metzler, *J. Am. Chem. Soc.* **1994**, *116*, 2691-2692, DOI: 10.1021/ja00085a088.
- [49] M. Veith, M. Grosser, *Zeitschrift für Naturforschung B* **1982**, *37*, 1375-1381, DOI: 10.1515/znb-1982-1103.
- [50] J. Barrau, G. Rima, *Coord. Chem. Rev.* **1998**, *178-180*, 593-622, DOI: 10.1016/S0010-8545(98)00076-9.
- [51] J. D. Andriamizaka, C. Couret, J. Escudié, J. Satgé, *Phosphorus and Sulfur and the Related Elements* **1982**, *12*, 265-278, DOI: 10.1080/03086648208078959.
- [52] O. Kühn, *Coord. Chem. Rev.* **2004**, *248*, 411-427, DOI: 10.1016/j.ccr.2003.12.004.

- [53] Z. Benedek, T. Szilvási, *RSC Adv.* **2015**, *5*, 5077-5086, DOI: 10.1039/C4RA14417A.
- [54] M. Asay, C. Jones, M. Driess, *Chem. Rev.* **2011**, *111*, 354-396, DOI: 10.1021/cr100216y.
- [55] C. Boehme, G. Frenking, *Organometallics* **1998**, *17*, 5801-5809, DOI: 10.1021/om980394r.
- [56] A. K. Guha, S. Sarmah, A. K. Phukan, *Dalton Trans.* **2010**, *39*, 7374-7383, DOI: 10.1039/C003266B.
- [57] F. Ullah, O. Kühl, G. Bajor, T. Veszprémi, P. G. Jones, J. Heinicke, *Eur. J. Inorg. Chem.* **2009**, *2009*, 221-229, DOI: 10.1002/ejic.200800849.
- [58] H. M. Tuononen, R. Roesler, J. L. Dutton, P. J. Ragogna, *Inorg. Chem.* **2007**, *46*, 10693-10706, DOI: 10.1021/ic701350e.
- [59] P. B. Hitchcock, M. F. Lappert, M. Layh, *J. Chem. Soc., Dalton Trans.* **1998**, 3113-3118, DOI: 10.1039/A804134B.
- [60] F. E. Hahn, D. Heitmann, T. Pape, *Eur. J. Inorg. Chem.* **2008**, *2008*, 1039-1041, DOI: 10.1002/ejic.200701260.
- [61] R. Dasgupta, S. Khan, in *Adv. Organomet. Chem., Vol. 74* (Ed.: P. J. Pérez), Academic Press, **2020**, pp. 105-152, DOI: 10.1016/bs.adomc.2020.04.001.
- [62] B. Gehrhus, P. B. Hitchcock, M. F. Lappert, *J. Chem. Soc., Dalton Trans.* **2000**, 3094-3099, DOI: 10.1039/B005216G.
- [63] M. He, C. Hu, R. Wei, X.-F. Wang, L. L. Liu, *Chem. Soc. Rev.* **2024**, DOI: 10.1039/D3CS00784G.
- [64] V. Lavallo, Y. Canac, C. Präsang, B. Donnadiou, G. Bertrand, *Angew. Chem. Int. Ed.* **2005**, *44*, 5705-5709, DOI: 10.1002/anie.200501841.
- [65] M. Melaimi, R. Jazzar, M. Soleilhavoup, G. Bertrand, *Angew. Chem. Int. Ed.* **2017**, *56*, 10046-10068, DOI: 10.1002/anie.201702148.
- [66] R. Jazzar, M. Soleilhavoup, G. Bertrand, *Chem. Rev.* **2020**, *120*, 4141-4168, DOI: 10.1021/acs.chemrev.0c00043.
- [67] B. Rao, H. Tang, X. Zeng, L. L. Liu, M. Melaimi, G. Bertrand, *Angew. Chem. Int. Ed.* **2015**, *54*, 14915-14919, DOI: 10.1002/anie.201507844.
- [68] C. M. Weinstein, G. P. Junor, D. R. Tolentino, R. Jazzar, M. Melaimi, G. Bertrand, *J. Am. Chem. Soc.* **2018**, *140*, 9255-9260, DOI: 10.1021/jacs.8b05518.
- [69] Z. R. McCarty, D. N. Lastovickova, C. W. Bielawski, *Chem. Commun.* **2016**, *52*, 5447-5450, DOI: 10.1039/C6CC01376G.
- [70] J. P. Moerdyk, D. Schilter, C. W. Bielawski, *Acc. Chem. Res.* **2016**, *49*, 1458-1468, DOI: 10.1021/acs.accounts.6b00080.
- [71] M. B. Gildner, T. W. Hudnall, *Chem. Commun.* **2019**, *55*, 12300-12303, DOI: 10.1039/C9CC05280A.
- [72] D. Munz, *Organometallics* **2018**, *37*, 275-289, DOI: 10.1021/acs.organomet.7b00720.
- [73] R. S. Ghadwal, *Angew. Chem. Int. Ed.* **2023**, *62*, e202304665, DOI: 10.1002/anie.202304665.
- [74] R. Maity, B. Sarkar, *JACS Au* **2022**, *2*, 22-57, DOI: 10.1021/jacsau.1c00338.
- [75] Á. Vivancos, C. Segarra, M. Albrecht, *Chem. Rev.* **2018**, *118*, 9493-9586, DOI: 10.1021/acs.chemrev.8b00148.
- [76] S. Gründemann, A. Kovacevic, M. Albrecht, J. W. Faller, R. H. Crabtree, *J. Am. Chem. Soc.* **2002**, *124*, 10473-10481, DOI: 10.1021/ja026735g.
- [77] S. Gründemann, A. Kovacevic, M. Albrecht, J. W. Faller Robert, H. Crabtree, *Chem. Commun.* **2001**, 2274-2275, DOI: 10.1039/B107881J.
- [78] O. Schuster, L. Yang, H. G. Raubenheimer, M. Albrecht, *Chem. Rev.* **2009**, *109*, 3445-3478, DOI: 10.1021/cr8005087.
- [79] D. Rottschäfer, T. Glodde, B. Neumann, H.-G. Stämmler, R. S. Ghadwal, *Chem. Commun.* **2020**, *56*, 2027-2030, DOI: 10.1039/C9CC09428H.
- [80] L. Benhamou, E. Chardon, G. Lavigne, S. Bellemin-Lapponnaz, V. César, *Chem. Rev.* **2011**, *111*, 2705-2733, DOI: 10.1021/cr100328e.
- [81] W. A. Herrmann, J. Schütz, G. D. Frey, E. Herdtweck, *Organometallics* **2006**, *25*, 2437-2448, DOI: 10.1021/om0600801.

- [82] A. J. Arduengo, R. Krafczyk, R. Schmutzler, H. A. Craig, J. R. Goerlich, W. J. Marshall, M. Unverzagt, *Tetrahedron* **1999**, *55*, 14523-14534, DOI: 10.1016/S0040-4020(99)00927-8.
- [83] E. Peris, in *N-Heterocyclic Carbenes in Transition Metal Catalysis* (Ed.: F. Glorius), Springer Berlin Heidelberg: Berlin, Heidelberg, **2007**, pp. 83-116, DOI: 10.1007/3418\_027.
- [84] D. J. Nelson, *Eur. J. Inorg. Chem.* **2015**, *2015*, 2012-2027, DOI: 10.1002/ejic.201500061.
- [85] C. Barnett, M. L. Cole, J. B. Harper, *ACS Omega* **2022**, *7*, 34657-34664, DOI: 10.1021/acsomega.2c04682.
- [86] D. J. Nelson, S. P. Nolan, *Chem. Soc. Rev.* **2013**, *42*, 6723-6753, DOI: 10.1039/C3CS60146C.
- [87] A. Comas-Vives, J. N. Harvey, *Eur. J. Inorg. Chem.* **2011**, *2011*, 5025-5035, DOI: 10.1002/ejic.201100721.
- [88] H. V. Huynh, *Chem. Rev.* **2018**, *118*, 9457-9492, DOI: 10.1021/acs.chemrev.8b00067.
- [89] A. A. Tukov, A. T. Normand, M. S. Nechaev, *Dalton Trans.* **2009**, 7015-7028, DOI: 10.1039/B906969K.
- [90] U. Radius, F. M. Bickelhaupt, *Coord. Chem. Rev.* **2009**, *253*, 678-686, DOI: 10.1016/j.ccr.2008.05.020.
- [91] R. Tonner, G. Heydenrych, G. Frenking, *Chem Asian J.* **2007**, *2*, 1555-1567, DOI: 10.1002/asia.200700235.
- [92] N. M. Scott, R. Dorta, E. D. Stevens, A. Correa, L. Cavallo, S. P. Nolan, *J. Am. Chem. Soc.* **2005**, *127*, 3516-3526, DOI: 10.1021/ja043249f.
- [93] T. Dröge, F. Glorius, *Angew. Chem. Int. Ed.* **2010**, *49*, 6940-6952, DOI: 10.1002/anie.201001865.
- [94] N. Konstandaras, M. H. Dunn, M. S. Guerry, C. D. Barnett, M. L. Cole, J. B. Harper, *Org. Biomol. Chem.* **2020**, *18*, 66-75, DOI: 10.1039/C9OB02258A.
- [95] M. H. Dunn, N. Konstandaras, M. L. Cole, J. B. Harper, *J. Org. Chem.* **2017**, *82*, 7324-7331, DOI: 10.1021/acs.joc.7b00716.
- [96] W. N. Olmstead, F. G. Bordwell, *J. Org. Chem.* **1980**, *45*, 3299-3305, DOI: 10.1021/jo01304a033.
- [97] Y. Chu, H. Deng, J.-P. Cheng, *J. Org. Chem.* **2007**, *72*, 7790-7793, DOI: 10.1021/jo070973i.
- [98] A. M. Magill, K. J. Cavell, B. F. Yates, *J. Am. Chem. Soc.* **2004**, *126*, 8717-8724, DOI: 10.1021/ja038973x.
- [99] T. L. Amyes, S. T. Diver, J. P. Richard, F. M. Rivas, K. Toth, *J. Am. Chem. Soc.* **2004**, *126*, 4366-4374, DOI: 10.1021/ja039890j.
- [100] A. M. Magill, B. F. Yates, *Aust. J. Chem.* **2004**, *57*, 1205-1210, DOI: 10.1071/CH04159.
- [101] G. Höfle, W. Steglich, H. Vorbrüggen, *Angew. Chem. Int. Ed. Engl.* **1978**, *17*, 569-583, DOI: 10.1002/anie.197805691.
- [102] M. N. Hopkinson, F. Glorius, in *N-Heterocyclic Carbenes in Organocatalysis* (Ed.: A. T. Biju), Wiley-VCH: Weinheim, Germany, **2018**, pp. 1-35, DOI: 10.1002/9783527809042.ch1.
- [103] H. Mayr, A. R. Ofial, *J. Phys. Org. Chem.* **2008**, *21*, 584-595, DOI: 10.1002/poc.1325.
- [104] B. Maji, M. Breugst, H. Mayr, *Angew. Chem. Int. Ed.* **2011**, *50*, 6915-6919, DOI: 10.1002/anie.201102435.
- [105] H. V. Huynh, Y. Han, R. Jothibas, J. A. Yang, *Organometallics* **2009**, *28*, 5395-5404, DOI: 10.1021/om900667d.
- [106] Q. Teng, H. V. Huynh, *Dalton Trans.* **2017**, *46*, 614-627, DOI: 10.1039/C6DT04222H.
- [107] M. Meier, T. T. Y. Tan, F. E. Hahn, H. V. Huynh, *Organometallics* **2017**, *36*, 275-284, DOI: 10.1021/acs.organomet.6b00736.
- [108] S. Guo, H. Sivaram, D. Yuan, H. V. Huynh, *Organometallics* **2013**, *32*, 3685-3696, DOI: 10.1021/om400313r.
- [109] H. V. Huynh, *Chem. Lett.* **2021**, *50*, 1831-1841, DOI: 10.1246/cl.210435.
- [110] Y. Han, H. V. Huynh, G. K. Tan, *Organometallics* **2007**, *26*, 6447-6452, DOI: 10.1021/om700753d.

- [111] D. Yuan, H. V. Huynh, *Organometallics* **2012**, *31*, 405-412, DOI: 10.1021/om2010029.
- [112] H. Clavier, S. P. Nolan, *Chem. Commun.* **2010**, *46*, 841-861, DOI: 10.1039/B922984A.
- [113] W. Wu, Q. Teng, Y.-Y. Chua, H. V. Huynh, H. A. Duong, *Organometallics* **2017**, *36*, 2293-2297, DOI: 10.1021/acs.organomet.7b00180.
- [114] O. Back, M. Henry-Ellinger, C. D. Martin, D. Martin, G. Bertrand, *Angew. Chem. Int. Ed.* **2013**, *52*, 2939-2943, DOI: 10.1002/anie.201209109.
- [115] A. Liske, K. Verlinden, H. Buhl, K. Schaper, C. Ganter, *Organometallics* **2013**, *32*, 5269-5272, DOI: 10.1021/om400858y.
- [116] A. Merschel, D. Rottschäfer, B. Neumann, H.-G. Stämmler, R. S. Ghadwal, *Organometallics* **2020**, *39*, 1719-1729, DOI: 10.1021/acs.organomet.0c00045.
- [117] C. Barnett, M. L. Cole, J. B. Harper, *Eur. J. Inorg. Chem.* **2021**, *2021*, 4954-4958, DOI: 10.1002/ejic.202100796.
- [118] C. Barnett, M. L. Cole, J. B. Harper, *Chemistry–Methods* **2021**, *1*, 374-381, DOI: 10.1002/cmtd.202100043.
- [119] R. R. Rodrigues, C. L. Dorsey, C. A. Arceneaux, T. W. Hudnall, *Chem. Commun.* **2014**, *50*, 162-164, DOI: 10.1039/C3CC45134H.
- [120] D. J. Nelson, F. Nahra, S. R. Patrick, D. B. Cordes, A. M. Z. Slawin, S. P. Nolan, *Organometallics* **2014**, *33*, 3640-3645, DOI: 10.1021/om500610w.
- [121] K. Verlinden, H. Buhl, W. Frank, C. Ganter, *Eur. J. Inorg. Chem.* **2015**, *2015*, 2416-2425, DOI: 10.1002/ejic.201500174.
- [122] G. Meng, L. Kakalis, S. P. Nolan, M. Szostak, *Tetrahedron Lett.* **2019**, *60*, 378-381, DOI: 10.1016/j.tetlet.2018.12.059.
- [123] C. A. Tolman, *Chem. Rev.* **1977**, *77*, 313-348, DOI: 10.1021/cr60307a002.
- [124] E. L. Rosen, C. D. Varnado, Jr., A. G. Tennyson, D. M. Khramov, J. W. Kamplain, D. H. Sung, P. T. Cresswell, V. M. Lynch, C. W. Bielawski, *Organometallics* **2009**, *28*, 6695-6706, DOI: 10.1021/om900698x.
- [125] A. R. Chianese, A. Kovacevic, B. M. Zeglis, J. W. Faller, R. H. Crabtree, *Organometallics* **2004**, *23*, 2461-2468, DOI: 10.1021/om049903h.
- [126] M. Braun, W. Frank, G. J. Reiss, C. Ganter, *Organometallics* **2010**, *29*, 4418-4420, DOI: 10.1021/om100728n.
- [127] A. B. P. Lever, *Inorg. Chem.* **1990**, *29*, 1271-1285, DOI: 10.1021/ic00331a030.
- [128] U. Siemeling, C. Färber, M. Leibold, C. Bruhn, P. Mücke, R. F. Winter, B. Sarkar, M. von Hopffgarten, G. Frenking, *Eur. J. Inorg. Chem.* **2009**, *2009*, 4607-4612, DOI: 10.1002/ejic.200900863.
- [129] G. A. Blake, J. P. Moerdyk, C. W. Bielawski, *Organometallics* **2012**, *31*, 3373-3378, DOI: 10.1021/om3001586.
- [130] S. Leuthäuser, D. Schwarz, H. Plenio, *Chem. Eur. J.* **2007**, *13*, 7195-7203, DOI: 10.1002/chem.200700228.
- [131] D. G. Gusev, *Organometallics* **2009**, *28*, 763-770, DOI: 10.1021/om800933x.
- [132] R. Tonner, G. Frenking, *Organometallics* **2009**, *28*, 3901-3905, DOI: 10.1021/om900206w.
- [133] D. G. Gusev, *Organometallics* **2009**, *28*, 6458-6461, DOI: 10.1021/om900654g.
- [134] L. Perrin, E. Clot, O. Eisenstein, J. Loch, R. H. Crabtree, *Inorg. Chem.* **2001**, *40*, 5806-5811, DOI: 10.1021/ic0105258.
- [135] Z. Dong, J. T. Blaskovits, F. Fadaei-Tirani, R. Scopelliti, A. Sienkiewicz, C. Corminboeuf, K. Severin, *Chem. Eur. J.* **2021**, *27*, 11983-11988, DOI: 10.1002/chem.202101742.
- [136] A. K. Phukan, A. K. Guha, S. Sarmah, R. D. Dewhurst, *J. Org. Chem.* **2013**, *78*, 11032-11039, DOI: 10.1021/jo402057g.
- [137] P. Geerlings, F. De Proft, W. Langenaeker, *Chem. Rev.* **2003**, *103*, 1793-1874, DOI: 10.1021/cr990029p.
- [138] J. C. Bernhammer, G. Frison, H. V. Huynh, *Chem. Eur. J.* **2013**, *19*, 12892-12905, DOI: 10.1002/chem.201301093.
- [139] A. Gómez-Suárez, D. J. Nelson, S. P. Nolan, *Chem. Commun.* **2017**, *53*, 2650-2660, DOI: 10.1039/C7CC00255F.

- [140] P. de Frémont, N. M. Scott, E. D. Stevens, S. P. Nolan, *Organometallics* **2005**, *24*, 2411-2418, DOI: 10.1021/om050111c.
- [141] S. Kamijo, Y. Yamamoto, *Chem Asian J.* **2007**, *2*, 568-578, DOI: 10.1002/asia.200600418.
- [142] F. Nahra, D. J. Nelson, S. P. Nolan, *Trends in Chemistry* **2020**, *2*, 1096-1113, DOI: 10.1016/j.trechm.2020.10.003.
- [143] N. Kuhn, T. Kratz, *Synthesis* **1993**, *1993*, 561-562, DOI: 10.1055/s-1993-25902.
- [144] M. K. Denk, A. Hezarkhani, F.-L. Zheng, *Eur. J. Inorg. Chem.* **2007**, *2007*, 3527-3534, DOI: 10.1002/ejic.200700217.
- [145] G. W. Nyce, S. Csihony, R. M. Waymouth, J. L. Hedrick, *Chem. Eur. J.* **2004**, *10*, 4073-4079, DOI: 10.1002/chem.200400196.
- [146] R. B. Bedford, M. Betham, D. W. Bruce, A. A. Danopoulos, R. M. Frost, M. Hird, *J. Org. Chem.* **2006**, *71*, 1104-1110, DOI: 10.1021/jo052250+.
- [147] H. A. Duong, T. N. Tekavec, A. M. Arif, J. Louie, *Chem. Commun.* **2004**, 112-113, DOI: 10.1039/B311350G.
- [148] B. Bantu, G. M. Pawar, U. Decker, K. Wurst, A. M. Schmidt, M. R. Buchmeiser, *Chem. Eur. J.* **2009**, *15*, 3103-3109, DOI: 10.1002/chem.200802670.
- [149] M. Otto, S. Conejero, Y. Canac, V. D. Romanenko, V. Rudzevitch, G. Bertrand, *J. Am. Chem. Soc.* **2004**, *126*, 1016-1017, DOI: 10.1021/ja0393325.
- [150] C. M. Crudden, D. P. Allen, *Coord. Chem. Rev.* **2004**, *248*, 2247-2273, DOI: 10.1016/j.ccr.2004.05.013.
- [151] N. Ségaud, C. Johnson, A. Farre, M. Albrecht, *Chem. Commun.* **2021**, *57*, 10600-10603, DOI: 10.1039/D1CC02740A.
- [152] J. A. M. Lummiss, C. S. Higman, D. L. Fyson, R. McDonald, D. E. Fogg, *Chem. Sci.* **2015**, *6*, 6739-6746, DOI: 10.1039/C5SC02592C.
- [153] S. Díez-González, N. Marion, S. P. Nolan, *Chem. Rev.* **2009**, *109*, 3612-3676, DOI: 10.1021/cr900074m.
- [154] W. A. Herrmann, M. Elison, J. Fischer, C. Köcher, G. R. J. Artus, *Angew. Chem. Int. Ed. Engl.* **1995**, *34*, 2371-2374, DOI: 10.1002/anie.199523711.
- [155] W. A. Herrmann, *Angew. Chem. Int. Ed.* **2002**, *41*, 1290-1309, DOI: 10.1002/1521-3773(20020415)41:8<1290::AID-ANIE1290>3.0.CO;2-Y.
- [156] M. Poyatos, J. A. Mata, E. Peris, *Chem. Rev.* **2009**, *109*, 3677-3707, DOI: 10.1021/cr800501s.
- [157] N. U. D. Reshi, J. K. Bera, *Coord. Chem. Rev.* **2020**, *422*, 213334, DOI: 10.1016/j.ccr.2020.213334.
- [158] K. M. Hindi, M. J. Panzner, C. A. Tessier, C. L. Cannon, W. J. Youngs, *Chem. Rev.* **2009**, *109*, 3859-3884, DOI: 10.1021/cr800500u.
- [159] I. Ott, in *Adv. Inorg. Chem., Vol. 75* (Eds.: P. J. Sadler, R. van Eldik), Academic Press, **2020**, pp. 121-148, DOI: 10.1016/bs.adioch.2019.10.008.
- [160] S. A Patil, A. P Hoagland, S. A Patil, A. Bugarin, *Future Medicinal Chemistry* **2020**, *12*, 2239-2275, DOI: 10.4155/fmc-2020-0175.
- [161] K. Oisaki, Q. Li, H. Furukawa, A. U. Czaja, O. M. Yaghi, *J. Am. Chem. Soc.* **2010**, *132*, 9262-9264, DOI: 10.1021/ja103016y.
- [162] L. Mercks, M. Albrecht, *Chem. Soc. Rev.* **2010**, *39*, 1903-1912, DOI: 10.1039/B902238B.
- [163] K. V. S. Ranganath, J. Kloesges, A. H. Schäfer, F. Glorius, *Angew. Chem. Int. Ed.* **2010**, *49*, 7786-7789, DOI: 10.1002/anie.201002782.
- [164] C. A. Smith, M. R. Narouz, P. A. Lummis, I. Singh, A. Nazemi, C.-H. Li, C. M. Crudden, *Chem. Rev.* **2019**, *119*, 4986-5056, DOI: 10.1021/acs.chemrev.8b00514.
- [165] N. Kuhn, A. Al-Sheikh, *Coord. Chem. Rev.* **2005**, *249*, 829-857, DOI: 10.1016/j.ccr.2004.10.003.
- [166] S. Bellemin-Lapponnaz, S. Dagorne, *Chem. Rev.* **2014**, *114*, 8747-8774, DOI: 10.1021/cr500227y.
- [167] V. Nesterov, D. Reiter, P. Bag, P. Frisch, R. Holzner, A. Porzelt, S. Inoue, *Chem. Rev.* **2018**, *118*, 9678-9842, DOI: 10.1021/acs.chemrev.8b00079.

- [168] A. Doddi, M. Peters, M. Tamm, *Chem. Rev.* **2019**, *119*, 6994-7112, DOI: 10.1021/acs.chemrev.8b00791.
- [169] T. Ochiai, D. Franz, S. Inoue, *Chem. Soc. Rev.* **2016**, *45*, 6327-6344, DOI: 10.1039/C6CS00163G.
- [170] N. Kuhn, H. Bohnen, J. Kreutzberg, D. Bläser, R. Boese, *J. Chem. Soc., Chem. Commun.* **1993**, 1136-1137, DOI: 10.1039/C39930001136.
- [171] P. Bag, A. Porzelt, P. J. Altmann, S. Inoue, *J. Am. Chem. Soc.* **2017**, *139*, 14384-14387, DOI: 10.1021/jacs.7b08890.
- [172] L. Delaude, *Eur. J. Inorg. Chem.* **2009**, *2009*, 1681-1699, DOI: 10.1002/ejic.200801227.
- [173] D. Martin, M. Soleilhavoup, G. Bertrand, *Chem. Sci.* **2011**, *2*, 389-399, DOI: 10.1039/C0SC00388C.
- [174] E. L. Kolychev, E. Theuergarten, M. Tamm, in *Frustrated Lewis Pairs II: Expanding the Scope* (Eds.: G. Erker, D. W. Stephan), Springer Berlin Heidelberg: Berlin, Heidelberg, **2013**, pp. 121-155, DOI: 10.1007/128\_2012\_379.
- [175] G. D. Frey, V. Lavallo, B. Donnadiou, W. W. Schoeller, G. Bertrand, *Science* **2007**, *316*, 439-441, DOI: 10.1126/science.1141474.
- [176] V. Lavallo, Y. Canac, B. Donnadiou, W. W. Schoeller, G. Bertrand, *Angew. Chem. Int. Ed.* **2006**, *45*, 3488-3491, DOI: 10.1002/anie.200600987.
- [177] J. D. Masuda, W. W. Schoeller, B. Donnadiou, G. Bertrand, *Angew. Chem. Int. Ed.* **2007**, *46*, 7052-7055, DOI: 10.1002/anie.200703055.
- [178] D. Enders, O. Niemeier, A. Henseler, *Chem. Rev.* **2007**, *107*, 5606-5655, DOI: 10.1021/cr068372z.
- [179] S. M. Langdon, K. Parmar, M. M. D. Wilde, M. Gravel, in *N-Heterocyclic Carbenes in Organocatalysis*, **2018**, pp. 37-57, DOI: 10.1002/9783527809042.ch2.
- [180] K. S. Smith, H. L. O. Huyck, G. S. Plumlee, M. J. Logsdon, L. F. Filipek, in *The Environmental Geochemistry of Mineral Deposits: Part A: Processes, Techniques, and Health Issues Part B: Case Studies and Research Topics, Vol. 6*, Society of Economic Geologists, **1997**, pp. 29-70, DOI: 10.5382/Rev.06.02.
- [181] A. Fürstner, *ACS Central Science* **2016**, *2*, 778-789, DOI: 10.1021/acscentsci.6b00272.
- [182] J. F. Berry, E. Bill, E. Bothe, S. D. George, B. Mienert, F. Neese, K. Wieghardt, *Science* **2006**, *312*, 1937-1941, DOI: 10.1126/science.1128506.
- [183] P. J. Chirik, *Angew. Chem. Int. Ed.* **2006**, *45*, 6956-6959, DOI: 10.1002/anie.200603056.
- [184] B. Plietker, A. Dieskau, *Eur. J. Org. Chem.* **2009**, *2009*, 775-787, DOI: 10.1002/ejoc.200800893.
- [185] K. S. Egorova, V. P. Ananikov, *Angew. Chem. Int. Ed.* **2016**, *55*, 12150-12162, DOI: 10.1002/anie.201603777.
- [186] European Medicines Agency, Guideline on the Specification Limits for Residues of Metal Catalysts or Metal Reagents, EMEA/CHMP/SWP/4446/2000, London, February 21, 2008.
- [187] K. Riener, S. Haslinger, A. Raba, M. P. Hogerl, M. Cokoja, W. A. Herrmann, F. E. Kühn, *Chem. Rev.* **2014**, *114*, 5215-5272, DOI: 10.1021/cr4006439.
- [188] S. Rana, J. P. Biswas, S. Paul, A. Paik, D. Maiti, *Chem. Soc. Rev.* **2021**, *50*, 243-472, DOI: 10.1039/D0CS00688B.
- [189] R. Shang, L. Ilies, E. Nakamura, *Chem. Rev.* **2017**, *117*, 9086-9139, DOI: 10.1021/acs.chemrev.6b00772.
- [190] K. Junge, K. Schröder, M. Beller, *Chem. Commun.* **2011**, *47*, 4849-4859, DOI: 10.1039/C0CC05733A.
- [191] Q. Liang, D. Song, *Chem. Soc. Rev.* **2020**, *49*, 1209-1232, DOI: 10.1039/C9CS00508K.
- [192] R. Pony Yu, D. Hesk, N. Rivera, I. Pelczer, P. J. Chirik, *Nature* **2016**, *529*, 195-199, DOI: 10.1038/nature16464.
- [193] K. Öfele, *Angew. Chem. Int. Ed. Engl.* **1969**, *8*, 916-917, DOI: 10.1002/anie.196908891.

- [194] U. Kernbach, M. Ramm, P. Luger, W. P. Fehlhammer, *Angew. Chem. Int. Ed. Engl.* **1996**, *35*, 310-312, DOI: 10.1002/anie.199603101.
- [195] I. Nieto, F. Cervantes-Lee, J. M. Smith, *Chem. Commun.* **2005**, 3811-3813, DOI: 10.1039/B505985B.
- [196] A. A. Danopoulos, N. Tsoureas, J. A. Wright, M. E. Light, *Organometallics* **2004**, *23*, 166-168, DOI: 10.1021/om0341911.
- [197] M. C. Jahnke, F. E. Hahn, *Coord. Chem. Rev.* **2015**, *293-294*, 95-115, DOI: 10.1016/j.ccr.2015.01.014.
- [198] V. Tegethoff, T. Lübbering, C. Schulte to Brinke, B. Schirmer, J. Neugebauer, F. E. Hahn, *Organometallics* **2021**, *40*, 606-617, DOI: 10.1021/acs.organomet.0c00812.
- [199] A. Flores-Figueroa, O. Kaufhold, K.-O. Feldmann, F. E. Hahn, *Dalton Trans.* **2009**, 9334-9342, DOI: 10.1039/B915033A.
- [200] V. Blase, A. Flores-Figueroa, C. Schulte to Brinke, F. E. Hahn, *Organometallics* **2014**, *33*, 4471-4478, DOI: 10.1021/om5006947.
- [201] K. Öfele, C. G. Kreiter, *Chem. Ber.* **1972**, *105*, 529-540, DOI: 10.1002/cber.19721050218.
- [202] B. Cetinkaya, P. Dixneuf, M. F. Lappert, *J. Chem. Soc., Chem. Commun.* **1973**, 206-206, DOI: 10.1039/C39730000206.
- [203] M. F. Lappert, P. L. Pye, *J. Chem. Soc., Dalton Trans.* **1977**, 2172-2180, DOI: 10.1039/DT9770002172.
- [204] M. H. Quick, R. J. Angelici, *J. Organomet. Chem.* **1978**, *160*, 231-239, DOI: 10.1016/S0022-328X(00)91216-6.
- [205] V. G. Albano, S. Bordoni, D. Braga, L. Busetto, A. Palazzi, V. Zanotti, *Angew. Chem. Int. Ed. Engl.* **1991**, *30*, 847-849, DOI: 10.1002/anie.199108471.
- [206] K. M. Blatchford, C. J. Mize, S. Roy, D. M. Jenkins, *Dalton Trans.* **2022**, *51*, 6153-6156, DOI: 10.1039/D2DT00772J.
- [207] Z. Lu, S. A. Cramer, D. M. Jenkins, *Chem. Sci.* **2012**, *3*, 3081-3087, DOI: 10.1039/C2SC20628E.
- [208] S. Meyer, C. M. Orben, S. Demeshko, S. Dechert, F. Meyer, *Organometallics* **2011**, *30*, 6692-6702, DOI: 10.1021/om200870w.
- [209] J. Hohenberger, K. Ray, K. Meyer, *Nat. Commun.* **2012**, *3*, 720, DOI: 10.1038/ncomms1718.
- [210] M. J. Ingleson, R. A. Layfield, *Chem. Commun.* **2012**, *48*, 3579-3589, DOI: 10.1039/C2CC18021A.
- [211] P. P. Chandrachud, D. M. Jenkins, *Tetrahedron Lett.* **2015**, *56*, 2369-2376, DOI: 10.1016/j.tetlet.2015.03.110.
- [212] A. Biffis, M. Baron, C. Tubaro, in *Adv. Organomet. Chem., Vol. 63* (Ed.: P. J. Pérez), Academic Press, **2015**, pp. 203-288, DOI: 10.1016/bs.adomc.2015.02.002.
- [213] V. Charra, P. de Frémont, P. Braunstein, *Coord. Chem. Rev.* **2017**, *341*, 53-176, DOI: 10.1016/j.ccr.2017.03.007.
- [214] J. W. Kück, R. M. Reich, F. E. Kühn, *Chem. Rec.* **2016**, *16*, 349-364, DOI: 10.1002/tcr.201500233.
- [215] A. C. Lindhorst, S. Haslinger, F. E. Kühn, *Chem. Commun.* **2015**, *51*, 17193-17212, DOI: 10.1039/C5CC07146A.
- [216] S. M. Hölzl, P. J. Altmann, J. W. Kück, F. E. Kühn, *Coord. Chem. Rev.* **2017**, *352*, 517-536, DOI: 10.1016/j.ccr.2017.09.015.
- [217] C. Johnson, M. Albrecht, *Coord. Chem. Rev.* **2017**, *352*, 1-14, DOI: 10.1016/j.ccr.2017.08.027.
- [218] J. Cheng, L. Wang, P. Wang, L. Deng, *Chem. Rev.* **2018**, *118*, 9930-9987, DOI: 10.1021/acs.chemrev.8b00096.
- [219] A. H. Mageed, *J. Organomet. Chem.* **2019**, *902*, 120965, DOI: 10.1016/j.jorganchem.2019.120965.
- [220] R. Kumar, B. Pandey, A. Sen, M. Ansari, S. Sharma, G. Rajaraman, *Coord. Chem. Rev.* **2020**, *419*, 213397, DOI: 10.1016/j.ccr.2020.213397.
- [221] L. Roy, *ChemPlusChem* **2019**, *84*, 893-906, DOI: 10.1002/cplu.201900178.

- [222] B. N. Jha, N. Singh, A. Raghuvanshi, in *Organic Synthesis-A Nascent Reelook*, IntechOpen, **2020**, DOI: 10.5772/intechopen.90640.
- [223] G. G. Zámbo, J. F. Schlagintweit, R. M. Reich, F. E. Kühn, *Catal. Sci. Technol.* **2022**, *12*, 4940-4961, DOI: 10.1039/D2CY00127F.
- [224] B. Zhang, F. E. Kühn, *Journal of Energy Chemistry* **2023**, *79*, 559-561, DOI: 10.1016/j.jechem.2023.01.019.
- [225] F. E. Kühn, *J. Organomet. Chem.* **2023**, *1000*, 122824, DOI: 10.1016/j.jorganchem.2023.122824.
- [226] T. Duchanois, T. Etienne, C. Cebrián, L. Liu, A. Monari, M. Beley, X. Assfeld, S. Haacke, P. C. Gros, *Eur. J. Inorg. Chem.* **2015**, *2015*, 2469-2477, DOI: 10.1002/ejic.201500142.
- [227] Y. Liu, T. Harlang, S. E. Canton, P. Chábera, K. Suárez-Alcántara, A. Fleckhaus, D. A. Vithanage, E. Göransson, A. Corani, R. Lomoth, V. Sundström, K. Wärnmark, *Chem. Commun.* **2013**, *49*, 6412-6414, DOI: 10.1039/C3CC43833C.
- [228] M. Huber-Gedert, M. Nowakowski, A. Kertmen, L. Burkhardt, N. Lindner, R. Schoch, R. Herbst-Irmer, A. Neuba, L. Schmitz, T.-K. Choi, J. Kubicki, W. Gawelda, M. Bauer, *Chem. Eur. J.* **2021**, *27*, 9905-9918, DOI: 10.1002/chem.202100766.
- [229] T. Duchanois, L. Liu, M. Pastore, A. Monari, C. Cebrián, Y. Trolez, M. Darari, K. Magra, A. Francés-Monerris, E. Domenichini, M. Beley, X. Assfeld, S. Haacke, P. C. Gros, *Inorganics* **2018**, *6*, 63, DOI: 10.3390/inorganics6020063.
- [230] C. Herrero, A. Quaranta, W. Leibl, A. W. Rutherford, A. Aukauloo, *Energy & Environmental Science* **2011**, *4*, 2353-2365, DOI: 10.1039/C0EE00645A.
- [231] S. Ardo, G. J. Meyer, *Chem. Soc. Rev.* **2009**, *38*, 115-164, DOI: 10.1039/B804321N.
- [232] M. Pastore, S. Caramori, P. C. Gros, *Acc. Chem. Res.* **2024**, *57*, 439-449, DOI: 10.1021/acs.accounts.3c00613.
- [233] J. J. Scepaniak, C. S. Vogel, M. M. Khusniyarov, F. W. Heinemann, K. Meyer, J. M. Smith, *Science* **2011**, *331*, 1049-1052, DOI: 10.1126/science.1198315.
- [234] P. Chábera, Y. Liu, O. Prakash, E. Thyraug, A. E. Nahhas, A. Honarfar, S. Essén, L. A. Fredin, T. C. B. Harlang, K. S. Kjær, K. Handrup, F. Ericson, H. Tatsuno, K. Morgan, J. Schnadt, L. Häggström, T. Ericsson, A. Sobkowiak, S. Lidin, P. Huang, S. Styring, J. Uhlig, J. Bendix, R. Lomoth, V. Sundström, P. Persson, K. Wärnmark, *Nature* **2017**, *543*, 695-699, DOI: 10.1038/nature21430.
- [235] J. England, C. R. Davies, M. Banaru, A. J. P. White, G. J. P. Britovsek, *Adv. Synth. Catal.* **2008**, *350*, 883-897, DOI: 10.1002/adsc.200700462.
- [236] M. S. Chen, M. C. White, *Science* **2007**, *318*, 783-787, DOI: 10.1126/science.1148597.
- [237] A. Company, L. Gómez, M. Costas, in *Iron-Containing Enzymes: Versatile Catalysts of Hydroxylation Reactions in Nature*, The Royal Society of Chemistry, **2011**, pp. 148-208, DOI: 10.1039/9781849732987-00148.
- [238] M. R. Anneser, G. R. Elpitiya, J. Townsend, E. J. Johnson, X. B. Powers, J. F. DeJesus, K. D. Vogiatzis, D. M. Jenkins, *Angew. Chem.-Int. Edit.* **2019**, *58*, 8115-8118, DOI: 10.1002/anie.201903132.
- [239] S. B. Isbill, P. P. Chandrachud, J. L. Kern, D. M. Jenkins, S. Roy, *ACS Catalysis* **2019**, *9*, 6223-6233, DOI: 10.1021/acscatal.9b01306.
- [240] A. Raba, M. Cokoja, S. Ewald, K. Riener, E. Herdtweck, A. Pöthig, W. A. Herrmann, F. E. Kühn, *Organometallics* **2012**, *31*, 2793-2800, DOI: 10.1021/om2010673.
- [241] D. T. Weiss, P. J. Altmann, S. Haslinger, C. Jandl, A. Pöthig, M. Cokoja, F. E. Kühn, *Dalton Trans.* **2015**, *44*, 18329-18339, DOI: 10.1039/C5DT02386F.
- [242] D. T. Weiss, M. R. Anneser, S. Haslinger, A. Pöthig, M. Cokoja, J.-M. Basset, F. E. Kühn, *Organometallics* **2015**, *34*, 5155-5166, DOI: 10.1021/acs.organomet.5b00732.
- [243] A. Flores-Figueroa, T. Pape, J. J. Weigand, F. E. Hahn, *Eur. J. Inorg. Chem.* **2010**, *2010*, 2907-2910, DOI: 10.1002/ejic.201000467.
- [244] J. Steube, A. Kruse, O. S. Bokareva, T. Reuter, S. Demeshko, R. Schoch, M. A. Argüello Cordero, A. Krishna, S. Hohloch, F. Meyer, K. Heinze, O. Kühn, S. Lochbrunner, M. Bauer, *Nat. Chem.* **2023**, *15*, 468-474, DOI: 10.1038/s41557-023-01137-w.

- [245] M. R. Gau, P. Kurta, T. M. Keller, J. J. Scepaniak, *Eur. J. Inorg. Chem.* **2023**, 26, e202300064, DOI: 10.1002/ejic.202300064.
- [246] A. A. Danopoulos, J. A. Wright, W. B. Motherwell, *Chem. Commun.* **2005**, 784-786, DOI: 10.1039/B415562A.
- [247] L. Deng, R. H. Holm, *J. Am. Chem. Soc.* **2008**, 130, 9878-9886, DOI: 10.1021/ja802111w.
- [248] M. Chakrabarti, L. Deng, R. H. Holm, E. Münck, E. L. Bominaar, *Inorg. Chem.* **2010**, 49, 1647-1650, DOI: 10.1021/ic902050k.
- [249] S. T. Oyama, in *Mechanisms in Homogeneous and Heterogeneous Epoxidation Catalysis* (Ed.: S. T. Oyama), Elsevier: Amsterdam, **2008**, pp. 3-99, DOI: 10.1016/B978-0-444-53188-9.00001-8.
- [250] S. A. Hauser, M. Cokoja, F. E. Kühn, *Catal. Sci. Technol.* **2013**, 3, 552-561, DOI: 10.1039/C2CY20595E.
- [251] W. E. Evans, P. I. Chipman, Patent US6717001B2, **2004**.
- [252] AgileIntel Research (ChemIntel360). (2023). Market volume of ethylene oxide worldwide from 2015 to 2022, with a forecast for 2023 to 2030 (in million metric tons). Statista. Statista Inc.. Accessed: 01.04.2024. <https://www.statista.com/statistics/1245260/ethylene-oxide-market-volume-worldwide/>.
- [253] T. A. Nijhuis, M. Makkee, J. A. Moulijn, B. M. Weckhuysen, *Ind. Eng. Chem. Res.* **2006**, 45, 3447-3459, DOI: 10.1021/ie0513090.
- [254] M. Pell, E. I. Korchak, Patent US3439001A, **1969**.
- [255] H.-U. Blaser, B. Pugin, F. Spindler, *J. Mol. Catal. A: Chem.* **2005**, 231, 1-20, DOI: 10.1016/j.molcata.2004.11.025.
- [256] S. Huber, M. Cokoja, F. E. Kühn, *J. Organomet. Chem.* **2014**, 751, 25-32, DOI: 10.1016/j.jorganchem.2013.07.016.
- [257] B. Cornils, W. A. Herrmann, *J. Catal.* **2003**, 216, 23-31, DOI: 10.1016/S0021-9517(02)00128-8.
- [258] C. J. Thibodeaux, W.-c. Chang, H.-w. Liu, *Chem. Rev.* **2012**, 112, 1681-1709, DOI: 10.1021/cr200073d.
- [259] S. Grüşchow, D. H. Sherman, in *Aziridines and Epoxides in Organic Synthesis*, **2006**, pp. 349-398, DOI: 10.1002/3527607862.ch10.
- [260] J. Li, H.-J. Liao, Y. Tang, J.-L. Huang, L. Cha, T.-S. Lin, J. L. Lee, I. V. Kurnikov, M. G. Kurnikova, W.-c. Chang, N.-L. Chan, Y. Guo, *J. Am. Chem. Soc.* **2020**, 142, 6268-6284, DOI: 10.1021/jacs.0c00484.
- [261] L. J. Rather, T. Weinert, U. Demmer, E. Bill, W. Ismail, G. Fuchs, U. Ermler, *J. Biol. Chem.* **2011**, 286, 29241-29248, DOI: 10.1074/jbc.M111.236893.
- [262] Y. Wu, C. E. Paul, F. Hollmann, *Green Carbon* **2023**, 1, 227-241, DOI: 10.1016/j.greenca.2023.10.004.
- [263] M. Costas, M. P. Mehn, M. P. Jensen, L. Que, *Chem. Rev.* **2004**, 104, 939-986, DOI: 10.1021/cr020628n.
- [264] T. Kubo, M. W. Peters, P. Meinhold, F. H. Arnold, *Chem. Eur. J.* **2006**, 12, 1216-1220, DOI: 10.1002/chem.200500584.
- [265] E. D. Babot, C. Aranda, J. Kiebist, K. Scheibner, R. Ullrich, M. Hofrichter, A. T. Martínez, A. Gutiérrez, *Antioxidants* **2022**, 11, 522, DOI: 10.3390/antiox11030522.
- [266] S. W. May, *Enzyme Microb. Technol.* **1979**, 1, 15-22, DOI: 10.1016/0141-0229(79)90005-X.
- [267] P. R. O. d. Montellano, *Cytochrome P-450 Structure, Mechanism and Biochemistry*, Springer New York, NY: New York, **2005**, DOI: 10.1007/b139087.
- [268] H. Yamazaki, *Fifty Years of Cytochrome P450 Research*, Springer Japan: **2014**, DOI: 10.1007/978-4-431-54992-5.
- [269] P. D. Oldenburg, R. Mas-Ballesté, L. Que, in *Mechanisms in Homogeneous and Heterogeneous Epoxidation Catalysis* (Ed.: S. T. Oyama), Elsevier: Amsterdam, **2008**, pp. 451-469, DOI: 10.1016/B978-0-444-53188-9.00018-3.
- [270] T. L. Poulos, *Chem. Rev.* **2014**, 114, 3919-3962, DOI: 10.1021/cr400415k.

- [271] D. Dolphin, T. G. Traylor, L. Y. Xie, *Acc. Chem. Res.* **1997**, *30*, 251-259, DOI: 10.1021/ar960126u.
- [272] M. Costas, K. Chen, L. Que, *Coord. Chem. Rev.* **2000**, *200-202*, 517-544, DOI: 10.1016/S0010-8545(00)00320-9.
- [273] K. A. Srinivas, A. Kumar, S. M. S. Chauhan, *Chem. Commun.* **2002**, 2456-2457, DOI: 10.1039/B207072N.
- [274] W. Nam, Y. O. Ryu, W. J. Song, *J. Biol. Inorg. Chem.* **2004**, *9*, 654-660, DOI: 10.1007/s00775-004-0577-5.
- [275] J. H. Dawson, *Science* **1988**, *240*, 433-439, DOI: 10.1126/science.3358128.
- [276] H. Fujii, *Coord. Chem. Rev.* **2002**, *226*, 51-60, DOI: 10.1016/S0010-8545(01)00441-6.
- [277] O. Shoji, Y. Watanabe, in *Fifty Years of Cytochrome P450 Research* (Ed.: H. Yamazaki), Springer Japan: Tokyo, **2014**, pp. 107-124, DOI: 10.1007/978-4-431-54992-5\_6.
- [278] N. A. Stephenson, A. T. Bell, *J. Mol. Catal. A: Chem.* **2007**, *272*, 108-117, DOI: 10.1016/j.molcata.2007.03.030.
- [279] I. D. Cunningham, T. N. Danks, J. N. Hay, I. Hamerton, S. Gunathilagan, C. Janczak, *J. Mol. Catal. A: Chem.* **2002**, *185*, 25-31, DOI: 10.1016/S1381-1169(02)00057-2.
- [280] D. Jeong, J. Selverstone Valentine, J. Cho, *Coord. Chem. Rev.* **2023**, *480*, 215021, DOI: 10.1016/j.ccr.2023.215021.
- [281] K. Chen, L. Que Jr, *Angew. Chem. Int. Ed.* **1999**, *38*, 2227-2229, DOI: 10.1002/(sici)1521-3773(19990802)38:15<2227::Aid-anie2227>3.0.Co;2-b.
- [282] R. Mas-Ballesté, M. Costas, T. van den Berg, L. Que Jr., *Chem. Eur. J.* **2006**, *12*, 7489-7500, DOI: 10.1002/chem.200600453.
- [283] E. P. Talsi, K. P. Bryliakov, *Coord. Chem. Rev.* **2012**, *256*, 1418-1434, DOI: 10.1016/j.ccr.2012.04.005.
- [284] R. Mas-Ballesté, L. Que, *J. Am. Chem. Soc.* **2007**, *129*, 15964-15972, DOI: 10.1021/ja075115i.
- [285] E. A. Mikhalyova, O. V. Makhlynets, T. D. Palluccio, A. S. Filatov, E. V. Rybak-Akimova, *Chem. Commun.* **2012**, *48*, 687-689, DOI: 10.1039/C1CC15935F.
- [286] A. Company, L. Gómez, X. Fontrodona, X. Ribas, M. Costas, *Chem. Eur. J.* **2008**, *14*, 5727-5731, DOI: 10.1002/chem.200800724.
- [287] W. Nam, R. Ho, J. S. Valentine, *J. Am. Chem. Soc.* **1991**, *113*, 7052-7054, DOI: 10.1021/ja00018a062.
- [288] D. Decembrino, D. Cannella, *Biotechnol. Adv.* **2024**, *72*, 108321, DOI: 10.1016/j.biotechadv.2024.108321.
- [289] P. Altmann, M. Cokoja, F. E. Kühn, *Eur. J. Inorg. Chem.* **2012**, *2012*, 3235-3239, DOI: 10.1002/ejic.201200120.
- [290] A. Schmidt, N. Grover, T. K. Zimmermann, L. Graser, M. Cokoja, A. Pöthig, F. E. Kühn, *J. Catal.* **2014**, *319*, 119-126, DOI: 10.1016/j.jcat.2014.08.013.
- [291] E. T. Farinas, M. Alcalde, F. Arnold, *Tetrahedron* **2004**, *60*, 525-528, DOI: 10.1016/j.tet.2003.10.099.
- [292] J. W. Kück, A. Raba, I. I. E. Markovits, M. Cokoja, F. E. Kühn, *ChemCatChem* **2014**, *6*, 1882-1886, DOI: 10.1002/cctc.201402063.
- [293] A. C. Lindhorst, J. Schütz, T. Netscher, W. Bonrath, F. E. Kühn, *Catal. Sci. Technol.* **2017**, *7*, 1902-1911, DOI: 10.1039/C7CY00557A.
- [294] S. Haslinger, A. Raba, M. Cokoja, A. Pöthig, F. E. Kühn, *J. Catal.* **2015**, *331*, 147-153, DOI: 10.1016/j.jcat.2015.08.026.
- [295] A. Raba, M. Cokoja, W. A. Herrmann, F. E. Kühn, *Chem. Commun.* **2014**, *50*, 11454-11457, DOI: 10.1039/C4CC02178A.
- [296] A. C. Lindhorst, M. Drees, W. Bonrath, J. Schütz, T. Netscher, F. E. Kühn, *J. Catal.* **2017**, *352*, 599-605, DOI: 10.1016/j.jcat.2017.06.018.
- [297] J. W. Kück, M. R. Anneser, B. Hofmann, A. Pöthig, M. Cokoja, F. E. Kühn, *ChemSusChem* **2015**, *8*, 4056-4063, DOI: 10.1002/cssc.201500930.
- [298] M. R. Anneser, S. Haslinger, A. Pöthig, M. Cokoja, J.-M. Basset, F. E. Kühn, *Inorg. Chem.* **2015**, *54*, 3797-3804, DOI: 10.1021/ic503043h.

- [299] M. A. Bernd, F. Dyckhoff, B. J. Hofmann, A. D. Böth, J. F. Schlagintweit, J. Oberkofler, R. M. Reich, F. E. Kühn, *J. Catal.* **2020**, *391*, 548-561, DOI: 10.1016/j.jcat.2020.08.037.
- [300] M. R. Anneser, S. Haslinger, A. Pöthig, M. Cokoja, V. D'Elia, M. P. Högerl, J.-M. Basset, F. E. Kühn, *Dalton Trans.* **2016**, *45*, 6449-6455, DOI: 10.1039/C6DT00538A.
- [301] F. Dyckhoff, J. F. Schlagintweit, R. M. Reich, F. E. Kühn, *Catal. Sci. Technol.* **2020**, *10*, 3532-3536, DOI: 10.1039/D0CY00631A.
- [302] M. R. Bukowski, P. Comba, A. Lienke, C. Limberg, C. Lopez de Laorden, R. Mas-Ballesté, M. Merz, L. Que Jr., *Angew. Chem. Int. Ed.* **2006**, *45*, 3446-3449, DOI: 10.1002/anie.200504357.
- [303] S. Kal, S. Xu, L. Que Jr., *Angew. Chem. Int. Ed.* **2020**, *59*, 7332-7349, DOI: 10.1002/anie.201906551.
- [304] S. Panke, M. Held, M. G. Wubbolts, B. Witholt, A. Schmid, *Biotechnol. Bioeng.* **2002**, *80*, 33-41, DOI: 10.1002/bit.10346.
- [305] E. Rose, Q.-Z. Ren, B. Andrioletti, *Chem. Eur. J.* **2004**, *10*, 224-230, DOI: 10.1002/chem.200305222.
- [306] N. Zwettler, J. A. Schachner, F. Belaj, N. C. Mösch-Zanetti, *Molecular Catalysis* **2017**, *443*, 209-219, DOI: 10.1016/j.mcat.2017.09.036.
- [307] S. Kal, A. Draksharapu, L. Que, Jr., *J. Am. Chem. Soc.* **2018**, *140*, 5798-5804, DOI: 10.1021/jacs.8b01435.
- [308] J. F. Schlagintweit, F. Dyckhoff, L. Nguyen, C. H. G. Jakob, R. M. Reich, F. E. Kühn, *J. Catal.* **2020**, *383*, 144-152, DOI: 10.1016/j.jcat.2020.01.011.
- [309] O. Cussó, X. Ribas, M. Costas, *Chem. Commun.* **2015**, *51*, 14285-14298, DOI: 10.1039/C5CC05576H.
- [310] M. Costas, J. Que, Lawrence, *Angew. Chem. Int. Ed.* **2002**, *41*, 2179-2181, DOI: 10.1002/1521-3773(20020617)41:12<2179::AID-ANIE2179>3.0.CO;2-F.
- [311] R. Mas-Ballesté, M. Costas, T. van den Berg, L. Que Jr., *Chem. Eur. J.* **2006**, *12*, 7489-7500, DOI: 10.1002/chem.200600453.
- [312] S. Kal, L. Que Jr., *Angew. Chem. Int. Ed.* **2019**, *58*, 8484-8488, DOI: 10.1002/anie.201903465.
- [313] E. N. Jacobsen, F. Kakiuchi, R. G. Konsler, J. F. Larrow, M. Tokunaga, *Tetrahedron Lett.* **1997**, *38*, 773-776, DOI: 10.1016/S0040-4039(96)02414-8.
- [314] M. Mitra, O. Cusso, S. S. Bhat, M. Sun, M. Cianfanelli, M. Costas, E. Nordlander, *Dalton Trans.* **2019**, *48*, 6123-6131, DOI: 10.1039/C8DT04449J.
- [315] H. Adolfsson, D. Balan, in *Aziridines and Epoxides in Organic Synthesis*, **2006**, pp. 185-228, DOI: 10.1002/3527607862.ch6.
- [316] Y. Zhu, Q. Wang, R. G. Cornwall, Y. Shi, *Chem. Rev.* **2014**, *114*, 8199-8256, DOI: 10.1021/cr500064w.
- [317] T. Katsuki, K. B. Sharpless, *J. Am. Chem. Soc.* **1980**, *102*, 5974-5976, DOI: 10.1021/ja00538a077.
- [318] R. Irie, K. Noda, Y. Ito, N. Matsumoto, T. Katsuki, *Tetrahedron Lett.* **1990**, *31*, 7345-7348, DOI: 10.1016/S0040-4039(00)88562-7.
- [319] R. Irie, K. Noda, Y. Ito, T. Katsuki, *Tetrahedron Lett.* **1991**, *32*, 1055-1058, DOI: 10.1016/S0040-4039(00)74486-8.
- [320] R. Irie, K. Noda, Y. Ito, N. Matsumoto, T. Katsuki, *Tetrahedron: Asymmetry* **1991**, *2*, 481-494, DOI: 10.1016/S0957-4166(00)86102-9.
- [321] W. Zhang, J. L. Loebach, S. R. Wilson, E. N. Jacobsen, *J. Am. Chem. Soc.* **1990**, *112*, 2801-2803, DOI: 10.1021/ja00163a052.
- [322] E. N. Jacobsen, W. Zhang, A. R. Muci, J. R. Ecker, L. Deng, *J. Am. Chem. Soc.* **1991**, *113*, 7063-7064, DOI: 10.1021/ja00018a068.
- [323] W. Zhang, E. N. Jacobsen, *J. Org. Chem.* **1991**, *56*, 2296-2298, DOI: 10.1021/jo00007a012.
- [324] K. B. Sharpless, *Angew. Chem. Int. Ed.* **2002**, *41*, 2024-2032, DOI: 10.1002/1521-3773(20020617)41:12<2024::AID-ANIE2024>3.0.CO;2-O.
- [325] M. Freindorf, E. Kraka, *Catalysts* **2022**, *12*, 789, DOI: 10.3390/catal12070789.
- [326] T. Katsuki, *Coord. Chem. Rev.* **1995**, *140*, 189-214, DOI: 10.1016/0010-8545(94)01124-T.

- [327] G. De Faveri, G. Ilyashenko, M. Watkinson, *Chem. Soc. Rev.* **2011**, *40*, 1722-1760, DOI: 10.1039/C0CS00077A.
- [328] M. Wu, C.-X. Miao, S. Wang, X. Hu, C. Xia, F. E. Kühn, W. Sun, *Adv. Synth. Catal.* **2011**, *353*, 3014-3022, DOI: 10.1002/adsc.201100267.
- [329] P. Fackler, S. M. Huber, T. Bach, *J. Am. Chem. Soc.* **2012**, *134*, 12869-12878, DOI: 10.1021/ja305890c.
- [330] Q. H. Xia, H. Q. Ge, C. P. Ye, Z. M. Liu, K. X. Su, *Chem. Rev.* **2005**, *105*, 1603-1662, DOI: 10.1021/cr0406458.
- [331] E. Rose, B. Andrioletti, S. Zrig, M. Quelquejeu-Ethève, *Chem. Soc. Rev.* **2005**, *34*, 573-583, DOI: 10.1039/B405679P.
- [332] T. Sawano, H. Yamamoto, *Eur. J. Org. Chem.* **2020**, *2020*, 2369-2378, DOI: 10.1002/ejoc.201901656.
- [333] "The Nobel Prize in Chemistry 2021", can be found under <https://www.nobelprize.org/prizes/chemistry/2021/popular-information/>, accessed: 10.04.2024.
- [334] O. Lifchits, M. Mahlau, C. M. Reisinger, A. Lee, C. Farès, I. Polyak, G. Gopakumar, W. Thiel, B. List, *J. Am. Chem. Soc.* **2013**, *135*, 6677-6693, DOI: 10.1021/ja402058v.
- [335] F. Dyckhoff, J. F. Schlagintweit, M. A. Bernd, C. H. G. Jakob, T. P. Schlachta, B. J. Hofmann, R. M. Reich, F. E. Kühn, *Catal. Sci. Technol.* **2021**, *11*, 795-799, DOI: 10.1039/D0CY02433C.
- [336] J. Chen, R. J. M. Klein Gebbink, *ACS Catalysis* **2019**, *9*, 3564-3575, DOI: 10.1021/acscatal.8b04463.
- [337] L. Gómez, I. Garcia-Bosch, A. Company, J. Benet-Buchholz, A. Polo, X. Sala, X. Ribas, M. Costas, *Angew. Chem. Int. Ed.* **2009**, *48*, 5720-5723, DOI: 10.1002/anie.200901865.
- [338] N. A. Vermeulen, M. S. Chen, M. Christina White, *Tetrahedron* **2009**, *65*, 3078-3084, DOI: 10.1016/j.tet.2008.11.082.
- [339] M. Costas, *Coord. Chem. Rev.* **2011**, *255*, 2912-2932, DOI: 10.1016/j.ccr.2011.06.026.
- [340] B. Meunier, *Chem. Rev.* **1992**, *92*, 1411-1456, DOI: 10.1021/cr00014a008.
- [341] M. R. Bukowski, S. Zhu, K. D. Koehntop, W. W. Brennessel, L. Que, *J. Biol. Inorg. Chem.* **2004**, *9*, 39-48, DOI: 10.1007/s00775-003-0494-z.
- [342] J. Y. Ryu, J. Kim, M. Costas, K. Chen, W. Nam, L. Que Jr, *Chem. Commun.* **2002**, 1288-1289, DOI: 10.1039/B203154J.
- [343] M. C. White, A. G. Doyle, E. N. Jacobsen, *J. Am. Chem. Soc.* **2001**, *123*, 7194-7195, DOI: 10.1021/ja015884g.
- [344] T. P. Schlachta, J. F. Schlagintweit, M. R. Anneser, E.-M. H. J. Esslinger, M. Muhr, S. Haslinger, F. E. Kühn, *Inorg. Chim. Acta* **2021**, *518*, 120228, DOI: 10.1016/j.ica.2020.120228.
- [345] Z. S. Ghavami, M. R. Anneser, F. Kaiser, P. J. Altmann, B. J. Hofmann, J. F. Schlagintweit, G. Grivani, F. E. Kühn, *Chem. Sci.* **2018**, *9*, 8307-8314, DOI: 10.1039/C8SC01834K.
- [346] T. P. Schlachta, M. R. Anneser, J. F. Schlagintweit, C. H. G. Jakob, C. Hintermeier, A. D. Böth, S. Haslinger, R. M. Reich, F. E. Kühn, *Chem. Commun.* **2021**, *57*, 6644-6647, DOI: 10.1039/D1CC02027G.
- [347] A. J. Jasniewski, L. Que, *Chem. Rev.* **2018**, *118*, 2554-2592, DOI: 10.1021/acs.chemrev.7b00457.
- [348] A. L. Feig, S. J. Lippard, *Chem. Rev.* **1994**, *94*, 759-805, DOI: 10.1021/cr00027a011.
- [349] T. C. Brunold, *Proc. Natl. Acad. Sci. U.S.A* **2007**, *104*, 20641, DOI: 10.1073/pnas.0710734105.
- [350] P. Nordlund, P. Reichard, *Annu. Rev. Biochem* **2006**, *75*, 681-706, DOI: 10.1146/annurev.biochem.75.103004.142443.
- [351] A. Draksharapu, S. Xu, L. Que Jr., *Angew. Chem. Int. Ed.* **2020**, *59*, 22484-22488, DOI: 10.1002/anie.202010027.
- [352] H.-F. Hsu, Y. Dong, L. Shu, V. G. Young, L. Que, *J. Am. Chem. Soc.* **1999**, *121*, 5230-5237, DOI: 10.1021/ja983666q.

- [353] A. Ghosh, F. Tiago de Oliveira, T. Yano, T. Nishioka, E. S. Beach, I. Kinoshita, E. Münck, A. D. Ryabov, C. P. Horwitz, T. J. Collins, *J. Am. Chem. Soc.* **2005**, *127*, 2505-2513, DOI: 10.1021/ja0460458.
- [354] G. G. Zábó, J. Mayr, M. J. Sauer, T. P. Schlachta, R. M. Reich, F. E. Kühn, *Dalton Trans.* **2022**, *51*, 13591-13595, DOI: 10.1039/D2DT02561B.
- [355] T. P. Schlachta, G. G. Zábó, M. J. Sauer, I. Rüter, C. A. Hoefler, S. Demeshko, F. Meyer, F. E. Kühn, *J. Catal.* **2023**, *426*, 234-246, DOI: 10.1016/j.jcat.2023.07.018.
- [356] T. P. Schlachta, L. F. Richter, F. E. Kühn, *Results in Chemistry* **2024**, *7*, 101421, DOI: 10.1016/j.rechem.2024.101421.
- [357] W. Stroek, M. Keilwerth, D. M. Pividori, K. Meyer, M. Albrecht, *J. Am. Chem. Soc.* **2021**, *143*, 20157-20165, DOI: 10.1021/jacs.1c07378.
- [358] W. R. E. Büchele, T. P. Schlachta, A. L. Gebendorfer, J. Pamperin, L. F. Richter, M. J. Sauer, A. Prokop, F. E. Kühn, *RSC Adv.* **2024**, *14*, 10244-10254, DOI: 10.1039/D4RA01195C.
- [359] S. Haslinger, A. C. Lindhorst, J. W. Kück, M. Cokoja, A. Pöthig, F. E. Kühn, *RSC Adv.* **2015**, *5*, 85486-85493, DOI: 10.1039/C5RA18270K.
- [360] S. Haslinger, J. W. Kück, E. M. Hahn, M. Cokoja, A. Pöthig, J.-M. Basset, F. E. Kühn, *Inorg. Chem.* **2014**, *53*, 11573-11583, DOI: 10.1021/ic501613a.
- [361] M. S. Ahmad, I. N. Pulidindi, C. Li, *New J. Chem.* **2020**, *44*, 17177-17197, DOI: 10.1039/D0NJ01996H.
- [362] T. Lu, X. Zhuang, Y. Li, S. Chen, *J. Am. Chem. Soc.* **2004**, *126*, 4760-4761, DOI: 10.1021/ja031874z.
- [363] A. Z. Spentzos, M. R. Gau, P. J. Carroll, N. C. Tomson, *Chem. Commun.* **2020**, *56*, 9675-9678, DOI: 10.1039/D0CC03521A.
- [364] A. Gurrane, E. Álvarez, J. Alberó, H. García, A. Corma, *Dalton Trans.* **2016**, *45*, 5444-5450, DOI: 10.1039/C6DT00370B.
- [365] S. M. M. Knapp, T. J. Sherbow, J. J. Juliette, D. R. Tyler, *Organometallics* **2012**, *31*, 2941-2944, DOI: 10.1021/om300047b.
- [366] R. J. Lewis, Sr., *Hazardous chemicals desk reference*, John Wiley & Sons: **2008**.
- [367] S. J. Blanksby, G. B. Ellison, *Acc. Chem. Res.* **2003**, *36*, 255-263, DOI: 10.1021/ar020230d.
- [368] D. J. Goebbert, L. Velarde, D. Khuseynov, A. Sanov, *J. Phys. Chem. Lett.* **2010**, *1*, 792-795, DOI: 10.1021/jz900379t.
- [369] G. P. Miscione, A. Bottoni, *Organometallics* **2014**, *33*, 4173-4182, DOI: 10.1021/om500094e.
- [370] J. L. Crossland, D. R. Tyler, *Coord. Chem. Rev.* **2010**, *254*, 1883-1894, DOI: 10.1016/j.ccr.2010.01.005.
- [371] Y. Sunada, T. Imaoka, H. Nagashima, *Organometallics* **2013**, *32*, 2112-2120, DOI: 10.1021/om3012322.
- [372] T. Takeshita, K. Sato, Y. Nakajima, *Dalton Trans.* **2018**, *47*, 17004-17010, DOI: 10.1039/C8DT04168G.
- [373] C. T. Saouma, C. E. Moore, A. L. Rheingold, J. C. Peters, *Inorg. Chem.* **2011**, *50*, 11285-11287, DOI: 10.1021/ic2016066.
- [374] N. I. Regenauer, H. Wadepohl, D.-A. Roşca, *Inorg. Chem.* **2022**, *61*, 7426-7435, DOI: 10.1021/acs.inorgchem.2c00459.
- [375] D. L. M. Suess, J. C. Peters, *J. Am. Chem. Soc.* **2013**, *135*, 4938-4941, DOI: 10.1021/ja400836u.
- [376] S. F. McWilliams, P. C. Bunting, V. Kathiresan, B. Q. Mercado, B. M. Hoffman, J. R. Long, P. L. Holland, *Chem. Commun.* **2018**, *54*, 13339-13342, DOI: 10.1039/C8CC07294A.
- [377] N. X. Gu, P. H. Oyala, J. C. Peters, *J. Am. Chem. Soc.* **2018**, *140*, 6374-6382, DOI: 10.1021/jacs.8b02603.
- [378] C. A. Hoefler, N. K. Dietl, G. G. Zábó, T. P. Schlachta, R. M. Reich, F. E. Kühn, *J. Organomet. Chem.* **2024**, *1006*, 123018, DOI: 10.1016/j.jorganchem.2024.123018.
- [379] A. Holas, C. Y. Koch, J. Leibold, A. Prendi, T. P. Schlachta, A. S. Schmid, L. Schmitt, *Environ. Res. Commun.* **2022**, *4*, 061002, DOI: 10.1088/2515-7620/ac77df.

- [380] W. L. Armarego, *Purification of laboratory chemicals*, Butterworth-Heinemann: **2017**, <https://www.sciencedirect.com/book/9780128054574/purification-of-laboratory-chemicals#book-description>.
- [381] G. R. Fulmer, A. J. M. Miller, N. H. Sherden, H. E. Gottlieb, A. Nudelman, B. M. Stoltz, J. E. Bercaw, K. I. Goldberg, *Organometallics* **2010**, *29*, 2176-2179, DOI: 10.1021/om100106e.
- [382] R. P. Sear, *CrystEngComm* **2014**, *16*, 6506-6522, DOI: 10.1039/C4CE00344F.
- [383] H. R. Pruppacher, J. D. Klett, *Microphysics of Clouds and Precipitation*, Springer Dordrecht: **1997**, DOI: 10.1007/978-0-306-48100-0.
- [384] D. Deng, M. Gopiraman, S. H. Kim, I.-M. Chung, I. S. Kim, *ACS Sustainable Chemistry & Engineering* **2016**, *4*, 5409-5414, DOI: 10.1021/acssuschemeng.6b01689.
- [385] X. Liu, W. Zhou, L. Yang, L. Li, Z. Zhang, Y. Ke, S. Chen, *Journal of Materials Chemistry A* **2015**, *3*, 8840-8846, DOI: 10.1039/C5TA01209K.
- [386] S. D. Haveli, P. Walter, G. Patriarche, J. Ayache, J. Castaing, E. Van Elslande, G. Tsoucaris, P.-A. Wang, H. B. Kagan, *Nano Lett.* **2012**, *12*, 6212-6217, DOI: 10.1021/nl303107w.
- [387] P. Walter, E. Welcomme, P. Hallégot, N. J. Zaluzec, C. Deeb, J. Castaing, P. Veyssière, R. Bréniaux, J.-L. Lévêque, G. Tsoucaris, *Nano Lett.* **2006**, *6*, 2215-2219, DOI: 10.1021/nl061493u.
- [388] B. Dereka, N. H. C. Lewis, J. H. Keim, S. A. Snyder, A. Tokmakoff, *J. Phys. Chem. B* **2022**, *126*, 278-291, DOI: 10.1021/acs.jpcc.1c09572.
- [389] S. Zhang, H. Jia, M. Song, H. Shen, L. Dongfei, L. Haibo, *Spectrochim. Acta A Mol. Biomol. Spectrosc.* **2021**, *246*, 119065, DOI: 10.1016/j.saa.2020.119065.

## List of Figures:

Figure 1. First NHC metal complexes reported by Wanzlick, Schönherr and Öfele, the first isolable carbene by Bertrand <i>et al.</i> and the first isolable NHC published by Arduengo <i>et al.</i> <sup>[5-8]</sup> .....	1
Figure 2. a) Schematic representation of singlet and triplet electronic ground state for carbenes (adapted from <sup>[10, 12]</sup> ). b) Schematic representation of the electronic stabilization of the singlet carbene by the adjacent nitrogen atoms (adapted from <sup>[1-2]</sup> ). .....	2
Figure 3. Structural features of NHCs and their effects displayed on the first stable, isolated NHC by Arduengo <i>et al.</i> <sup>[8]</sup> (adapted from <sup>[1, 10]</sup> ).....	3
Figure 4. Targeted design of NHC ligands illustrated using the example of ruthenium-catalyzed homogeneous olefin metathesis (adapted from <sup>[17]</sup> ). Mes = mesityl, PEG = polyethylene glycol, Me = methyl, Ph = phenyl, <sup>i</sup> Pr = isopropyl. ....	3
Figure 5. Selected most relevant groups of NHCs and exemplary resonance structures (adapted from <sup>[4, 28, 32-34]</sup> ). Heavier NHC homologues are shown for completeness.....	4
Figure 6. From left to right: Schematic representation of the planar nitrogen atoms in a calculated NHC (left) and pyramidalized phosphorus atoms in a calculated PHC (second from left, adapted from <sup>[42]</sup> ). Middle: first stable isolated PHC by Bertrand <i>et al.</i> <sup>[35]</sup> R = 2,4,6-tri- <i>tert</i> -butylphenyl. Second from right: first stable isolated NHSi by Denk <i>et al.</i> <sup>[48]</sup> Right: first stable isolated NHGe by Veith <i>et al.</i> <sup>[49]</sup> .....	5
Figure 7. Visualization of the $\sigma$ -donor and $\pi$ -accepting properties of the discussed classes of NHCs.....	7
Figure 8. $pK_a$ values of a few azolium salts, measured in DMSO if not stated else. <sup>[93-95, 97-100]</sup> .....	9
Figure 9. Nucleophilicity parameter $N$ and Lewis basicity (MCA) of several NHCs and reference examples. <sup>[86, 102-104]</sup> .....	9
Figure 10. Working principle of HEP (adapted from <sup>[11, 109]</sup> ). <sup>i</sup> Pr <sub>2</sub> -bimy = 1,3-diisopropylbenzimidazol-2-ylidene, L = ligand to be measured. ....	10
Figure 11. HEP values of some ligands. The $\sigma$ -donor strength increases to higher HEP values. <sup>[85, 88, 105, 108, 110-113]</sup> .....	11
Figure 12. Left: Resonance forms of carbene-phosphinidene adducts and selenoureas (adapted from <sup>[115]</sup> ). Right: <sup>31</sup> P and <sup>77</sup> Se chemical shift of some ligands. <sup>31</sup> P NMR measured in C <sub>6</sub> D <sub>6</sub> , <sup>77</sup> Se NMR measured in CDCl <sub>3</sub> , if not stated otherwise. <sup>[85, 88, 114-115, 118-120]</sup> Lewis structures of the NHCs only, without P-Ph/Se rest.....	12
Figure 13. Left: Selected azolium salts with their corresponding <sup>1</sup> J <sub>CH</sub> coupling constant. <sup>1</sup> H and <sup>13</sup> C NMR measured in DMSO- <i>d</i> <sub>6</sub> ( <sup>1</sup> J <sub>CH</sub> ). <sup>[122]</sup> Right: Selected NHCs and the <sup>1</sup> J <sub>CSe</sub> coupling constant of the corresponding selenoureas. <sup>13</sup> C NMR measured in CDCl <sub>3</sub> ( <sup>1</sup> J <sub>CSe</sub> ). <sup>[85, 118]</sup> .....	12

Figure 14. TEP values (calculated based on interconversion equations) of some NHCs. <sup>[85]</sup> 88, 102, 124-126] .....	13
Figure 15. Redox potentials for some NHC ligands. <sup>[88, 129-130]</sup> .....	14
Figure 16. Calculated energy of the HOMO, LUMO and singlet-triplet gap ( $E_S-E_T$ ) of selected calculated NHCs. <sup>[31]</sup> .....	15
Figure 17. Principle of percent buried volume ( $\% V_{bur}$ , adapted from <sup>[1]</sup> ). $\% V_{bur}$ of some NHCs. <sup>[139-140]</sup> .....	15
Figure 18. Selected iron NHC complexes with various characteristics (adapted from <sup>[192, 233- 234, 243-248]</sup> ). <i>p</i> -Tol = <i>para</i> -toluene. Formally Fe <sup>II</sup> atoms in <b>F</b> ( $[\text{Fe}_4\text{S}_4]^0 \triangleq 4\text{Fe}^{2+} + 4\text{S}^{2-}$ ). <sup>t</sup> Bu = <i>tert</i> -butyl. ....	20
Figure 19. Active species of cytochromes P450, Fe <sup>IV</sup> =O(por•), also called compound I (left). The porphyrin framework is marked blue. Selected examples of nonheme iron(II) complexes applied in epoxidation catalysis (right, adapted from <sup>[10, 237, 269-270, 277, 282, 286-288]</sup> ). Cys = cysteine, OTf = triflate anion. ....	23
Figure 20. Two most active Re and Mo complexes in epoxidation catalysis (adapted from <sup>[289-290]</sup> ). ....	23
Figure 21. Iron(II) and iron(III) NHC complexes employed in epoxidation catalysis (adapted from <sup>[11, 240, 297-300]</sup> ). ....	24
Figure 22. Iron(II) NHC complexes with <i>cis</i> labile coordination sites employed in epoxidation catalysis (adapted from <sup>[308]</sup> ). Dipp = 1,5-diisopropylphenyl. Bn = benzyl. ....	27
Figure 23. First chiral Mn(III) salen complexes developed by Jacobsen and Katsuki for the enantioselective epoxidation of general unfunctionalized alkenes (adapted from <sup>[318, 321-322]</sup> ). ..	28
Figure 24. Example for an organocatalyst developed by List <i>et al.</i> for the enantioselective epoxidation of $\alpha,\beta$ -disubstituted enals (adapted from <sup>[316, 334]</sup> ). ....	29
Figure 25. ORTEP-style representation of the cationic fragment of <b>14</b> . <sup>[346]</sup> Hydrogen atoms and PF <sub>6</sub> <sup>-</sup> anions are omitted for clarity and thermal ellipsoids are shown at a 50% probability level. Selected bond lengths (Å) and angles (°): Fe1–C1 1.929(2), Fe2–C17 1.931(3), Fe1–O1 1.7272(17), Fe2–O1 1.7298(17), Fe1–N17 1.984(2), Fe2–N18 1.987(2), Fe1–O1–Fe2 176.34(11), C1–Fe1–C5 89.43(10), C1–Fe1–O1 95.55(9), O1– Fe1–N17 178.09(8). Reproduced from Ref. <sup>[346]</sup> with permission from the Royal Society of Chemistry. ....	35
Figure 26. Modified iron NHC complexes employed in epoxidation catalysis (adapted from <sup>[355]</sup> ). ....	38
Figure 27. Synthesized chiral imidazolium and triazolium NHC ligand precursors (adapted from <sup>[356]</sup> ). ....	40
Figure 28. Synthesized transition metal complexes (Pd <sup>II</sup> , Pt <sup>II</sup> , Au <sup>III</sup> ) with an open-chain tetracarbene ligand with saturated backbone (imidazolin-2-ylidene units, <b>22</b> , <b>23</b> ), with a	

cyclic tetracarbene ligand with saturated backbone (imidazolin-2-ylidene units, <b>24</b> , <b>25</b> ) and a cyclic tetracarbene ligand with unsaturated backbone (imidazol-2-ylidene units, <b>26-29</b> ) (adapted from <sup>[358]</sup> ).....	42
Figure 29. ORTEP-style representation of the cationic fragment of <b>27</b> . Hydrogen atoms and PF <sub>6</sub> <sup>-</sup> anions are omitted for clarity and thermal ellipsoids are shown at a 50% probability level. Left: Top perspective, right: side perspective. Selected bond lengths (Å) and angles (°): C1–Pd 2.019(2), C1–Pd1–C1_b 172.03(12), C1–Pd1–C1_d–N2_d 53.62, C5–Pd1–C5_b 98.97°. Reproduced and modified from Ref. <sup>[358]</sup> with permission from the Royal Society of Chemistry.....	42
Figure 30. Modified iron NHC complex <b>30</b> containing benzimidazol-2-ylidene units applied in epoxidation catalysis.....	44
Figure 31. Left: Diiron end-on $\mu_2\text{-}\eta^1\text{:}\eta^1\text{-CN}$ bridged complex [(MeCN)(NHC)Fe] <sub>2</sub> ( $\mu_2\text{-}\eta^1\text{:}\eta^1\text{-CN}$ )(PF <sub>6</sub> ) <sub>3</sub> ( <b>31</b> ). Right: ORTEP-style representation of <b>31</b> . Hydrogen atoms and hexafluorophosphate anions are omitted for clarity. Thermal ellipsoids are shown at a 50% probability level. Notable are the strongly bent NHC ligands, in contrast to <b>30</b> , and their rotation towards each other of 160.7°.....	46
Figure 32. Crystallization setup of <b>31</b> .....	91
Figure 33. <sup>1</sup> H NMR spectrum of <b>30</b> in CD <sub>3</sub> CN before crystallization. Unreacted NHC ligand precursor is visible as impurity.....	91
Figure 34. ESI-MS spectrum of the batch of <b>30</b> before crystallization. Unreacted NHC ligand precursor is present as impurity. ....	92
Figure 35. FT-IR spectrum of MeCN. The values are in accordance to the literature. <sup>[388]</sup> .....	92
Figure 36. FT-IR spectrum of CD <sub>3</sub> CN. The values are in accordance to the literature. <sup>[388]</sup> ....	93
Figure 37. FT-IR spectrum of <b>30</b> . No CN band is visible. ....	93
Figure 38. FT-IR spectrum of crude material of the crystallization batch of <b>31</b> . No CN band is visible.....	94
Figure 39. Close up of the FT-IR spectrum of crude material of the crystallization batch of <b>31</b> . No CN band is visible. ....	94
Figure 40. Raman spectrum of <b>30</b> . The signals at 2291, 2327 and 2941 cm <sup>-1</sup> can be assigned to MeCN vibrations according to the literature. <sup>[389]</sup> .....	95
Figure 41. Raman spectrum of crystalline crude material of the crystallization batch of <b>31</b> . No NN band is visible. ....	95
Figure 42. Raman spectrum of crude material of the crystallization batch of <b>31</b> . No NN band is visible.....	96

## List of Schemes:

Scheme 1. Common routes to NHCs (adapted from <sup>[93]</sup> ). TMS = trimethylsilyl. ....	16
Scheme 2. Common pathways to Fe NHC complexes (adapted from <sup>[187, 208]</sup> ). $n = -2$ to $+6$ , $m = 3-5$ .....	19
Scheme 3. Catalytic epoxidation of olefins (left). Heterogeneous oxidation of ethylene to ethylene oxide (right, adapted from <sup>[249, 251]</sup> ). X = conversion, S = selectivity, TOF = turnover frequency. ....	21
Scheme 4. Chlorohydrin process (top) and Halcon process (bottom, adapted from <sup>[249, 253- 254]</sup> ). ....	21
Scheme 5. Proposed mechanism for the epoxidation of olefins by iron NHCs, based on the mechanistic studies of <i>N</i> -ligated iron complexes (adapted from <sup>[216, 223, 225]</sup> ). Compounds marked in red have been isolated.....	25
Scheme 6. Proposed mechanism for the epoxidation of olefins by nonheme iron complexes without <i>cis</i> -labile sites (adapted from <sup>[10, 216, 302]</sup> ). ....	26
Scheme 7. Sharpless-Katsuki asymmetric epoxidation of allyl alcohols, published in 1980 (adapted from <sup>[325]</sup> ). ....	28
Scheme 8. Excluded (path B and path C) and determined degradation pathways (path A and path D) for iron tetracarbene complexes <b>2/3</b> in epoxidation catalysis (adapted from <sup>[11, 335, 345]</sup> ). Nuc = generic nucleophile.....	33
Scheme 9. Reactivity of <b>8</b> (adapted from <sup>[346]</sup> ). Th = thianthrene, r.t. = room temperature. ....	35
Scheme 10. Simplified synthesis of <b>16</b> (adapted from <sup>[11, 354]</sup> ). TIPS = triisopropylsilyl.....	36

**List of Tables:**

Table 1. Selected catalytic performance of **2**, **3** and **8** in the epoxidation of *cis*-cyclooctene.<sup>[297, 301]</sup> .....25

Table 2. Contributions of T. P. Schlachta to the publications. # Equally contributing first authors (referring to publications [1], [3], [10]). \* Corresponding author (referring to publication [4]). § All authors contributed equally and are in alphabetical order (referring to publication [4]).....58

## 10. Appendix

### 10.1. Formation of a diiron-( $\mu_2$ - $\eta^1$ : $\eta^1$ -CN) complex from acetonitrile solution – supporting data

This section contains supporting experimental data regarding the diiron-( $\mu_2$ - $\eta^1$ : $\eta^1$ -CN) complex obtained from acetonitrile solution (see 4.2).

#### General procedures and analytical methods

Complex **30** was synthesized according to the literature (see 4.1). Solvents were purified, dried and degassed using standard methods<sup>[380]</sup> or received from a solvent purification system by M. Braun. All other chemicals were obtained from commercial suppliers and were used without further purification. NMR spectra were recorded on a Bruker Avance Ultrashield AV400 (<sup>1</sup>H NMR, 400.13 MHz; <sup>13</sup>C NMR, 100.53 MHz). The chemical shifts are given in  $\delta$  values in ppm (parts per million) relative to tetramethylsilane and are reported relative to the residual deuterated solvent signal.<sup>[381]</sup> Electrospray ionization mass spectrometry (ESI-MS) data were measured on a Thermo Fisher Ultimate 3000. FT-IR measurements were conducted on a *PerkinElmer* Frontier FT-IR spectrometer (ATR). The "inVia Reflex Raman System" comprises a research grade optical microscope (Leica DM2700M, Magnification 5x, 20x, 50x (in this case 50x was used)) coupled to a high performance Raman spectrometer (Renishaw). The 633nm wavelength laser was used: RL633, Class 3B, Company: Renishaw.

#### Crystallographic data of **31**

Single crystals suitable for X-ray diffraction were obtained by slow evaporation of a solution of **30** in CD<sub>3</sub>CN over 6 months at r.t. under ambient atmosphere near a window with sunlight (see Figure 32):

A solution of **30** (around 1-2 mg) in CD<sub>3</sub>CN (around 0.4 mL, dry and degassed) from an NMR tube (Figure 33, Figure 34) was placed in a 10 mL vial under ambient atmosphere. A human hair from the first author was fixed with adhesive tape to the inside of the vial, reaching into the solution. Heterogeneous nucleation occurs more frequently than homogeneous nucleation<sup>[382-383]</sup> and human hair has been used for growth of nanoparticles or as catalyst support material.<sup>[384-387]</sup> The vial was closed, and the cap was punctured with a cannula. The vial was left 6 months at r.t. under ambient conditions near a window with sunlight, allowing the solvent to slowly evaporate and orange crystals suitable for SC-XRD were obtained.



T: ITMS + c ESI Full ms [50.00-1000.00]

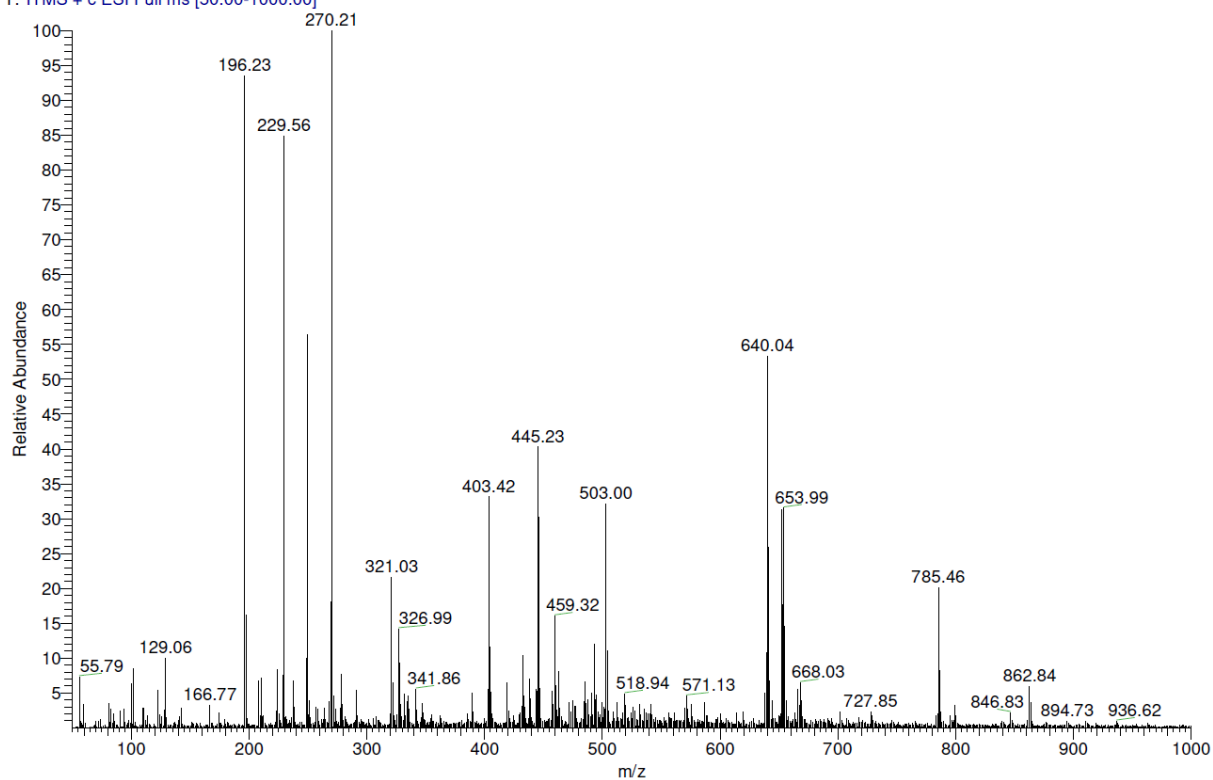


Figure 34. ESI-MS spectrum of the batch of **30** before crystallization. Unreacted NHC ligand precursor is present as impurity.

### FT-IR measurements

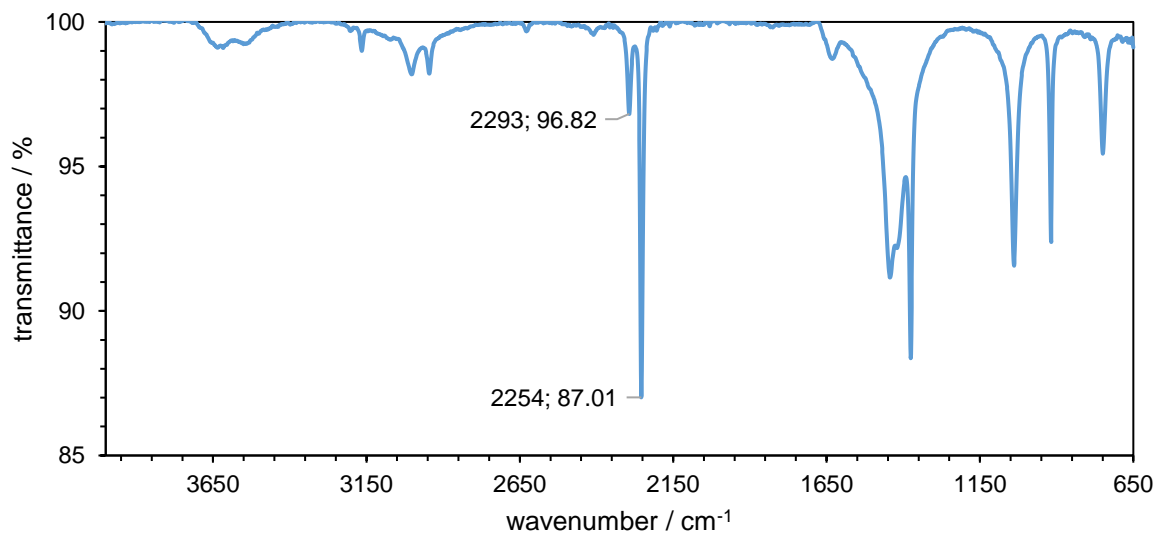


Figure 35. FT-IR spectrum of MeCN. The values are in accordance to the literature.<sup>[388]</sup>

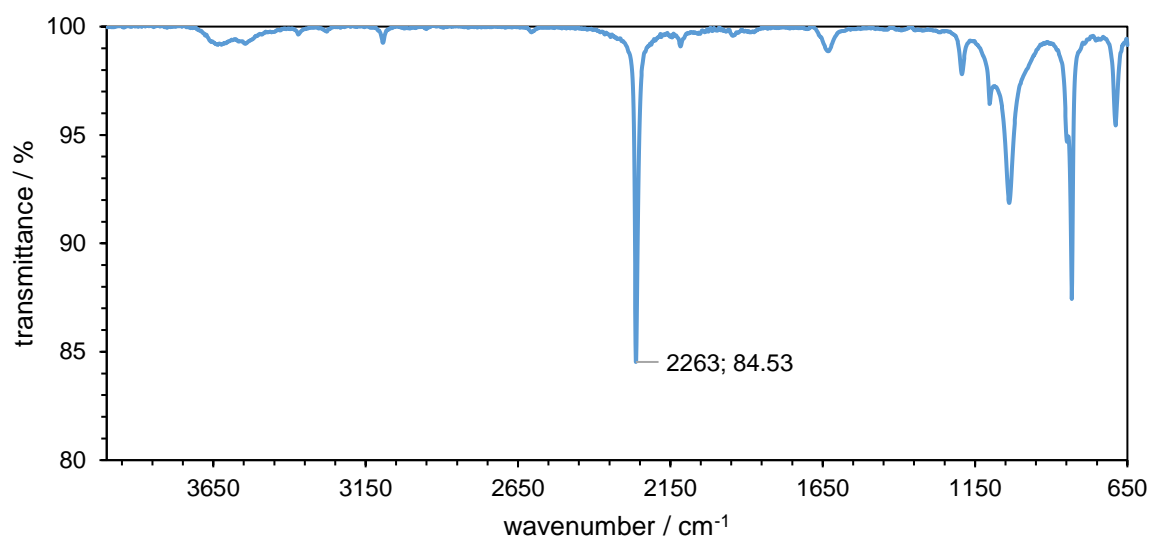


Figure 36. FT-IR spectrum of CD<sub>3</sub>CN. The values are in accordance to the literature.<sup>[388]</sup>

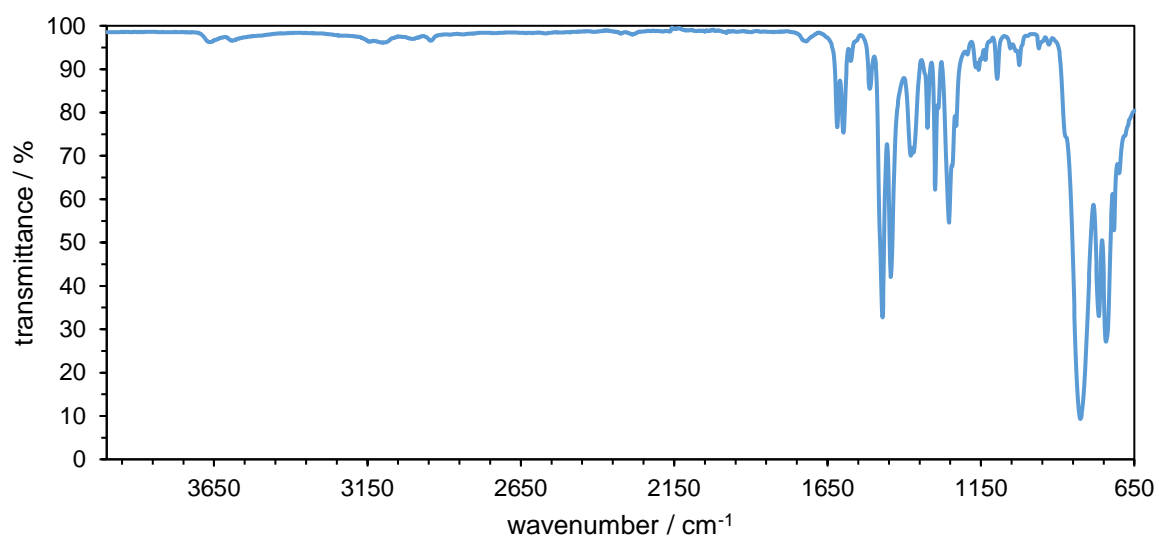


Figure 37. FT-IR spectrum of **30**. No CN band is visible.

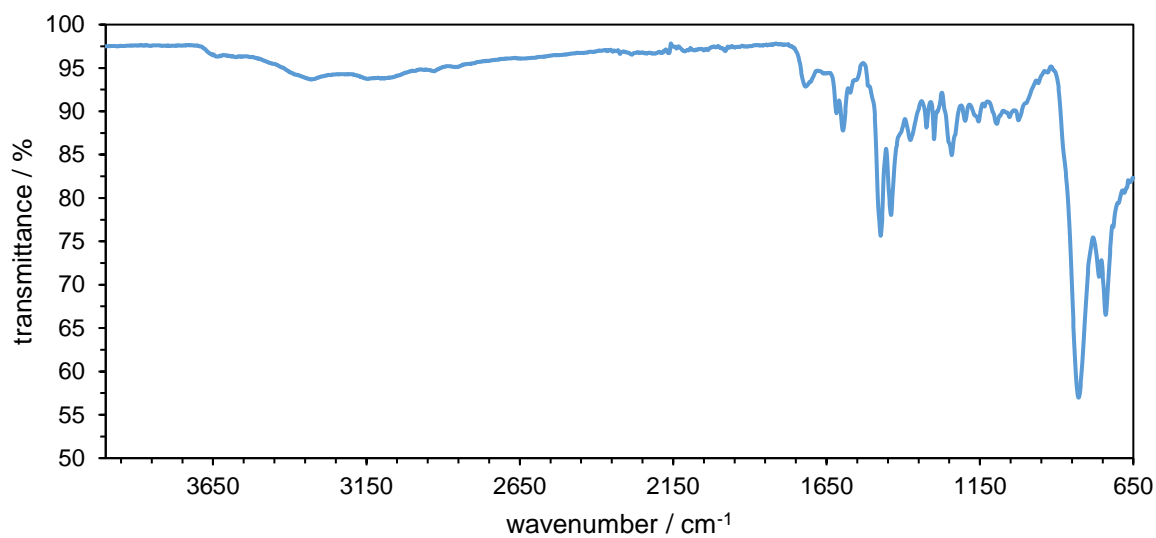


Figure 38. FT-IR spectrum of crude material of the crystallization batch of **31**. No CN band is visible.

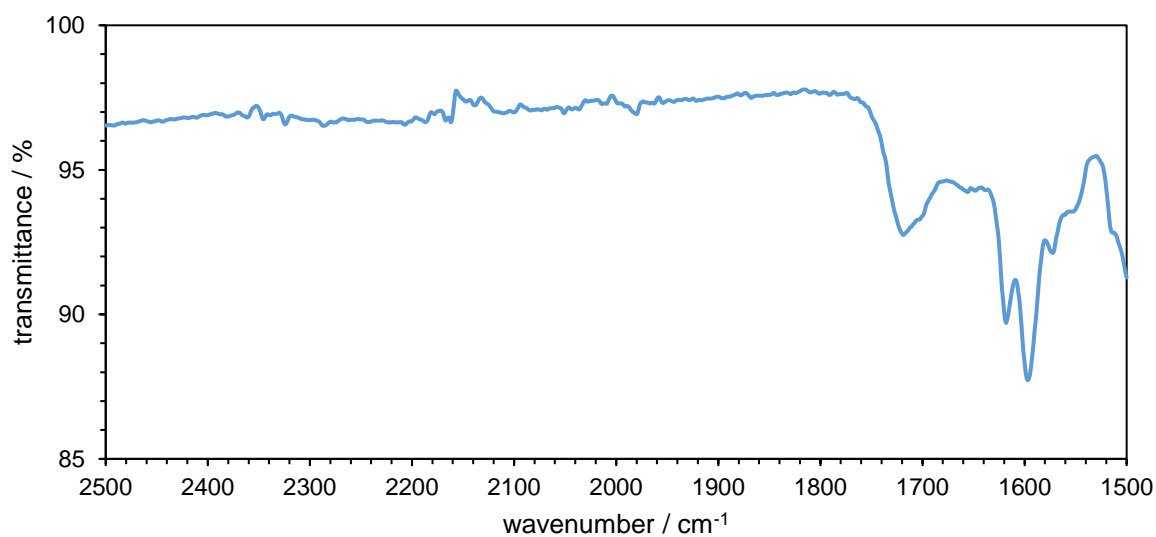


Figure 39. Close up of the FT-IR spectrum of crude material of the crystallization batch of **31**. No CN band is visible.

## Raman measurements

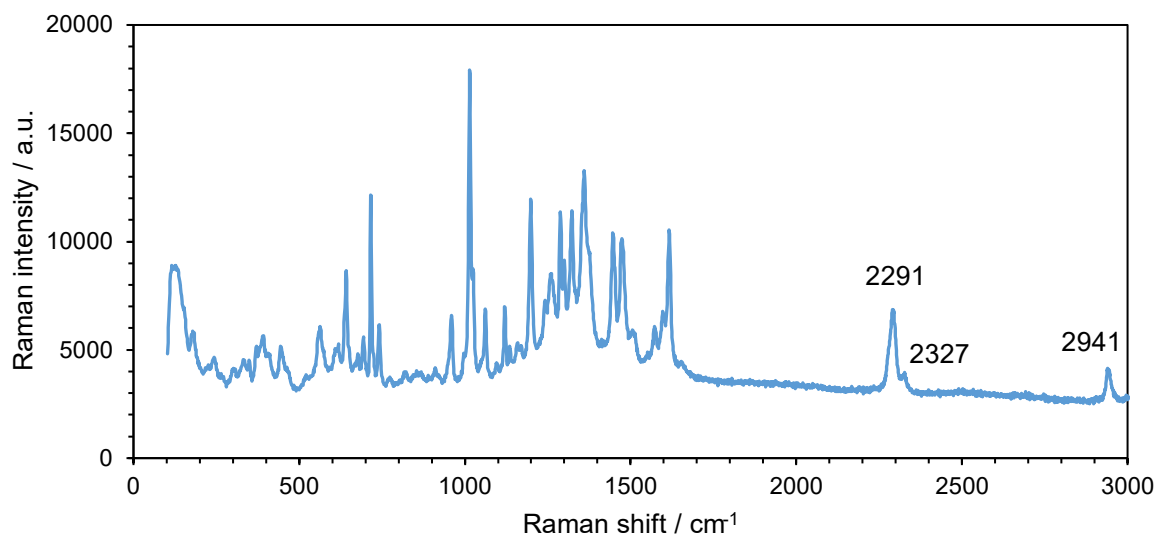


Figure 40. Raman spectrum of **30**. The signals at 2291, 2327 and 2941 cm<sup>-1</sup> can be assigned to MeCN vibrations according to the literature.<sup>[389]</sup>

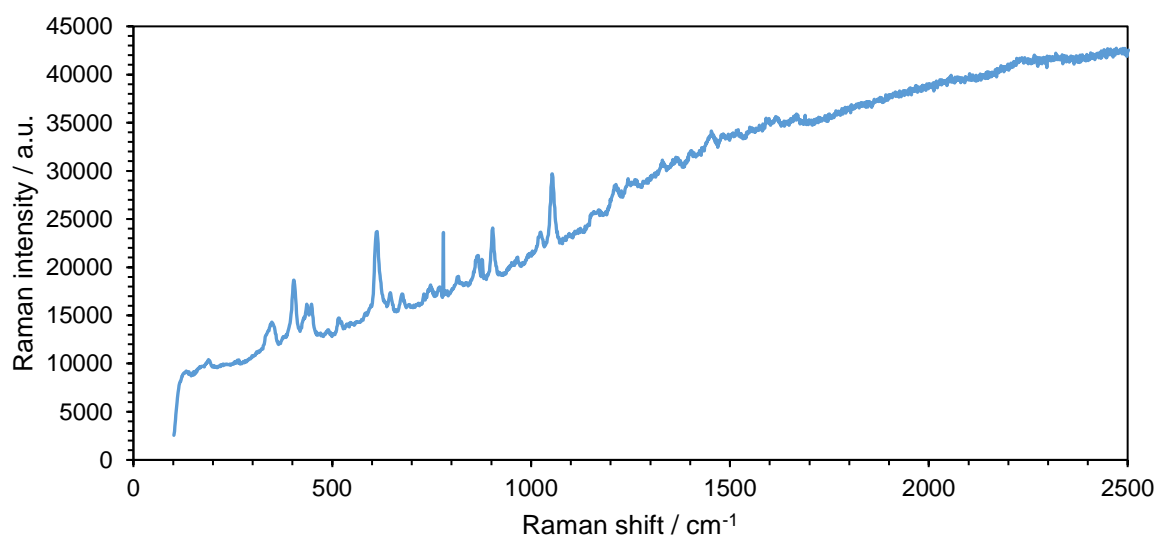


Figure 41. Raman spectrum of crystalline crude material of the crystallization batch of **31**. No NN band is visible.

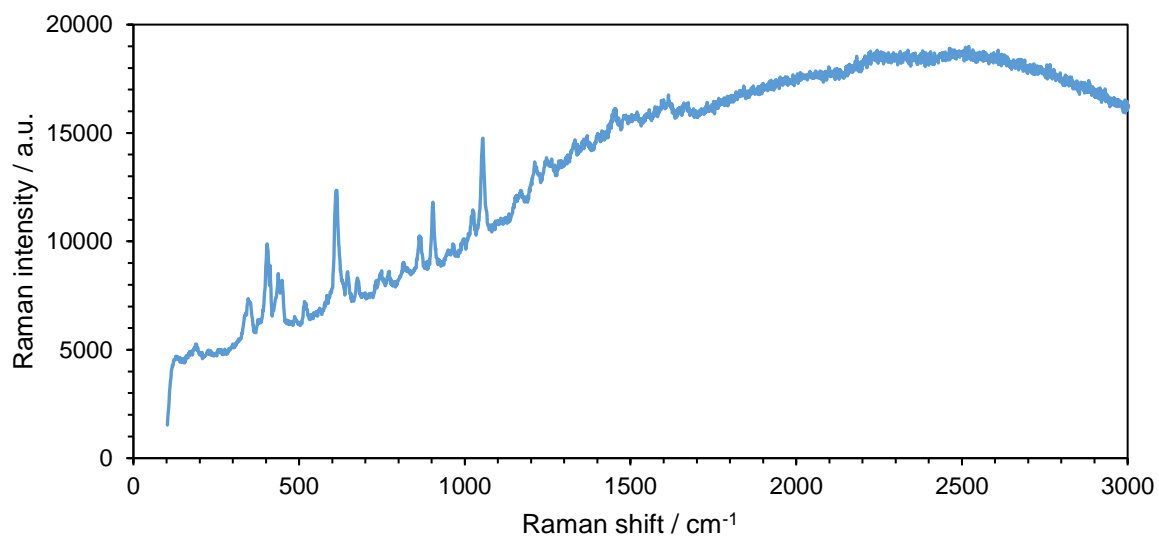


Figure 42. Raman spectrum of crude material of the crystallization batch of **31**. No NN band is visible.

Cite this: *Catal. Sci. Technol.*, 2021, 11, 795Received 22nd December 2020,  
Accepted 8th January 2021

DOI: 10.1039/d0cy02433c

rsc.li/catalysis

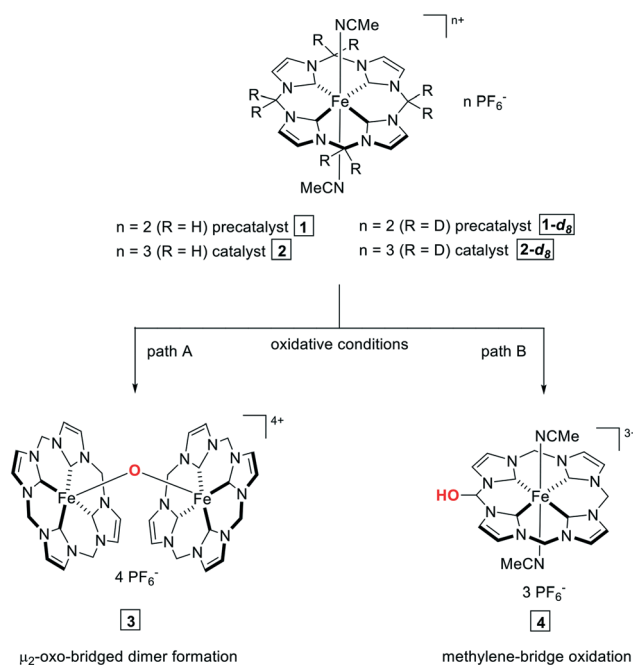
Pivotal degradation pathways of the most active non-heme iron epoxidation catalyst to date are investigated in detail. In-depth HR-ESI-MS and NMR spectroscopy decomposition studies and comparative catalytic experiments exclude the generally accepted literature paths of  $\mu_2$ -oxo bridged  $\text{Fe}^{\text{III}}\text{-O-Fe}^{\text{III}}$  dimer formation and methylene bridge oxidation. Instead, the Fe–NHC bond has been identified as the “weak spot”. It is shown that direct oxidation of one of the carbenes ( $\text{ImC=O}$ ) results in its de-coordination and induces protonation of the other NHC moieties, thus completely deactivating the catalyst. Evidence for protonation prior to carbene oxidation has not been found in this study.

Olefin epoxidation is of significant importance for the synthesis of both bulk and fine chemicals in industry.<sup>1</sup> So far, the most efficient organometallic epoxidation catalysts are based on molybdenum and rhenium.<sup>2–6</sup> However, their rather toxic and environmentally hazardous nature in combination with high cost directed research toward alternatives. Iron has attracted increasing attention over the past decade, as it is largely available and considered environmentally benign and “non-toxic”.<sup>7–11</sup> Inspired by metalloenzymes such as cytochrome P450 monooxygenase, iron is considered to be the ideal candidate for the development of sustainable oxidation catalysts.<sup>3,12–16</sup> Recent advances in terms of stability and activity of non-heme iron catalysts in the epoxidation of *cis*-cyclooctene with  $\text{H}_2\text{O}_2$  entailed the highest reported turnover frequencies (up to  $410\,000\ \text{h}^{-1}$ ) and turnover numbers (up to 1200) at  $20\ ^\circ\text{C}$  employing a macrocyclic tetradentate iron–NHC (N-heterocyclic carbene) complex as catalyst supported by strong Lewis acidic additives.<sup>17–19</sup>  $\text{Sc}^{3+}$  has been shown to promote the instantaneous one-electron

## Degradation pathways of a highly active iron(III) tetra-NHC epoxidation catalyst†‡

Florian Dyckhoff, Jonas F. Schlagintweit,<sup>id</sup> Marco A. Bernd,<sup>id</sup> Christian H. G. Jakob, Tim P. Schlachta,<sup>id</sup> Benjamin J. Hofmann,<sup>id</sup> Robert M. Reich<sup>id</sup> and Fritz E. Kühn<sup>id</sup>\*

oxidation of the  $\text{Fe}^{\text{II}}$  pre-catalyst (**1**) to the catalytically active  $\text{Fe}^{\text{III}}$  complex (**2**) upon addition of  $\text{H}_2\text{O}_2$ . Furthermore,  $\text{Sc}^{3+}$  enables the reactivation of a catalytically rather inactive  $\mu_2$ -oxodiiron(III)  $\text{Fe}^{\text{III}}\text{-O-Fe}^{\text{III}}$  dimer species (**3**) which is formed under oxidative conditions (Scheme 1, path A).<sup>17,20</sup> The beneficial influence of Lewis acids – so far known for an increased activity of non-heme iron catalysts – has therefore been expanded to the stability of such catalysts.<sup>7,21–26</sup> However, despite the unambiguous improvements with regard to stability and the progress in the understanding of the particular roles of Lewis acids such as  $\text{Sc}^{3+}$  in oxidation reactions with  $\text{H}_2\text{O}_2$  catalysed by iron (or manganese)



**Scheme 1** Literature derived degradation pathways of catalysts **1** and **2** under oxidative conditions. Path A:  $\mu_2$ -oxo-bridged  $\text{Fe}^{\text{III}}\text{-O-Fe}^{\text{III}}$  dimer (**3**) formation; path B: methylene bridge C–H oxidation (**4**). All methylene-bridge deuterated compounds are indicated with a  $-\text{d}_8$ .<sup>26</sup>

*Molecular Catalysis, Catalysis Research Center and Department of Chemistry, Technische Universität München, Lichtenbergstr. 4, 85748 Garching bei München, Germany. E-mail: fritz.kuehn@ch.tum.de*

† Electronic supplementary information (ESI) available: Catalytic procedures, synthetic procedures and analytical methods,  $^1\text{H-NMR}$  spectra of base reactions, UV/vis spectra, ESI-MS spectra and experimental procedure. See DOI: 10.1039/d0cy02433c

‡ All authors have given approval to the final version of the manuscript.

complexes, they still fall short with respect to real-life application due to rapid deactivation and degradation.<sup>23–25,27–38</sup> In literature,  $\mu_2$ -oxo bridged  $\text{Fe}^{\text{III}}\text{-O-Fe}^{\text{III}}$  dimer formation and C–H oxidation of the methylene bridges ultimately resulting in dissociation of the ligand are generally accepted as the most imminent decomposition pathways of non-heme iron oxidation catalysts, although varying in the particular impact throughout different ligand structures, as recently demonstrated by Chen and Klein Gebbink.<sup>27,39–46</sup> However, by far most studied iron catalysts bear tetradentate exclusively N-donating ligand motifs.<sup>10,47–51</sup> Accordingly, degradation of Fe–NHC catalysts may differ from decomposition of iron centres coordinated only by N-donors. Therefore, beside  $\text{Fe}^{\text{III}}\text{-O-Fe}^{\text{III}}$  dimer formation and methylene bridge oxidation, irreversible ligand protonation at the carbene C-donors with subsequent dissociation and/or oxidation of the ligand could play a pivotal role in the overall stability of Fe–NHCs in oxidation catalysis.<sup>52</sup>

To investigate the potential decomposition pathway of methylene-bridge oxidation (Scheme 1, path B) with respect to the non-heme iron epoxidation catalyst **2**, a methylene bridge deuterated analogue of catalyst **2** was synthesized (**2-d<sub>8</sub>**, see ESI† for synthetic details) and employed in comparative catalytic epoxidation experiments. Decomposition products formed during catalytic experiments were identified using detailed HR-ESI-MS and <sup>1</sup>H-NMR spectroscopic studies. As ligand C-protonation might play a sustentative role in the decomposition of the catalyst, several NMR, UV/vis and catalytic experiments were conducted to evaluate the effects of adding a soluble base (*i.e.*  $\text{NEt}_3$ , 1,8-bis(dimethylamino)naphthalene) to the epoxidation of *cis*-cyclooctene with  $\text{H}_2\text{O}_2$  catalysed by **2**, with the goal to intercept any protons forming during the reaction. The influence of the pH value of the reaction medium in non-heme iron catalysed oxidation with  $\text{H}_2\text{O}_2$  has already been reported by Banse and coworkers, however, only with respect to active species formation.<sup>53</sup> In order to investigate the kinetic isotope effect (KIE) the deuterated catalyst **2-d<sub>8</sub>** would display, if methylene bridge oxidation played a distinctive role in catalyst degradation, **2** and **2-d<sub>8</sub>** are employed as catalysts in comparative epoxidation reactions with  $\text{H}_2\text{O}_2$  as oxidant and *cis*-cyclooctene as a model substrate. Kinetic approaches (Fig. 1) at a reaction temperature of  $-10\text{ }^\circ\text{C}$  and 0.05 mol% catalyst concentration are conducted to facilitate the observance of potential differences in catalytic behaviour between **2** and **2-d<sub>8</sub>**. Neither the results of the kinetic experiments at  $-10\text{ }^\circ\text{C}$ , nor a TON comparison at  $20\text{ }^\circ\text{C}$  (table in Fig. 1) show a distinctive difference in stability or overall reaction progression. The determined TONs of **2** and **2-d<sub>8</sub>** in absence and presence of  $\text{Sc}(\text{OTf})_3$  at  $20\text{ }^\circ\text{C}$  coincide with the results reported previously for catalyst **2**.<sup>17</sup> Therefore, in addition to path A, which is easily suppressed by addition of Lewis acids,<sup>17</sup> path B (Scheme 1) can be excluded from being involved in the actual degradation mechanism of catalyst **2**. In consequence, other possible pathways such as ligand protonation (Scheme 2, path C) and/or oxidation (path D) of

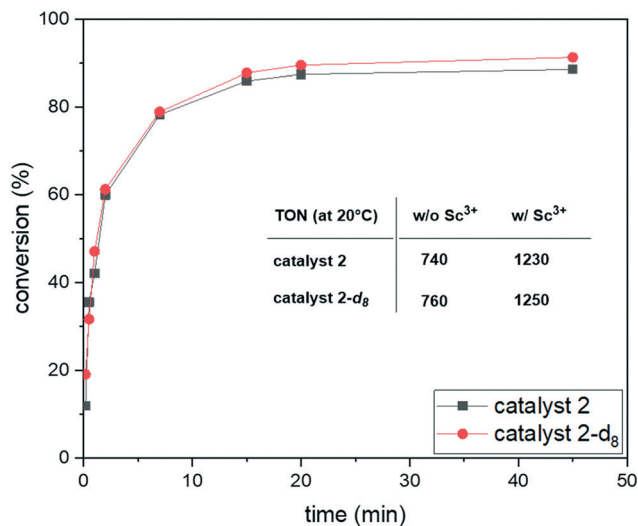
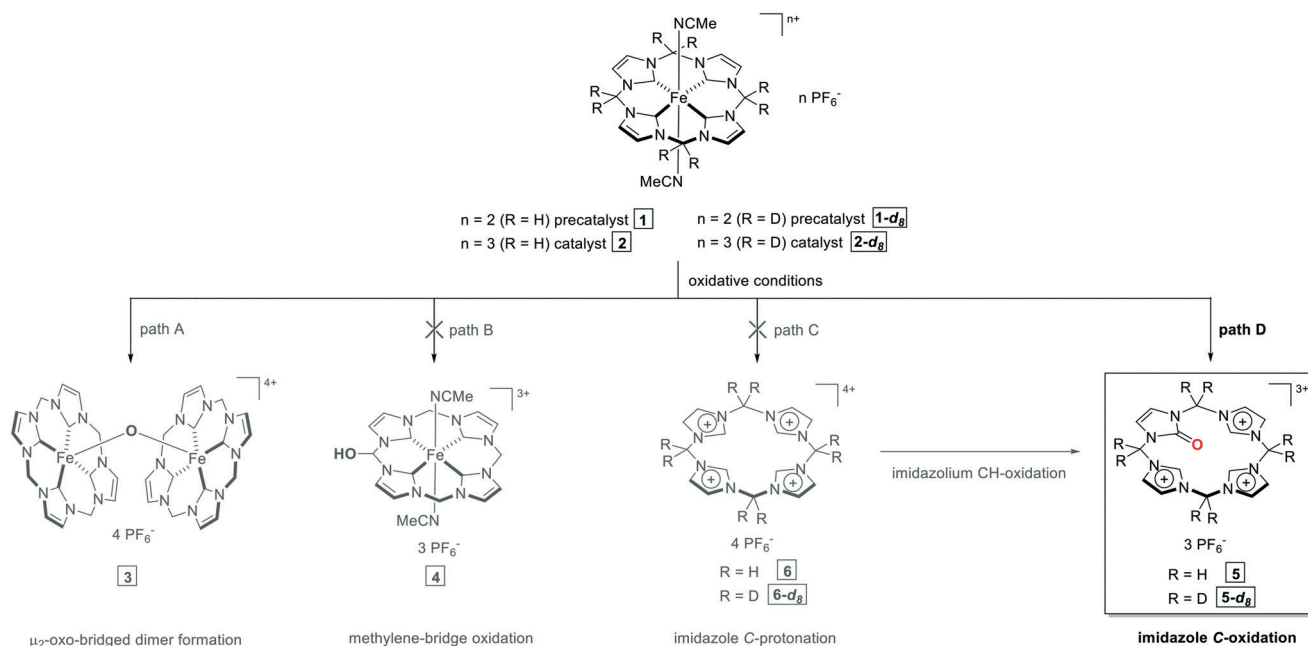


Fig. 1 Time-dependent conversions of catalysts (0.05 mol%) **2** and **2-d<sub>8</sub>** in the epoxidation of *cis*-cyclooctene with  $\text{H}_2\text{O}_2$  in MeCN at  $-10\text{ }^\circ\text{C}$ . Selectivity >99% in all reactions.

the carbene C-positions are investigated. <sup>1</sup>H-NMR spectroscopic studies reacting catalyst **2** with 10 eq.  $\text{H}_2\text{O}_2$  in  $\text{CD}_3\text{CN}$  reveal the formation of one dominant decomposition product (see ESI† Fig. S4, top). The signals conform to a mono-oxidised and three-fold protonated ligand species **5** (*cf.* Scheme 2) which has also reportedly been formed from the  $\text{Cu}^{\text{III}}$  analogue of **2** when treated with  $\text{AcOH}$ .<sup>54</sup> Interestingly, no traces of a compound with more than one oxidised carbene C-positions are observed. However, the question of whether this decomposition species is formed through direct carbene oxidation or imidazolium C–H oxidation with prior carbene protonation still remains.

If carbene protonation plays a decisive role in the oxidation of the ligand, an additive base could have a beneficial effect on the overall stability of catalyst **2**. Therefore, several catalytic experiments with a coordinating and non-coordinating base (*i.e.*  $\text{NEt}_3$ , 1,8-bis(dimethylamino)naphthalene (BDAN)) at a catalyst/base ratio of 1:10 in MeCN were conducted, in order to investigate their effects (*i.e.* intercepting any forming protons during the reaction) on the performance of catalyst **2**. However, all epoxidation attempts of *cis*-cyclooctene with  $\text{H}_2\text{O}_2$  catalysed by **2** result in an almost instantaneous colour change from purple (compound **2**) to pale yellow upon addition of the base and only negligible epoxide formation (see ESI† Table S1). <sup>1</sup>H-NMR spectroscopic studies adding  $\text{NEt}_3$  or BDAN to a solution of complex **2** in  $\text{CD}_3\text{CN}$  (1:1) using EtOAc as a standard, respectively, reveal an instantaneous reduction of the active  $\text{Fe}^{\text{III}}$  catalyst **2** to the  $\text{Fe}^{\text{II}}$  pre-catalyst **1** accompanied by formation of **3** under ambient conditions (see ESI† Fig. S2). This instantaneous reduction constitutes an exact opposite effect in comparison to the addition of Lewis acids (*e.g.*  $\text{Sc}(\text{OTf})_3$ ) to  $\text{Fe}^{\text{II}}$  complex **1**.<sup>17</sup> Using standard glovebox techniques, a considerably slower colour change (purple **2** → yellow **1**) is observed indicating that traces of water might be



**Scheme 2** Formation of mono-oxidised and three-fold protonated ligand **5** (path D) possibly via a four-fold protonated ligand species **6** in the degradation of catalysts **1** and **2** under oxidative conditions. Paths A–C – coloured in grey – were ultimately excluded via several experiments in the course of this work. All methylene-bridge deuterated compounds are indicated with a -**d<sub>8</sub>**.

oxidised forming hydroxyl radicals. Consequently, these radicals are able to oxidise acetonitrile, a solvent containing rather activated C–H bonds due to the neighbouring nitrile group. The oxidation of acetonitrile to glycolonitrile is verified by  $^1\text{H-NMR}$  spectroscopic measurements (solvent:  $\text{CD}_3\text{CN}$  with 5%  $\text{CH}_3\text{CN}$ ), as of the appearance of a distinctive formaldehyde signal, which is formed upon decay of glycolonitrile under basic conditions (see ESI† Fig. S3).<sup>55</sup> Several catalytic and UV/vis spectroscopic experiments were conducted applying derivatives of **2**, whereat both apical acetonitrile ligands are exchanged by *tert*-butylnitrile and benzonitrile, respectively.<sup>56</sup> Therein, no beneficial effects of varying the nitrile ligand in combination with applying an additive base were observed (see ESI† for a detailed discussion of the results).

Additional in-depth degradation studies of catalyst **2** via high resolution (HR) ESI-MS reveal the formation of one dominant decomposition product under oxidative conditions (*i.e.* 10 eq. of added  $\text{H}_2\text{O}_2$ ), coinciding with the results obtained via  $^1\text{H-NMR}$  (ESI† Fig. S4). The mono-oxidised and three-fold protonated compound **5** formed instantly upon addition of  $\text{H}_2\text{O}_2$  (see ESI† Fig. S32 and S33) render path D (*cf.* Scheme 2) highly likely as the crucial decomposition pathway. The fact that there is no protonated and unoxidised ligand **6** found via ESI-MS further supports a direct oxidation mechanism in the formation of compound **5** without prior protonation (path C) of the carbene C-atom to generate a C–H bond, otherwise a four-fold protonated ligand should be present among the decomposition species. The presence of a species comprising of an oxidised and deprotonated ligand still being coordinated to an  $\text{Fe}^{\text{III}}$  centre

confirms this assumption and a feasible structure of this intermediary species was calculated via DFT methods (see ESI† Fig. S33–S35 and S40). Furthermore, reacting complex **2** (1.0 eq.) with  $\text{H}_2\text{O}_2$  (10 eq.) in the presence of an excess of the bridge-deuterated ligand **6-d<sub>8</sub>** (5.0 eq.) did not result in any formation of an oxidised and deuterated species **5-d<sub>8</sub>** (see ESI† Fig. S38 and S39). Conclusively, oxidation of one of the ligand's carbene C-positions occurs prior to de-coordination and protonation of the remaining carbenes.

## Conclusions

In summary, different degradation pathways of catalyst **2** in the epoxidation of *cis*-cyclooctene with  $\text{H}_2\text{O}_2$  are investigated. Detailed HR-ESI-MS and  $^1\text{H-NMR}$  spectroscopy studies reveal direct oxidation of one carbene C-position with subsequent dissociation of the ligand from the Fe-centre to be the most imminent pathway of catalyst degradation. Methylene bridge oxidation was eliminated from being involved in catalyst decomposition via ESI-MS and comparative catalytic epoxidation experiments by synthesizing and employing a methylene bridge-deuterated analogue of **2** (*i.e.* **2-d<sub>8</sub>**). In these cases, no distinct differences in performance of **2** and **2-d<sub>8</sub>** were observed. Furthermore, excluding complete ligand protonation with and without subsequent oxidation at one of the generated imidazolium C–H positions was performed via ESI-MS and by adding a  $\text{H}^+$  intercepting base to a catalytic epoxidation reaction of **2**, resulting in no stability improvements of the catalyst. An intermediary degradation species, comprising of a mono-oxidised ligand still coordinating to an  $\text{Fe}^{\text{III}}$  centre, was found via HR-ESI-MS and

calculated by DFT methods, unequivocally confirming the oxidation of the ligand to occur prior to protonation and decoordination. Such a deactivation pathway has not been reported before for any other iron-based oxidation catalysts. The identified decomposition pathway is limited to N-heterocyclic carbene catalysts and so far only verified for 2. Further investigations on the exact mechanism of the oxygen transfer are currently ongoing in our laboratories.

## Conflicts of interest

There are no conflicts to declare.

## Notes and references

- F. Cavani and J. H. Teles, *ChemSusChem*, 2009, **2**(6), 508–534.
- S. A. Hauser, M. Cokoja and F. E. Kühn, *Catal. Sci. Technol.*, 2013, **3**(3), 552–561.
- J. W. Kück, R. M. Reich and F. E. Kühn, *Chem. Rec.*, 2016, **16**(1), 349–364.
- P. Altmann, M. Cokoja and F. E. Kühn, *Eur. J. Inorg. Chem.*, 2012, **2012**(19), 3235–3239.
- A. Schmidt, N. Grover, T. K. Zimmermann, L. Graser, M. Cokoja, A. Pöthig and F. E. Kühn, *J. Catal.*, 2014, **319**, 119–126.
- F. Dyckhoff, S. Li, R. M. Reich, B. J. Hofmann, E. Herdtweck and F. E. Kühn, *Dalton Trans.*, 2018, **47**(29), 9755–9764.
- S. M. Hölzl, P. J. Altmann, J. W. Kück and F. E. Kühn, *Coord. Chem. Rev.*, 2017, **352**, 517–536.
- F. Jia and Z. Li, *Org. Chem. Front.*, 2014, **1**(2), 194–214.
- A. C. Lindhorst, S. Haslinger and F. E. Kühn, *Chem. Commun.*, 2015, **51**(97), 17193–17212.
- L. Que Jr and W. B. Tolman, *Nature*, 2008, **455**, 333.
- R. Jennerjahn, R. Jackstell, I. Piras, R. Franke, H. Jiao, M. Bauer and M. Beller, *ChemSusChem*, 2012, **5**(4), 734–739.
- M. R. Anneser, G. R. Elpitiya, X. B. Powers and D. M. Jenkins, *Organometallics*, 2019, **38**(4), 981–987.
- I. Bauer and H.-J. Knölker, *Chem. Rev.*, 2015, **115**(9), 3170–3387.
- M. S. Chen and M. C. White, *Science*, 2010, **327**(5965), 566.
- S. Enthaler, K. Junge and M. Beller, *Angew. Chem., Int. Ed.*, 2008, **47**(18), 3317–3321.
- Q. Liang and D. Song, *Chem. Soc. Rev.*, 2020, **49**(4), 1209–1232.
- F. Dyckhoff, J. F. Schlagintweit, R. M. Reich and F. E. Kühn, *Catal. Sci. Technol.*, 2020, **10**(11), 3532–3536.
- J. W. Kück, M. R. Anneser, B. Hofmann, A. Pöthig, M. Cokoja and F. E. Kühn, *ChemSusChem*, 2015, **8**(23), 4056–4063.
- M. A. Bernd, F. Dyckhoff, B. J. Hofmann, A. D. Böth, J. F. Schlagintweit, J. Oberkofler, R. M. Reich and F. E. Kühn, *J. Catal.*, 2020, **391**, 548–561.
- M. R. Anneser, S. Haslinger, A. Pöthig, M. Cokoja, V. D'Elia, M. P. Högerl, J.-M. Basset and F. E. Kühn, *Dalton Trans.*, 2016, **45**(15), 6449–6455.
- K. Chen and L. Que, *J. Am. Chem. Soc.*, 2001, **123**(26), 6327–6337.
- A. Company, L. Gómez, X. Fontrodona, X. Ribas and M. Costas, *Chem. – Eur. J.*, 2008, **14**(19), 5727–5731.
- S. Kal, A. Draksharapu and L. Que, *J. Am. Chem. Soc.*, 2018, **140**(17), 5798–5804.
- R. Mas-Ballesté and L. Que, *J. Am. Chem. Soc.*, 2007, **129**(51), 15964–15972.
- S. Kal, S. Xu and L. Que Jr, *Angew. Chem., Int. Ed.*, 2020, **59**(19), 7332–7349.
- J. F. Schlagintweit, F. Dyckhoff, L. Nguyen, C. H. G. Jakob, R. M. Reich and F. E. Kühn, *J. Catal.*, 2020, **383**, 144–152.
- J. Chen and R. J. M. Klein Gebbink, *ACS Catal.*, 2019, **9**(4), 3564–3575.
- S. Fukuzumi, Y. Morimoto, H. Kotani, P. Naumov, Y.-M. Lee and W. Nam, *Nat. Chem.*, 2010, **2**(9), 756–759.
- S. Kal and L. Que Jr, *Angew. Chem., Int. Ed.*, 2019, **58**(25), 8484–8488.
- Z. Lv, C. Choe, Y. Wu, H. Wang, Z. Chen, G. Li and G. Yin, *Mol. Catal.*, 2018, **448**, 46–52.
- J. D. Steen, S. Stepanovic, M. Parvizian, J. W. de Boer, R. Hage, J. Chen, M. Swart, M. Gruden and W. R. Browne, *Inorg. Chem.*, 2019, **58**(21), 14924–14930.
- M. Swart, *Chem. Commun.*, 2013, **49**(59), 6650–6652.
- J. Zhang, W.-J. Wei, X. Lu, H. Yang, Z. Chen, R.-Z. Liao and G. Yin, *Inorg. Chem.*, 2017, **56**(24), 15138–15149.
- S. Banerjee, A. Draksharapu, P. M. Crossland, R. Fan, Y. Guo, M. Swart and L. Que, *J. Am. Chem. Soc.*, 2020, **142**(9), 4285–4297.
- S. Xu, A. Draksharapu, W. Rasheed and L. Que, *J. Am. Chem. Soc.*, 2019, **141**(40), 16093–16107.
- Y.-H. Lin, Y. Kutin, M. van Gastel, E. Bill, A. Schnegg, S. Ye and W.-Z. Lee, *J. Am. Chem. Soc.*, 2020, **142**(23), 10255–10260.
- A. H. Mageed, *J. Organomet. Chem.*, 2019, **902**, 120965.
- Q. Zhao, G. Meng, S. P. Nolan and M. Szostak, *Chem. Rev.*, 2020, **120**(4), 1981–2048.
- C. Cordes, M. Morganti, I. Klawitter, C. Schremmer, S. Dechert and F. Meyer, *Angew. Chem., Int. Ed.*, 2019, **58**(32), 10855–10858.
- L. Gómez, I. Garcia-Bosch, A. Company, J. Benet-Buchholz, A. Polo, X. Sala, X. Ribas and M. Costas, *Angew. Chem., Int. Ed.*, 2009, **48**(31), 5720–5723.
- N. A. Vermeulen, M. S. Chen and M. C. White, *Tetrahedron*, 2009, **65**(16), 3078–3084.
- M. Costas, *Coord. Chem. Rev.*, 2011, **255**(23), 2912–2932.
- B. Meunier, *Chem. Rev.*, 1992, **92**(6), 1411–1456.
- M. R. Bukowski, S. Zhu, K. D. Koehn-top, W. W. Brennessel and L. Que, *J. Biol. Inorg. Chem.*, 2004, **9**(1), 39–48.
- J. Y. Ryu, J. Kim, M. Costas, K. Chen, W. Nam and L. Que Jr, *Chem. Commun.*, 2002(12), 1288–1289.
- M. C. White, A. G. Doyle and E. N. Jacobsen, *J. Am. Chem. Soc.*, 2001, **123**(29), 7194–7195.
- A. Company, L. Gómez, M. Güell, X. Ribas, J. M. Luis, L. Que and M. Costas, *J. Am. Chem. Soc.*, 2007, **129**(51), 15766–15767.
- J. T. Groves, T. E. Nemo and R. S. Myers, *J. Am. Chem. Soc.*, 1979, **101**(4), 1032–1033.
- R. A. Leising, R. E. Norman and L. Que, *Inorg. Chem.*, 1990, **29**(14), 2553–2555.

- 50 W. Nam, *Acc. Chem. Res.*, 2007, **40**(7), 522–531.
- 51 W. Nam, R. Ho and J. S. Valentine, *J. Am. Chem. Soc.*, 1991, **113**(18), 7052–7054.
- 52 Y. Zhang, B. Liu, H. Wu and W. Chen, *Chin. Sci. Bull.*, 2012, **57**(19), 2368–2376.
- 53 A. Bohn, C. Chinaux-Chaix, K. Cheaib, R. Guillot, C. Herrero, K. Sénéchal-David, J.-N. Rebilly and F. Banse, *Dalton Trans.*, 2019, **48**(45), 17045–17051.
- 54 Z. S. Ghavami, M. R. Anneser, F. Kaiser, P. J. Altmann, B. J. Hofmann, J. F. Schlagintweit, G. Grivani and F. E. Kühn, *Chem. Sci.*, 2018, **9**(43), 8307–8314.
- 55 R. J. Lewis, *Hazardous Chemicals Desk Reference*, John Wiley & Sons, 6th edn, 2008.
- 56 T. P. Schlachta, J. F. Schlagintweit, M. R. Anneser, E.-M. H. J. Esslinger, M. Muhr, S. Haslinger and F. E. Kühn, *Inorg. Chim. Acta*, 2020, 120228, in press.


 Cite this: *Chem. Commun.*, 2021, 57, 6644

 Received 16th April 2021,  
 Accepted 7th June 2021

DOI: 10.1039/d1cc02027g

rsc.li/chemcomm

# Mimicking reactive high-valent diiron- $\mu_2$ -oxo intermediates of nonheme enzymes by an iron tetracarbene complex†

 Tim P. Schlachta,<sup>‡</sup> Markus R. Anneser,<sup>‡</sup> Jonas F. Schlagintweit,<sup>‡</sup> Christian H. G. Jakob, Carolin Hintermeier, Alexander D. Böth,<sup>‡</sup> Stefan Haslinger, Robert M. Reich and Fritz E. Kühn<sup>‡</sup> \*

**The first diiron(III,IV)- $\mu_2$ -oxo tetracarbene complex is isolated and characterized by SC-XRD, UV/Vis, EPR, Evans' NMR and elemental analysis. CV indicates the presence of a transient high-valent diiron(IV)- $\mu_2$ -oxo species. Its formation and decay is investigated via UV/Vis kinetics and NMR.**

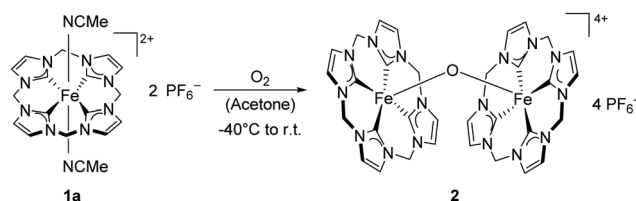
Nonheme diiron metalloenzymes are a subclass of enzymes that activate dioxygen to catalyze a broad variety of reactions, such as the desaturation of fatty acids, the hydroxylation of aromatic hydrocarbons or the six-electron oxidation of aminoarenes to nitroarenes in the biosynthesis of antibiotics.<sup>1</sup> Their reaction mechanism involves the formation of highly reactive intermediates, including diiron(II,III)-superoxo, diiron(III)-peroxo, diiron(III,IV)- $\mu_2$ -oxo or diiron(IV)- $\mu_2$ -oxo species. These species are responsible for the respective substrate oxidation.<sup>1</sup> One of the most prominent representatives containing a diiron active site is soluble methane monooxygenase (sMMO), catalyzing the challenging C–H oxidation of inert methane to methanol under mild conditions using dioxygen.<sup>2</sup> Its reaction mechanism involves the cleavage of the O–O bond of a diiron(III)-peroxo species, forming intermediate Q, a diiron(IV)- $\mu_2$ -oxo species, which is even more reactive and facilitates the hydroxylation of the strong C–H bond in methane.<sup>1,3</sup> An example for a high-valent<sup>4</sup> diiron(III,IV)- $\mu_2$ -oxo intermediate can be found in ribonucleotide reductases. This intermediate generates tyrosyl radicals that are catalytically essential to convert ribonucleotides to deoxyribonucleotides.<sup>5</sup>

The nature of these enzymes has attracted many researchers to develop model systems to study the reaction mechanisms and mimic their catalytic reactivity.<sup>6–9</sup> However, artificial models for high-valent diiron intermediates, such as intermediate Q, remain

scarce, as they are highly reactive and thus difficult to isolate and study.<sup>1,6</sup> The vast majority of these biomimetic complexes contains *N*-donor ligands.<sup>1</sup> So far, only one diiron(III,IV)- $\mu_2$ -oxo<sup>10</sup> and one diiron(IV)- $\mu_2$ -oxo complex<sup>11</sup> could be isolated and structurally characterized.

In 2015, a bio-inspired non-heme iron *N*-heterocyclic tetracarbene (cCCCC) complex (**1a**, Scheme 1) was reported exhibiting close structural and electronic properties to heme systems.<sup>12,13</sup> Indeed, similar to cytochrome P450, complex **1a**, and especially its oxidized iron(III) counterpart (**1b**, Scheme 2), are excellent epoxidation catalysts with unprecedented activity.<sup>14,15</sup> **1a** is capable of activating dioxygen in acetone at  $-40^\circ\text{C}$  to yield an iron(III)-superoxo species, subsequently forming a diiron(III)- $\mu_2$ -oxo complex (**2**) upon warming to room temperature (r.t., Scheme 1).<sup>12</sup> **2** can act as an oxygen atom transfer agent, as showcased in the fast oxidation of triphenylphosphane or hydroquinone.<sup>12</sup>

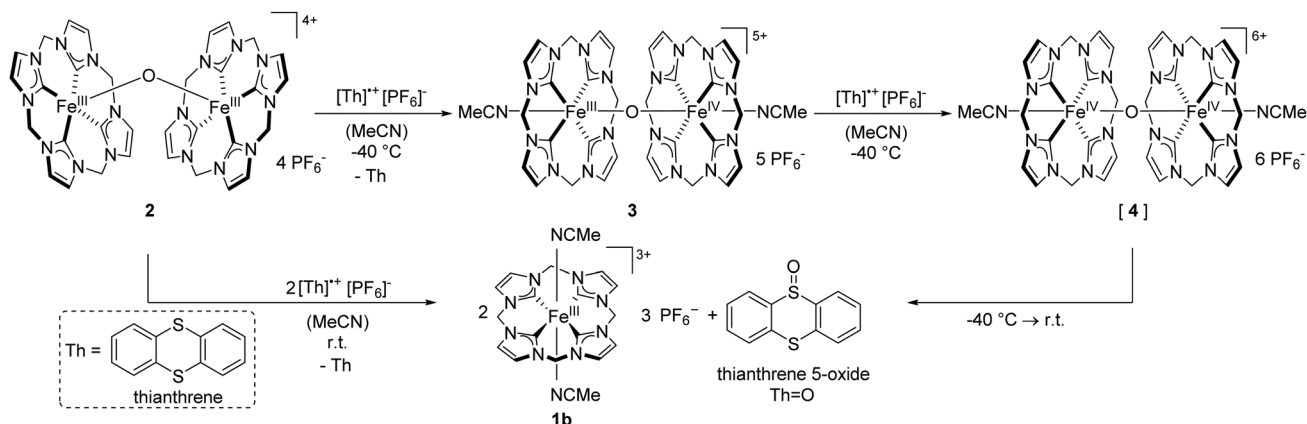
In this work, the synthesis of the high-valent diiron(III,IV)- $\mu_2$ -oxo tetracarbene complex [(MeCN)(cCCCC)Fe<sup>III</sup>–O–Fe<sup>IV</sup>(cCCCC)(MeCN)]<sup>5+</sup> (**3**, Scheme 2) is described. It is obtained from **2** via one-electron oxidation using thianthrenyl hexafluorophosphate (ThPF<sub>6</sub>). Even though such complexes are considered highly reactive,<sup>1</sup> **3** has been isolated and characterized by single crystal X-ray diffraction (SC-XRD, Fig. 2). In addition, it has been characterized by UV/Vis spectroscopy, cyclic voltammetry (CV), Evans' NMR and elemental analysis. Subsequent one-electron oxidation of **3** with another equivalent of ThPF<sub>6</sub> indicates the formation of a diiron(IV)- $\mu_2$ -oxo complex **4** (Scheme 2). Due to its even higher reactivity compared to **3**,


 Scheme 1 Activation of dioxygen by **1a**.

*Molecular Catalysis, Catalysis Research Center and Department of Chemistry, Technische Universität München, Lichtenbergstr. 4, 85748 Garching bei München, Germany. E-mail: fritz.kuehn@ch.tum.de*

† Electronic supplementary information (ESI) available: Experimental details, crystallographic data, UV/Vis, EPR and <sup>1</sup>H-NMR spectra, Evans' NMR method. CCDC 2077633. For ESI and crystallographic data in CIF or other electronic format see DOI: 10.1039/d1cc02027g

‡ Tim P. Schlachta and Markus R. Anneser contributed equally to this work.



**Scheme 2** One-electron oxidation of **2** using  $\text{ThPF}_6$  to form the diiron(III,IV)- $\mu_2$ -oxo complex **3** and subsequent one-electron oxidation to obtain the diiron(IV)- $\mu_2$ -oxo species **4**. **4** cannot be isolated and is reduced to **1b** after a short period by oxygen transfer to thianthrene. Using two equivalents of  $\text{ThPF}_6$  at r.t., **2** quickly results in **1b**, presumably *via* the formation of **3** and **4**.  $\text{Th}^{*+}$  = thianthrenyl, Th = thianthrene,  $\text{Th}=\text{O}$  = thianthrene 5-oxide.

the formation and decay of **4** can only be investigated *in situ* by UV/Vis kinetic studies. To the best of our knowledge, the compounds **3** and **4** are the first examples of diiron(III,IV)- $\mu_2$ -oxo and diiron(IV)- $\mu_2$ -oxo complexes bearing N-heterocyclic carbene ligands (NHCs). In fact, **3** is only the second example of a structurally characterized  $\mu_2$ -oxo bridged diiron(III,IV) complex<sup>10</sup> and the third example for a high-valent diiron- $\mu_2$ -oxo complex.<sup>1,11</sup>

In most cases, the generation of high-valent nonheme diiron complexes is performed by chemical oxidation.<sup>6,16–18</sup> For example, a recently described method includes the formation of a diiron(III)- $\mu_2$ -peroxo complex by reaction with dioxygen in the presence of a base and subsequent cleavage of the O–O bond promoted by the Lewis acid  $\text{Sc}(\text{OTf})_3$ .<sup>17</sup> However, bulk electrolysis has also been utilized to transform a diiron(III,IV)- $\mu_2$ -oxo complex nearly quantitatively to its diiron(IV)- $\mu_2$ -oxo counterpart.<sup>19</sup>

Therefore, preliminary CV studies of **2** were performed to investigate its redox behavior (Fig. 1). Indeed, two reversible one-electron redox processes could be observed. The first one,

assignable to the diiron(III)/(III,IV) redox couple, exhibits a half-cell potential of  $E_{1/2} = 0.19$  V. This is significantly lower than half-cell potentials of similar compounds, *e.g.* of a diiron(III,IV)- $\mu_2$ -oxo complex bearing a tris(2-pyridylmethyl)amine (TPA) ligand ( $E_{1/2} = 0.56$  V, diiron(III,IV)/(III) couple).<sup>16,20</sup> This observation can be attributed to the strong  $\sigma$ -donor properties of the tetra-NHC ligands increasing the electron density of the iron center, resulting in a lower potential for the one-electron oxidation at 0.25 V. For comparison, the half-cell potential of the mononuclear complex **1a** lies at 0.15 V and the substitution of the axial acetonitrile ligands of **1a** with benzonitrile or *tert*-butylisocyanide as better  $\pi$ -acceptors yields 0.27 V and 0.47 V, respectively.<sup>13,21,22</sup> The diiron(III,IV)/(IV) redox couple appears at  $E_{1/2} = 1.07$  V, which is in the same range, but slightly higher ( $\sim 170$  mV) compared to a bis( $\mu_2$ -oxo)diiron(III,IV) TPA complex.<sup>19</sup> These results indicate, that

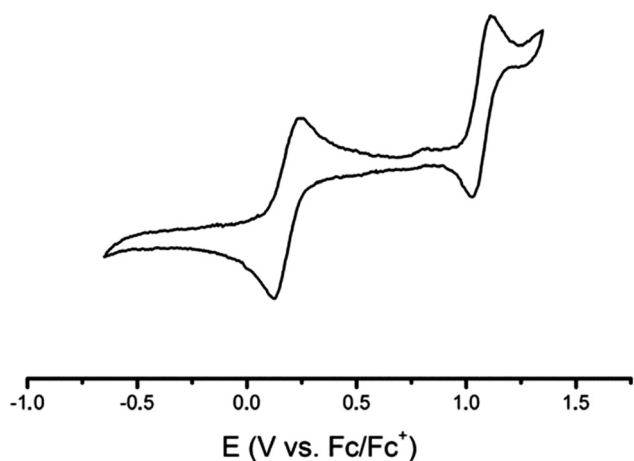


**Fig. 1** Cyclic voltammogram of **2** in MeCN at  $-40$  °C. Half-cell potentials are determined to  $E_{1/2} = 0.19$  V and  $E_{1/2} = 1.07$  V.

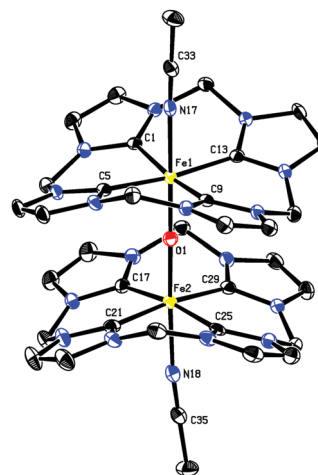


**Fig. 2** ORTEP-style representation of the cationic fragment of **3**. Hydrogen atoms and  $\text{PF}_6^-$  anions are omitted for clarity and thermal ellipsoids are shown at a 50% probability level. Selected bond lengths ( $\text{\AA}$ ) and angles ( $^\circ$ ): Fe1–C1 1.929(2), Fe2–C17 1.931(3), Fe1–O1 1.7272(17), Fe2–O1 1.7298(17), Fe1–N17 1.984(2), Fe2–N18 1.987(2), Fe1–O1–Fe2 176.34(11), C1–Fe1–C5 89.43(10), C1–Fe1–O1 95.55(9), O1–Fe1–N17 178.09(8).

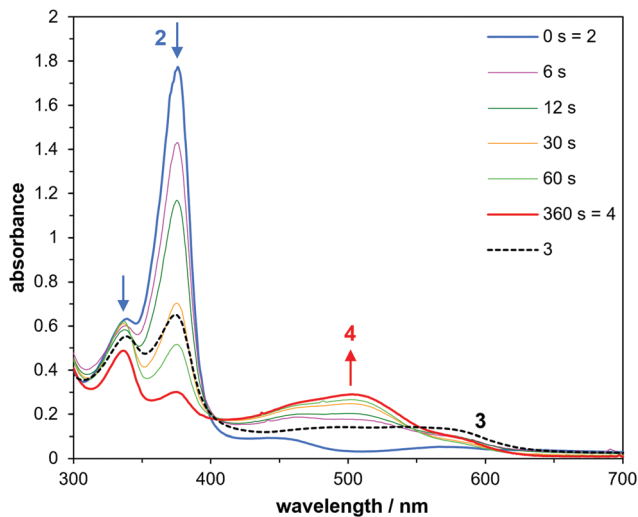


Fig. 3 UV/Vis spectrum of the formation of **4** from **2** via **3** upon addition of 2 eq. ThPF<sub>6</sub>. The spectrum of **3** was measured separately from isolated **3** and was included for comparison.  $T = -40\text{ }^{\circ}\text{C}$ ,  $c = 3.5 \times 10^{-4}\text{ M}$  in dry and degassed MeCN.

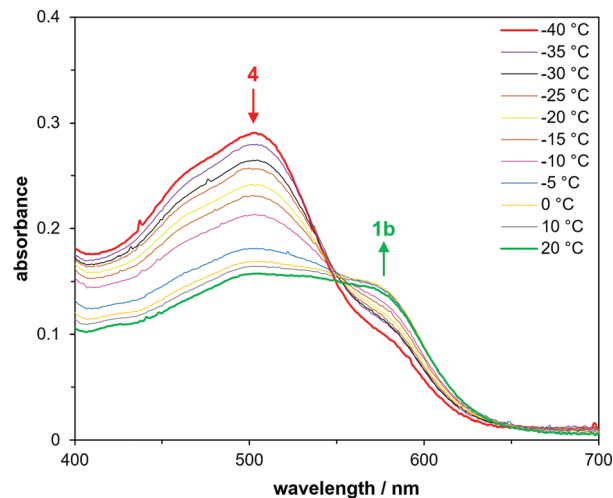


Fig. 4 UV/Vis spectrum of the decay of **4** to **1b** upon rising temperature. Each temperature was changed after 25 s.  $c = 3.5 \times 10^{-4}\text{ M}$  in dry and degassed MeCN.

not only one but two one-electron oxidations of **2** are feasible resulting in the new high-valent species **3** and **4**.

ThPF<sub>6</sub> is an one-electron oxidant which has been used to selectively oxidize iron(II) to iron(III) complexes.<sup>15,23</sup> The addition of one equivalent of ThPF<sub>6</sub> to **2** in acetonitrile at  $-40\text{ }^{\circ}\text{C}$  results in a burgundy solution. Upon precipitation with diethyl ether **3** is obtained as burgundy powder in 85% yield (ESI<sup>†</sup>). In solid form **3** is remarkably stable and can be stored for several months at  $-37\text{ }^{\circ}\text{C}$  in argon atmosphere without showing any signs of decomposition. In the typical range of <sup>1</sup>H-NMR spectroscopy, no signals are observable indicating a paramagnetic character of compound **3**. According to SC-XRD and contrary to **2**, the new complex **3** contains two axial acetonitrile ligands and five counterions (Fig. 2) proving the successful one-electron oxidation (Scheme 2). The composition determined by SC-XRD is also in alignment with elemental analysis (ESI<sup>†</sup>).

While complex **2** exhibits a slightly distorted square pyramidal geometry,<sup>12</sup> the two iron centers in the binuclear iron(III,IV)- $\mu_2$ -oxo complex **3** are coordinated in a slightly distorted octahedral fashion. The average of the Fe-C<sub>carbene</sub> distances is 1.931(5) Å and slightly shorter than in **2** (1.949(14) Å)<sup>12</sup> or another comparable  $\mu_2$ -oxo bridged diiron(III) tetracarbene complex (1.99 Å).<sup>24</sup> The Fe-N and Fe-O distances are longer than in **1a,1b** (1.914(2)–1.933(3) Å)<sup>13,15</sup> and similar to **2** (1.7322(7) Å),<sup>12</sup> respectively. However, in stark contrast to **2** (Fe-O-Fe 162.7°),<sup>12</sup> the vertical axis intersecting the axial MeCN ligands and the  $\mu_2$ -oxo bridged iron centers is close to 180° with the Fe-O-Fe angle of 176.34° and the O-Fe-N angles around 177.64°.

Evans' NMR method is applied to elucidate the magnetic moment of the complexes **2** and **3** (ESI<sup>†</sup>).<sup>25</sup> For **2** no relative shift of the respective solvent signals is determined, even though both iron centers in **2** are in 3d<sup>5</sup> electron configuration. The apparent

diamagnetic behavior of complex **2** is most likely resulting from antiferromagnetic coupling of the unpaired electrons facilitated by the bridging  $\mu_2$ -oxo ligand.<sup>12</sup> This is furthermore supported by EPR measurements, as no signal could be observed (ESI<sup>†</sup>, Fig. S7). **3** on the other hand is paramagnetic and exhibits a magnetic moment of  $\mu = 1.72\ \mu_{\text{B}}$ . A thin, axial signal can be observed in the EPR spectrum of **3** (Fig. 5, bottom), indicative of a  $S = 0.5$  system. Simulation was achieved with  $g = (2.0572, 2.0574, 2.0026)$  and  $A_{\text{Fe}}^{57} = (183, 97, 136)\text{ MHz}$ .

Due to the potential existence of the diiron(IV)- $\mu_2$ -oxo species **4** suggested by CV (Fig. 1), the one-electron oxidation of complex **3** was studied as well. The addition of one equivalent ThPF<sub>6</sub> to a burgundy acetonitrile solution of **3** at  $-40\text{ }^{\circ}\text{C}$  leads to a brightening of the color to a light red solution indicating the proposed formation of diiron(IV)- $\mu_2$ -oxo complex **4**. Despite many efforts, this intermediate

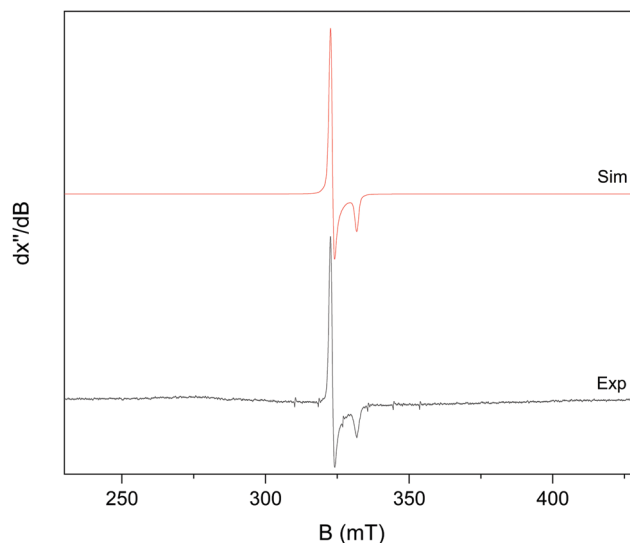


Fig. 5 EPR X-band spectrum of complex **3** (experimental, black, bottom, 173 K,  $4.6 \times 10^{-4}\text{ mol L}^{-1}$  and simulated, red, top).

could not be isolated, as it readily oxidizes thianthrene (Th) to thianthrene 5-oxide (Th=O, ESI,† Fig. S3 and S4). In similar fashion, two equivalents ThPF<sub>6</sub> added to a solution of **2** at r.t. result in the formation of mononuclear iron(III) complex **1b**, Th=O and Th, as assigned by <sup>1</sup>H-NMR spectroscopy (ESI,† Fig. S3 and S4).

The formation of **4** is monitored by *in situ* UV/Vis kinetics. The diiron(III)-μ<sub>2</sub>-oxo complex **2** shows a characteristic absorption maximum at 376 nm (Fig. 3 and Fig. S2, ESI†). Upon addition of two equivalents ThPF<sub>6</sub> at -40 °C in acetonitrile, the maximum rapidly decreases while a new broad band at 503 nm is observed. The reaction is completed in 360 s at -40 °C (Fig. 3). This species is unequivocally differentiated from the diiron(III,IV)-μ<sub>2</sub>-oxo complex **3** that shows a broad absorption maximum at 541 nm. Thus, this highly temperature sensitive species is assumed to be the diiron(IV)-μ<sub>2</sub>-oxo intermediate **4**.

To examine its stability under the afore mentioned condition, the -40 °C cold solution is warmed at a constant rate of 5 °C per 25 s and monitored by UV/Vis. The absorption maximum of **4** at 503 nm gradually declines and a broad absorption maximum is formed with its maximum at 505 nm (Fig. 4). It was assigned previously to the formation of the mononuclear iron(III) complex **1b**<sup>15</sup> resulting from the reduction of **4** by oxygen transfer to Th and consequently the formation of Th=O in line with the NMR experiment (ESI,† Fig. S3 and S4). While these two absorption maxima are close to each other, their shape is clearly distinguishable, with the broad maximum of **1b** being considerably more red-shifted.

The CV studies and NMR experiment in conjunction with the UV/Vis kinetics and the isolation of compound **3** conclusively support the mechanism shown in Scheme 2. After two subsequent one-electron oxidations of diiron(III)-μ<sub>2</sub>-oxo complex **2**, highly reactive diiron(IV)-μ<sub>2</sub>-oxo intermediate **4** is formed, followed by its decay and oxygen transfer to Th forming **1b** and Th=O.

In summary, the synthesis of the high-valent diiron(III,IV)-μ<sub>2</sub>-oxo tetracarbene complex **3** is described and its reactivity evaluated. It is formed from the diiron(III)-μ<sub>2</sub>-oxo complex **2** *via* one-electron oxidation using ThPF<sub>6</sub>. SC-XRD reveals, that during this oxidation, the Fe–O–Fe angle significantly changes to result in a nearly linear arrangement of the central Fe–O–Fe motive. In addition, two axial acetonitrile ligands are stabilizing the new structure. Such an acetonitrile adduct has not been observed for **2**. EPR indicates an overall spin *S* = 0.5 for complex **3**. CV demonstrates, that a consecutive second oxidation of **2** is feasible, leading to a diiron(IV)-μ<sub>2</sub>-oxo complex **4**. Its formation as well as its decay are observed *in situ* in UV/Vis kinetic experiments. The complex is highly active and oxidizes the oxophilic sulfur compound Th to Th=O, as shown by NMR spectroscopy. The novel compounds **3** and **4** are the first examples of high-valent diiron(III,IV)-μ<sub>2</sub>-oxo and diiron(IV)-μ<sub>2</sub>-oxo complexes bearing NHC ligands. Furthermore, **3** is only the third example of a crystallized high-valent diiron-μ<sub>2</sub>-oxo complex. The synthesis of **3** and **4** can serve as example to

obtain high-valent μ<sub>2</sub>-oxo iron complexes. Both complexes will be employed in reactivity and catalytic studies as artificial models for high-valent diiron intermediates of metalloenzymes for the ultimate goal of mimicking the reactivity of natural enzymes by oxidizing methane to methanol.

T. P. S., J. F. S., C. H. G. J. and A. D. B. gratefully acknowledge support from TUM graduate school. Oksana Storcheva is thanked for EPR measurements.

## Conflicts of interest

There are no conflicts to declare.

## Notes and references

- 1 A. J. Jasniewski and L. Que, *Chem. Rev.*, 2018, **118**, 2554–2592.
- 2 A. L. Feig and S. J. Lippard, *Chem. Rev.*, 1994, **94**, 759–805.
- 3 T. C. Brunold, *Proc. Natl. Acad. Sci. U. S. A.*, 2007, **104**, 20641.
- 4 High-valent iron complexes are complexes where the iron center has a higher oxidation number than the common +II or +III states.
- 5 P. Nordlund and P. Reichard, *Annu. Rev. Biochem.*, 2006, **75**, 681–706.
- 6 A. Draksharapu, S. Xu and L. Que Jr., *Angew. Chem., Int. Ed.*, 2020, **59**, 22484–22488.
- 7 B. E. R. Snyder, M. L. Bols, R. A. Schoonheydt, B. F. Sels and E. I. Solomon, *Chem. Rev.*, 2018, **118**, 2718–2768.
- 8 L. Que and W. B. Tolman, *Nature*, 2008, **455**, 333–340.
- 9 A. Kejriwal, P. Bandyopadhyay and A. N. Biswas, *Dalton Trans.*, 2015, **44**, 17261–17267.
- 10 H.-F. Hsu, Y. Dong, L. Shu, V. G. Young and L. Que, *J. Am. Chem. Soc.*, 1999, **121**, 5230–5237.
- 11 A. Ghosh, F. Tiago de Oliveira, T. Yano, T. Nishioka, E. S. Beach, I. Kinoshita, E. Münck, A. D. Ryabov, C. P. Horwitz and T. J. Collins, *J. Am. Chem. Soc.*, 2005, **127**, 2505–2513.
- 12 M. R. Anneser, S. Haslinger, A. Pöthig, M. Cokoja, V. D'Elia, M. P. Högerl, J.-M. Basset and F. E. Kühn, *Dalton Trans.*, 2016, **45**, 6449–6455.
- 13 M. R. Anneser, S. Haslinger, A. Pöthig, M. Cokoja, J.-M. Basset and F. E. Kühn, *Inorg. Chem.*, 2015, **54**, 3797–3804.
- 14 F. Dyckhoff, J. F. Schlagintweit, R. M. Reich and F. E. Kühn, *Catal. Sci. Technol.*, 2020, **10**, 3532–3536.
- 15 J. W. Kück, M. R. Anneser, B. Hofmann, A. Pöthig, M. Cokoja and F. E. Kühn, *ChemSusChem*, 2015, **8**, 4056–4063.
- 16 Y. Dong, H. Fujii, M. P. Hendrich, R. A. Leising, G. Pan, C. R. Randall, E. C. Wilkinson, Y. Zang and L. Que, *J. Am. Chem. Soc.*, 1995, **117**, 2778–2792.
- 17 S. Banerjee, A. Draksharapu, P. M. Crossland, R. Fan, Y. Guo, M. Swart and L. Que, *J. Am. Chem. Soc.*, 2020, **142**, 4285–4297.
- 18 G. Xue, A. T. Fiedler, M. Martinho, E. Münck and L. Que, *Proc. Natl. Acad. Sci. U. S. A.*, 2008, **105**, 20615.
- 19 G. Xue, D. Wang, R. De Hont, A. T. Fiedler, X. Shan, E. Münck and L. Que, *Proc. Natl. Acad. Sci. U. S. A.*, 2007, **104**, 20713–20718.
- 20 H.-M. Koeppe, H. Wendt and H. Strehlow, *Bunsen-Ges. Phys. Chem., Ber.*, 1960, **64**, 483–491.
- 21 T. P. Schlachta, J. F. Schlagintweit, M. R. Anneser, E.-M. H. J. Esslinger, M. Muhr, S. Haslinger and F. E. Kühn, *Inorg. Chim. Acta*, 2021, **518**, 120228.
- 22 J. F. Schlagintweit, C. Hintermeier, M. R. Anneser, E.-M. H. J. Esslinger, S. Haslinger and F. E. Kühn, *Chem. – Asian J.*, 2020, **15**, 1896–1902.
- 23 J. M. Smith and J. R. Long, *Inorg. Chem.*, 2010, **49**, 11223–11230.
- 24 S. Meyer, I. Klawitter, S. Demeshko, E. Bill and F. Meyer, *Angew. Chem., Int. Ed.*, 2013, **52**, 901–905.
- 25 D. F. Evans, *J. Chem. Soc.*, 1959, 2003–2005.



Cite this: *Dalton Trans.*, 2022, **51**, 13591

Received 5th August 2022,  
Accepted 23rd August 2022

DOI: 10.1039/d2dt02561b

rsc.li/dalton

## The first macrocyclic abnormally coordinating tetra-1,2,3-triazole-5-ylidene iron complex: a promising candidate for olefin epoxidation†

Greta G. Zámbo,  Johannes Mayr, Michael J. Sauer, Tim P. Schlachta,   
Robert M. Reich  and Fritz E. Kühn \*

The first macrocyclic and abnormally coordinating, mesoionic *N*-heterocyclic carbene iron complex has been synthesised and characterised via ESI-MS, EA, SC-XRD, CV, NMR and UV/Vis spectroscopy. <sup>13</sup>C-NMR spectroscopy and CV measurements indicate a strong  $\sigma$ -donor ability of the carbene moieties, suggesting an efficient catalytic activity of the iron complex in oxidation reactions. Initial tests in the epoxidation of *cis*-cyclooctene as a model substrate confirm this assumption.

Inspired by the activity of iron metalloenzymes,<sup>1</sup> several non-heme macrocyclic tetradentate iron complexes have been designed over the last decade,<sup>2,3</sup> mimicking, *inter alia*, their capability of oxidation of hydrocarbons as well as for oxygen transport.<sup>2–4</sup> In this context, metal supporting *N*-heterocyclic carbenes (NHC) have received attention as ligands stabilising high oxidation state transition metals.<sup>5</sup> Accordingly, iron tetra (NHC) complexes have been successfully applied in oxidation catalysis,<sup>2–4,6</sup> including aziridination, epoxidation and C–H activation. Based on the extensive work of Que *et al.*<sup>1,7–9</sup> and Costas *et al.*<sup>7,10</sup> high valent iron intermediates are considered to be the active species in these reactions. A remarkable activity in the catalytic oxidation of olefins is displayed by an imidazole based cyclic tetra(NHC) iron complex with turnover frequencies (TOFs) up to 410 000 h<sup>–1</sup> (Fig. 1, middle). However, limited catalyst stability (TON = 1200) overshadows its high activity.<sup>11</sup> Tuning of its electronic properties by insertion of substituents varying the NHC backbone affects not only catalyst stability but also its activity, emphasising once more the role of ligand design.<sup>12</sup> Pioneering work on bio-inspired non-heme macrocyclic iron tetra(NHCs) has been done by

Jenkins *et al.*<sup>13–18</sup>, Meyer *et al.*<sup>19–21</sup> and our group.<sup>12,22–26</sup> During these studies several bridged tetra(imidazole-2-ylidene) iron complexes have been prepared and characterised (Fig. 1, left).

Abnormally coordinating NHC moieties (aNHCs) are considered to be stronger  $\sigma$ -donors and post-modification of the ligand macrocycle is possible.<sup>27–29</sup> However, all macrocyclic tetra(NHC) iron complexes reported so far are based on normally coordinating imidazole-2-ylidenes, where the ligand modification occurs in the very first synthetic step. On the other hand, application of aNHCs as ligands in transition metal catalysis proved to be a powerful tool for tuning the electronic nature of the central metal and improving the catalytic performance.<sup>29,30</sup> In this context, 1,2,3-triazol-5-ylidenes (trz) come into mind, representing a promising subclass of aNHCs with easy synthetic access *via* click chemistry.<sup>27,31</sup> To date, only a rather limited number of trz-iron complexes is known. Besides a homoleptic C,O-chelating trz-iron complex,<sup>32</sup> three different general complex scaffolds have been described so far, where the ligands have an open chain shape: (a) cyclopentadienyl iron half sandwich complexes bearing one trz ligand,<sup>33–35</sup> (b) hetero- and homoleptic iron complexes bearing two or three bis(trz) in octahedral fashion<sup>36–38</sup> and (c) a class that contains one or two pincer-type bis(trz) entities, bridged *via* pyridine, that latter acting as additional *N*-donor.<sup>39,40</sup>

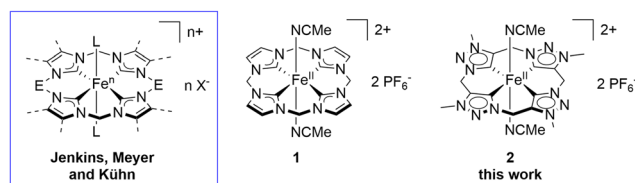


**Fig. 1** General framework of macrocyclic tetra(NHC) iron complexes reported by Jenkins, Meyer and Kühn (left) with E = CH<sub>2</sub>, C<sub>2</sub>H<sub>4</sub> or BMe<sub>2</sub>, L = ligand, n = 2 or 3, X = PF<sub>6</sub> or OTf and this work (**2**, right), and the chemical structure of the most active (pre-)catalyst Fe<sup>II</sup>[cCCCC]<sub>im</sub> **1** in the epoxidation of *cis*-cyclooctene with H<sub>2</sub>O<sub>2</sub> (middle).

*Molecular Catalysis, Department of Chemistry and Catalysis Research Centre, Technische Universität München, Lichtenbergstr. 4, 85784 Garching bei München, Germany. E-mail: fritz.kuehn@ch.tum.de*

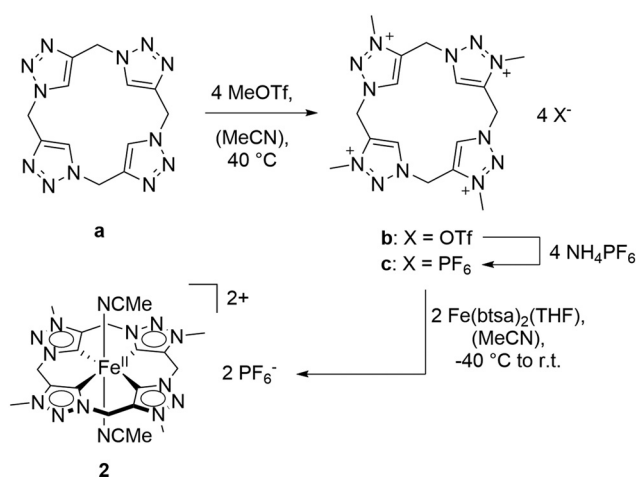
† Electronic supplementary information (ESI) available: Experimental details, analytical methods, crystallographic data, ORTEP-style structure of **1**, <sup>1</sup>H-, <sup>13</sup>C-, <sup>31</sup>P-, <sup>19</sup>F-NMR-spectra and catalytic procedure. CCDC 2184662 and 2184663. For ESI and crystallographic data in CIF or other electronic format see DOI: <https://doi.org/10.1039/d2dt02561b>

In this work, the synthesis and characterisation of the – to the best of our knowledge – first macrocyclic aNHC iron complex is reported (Fig. 1, right). A synthetic strategy, differing from the literature known calix[4]1,2,3-triazole,<sup>41</sup> proceeding *via* repeated click reactions and azidations, is described. Subsequent alkylation with MeOTf results in the formation of the cyclic tetra(trz) ligand precursor. *In situ* deprotonation and complexation yields the methyl bridged tetra(aNHC) iron complex Fe<sup>II</sup>[cCCCC]<sub>trz</sub> **2**. Application of **2** for initial catalytic investigations demonstrates its activity in the epoxidation of *cis*-cyclooctene with hydrogen peroxide.

The modified synthesis of methylene bridged calix[4]1,2,3-triazole is based on the copper(i) catalysed click reaction of a terminal alkyne with an azide, introduced by Sharpless *et al.*<sup>42</sup> and Meldal *et al.*<sup>43</sup> to form 1,4-substituted 1,2,3-triazoles.<sup>31</sup> Starting from propargyl bromide the ligand synthesis includes eleven steps (ESI, Scheme S1<sup>†</sup>). First, the terminal alkyne has to be protected with a triisopropylsilyl (TIPS) group to avoid an undesired second click reaction in the following steps. Afterwards, the bromide is replaced by an azide group. Then, a click reaction with propargyl alcohol occurs initially, followed by an Appel reaction<sup>44</sup> of the alcohol with PPh<sub>3</sub> and CBr<sub>4</sub> and an *in situ* azidation with NaN<sub>3</sub>. These steps are subsequently repeated for two more times until three triazole moieties are formed within the chain. The cyclisation occurs *via* an *in situ* deprotection and an intramolecular click reaction. Post modification of the macrocycle by alkylation of the N3 positions with an excess of methyl triflate yields calix[4]3-methyl-1,2,3-triazolium triflate **b** (72% isolated yield, Scheme 1, for SC-XRD data see ESI<sup>†</sup>). Methylation with significant less reactive methyl iodide in DMF, which has been applied in previous synthetic approaches for the alkylation of 1,2,3-triazoles<sup>34,45</sup> does not result in any product formation, even at temperatures of up to 70 °C. Subsequently, salt metathesis of **b** with NH<sub>4</sub>PF<sub>6</sub> quantitatively yields the hexafluorophosphate salt trz precursor **c** (Scheme 1). Recently, a second salt analogue of **b** and **c** with

BF<sub>4</sub><sup>-</sup> anion was described and synthesised *via* grinding with a vibration ball mill of **a** with the corresponding *Meerwein* salt.<sup>46</sup>

Iron bis(trimethylsilyl)amide (btsa, N(SiMe<sub>3</sub>)<sub>2</sub>) THF adduct Fe(btsa)<sub>2</sub>(THF) proved to be a viable agent to form iron(II) complexes.<sup>19,22</sup> Deprotonation of 1.00 eq. alkylated calix[4]1,2,3-triazole salt **c** by the internal base of 2.00 eq. Fe(btsa)<sub>2</sub>(THF) under formation of the free carbene in immediate metal vicinity gives Fe<sup>II</sup>[cCCCC]<sub>trz</sub> complex **2** in 78% yield (Scheme 1). During the synthesis of **1**, [Fe(MeCN)<sub>6</sub>](PF<sub>6</sub>)<sub>2</sub> is formed as a by-product, due to the excess of Fe(btsa)<sub>2</sub>(THF) in MeCN.<sup>22</sup> Under optimal conditions, complex **2** precipitates directly as orange solid, which makes further purification *via e.g.* column chromatography or fractional precipitation unnecessary. <sup>13</sup>C-NMR spectroscopy shows the coordinating carbene carbon signals at δ(<sup>13</sup>C) = 190 ppm (ESI, Fig. S32<sup>†</sup>). The carbene carbon signal is significantly high field shifted, compared to imidazole-2-ylidene iron complexes (δ(<sup>13</sup>C)<sub>C<sub>NHC</sub></sub> = 205–194 ppm)<sup>12,13,15,20,22,47</sup> and especially its imidazole counterpart **1** Fe[cCCCC]<sub>im</sub>, where the carbene signals appear at δ(<sup>13</sup>C) = 205 ppm.<sup>22</sup> The observed <sup>13</sup>C shifts indicates a high electron density environment at the iron centre, as expected for a strong σ-donation. Single crystals of **2** suitable for SC-XRD were obtained by the slow diffusion of diethyl ether into a solution of **2** in acetonitrile. The complex exhibits a distorted octahedral coordination sphere around the iron (Fig. 2). The aNHC ligand is ideal square-planar, differing from the previously characterised macrocyclic tetra(NHC) iron complexes, which are showing a saddle-distorted conformation for the NHC ligand (ESI, Fig. S3<sup>†</sup>). Axial positions are occupied by two acetonitrile ligands. The Fe–C<sub>NHC</sub> distances of **2** with 1.925(2) and 1.931(2) Å are slightly longer than observed for the saddle-distorted NHC iron complexes. Selected bond length and angles of complexes **1** and **2** are compared in Table S3 (ESI<sup>†</sup>).



**Scheme 1** Synthesis of the calix[4]1,2,3-triazolium salts **b** and **c** and subsequent iron complexation to complex **2**.

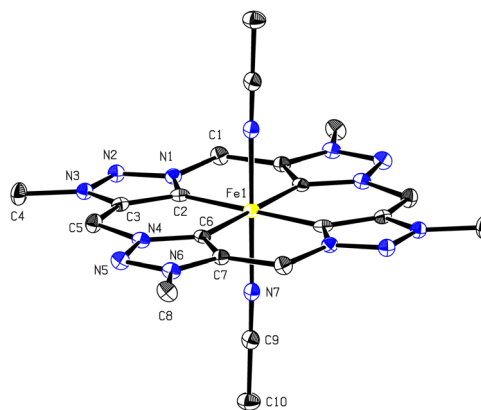


**Fig. 2** ORTEP-style representation of the cationic fragment of compound **2**. Hydrogen atoms and PF<sub>6</sub><sup>-</sup> anions, as well as a co-crystallised MeCN molecule are omitted for clarity and thermal ellipsoids are shown at a 50% probability level. Due to the inversion centre only half of the atoms are labelled. Selected bond lengths (Å) and angles (°): Fe1–C2 1.925(2), Fe1–C6 1.931(2), Fe1–N 1.9247(17), N7–Fe1–N7\* 180.00(0), C2–Fe1–C2\* 180.00(0), C6–Fe1–C6\* 180.00(0), C2–Fe1–C6 90.15(8), C2–Fe1–C6\* 89.85(8). Symmetry code:  $-x + 1, -y + 2, -z + 1$ .

To get further insights of the electronic structure of  $\text{Fe}[\text{cCCCC}]_{\text{trz}}$  complex **2**, cyclic voltammetry (CV) measurements were performed in acetonitrile solution with  $[\text{N}(n\text{-Bu})_4]\text{PF}_6$  as the supporting electrolyte. The cyclic voltammogram shows a fully reversible one-electron redox process, assigned to the  $\text{Fe}^{\text{II}}/\text{Fe}^{\text{III}}$  redox couple (ESI, Fig. S4†). The half-cell potential is  $E_{1/2} = -0.34$  V ( $\text{Fe}^{\text{II}}/\text{Fe}^{\text{III}}$ ) and oxidation/reduction potentials are determined to be  $E_{\text{ox}} = -0.31$  V and  $E_{\text{red}} = -0.38$  V. The insertion of the aNHC ligand significantly decreases the half-cell potential compared to similar macrocyclic imidazol-2-ylidene iron complexes with  $E_{1/2} = 0.00$ – $0.44$  V vs.  $\text{Fc}/\text{Fc}^+$  (ref. 12, 15, 17, 28 and 47) (e.g.  $E_{1/2} = 0.15$  V vs.  $\text{Fc}/\text{Fc}^+$  for **1**),<sup>23</sup> indicating an easier oxidation of  $\text{Fe}^{\text{II}}$  to  $\text{Fe}^{\text{III}}$ . As defined by the *Lever's Electronic Parameter* (LEP),<sup>48</sup> the stronger the donor capability of a ligand, the lower the resulting  $E_{1/2}$  values,<sup>49</sup> due to the high electron density at the iron centre induced by the strong  $\sigma$ -donor properties of the aNHC. These results suggest the applicability of **2** as suitable pre-catalyst for oxidation reactions, as recent investigation on the catalytic mechanism of iron complexes in oxidation catalysis, such as epoxidation and C–H activation, indicate an one electron oxidation of  $\text{Fe}^{\text{II}}$  to  $\text{Fe}^{\text{III}}$  as prerequisite to form the active catalyst.<sup>11,50</sup> UV/Vis spectrometry of complex **2** was performed in acetonitrile at 20 °C. Two absorption bands are visible at 405 nm and 480 nm (Fig. 3). In order to gain information about the formation of iron(III), one equivalent of thianthrenyl hexafluorophosphate ( $\text{ThPF}_6$ ) was added to the solution of complex **2** in acetonitrile under inert conditions.  $\text{ThPF}_6$  as one-electron oxidising agent has been successfully used for the selective oxidation of iron(II) to iron(III) complexes.<sup>23,51,52</sup> The measured UV/Vis spectrum shows the disappearance of the two absorption bands by generating a new band around 431 nm, indicating the occurrence of an oxidation process (Fig. 3).

Building on the characteristic findings and electronic properties, complex **2** is examined as pre-catalyst in the epoxidation of *cis*-cyclooctene, being widely applied as model substrate using  $\text{H}_2\text{O}_2$  as oxidising agent. First time-dependant catalytic studies using standard conditions (269  $\mu\text{mol}$  *cis*-

cyclooctene, 403  $\mu\text{mol}$   $\text{H}_2\text{O}_2$ ) and 0.50 mol% of **2** have been performed at variable temperatures in MeCN (Fig. 4, left). No side product formation occurs with an epoxide selectivity of >99%. At 20 °C, maximal conversion of 37% is reached after 30 s. Lowering the temperature enhances the catalyst stability, as a consequence of a longer catalyst lifetime.<sup>23</sup> After 10 min the conversion increases from 49% for 10 °C over 72% for 0 °C to 89% for –10 °C. In previous catalytic studies strong Lewis acids like  $\text{Sc}(\text{OTf})_3$  are utilised in the oxidation process with  $\text{Fe}^{\text{II}}[\text{cCCCC}]_{\text{im}}$  complex **1** as catalyst, resulting in a significantly improved performance.<sup>11</sup>  $\text{Sc}^{3+}$  initiates the *in situ* oxidation of  $\text{Fe}^{\text{II}}$  complex to the active  $\text{Fe}^{\text{III}}$  catalyst.<sup>11</sup> Although an epoxidation mechanism with iron carbenes as catalyst precursors is not yet established beyond any doubt, it can be assumed, based on observations of related catalysts, that heterolytic O–O bond cleavage of a  $\text{Fe}^{\text{III}}\text{-OOH}$  species, which is initially formed upon reaction of the  $\text{Fe}^{\text{III}}$  catalyst with  $\text{H}_2\text{O}_2$ , is facilitated by  $\text{Sc}(\text{OTf})_3$ , resulting in the formation of an active iron(v) oxo species.<sup>1,7–10</sup> Furthermore, the addition of Lewis acids to the catalytic reaction proved to reactivate  $\mu_2$ -oxodiiron(III)  $\text{Fe}^{\text{III}}\text{-O-Fe}^{\text{III}}$  species, which has been identified as important deactivation product.<sup>11,47</sup> With the addition of 0.10 eq.  $\text{Sc}(\text{OTf})_3$  to the reaction under standard conditions at 20 °C and 0.50 mol% of **2**, the reaction is completed after 30 min and a 97% conversion is reached with a cyclooctene oxide yield of 93% (Fig. 4). After 5 min the formation of side products starts, including 1,2-cyclooctandiol, decreasing the selectivity from initial >99% to 96%. The 1,2-cyclooctandiol yield remains at 2%. The TOF has been determined after 10 s to be 41 000  $\text{h}^{-1}$ , which is lower than that of its imidazole counterpart **1**, but in the range of the homogeneous laboratory benchmark catalyst methyltrioxorhenium(vII) ( $\text{TOF} < 40\,000\ \text{h}^{-1}$ )<sup>53</sup> and the area of magnitude of some of the most active molybdenum based epoxidation complexes ( $\text{TOF ca. } 41\,000\ \text{h}^{-1}$ ).<sup>54</sup>

In summary, the first macrocyclic, aNHC iron complex  $\text{Fe}^{\text{II}}[\text{cCCCC}]_{\text{trz}}$  was successfully synthesised. SC-XRD shows an octahedral geometry with the tetradentate ligand in an ideal square-planar coordination. As indicated by the carbene shifts in the <sup>13</sup>C-spectra, as well as by its half-cell potential the complex displays a remarkably electron-rich iron centre, corre-

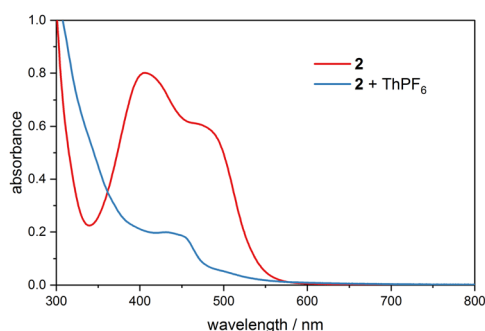


**Fig. 3** UV/Vis spectrum of **2** (red);  $c = 0.20$  mM,  $T = 20$  °C in MeCN. Two absorption bands appear at 405 nm and 480 nm. Addition of 1.00 eq.  $\text{ThPF}_6$  to the light orange solution results in a light yellow solution. The two absorption bands of **2** disappear and a new band around 431 nm occurs ( $c = 0.2$  mM,  $T = 20$  °C in MeCN).

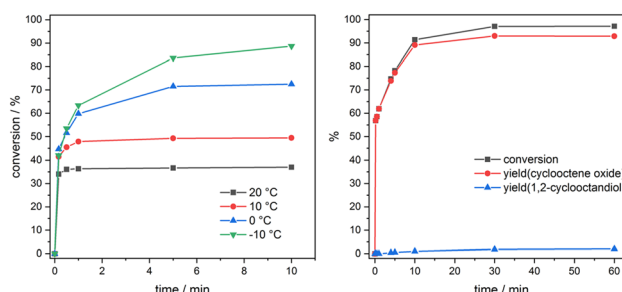


**Fig. 4** Time-dependant epoxidation of *cis*-cyclooctene (403  $\mu\text{mol}$ , 1.50 eq.), in MeCN using **2** as catalyst (1.35  $\mu\text{mol}$ , 0.005 eq.), and  $\text{H}_2\text{O}_2$  (403  $\mu\text{mol}$ , 1.50 eq.) as oxidising agent at variable temperatures (left) and at 20 °C using  $\text{Sc}(\text{OTf})_3$  (26.9  $\mu\text{mol}$ , 0.10 eq.) as additive (right). Yields and conversions are determined by GC-FID.

lating to a high  $\sigma$ -donor strength of the aNHCs. CV measurements and UV/Vis experiments suggest the possible oxidation to the Fe<sup>III</sup> derivative, which is crucial for the catalytic activity in oxidation reactions, including epoxidation and C–H activation. First epoxidation reactions applying **2** as catalyst show a substrate conversion up to 97% (TOF = 41 000 h<sup>-1</sup>). As simple modification inserting different N3 substituents on the ligand after cyclisation is expected to be possible, this already highly suitable ligand can be modified to further tune its electronic and steric environment. The application of 1,2,3-triazol-5-ylidenes as ligands offers two major advantages over imidazole-2-ylidene iron complexes: (a) a significantly higher  $\sigma$ -donation of the NHC moieties and (b) post modification of the ligand, which is not possible for imidazole-2-ylidene ligand precursors, where the NHC moieties are defined within the very first synthetic step. This new ligand system opens great opportunities for the design of selective and stable (immobilisation) Fe<sup>II/III</sup> metal complexes (e.g. for the (ep)oxidation of olefins). Further catalytic in-depth studies, as well as the synthetic modification of the macrocycle are currently ongoing in our laboratories.

## Conflicts of interest

There are no conflicts to declare.

## Acknowledgements

G. G. Z., M. J. S., and T. P. S. gratefully acknowledge support from TUM Graduate School.

## References

- 1 A. J. Jasniewski and L. Que Jr., *Chem. Rev.*, 2018, **118**, 2554–2592.
- 2 S. M. Hölzl, P. J. Altmann, J. W. Kück and F. E. Kühn, *Coord. Chem. Rev.*, 2017, **352**, 517–536.
- 3 G. G. Zámbo, J. F. Schlagintweit, R. M. Reich and F. E. Kühn, *Catal. Sci. Technol.*, 2022, **12**, 4949–4961.
- 4 K. Riener, S. Haslinger, A. Raba, M. P. Högerl, M. Cokoja, W. A. Herrmann and F. E. Kühn, *Chem. Rev.*, 2014, **114**, 5215–5272.
- 5 M. N. Hopkinson, C. Richter, M. Schedler and F. Glorius, *Nature*, 2014, **510**, 485–496.
- 6 J. W. Kück, R. M. Reich and F. E. Kühn, *Chem. Rec.*, 2016, **16**, 349–364.
- 7 M. Borrell, E. Andris, R. Navrátil, J. Roithová and M. Costas, *Nat. Commun.*, 2019, **10**, 1–9.
- 8 X. Lu, X.-X. Li, Y.-M. Lee, Y. Jang, M. S. Seo, S. Hong, K.-B. Cho, S. Fukuzumi and W. Nam, *J. Am. Chem. Soc.*, 2020, **142**, 3891–3904.
- 9 S. Kal and L. Que Jr., *Angew. Chem., Int. Ed.*, 2019, **58**, 8484–8488.
- 10 K. Chen, M. Costas, J. Kim, A. K. Tipton and L. Que, *J. Am. Chem. Soc.*, 2002, **124**, 3026–3035.
- 11 F. Dyckhoff, J. F. Schlagintweit, R. M. Reich and F. E. Kühn, *Catal. Sci. Technol.*, 2020, **10**, 3532–3536.
- 12 M. A. Bernd, F. Dyckhoff, B. J. Hofmann, A. D. Böth, J. F. Schlagintweit, J. Oberkofler, R. M. Reich and F. E. Kühn, *J. Catal.*, 2020, **391**, 548–561.
- 13 M. R. Anneser, G. R. Elpitiya, X. B. Powers and D. M. Jenkins, *Organometallics*, 2019, **38**, 981–987.
- 14 J. F. DeJesus and D. M. Jenkins, *Chem. – Eur. J.*, 2020, **26**, 1429–1435.
- 15 S. A. Cramer and D. M. Jenkins, *J. Am. Chem. Soc.*, 2011, **133**, 19342–19345.
- 16 P. P. Chandrachud, H. M. Bass and D. M. Jenkins, *Organometallics*, 2016, **35**, 1652–1657.
- 17 K. M. Blatchford, C. J. Mize, S. Roy and D. M. Jenkins, *Dalton Trans.*, 2022, **51**, 6153–6156.
- 18 M. R. Anneser, G. R. Elpitiya, J. Townsend, E. J. Johnson, X. B. Powers, J. F. DeJesus, K. D. Vogiatzis and D. M. Jenkins, *Angew. Chem.*, 2019, **131**, 8199–8202.
- 19 S. Meyer, I. Klawitter, S. Demeshko, E. Bill and F. Meyer, *Angew. Chem.*, 2013, **125**, 935–939.
- 20 C. Schremmer, C. Cordes, I. Klawitter, M. Bergner, C. E. Schiewer, S. Dechert, S. Demeshko, M. John and F. Meyer, *Chem. – Eur. J.*, 2019, **25**, 3918–3929.
- 21 A. A. Massie, C. Schremmer, I. Ruter, S. Dechert, I. Siewert and F. Meyer, *ACS Catal.*, 2021, **11**, 3257–3267.
- 22 M. R. Anneser, S. Haslinger, A. Pöthig, M. Cokoja, J.-M. Basset and F. E. Kühn, *Inorg. Chem.*, 2015, **54**, 3797–3804.
- 23 J. W. Kück, M. R. Anneser, B. Hofmann, A. Pöthig, M. Cokoja and F. E. Kühn, *ChemSusChem*, 2015, **8**, 4056–4063.
- 24 T. P. Schlachta, J. F. Schlagintweit, M. R. Anneser, E.-M. H. Esslinger, M. Muhr, S. Haslinger and F. E. Kühn, *Inorg. Chim. Acta*, 2021, **518**, 120228.
- 25 J. F. Schlagintweit, C. Hintermeier, M. R. Anneser, E. M. H. Esslinger, S. Haslinger and F. E. Kühn, *Chem. – Asian J.*, 2020, **15**, 1896–1902.
- 26 M. R. Anneser, S. Haslinger, A. Pöthig, M. Cokoja, V. D'Elia, M. P. Högerl, J.-M. Basset and F. E. Kühn, *Dalton Trans.*, 2016, **45**, 6449–6455.
- 27 D. Schweinfurth, L. Hettmanczyk, L. Suntrup and B. Sarkar, *Z. Anorg. Allg. Chem.*, 2017, **643**, 554–584.
- 28 J. D. Crowley, A.-L. Lee and K. J. Kilpin, *Aust. J. Chem.*, 2011, **64**, 1118–1132.
- 29 O. Schuster, L. Yang, H. G. Raubenheimer and M. Albrecht, *Chem. Rev.*, 2009, **109**, 3445–3478.
- 30 R. H. Crabtree, *Coord. Chem. Rev.*, 2013, **257**, 755–766.
- 31 L. Liang and D. Astruc, *Coord. Chem. Rev.*, 2011, **255**, 2933–2945.
- 32 W. Stroek, M. Keilwerth, D. M. Pividori, K. Meyer and M. Albrecht, *J. Am. Chem. Soc.*, 2021, **143**, 20157–20165.
- 33 Q. Liang, K. Hayashi, K. Rabeda, J. L. Jimenez-Santiago and D. Song, *Organometallics*, 2020, **39**, 2320–2326.

- 34 P. V. Nylund, N. C. Ségaud and M. Albrecht, *Organometallics*, 2021, **40**, 1538–1550.
- 35 C. Johnson and M. Albrecht, *Organometallics*, 2017, **36**, 2902–2913.
- 36 Y. Liu, K. S. Kjær, L. A. Fredin, P. Chábera, T. Harlang, S. E. Canton, S. Lidin, J. Zhang, R. Lomoth and K. E. Bergquist, *Chem. – Eur. J.*, 2015, **21**, 3628–3639.
- 37 P. Chábera, K. S. Kjaer, O. Prakash, A. Honarfar, Y. Liu, L. A. Fredin, T. C. Harlang, S. Lidin, J. Uhlig and V. Sundström, *J. Phys. Chem. Lett.*, 2018, **9**, 459–463.
- 38 P. Chábera, Y. Liu, O. Prakash, E. Thyraug, A. E. Nahhas, A. Honarfar, S. Essén, L. A. Fredin, T. C. Harlang and K. S. Kjær, *Nature*, 2017, **543**, 695–699.
- 39 Y. Liu, P. Persson, V. Sundström and K. Wärnmark, *Acc. Chem. Res.*, 2016, **49**, 1477–1485.
- 40 H. Iwasaki, Y. Teshima, Y. Yamada, R. Ishikawa, Y. Koga and K. Matsubara, *Dalton Trans.*, 2016, **45**, 5713–5719.
- 41 I. Kim, K. C. Ko, W. R. Lee, J. Cho, J. H. Moon, D. Moon, A. Sharma, J. Y. Lee, J. S. Kim and S. Kim, *Org. Lett.*, 2017, **19**, 5509–5512.
- 42 V. V. Rostovtsev, L. G. Green, V. V. Fokin and K. B. Sharpless, *Angew. Chem.*, 2002, **114**, 2708–2711.
- 43 C. W. Tornøe, C. Christensen and M. Meldal, *J. Org. Chem.*, 2002, **67**, 3057–3064.
- 44 R. Appel, *Angew. Chem., Int. Ed. Engl.*, 1975, **14**, 801–811.
- 45 J. F. Schlagintweit, C. H. Jakob, N. L. Wilke, M. Ahrweiler, C. Frias, J. Frias, M. König, E.-M. H. Esslinger, F. Marques and J. F. Machado, *J. Med. Chem.*, 2021, **64**, 15747–15757.
- 46 J. Cho, J. Shin, M. Kang, P. Verwilt, C. Lim, H. Yoo, J. G. Kim, X. Zhang, C. S. Hong and J. S. Kim, *Chem. Commun.*, 2021, **57**, 12139–12142.
- 47 F. Dyckhoff, J. F. Schlagintweit, M. A. Bernd, C. H. Jakob, T. P. Schlachta, B. J. Hofmann, R. M. Reich and F. E. Kühn, *Catal. Sci. Technol.*, 2021, **11**, 795–799.
- 48 A. Lever, *Inorg. Chem.*, 1990, **29**, 1271–1285.
- 49 V. N. Nemykin, D. E. Nevonon, W. R. Osterloh, L. S. Ferch, L. A. Harrison, B. S. Marx and K. M. Kadish, *Inorg. Chem.*, 2021, **60**, 16626–16644.
- 50 S. Kal, S. Xu and L. Que Jr., *Angew. Chem., Int. Ed.*, 2020, **59**, 7332–7349.
- 51 J. M. Smith and J. R. Long, *Inorg. Chem.*, 2010, **49**, 11223–11230.
- 52 T. P. Schlachta, M. R. Anneser, J. F. Schlagintweit, C. H. Jakob, C. Hintermeier, A. D. Böth, S. Haslinger, R. M. Reich and F. E. Kühn, *Chem. Commun.*, 2021, **57**, 6644–6647.
- 53 P. Altmann, M. Cokoja and F. E. Kühn, *J. Organomet. Chem.*, 2012, **701**, 51–55.
- 54 A. Schmidt, N. Grover, T. K. Zimmermann, L. Graser, M. Cokoja, A. Pöthig and F. E. Kühn, *J. Catal.*, 2014, **319**, 119–126.



Cite this: *Chem. Soc. Rev.*, 2023, 52, 2238

## Cyclic iron tetra N-heterocyclic carbenes: synthesis, properties, reactivity, and catalysis

Tim P. Schlachta  and Fritz E. Kühn \*

Cyclic iron tetracarbenes are an emerging class of macrocyclic iron N-heterocyclic carbene (NHC) complexes. They can be considered as an organometallic compound class inspired by their heme analogs, however, their electronic properties differ, e.g. due to the very strong  $\sigma$ -donation of the four combined NHCs in equatorial coordination. The ligand framework of iron tetracarbenes can be readily modified, allowing fine-tuning of the structural and electronic properties of the complexes. The properties of iron tetracarbene complexes are discussed quantitatively and correlations are established. The electronic nature of the tetracarbene ligand allows the isolation of uncommon iron(III) and iron(IV) species and reveals a unique reactivity. Iron tetracarbenes are successfully applied in C–H activation, CO<sub>2</sub> reduction, aziridination and epoxidation catalysis and mechanisms as well as decomposition pathways are described. This review will help researchers evaluate the structural and electronic properties of their complexes and target their catalyst properties through ligand design.

Received 28th December 2022

DOI: 10.1039/d2cs01064j

[rsc.li/chem-soc-rev](http://rsc.li/chem-soc-rev)

### 1. Introduction

Since the first isolation of stable N-heterocyclic carbenes (NHCs) by A. J. Arduengo *et al.*,<sup>1,2</sup> they have been widely employed as ligands in coordination chemistry.<sup>3</sup> NHCs are subvalent compounds, as the divalent carbon atom exhibits an electron sextet.

The carbene carbon atom has an occupied  $\sigma$  orbital and an unoccupied  $p_z$  orbital. The  $\pi$ -electron-donating properties of the two adjacent nitrogen atoms stabilize the singlet ground state of the carbene carbon atom mesomerically by donating electron density into the empty  $p_z$  orbital and inductively by lowering the energy of the occupied  $\sigma$  orbital of the carbon atom with their  $\sigma$ -electron-withdrawing effects due to their higher electronegativity, also called +M/–I push–pull effect.<sup>4</sup> Due to their electron configuration, NHCs are known to be strong two-electron- $\sigma$ -donors but possess a weak  $\pi$ -acceptor character. NHCs are stronger  $\sigma$ -donors in comparison to widespread

*Technical University of Munich, School of Natural Sciences, Department of Chemistry and Catalysis Research Center, Molecular Catalysis, Lichtenbergstraße 4, 85748 Garching, Germany. E-mail: fritz.kuehn@ch.tum.de; Fax: (+49) 89 289 13247; Tel: (+49) 89 289 13096*



**Tim P. Schlachta**

Tim Pascal Schlachta obtained his BSc (2018) and MSc degree (2020) in chemistry at the Technical University of Munich (TUM). For completion of the master's program with honors, he received the Jürgen Manchot Study Award. From 2020 to 2022, he participated in the TUM: Junge Akademie scholarship program for exceptionally talented and dedicated students and investigated the energy consumption of online and on-site lectures. Since 2021, he has been a PhD student under the supervision of Fritz E. Kühn conducting research on the synthesis and reactivity of iron NHC complexes and their application in oxidation catalysis.



**Fritz E. Kühn**

Fritz E. Kühn received his doctoral degree as fellow of the Hermann-Schlosser-foundation (Degussa) at TUM in 1994, and worked at Texas A&M University as postdoctoral research associate supported by a Feodor Lynen-grant (Alexander von Humboldt-foundation). He finished his "Habilitation" at TUM in 2000. In 2005 he accepted a position as Principal Investigator at the Instituto Tecnológico e Nuclear (ITN) in Sacavém (Portugal). In Dec. 2006 he was appointed Professor of Molecular Catalysis at TUM. He is author/co-author of more than 500 publications and ca. 25 patents. His h-index is currently 66.

phosphane ligands, resulting in stronger metal-ligand bonding.<sup>5,6</sup> Therefore, NHC complexes often are less prone to oxidation and more thermally stable than their phosphane analogs.<sup>7–10</sup> In addition, the substitution of phosphane with NHC ligands can lead to a higher catalytic activity, as *e.g.* showcased in olefin metathesis or cross-coupling reactions.<sup>11–13</sup> These reactions led to a Nobel Prize, both in 2005 and in 2010, underscoring the significance of NHCs as ligands in catalysis, where 4d and 5d transition metal complexes play an important role.<sup>4,14</sup> However, the used precious metals are expensive and scarce. Hence, replacing those elements with earth-abundant metals is of major interest. The challenge is to match the skillset of the more expensive model catalysts, such as mild reaction conditions or catalytic activity. One potential candidate is iron, being the fourth most abundant element in the geosphere with 4.7%.<sup>15</sup>

Polydentate carbene complexes benefit from the strong  $\sigma$ -donation of multiple NHCs and a chelate effect. Thus, the ligand can support metals in high oxidation states, which often are important intermediates in catalytic reactions. Depending on the structural properties, metals in unusual high oxidation states and certain rare, reactive species can be isolated and characterized, such as  $\text{Fe}^{\text{V}}\equiv\text{N}$ ,<sup>16</sup>  $\text{Co}^{\text{IV}}\equiv\text{N}^{17}$  or  $\text{Ni}^{\text{IV}}\text{-halide}^{18}$  complexes, to name a few.<sup>19</sup>

Cyclic tetracarbenes are a subgroup amongst polydentate carbene ligands, resembling porphyrins structurally, but being electronically distinct. The first cyclic tetra(NHC) ligands have been implemented in catalysts around two decades ago, featuring complexes with, among others, Ag, Au, Pd, Pt, Co and Ni.<sup>20–24</sup> Tetracarbene complexes with iron can be seen as artificial heme analogs. Exploring their reactivity has attracted researchers since the last decade. Eventually mimicking the reactivity of their models in nature, extending the reaction scope, or even obtaining superior catalytic systems based on the different electronic properties of NHCs would be highly desirable. Reactions known to be catalyzed by biological iron porphyrins include oxygen transport and storage, electron transfer and oxidation/oxygenation reactions.<sup>25</sup> Artificial iron porphyrin complexes have extended this scope, for instance, with reduction reactions, such as oxygen or  $\text{CO}_2$  reduction.<sup>26,27</sup>

Certain aspects in the field of iron NHC complexes and polydentate NHC ligands have been reviewed in the past decade, which the reader is referred to for additional information. In 2012, high-valent iron-oxo and iron-nitrido complexes have been summarized, featuring mostly N-donor ligands but NHCs as well.<sup>28</sup> Another article in 2012 focused on fundamentals and applications of iron NHCs,<sup>29</sup> followed by a comprehensive review on the chemistry of iron NHCs in 2014.<sup>30</sup> In 2015, the role of high-valent iron(IV) in oxidation catalysis was described.<sup>31</sup> In the same year, polydentate NHC complexes of transition metals were reviewed,<sup>32</sup> extended by an article on polydentate NHC complexes of 3d metals in 2017.<sup>33</sup> Iron NHC complexes in C–H oxygenation and epoxidation reactions were illustrated in 2015 and 2016, respectively.<sup>34,35</sup> The role of iron(III)-hydroperoxo species in epoxidation<sup>36</sup> and piano-stool iron NHC complexes<sup>11</sup> have been discussed in 2017. In 2018, 3d metals in high oxidation state ligated by NHC ligands were summarized.<sup>19</sup>

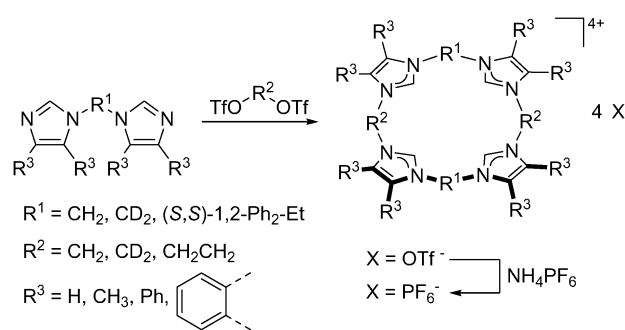
In the same year, a general overview on tetracarbene complexes was published.<sup>37</sup> Different factors determining the reactivity of high-valent  $\text{Fe}^{\text{IV}}=\text{O}$  species were theoretically reviewed both in 2019 and 2020.<sup>38,39</sup> Iron NHC complexes in homogenous catalysis were described twice in 2020,<sup>40,41</sup> followed by a summary of 3d metal NHC complexes in oxidation catalysis in 2022.<sup>42</sup>

As listed above, there are many reviews in the field of iron NHC complexes. However, the topic of iron tetracarbenes has only been loosely touched. This review aims to introduce the reader to the field of cyclic iron tetracarbenes and summarizes all articles published up to and including January 2023. Their synthesis and properties are described in-depth and, if applicable, structure-response relationships are discussed based on the complexes' reactivity and catalytic activity. These findings are expected to be helpful in future research, particularly in the area of ligand design by fine-tuning of the structural and electronic properties, to steer the reactivity and catalytic performance of the complexes.

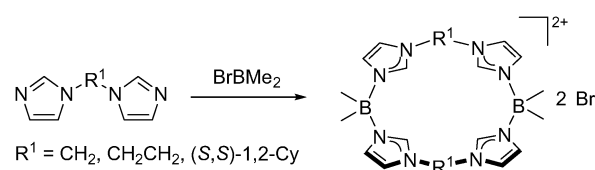
## 2. Synthesis

### 2.1. Ligand precursors

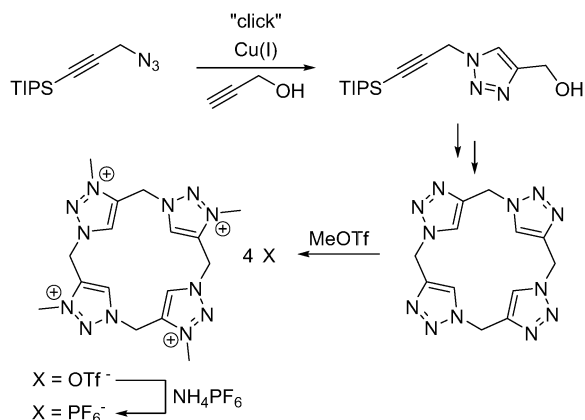
While cyclic tetracarbene complexes can be obtained *via* a template synthesis,<sup>23</sup> the common route involves the synthesis of the ligand precursor prior to complexation. First syntheses of macrocyclic imidazolium salts were reported around 20 years ago.<sup>20,43–45</sup> The synthetic strategy (Scheme 1) usually involves the synthesis of a bis(imidazolium) unit first. Two units are then connected using a coupling agent with good leaving groups, like triflate ( $\text{OTf}^-$ ), to form the macrocycle. In the case of imidazolylborane compounds, bromodimethylborane is used as coupling agent (Scheme 2). To avoid intermolecular coupling, dilute conditions can be applied (Ruggli-Ziegler dilution principle<sup>46</sup>).



Scheme 1 Synthesis of macrocyclic imidazolium salts.



Scheme 2 Synthesis of zwitterionic macrocyclic imidazolium salts.



Scheme 3 Synthesis of macrocyclic 1,2,3-triazolium salt.

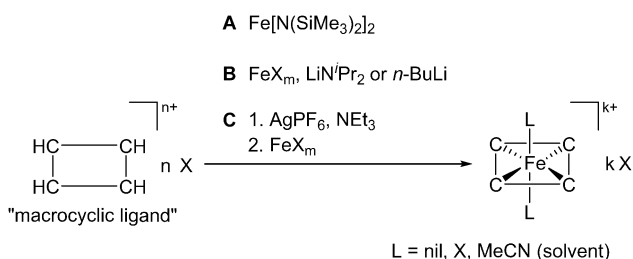
The synthesis of the macrocyclic 1,2,3-triazolium salt is following a multi-step synthesis involving the copper(I) catalyzed click reaction of a terminal alkyne with an azide as developed by the 2022 Nobel laureates Sharpless and Meldal (Scheme 3).<sup>47–52</sup> The calix[4]1,2,3-triazole is subsequently methylated using MeOTf.<sup>53</sup>

The imidazolium salts can be purified by anion exchange with the weakly coordinating anion hexafluorophosphate. This does not only increase the solubility of the macrocycle towards organic solvents, but also is an effective way to remove larger rings as side-products.<sup>54</sup> Additionally, the axial positions remain accessible to labile ligands or substrates after complexation, which is important for potential catalytic use of the complexes. Zwitterionic imidazolylborane macrocycles already exhibit good solubility in nonpolar solvents, which increases the range of solvents of their complexes for applications.<sup>55</sup>

## 2.2. Complex synthesis

The three routes followed for the synthesis of iron tetracarbene complexes are the direct metalation using an internal base (A, Scheme 4), the use of an external base (B) or the transmetalation (C). They also represent the most common ways in the field of iron NHC complexes.<sup>56</sup>

Direct metalation is an effective way to obtain the respective iron(II) complexes by use of the iron(II) precursor and internal base iron bis(trimethylsilyl)amide,  $\text{Fe}[\text{N}(\text{SiMe}_3)_2]_2$ .<sup>57</sup> The amide is a strong, non-nucleophilic base ( $\text{p}K_a \sim 26$ ),<sup>58</sup> which deprotonates the ligand precursor, while iron coordinates immediately to the formed carbenes. The resulting amine  $\text{HN}(\text{SiMe}_3)_2$  is easily removable in vacuum. Deprotonation of the imidazolium salts



Scheme 4 Synthetic routes to cyclic iron tetracarbene complexes.

requires slight excess of two equivalents of the iron precursor. This leads to an inorganic byproduct *e.g.*  $[\text{Fe}(\text{MeCN})_6](\text{PF}_6)_2$  if acetonitrile is used as solvent and hexafluorophosphate is applied as counterion.<sup>59</sup> The byproduct can be removed by filtration over a plug of silica or several washing steps.<sup>54,59–61</sup> A drawback of this route is the high sensitivity of the iron precursor towards oxygen and water, requiring inert conditions.<sup>62</sup>

A combination of an external base and iron halide is used when the iron precursor and internal base  $\text{Fe}[\text{N}(\text{SiMe}_3)_2]_2$  fails to fully deprotonate the imidazolium salt.<sup>63–66</sup> Bases of choice can be lithium diisopropylamide ( $\text{p}K_a \sim 36$ )<sup>67</sup> or *n*-butyllithium ( $\text{p}K_a \sim 50$ ).<sup>68</sup> Depending on the iron salts used, the respective iron(II) or iron(III) tetracarbenes are obtained. The latter usually contains one halide in axial position, which can be removed by reduction to the iron(II) tetracarbene with sodium amalgam.<sup>64</sup> Purification of the complexes by several extractions and filtration over Celite is necessary to separate them from the respective lithium salts as byproducts in this route.<sup>63</sup>

The transmetalation route is less frequently applied. The group of Jenkins used this strategy successfully to avoid selectivity issues during the deprotonation of the ligand precursor, due to similar  $\text{p}K_a$  values of the imidazolium protons and the ethylene bridge stereogenic protons.<sup>69</sup> In another case, the yield of an iron tetracarbene complex could significantly be increased by shifting from using an external base and iron halide to the transmetalation route with  $\text{AgPF}_6$ .<sup>70</sup> The obtained silver complexes can subsequently be treated with an iron halide and the formed silver halide be removed by filtration over Celite to receive the respective iron complexes.<sup>69,70</sup>

## 2.3. Summary

The macrocyclic ligand precursor is always synthesized prior to complexation. The respective iron tetracarbenes are mainly obtained through direct metalation using  $\text{Fe}[\text{N}(\text{SiMe}_3)_2]_2$  as internal base or iron halide in combination with a stronger external base if necessary. In special cases, transmetalation *via* the corresponding silver complexes may be an alternative.

## 3. Properties

All cyclic iron tetracarbene complexes reported in literature – all of them being a direct result of a complexation reaction described in 2.2 or a one-electron redox reaction of the former – are depicted in Fig. 1. Their ligands vary in ring size (16 or 18 membered), modifications in the NHC backbone and/or bridging units. Until recently, only tetracarbenes with imidazolylidenes have been reported. Complex 70 is the first abnormally coordinating iron tetracarbene with 1,2,3-triazole-5-ylidenes. The influence of these changes on the structural and electronic properties of the displayed iron complexes will be discussed in the following based on selected structural and spectroscopic parameters (Tables 1 and 2). The prerequisites for such parameters are, on the one hand, that they are meaningful and, on the other hand, that they are available in sufficient numbers for comparison, *i.e.* that they are routinely measured. Therefore, the  $^{13}\text{C}_{\text{NHC}}$  NMR signal, the

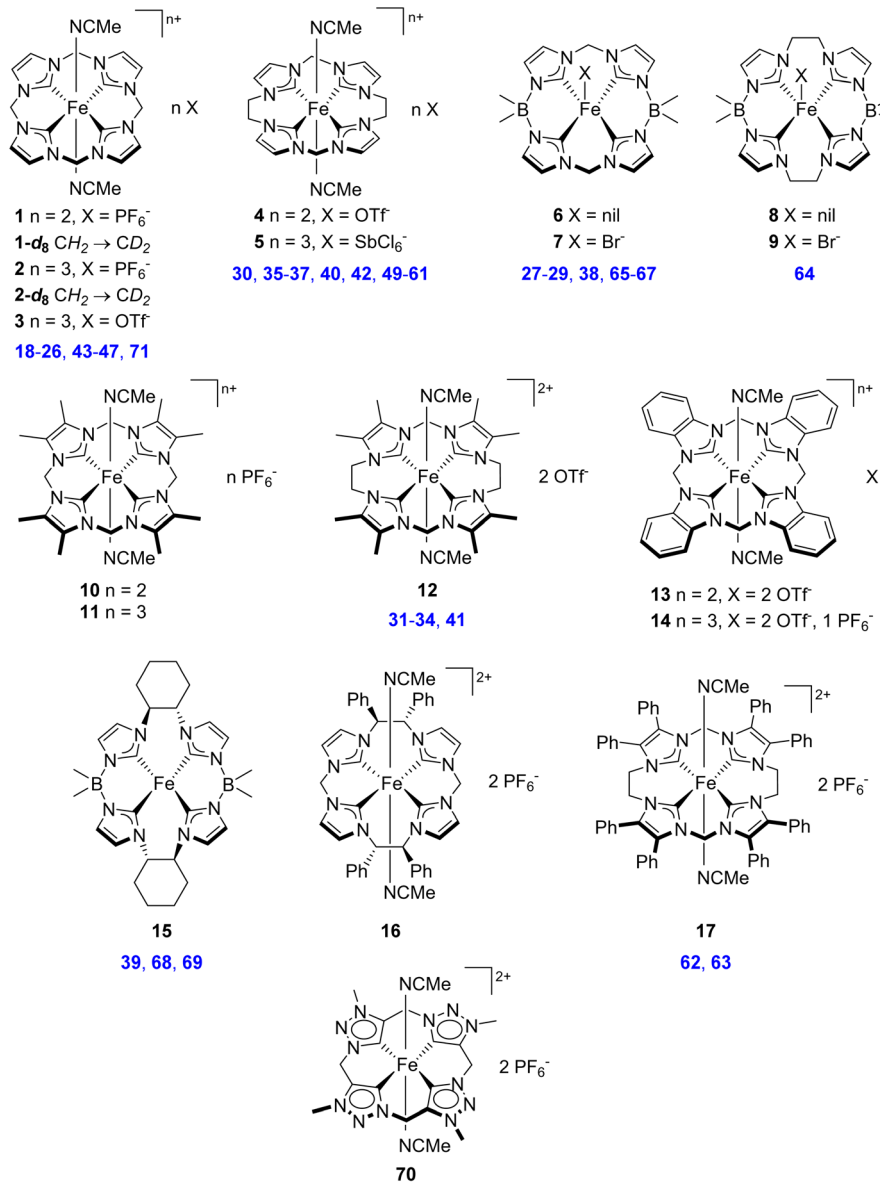


Fig. 1 Cyclic iron(II) and iron(III) tetracarbenes being a direct result of a complexation reaction described in 2.2 or a one-electron redox reaction of the former. The numbers of all other iron tetracarbene complexes are assigned to their primary iron tetracarbenes and are highlighted in blue.

$\text{Fe}^{2+}/\text{Fe}^{3+}$  half-cell potential, SC-XRD and Mössbauer spectroscopy are chosen to compare and discuss the structural and electronic properties of cyclic iron tetracarbenes. The resulting reactivity and catalytic performance of the complexes will be showcased in Sections 4 and 5, respectively.

### 3.1. $^{13}\text{C}_{\text{NHC}}$ NMR signal

The chemical shift of the carbene signal in the  $^{13}\text{C}$  NMR is quite sensitive towards changes in the electronic properties of the metal center, which gave rise for Huynh *et al.* to introduce this observation as Huynh Electronic Parameter (HEP).<sup>84</sup> The HEP measures the shift of the  $^{13}\text{C}_{\text{NHC}}$  signal of a reference NHC ligand in a hetero-bis-NHC palladium complex, where the opposing NHC ligand in *trans* position is formally exchanged (Fig. 2). Based on the shift of the reference carbene in the

$^{13}\text{C}$  NMR, the  $\sigma$ -donation strength of the new ligand can be assessed, where a downfield shift is assigned to a strong  $\sigma$ -donation and *vice versa*. Free NHCs possess large downfield carbene chemical shifts of  $>200$  ppm. In the free carbene, the probability of a transition of an electron from the occupied  $\sigma$  orbital to the formally empty  $p_z$  orbital, singlet-triplet transition, is higher. This transition is contributing the most to the paramagnetic shielding term, resulting in the observed downfield shift.<sup>85</sup> Upon coordination to a metal center, the carbene experiences a significant upfield shift, as the lone pair of the NHC is coordinating into the empty metal orbitals, reducing the likelihood of the singlet-triplet transition. In contrast, when a strong  $\sigma$ -donor ligand is placed in *trans* position of the reference NHC ligand of the palladium complex, the Pd-reference NHC bond is weakened, leading to a more pronounced “free carbene” character and thus

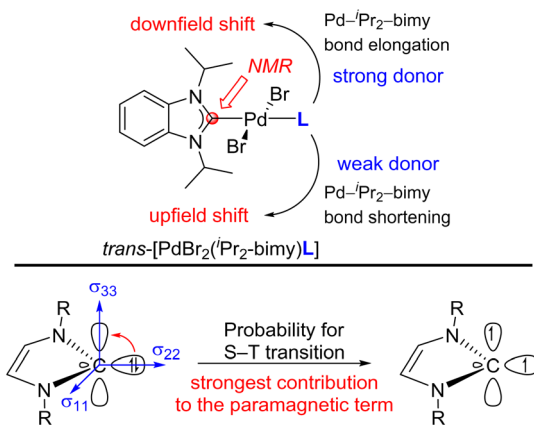


Fig. 2 Working principle of HEP.<sup>86</sup>

downfield shift of the  $^{13}\text{C}$  carbene signal of the reference ligand.<sup>86,87</sup>

The argumentation of the HEP is partly applied in the following, but due to the equatorial cyclic symmetrical ligands, no opposing NHC ligand with different donor properties is present and hence, no *trans* effect is occurring. Therefore, the chemical shift of the tetracarbene ligands (Fig. 3) is explained by a major contribution of the diamagnetic shielding term, influenced by backbone and wingtip/bridging unit modifications. The decreased paramagnetic shielding term explains the upfield shift of the  $^{13}\text{C}_{\text{NHC}}$  signals upon coordination and increasing Lewis acidity of the iron center (Fig. 4).<sup>85</sup> The  $^{13}\text{C}_{\text{NHC}}$  signals of the tetracarbene ligands from the iron complexes shown in Fig. 1 are ranked against each other in Fig. 3. The chemical shift is a suitable indicator of the electron donating capabilities of the tetracarbene ligands towards the iron center, as long as the electronic surroundings of the complex are comparable, *i.e.* exhibiting the same axial ligands.

Modifications of the imidazole backbone have a significant influence on the electronic donating properties of tetracarbene

ligands. Free benzimidazolylienes have a slightly smaller singlet-triplet gap than imidazolylienes, which results in a larger downfield shift of the former ( $\sim 223\text{--}232$  ppm) in comparison to the latter ( $\sim 211\text{--}221$  ppm). The observed shift differences vary therefore between *ca.* 10 and 20 ppm.<sup>87</sup> The benzimidazolyliene ligand of **13** ( $\delta(^{13}\text{C}) = 216$  ppm) is shifted downfield 11 ppm in comparison to the imidazolyliene ligand of **1** ( $\delta(^{13}\text{C}) = 205$  ppm, Fig. 3). The chemical shift of  $^{31}\text{P}$  or  $^{77}\text{Se}$  in the respective phosphinidene adducts and selenoureas can be used to report the  $\pi$ -accepting properties of NHCs, where an upfield shift is correlated with primarily  $\sigma$ -donation and *vice versa*.<sup>87–89</sup> Benzimidazolyliene appears to be a slightly better  $\pi$ -acceptor than imidazolyliene, based on their  $^{31}\text{P}$  or  $^{77}\text{Se}$  chemical shifts, which might explain part of the observed downfield shift of **13**. However, in general, all NHC units of the tetracarbene ligands mentioned in this review are in a range of rather low to negligible  $\pi$ -backdonation,<sup>87</sup> therefore the changes in electronic properties are dominated by the  $\sigma$ -donation of the tetracarbenes. The  $-M$  effect of the enlarged aromatic ring of the benzimidazolyliene ligand is lowering the electron density at the carbene carbon atom, resulting in the downfield shift of **13** in comparison to **1** (Fig. 3), due to diamagnetic deshielding. In contrast, the methyl groups in the backbone of **10** donate electron density to the carbene carbon atom with their  $+I$  effect, increasing the diamagnetic shielding term and leading to an upfield shift of the  $^{13}\text{C}_{\text{NHC}}$  signal of about 1 ppm, compared to **1**. The uncertainty of a  $^{13}\text{C}$  NMR measurement is expected to be below 0.1 ppm, hence using three times the weighted standard deviation, a difference of  $>0.4$  ppm is required for a significant difference, exceeding statistic uncertainty.<sup>84</sup> Therefore, **1** and **10** show a sufficiently different chemical shift to be discussed, whereas **1** and **1-d<sub>8</sub>** lay within the  $3\sigma$  interval and have to be considered as equal with respect to the error range. **4** and **12** follow the same pattern ( $\Delta\delta(^{13}\text{C}) = 3$  ppm) as **1** and **10**, but both are upfield shifted *ca.* 7–8 ppm due to the larger  $+I$  effect of the ethyl wingtips. The upfield shift of **17** is unexpected, as the enlarged aromatic system

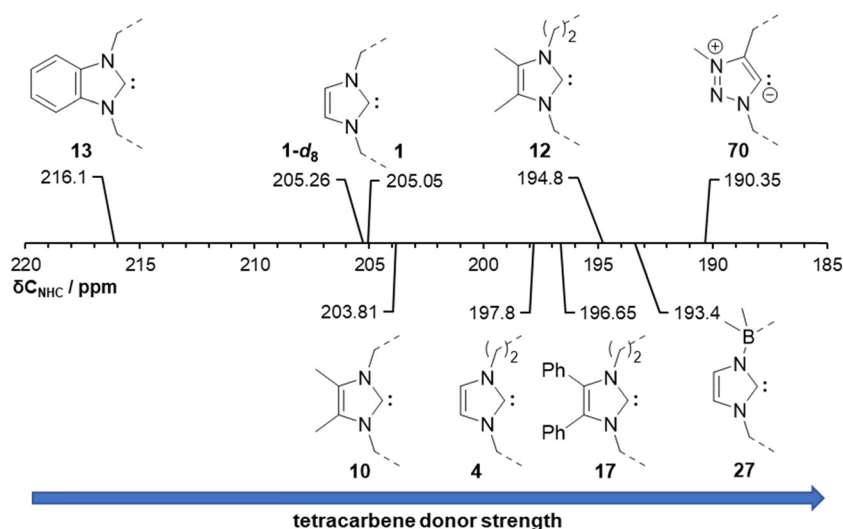


Fig. 3  $^{13}\text{C}$  NMR carbene signals of iron tetracarbenes with MeCN as axial ligands.

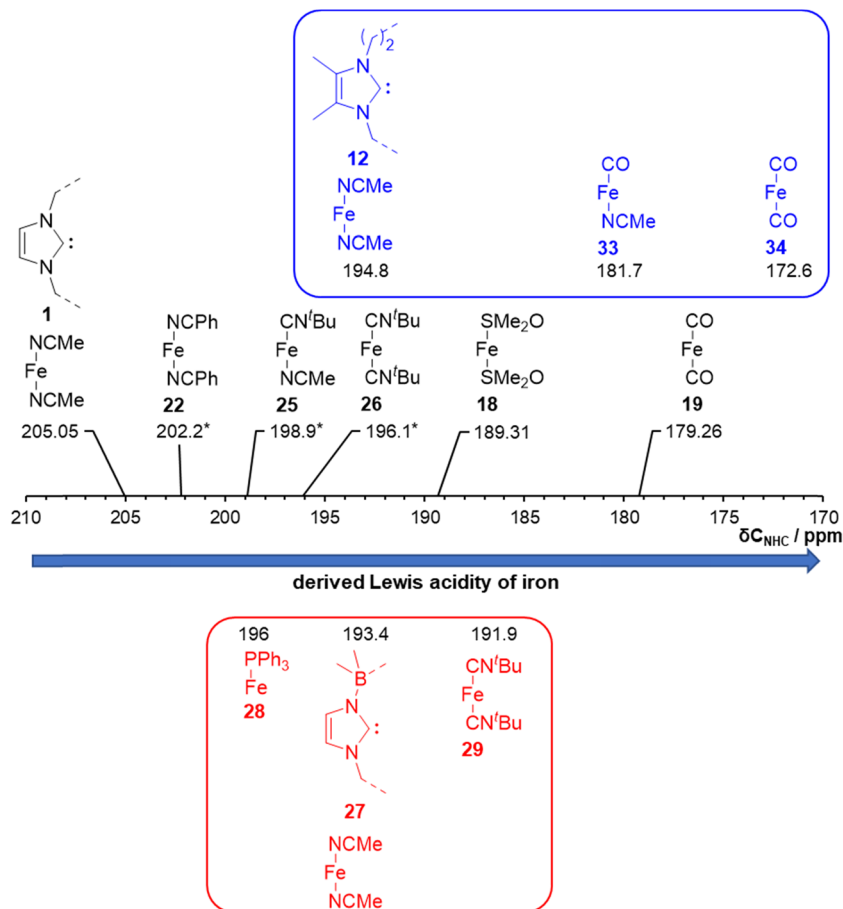


Fig. 4 Effect of axial ligand exchange on the  $^{13}\text{C}$  NMR carbene signals of iron tetracarbenes. The colors black (**1**), red (**27**) and blue (**12**) represent the same tetracarbene frameworks. Signals marked with \* were measured in acetone- $d_6$ . The Lewis acidity of iron can only be compared between the same tetracarbene frameworks.

with the two phenyl groups in the backbone is supposed to result in a downfield shift, as is the case for **13**. SC-XRD reveals that the phenyl rings are twisted and not in the same plane as the imidazole ring, which is known for similar compounds as well,<sup>90,91</sup> and probably makes  $\pi$  interactions unfavorable.<sup>65,92</sup> The imidazolylborane ligand of **27** (Scheme 6) exhibits the second highest electron donating properties in this series with a chemical shift of 193.4 ppm, due to the strong +I effect of the negatively charged boron bridging unit. The abnormally coordinating NHC (aNHC) ligand of **70** shows the highest donating capability, which can be explained by the removal of one adjacent electron-withdrawing nitrogen atom, increasing the electron density at the carbene atom. HEP for biscarbene systems and Tolman electronic parameter data are in line with the discussed electronic trends.<sup>87,93,94</sup>

The  $^{13}\text{C}_{\text{NHC}}$  signal is further influenced by the oxidation state of the iron center and by exchanging the axial ligands of the iron tetracarbene complex. For instance, a higher oxidation state in an Fe–N–Fe complex led to an upfield shift of the carbene signal from 187.5 ppm for  $\text{Fe}^{\text{III}}\text{–N–Fe}^{\text{III}}$  (**55**, Scheme 22) to 163.7 ppm for  $\text{Fe}^{\text{IV}}\text{–N–Fe}^{\text{IV}}$  complex (**58**, Scheme 22) (see Section 4.5).<sup>83</sup> This can be explained by the higher Lewis acidity of the iron center at higher oxidation states leading to a larger upfield shift of the  $^{13}\text{C}_{\text{NHC}}$  signal due to a lower paramagnetic

shielding term, and lower Fe  $\rightarrow$  NHC backbonding.<sup>83,85,86,89</sup> The significant shift of the  $^{13}\text{C}_{\text{NHC}}$  signal upon exchange of the axial ligands of one iron tetracarbene framework (Fig. 4 and Table 2) can also be explained with the Lewis acidity of iron. Upon complexation of a NHC ligand, part of the electronic density is transferred to the iron center by  $\sigma$ -donation, which leads to the observed upfield shift, a less likely singlet-triplet transition and therefore smaller paramagnetic shielding term.<sup>85</sup> This effect appears to be more pronounced with an increased Lewis acidic center “pulling” the electron density. A stronger electron donating ligand, *e.g.*  $\sigma$ -donor  $\text{PPh}_3$  (**28**), results in a downfield shift of the carbene signal and a more accepting ligand, *e.g.*  $\pi$ -acceptor  $\text{CN}^t\text{Bu}$  (**29**, Scheme 6), leads to an upfield shift with increased Lewis acidity of iron. Once the tetracarbene framework remains the same, the  $^{13}\text{C}_{\text{NHC}}$  chemical shift can be used to rank the electronic properties of different axial ligands and to estimate the resulting Lewis acidity of the iron center within this series.

The observed differences in the chemical shift of the  $^{13}\text{C}_{\text{NHC}}$  signal might also evolve through a higher diamagnetic shielding of the carbene carbon atom, complementary to a decreased paramagnetic shielding term: To compensate the electron density loss at the iron center upon coordination of an electron

withdrawing axial ligand, the carbene carbon atom experiences a higher diamagnetic shielding, *i.e.* higher electron density ( $\rightarrow$ upfield shift), as the electron density is drawn/donated from the residual carbene ring system and the wingtips. This leads to a reduced electron density at these positions and diamagnetic deshielding ( $\rightarrow$ downfield shift). Indeed, the  $^{13}\text{C}$  signals of the backbone (CH) are downfield shifted 2 ppm from **1** ( $\delta(^{13}\text{C}) = 122.62$  ppm) to bis(DMSO) complex **18** ( $\delta(^{13}\text{C}) = 124.57$  ppm) and bis(CO) complex **19** ( $\delta(^{13}\text{C}) = 124.49$  ppm, Scheme 5). The wingtip ( $\text{CH}_2$ )  $^{13}\text{C}$  signals remain rather constant.<sup>59</sup> In a similar fashion, the downfield shift of the  $^{13}\text{C}$  signals of the backbone (CH) of **12** ( $\delta(^{13}\text{C}) = 128.2; 126.6$  ppm) increase upon addition of one CO (**33**:  $\delta(^{13}\text{C}) = 128.6; 127.4$  ppm) and two axial CO ligands (**34**:  $\delta(^{13}\text{C}) = 130.1; 128.3$  ppm, Scheme 7).<sup>61,79</sup> Another downfield shift can be observed in the backbone of the diiron(III)- $\mu_2$ -nitrido complex (**55**:  $\delta(^{13}\text{C}) = 123.0; 122.5$  ppm) upon higher oxidation state and Lewis acidity of the iron centers in diiron(IV)- $\mu_2$ -nitrido complex (**58**:  $\delta(^{13}\text{C}) = 126.8; 126.9$  ppm, Scheme 22).<sup>83</sup> The rather small difference in  $^{13}\text{C}_{\text{NHC}}$  signals in the series of the neutral iron tetracarbene **27** (Scheme 6) does not lead to noticeable changes in the backbone  $^{13}\text{C}$  signals.

The showcased trends in Fig. 4 are in accordance with HEP and TEP parameters, where available.<sup>84,87,93</sup> CO is at the end of the row with the strongest  $\pi$ -accepting properties in the two series developed from **1** and **12**, reducing the electron density at the iron center and increasing its Lewis acidity. The correlation of the Lewis acidity of the metal center with the  $^{13}\text{C}_{\text{NHC}}$  chemical shift was established for various other

complexes as well, apart from the bis-NHC palladium complex of HEP.<sup>85,95,96</sup>

### 3.2. Half-cell potential

Redox potentials of complexes can be influenced by the electronic properties of the surrounding ligands. In fact, experimentally determined parameters of the respective ligands (Lever electronic parameter)<sup>97</sup> can be used to predict the redox potential of a complex of interest.<sup>87,98</sup> By formally exchanging one ligand in a complex while keeping the co-ligands the same, the difference in the redox potentials of the two complexes can provide information about the donor strength of the different ligands, with a lower redox potential being due to a stronger donor. This effect is related to the ability of the ligand to facilitate the redox process, *e.g.* oxidation from  $\text{Fe}^{\text{II}}$  to  $\text{Fe}^{\text{III}}$  in the case of iron complexes, and to stabilize the new (higher) oxidation state,  $\text{Fe}^{\text{III}}$ .<sup>87</sup> Therefore, the half-cell potential  $E_{1/2}$  of the  $\text{Fe}^{2+}/\text{Fe}^{3+}$  redox couple is another useful parameter to rank the different electronic properties of cyclic iron tetracarbenes.

The different redox potentials of mononuclear iron tetracarbenes are listed in Fig. 5, as well as Tables 1 and 2. Interestingly, while the  $^{13}\text{C}_{\text{NHC}}$  signal of **70** is more upfield shifted in comparison to **27** (Scheme 6), the latter exhibits a more negative redox potential. On the other end, the benzimidazolylidene ligand of **13** is reducing the electron density of the iron center the most, resulting in the highest half-cell potential amongst the tetracarbene ligand modifications. Similar to 3.1, the axial ligands can significantly affect the redox properties of an iron tetracarbene

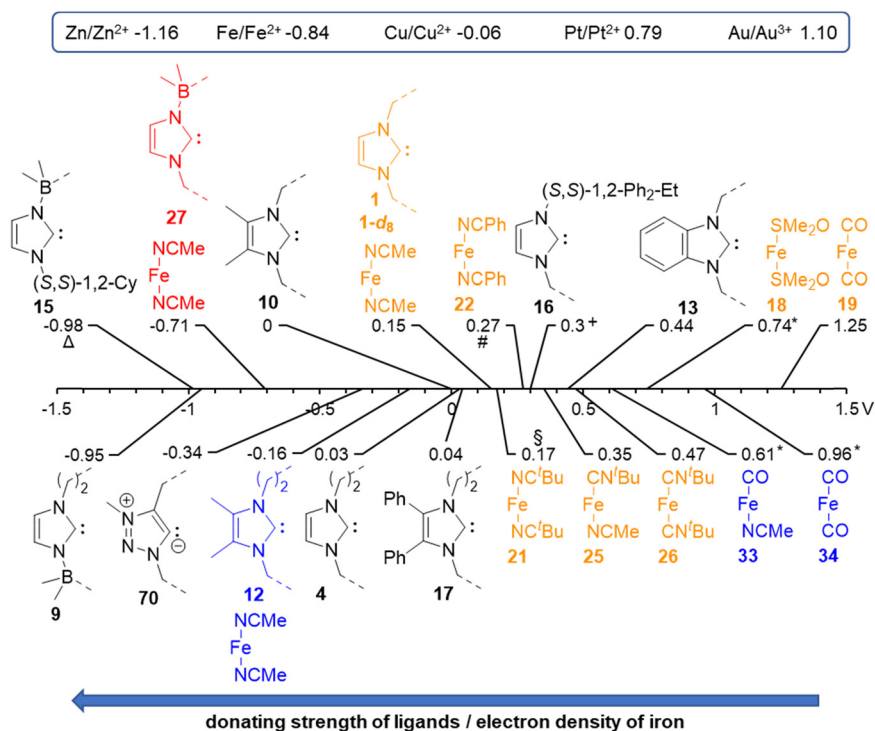


Fig. 5 Effect of the electronic surroundings on the half-cell potential  $E_{1/2}$  of iron tetracarbenes (V versus  $\text{Fc}/\text{Fc}^+$ ). The colors red (**27**), blue (**12**) and orange (**1**) represent the same tetracarbene frameworks and indicate axial ligand exchange. \* Oxidation potentials only.  $\Delta$  measured in THF.  $\S$  measured in  $^t\text{BuCN}$ . # measured in PhCN. + estimated graphically. Standard potentials of selected metals as comparison referenced to  $\text{Fc}/\text{Fc}^+$ .<sup>99</sup>

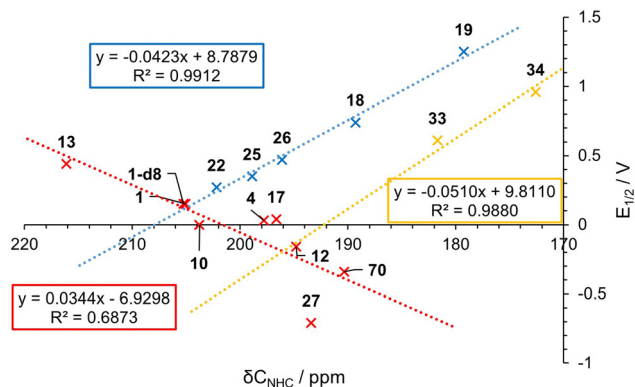


Fig. 6 Correlation of the  $^{13}\text{C}_{\text{NHC}}$  chemical shift and redox potential of iron tetracarbenes. Iron complexes with variable tetracarbene ligands are marked red and with variable axial ligands marked blue (based on **1**) and yellow (based on **12**). Oxidation potentials for **18**, **33** and **34**. **22**: CV measured in PhCN. **22**, **25** and **26**:  $^{13}\text{C}$  NMR measured in acetone- $d_6$ .

complex. For example, the two axial CO ligands of **19** (Scheme 5) as strong  $\pi$ -acceptors induce a maximum redox potential of 1.25 V.

The  $^{13}\text{C}_{\text{NHC}}$  chemical shift can be set in correlation to the redox potential (Fig. 6). Iron tetracarbene complexes with variations of the tetracarbene ligands are marked red. A stronger  $\sigma$ -donor tetracarbene results both in an upfield shift of the  $^{13}\text{C}_{\text{NHC}}$  signal and a lower half-cell potential. In return, axial ligand modifications, marked blue (based on **1**) and orange (based on **12**), steer the Lewis acidity of the iron center when the tetracarbene ligand remains unchanged. As discussed above, a higher Lewis acidity, *i.e.* less electron rich iron center, leads to an upfield shift of the  $^{13}\text{C}_{\text{NHC}}$  signals and a higher redox potential, *i.e.* hindered redox process and less stabilized  $\text{Fe}^{\text{III}}$  oxidation state.

A change of the equatorial tetracarbene ligands follows a rather loose linear trend (Fig. 6). In contrast, substitution of the axial ligands of a remaining iron tetracarbene framework appears to have a nearly linear correlation, especially when more datapoints are available, as it is the case for the series of **1**. Here, once one parameter is known, *e.g.* the  $^{13}\text{C}_{\text{NHC}}$  signal, the other variable, in this case the redox potential, can be calculated.

### 3.3. SC-XRD

Most of the published iron tetracarbenes are characterized by SC-XRD (Tables 1 and 2). Here, useful information about the structural and electronic properties of the complex can be obtained.

The rigidity of a ligand is a crucial factor for the reactivity of the complex. The  $\text{Fe}-\text{C}_{\text{NHC}}$  bond lengths can be used as a rule of thumb for the rigidity of the ligand, especially for similar tetracarbene frameworks. A smaller, more rigid ligand enables closer interaction of the carbene carbon with the iron center, while a larger ligand might experience a higher internal steric tension upon coordination, and thus creates a larger macrocycle around the iron center with elongated  $\text{Fe}$ -carbene bonds. The iron complex **2** is a highly active precursor for epoxidation of olefins (see Section 5.3),<sup>73</sup> supported by a rigid 16-membered

tetracarbene ligand. For C-H oxidation and epoxidation reactions, a higher ligand rigidity has been attributed to a higher activity, selectivity and stability of the catalysts.<sup>100–102</sup> The 18-membered tetracarbene of **4** ( $(\text{Fe}-\text{C}_{\text{NHC}})_{\text{av}} = 1.996(11) \text{ \AA}$ ) is stabilizing an  $\text{Fe}^{\text{IV}}=\text{O}$  complex (**42**, Scheme 11) through intramolecular hydrogen bonds between the ethylene bridges and the oxygen atom<sup>60</sup> and probably to a certain extent steric shielding due to the bent ligand (Fig. 10). This has not been reported in the oxygen transfer reactions of the more rigid equivalent iron tetracarbene **1** ( $(\text{Fe}-\text{C}_{\text{NHC}})_{\text{av}} = 1.907(3) \text{ \AA}$ ), even though hydrogen bonding was also assumed for this tetracarbene framework in an iron(III)-superoxo adduct (**43**, Fig. 11).<sup>74</sup> While **8** ( $(\text{Fe}-\text{C}_{\text{NHC}})_{\text{av}} = 1.990(12) \text{ \AA}$ ) is capable of catalyzing aziridination reactions,<sup>64</sup> its more rigid 16-membered analog **6** ( $(\text{Fe}-\text{C}_{\text{NHC}})_{\text{av}} = 1.940(2) \text{ \AA}$ ) is ineffective for this reaction.<sup>76</sup> This can be explained by the proposed mechanism, which requires a flexible ligand (Scheme 33).<sup>103</sup> In return, the strong  $\sigma$ -donation and rigidity of the smaller tetracarbene of **6** allows to stabilize five-coordinate iron(IV) imide complexes as proposed intermediates in aziridination.<sup>76</sup>

Upon higher oxidation states of the iron center within one ligand system, the  $\text{Fe}-\text{C}_{\text{NHC}}$  bond lengths can become slightly up to significantly elongated in terms of statistic uncertainty (*i.e.* three times the weighted standard deviation for the latter). For example, the oxidation from iron(II) to iron(III) results in lengthening of the  $\text{Fe}-\text{NHC}$  bonds from 1.907(3)  $\text{ \AA}$  for **1**, to 1.941(2)  $\text{ \AA}$  for **2**. This is contrary to expectations, as the stronger Lewis acidity of iron should lead to a stronger bound tetracarbene as Lewis base and thus a shorter  $\text{Fe}-\text{NHC}$  bond. In fact, this observation is likely due to the removal of an electron from a molecular orbital involved in  $\text{Fe} \rightarrow \text{NHC}$  backbonding, resulting in diminished backbonding and weaker  $\text{Fe}-\text{NHC}$  interaction and consequently a longer  $\text{Fe}-\text{NHC}$  bond.<sup>83,104,105</sup> A holistic analysis can however become quite complex.<sup>104</sup>

A weakening of the  $\text{MeCN}-\text{Fe}$  bond in dependence to the  $\sigma$ -donation strength of the tetracarbene, as one might expect based on HEP,<sup>86</sup> cannot be found. However, the significant impact of the axial ligands on the Lewis acidity of iron, as described above, can partly be monitored by means of the  $\text{Fe}-\text{X}$  bond lengths. For example, the  $\text{Fe}-\text{CO}$  length increases from 1.717(4)  $\text{ \AA}$  (**33**) to 1.803(11)  $\text{ \AA}$  (**34**, Scheme 7) upon formal substitution of MeCN of **33** with a second CO ligand, resulting in two axial ligands competing for  $\pi$ -backbonding. This elongation in the  $\text{Fe}-\text{X}$  bonds can also be observed between mono and bis  $\text{CN}^t\text{Bu}$  substituted iron tetracarbenes **25** and **26**, respectively (Scheme 5). Here, the length is increased from 1.819(3)  $\text{ \AA}$  for mono substituted **25** to 1.868(8)  $\text{ \AA}$  for bis  $\text{CN}^t\text{Bu}$  containing **26** with shared  $\pi$ -backbonding. Due to the same tetracarbene frameworks of each pair of complexes, the slight decrease of the  $\text{Fe}-\text{C}_{\text{NHC}}$  bonds for both bis substituted compounds, **34** and **26**, might be related to the higher Lewis acidity of the iron center.

The *trans* NHC- $\text{Fe}$ -NHC angles give useful information about the geometry of the iron tetracarbene complex. While the common angle converges to 180°, the smaller angles of **7** (155.29(11)°) and **9** (153.12(67)°) reveal that the iron is slightly out of plane of the macrocyclic carbene atoms. This is supported

by the NHC–Fe–X angle, which is deviating from the usual  $\sim 90^\circ$  degrees. The typical X–Fe–X angle is converging  $180^\circ$  as well; deviations can be a sign for a larger steric demand of the axial ligands or the tetracarbene.

Generally speaking, no significant correlation between the Fe–NHC bond length and the Lewis acidity of the iron center controlled by the  $\sigma$ -donation strength of the tetracarbene ligand or axial ligand exchange can be found across the different iron tetracarbene complexes. A relation of the Fe–NHC bond length and the Lewis acidity can only be found, when changing the oxidation state of the iron center – and thus the Lewis acidity – within one system, *i.e.* keeping the same ligand framework (*vide supra*). Instead, the Fe–NHC bonds are highly dependent on the geometry of the surrounding tetracarbene. Furthermore, it has to be considered, that structural parameters in SC-XRD are affected by various factors like the quality of the single crystals, crystal packing, temperature of analysis and presence of solvates.<sup>86</sup> Therefore, the  $^{13}\text{C}_{\text{NHC}}$  signal and half-cell potentials are more suitable and sensitive measures regarding the electronic properties of iron tetracarbenes. Nevertheless, using SC-XRD, unexpected electronic properties can be explained, *e.g.* the upfield shift of the  $^{13}\text{C}_{\text{NHC}}$  signal of 17 in relation to the other signals in Fig. 3 due to suppressed  $-M$  effect of the out of plane aligned phenyl rings.

### 3.4. Mössbauer spectroscopy

Mössbauer spectroscopy, often supported by DFT calculations, is useful for gaining further information on the electronic properties of iron tetracarbenes, allowing to make statements concerning oxidation state, spin state and electronic surroundings of iron tetracarbenes.<sup>106–108</sup> EPR is usually conducted in addition to Mössbauer measurements to identify the spin state of the complex. Magnetic susceptibility measurements through SQUID magnetometry and Evans NMR spectroscopic method<sup>109</sup> can confirm the spin state assignment.

The isomer shift  $\delta$  and electronic quadrupole splitting  $|\Delta E_Q|$  are the two parameters that are usually of interest. The isomer

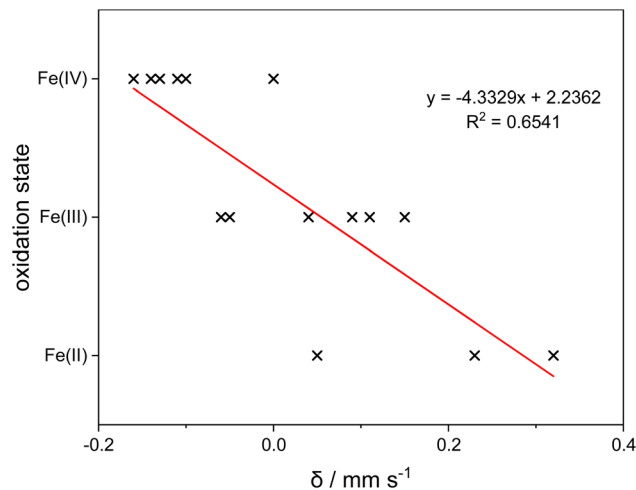


Fig. 8 Correlation of the isomer shift and the oxidation state of iron tetracarbenes based on the tetracarbene framework of **4**. While there is some overlap in the ranges of measured isomer shift associated with each oxidation state, the overall trend is still discernible.

shift is proportional to the electron density at the iron atom, which primarily originates from the 4s-electrons at the nucleus. The isomer shift is significantly affected by the oxidation state, in fact, a (nearly) linear negative correlation between the isomer shift and the oxidation state of the iron atom has been observed for a series of iron cyclam (1,4,8,11-tetraazacyclotetradecane) and iron (oxo) tetracarbene complexes (Fig. 7 and Table 1).<sup>60,61,110</sup> For such relations it is important to keep variations in the coordination sphere of the iron complexes at a minimum.<sup>110</sup> The overall trend is, however, discernible even for a larger group of iron tetracarbenes based on the tetracarbene framework of **4** (Fig. 8 and Tables 1, 2). The above described observation can be explained by the increased shielding of the nuclear potential of iron in lower oxidation states by more electrons in the valence shell, *e.g.* six 3d-electrons of iron(II) in comparison to five 3d-electrons of iron(III). Therefore, more expansion of the s-orbitals is allowed, which results in a lower electron density around the nucleus and thus larger (more positive) isomer shift of the complex with lower oxidation state.<sup>106</sup>

For a holistic interpretation of the isomer shift, the iron–ligand bond lengths, electronic properties of the ligands (somewhat related to the former), coordination number and structural properties, have to be considered. The coordination of the ligand to the iron atom leads to a compression of the radial distribution of the 3s- and 4s-iron orbitals, which changes the electron density at the nucleus. Four-fold coordination induces shorter Fe–ligand bonds and, because of the accompanying higher compression of the s-orbitals resulting in a higher electron density, a lower (more negative) isomer shift, in comparison to six-fold coordination and longer Fe–ligand bonds. High-spin states afford longer bond lengths and higher isomer shifts as opposed to low-spin states.<sup>106</sup> The electronic properties of the surrounding ligands also play a crucial role and are partly related to the iron–ligand bonds. While the Fe–NHC bonds are more dependent on the geometry and rigidity of the tetracarbene

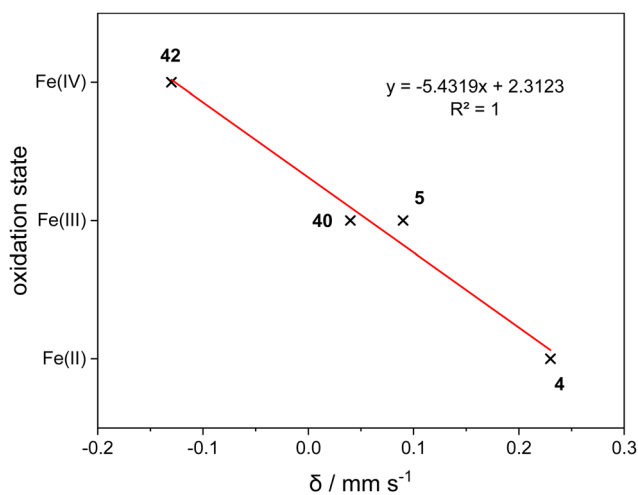


Fig. 7 Nearly linear correlation of the isomer shift and the oxidation state between a series of iron (oxo) tetracarbenes, **4**, **5**, **40**, **42**.<sup>60,61</sup>

(see Section 3.3), the iron–axial ligand bonds are more proportional to the respective axial ligand's electronic characteristics. The strong  $\sigma$ -donation of the equatorial tetracarbene into the 4s-orbital of iron is demonstrated by the significantly lower isomer shifts (Table 1), in comparison to tetradentate N-donor ligands ( $\Delta\delta > 0.2 \text{ mm s}^{-1}$ ).<sup>60,110</sup> Strong  $\pi$ -accepting axial ligands are effectively depopulating the 3d-orbitals, consequently deshielding the 4s-iron orbital and, in addition to the compression due to expected shorter Fe–X bond lengths, result in a lower isomer shift of the iron tetracarbene.<sup>81</sup> Iron(II) complexes **33** and **34** (Scheme 7) illustrate this effect in an extreme manner with one and two axial CO ligands as strong  $\pi$ -acceptors, respectively. The isomer shift is significantly lowered from  $0.23 \text{ mm s}^{-1}$  for **12** (Table 1) upon exchange of axial MeCN with one CO to  $0.00 \text{ mm s}^{-1}$  for **33** and with two CO ligands to  $-0.04 \text{ mm s}^{-1}$  for **34** (Table 2). The structural properties of the iron tetracarbene further play a decisive role. For instance, the metal centered reduction of iron nitrosyl complex **35** to **36** (Scheme 8) not only leads to a larger shielding of the s-orbitals but the iron atom is somewhat more displaced from the equatorial plane of the tetracarbene in **35**. Hence, the  $\sigma$ -interactions of the iron center with the tetracarbene are reduced. Both effects result in a lower electron density at the nucleus and a higher isomer shift. However, in this particular case, the described effects are counterbalanced by shorter Fe–NHC bonds and increased  $\pi$ -backbonding of the axial NO ligand in **36**, inducing a higher electron density at the iron and deshielding of the 4s-orbital, respectively. Therefore, the isomer shift nearly stays the same with  $-0.01 \text{ mm s}^{-1}$  for **35** and  $0.02 \text{ mm s}^{-1}$  for **36**.<sup>81</sup> This is a good example of the fact that a correct interpretation of the isomer shift is only possible if all aspects are taken into account, since at first glance this marginal change in isomer shift could also have indicated a ligand centered reduction, which would not have been unusual.<sup>81,111,112</sup>

Quadrupole splitting  $|\Delta E_Q|$  is occurring when an electronic field gradient is present at the Mössbauer nucleus.<sup>107,113</sup> Iron tetracarbenes often show high quadrupole splitting because of the oblate (disk-shaped) charge distribution around the iron nucleus due to the large electronic charge donation into the Fe  $3d_{x^2-y^2}$  orbital by the equatorial tetracarbene.<sup>114</sup> This effect is more pronounced for tetracarbenes than for most N-donor ligands, likely due to the strong  $\sigma$ -donor properties of the former, which is showcased in the significantly larger quadrupole splitting of iron(IV)-oxo complex **42** ( $|\Delta E_Q| = 3.08 \text{ mm s}^{-1}$ , Scheme 11) in comparison to the majority of other iron(IV)-oxo complexes ( $0.16\text{--}1.39 \text{ mm s}^{-1}$ ).<sup>28,60,115</sup> When the electric field is more spherically symmetric distributed around the nucleus, a smaller quadrupole splitting can be observed: Upon reduction of **35** to **36** (Scheme 8), the quadrupole splitting is significantly decreased from  $2.36 \text{ mm s}^{-1}$  for **35** to  $0.85 \text{ mm s}^{-1}$  for **36**. The change can be assigned to the displacement of iron out of the tetracarbene plane in the latter complex, decreasing the charge donation of the tetracarbene, and thus decreasing the anisotropy.<sup>81</sup> The decline of the quadrupole splitting in the series of iron carbonyl complexes from 2.19 for **4** (Table 1), 1.76 for **33** (one axial CO) and 0.98  $\text{mm s}^{-1}$  for **34** (two axial CO, Table 2, Scheme 7)

corresponds to the more spherically symmetric electron distribution around the iron center presumably due to the strong  $\pi$ -accepting carbonyl moieties, balancing the charge donation of the tetracarbene. The five-coordinate iron(III) halide complexes such as **7** possess a distorted molecular symmetry and heterogeneous ligand coordination sphere ( $7: \text{C}_{\text{NHC}}\text{-Fe-C}_{\text{NHC}})_{\text{av}} = 155.29(11)^\circ$  and  $(\text{C}_{\text{NHC}}\text{-Fe-X})_{\text{av}} = 102.35(1.40)^\circ$ , (Table 1) – two effects that lead to a higher quadrupole splitting of these compounds of above  $4 \text{ mm s}^{-1}$ .<sup>107,108</sup> In addition, the  $-I$  effect of the axial ligand increases the anisotropy of the nucleus, which enlarges the quadrupole splitting in the order  $\text{Cl}^-$  (**30**) <  $\text{Br}^-$  (**7**) <  $\text{OTf}^-$  (**31**), where **7** is after **30** in contrast to the order of increasing  $-I$  effect, probably due to the stronger donating tetracarbene of **7**, and the stronger  $-I$  effect of  $\text{OTf}^-$  results in the largest observed quadrupole splitting of all iron tetracarbenes in this review,  $5.02 \text{ mm s}^{-1}$  for **31** (Scheme 7).

### 3.5. Comparison to Fe porphyrins

Iron tetracarbenes share some similarities with the heme group and have been sometimes described as organometallic heme analogs.<sup>59,63,74,79</sup> The structure of the heme unit is shown in Fig. 9. In contrast to iron tetracarbenes, the ligand contains a conjugated cyclic aromatic system with 18  $\pi$ -electrons and is coordinated to the iron atom through the nitrogen atoms.<sup>116</sup> Furthermore, it is planar,<sup>117–121</sup> whereas many iron tetracarbenes possess a saddle-distorted conformation. Porphyrins readily undergo one-electron-transfer reactions leading to the respective radical cations or anions. The unpaired electron is effectively delocalized in the conjugated aromatic circuit.<sup>116,122</sup> Radical porphyrins play an important role as intermediates in enzymatic cycles, e.g. a cationic radical is involved in C–H oxidation catalyzed by cytochromes P450.<sup>122–125</sup> Instead, the tetracarbene ligand is redox inactive which can simplify mechanistic investigations as the redox processes are limited to the metal center. In addition, while the heme is not charged, most iron(II) tetracarbenes have two counterions. In this regard, the 16-membered iron complex **6** has the most porphyrinoid character of all compounds mentioned in this review, exhibiting a neutral charge due to its dianionic tetracarbene ligand. Finally, the four connected NHC moieties of the tetracarbene ligand result in a strong  $\sigma$ -donation in equatorial plane towards the iron atom. This pushes the  $d_{x^2-y^2}$  orbital above the  $d_{z^2}$  orbital and can lead to a different reactivity as

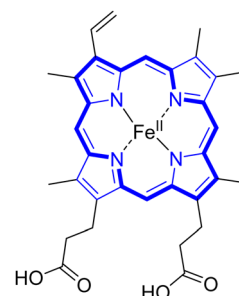


Fig. 9 Heme unit, more specifically called heme B or iron protoporphyrin IX.<sup>3,126</sup> The skeletal structure of porphyrin is marked blue. The conjugated aromatic circuit with 18  $\pi$ -electrons is marked in bold.

Table 1 Selected structural and spectroscopic parameters of cyclic iron tetracarbenes obtained directly from complexation reaction or one-electron redox reaction

Complex	$\delta_{\text{NHC}}^a$	$E_{1/2} [V]$ vs. $\text{Fc}/\text{Fc}^+$ <sup>b</sup>	$(\text{Fe}-\text{X})_{\text{av}}^c$ [Å]	$(\text{Fe}-\text{C}_{\text{NHC}})_{\text{av}}^d$ [Å]	$(\text{C}_{\text{NHC}}-\text{Fe}-\text{C}_{\text{NHC}})_{\text{av}}^e$ [°]	$(\text{C}_{\text{NHC}}-\text{Fe}-\text{X})_{\text{av}}^f$ [°]	$\text{X}-\text{Fe}-\text{X}^g$ [°]	$\delta^h$ [mm s <sup>-1</sup> ]	$ \Delta E_Q ^i$ [mm s <sup>-1</sup> ]	Ref.	Additional
1	205.05	0.15	1.932(3)	1.907(3)	90.00(24), 178.93(67)	90.00(66)	177.09(10)	0.08	3.45	59 and 71	Fe(II) $\tilde{\nu}_{\text{NC}} = 2291 \text{ cm}^{-1}$ $S = 0$
1-d <sub>8</sub>	205.26	0.15	—	—	—	—	—	—	—	72	Fe(II)
2	—	—	1.922(8)	1.941(2)	90.01(32), 179.09(8)	90.00(23)	179.04(9)	0.01	3.73	71, 73 and 74	Fe(III) $S = 1/2$ $g = 2.10$
2-d <sub>8</sub>	—	—	—	—	—	—	—	—	—	72	Fe(III)
3	—	—	1.926(3)	1.940(2)	90.00(47), 179.30(15)	90.00(42)	179.19(14)	—	—	75	Fe(III)
4	197.8	0.03	1.921(7)	1.996(11)	90.03(1.84), 176.78(46)	90.00(49)	179.47(7)	0.23	2.10	60 and 61	Fe(II)
5	—	—	1.929(6)	2.020(17)	89.98(2.46), 174.59(37)	90.04(67)	177.22(13)	0.09	0.63	61	Fe(III) $S = 1/2$ $g = 2.037$
6	—	—	—	1.940(2)	89.99(49), 178.74(47)	—	—	—	—	63	Fe(II) paramagnetic $S = 1$
7	—	Irrev., $E_{\text{ox}} = +0.36$ , $E_{\text{red}} = -1.25$	2.4493(9)	1.986(3)	87.37(18), 155.29(11)	102.35(1.40)	—	0.07	4.91	63 and 76	Fe(III) $S = 1/2$
8	—	—	—	1.990(12)	89.99(1.90), 177.23(2.34)	—	—	—	—	64	Fe(II) paramagnetic $S = 1$ $\mu = 2.8\mu_{\text{B}}$
9	—	-0.95	2.5016(2)	2.037(8)	87.04(2.33), 153.12(67)	103.31(2.59)	—	—	—	64	Fe(III) $S = 1/2$ $\mu = 1.7\mu_{\text{B}}$
10	203.81	0.00	—	—	—	—	—	—	—	54	Fe(II)
11	—	—	1.933(1)	1.934(2)	90.00(7), 179.89(12)	90.00(44)	177.52(6)	—	—	54	Fe(III)
12	194.8	-0.16	1.921(3)	2.003(19)	90.13(1.55), 174.28(2.53)	90.00(1.37)	176.86(18)	0.23	2.19	61	Fe(II) $S = 0$
13	216.10	0.44	1.929(2)	1.910(2)	90.01(13), 179.14(9)	90.00(43)	178.90(6)	—	—	54	Fe(II)
14	—	—	1.925(4)	1.937(2)	89.98(38), 177.83(17)	90.00(65)	177.67(10)	—	—	54	Fe(III)
15	—	-0.98 (in THF)	—	1.989(17)	89.70(98), 170.76(4.12)	—	—	—	—	66	Fe(II) paramagnetic $S = 1$ $\mu = 3.4\mu_{\text{B}}$
16	—	~0.3 (est. graphically)	1.918(15)	1.963(20)	89.88(78), 173.70(3.50)	89.99(1.37)	178.7(2)	—	—	69	Fe(II)
17	196.65	+0.04	1.924(7)	2.011(18)	90.33(1.42), 171.21(1.48)	90.00(1.73)	178.20(9)	—	—	65	Fe(II)
70	190.35	-0.34 V	1.9247(13)	1.928(2)	90.0(1) 180.00	90.00(34)	180.00	—	—	53	Fe(II)

Average XRD parameters are given as arithmetic mean and the error (in bars) are calculated by combining the standard error of the mean of the measured bond lengths with the Gaussian error propagation for the measurement error. <sup>a</sup> <sup>13</sup>C-NMR carbene signal,  $\delta$  in ppm in CD<sub>3</sub>CN. <sup>b</sup> Half-cell potential  $E_{1/2}$  [V] vs.  $\text{Fc}/\text{Fc}^+$  in MeCN. <sup>c</sup> Average distance between iron center and axial ligands. <sup>d</sup> Average distance between iron center and carbene carbon atom. <sup>e</sup> Average angle between carbene, iron center and neighboring or opposing carbene carbon atom. <sup>f</sup> Average angle between carbene carbon atom, iron center and axial ligand. <sup>g</sup> Angle of the vertical axis intersecting both axial ligands and the iron center. <sup>h</sup> Isomer shift. <sup>i</sup> Quadrupole splitting.

demonstrated in C–H activation (see Section 4.4). The strong electron donation also promotes lower spin states, making, for example a high-spin configuration ( $S = 5/2$ ) of **30** unfavorable (see Section 4.2.1, Scheme 7). In the following sections, the properties and resulting reactivity of iron tetracarbenes are compared with iron porphyrins and iron nonheme complexes at appropriate sites.

### 3.6. Summary

Cyclic iron tetracarbenes cover a wide range of structural and electronic properties. The equatorial tetracarbene ligand needs to be designed based on the scope and required capabilities of the target complex, which can be accomplished by modification of the backbone, bridging units and type of NHC. Post-processing of the electronic properties of the iron tetracarbene can be easily achieved by substitution of the axial ligands. The structural and electronic properties of iron tetracarbenes can be evaluated and compared based on the  $^{13}\text{C}_{\text{NHC}}$  NMR signal, the  $\text{Fe}^{2+}/\text{Fe}^{3+}$  half-cell potential, SC-XRD and Mössbauer spectroscopy.

The chemical shift of the  $^{13}\text{C}_{\text{NHC}}$  NMR signal provides information about the  $\sigma$ -donor strength of the tetracarbene ligand. Backbone modifications of the NHCs and different wingtips have a significant impact on the donating properties of the tetracarbene ligand, as observed in the carbene chemical shift in NMR spectroscopy. By substitution of the axial ligands of the finished complex, the  $^{13}\text{C}_{\text{NHC}}$  NMR signal of the tetracarbene ligand is shifted, and information about the electronic properties of the axial ligands and the resulting Lewis acidity of the iron center can be obtained. The electronic changes are also noticeable in the  $^{13}\text{C}$  signals of the NHC backbone.

The half-cell potential of the  $\text{Fe}^{2+}/\text{Fe}^{3+}$  redox couple allows the comparison of the electronic properties of iron tetracarbenes like the donor strength of the axial or equatorial ligands and the Lewis acidity of the iron center. The  $^{13}\text{C}_{\text{NHC}}$  chemical shift and the half-cell potential correlate with each other allowing the prediction of one of the parameters of an iron tetracarbene before it is measured.

SC-XRD reveals the structural properties of iron tetracarbenes. The rigidity of the tetracarbene ligand has a decisive influence on the reactivity of the respective complex; for example, of the two iron tetracarbenes **6** and **8** with similar electronic properties, only **8**, which contains a larger tetracarbene ligand, is effective in aziridination reaction. Furthermore, the changes of the electronic properties can be monitored in SC-XRD, like the dependency of the iron-axial ligand bond lengths on the Lewis acidity of the iron center.

Mössbauer spectroscopy is important for the holistic consideration of the electronic properties of iron tetracarbenes, such as the oxidation state, spin state and electronic surroundings. Of interest are the isomer shift and the quadrupole splitting. The isomer shift is affected by the oxidation state, and a linear negative correlation can be observed between the isomer shift and the oxidation state within one iron tetracarbene system. The significantly lower isomer shifts of iron tetracarbenes in comparison to tetradentate N-ligated complexes demonstrate the strong  $\sigma$ -donation of the equatorial tetracarbene. Furthermore, it is the reason for the high

quadrupole splitting of iron tetracarbenes due to the oblate (disk-shaped) charge distribution around the iron nucleus.

Finally, iron tetracarbenes differ electronically from iron porphyrins in that they do not have a conjugated aromatic system and, unlike the latter, are redox inactive. The strong  $\sigma$ -donation of the tetracarbene ligand in equatorial plane towards the iron center pushes the  $d_{x^2-y^2}$  orbital above the  $d_{z^2}$  orbital leading to a different reactivity in C–H activation (see Section 4.4) and promotes lower spin states.

## 4. Reactivity

In the following, the reactivity of the cyclic iron tetracarbenes shown in Fig. 1 is described. The structural and electronic properties of the newly obtained complexes are exemplified. However, the reader is referred to the previous chapter for a more detailed discussion of the respective parameters.

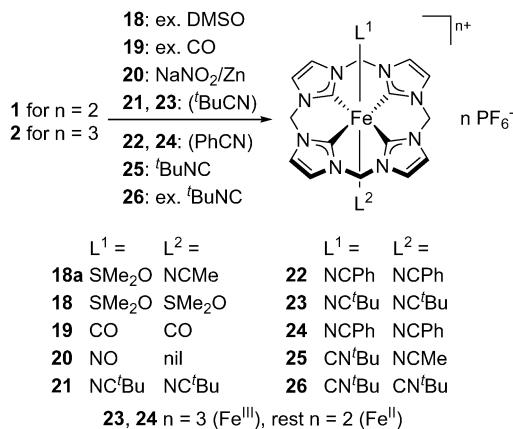
### 4.1. Modification of the oxidation state

Iron tetracarbenes are usually obtained as iron(II) complexes (see Section 2.2) but can be readily oxidized to obtain the respective iron(III) counterparts (*e.g.* Scheme 7). Chemical redox agents include [(4-BrC<sub>6</sub>H<sub>4</sub>)<sub>3</sub>N]SbCl<sub>6</sub> ( $E^0 = +0.67$  V in MeCN<sup>127,128</sup>), AgOTf ( $E^0 = +0.65$  V in DCM<sup>128,129</sup>), AgNO<sub>3</sub> ( $E^0 = +0.04$  V in MeCN<sup>128,129</sup>), NOBF<sub>4</sub> ( $E^0 = +0.87$  V in MeCN<sup>128,130</sup>) or thianthrethryl hexafluorophosphate (ThPF<sub>6</sub>,  $E^0 = +0.86$  in MeCN<sup>128,131</sup>) and with exception of the first all have been applied in the oxidation to iron(IV) centers (*vide infra*).<sup>54,61,73,82,83,132</sup> The choice of oxidant depends on *e.g.* the solubility of the complex, the required oxidant strength or the counterion of the iron tetracarbene. [(4-BrC<sub>6</sub>H<sub>4</sub>)<sub>3</sub>N]SbCl<sub>6</sub> has the drawback of potential chloride abstraction and coordination from SbCl<sub>6</sub><sup>−</sup> by the Lewis-acidic iron center.<sup>61</sup> AgOTf, AgNO<sub>3</sub> and NOBF<sub>4</sub> also contain coordinating ions, possibly leading to unwanted counterions for the iron complexes but can also be used to steer the electronic properties of the complex by introduction of axial ligands.<sup>61,83</sup> However, (partial) anion exchange of the resulting iron complex has to be considered. Reduction of iron(III) tetracarbenes is possible with CoCp<sub>2</sub> ( $E^0 = ca. -1.3$  V)<sup>128,133</sup> and, additionally remove coordinated halides, with sodium amalgam ( $E^0 = -2.36$  V).<sup>64,81,128,134</sup>

### 4.2. Axial ligand modifications

As showcased in the previous chapter, axial ligand exchange can have a significant impact on the electronic properties of iron tetracarbenes. The axial ligand substitution can be readily achieved by adding the new ligand to a solution of the iron tetracarbene, letting it stir for a certain time, usually at room temperature, and obtaining the modified complex by precipitation with Et<sub>2</sub>O or by extraction. Precipitation is applied for the ionic iron tetracarbenes (Schemes 5 and 7), whereas the neutral iron tetracarbenes **28** and **29** (Scheme 6) are extracted.

Addition of excess DMSO to iron tetracarbene **1** in MeCN leads to a mixture of mono-substituted **18a**, bis(DMSO)-complex **18** and **1** (Scheme 5). The equilibrium is shifted to

Scheme 5 Ligand substitution reactions of **1** and **2**.<sup>59,77,78</sup>

**18a** and **18** with increasing amount of DMSO and at more than 50-fold excess only **18** is present. When changing the solvent to acetone as weakly coordinating solvent, exclusively **18** has been obtained in 95% yield with almost planar geometry of the tetracarbenic.<sup>59</sup> A rather rare example for a stable, cationic bis(carbonyl)-iron NHC complex, **19**, can be synthesized in CO atmosphere at 2.5 atm and 40 °C in 77% yield.<sup>59</sup> It shows a similar saddle-distorted tetracarbenic conformation to **1**. Other iron(II) NHC complexes usually only contain one carbonyl ligand.<sup>135</sup> Some examples for cationic bis(CO)-iron complexes have been published for heme systems.<sup>136–138</sup> A mono(carbonyl)-complex could be observed in CV at higher scan rates ( $>400 \text{ mV s}^{-1}$ ) at  $E_{1/2} = 0.83 \text{ V}$  and represents an intermediate in the decomposition of **19** to **1** over time under these conditions. The isolation of complexes **19** and **34** (Scheme 7) demonstrates yet again the strong  $\sigma$ -donating properties of tetracarbenic ligands, resulting in a high electron density at iron. Exchange of the labile MeCN ligands of **1** with ligands exhibiting similar electronic properties, like <sup>t</sup>BuCN and PhCN, requires MeCN-free conditions to obtain the fully substituted complexes. Hence, complexes **21–24** were synthesized using the respective ligand as solvent. To ensure full substitution, the crude products have to be stirred again in <sup>t</sup>BuCN or PhCN after the first precipitation with Et<sub>2</sub>O to obtain the complexes **21–24** in 46 to 57% yield. All analytics to characterize these compounds have been performed in weakly coordinating acetone or <sup>t</sup>BuCN and PhCN.<sup>77</sup> The overall geometry of the complexes is comparable to **1**, but the Fe–X bonds of **22** are significantly shorter (Table 2), assignable to the better  $\pi$ -accepting properties of PhCN due to the –M effect of its phenyl group. This also leads to a decreased electron density of iron, resulting in a higher redox potential of 0.27 V. Introduction of axial isocyanide ligands, e.g. <sup>t</sup>BuNC, is possible in MeCN as solvent,<sup>63,139</sup> but has been conducted in acetone using one equivalent or excess of <sup>t</sup>BuNC to obtain mono(<sup>t</sup>BuNC)-complex **25** (90% yield) and bis substituted complex **26** (87% yield), respectively.<sup>78</sup> The strong  $\pi$ -accepting ligands of **25** and **26** lead to higher redox potentials of 0.35 V and 0.47 V, respectively. Complexes **21–26** have been applied in epoxidation catalysis to elucidate the effect of axial substitution in comparison to the performance of their model catalysts **1** and **2** (see Section 5.3).

**4.2.1. Spin state variations.** Square planar, neutral iron(II) complex **6** exhibits an intermediate-spin  $S = 1$ , similar to isostructural iron porphyrin complexes.<sup>63,140</sup> Upon coordination with a strong donor axial ligand, the complex changes to a low-spin iron(II) complex with  $S = 0$  (Scheme 6). Dissolving **6** in MeCN gives bis(MeCN)-complex **27**, which is diamagnetic and thus allows the evaluation of the  $\sigma$ -donation strength of the dianionic tetracarbenic of **6**. This reactivity is in contrast to its larger counterpart **8**, which remains paramagnetic ( $S = 1$ ) in MeCN solutions.<sup>64</sup> The large upfield shift of the <sup>13</sup>C<sub>NHC</sub> signal (193.4 ppm) and the negative redox potential (–0.71 V, Table 2) reveal the stronger electron donating capabilities of this ligand in comparison to neutral tetracarbenes (see Section 3). However, **27** could not be isolated, as evaporation of MeCN as solvent leads to the recovery of the starting material **6**. Hence, characterization was performed *in situ*. Addition of one equivalent of PPh<sub>3</sub> or excess of <sup>t</sup>BuNC to a solution of **6** in MeCN (*i.e.* effectively **27**) gave the respective mono (**28**, 65% yield) and bis-substituted (**29**, 88% yield) low-spin iron(II) complexes. Remaining PPh<sub>3</sub> or <sup>t</sup>BuNC were removed by extraction with pentane.<sup>63</sup>

The impact of ligand substitutions on the spin state were further investigated with complexes **4** and **12** (Scheme 7). On that occasion, the ring-flip of the saddle-shaped tetracarbenic ligands of **4** and **12** was analyzed by means of variable temperature NMR spectroscopy, giving  $\Delta G_{298}^{\ddagger} = 12.1 \text{ kcal mol}^{-1}$  for **4** and  $13.4 \text{ kcal mol}^{-1}$  for **12** for the barrier of the conformational ring inversion.<sup>61</sup> A similar iron complex with a macrocyclic NHC/pyridine hybrid ligand has a slightly higher value of  $\Delta G_{298}^{\ddagger} = 16.5 \text{ kcal mol}^{-1}$ .<sup>141</sup> In contrast, the related smaller iron complex **1** does not show any line broadening even at –40 °C in the NMR spectrum, indicating a fast inversion of its tetracarbenic.<sup>59</sup> Oxidation of **4** with [(4-BrC<sub>6</sub>H<sub>4</sub>)<sub>3</sub>N]SbCl<sub>6</sub> (see Section 4.1) in MeCN at –35 °C leads to species **5** in 31% yield, which is rather unstable in solution and forms **30** upon chloride abstraction from SbCl<sub>6</sub><sup>–</sup> by the Lewis acidic iron center over time. The latter can be directly obtained from **4** by preparation of **5** *in situ* in 83% yield. **30** exhibits a square-pyramidal geometry, similar to other halide iron tetracarbenes like **7** or **9**.<sup>63,64</sup> EPR measurements were conducted to assign **5** to a low-spin ( $S = 1/2$ ) and **30** to an intermediate-spin ( $S = 3/2$ ) complex, confirmed by a variable-temperature SQUID measurement.<sup>61</sup> This is similar to iron(III)

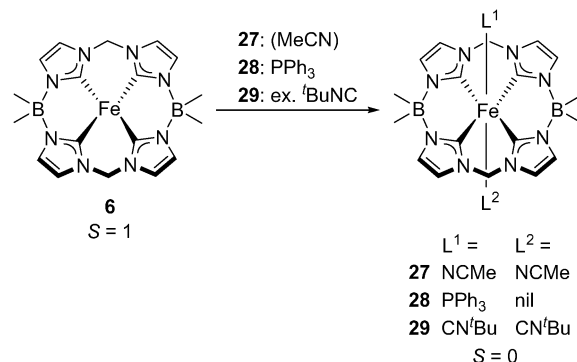
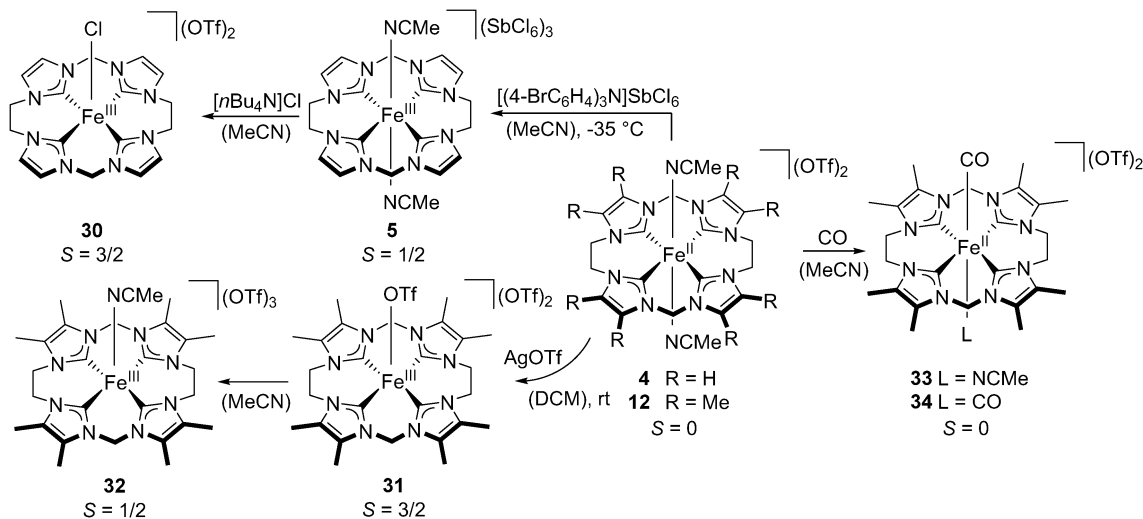
Scheme 6 Addition of axial ligands to **6**.<sup>63</sup>

Table 2 Selected structural and spectroscopic parameters of cyclic iron tetracarbenes with axial ligand modifications

Complex	$\delta_{\text{CNHC}}^a$	$E_{1/2} [V]_{\text{vs. FC/FC}^+}$	$(\text{Fe-X})_{\text{av}}^c [\text{\AA}]$	$(\text{Fe-CNHC})_{\text{av}}^d [\text{\AA}]$	$(\text{CNHC-Fe-CNHC})_{\text{av}}^e [^\circ]$	$(\text{CNHC-Fe-X})_{\text{av}}^f [^\circ]$	X-Fe-X <sup>g</sup> [°]	$\delta^h$ [mm s <sup>-1</sup> ]	$ \Delta E_{\text{O}_2} ^i$ [mm s <sup>-1</sup> ]	Ref.	Additional
18	189.31	0.74 (ox.)	2.1982(4)	1.935(1)	90.00(30)	90.00(1.20)	180.00	—	—	59	Fe(II) $\tilde{\nu}_{\text{SO}} = 1100 \text{ cm}^{-1}$
19	179.26	1.25	1.821(6)	1.915(2)	90.00(27)	90.01(82)	177.10(16)	—	—	59	Fe(II) $\tilde{\nu}_{\text{CO}} = 2010 \text{ cm}^{-1}$
20	170.43	-1.06 (irrev. red.)	Fe-N: 1.673(3), N-O: 1.160(4)	1.944(4)	86.79(20)	103.69(1.32)	Fe-N-O: 172.1(3)	—	—	59	{FeNO} <sup>+</sup> $g = 1.988$ $\tilde{\nu}_{\text{NO}} = 1729 \text{ cm}^{-1}$
21	—	0.17	1.915(7)	1.899(4)	90.00(20)	90.01(87)	173.94(13)	—	—	77	Fe(II)
22	202.2 <sup>j</sup>	0.27	1.905(4)	1.906(3)	178.88(26)	90.00(31)	177.74(8)	—	—	77	Fe(II)
23	—	—	—	—	—	—	—	—	—	77	Fe(II)
24	—	—	—	—	—	—	—	—	—	77	Fe(II)
25	198.9 <sup>j</sup>	0.35	Fe-N: 1.974(2), Fe-C: 1.819(3)	1.905(3)	90.00(18)	C-Fe-C <sub>ax</sub> : 90.23(1.17) C-Fe-N: 89.77(75)	177.95(10)	—	—	78	Fe(II)
26	196.1 <sup>j</sup>	0.47	1.868(8)	1.899(3)	89.97(36)	90.00(75)	176.44(17)	—	—	78	Fe(II)
27	193.4	-0.71	—	—	88.98(3.23)	98.12(1.59)	—	—	—	63	Fe(II) $S = 0$
28	196.0	—	—	—	163.70(5.40)	101.59(38)	—	—	—	63	Fe(II) $S = 0$
29	191.9	—	—	—	156.55(90)	—	—	—	—	63	Fe(II) $S = 0$
30	—	—	2.2656(9)	2.009(19)	87.70(1.71)	—	—	0.11	4.52	61	Fe(II) $S = 3/2$ $g = 4.300, 2.095, 2.095$
31	—	—	2.034(3)	2.008(15)	156.55(90)	—	—	0.16	5.02	61	Fe(II) $S = 3/2$ $g = 4.950, 2.700, 1.900$
32	—	—	—	—	—	—	—	—	—	61	Fe(II) $S = 1/2$
33	181.7	0.61 (ox.)	Fe-CO: 1.717(4), Fe-N: 1.984(4), C-O: 1.133(5)	2.014(13)	90.12(1.62)	N-Fe-C: 89.84(1.49)	—	—	—	61	Fe(II)
34	172.6	0.96 (ox.)	Fe-CO: 1.803(11) C-O: 1.140(10)	1.992(19)	174.84(34)	OC-Fe-C: 90.16(1.49)	180.0	0.00	1.76	79	$\tilde{\nu}_{\text{CO}} = 1938 \text{ cm}^{-1}$
35	—	-0.98 (rev. red.)	1.670(3), N-O: 1.166(4)	1.994(18)	90.00(2.32)	90.04(69)	175.5(3)	-0.04	0.98	79	Fe(II)
36	195.85	—	1.660(2), N-O: 1.207(3)	1.968(17)	176.35(76)	101.88(2.38)	Fe-N-O: 176.9(3)	-0.01	2.36	80	$\tilde{\nu}_{\text{CO}} = 1981 \text{ cm}^{-1}$ $g = 2.029, 2.014, 1.996$ FeNO <sup>+</sup> {FeNO} <sup>+</sup> $S = 1/2$
37	167.7	-1.00 (rev. red.)	Fe-N: 1.625(4) Fe-O: 1.979(3) N-O: 1.162(4) ON=O: 1.201(5) FeO-N: 1.305(4)	2.008(15)	87.86(40)	156.22(8.12)	—	—	—	80 and 81	{FeNO} <sup>+</sup> $S = 0$
45	—	—	—	—	85.62(74)	106.37(2.69)	Fe-N-O: 169.13(18)	0.02	0.85	80 and 81	{FeNO} <sup>+</sup> $S = 0$
51	186.33	—	Fe-C: 1.740(4), Fe-P: 2.4997(12), P=C: 1.635(5), PC=O: 1.171(6), FeC-O: 1.142(5)	1.996(19)	147.23(6.62)	—	—	—	—	81	Low-spin
60	—	—	2.11(2)	1.987(28)	89.98(2.35)	90.08(1.73)	174.4(12), Fe-N-N: 127.5(8.5)	0.32	2.39	83	Fe(II) $\tilde{\nu}_{\text{N}_3} = 2022 \text{ cm}^{-1}$
61	—	—	1.919(5), Fe-N <sub>3</sub> : 2.056(5)	1.986(15)	175.75(1.99)	90.78(1.66)	176.21(18), Fe-N-N: 120.4(4)	—	—	83	Fe(II)

Annotations *a-i* see Table 1. <sup>j</sup>JNMR measured in acetone-*d*<sub>6</sub>.



Scheme 7 Ligand substitution reactions of **4** and **12**. **30** was synthesized directly from **4**.<sup>61,79</sup>

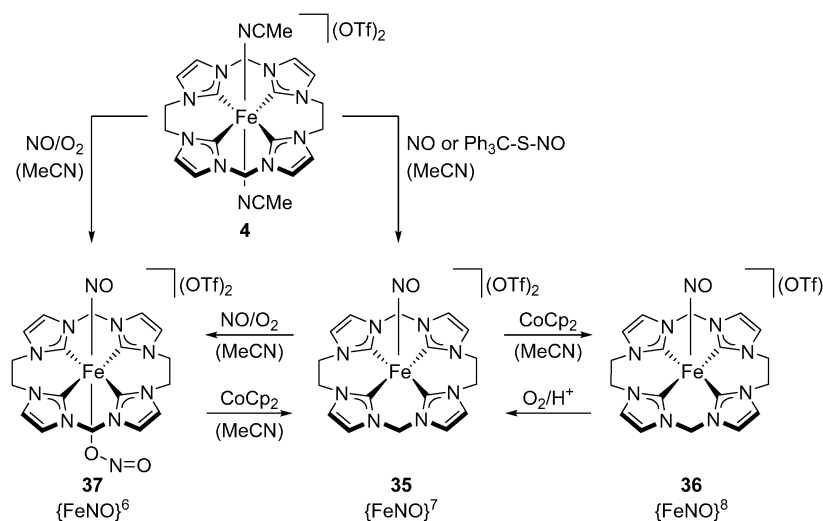
porphyrins, where complexes with two axial ligands usually show  $S = 1/2$  and five-coordinate complexes with weak axial ligands can adopt  $S = 3/2$ .<sup>140</sup> Due to the strong  $\sigma$ -donating properties of the tetracarbene, a high-spin ( $S = 5/2$ ) configuration is unfavored, as determined by DFT calculations.<sup>61</sup> This is probably the reason for the halide complexes **7** and **9** exhibiting  $S = 1/2$  configuration in contrast to **30** or **31**, due to the significant stronger electron donating character of the equatorial ligand. Oxidation of **12** with AgOTf in DCM results in the halide iron complex **31** (96% yield), resembling the other halide complexes structurally and featuring intermediate-spin state ( $S = 3/2$ ) like **30**. The axial ligand of **31** is replaced upon addition of MeCN to result in the low-spin ( $S = 1/2$ ) complex **32**. This rather unstable compound could not be isolated, but the structure was proposed to contain one axial MeCN and eventually one OTf<sup>-</sup> ligand in *trans* position based on the EPR findings.<sup>61</sup>

Bis(CO)-complex **34** can be obtained by replacing the inert atmosphere of a solution of **12** in MeCN with CO gas using

freeze-pump-thaw technique and stirring it for 2 days (Scheme 7). **34** is received after precipitation with Et<sub>2</sub>O and recrystallization from DCM/Et<sub>2</sub>O (no yield given).<sup>79</sup> Removing excess CO results in a mixture of **33** and **34**. Isolation of mono(CO)-complex **33** has been achieved by direct synthesis from **12** similar to **34**, however it was only stirred overnight, the CO atmosphere was removed afterwards and multiple recrystallizations steps by slow diffusion of Et<sub>2</sub>O into a concentrated solution of **33** in MeCN were performed. **12** and **33** have been employed in the electrocatalytic CO<sub>2</sub> reduction to CO (see Section 5.1).

#### 4.2.2. Iron nitrosyl complexes: {FeNO}<sup>6</sup>, {FeNO}<sup>7</sup> and {FeNO}<sup>8</sup>.

Iron nitrosyl complex **20** can be obtained by generation of NO *in situ* from NaNO<sub>2</sub> using zinc powder, iron powder or hydroquinone as reducing agents (73% yield, Scheme 5).<sup>59</sup> The iron atom is placed 0.475 Å above the tetracarbene plane, resulting in a ruffled macrocycle, similar to **35** (Scheme 8). **20**



Scheme 8 Synthesis and reactivity of iron nitrosyl complexes based on **4**.<sup>80,81</sup>

can be assigned as  $\{\text{FeNO}\}^7$  complex using Enemark–Feltham notation.<sup>142,143</sup> Interestingly, **20** exhibits sharp, not paramagnetic-shifted NMR signals, being rather uncommon for  $\{\text{FeNO}\}^7$  compounds.<sup>80,144</sup> In addition, no oxidation of **20** to  $\{\text{FeNO}\}^6$  can be observed in CV. The result of the CV is, however, identical to that obtained for **35**. Both **35** and **20** show a reduction wave indicating the formation of  $\{\text{FeNO}\}^8$ . Contrary to the isolation of  $\{\text{FeNO}\}^8$  complex **36** by reduction of **35**, the  $\{\text{FeNO}\}^8$  species generated from **20** is unstable and thus only an irreversible reduction wave is visible.<sup>59</sup> Iron nitrosyl complex **35**, the larger  $\{\text{FeNO}\}^7$  counterpart to **20**, has been synthesized by addition of gaseous NO or one equivalent of NO transfer reagent  $\text{Ph}_3\text{CSNO}$ <sup>145</sup> to a solution of **4** in MeCN at  $-35^\circ\text{C}$  (54% yield, Scheme 8).<sup>80</sup> **35** shows a nearly linear Fe–N–O moiety with an angle of  $176.9(3)^\circ$ , similar to **20**, and unusual for  $\{\text{FeNO}\}^7$  complexes. In addition, both complexes have shorter Fe–N distances than other heme and non-heme  $\{\text{FeNO}\}^7$  compounds.<sup>59,80</sup> **35** has been assigned to a low-spin ( $S = 1/2$ ) complex based on a SQUID magnetic susceptibility measurement. The IR spectrum shows an absorption of  $\tilde{\nu}_{\text{NO}} = 1742\text{ cm}^{-1}$  for **35**, which is similar to **20** ( $\tilde{\nu}_{\text{NO}} = 1729\text{ cm}^{-1}$ ) at slightly higher energy in comparison to other low-spin  $\{\text{FeNO}\}^7$  complexes (around  $1600\text{--}1700\text{ cm}^{-1}$ ), with high-spin  $\{\text{FeNO}\}^7$  complexes showing an absorption around  $1700\text{--}1850\text{ cm}^{-1}$ .<sup>146,147</sup> While the NO stretching frequency is influenced by the oxidation and spin state of the iron center, linear Fe–NO units tend to have higher values than their bent equivalents.<sup>80,148,149</sup> Considering the linear Fe–NO structure of **35**, indicating a  $\text{NO}^+$  ligand, and DFT calculations, a  $\text{Fe}^+\text{NO}^+$  character has been proposed.

As mentioned above,  $\{\text{FeNO}\}^8$  complex **36** could be synthesized by adding  $\text{CoCp}_2$  as reducing agent to a MeCN solution of **35** at  $-35^\circ\text{C}$  (47% yield).<sup>81</sup>  $\{\text{FeNO}\}^8$  complexes are known to form the respective  $\{\text{FeNO}\}^7$  complex upon protonation of the former *via* a  $\{\text{FeNHO}\}^8$  intermediate and release of  $\text{H}_2$  after disproportionation.<sup>147,150–152</sup> However, **36** does not show such a reactivity in the presence of Brønsted acids, which has been related to the electron density being centered at the iron rather than at the NO ligand, making the protonation somewhat unfavorable.<sup>81</sup> In the presence of oxygen, the formation of  $\{\text{FeNO}\}^7$  is observed, but with a large amount of decomposition products. Combination of Brønsted acids and oxygen leads to a quick formation of  $\{\text{FeNO}\}^7$  compound **35** from **36**, without recognizable decomposition.<sup>81</sup> The overall geometry of **36** is similar to **35**, but the iron atom is more out of plane ( $0.56\text{ \AA}$ ) than in **35**, which reduces the interaction with the tetracarbene ligand. The implications of that and other factors on the electronic properties are discussed in 3.4. The Fe–NO moiety is more deviated from  $180^\circ$  ( $169.13(18)^\circ$ ) in **36** than in **35** ( $176.9(3)^\circ$ ). The bending appears to originate from lower electronic repulsion between the more electron rich, reduced iron atom and the NO ligand, and furthermore enables better Fe  $\rightarrow$  NO  $\pi$ -backbonding, resulting in a shorter Fe–NO bond rather than elongation in the case of enhanced electronic repulsion.<sup>81</sup>

$\{\text{FeNO}\}^6$  complex **37**, featuring an unusual axial O–nitrito ligand, can be obtained in 63% yield by a two-step procedure. First, a MeCN solution of **4** is treated with NO gas, effectively

generating the  $\{\text{FeNO}\}^7$  compound **35** *in situ*, then oxygen is added (Scheme 8).<sup>81</sup> A proposed mechanism involves the formation of  $\text{NO}_2$  in the gas phase, which subsequently undergoes a redox reaction with  $\{\text{FeNO}\}^7$  complex **35** to form  $\{\text{FeNO}\}^6(\text{ONO}^-)$  complex **37**. The mechanism was supported by  $^{18}\text{O}_2$  labeling experiments and DFT calculations. Direct oxidation of **35** to a five-coordinated  $\{\text{FeNO}\}^6$  complex has not been achieved as well as nitrite salts do not lead to a reaction. Identical to **20**, **35** does not show any oxidation peak in CV up to  $+1.5\text{ V}$ . However, in presence of a nitrite salt, a redox transition assignable to  $\{\text{FeNO}\}^7/\{\text{FeNO}\}^6$  is observed in CV, underlining the requirement of binding of a sixth ligand *trans* to NO for the oxidation of **35**. The low isomer shift ( $-0.16\text{ mm s}^{-1}$ ) of **37** is evidence for the metal-centered oxidation and the large quadrupole splitting ( $3.12\text{ mm s}^{-1}$ ) is caused by the extensive charge donation of the tetracarbene into the iron  $3d_{x^2-y^2}$  orbital leading to an oblate charge distribution around the iron nucleus (see Section 3.4). Reduction of **37** with one equivalent of  $\text{CoCp}_2$  releases the weakly bound nitrito ligand and forms **35**, and two equivalents of  $\text{CoCp}_2$  give **36** (Scheme 8).  $K\beta$  X-ray emission spectroscopy has been performed to confirm the low-spin state of all three complexes **35**, **36** and **37**.<sup>81</sup>

### 4.3. Oxygen activation and transfer

In nature, many metalloproteins show defined reactivity towards oxygen due to adaptation to an aerobic environment.<sup>124</sup> Activation of oxygen for *e.g.* oxygen transport or oxidation reactions involves reactive, high-valent metal-oxo intermediates.<sup>153</sup> Iron tetracarbenes as biomimetic heme analogs are therefore investigated regarding their reactivity towards oxygen. Some high-valent iron-oxo species have been isolated and represent artificial models of intermediates in oxygen activation in enzymes, enabling the study of their reactivity as well as electronic and structural properties (Table 3).

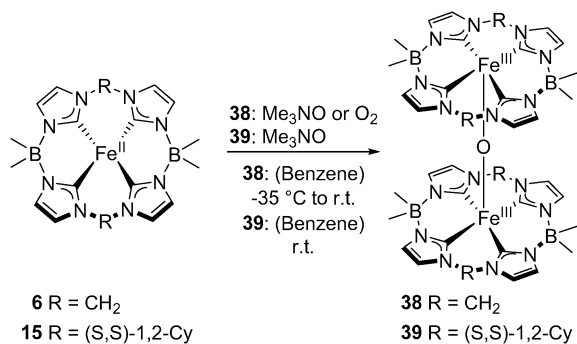
The neutral iron(II) complex **6** has been reacted with  $\text{Me}_3\text{NO}$  or oxygen/air to form diiron(III)- $\mu_2$ -oxo complex **38** in 74% yield (Scheme 9).<sup>63</sup> Similarly, **39** is obtained in 88% yield from **15** using  $\text{Me}_3\text{NO}$ .<sup>66</sup> Based on this reactivity, the bridged diiron complex often times is the primary impurity if traces of oxygen or water are present.<sup>63</sup> **38** is stable under air and moisture and oxidized  $\text{PPh}_3$  slowly with only 15% conversion to **28** (Scheme 6) after 4 days, in contrast to the fast oxidation of  $\text{PPh}_3$  shown by **44** (Scheme 14).<sup>74</sup> **38** shows a linear Fe–O–Fe axis, similar to **39** and all other described  $\mu_2$ -oxo-bridged diiron complexes, except for **44**, exhibiting a bent axis. Despite iron formally having 15 valence electrons, these oxo-bridged diiron complexes commonly are diamagnetic due to the antiferromagnetic coupling of the unpaired electrons over the bridging oxide.<sup>74</sup> The protons of cyclohexane from **39** pointing toward the oxo ligand are shifted downfield in the NMR spectrum, suggesting significant hydrogen bonding, which is further visible in the XRD structure.

When cationic iron tetracarbenes **4** and **12** are stirred under ambient atmosphere, diiron(III)- $\mu_2$ -oxo complexes **40** (98% yield, Scheme 10)<sup>60</sup> and **41** (76% yield)<sup>61</sup> are obtained. **40** is also obtained by oxidation of **4** with *m*CPBA,  $\text{Me}_3\text{NO}$  or, in contrast to the generation of iron(IV)-oxo complex **42** with

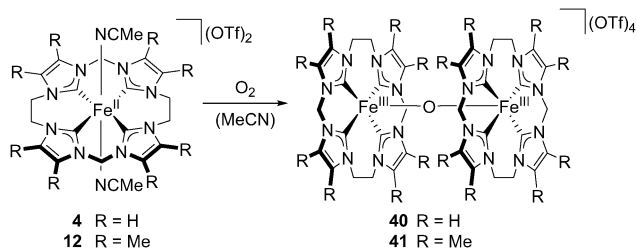
Table 3 Selected structural and spectroscopic parameters of bridged diiron tetracarbene complexes

Complex	$\delta C_{NHC}^a$	$E_{1/2} [V]$ vs. $Fe/Fe^{+b}$	$(Fe-X)_{av}^c$ [Å]	$(Fe-C_{NHC})_{av}^d$ [Å]	$(C_{NHC}-Fe-C_{NHC})_{av}^e$ [°]	$(C_{NHC}-Fe-X)_{av}^f$ [°]	Fe-X-Fe <sup>g</sup> [°]	$\delta^h$ [mm s <sup>-1</sup> ]	$[\Delta E_Q]^i$ [mm s <sup>-1</sup> ]	Ref.	Additional
38	179.6	—	1.7302(11)	1.9668(11) 161.03(46)	88.45(20)	99.49(15)	180.0	-0.02	2.8	63 and 154	Fe(III) S = 0
39	—	-0.28 (+3/+4) -2.71 (+3/+2) in THF	1.816(1)	2.042(16)	85.54(57) 147.22(4.85)	—	177.33(15)	—	—	66	Fe(III)
40	—	-1.33, -2.03 (r), +0.87 (o)	1.752(1)	1.996(11)	87.49(44) 155.11(3.40)	102.43(1.15)	178.79(16)	0.04	2.56	60 and 82	Fe(III) S = 3/2
41	—	—	—	—	—	—	177.0	0.03	2.60	61	Fe(III) S = 0, S <sub>1</sub> = 3/2
44	175	0.19 (+3/+3,4) 1.07 (+3,4/+4)	1.7321(12)	1.950(6)	87.31(21) 154.93(1.20)	102.53(1.03)	162.72(17)	—	—	74 and 132	Fe(III)
46	—	—	Fe-O: 1.7286(19) Fe-N: 1.986(2)	1.931(2)	89.69(18) 171.54(46)	O-Fe-C: 94.23(63) N-Fe-C: 85.77(30)	O-Fe-N: 177.63(46) Fe-O-Fe: 176.34(11)	—	—	132	Fe(III,IV) S = 1/2 $\mu = 1.72\mu_B$ $g = 2.0572, 2.0574,$ 2.0026
47	—	—	—	—	—	—	—	—	—	132	Fe(IV)
50	—	—	Fe-S: 2.1476(16) Fe-N: 1.993(5) S-S: 2.023(3) Fe-P: 1.996(3)	2.022(14)	90.0(2.1) 175.0(6)	C-Fe-S: 91.52(49) C-Fe-N: 88.48(66)	N-Fe-S: 178.96(15), Fe-S-S: 112.59(9)	0.15	2.76	155	Fe(III) S = 0, S <sub>1</sub> = 1/2
52	180.94, 191.45	-1.95, -2.26 (rr) -0.6 (ro 2e <sup>-</sup> ) -0.6 (ro 2e <sup>-</sup> ) ~ -0.7 (ro), -2.0, -2.3 (rr) <sup>j</sup>	—	1.982(11)	89.4(1.9) 165.4(4.8)	97.31(1.58)	178.25(12)	0.01	1.94	82	Fe(III) S = 0
53	—	—	—	—	—	—	—	0.02/0.01	1.96/2.68	82	Fe(III,IV), S = 1/2 $g_{xy} = 2.1059$ $g_z = 2.0022$
54	162.6	-0.67 (ro), ~ -2.0, -2.3 (rr) <sup>j</sup>	Fe-N: 2.004(9) Fe-P: 2.0048(32)	2.017(9)	89.99(70) 172.33(3.81)	C-Fe-N: 86.38(1.38) C-Fe-P: 93.62(1.37)	N-Fe-P: 178.58(1.22) Fe-P-Fe: 179.61(4)	0.00	2.69	82	Fe(IV) S = 0
55	187.5	-2.16 (r), -2.51 (r), -0.65 (o), 0.47 (ro)	1.690(1)	1.988(11)	87.75(7) 156.47(3.28)	101.77(1.12)	178.49(13)	-0.06	1.27	83	Fe(III) S = 0 {Fe <sub>2</sub> N} <sup>14</sup>
56	—	—	1.699(15) Fe-NCMe: 2.092(8)	2.001(13)	88.1(9) 160.4(6.0)	99.78(1.99) C-Fe-NCMe: 84.90(1.26)	178.5(3)	(+3): -0.05, (+4): -0.11	(+3): 2.11, 83 (+4): 2.40	83	Fe(III,IV) S = 2.095, 2.085, 2.013 $g = 1/2$ {Fe <sub>2</sub> N} <sup>13</sup>
57	—	—	1.700(11) Fe-O: 2.201(3)	2.006(12)	88.23(66) 160.77(4.83)	99.61(1.59) C-Fe-O: 84.15(2.01)	179.8(2), N-Fe-O: 175.31(13)	(+3): -0.06, (+4): 0.10	(+3): 1.96, 83 (+4): 2.74	83	Fe(III,IV) S = 2.094, 2.080, 2.010 S = 1/2 {Fe <sub>2</sub> N} <sup>13</sup>
58	163.7	—	—	—	—	—	—	-0.14	2.84	83	Fe(IV) S = 0
59	169.7	—	Fe-O: 2.075(10) Fe-N: 1.6838(4)	2.016(18)	89.2(9) 165.4(4.8)	97.26(1.42) C-Fe-O: 82.74(1.04)	179.5(3), N-Fe-O: 179.0(7)	-0.16	3.12	83	Fe(IV) S = 0 {Fe <sub>2</sub> N} <sup>12</sup>

Annotations a, c-i see Table 1. Half-cell potential  $E_{1/2}$  [V] vs.  $Fe/Fe^+$  in MeCN. r = reduction, o = oxidation, = oxidation, rr = reversible reduction, ro = reversible oxidation, ir = irreversible oxidation. <sup>j</sup>Estimated graphically. + 2, +3, +4 represent the iron oxidation states. +3,4 stands for iron(III,IV). Monomeric iron(IV) adducts.



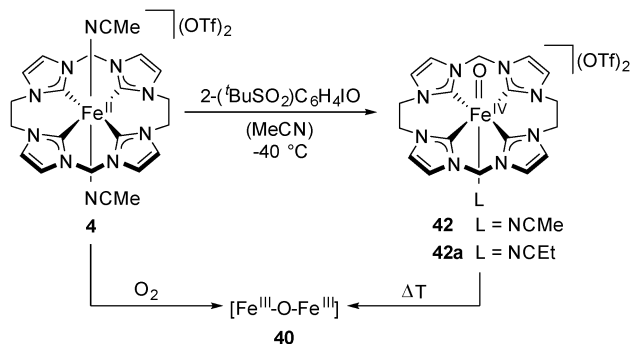
Scheme 9 Synthesis of  $\mu_2$ -oxo-bridged diiron complexes from **6** and **15**.<sup>63,66</sup>



Scheme 10 Activation of oxygen by **4** and **12**.<sup>60,61</sup>

2-(<sup>t</sup>BuSO<sub>2</sub>)C<sub>6</sub>H<sub>4</sub>IO (Scheme 11), with C<sub>6</sub>H<sub>4</sub>IO. The molecular structure of both complexes resembles **38** and **39** with an effectively linear Fe–O–Fe axis. **40** and **41** are diamagnetic ( $S = 0$ ) as well due to antiferromagnetic coupling. In fact, the antiferromagnetic coupling of **40** was found to be very strong ( $J = -606 \text{ cm}^{-1}$ ).<sup>60</sup> Based on the Mössbauer parameters and supporting DFT calculations, both **40** and **41** have intermediate-spin  $S_i = 3/2$  iron centers,<sup>61,155</sup> revising the earlier drawn conclusion of **40** being a rare example for a low-spin diiron(III)- $\mu_2$ -oxo complex.<sup>60</sup> The isomer shift of **41** ( $0.03 \text{ mm s}^{-1}$ , Table 3) is similar to **40** ( $0.04 \text{ mm s}^{-1}$ ), supporting the nearly linear correlation of oxidation state and isomer shift displayed in Fig. 7, despite its different backbone modification resulting in a more electron rich iron center.

A first example of an organometallic Fe<sup>IV</sup>=O complex (**42**) has been isolated by reaction of **4** with oxo-transfer agent 2-(<sup>t</sup>BuSO<sub>2</sub>)C<sub>6</sub>H<sub>4</sub>IO<sup>156</sup> at  $-40^\circ\text{C}$  in MeCN in 16% yield (Scheme 11 and



Scheme 11 Generation and reactivity of **42** from **4**.<sup>60</sup>

Table 4).<sup>60</sup> Interestingly, reaction with analog C<sub>6</sub>H<sub>4</sub>IO yields **40** directly. **40** is stable at  $-40^\circ\text{C}$  for at least one month. Upon warming to room temperature, **42** is reduced to binuclear diiron(III)- $\mu_2$ -oxo complex **40** (Scheme 11). Single crystals of the oxoiron(IV) complex suitable for XRD were obtained by slow diffusion of Et<sub>2</sub>O into a EtCN solution at  $-40^\circ\text{C}$  (**42a**).<sup>60</sup> The molecular structure reveals a nearly linear N–Fe–O angle and weak intramolecular hydrogen bonds between the ethylene bridges and the oxygen atom (Fig. 10), which, together with steric shielding of the ligand, probably stabilize the high-valent oxygen adduct. The hydrogen bonding strength was calculated to be  $1.9 \text{ kcal mol}^{-1}$ .<sup>157</sup> **42** can be assigned to an intermediate-spin ( $S = 1$ ) based on a SQUID measurement, being stabilized by the strong  $\sigma$ -donation of the tetracarbene ligand over  $S = 2$  spin state by rising of the iron  $3d_{x^2-y^2}$  orbital. Fe<sup>IV</sup>=O porphyrins also exclusively adopt the  $S = 1$  configuration of the metal center.<sup>158</sup> The reactivity of iron(IV)-oxo complex **42** in C–H bond activation and further details on the electronic properties of **42** are discussed in 4.4.

In contrast to diiron-oxo systems **40** and **41**, stirring of **1** under ambient atmosphere in MeCN does not yield a  $\mu_2$ -oxo bridged diiron complex, but iron(III) analog **2** (Scheme 12).<sup>74</sup> The transformation has been proposed to proceed *via* a stoichiometric reaction of **1** and O<sub>2</sub> by monitoring of the oxygen pressure. The oxidation of **1** to **2** by molecular oxygen is complete within 5 h at room temperature. Higher oxygen pressures of 3.5 bar promote the reaction. In return, addition of DMSO to **1** leads to no detectable formation of **2**, but rather the stable bis(DMSO) complex **18** (Scheme 5). Therefore, it has been hypothesized that the key step in the oxidation of **1** to **2** is an oxygen-axial ligand exchange that is hindered by axial ligand coordination.<sup>74</sup> However, no iron-oxo intermediates or oxygenated products could be observed. This finding has been explained by the oxidation of the solvent, MeCN, to form

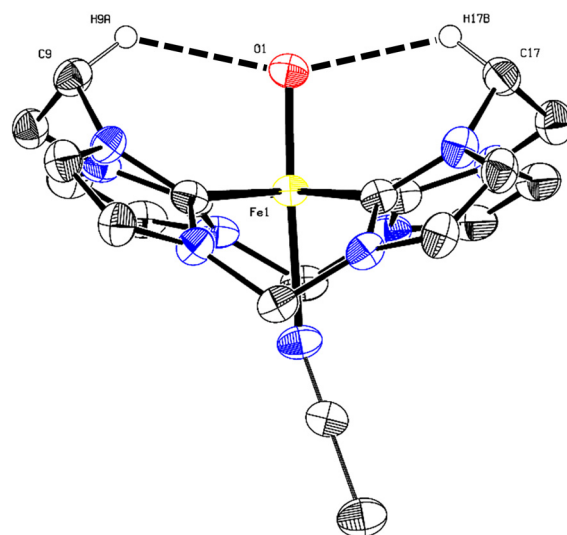
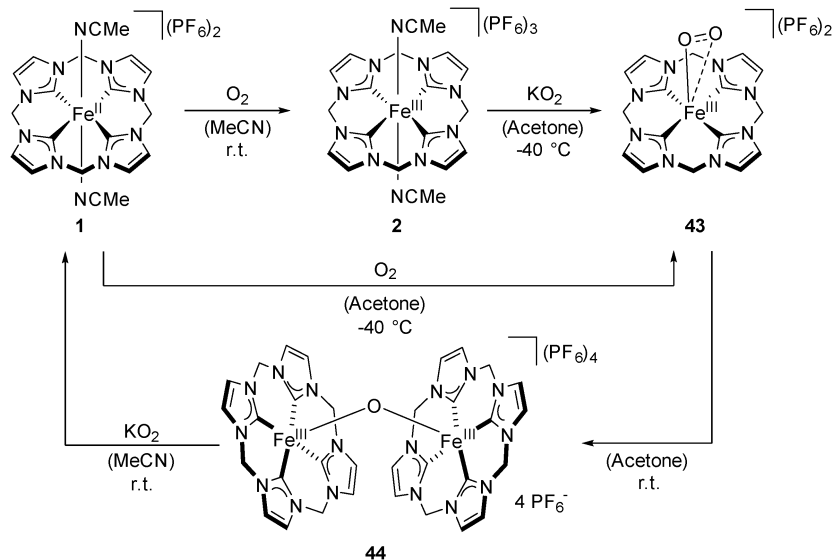


Fig. 10 ORTEP-style representation of the cationic fragment of **42a**. Selected atom distances [Å] and angles [°]: Fe–O1: 1.661(3), O1···H9A: 2.31, O1···H17B: 2.35, O1···C9: 3.036(6), O1···C17: 3.078(6); C9···O1: 130.5, C17···H17B···O1: 131.6.

Scheme 12 Reactivity of **1** in oxygen transfer reactions.<sup>74</sup>

glycolonitrile followed by decomposition to gaseous formaldehyde and HCN.<sup>72,74</sup> Indeed, when using *t*BuCN, PhCN or acetone as solvents bearing less activated C–H bonds, a  $\mu_2$ -oxo bridged diiron(III) complex **44** is obtained (67% yield for acetone, Scheme 12).<sup>74,77</sup> The above described reactivity has – so far – not been reported for other  $\mu_2$ -oxo diiron complexes. Nevertheless, the oxidation of **1** to **2** by O<sub>2</sub> without detectable formation of an Fe–O–Fe dimer is analogous to the oxidation of hemoglobin (Fe<sup>II</sup>) to methemoglobin (Fe<sup>III</sup>) and a superoxide.<sup>74,161</sup> Complex **44** is diamagnetic. However, it is the only diiron(III)- $\mu_2$ -oxo complex in this review, which does not exhibit a linear Fe–O–Fe moiety, displaying an 162.72(17)° angle, presumably due to the lower steric demand of the small tetracarbene.<sup>61</sup>

On the pathway to **44**, a superoxo iron(III) complex **43** has been isolated at –40 °C in acetone in 64% yield (Scheme 12 and Table 4), stable in solution or as solid at these temperatures for a few days.<sup>74</sup> **43** is diamagnetic, which has been explained by the antiferromagnetic coupling of the iron(III) center and the superoxide ligand.<sup>74,162,163</sup> The superoxidic nature of **43** is confirmed by EPR experiments using 5,5-dimethyl-1-pyrroline *N*-oxide (DMPO) as superoxide trapping reagent. Oxygen centered radicals are expected to form EPR active oxidation products upon reaction with DMPO.<sup>74,164–166</sup> EPR measurement of **43** + DMPO under inert atmosphere gives two independent signals with the first,  $g = 1.97$ , corresponding to an experiment of **2** + DMPO, indicating a partial decomposition of **43** to **2** under the reaction conditions. The second,  $g = 1.95$ , is related to an experiment of **1** + DMPO + O<sub>2</sub>, proposing the same formed oxygen centered radical for the reaction of **1** + DMPO + O<sub>2</sub> and **43** + DMPO. As the latter experiment of **43** + DMPO has been conducted under inert conditions, the oxygen radical is supposed to be bound to the iron center of **43**, corroborating **43** as iron(III)-superoxo complex. Both the NMR spectrum and the structure obtained from DFT calculations do not show axial

MeCN ligands. DFT calculations suggest a side-on coordination of the superoxide and stabilizing hydrogen bonds between the methylene bridges and the superoxide (Fig. 11), similar to the Fe<sup>IV</sup>=O complex **42** (Fig. 10). **43** can also be obtained from reaction of **2** with KO<sub>2</sub> at –40 °C in acetone (Scheme 12), which forms **44** upon warming to room temperature. **44** in turn is reduced by KO<sub>2</sub> to retrieve the starting material of the redox cycle, iron(II) complex **1**.<sup>74</sup>

Iron(III)-superoxo complex **43** has been reacted with more nucleophilic ligands DMSO and PPh<sub>3</sub>, replacing the superoxide and leading to iron(II) complexes **18** and **45** (Scheme 13). Upon addition of MeCN, iron(III) complex **2** is obtained, which is in accordance to the reactivity of **1** with O<sub>2</sub> to form **2**.<sup>74</sup> Iron dimer **44** oxidizes PPh<sub>3</sub> to O=PPh<sub>3</sub> forming **1** (Scheme 14). Furthermore, reducing agents like Zn or Fe powder, hydroquinone or KO<sub>2</sub> also reduce **44** to **1**. The oxidation of MeCN by **44** has been monitored *via* NMR or UV/Vis spectroscopy. In solvents with less activated C–H bonds like *t*BuCN or PhCN, the decay of **44** to **1** is significantly decelerated or even suppressed.<sup>74,77</sup> Deoxygenation of **44** to **2** is achieved by addition of Brønsted acids such as HBF<sub>4</sub> or HPF<sub>6</sub> at room temperature.<sup>74</sup>

Diiron(III)- $\mu_2$ -oxo complex **44** can be oxidized using ThPF<sub>6</sub> (see Section 4.1) in MeCN at –40 °C to form a rare example of a diiron(III,IV)- $\mu_2$ -oxo complex **46** in 85% yield (Scheme 15).<sup>132</sup> **46** is remarkably stable and can be stored several months at –37 °C as solid. Upon oxidation to **46**, the Fe–O–Fe angle significantly changes from 162.72(17)° to nearly linear 176.34(11)° as shown in the crystal structure (Fig. 12) and similar to all other diiron(III)- $\mu_2$ -oxo complexes in this review. In contrast, **46** contains two axial MeCN ligands, presumably due to the higher Lewis acidity of the iron center. **46** is paramagnetic and has been assigned as a  $S = 1/2$  system by EPR spectroscopy, whereas **44** is EPR-silent due to antiferromagnetic coupling (*vide supra*). CV suggests possible oxidation of **46** to a diiron(IV)- $\mu_2$ -oxo complex **47**. Indeed, a change in

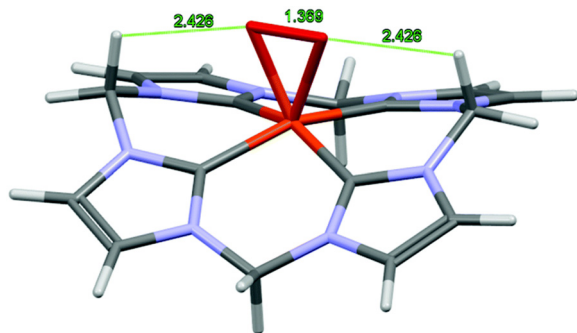


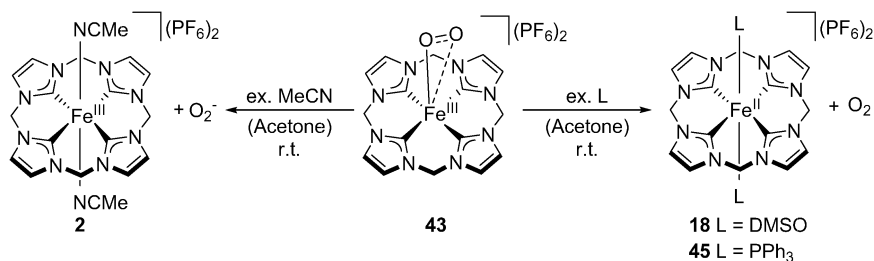
Fig. 11 DTF-derived structure of the cationic fragment of **43**. Reproduced from ref. 74 with permission from the Royal Society of Chemistry.

color can be observed when adding one equivalent of  $\text{ThPF}_6$  to **46** in MeCN at  $-40^\circ\text{C}$ . However, this intermediate has not been isolated as thianthrene is readily oxidized to thianthrene

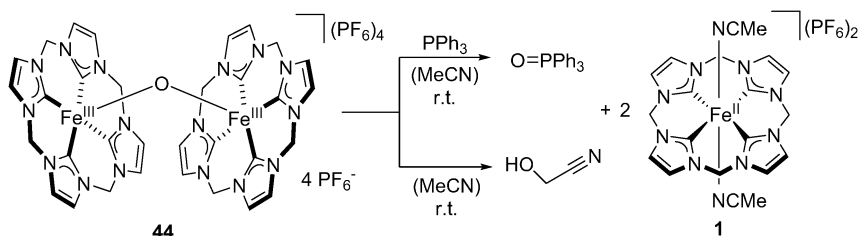
5-oxide. Similarly, the reaction of **44** with two equivalents of  $\text{ThPF}_6$  gives iron(III) complex **3**, oxidized thianthrene 5-oxide and thianthrene. However, UV/Vis kinetic studies provide further evidence for **47**, showing the formation of a new species after the addition of two equivalents of  $\text{ThPF}_6$  to **44** in MeCN at  $-40^\circ\text{C}$ , which is distinctly different from diiron(III,IV)- $\mu_2$ -oxo complex **46**. This species is highly temperature sensitive and decays to **2** upon warming to room temperature.

#### 4.4. C–H bond activation

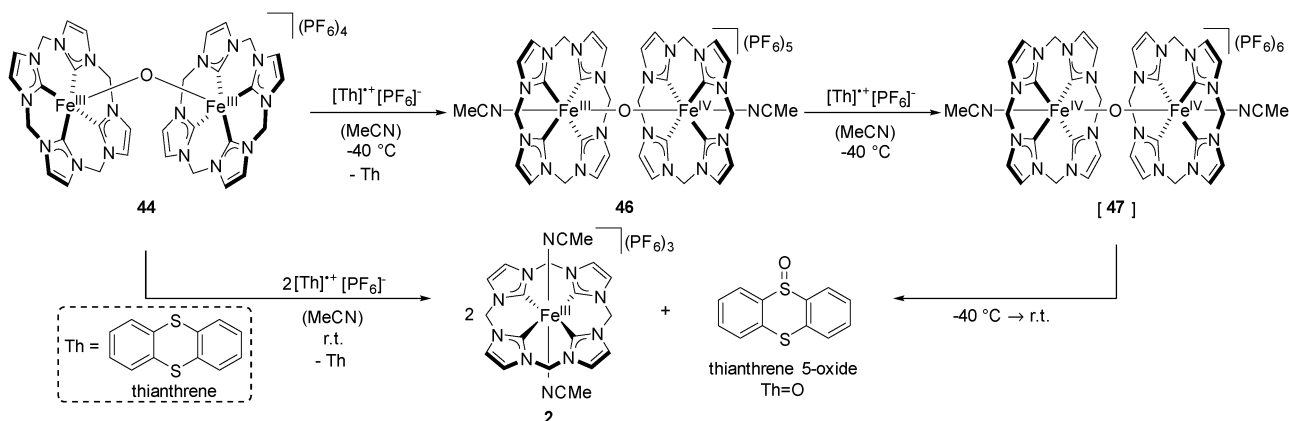
The electronic structure of the iron(IV)-oxo complex **42** (Fig. 13) has been investigated in detail using helium tagging infrared photodissociation, absorption, and magnetic circular dichroism spectroscopy, coupled with theoretical calculations.<sup>167</sup> Thus, relevant ligand field transitions have been unambiguously assigned. Like **42**, the majority of iron(IV)-oxo complexes



Scheme 13 Reactivity of iron(III)-superoxo complex **43**.<sup>74</sup>



Scheme 14 Oxidative reactivity of **44**.<sup>74</sup>



Scheme 15 Reactivity pattern of **44**.<sup>132</sup>

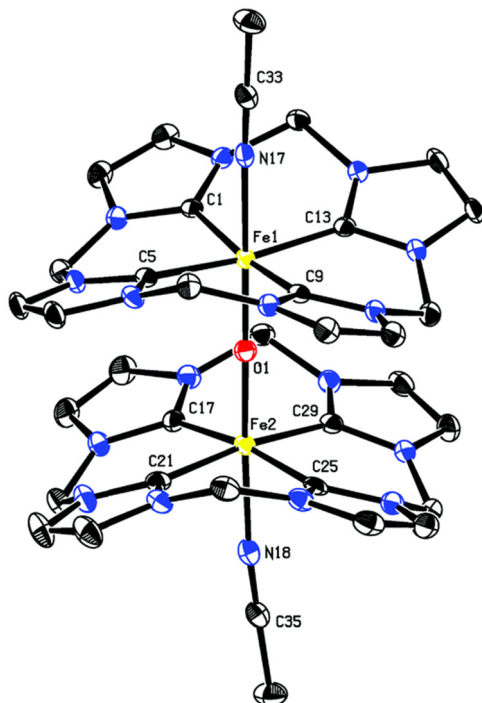


Fig. 12 ORTEP-style representation of the cationic fragment of **46**. Reproduced from ref. 132 with permission from the Royal Society of Chemistry. Selected (average) atom distances [Å] and angles [°]: Fe–O: 1.7286(19), Fe–C<sub>NHC</sub>: 1.931(2), Fe–O–Fe: 176.34(11), O–Fe–C<sub>NHC</sub>: 94.23(63).

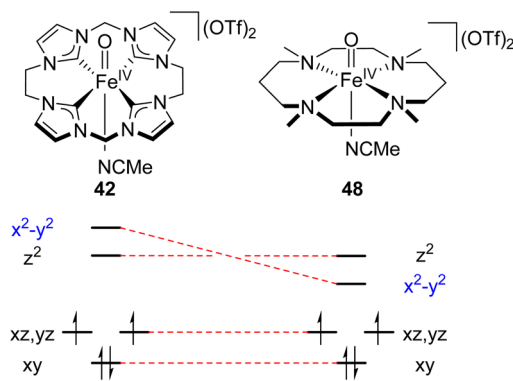


Fig. 13 Electronic structures of **42** and **48**.<sup>159</sup>

possesses a  $S = 1$  triplet ground state,<sup>115</sup> but a few compounds are known to have a  $S = 2$  quintet ground state (Fig. 14).<sup>167–170</sup> The quintet ground state can be favored by lowering of the  $x^2-y^2$  orbital by use of a weak field ligand ( $\text{H}_2\text{O}$ ) or elongation of the Fe–ligand bonds in equatorial plane through steric demand. In the case of **42**, the opposite effect is achieved by the strong  $\sigma$ -donation of the tetracarbenic ligand in equatorial plane to rise the  $x^2-y^2$  orbital.<sup>167</sup> In fact, the excitation energies of the  $d_{xz,yz} \rightarrow d_{z^2}$  transitions of **42** are found to be much lower than the  $d_{xz,yz} \rightarrow d_{x^2-y^2}$  transitions. This reveals the unusual electronic structure of **42**, in which the  $d_{x^2-y^2}$  orbital is placed above the  $d_{z^2}$  orbital, opposite to N-ligated **48**<sup>171</sup> and related complexes, as shown in Fig. 13. The equatorial tetracarbenic ligand appears to have no discernible impact on the bonding in the iron(IV)–oxo unit but pushes the  $x^2-y^2$  orbital above the  $z^2$  orbital with its strong  $\sigma$ -donation. The Fe–O stretching vibration of **42** is  $832(3) \text{ cm}^{-1}$  for the ground state and a vibration at  $616(15) \text{ cm}^{-1}$  has been calculated for the excited state.<sup>167</sup> The former is in the range of  $815$  to  $855 \text{ cm}^{-1}$  for other iron(IV)–oxo complexes.<sup>115</sup> The triplet–quintet energy gap for complexes bearing polydentate N-donor ligands usually is quite low around  $3 \text{ kcal mol}^{-1}$  (Fig. 14). Here, the iron–ligand bonds in equatorial plane are expected to increase slightly upon excitation of one electron from the  $d_{xy}$  to the  $d_{x^2-y^2}$  orbital for the quintet state, while the Fe–O bond rather remains the same.<sup>167,172–174</sup> In contrast, the calculated Fe–O bond of **42** ( $1.73 \text{ Å}$ ) for the quintet state is significantly larger than in the triplet ground state ( $1.661(3) \text{ Å}$ , Table 4), due to one electron being in the  $d_{z^2}$  orbital. This leads to considerably larger triplet–quintet energy gaps of  $18.7 \text{ kcal mol}^{-1}$  and  $28.3 \text{ kcal mol}^{-1}$ , derived by DTF or state-specific CASSCF/NEVPT2 calculations, respectively.<sup>167</sup> The calculated triplet–quintet energy gap of a hypothetical iron(IV)–oxo complex of **1** is  $15 \text{ kcal mol}^{-1}$ .<sup>175</sup>

High valent iron(IV)–oxo species are key intermediates in enzymatic cycles in nature that carry out challenging substrate transformations including the oxygenation of unreactive C–H bonds under mild conditions.<sup>176,177</sup> Therefore, the development and study of synthetic models is of high interest. The iron(IV)–oxo species is expected to cleave the C–H bond first by hydrogen atom transfer (HAT) to yield a radical and  $\text{Fe}^{\text{III}}\text{–OH}$  intermediate (Scheme 16).<sup>38,157,178</sup>

The C–H bond activation for  $S = 1$  complexes like **48** does not necessarily proceed *via* the triplet ground state but can also

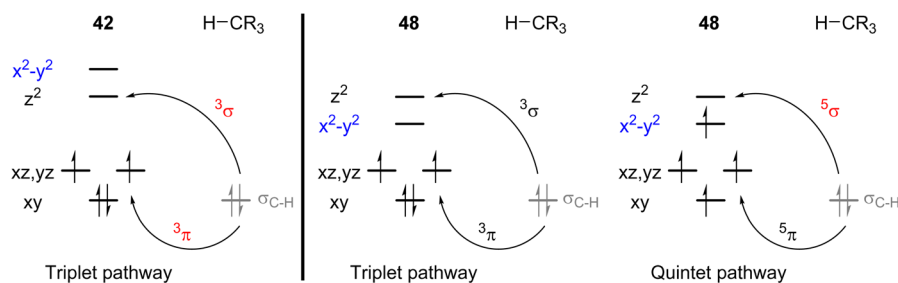
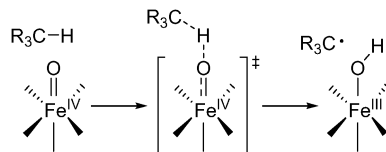
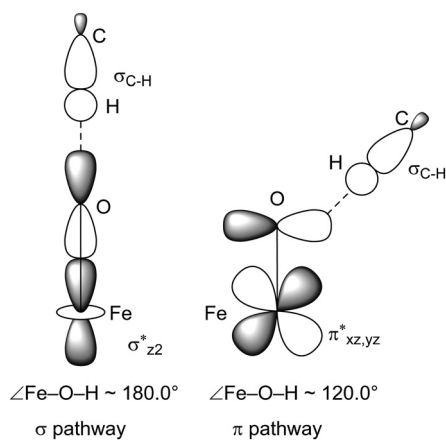
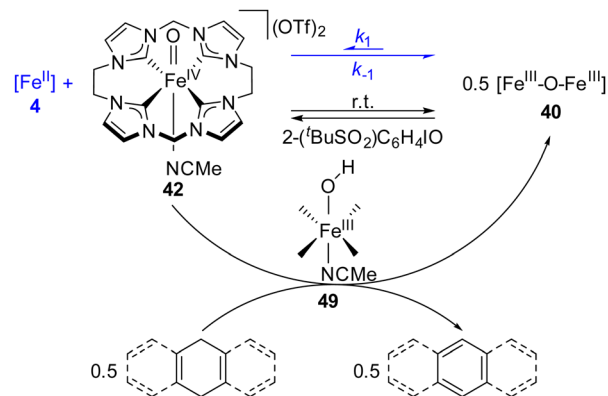


Fig. 14 Electron transfer pathways for the HAT process mediated by **42** and **48**. The most favorable substrate attack trajectories are highlighted in red, determined by computational methods.<sup>159</sup>

Scheme 16 Iron(IV)-oxo mediated C–H bond activation.<sup>157</sup>

involve the excited quintet state due to the low triplet–quintet energy gap, *vide supra*, called two-state reactivity (Fig. 14).<sup>159,167,179,180</sup> The quintet state is expected to be more reactive and have a lower activation barrier, but no distinct conclusion has been drawn so far, as experimental data from  $S = 2$  complexes is hampered by their low stability or steric hindrance.<sup>159,167,181,182</sup> Furthermore, the C–H bond activation can run *via* two routes,  $\sigma$  and  $\pi$ . In the  $\sigma$ -pathway, the  $d_{z^2}$  orbital accepts one electron, and the Fe–O–H angle is around  $180^\circ$ , whereas in the  $\pi$ -trajectory the  $d_{xz,yz}$  is the electron accepting orbital and the Fe–O–H angle is close to  $120^\circ$  (Fig. 15).<sup>157,175,183,184</sup> In terms of mechanistic studies, a simple model exclusively showing triplet reactivity is desired to restrict the possible four pathways to two. In the case of complex **42**, the large triplet–quintet energy gap should lead to a triplet-only pathway. This has also been proposed for the hypothetical  $\text{Fe}^{\text{IV}}=\text{O}$  complex of **1**.<sup>175</sup> Therefore, the reactivity of complex **42** in C–H activation has been investigated and compared to **48**.<sup>159,167</sup>

**42** reacts with several substrates containing rather weak C–H bonds like 1,4-cyclohexadiene (CHD), 9,10-dihydroanthracene (DHA), 9*H*-xanthene and 9*H*-fluorene at  $-40^\circ\text{C}$  in MeCN to avoid self-decay of **42** to diiron(III)- $\mu_2$ -oxo complex **40** (Scheme 17).<sup>159</sup> The proposed mechanism proceeds *via* an iron(III)-hydroxo intermediate **49** and yields **40** in the end, as evidenced by UV/Vis and mass spectroscopy experiments.<sup>159</sup> However, **40** is not a dead-end product in this case, contrary to usual  $\mu_2$ -oxo bridged diiron(III) complexes. As revealed in a follow-up study, **40** thermally disproportionates in MeCN solution at room temperature into **42** and **4** without additional oxidant (Scheme 17, blue).<sup>185</sup> The equilibrium constant is small with  $K_{\text{eq}} = 7.5(2.5) \times 10^{-8}$  M.

Fig. 15 Optimal substrate attack geometry of the substrate for the  $\sigma$ - and  $\pi$ -pathway.<sup>157</sup>Scheme 17 C–H activation of **42** of CHD and DHA as substrates.<sup>159</sup>

The formed **42** can continue with C–H activation and a selective, full conversion was achieved.

The decrease of **42** during C–H activation has been measured as  $k_{\text{obs}}$  and appears to be independent from the concentration of **42**, meaning that the process follows pseudo-first-order kinetics and is bimolecular. In Fig. 16 (left), the linear correlation of  $k_{\text{obs}}$  versus the concentration of the substrate is shown. A plot of  $\log(k_2')$  versus the bond dissociation energy of the weakest C–H bonds is presented in Fig. 16 (right), as well.  $k_2'$  is defined as the second order rate constant  $k_2$  divided by the number of equivalent C–H bonds on the substrate.<sup>159</sup> A linear correlation is observed with a slope of  $-0.39$ , similar to other iron(IV)-oxo complexes.<sup>159,186–189</sup> **42** shows no reactivity towards substrates with a stronger C–H bond like cyclohexane ( $99.5 \text{ kcal mol}^{-1}$ )<sup>190</sup> under these conditions. The kinetic isotope effect (KIE) has been investigated by employing DHA- $d_4$  as substrate and  $k_{\text{H}}/k_{\text{D}} = 32(8)$  at  $-40^\circ\text{C}$ , 18 at  $-20^\circ\text{C}$  and 11 at  $0^\circ\text{C}$  were found.<sup>159</sup> Complex **48** has a KIE value of 10 at  $25^\circ\text{C}$ .<sup>188</sup> The large KIE values indicate HAT as rate determining step and the reaction to proceed along the triplet pathway ( $S = 1$ , Fig. 14).<sup>159,191,192</sup> The KIE values decrease with an increasing temperature, explained by an increasing impact of the differences in entropy (DHA:  $\Delta S^\ddagger = -22.4(7) \text{ cal K}^{-1} \text{ mol}^{-1}$  vs. DHA- $d_4$ :  $\Delta S^\ddagger = -11.6(2.0) \text{ cal K}^{-1} \text{ mol}^{-1}$ ) and decreasing influence of the activation enthalpy between C–H and C–D (DHA:  $\Delta H^\ddagger = 8.5(2) \text{ kcal mol}^{-1}$  vs. DHA- $d_4$ :  $\Delta H^\ddagger = 13.0(5) \text{ kcal mol}^{-1}$ ). During C–H activation of DHA, 64% of the theoretical maximum yield is obtained after 100 s (0.32 equivalents of maximum 0.5 equivalents), whereas 74% is reached after 1 h. This fast initial conversion supports the proposed formation of an  $\text{Fe}^{\text{III}}\text{-OH}$  intermediate. Anthracene is the sole product, and no oxygen atom transfer has been observed. The bimolecular reaction rates  $k_2$  of **42** are 2–3 orders of magnitude higher than those of **48** but up to 4 orders of magnitude lower than the most active systems, which are capable of oxidizing cyclohexane, a model substrate in C–H oxidation.<sup>159,169,193–195</sup> For comparison, Compound I, the reactive  $\text{Fe}^{\text{IV}}=\text{O}$  intermediate of cytochrome P450, is capable of cleaving unactivated C–H bonds with a rate constant of  $1.1 \times 10^7 \text{ M}^{-1} \text{ s}^{-1}$ .<sup>196</sup>

Variations in the ligand environment can have a significant influence on the structural and electronic properties of the complex, as showcased in Section 3. These changes can impact the C–H activation activity as observed between **42** and **48**.

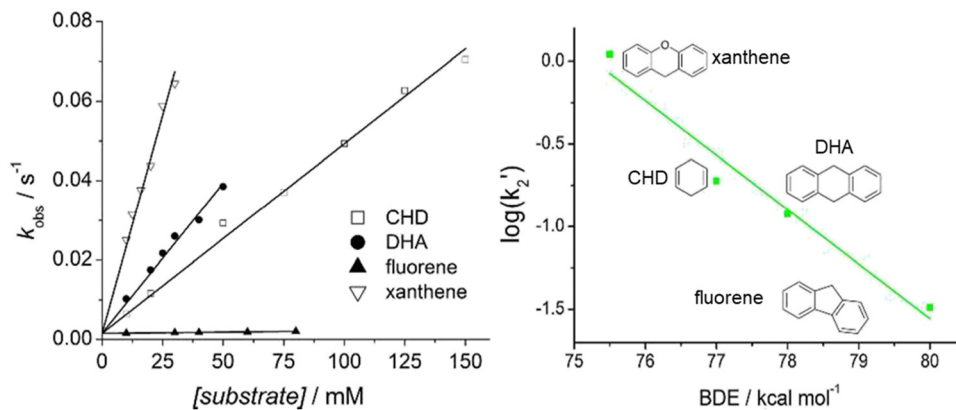


Fig. 16 Left: Kinetic data for **42** at 233 K in MeCN. Right: Plot of  $\log(k_2')$  against the weakest C–H bond dissociation energy of various substrates for **42**. Reprinted and adapted with permission from ref. 159. Copyright 2017 American Chemical Society.

Another example is an iron(IV)–oxo complex resembling **48** but with a smaller equatorial tetradentate ligand (an ethylene instead of a propylene bridge), resulting in a 3 orders of magnitude higher activity compared to **48**.<sup>197</sup>

Computational studies on the mechanism of HAT suggest a dissociation of the *trans* axial MeCN ligand in **42**, in contrast to **48**, as the resulting five-coordinated complex appears to have enhanced reactivity in HAT.<sup>159,175</sup> The HAT is predicted to follow a radical reaction pathway, as shown in Scheme 16, beginning with the formation of an oxyl-iron(III) ( $\text{Fe}^{\text{III}}\text{-O}^{\bullet-}$ ) species from **42** into the iron(III)-hydroxo intermediate **49** and a hydrocarbon radical.<sup>157,159</sup> Furthermore, HAT is proposed to proceed *via* the  $\pi$ -trajectory in the triplet pathway and a potential following hydroxylation step *via* the  $\sigma$ -trajectory.<sup>157,183</sup> Large kinetic barriers are calculated for C–H bond activation and hydroxylation.<sup>157</sup>

The C–H activation arising from the disproportionation of **40** to **42** can be significantly retarded upon addition of **4** and consequently shifting the equilibrium towards **40** (Scheme 17).<sup>185</sup> Cleavage of the Fe–O–Fe bridge and subsequent disproportionation was suggested to be initiated by axial coordination of the  $\text{Fe}^{\text{IV}}\text{=O}$  unit to one iron center of **40**. An isolated molecular structure of a **42**·**40**·**42** adduct is indicative of this conjecture (Fig. 17). Furthermore,

this adduct supports the proposed highly nucleophilic character of the oxo-ligand in **42**, which unusually does not show oxygen atom transfer with common substrates like MeSPh or  $\text{PPh}_3$ .<sup>159,185</sup>

#### 4.5. Further Fe–X–Fe (X = S–S, P, N) complexes

A *trans*-1,2-disulfide-bridged (*trans*- $\mu$ - $\eta^1$ : $\eta^1$ - $\text{S}_2$ )-diiron(III) complex (**50**) has been obtained after reaction of an excess of elemental sulfur with **4** in THF and subsequent precipitation from a MeCN solution with  $\text{Et}_2\text{O}$  at  $-35^\circ\text{C}$  in 20% yield.<sup>155,198–200</sup> The rather low yield is a result of decomposition of **50** in MeCN to the starting complex **4** when exposed to higher temperatures (Scheme 18). Under ambient conditions, **50** shows the same reactivity as **4** and forms the  $\mu_2$ -oxo bridged diiron complex **40**. XRD results reveal the molecular structure drawn in Scheme 18. The N–Fe–S angles are nearly linear ( $178.96(15)^\circ$ , Table 3) and the Fe–S–S moiety is bent with an angle of  $112.59(9)^\circ$ .<sup>155</sup> Generally, the disulfide–diiron unit can resonate between three structures including different oxidation states (Scheme 19).<sup>155,201</sup> However, the S–S bond length ( $2.023(3)\text{ \AA}$ ) is closer to the one in  $\text{H}_2\text{S}_2$  ( $2.055\text{ \AA}$ )<sup>202</sup> than to free  $\text{S}=\text{S}$  ( $1.887\text{ \AA}$ ),<sup>203</sup> indicating single bond character.<sup>155</sup> **50** has been found to be diamagnetic ( $S = 0$ ) due to extremely strong antiferromagnetic coupling ( $J = -836\text{ cm}^{-1}$ ), similar to **40** ( $J = -606\text{ cm}^{-1}$ ).<sup>60,155</sup> Mössbauer spectroscopy

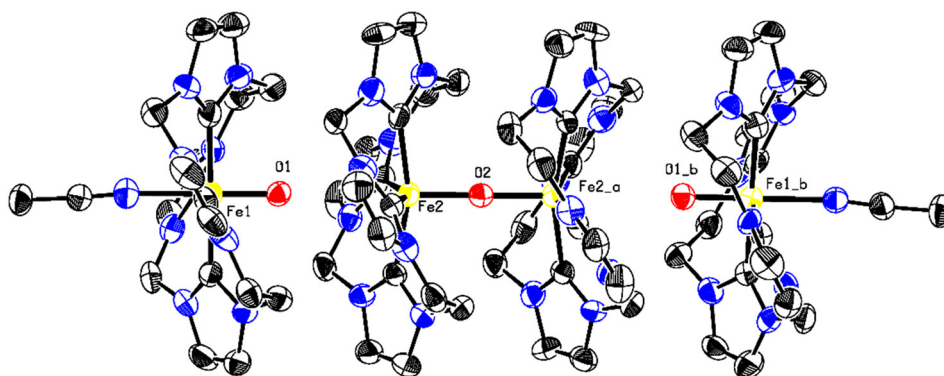
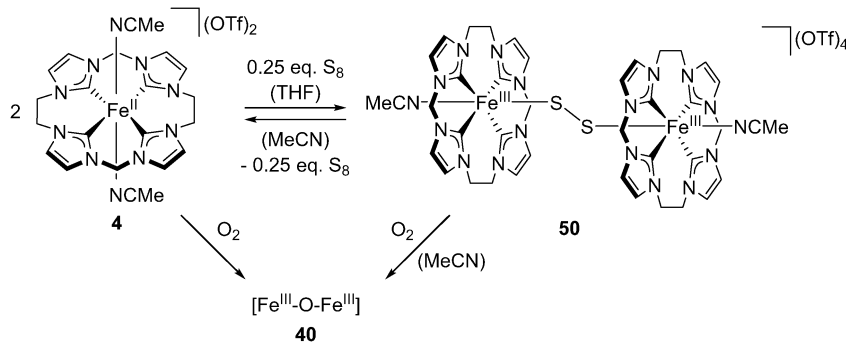
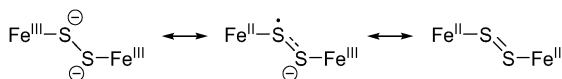


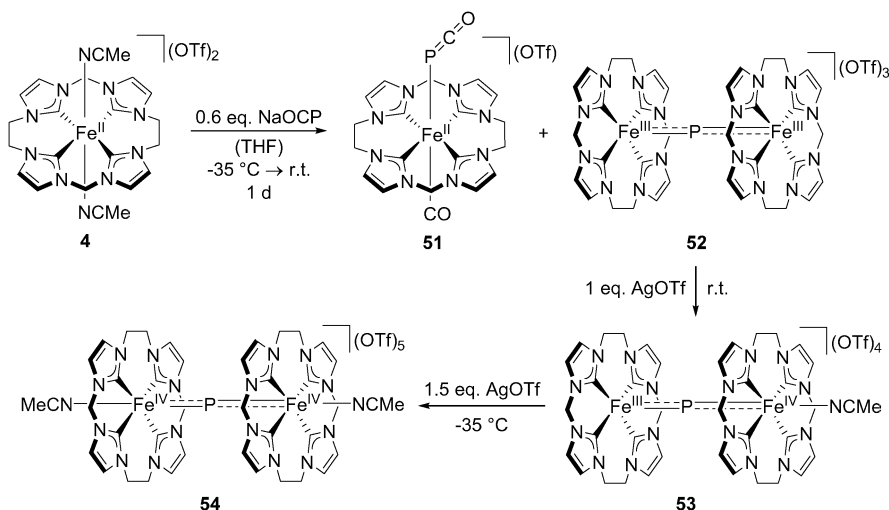
Fig. 17 Molecular structure of the **42**·**40**·**42** adduct. Selected atom distances [ $\text{\AA}$ ] and angles [ $^\circ$ ]: Fe1–O1: 1.673(4), Fe2–O2: 1.7685(9), O1...Fe2: 3.193(5), Fe1...Fe2: 4.8647(13), Fe2...Fe2\_a: 3.5369(13), O1–Fe1–N9: 179.4(4), Fe1–O1...Fe2: 178.2(3), Fe2–O2–Fe2\_a: 179.7(8).

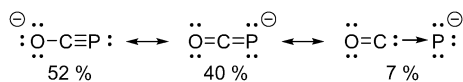
Scheme 18 Synthesis and reactivity of (*trans*- $\mu$ - $\eta^1$ : $\eta^1$ -S<sub>2</sub>)-diiron(III) complex **50**.<sup>155</sup>Scheme 19 Resonance structures of the *trans*-disulfide-diiron moiety.<sup>155,201</sup>

indicates identical local iron sites, excluding a mixed-valence configuration (Scheme 19, middle). The lower isomer shift of **50** (0.15 mm s<sup>-1</sup>) in comparison to iron(II) parent complex **4** (0.23 mm s<sup>-1</sup>) suggests low-spin iron(III) centers ( $S_i = 1/2$ ), which is supported by DTF calculations.<sup>155</sup>

A first example of a Fe–P–Fe complex containing a single-atom “naked” phosphorus bridge has been reported by reaction of Na(OCP)<sup>204,205</sup> as a P-anion transfer reagent with **4** in THF at –35 °C, forming a green precipitate (Scheme 20). It was characterized as the diiron(III)- $\mu_2$ -phosphido complex **52**. Mononuclear iron(II) complex **51** can be obtained as single crystals from the THF solution. Both **51** and **52** are formed in equal amounts in total about 60% yield.<sup>82</sup> **51** contains an axial P-bound OCP<sup>-</sup> ligand and a CO ligand.<sup>206,207</sup> The P–Fe–CO and P–C–O angles in **51** are nearly linear (174.73(13)° and 178.1(5)°, Table 2) and the C–P–Fe angle is 95.32(16)°. **51** is diamagnetic and the low-spin ( $S = 0$ )

configuration is confirmed by Mössbauer spectroscopy, even though its isomer shift is lower (0.05 mm s<sup>-1</sup>) in comparison to starting iron(II) complex **4** (0.23 mm s<sup>-1</sup>),<sup>60</sup> which has been explained by the different  $\pi$ -backbonding capabilities of the axial ligands.<sup>82</sup> The diiron(III)- $\mu_2$ -phosphido complex **52** shows a nearly linear Fe–P–Fe angle (178.25(12)°, Table 3) and is diamagnetic, similar to other bridged diiron complexes (except **44**, which has a bent angle but is also diamagnetic, see Scheme 12). A very strong antiferromagnetic coupling is observed between the two iron centers ( $|2J| \geq 1200$  cm<sup>-1</sup>) close to **40** ( $J = -606$  cm<sup>-1</sup>).<sup>60,82</sup> The  $S = 0$  ground state and the formal iron(III) centers of **52** have been confirmed by Mössbauer spectroscopy. The signal of the P nucleus appears at 1480 ppm in <sup>31</sup>P NMR. Furthermore, three conformational isomers have been detected in NMR. The reaction of **4** with NaOCP is assumed to form [LFe(PCO)(MeCN)]<sup>+</sup> first, which quickly releases CO. The ease of decarbonylation of OCP<sup>-</sup> can be explained with its resonance structures (Scheme 21, right). The release of CO might result in [LFe(P)(MeCN)]<sup>+</sup>, which reacts with **4** to **52**, but might also be triggered from the coordination of [LFe(PCO)(MeCN)]<sup>+</sup> with **4** to form **52**, without a terminal phosphido intermediate. **51** might be formed by substitution of MeCN with CO of [LFe(PCO)(MeCN)]<sup>+</sup>, apparently stabilizing the P-bound OCP<sup>-</sup> ligand.

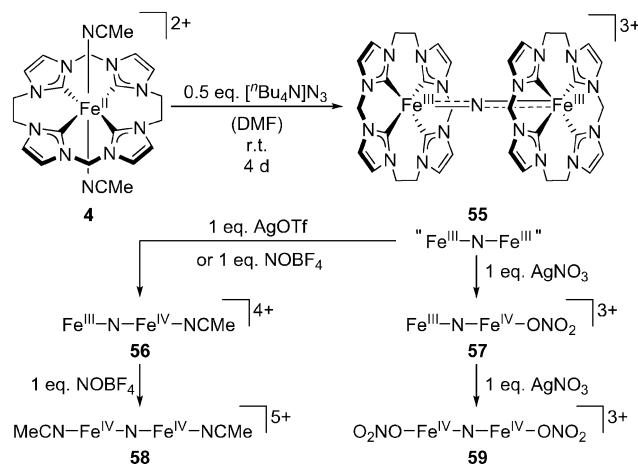
Scheme 20 Synthesis and one-electron oxidations of **52**.<sup>82</sup>



**Scheme 21** Resonance structures of  $\text{OCP}^-$  and their weights obtained from natural resonance theory analysis.<sup>204</sup>

UV/Vis monitored CV suggests the possibility of oxidizing **52** twice. Indeed, oxidation of **52** in MeCN with one equivalent or 2.5 equivalent of AgOTf leads to diiron(III,IV)- $\mu_2$ -phosphido complex **53** and diiron(IV)- $\mu_2$ -phosphido complex **54**, respectively, after precipitation with  $\text{Et}_2\text{O}$  (Scheme 20). The second oxidation is kinetically hindered and the product, **54**, is unstable at temperatures above *ca.*  $-10^\circ\text{C}$ . **53** contains one additional axial MeCN ligand stabilizing the higher oxidation state, but more information is not yet available due to the comparatively poor quality of the obtained crystallographic data. The molecular structure of **54** is similar to **52** and the Fe–P–Fe angle remains linear ( $179.61(4)^\circ$ ).<sup>82</sup> Based on the structures of **53** and **54**, the electrochemical irreversibility at lower temperatures has been assigned to coordination/dissociation processes of the axial MeCN ligands. The isomer shift of the three  $\mu_2$ -phosphido bridged complexes **52**, **53**, **54** barely changes upon oxidation, which might be assigned to a ligand-centered oxidation at first glance. However, the situation is similar to the series of  $\{\text{FeNO}\}^x$  complexes (see Sections 3.4, 4.2.2) and represents a metal-centered oxidation. The effect of deshielding of the 4s-iron orbital upon higher oxidation state, resulting in a higher electron density around the nucleus and thus smaller, more negative isomer shift, is counterbalanced by the longer Fe–NHC bonds in **54** ( $2.017(9)\text{ \AA}$ ) compared to **52** ( $1.982(11)\text{ \AA}$ ), leading to reduced  $\sigma$ -interactions, a lower compression of the 4s-iron orbital, a lower electron density around the nucleus and hence a higher, more positive isomer shift. SQUID magnetometry was used to assign paramagnetic **53** to a  $S = 1/2$  and diamagnetic **54** to a  $S = 0$  system.

Molecular iron nitrido complexes are of interest as models of key intermediates in the industrially highly desirable conversion of  $\text{N}_2$  to  $\text{NH}_3$  under mild conditions, as also observed in certain organisms. Addition of  $[\text{t}^{\text{Bu}}_4\text{N}]\text{N}_3$  to **4** in DMF and precipitation with  $\text{Et}_2\text{O}$  yields diiron(III)- $\mu_2$ -nitrido complex **55** (69% yield, Scheme 22).<sup>83</sup> The original formation of a  $[\text{LFe}^{\text{II}}(\text{N}_3)]^+$  species has been assumed, subsequently combining with **4** to release  $\text{N}_2$  and form **55**, possibly *via* a high-valent  $[\text{LFe}^{\text{IV}}=\text{N}]^+$  intermediate. The quantitative isolation of  $[\text{LFe}^{\text{II}}(\text{N}_3)_2]$  (**60**) and  $[\text{LFe}^{\text{II}}(\text{N}_3)](\text{OTf})$  (**61**) from reaction of **4** with an excess of  $[\text{t}^{\text{Bu}}_4\text{N}]\text{N}_3$  at  $-35^\circ\text{C}$  supports this idea. The high isomer shift of **60** ( $0.32\text{ mm s}^{-1}$ , Table 2) is indicative of an iron(II) oxidation state. Both molecular structures resemble **4** with nearly linear N–Fe–N angles (**60**:  $174.4(12)^\circ$ ; **61**:  $176.21(18)^\circ$ ) but the azido ligands are tilted, *i.e.* the Fe–N–N angles are bent (**60**:  $127.5(8.5)^\circ$ ; **61**:  $120.4(4)^\circ$ ). The molecular structure of diiron(III)- $\mu_2$ -nitrido complex **55** is similar to  $\mu_2$ -oxo complex **40** (Scheme 10), but the Fe–N bonds are shorter ( $1.690(1)\text{ \AA}$ ) than the Fe–O bonds ( $1.752(1)\text{ \AA}$ ), indicating multiple bond character in **55**, similar to the situation in **52** (Scheme 20 and Table 3). As is compound **40** and other bridged diiron(III) complexes in this review, **55** is diamagnetic ( $S = 0$ ) due



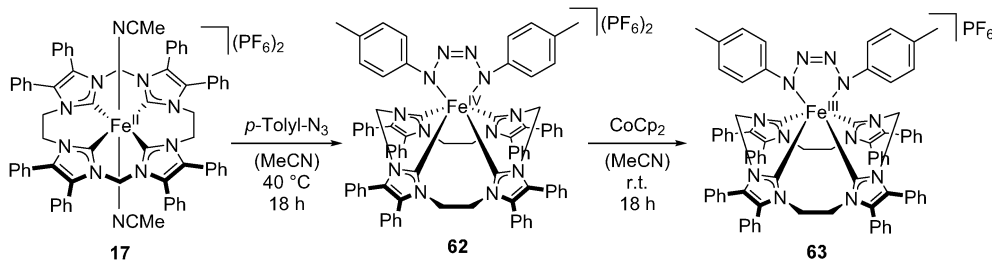
**Scheme 22** Synthesis and one-electron oxidations of diiron(III)- $\mu_2$ -nitrido complex **55**. The latter were conducted in MeCN at  $-35^\circ\text{C}$ . The counterions of **4**, **55**, **57** and **59** are  $\text{OTf}^-$ , whereas **56** and **58** can experience partial anion exchange.<sup>83</sup>

to very strong antiferromagnetic coupling ( $J > -700\text{ cm}^{-1}$ , stronger than **40** but weaker than **50**, see Scheme 18). The  $^1\text{H}$  NMR spectrum shows three different isomers with and without twisted tetracarbene ligands around the Fe–N–Fe axis.<sup>83</sup>

One-electron oxidation of **55**, as indicated in CV, has been achieved with AgOTf,  $\text{AgSbF}_6$  or  $\text{NOBF}_4$  (see Section 4.1) to obtain the mixed-valent diiron(III,IV)- $\mu_2$ -nitrido compound **56** (70% yield, Scheme 22).<sup>83</sup> Here, similar to **53** (Scheme 20), an axial MeCN ligand is coordinating to the iron(IV) center. Oxidation of **55** with  $\text{AgNO}_3$  leads to a mixed-valent complex (**57**, 83% yield) with an axial O-bound nitrate at the iron(IV) site. In excess of  $\text{AgNO}_3$ , a diiron(IV)- $\mu_2$ -nitrido species (**59**) with two axial O-bound nitrates is formed in 77% yield. Complementary, excess of  $\text{NOBF}_4$  with **55** gives the respective diiron(IV)- $\mu_2$ -nitrido complex (**58**, quantitative yield) with two axial MeCN ligands, which is slightly less stable than its counterpart **59**. The molecular structures resemble those of other bridged diiron complexes and the Fe–NHC bonds slightly increase upon higher oxidation state (**55**:  $1.988(11)\text{ \AA}$ ; **59**:  $2.016(18)\text{ \AA}$ , Table 3). Mössbauer spectroscopy and EPR measurements lead to an assignment of **56** and **57** to  $S = 1/2$  systems whereas **58** and **59** have  $S = 0$  ground states. The observed high covalency in the Fe–N–Fe moiety across the redox series suggests the use of Enemark–Feltham notation:  $\{\text{Fe}_2\text{N}\}^{n+4}$  with the nitrido ligand ( $\text{N}^{3-}$ ) as  $2e^- \sigma$  donor and  $4e^- \pi$  donor, and  $n$  the number of d-electrons. Thus, **55** can be written as  $\{\text{Fe}_2\text{N}\}^{14}$ , **56** and **57** as  $\{\text{Fe}_2\text{N}\}^{13}$  and **58** and **59** as  $\{\text{Fe}_2\text{N}\}^{12}$  complexes.<sup>83</sup>

#### 4.6. Monomeric iron(IV) adducts

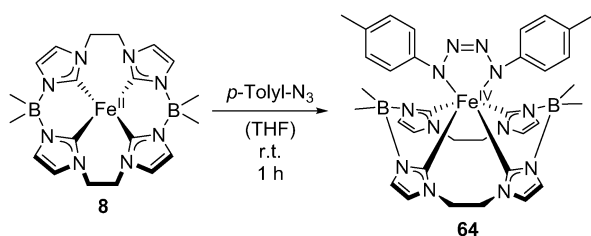
Iron(IV) imides are proposed to be intermediates in the aziridination of olefins (see Section 5.2).<sup>103</sup> In an attempt to isolate a potential iron(IV) imide species from an iron(II) aziridination catalyst, **17**,<sup>65</sup> an iron tetrazene complex has been isolated instead: Addition of *p*-tolyl azide to a solution of **17** in MeCN at  $40^\circ\text{C}$  yields the iron(IV) tetrazene complex **62** (74% yield, Scheme 23).<sup>160</sup> **62** is diamagnetic ( $S = 0$ ) and displays a trigonal prismatic geometry. The N–N bond lengths suggest a double

Scheme 23 Synthesis of iron(IV) tetrazene complex **62** and its reduction to **63**.<sup>160</sup>

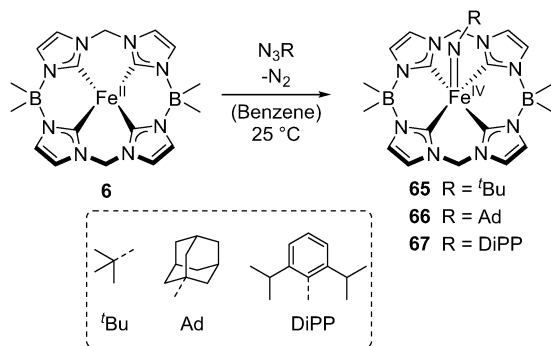
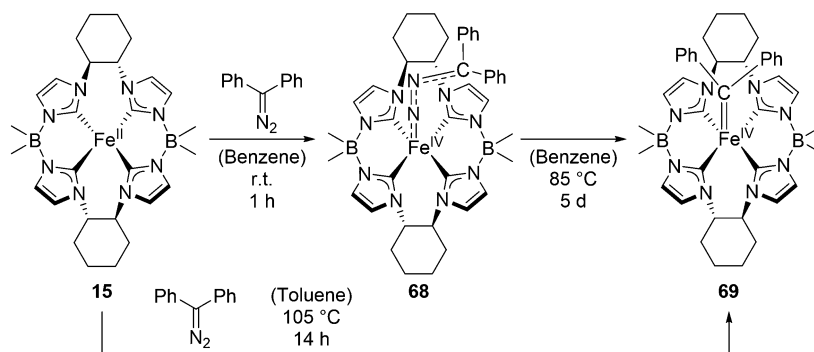
bond between the central nitrogen atoms, indicative of a dianionic tetrazene ligand (Table 4). Reduction of **62** has been achieved with  $\text{CoCp}_2$  to give its low-spin ( $S = 1/2$ ) iron(III) tetrazene analog **63**. The reduction has been assigned to be metal-centered based on the results of Mössbauer and EPR

spectroscopy in contrast to other cases, where the tetrazene ligand has been found to be redox active.<sup>160,208,209</sup> The overall geometry is similar to **62**.

Another iron(IV) tetrazene (**64**) has been obtained from reaction of excess *p*-tolyl azide with neutral iron(II) aziridination catalyst **8** in THF at room temperature in 14% yield (Scheme 24). **64** adopts a distorted trigonal prismatic geometry resembling **62**.<sup>103</sup>

Scheme 24 Synthesis of iron(IV) tetrazene complex **64**.<sup>103</sup>

Reaction of rather steric demanding azide compounds with the smaller, more rigid iron(II) complex **6** did not yield iron(IV) tetrazenes, instead, it gave the first examples for five-coordinated iron(IV) imides. Addition of *tert*-butyl azide, adamantyl azide or 2,6-diisopropylphenyl azide to a solution of **6** in benzene forms iron(IV) imides in 90% (**65**), 83% (**66**) and 78% yield (**67**), respectively (Scheme 25).<sup>76</sup> The complexes are thermally stable but react with traces of water to result in free amine and the  $\mu_2$ -oxo-bridged diiron(III) complex **38**. Complex **6** is ineffective for aziridination reaction and the iron(IV) imide complexes are as well (see Section 5.2). **65** and **66** show a similar distorted square-pyramidal structure with the imide nitrogen atom tilted towards one side of the macrocycle.<sup>76</sup> The Fe–N–C angles are more bent for **65** ( $150.07(10)^\circ$ , Table 4) and **66** ( $149.4(3)^\circ$ ) in comparison to **67** ( $163.04(11)^\circ$ ). **67** exhibits a symmetric structure, where the imide ligand is placed in the middle of the tetracarbene. The bending of the tetracarbene ligand upon formation of the iron(IV) imides can be recognized by the change of the NHC–Fe–NHC angles from square planar **6** ( $178.74(47)^\circ$ ) to around  $145^\circ$ . **67** has a significantly longer Fe–N bond ( $1.7300(12) \text{ \AA}$ ) than **65** or **66** ( $\sim 1.65 \text{ \AA}$ ). As **67** is paramagnetic, it has been assigned an intermediate ( $S = 1$ ) spin

Scheme 25 Synthesis of iron(IV) imide **65**, **66** and **67**.<sup>76</sup>Scheme 26 Synthesis of iron(IV) diazoalkane **68** and iron(IV) alkyldiene **69**.<sup>66</sup>

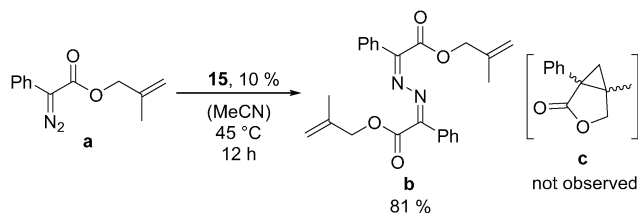
state using Evans NMR method. **65** and **66** are diamagnetic ( $S = 0$ ). The iron(IV) oxidation state was confirmed by Mössbauer spectroscopy.  $^{15}\text{N}$  isotope labelling of **65** has been achieved (83% yield), which allowed the measurement of the  $^{15}\text{N}$  NMR resonance of the  $^{15}\text{N}$  imide at  $-413$  ppm.

The reaction of oxidant  $\text{N}_2\text{CPh}_2$  with **15** gives a paramagnetic iron(IV) diazoalkane complex **68** (76% yield, Scheme 26).<sup>66</sup> The axial ligand is suggested to be in a hydrazonido(2-) [ $\text{Fe}^{\text{IV}}=\text{N}^+=\text{N}-\text{C}^-\text{Ph}_2$ ] conformation<sup>210</sup> with an Fe–N–N angle of  $174.5(4)^\circ$  and a N–N–C angle of  $140.4(5)^\circ$ . **68** has a spin state  $S = 1$ .<sup>66</sup> Reaction of **15** with  $\text{N}_2\text{CPh}_2$  at  $105^\circ\text{C}$  in toluene forms a purely organometallic iron(IV) alkylidene complex (**69**, Scheme 26). **69** is diamagnetic ( $S = 0$ ) and can also be obtained from heating of **68** at  $85^\circ\text{C}$  albeit **15** is also generated. In contrast to iron porphyrin alkylidenes, where suggested iron(IV) states have been corrected to iron(II),<sup>211</sup> the iron(IV) oxidation state of **69** has been verified by CV measurements.<sup>66</sup>

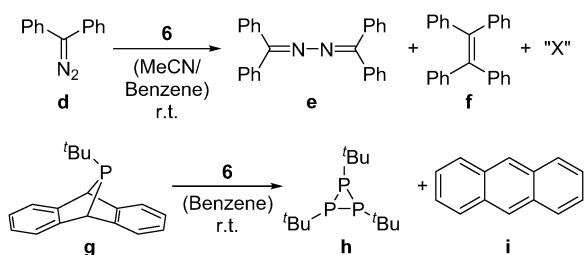
#### 4.7. Carbene and phosphinidene transfer

Iron carbene adducts like **69** (Scheme 26) have been reported to act as useful cyclopropanating agents.<sup>212,213</sup> Test reactions of **69** in chiral cyclopropanation did not show a carbene transfer, probably due to rather little space at the iron center for disubstituted alkenes.<sup>66</sup> Complex **15** also did not yield the cyclopropane (**c**, Scheme 27) but a dimeric azine (**b**).<sup>66</sup>

Further studies on carbene transfer using  $\text{N}_2\text{CPh}_2$  have been performed with **6**, **7** and **38** (Scheme 9).<sup>63</sup> Only **6** (25% load) shows conversion of  $\text{N}_2\text{CPh}_2$  at r.t. within 1 h. Three products are found in a 50 (**e**)/35 (**f**)/15 molecular ratio with an unidentified compound ("X", Scheme 28). **e** and **f** are known side products in the decomposition of  $\text{N}_2\text{CPh}_2$  after prolonged heating, but control experiments without **6** do not yield these compounds, evidencing a certain catalytic activity of **6** albeit at low selectivity.<sup>63,214,215</sup>



Scheme 27 Cyclopropanation test reaction with **6**.<sup>66</sup>

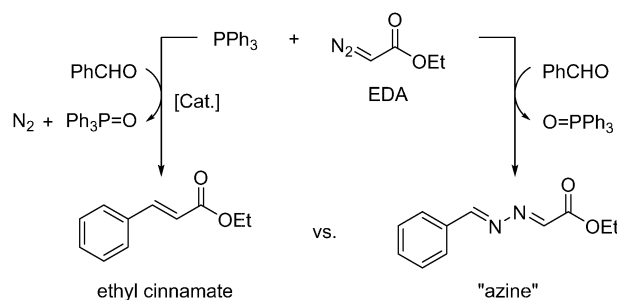


Scheme 28 Carbene and phosphinidene transfer test reactions.<sup>63</sup>

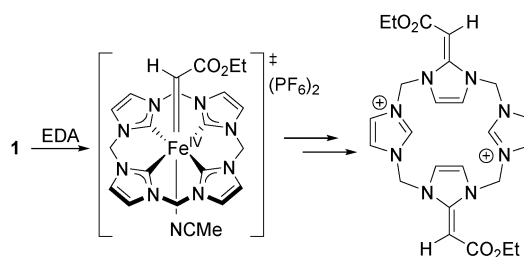
Phosphinidene transfer has been tested using  $\text{g}^{216}$  and complexes **6**, **7**, **8** and **38** (Scheme 28). Again, only **6** (10% load) shows conversion of **g** at r.t. within 2 h. The major product **h** is generated in high selectivity and a control reaction without **6** shows minor decomposition of **g**. It should be mentioned, that **8**, although structurally very similar to **6**, does not show any reactivity.<sup>63</sup> In return, **8** is active in aziridination reaction, whereas **6** is not.<sup>64,76</sup>

#### 4.8. Olefination of aldehydes

Catalytic olefination of aldehydes in Wittig reactions are known with transition metal complexes containing, for example, Mo, Re, Ru and Fe, and have the advantage to not require the preformation of the ylide as in an un-catalyzed Wittig reaction.<sup>217–219</sup> While many described systems need high catalyst loadings and harsh conditions, an iron(II) porphyrin was reported as a first highly active catalyst working at r.t. at low concentrations.<sup>219–222</sup> Hence, iron(II) tetracarbene **1** as organometallic heme analog has been tested in the catalytic olefination of aldehydes using 4 mol% of **1** and benzaldehyde, ethyl diazoacetate (EDA) and triphenylphosphine at  $70^\circ\text{C}$  for 4 h. However, no olefin formation but undesired azine has been observed in 63% yield (Scheme 29). This has been assigned to the decomposition of the tetracarbene ligand of **1** in the presence of EDA, resulting in de-coordination of iron and thus un-catalyzed azine formation. The degradation is suggested to proceed *via* an unstable iron(IV) carbene species (Scheme 30), as for other iron complexes, which would resemble the reactivity of **15** yielding iron(IV) alkylidene **69** (Scheme 26).<sup>66,219</sup>



Scheme 29 Catalytic olefination of aldehydes (left) and un-catalyzed competing reaction (right).<sup>219</sup>



Scheme 30 Degradation of **1** in the presence of EDA.<sup>219</sup>

Table 4 Selected structural and spectroscopic parameters of monomeric iron tetracarbenes adducts

Complex	$\delta C_{\text{NHC}}^a$	$E_{1/2}$ [V] vs. Fe/Fe <sup>+</sup> <sub>b</sub>	(Fe-X) <sub>av</sub> <sup>c</sup> [Å]	(Fe-C <sub>NHC</sub> ) <sub>av</sub> <sup>d</sup> [Å]	(C <sub>NHC</sub> -Fe-C <sub>NHC</sub> ) <sub>av</sub> <sup>e</sup> [°]	(C <sub>NHC</sub> -Fe-X) <sub>av</sub> <sup>f</sup> [°]	$\delta^h$ [mm s <sup>-1</sup> ]	$ \Delta E_Q ^i$ [mm s <sup>-1</sup> ]	Ref.	Additional
42 (42a)	—	—	1.661(3) Fe-N: 2.104(4)	2.010(18)	89.88(2.39) 173.46(56)	O-Fe-C: 92.69(36) O-Fe-N: 176.65(17), C-Fe-N: 87.36(1.25)	-0.13	3.08	60	Fe(IV) S = 1 $\nu_{\text{FeO}} = 832(3) \text{ cm}^{-1}$ Fe(III) $g = 1.95$
43	—	—	—	—	—	—	—	—	74	Fe(III)
49	—	—	—	—	—	—	—	—	159	Fe(III)
62	169.79	-1.05 (FeIV/III)	1.909(13) N-N: 1.344(2) N=N: 1.292(3)	1.976(14)	80.17(2.56) 130.89(5.45)	87.25(1.45) 126.10(1.52) 143.63(36)	-0.01	0.62	160	Fe(IV) S = 0
63	—	—	1.964(17) N-N: 1.373(5) N=N: 1.272(3)	1.965(4)	81.79(2.76) 132.96(14.86)	N-Fe-N: 77.13(9) 88.10(1.39) 116.08(2.27) 150.77(27)	0.10	1.13	160	Fe(III) S = 1/2
64	—	—	1.907(5) N-N: 1.353(4) N=N: 1.294(5)	1.980(5)	79.11(2.50) 126.06(15.14)	N-Fe-N: 76.08(9) 89.86(28) 121.00(12) 152.25(40)	—	—	103	Fe(IV)
65	176.2	—	1.6552(12)	1.961(18)	83.97(97) 142.13(94)	N-Fe-N: 78.22(13) 108.71(6.20)	-0.18	0.97	154	Fe(IV) S = 0
66	175.9	—	1.654(4)	1.957(19)	84.83(69) 145.02(95)	Fe=N-C: 150.07(10) 107.29(6.41)	-0.18	1.11	154	Fe(IV) S = 0
67	—	—	1.7300(12)	1.980(3)	86.61(16) 151.82(99)	Fe=N-C: 149.4(3) 104.09(87)	-0.11	2.67	154	Fe(IV) S = 1 $\mu = 2.6 \mu_B$
68	—	—	1.779(4), N=N: 1.215(5), N=C: 1.327(6)	2.005(13)	86.33(42) 150.55(2.05)	Fe=N-C: 163.04(11) Fe=N-N: 174.5(4), N=N=C: 140.4(5)	—	—	66	Fe(IV) S = 1 $\mu = 2.5 \mu_B$
69	188.8 (NHC), 172.4 (NHC), 309.8 (Fe = C) <sup>j</sup>	-2.21 (FeIV/FeIII)	1.814(4)	1.995(13)	88.06(50) 158.33(4.35)	Fe=C-C: 123.3(3)	—	—	66	Fe(IV) S = 0
71	—	—	—	—	—	—	-0.21	4.05	71	Fe(IV) S = 1

Annotations *a-i* see Table 1. <sup>j</sup> in C<sub>6</sub>D<sub>6</sub>.

#### 4.9. Summary

Iron tetracarbenes exhibit a manifold reactivity. Axial ligand substitution is easy to perform and provides a simple but powerful tool for post-modification of the electronic properties of iron tetracarbenes. The choice and number of axial ligands can be decisive regarding the spin state of the complex, *e.g.*  $S = 0$  or  $1$  for iron(II) or  $S = 1/2$  or  $3/2$  for iron(III) complexes, similar to iron porphyrins, but configurations with high-spin are unfavored due to the strong  $\sigma$ -donation of the tetracarbene.

Iron tetracarbenes show a great affinity to oxygen and various  $\mu_2$ -oxo bridged diiron, a superoxo and an iron(IV)-oxo complex have been reported. The iron(IV)-oxo complex as a synthetic model of the active key intermediates in enzymatic cycles of C-H oxygenation has been studied in C-H bond activation. The strong electron donation of the tetracarbene into the equatorial plane rises the  $x^2-y^2$  orbital above the  $z^2$  orbital, which is unusual and opposite to the electronic structure of most N-ligated iron complexes. This results in a considerable larger triplet–quintet energy gap and thus exclusively triplet reactivity in hydrogen atom transfer. The reaction rates are on an intermediate level compared to the literature, but no oxygen atom transfer has been achieved.

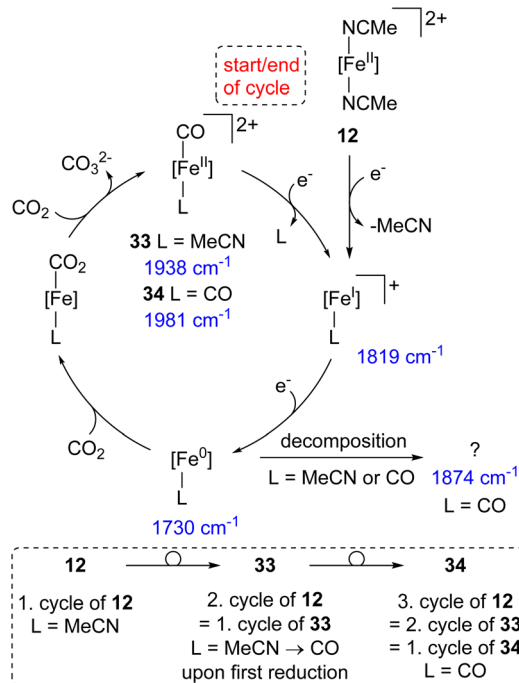
Similar to oxygen, N, P and  $S_2$  containing diiron complexes have been reported. These bridged diiron(III) complexes are diamagnetic due to very high antiferromagnetic coupling and can be stepwise oxidized to diiron(IV) compounds. The chelating, electron donating nature of the tetracarbene ligand is beneficial for the isolation of stable iron tetracarbenes in high oxidation state (*i.e.*  $Fe^{IV}$ ). Monomeric iron(IV) compounds also have been obtained, such as iron(IV) tetrazenes and first examples of five-coordinated iron(IV) imides – both being intermediates in the aziridination reaction –, an iron(IV) diazoalkane, an iron(IV) alkylidene and of course the already mentioned iron(IV)-oxo complex.

## 5. Catalysis

### 5.1. Electrochemical $CO_2$ reduction

The reduction of  $CO_2$  in general, but especially using molecular catalysts with abundant metals mostly based on porphyrin or other N-donor based systems, has experienced a revival in the last 15 years. The idea is to remove excess greenhouse gas  $CO_2$ , a major cause of the climate change, from the atmosphere and use it as feedstock.<sup>223,224</sup> Iron(II) tetracarbene **12** represents one of the first examples of an iron NHC complex to be employed in electrochemical  $CO_2$  reduction.<sup>79,225</sup> Iron tetracarbenes are interesting systems to be investigated in  $CO_2$  reduction, as they are structurally similar, but electronic distinct to iron porphyrin systems, which are capable and stable catalysts achieving selective  $CO_2$  to CO reduction at very high turnover frequencies (TOF) up to  $10^6 s^{-1}$ .<sup>223,226</sup>

**12** converts  $CO_2$  to CO selectively at  $-2.21 V$  vs.  $Fc^{+/0}$  with a faradaic efficiency of 92% in MeCN. A very high TOF of  $3300 s^{-1}$  is reached, which is in the range of other highly active first-row transition metal catalysts without a proton source.<sup>79</sup> The turnover

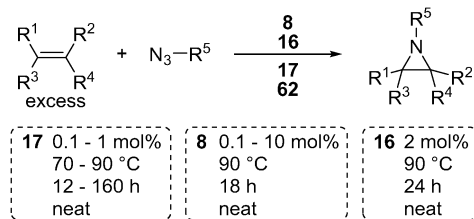


Scheme 31 Proposed mechanism for the reduction of  $CO_2$  to CO by **12** and **33**.<sup>79</sup>

number (TON) of 4 is only modest. Mono- and bis(CO) complexes **33** and **34** (Scheme 7) are expected to be intermediates in the catalytic cycle. Hence, **33** has been tested in the reduction of  $CO_2$  at  $-2.21 V$  and achieved a slightly lower TOF ( $3100 s^{-1}$ ) but higher TON (7). Linear sweep voltammetry spectroelectro-IR studies together with DTF calculations suggest the catalytic mechanism represented in Scheme 31. **12** is expected to lose one axial MeCN ligand upon first reduction to give  $[LFe^I(MeCN)]^+$ . It is consecutively reduced to iron(0) and a  $CO_2$  molecule coordinates to the highly nucleophilic iron center with presumably occupied  $d_{z^2}$  orbital due to the strong  $\sigma$ -donating properties of the tetracarbene (see Section 4.4 for details).<sup>227</sup> This is in contrast to iron porphyrin complexes, where the reduction is ligand-centered and an intermediate-spin iron(II) center which is antiferromagnetically coupled to a porphyrin diradical anion is proposed.<sup>228,229</sup> The formation of CO in the absence of a proton source proceeds *via* disproportionation of two formal  $CO_2^{\bullet-}$  radical species to CO and  $CO_3^{2-}$ .<sup>79,230</sup> One can visualize the first CO to be bound to the iron center still after the first cycle of **12**, representing the mono(CO) iron(II) complex **33**. The following cycles of the initial complex **12** are the same as for the first and consecutive cycles of **33**: The MeCN ligand is removed upon first reduction of **33** to give  $[LFe^I(CO)]^+$ . The same steps mentioned above are repeated to finish this catalytic cycle with bis(CO) complex **34**. The next and all subsequent catalytic cycles starting with **34** always involve the removal of one CO ligand from **34** upon first reduction.<sup>79</sup>

### 5.2. Aziridination

Aziridines, the smallest nitrogen-containing heterocycles, are important building blocks and synthetic targets that can be



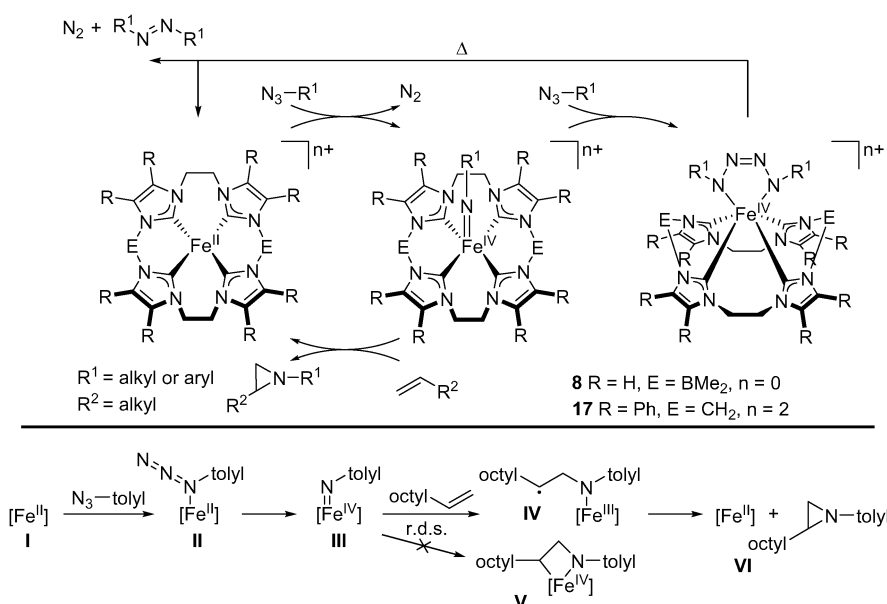
Scheme 32 Aziridination of olefins with organic azides catalyzed by **8**, **16**, and **62**.

found in natural products and pharmaceuticals.<sup>231,232</sup> Aziridines can be synthesized through addition of a nitrogen source to olefins, among other methods (Scheme 32).<sup>232</sup> Organic azides are easy to synthesize and are atom efficient and sustainable metal–nitrene precursors.<sup>103,232</sup> However, rather harsh conditions, such as heating or UV irradiation, have to be applied due to the low reactivity of azides.<sup>232</sup>

Iron(II) tetracarbene **17** has been employed as catalyst in aziridination of different substituted aliphatic alkenes with electron donating and withdrawing aryl azides.<sup>65</sup> The reactions are performed neat, *i.e.* using the substrate as solvent, different to Ru, Cu or Rh systems, which operate at lower temperatures in the presence of a solvent (Scheme 32).<sup>232</sup> The rather high temperatures seem to be required for the initial formation of the iron imide intermediate (*vide infra*). Due to the resulting low solubility of **17** at room temperature, the catalyst can be recovered and reused up to three times without significant decrease in yield.<sup>65</sup> An iron(IV) imide as potential intermediate in the aziridination has been detected in mass spectroscopy (Scheme 33). In an attempt to isolate the iron(IV) imide, an iron(IV) tetrazene complex **62** has been obtained instead (Scheme 23). **62** can be employed as aziridination catalyst and achieved a lower yield of **j** (77%) at higher catalyst loading

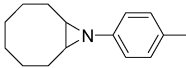
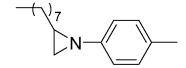
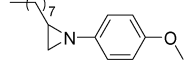
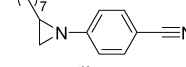
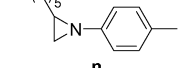
(0.2 mol%) in comparison to **17** (97%, 0.1 mol%, Table 5). Direct group transfer of **62** has also been reported and **17** can be regenerated after heating at 85 °C for 1 d in the presence of *cis*-cyclooctene.

Complex **8**, possessing a stronger  $\sigma$ -donating tetracarbene ligand than **17**, has been used as a first catalyst in aziridination of aliphatic alkenes with more challenging alkyl azides.<sup>64,233</sup> Furthermore, functionalized, aliphatic-aryl and bicyclic aziridines are synthesized. A higher yield (>80%) of aliphatic-alkyl aziridines is achieved with less steric demanding alkyl azides. More challenging functionalized aziridines are synthesized in modest yields (32–50%) and **8** also catalyzes intramolecular aziridinations. **8** reaches higher yields than **17**, *e.g.* 95% *vs.* 82% of **k** and is more functional group tolerant (Table 5). The higher yields of **8** are explained by the more electron rich iron center, which is expected to lower the required energy for the formation of the initial iron(IV) imide.<sup>64</sup> A higher electron affinity (EA) of the iron(IV) imide has also been set in correlation with higher aziridine yields.<sup>234</sup> For the respective iron(IV) imide of **8**, an EA of 70 kcal mol<sup>-1</sup> has been calculated and a value of 88 kcal mol<sup>-1</sup> for **17**,<sup>234</sup> which does however appear to not be the decisive factor in this case. Asymmetric aziridination has been tested with the chiral iron(II) complex **16**, which can be recovered after reaction like **17**, but to a lower extent. However, **16** is only moderately active in aziridination (55% yield of **k**, Table 5), does not react with alkyl azides like **17**, and achieves low enantiomeric excess of 4% in maximum.<sup>69</sup> Similar to **8**, more steric demanding aryl azides lead to lower yields or no reaction at all. This can be explained by a higher necessary activation energy for the initial iron(IV) imide formation step (*vide infra*). Generally speaking, it has to be pointed out, that the aziridination of alkenes with organic azides at these conditions already proceeds without an iron complex in low (2%) up to moderate yields (60%).<sup>64,65,69,103,235,236</sup> In extreme cases, this can make



Scheme 33 Proposed mechanism of aziridination of alkenes.<sup>103,160</sup>

**Table 5** Comparable catalytic results of **8**, **16**, **17** and **62**. All reactions were performed without solvent at 90 °C. Blank experiments are without an iron complex<sup>64,65,69,160</sup>

Entry	Complex	Catalyst loading	Time [h]	Yield	Blank
	<b>17</b>	0.1 mol%	12	97%	—
	<b>62</b>	0.2 mol%	16	77%	—
	<b>17</b>	1 mol%	18	82%	43%
	<b>8</b>	1 mol%	18	95%	—
	<b>16</b>	2 mol%	24	55%	32%
	<b>17</b>	5 mol%	18	65%	—
	<b>8</b>	5 mol%	18	80%	—
	<b>17</b>	1 mol%	18	38%	—
	<b>8</b>	1 mol%	18	68%	—
	<b>16</b>	2 mol%	24	65%	60%
	<b>8</b>	1 mol%	18	91%	—
	<b>8<sup>a</sup></b>	1 mol%	18	32%	—

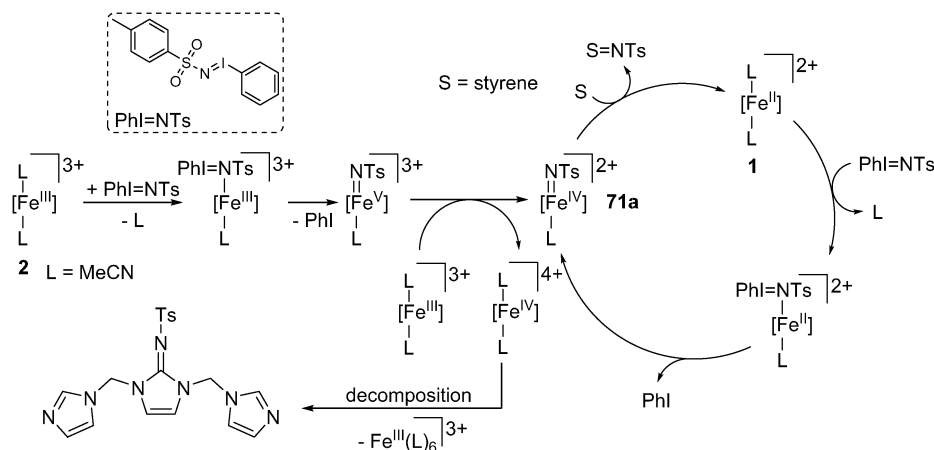
<sup>a</sup> Reaction in 5 equivalents of alkene and toluene as solvent.

the addition of the iron complex unnecessary: **16** yields **n** in 65%, whereas the control reaction without **16** gives 60%.<sup>69</sup>

The proposed mechanism of aziridination involving an iron(IV) imide has been more closely investigated using DFT calculations.<sup>103</sup> The initial iron imide formation (**III**, Scheme 33) proceeds *via* an  $\alpha$ -bound azide (**II**). Alkyl azides appear to require a higher activation energy than aryl azides. Additional experimental data show, that **8** exhibits a higher imide formation rate than **17** because of the higher electron density from the stronger donating tetracarbene. The reaction of the alkene with the iron imide is suggested to proceed *via* an open-chain radical intermediate (**IV**) rather than an azametallacyclobutane intermediate (**V**). Here, a flexible tetracarbene ligand is required to accommodate the alkene in proximity to the

imide as additional ligand is *cis* position,<sup>160</sup> giving reasons why the more rigid complex **6** is not an effective aziridination catalyst. This is the rate determining step (r.d.s.) of the aziridination in contrast to porphyrin systems, where the r.d.s. is the addition of the organic azide to the catalyst.<sup>103,237,238</sup> **8** already reacts with azides at room temperature, but aziridination occurs at higher temperatures only, supporting the r.d.s. assignment. The azametallacyclobutane intermediate is expected to retain the stereochemistry of the alkene in the aziridine, whereas the open-chain intermediate can change it, which was observed for **8**. However, although not mentioned by the authors, the control reaction without iron complex already yields a mixture of the respective diastereomers achieving around a half of the total yield with **8**.<sup>103</sup> **17** achieved a higher stereoselectivity at a lower yield. While the intramolecular rotational barrier is similar for both open-chain intermediates of **8** and **17**, **17** has a 6.7 kcal mol<sup>-1</sup> lower activation barrier than **8** for the formation of the aziridine from the open-chain intermediate (**VI**), resulting in a faster rate of aziridine generation and an enhanced stereocontrol. The role of the formation of the iron tetrazene as side product remains somewhat unclear as described by the authors. While aziridination with iron tetrazene **62** (Scheme 23) was reported previously,<sup>160</sup> the proposed mechanism describes the formation of iron tetrazene as competing reaction, which only yields a diazene upon regeneration of the iron(II) counterpart.<sup>103</sup> However, the major product from direct group transfer of **62** indeed was the diazene and as the iron(II) complex **17** could be regenerated from **62** below the catalysis temperature, the aziridination results of **62** might in reality mostly originate from reformed **17**. Therefore, the tetrazene can be considered to slow down the reaction rate and to consume organic azide to form (mainly) unwanted diazene. Nevertheless, the use of steric demanding organic azides is assumed to avoid the formation of the tetrazene. Indeed, effectively the same yield of aziridine is obtained with only 5 equivalents of alkene in toluene as solvent in comparison to an excess of alkene neat when using mesityl azide.<sup>103</sup>

Just recently, complexes **1** and **2** have been tested in aziridination.<sup>71</sup> In this case, (*p*-toluenesulfonylimino)benzene (PhI = NTs) as nitrene source and styrene as substrate have been used and both complexes achieved around 75% yield at r.t., indicating that both reactions involve the same active



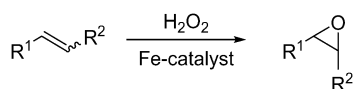
**Scheme 34** Proposed mechanism of aziridination/nitrene transfer employing **1** or **2**.<sup>71</sup>

species. Furthermore, **1** and **2** have been tested in the sulfimination of thioanisole (~98% yield) and the amination of ethylbenzene (~22% yield) and cyclohexane (~15% yield). No information about the yield without complex is given. The active species has been characterized as iodine adduct of an iron(IV) imide complex [LFe<sup>IV</sup> = NTs(PhI = NTs)]<sup>2+</sup> with *S* = 1 spin state (**71**, Table 4). However, the actual active species during catalysis is expected to be the analog MeCN adduct [LFe<sup>IV</sup> = NTs(MeCN)]<sup>2+</sup> (**71a**) after ligand exchange. Based on experimental and spectroscopic data, the displayed mechanism was proposed (Scheme 34). As imino and oxo iodine reagents commonly react through two-electron processes,<sup>239</sup> the formation of **71a** from iron(III) complex **2** proceeds through a comproportionation reaction, involving an iron(V) imide species and **2**. In turn, **71a** is directly formed from **1**. Similar to epoxidation reaction (*vide infra*), degradation of the catalyst was assigned to C-tosylation of one of the NHC units of the tetracarbene ligand, leading to Fe release.

### 5.3. Epoxidation

Cytochrome P450 are a family of hemoproteins catalyzing monooxygenation of inert C–H bonds and epoxidation of C=C double bonds under mild conditions with high regioselectivity and stereoselectivity.<sup>3,177,240,241</sup> Originally to study the reaction mechanisms of cytochrome P450, artificial Fe catalysts with porphyrin ligands were synthesized, to mimic the reactive character of the enzymes, as the chemistry of these hemoproteins takes place at the iron(II) porphyrin cofactor, called heme.<sup>125,242–245</sup> Iron(II) tetracarbenes as heme analogs are structurally similar, – albeit the heme unit is planar in opposite to some tetracarbenes<sup>117–121</sup> – but they are electronically distinct: the porphyrin ligand contains a conjugated cyclic aromatic system and is redox active, whereas tetracarbenes are not.<sup>116</sup> Furthermore, the strong  $\sigma$ -donation of the tetracarbene raises the  $d_{x^2-y^2}$  orbital, which can lead to a different reactivity (see Section 4.4).<sup>175</sup> Therefore, epoxidation of olefins was tested with **1** and **2** (Scheme 35).<sup>73</sup>

Both iron complexes catalyze the epoxidation of *cis*-cyclooctene as model substrate in full conversion at high selectivity without the formation of diol (Table 6).<sup>73</sup> *Trans* coordination of the axial MeCN ligands is known to strongly favor the epoxidation over the dihydroxylation, whereas for a *cis* coordination the epoxide is usually obtained in low yields without the use of coordinating additives, *e.g.* acetic acid.<sup>102,195,246–254</sup> Control experiments without **1** or **2** do not show any epoxide formation.<sup>73</sup> Iron complex (II) **1** is highly active with a TOF of 50 000 h<sup>-1</sup>, whereas iron(III) complex **2** reaches a TOF of 183 000 h<sup>-1</sup>, which is much higher than the most active homogenous catalysts based on Re (39 000 h<sup>-1</sup>) and Mo (53 000 h<sup>-1</sup>) or other iron catalysts based on N-donor ligands (20 000 h<sup>-1</sup>).<sup>249,255,256</sup>



Scheme 35 Epoxidation of olefins catalyzed by iron tetracarbenes.

Table 6 Selected catalytic performance of **1**, **2** and **44** in the epoxidation of *cis*-cyclooctene<sup>53,73,75</sup>

Cat.	Additive	Conv. <sup>a</sup> [%]	Sel. <sup>a</sup> [%]	TOF <sup>b</sup> [h <sup>-1</sup> ]	TON
<b>1</b>	—	24	94	50 000	480
<b>1</b>	Sc(OTf) <sub>3</sub>	59	>99	415 000	1180
<b>2</b>	—	51 <sup>c</sup>	>99	183 000	—
<b>2</b>	Sc(OTf) <sub>3</sub>	58	>99	413 000	1160
<b>44</b>	—	7	>99	23 000	140
<b>44</b>	Sc(OTf) <sub>3</sub>	58	>99	405 000	1160
<b>70</b>	—	37 <sup>de</sup>	>99	—	—
<b>70</b>	Sc(OTf) <sub>3</sub>	97 <sup>df</sup>	>96	41 000	—

Reaction conditions: *cis*-cyclooctene (269  $\mu$ mol, 100 mol%), H<sub>2</sub>O<sub>2</sub> (404  $\mu$ mol, 150 mol%), catalyst (0.135  $\mu$ mol, 0.05 mol% based on iron), additive (1.35  $\mu$ mol, 0.5 mol%); solvent: acetonitrile; *T* = 20 °C. <sup>a</sup> All conversions and selectivities were determined by GC-FID after a reaction time of 5 min. <sup>b</sup> TOFs were determined after 10 s. <sup>c</sup> Catalyst concentration: 0.1 mol%, conversion was determined after 10 s. <sup>d</sup> Catalyst concentration: 0.5 mol%. <sup>e</sup> Reaction time 30 s. <sup>f</sup> 0.1 eq. of Sc(OTf)<sub>3</sub>, reaction time 30 min.

Higher yields can be obtained at reduced temperature due to an enhanced catalyst stability, albeit at lower reaction rates. A TON of 4300 was found for **2** at –30 °C. Different oxidants have been tested, but H<sub>2</sub>O<sub>2</sub> gives the highest yields of epoxide. Regardless, H<sub>2</sub>O<sub>2</sub> is the oxidant of choice as it is the most atom economic and cheapest oxidant next to air, easy to handle and its byproduct, water, is environmentally benign.<sup>75,257–259</sup> Increasing H<sub>2</sub>O<sub>2</sub> over 250 mol% reduces the yield due to a lower catalyst stability. Lower oxidant concentrations than 150 mol% also result in lower yields due to catalytic decomposition of H<sub>2</sub>O<sub>2</sub> to a certain extent; however, additional H<sub>2</sub>O<sub>2</sub> can lead to a complete conversion, as the catalyst is still active in this case.<sup>73,260–262</sup> Furthermore, **2** does not exhibit a strong Fenton reactivity. Contrary to iron epoxidation catalysts with *cis*-labile coordination sites, further addition of H<sub>2</sub>O results in lower epoxide yields, indicating, that a water-assisted pathway does not apply for **2**. This is supported by the fact, that no <sup>18</sup>O is incorporated in formed epoxide in a H<sub>2</sub><sup>18</sup>O labeling experiment. Cyclic, acyclic and aryl alkenes can also be applied in the epoxidation using **2**. For acyclic alkenes, the *Z* isomer is favored over the *E* isomer similar to other iron complexes<sup>253</sup> and acyclic terminal alkenes are the most challenging. The affinity of **2** to highly substituted alkenes and its high selectivity are an indicator for the electrophilic nature of the active species.<sup>73,248</sup>

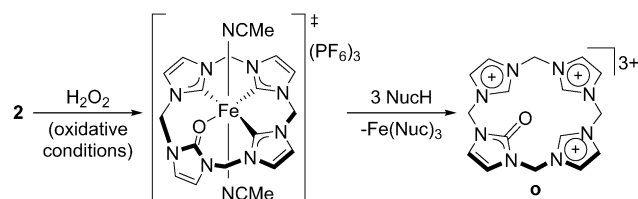
The oxidation of iron(II) complex **1** to iron(III) counterpart **2** is expected to be the initial step in the mechanism, as **1** has an induction period contrary to **2**.<sup>73</sup> No in-depth mechanistic studies on the epoxidation mechanism for **2** have been reported yet, but the mechanism for other N-ligated iron complexes suggests the formation of an Fe<sup>III</sup>–OOH intermediate as next step, followed by the rate-determining homolytic or heterolytic cleavage to give an iron(IV)- or iron(V)-oxo intermediate, respectively, and electrophilic attack on the alkene to yield the epoxide.<sup>36,42</sup> The reaction with the alkene is, based on an assumed Fe<sup>IV</sup>=O reactive species, proposed to proceed *via* the <sup>3</sup> $\sigma$ -pathway, as the <sup>3</sup> $\pi$ -pathway is calculated to be 10.6 kcal mol<sup>-1</sup> higher in energy for the epoxidation of propene and only the triplet state is accessible during catalysis (see Fig. 14 and Section 4.4).<sup>175</sup>

Stable diiron  $\mu_2$ -oxo-bridged complexes are known to be generated under oxidative conditions during catalysis and often are dead-end species decelerating the catalytic performance.<sup>75,263,264</sup> Indeed, the evolution of diiron(III)- $\mu_2$ -oxo complex **44** (Scheme 12) was observed in UV/Vis from **1** and **2** under oxidative conditions and possesses a low activity ( $23\,000\text{ h}^{-1}$ ).<sup>75</sup> Addition of Lewis acids was found to reactivate the deactivation product **44**. In fact, all complexes, **1**, **2** and **44** effectively show the same activity (TOF) and stability (TON) in the presence of Lewis acids, as the deactivation pathway to form the Fe–O–Fe product is suppressed and the same catalytically active complex **2** is formed in all reactions. Sc<sup>3+</sup>, Ce<sup>4+</sup> and Fe<sup>3+</sup> have the highest catalytic impact and enable a longer lifetime of the catalyst at room temperature (TON: 1200 vs. without additive **2**: 740; **1**: 390).<sup>73,75</sup> The Lewis acids are expected to facilitate OH<sup>•/–</sup> cleavage from the Fe<sup>III</sup>–OOH intermediate and shift the rate determining step towards olefin oxidation.<sup>75,175</sup>

The electronic properties of **1** and **2** can be changed through modifications of the ligand framework (see Section 3) and their influence on the catalytic performance was investigated. Substitution of the axial MeCN ligands of **1** with one (**25**) or two <sup>t</sup>BuNC molecules (**26**, Scheme 5) lowers the electron density at the iron center through their  $\pi$ -accepting character. Catalytic tests at room temperature show significantly lower TOFs (**25**:  $1400\text{ h}^{-1}$ ; **26**:  $240\text{ h}^{-1}$ ),<sup>265</sup> which can be explained by lower electron density at iron and by stronger coordinating axial ligands, corroborated by thermogravimetric analysis.<sup>59,265</sup> Higher temperatures ( $60\text{ }^\circ\text{C}$ ) might facilitate the dissociation of the <sup>t</sup>BuNC ligands, as higher TOFs can be achieved (**25**:  $25\,900\text{ h}^{-1}$ ; **26**:  $4300\text{ h}^{-1}$ ),<sup>265</sup> underlining the importance of accessible axial coordination sites for catalysis. Iron(II) **13** and iron(III) **14** complexes contain a tetracarbene ligand with benzimidazole units, which is providing less  $\sigma$ -donation compared to **1** and **2** and thus leading to a less electron rich iron atom (see Section 3).<sup>54</sup> A more electron rich iron center is assumed to be beneficial for the formation of the electrophilic iron(IV/V)-oxo species, which should increase the activity.<sup>54,266</sup> Indeed, both **13** and **14** ( $11\,000\text{ h}^{-1}$ ) are less active than **1** and **2** at room temperature, but **14** is comparably stable with a TON of 1000. While **14** is remarkable temperature-tolerant, the temperature has to be increased up to  $80\text{ }^\circ\text{C}$  in order to achieve a TOF of  $95\,000\text{ h}^{-1}$  for **14** (TON = 360). However, **14** appears to convert more challenging alkenes in higher yields, than **2**.<sup>54</sup> The two methyl groups in the backbone of the tetracarbene ligand in **10** (Fe<sup>II</sup>) and **11** (Fe<sup>III</sup>) are supposed to increase the electron density at the iron center (see Section 3). However, albeit being more active than **13** and **14**, **10** and **11** lack behind **1** and **2**, due to their low stability even at room temperature. The highest conversion for **10** can be achieved at  $-20\text{ }^\circ\text{C}$  ( $82\%$ ,  $>99\%$  selectivity). Interestingly, **10** reaches similar conversion ( $40\%$ ) compared to **11** ( $46\%$ ) at  $20\text{ }^\circ\text{C}$ , which probably is attributable to a fast initial Fe<sup>II</sup>  $\rightarrow$  Fe<sup>III</sup> oxidation (no induction period is observed in contrast to **13**) due to the electron rich iron center. Despite the low stability of **10** and **11**, DFT calculations suggest a considerable amount of  $\pi$ -backbonding, partly compensating the +I effect of the methyl groups at the imidazole backbone

and thus explaining the lower activity in comparison to **1** and **2**.<sup>54</sup> Just recently, abnormally coordinating iron(II) tetracarbene **70** (Fig. 1), possessing an even more electron-rich iron center in this series, has been preliminarily investigated as pre-catalyst in epoxidation catalysis.<sup>53</sup> However, the first results indicate that **70** lags behind its model, complex **1**, in terms of activity, as **70** reaches a TOF of  $41\,000\text{ h}^{-1}$  with Sc(OTf)<sub>3</sub>, whereas **1** exhibits a higher TOF ( $50\,000\text{ h}^{-1}$ ) in the absence of any additive (Table 6). The highest conversion of  $89\%$  without additive is reached at  $-10\text{ }^\circ\text{C}$  after 10 min, revealing a reduced stability at higher temperatures, like **1** and **2**.

While the found deactivation pathway, the formation of **44** from pre-catalyst **1** and catalytically active **2** during catalysis, can be suppressed using Lewis acids as additives, the lifetime of **1** and **2** still lacks behind in order to become suitable for real-life applications.<sup>72,75</sup> Hence, further studies on the decomposition pathways of **2** as active complex have been performed using high-resolution ESI-MS, NMR spectroscopy and DFT calculations. The C–H oxidation of the methylene bridges and the formation of a dead-end  $\mu_2$ -oxo-bridged Fe–O–Fe complex are the most common degradation pathways for non-heme iron oxidation catalysts, however mostly containing N-donor ligands.<sup>72,247,250,263,264,267–270</sup> The first can be excluded, as no kinetic isotope effect has been observed between catalytic experiments of **2** and **2-d<sub>8</sub>** with deuterated methylene bridges. In NMR, one dominant decomposition product is found, which can be assigned to a mono-oxidized and threefold-protonated ligand species **o** (Scheme 36). Carbene oxidation is proposed to occur prior to carbene protonation due to two reasons: (a) Addition of intercepting bases does not have a beneficial effect on the catalytic performance, instead **2** is quickly reduced back to **1**. Traces of water are expected to be oxidized to hydroxyl radicals, in turn oxidizing the solvent and axial ligands, MeCN (see Scheme 14). Employing **23** and **24** (Scheme 5) with axial <sup>t</sup>BuCN or PhCN ligands, respectively, bearing less activated C–H bonds, did not show a beneficial effect on the catalytic performance in the presence of bases and other solvents. (b) In mass spectroscopic experiments, only **o** and no fully protonated ligand has been observed. Furthermore, a species with mono-oxidized ligand still coordinated to the iron center has been present (Scheme 36, middle). Therefore, as intercepting bases do not enhance the catalytic lifetime of **2** (a), no protonated ligand can be found (b) and a transient species confirming the proposed mechanism can be detected, the oxidation of one carbene is expected to initiate de-coordination of the equatorial ligand and subsequent protonation of the remaining three carbenes.<sup>72</sup>



Scheme 36 Proposed degradation mechanism of **2** under oxidative conditions.

Whether this mechanism occurs intra- or intermolecular is yet unclear. In the case of an intermolecular mechanism, a possible solution could be to block one coordination site. However, it is challenging to keep the electronic properties of the complex constant, as **25** (Scheme 5), bearing one rather strong bound <sup>t</sup>BuNC ligand, does not show an enhanced lifetime of the catalyst, but in fact worse catalytic performance due to the less electron rich iron center (*vide supra*). An intramolecular mechanism might be suppressed with stronger NHC–Fe bonds. In theory, the stronger donating triazolylidene tetracarbene of **70** should result in stronger ligand-metal bonds, however, predicting the stability is not trivial.<sup>271</sup> Comprehensive catalytic studies of **70** on this topic are still pending.

#### 5.4. Summary

Cyclic iron tetracarbenes have been successfully applied as catalysts in several reactions. In CO<sub>2</sub> reduction, a high activity is reached and despite the structural proximity to iron porphyrins, a different mechanism is reported. Highly nucleophilic iron(0) is involved in the case of the iron tetracarbene due to the strong electron donating properties of the tetracarbene, whereas for iron porphyrin complexes an intermediate-spin iron(II) center antiferromagnetically coupled to a porphyrin diradical is assumed.

Aziridination of olefins is reported for various iron tetracarbenes. The reaction mechanism is expected to proceed *via* an iron(IV) imide intermediate. Stronger  $\sigma$ -donating tetracarbenes result in a more electron rich iron center, facilitating the formation of the iron(IV) imide intermediate and enabling higher yields. On the other hand, more steric demanding substrates can rise the activation energy required for the iron(IV) imide formation and thus lower the yields. The rate determining step of the aziridination reaction is the open-chain radical intermediate, in contrast to porphyrin systems where it is the addition of the organic azide to the catalyst. For this open-chain radical intermediate, a flexible tetracarbene ligand is required. Decomposition of the iron tetracarbene during catalysis has been assigned to the oxidation of one carbene carbon atom of the tetracarbene ligand and subsequent de-coordination.

In epoxidation of olefins, iron tetracarbenes have reached a very high activity, outperforming other iron catalysts with N-donor ligands or other homogeneous catalysts based on Re or Mo. Modifications of the electronic surroundings have a significant effect on the catalytic performance. However, the electronic properties of the unmodified iron tetracarbene appear to be optimal for the best catalytic results, as both stronger and weaker electron donating ligands lead to worse results. During catalysis, a diiron  $\mu_2$ -oxo-bridged complex has been identified as deactivation product, but addition of Lewis acids can suppress its formation and reactivate it. Similar to aziridination, oxidation of the carbene carbon atom of the tetracarbene ligand ultimately initiates the degradation of the catalyst.

## 6. Conclusion and outlook

Cyclic iron tetracarbenes possess a unique ligand framework consisting of two axial coordination sites in *trans* position and a

cyclic equatorial tetracarbene ligand coordinating fourfold to the iron center, ensuring a high comparability between the different systems. The facile modification of both the equatorial tetracarbene as well as the axial ligands allows fine-tuning of structural and electronic properties of the respective iron complexes. The structural and electronic properties of iron tetracarbenes can be evaluated and compared based on the <sup>13</sup>C<sub>NHC</sub> NMR signal, the Fe<sup>2+</sup>/Fe<sup>3+</sup> half-cell potential, SC-XRD and Mössbauer spectroscopy:

- The chemical shift of the <sup>13</sup>C<sub>NHC</sub> NMR signal provides information about the  $\sigma$ -donor strength of the tetracarbene ligand; an upfield shift compared to other tetracarbene ligands indicates a stronger electron donation. Modifications of the wingtip and backbone have a significant effect on the  $\sigma$ -donation. The donating capabilities of different axial ligands can be monitored on the basis of the shift of the <sup>13</sup>C<sub>NHC</sub> NMR signal of the tetracarbene ligand.

- The Fe<sup>2+</sup>/Fe<sup>3+</sup> half-cell potential is a parameter for the Lewis acidity of the iron center and the electron donation of the surrounding ligands; a lower, more negative half-cell potential indicates a more electron rich iron center due to stronger electron donating ligands. The <sup>13</sup>C<sub>NHC</sub> chemical shift and the half-cell potential correlate with each other allowing the prediction of parameters.

- SC-XRD gives insights on the structural properties. Changes of the electronic properties can be measured, and it can explain experimental findings.

- Mössbauer spectroscopy complements the evaluation of the properties and provides the oxidation state, spin state and electronic surroundings of iron tetracarbenes.

Future studies could introduce additional parameters for a better understanding of iron tetracarbenes, such as the stability of the iron–NHC bond, determined using thiones.<sup>271</sup> NHCs are known to be strong  $\sigma$ -donors, and even stronger in comparison to phosphane ligands. Combining four NHC moieties in one plane in the cyclic tetracarbene ligand results in a very strong electron donation in the equatorial plane to the iron center and often determines the overall properties and reactivity of iron tetracarbenes; the key insights are summarized in the following:

- The strong  $\sigma$ -donation of the tetracarbene ligand and its chelating effect stabilizes multiple uncommon species in high oxidation states, *i.e.* up to iron(IV).

- Iron tetracarbenes adopt low-spin or intermediate-spin complexes whereas high-spin is unfavorable due to the strong electron donation of the tetracarbene ligand.

- The strong electron donation of the tetracarbene into the equatorial plane rises the  $x^2-y^2$  orbital above the  $z^2$  orbital, which is contrary to the usual electronic structure of most N-ligated iron complexes. This leads to a significantly larger triplet–quintet energy gap and thus to exclusive triplet reactivity in hydrogen atom transfer and in epoxidation of olefins, without a usually occurring spin-crossover.

- Iron tetracarbenes are electronically distinct to iron porphyrins as the tetracarbene ligand does not have a conjugated aromatic system, is redox inactive and exhibits a strong  $\sigma$ -donation. This leads to a different reactivity, as exemplarily

demonstrated in the CO<sub>2</sub> reduction (iron(0) vs. iron(II) diradical), aziridination of olefins (open-chain radical intermediate as rate determining step) or hydrogen atom transfer and in epoxidation of olefins (triplet reactivity).

• Iron tetracarbenes can be successfully applied as catalysts in oxidation but also reduction reactions and structural or electronic changes can significantly impact the catalytic performance. In epoxidation catalysis, NHC ligation was found to be superior to N-donor ligands achieving unprecedented activities.

All in all, the findings of this review will serve chemists across disciplines to evaluate their complexes and interpret their experimental data, tailor their catalyst properties by ligand design, and investigate their catalytic mechanism and degradation pathway. Finally, they should of course stimulate this young research field in designing exciting new compounds and achieving major breakthroughs in the application of iron tetracarbenes. Just recently, the first abnormally coordinating tetracarbene was published, representing an inspiring example for possible new ligands containing other classes of NHCs. The isolation of iron tetracarbene complexes in rare higher oxidation states, e.g., iron(V), would also be desirable. However, several challenges remain for an application of iron tetracarbenes in laboratories or industry. To increase the stability while keeping the high activity is one of the biggest; but also recycling or immobilization are fields for future research. With the emergence of machine learning in chemical research in recent years,<sup>272,273</sup> the structural and spectroscopic parameters provided in this work, as well as established correlations, could support computational approaches to predict the best candidates for each purpose on the ease of modifiability of iron tetracarbenes, thus speeding up tedious laboratory research.

## Author contributions

Tim P. Schlachta: Conceptualization, data curation, formal analysis, investigation, methodology, visualization, writing – original draft, writing – review & editing; Fritz E. Kühn: conceptualization, project administration, supervision, writing – review & editing.

## Conflicts of interest

There are no conflicts to declare.

## Acknowledgements

T. P. Schlachta gratefully acknowledges support from TUM graduate school.

## References

- 1 A. J. Arduengo, R. L. Harlow and M. Kline, *J. Am. Chem. Soc.*, 1991, **113**, 361–363.
- 2 A. J. Arduengo, H. V. R. Dias, R. L. Harlow and M. Kline, *J. Am. Chem. Soc.*, 1992, **114**, 5530–5534.
- 3 C. Janiak, H.-J. Meyer, D. Gudat, R. Alsfasser, E. Riedel and H.-J. Meyer, *Riedel Moderne Anorganische Chemie*, De Gruyter, Berlin, Boston, 2012.
- 4 M. N. Hopkinson, C. Richter, M. Schedler and F. Glorius, *Nature*, 2014, **510**, 485–496.
- 5 C. Janiak, H.-J. Meyer, D. Gudat, P. Kurz and H.-J. Meyer, *Riedel Moderne Anorganische Chemie*, Walter de Gruyter, Berlin, Boston, 2018.
- 6 K. Öfele, W. A. Herrmann, D. Mihalios, M. Elison, E. Herdtweck, W. Scherer and J. Mink, *J. Organomet. Chem.*, 1993, **459**, 177–184.
- 7 W. A. Herrmann, M. Elison, J. Fischer, C. Köcher and G. R. J. Artus, *Angew. Chem., Int. Ed. Engl.*, 1995, **34**, 2371–2374.
- 8 N. Debono, A. Labande, E. Manoury, J.-C. Daran and R. Poli, *Organometallics*, 2010, **29**, 1879–1882.
- 9 M. S. Sanford, J. A. Love and R. H. Grubbs, *J. Am. Chem. Soc.*, 2001, **123**, 6543–6554.
- 10 G. C. Fortman and S. P. Nolan, *Chem. Soc. Rev.*, 2011, **40**, 5151–5169.
- 11 C. Johnson and M. Albrecht, *Coord. Chem. Rev.*, 2017, **352**, 1–14.
- 12 W. A. Herrmann, *Angew. Chem., Int. Ed.*, 2002, **41**, 1290–1309.
- 13 M. Eckhardt and G. C. Fu, *J. Am. Chem. Soc.*, 2003, **125**, 13642–13643.
- 14 P. Bellotti, M. Koy, M. N. Hopkinson and F. Glorius, *Nat. Rev. Chem.*, 2021, **5**, 711–725.
- 15 A. F. Holleman and N. Wiberg, *Nebengruppenelemente, Lanthanoide, Actinoide, Transactinoide*, De Gruyter, Berlin, Boston, 2017.
- 16 J. J. Scepaniak, C. S. Vogel, M. M. Khusniyarov, F. W. Heinemann, K. Meyer and J. M. Smith, *Science*, 2011, **331**, 1049–1052.
- 17 E. M. Zolnhofer, M. Käß, M. M. Khusniyarov, F. W. Heinemann, L. Maron, M. van Gastel, E. Bill and K. Meyer, *J. Am. Chem. Soc.*, 2014, **136**, 15072–15078.
- 18 G. E. Martinez, C. Ocampo, Y. J. Park and A. R. Fout, *J. Am. Chem. Soc.*, 2016, **138**, 4290–4293.
- 19 J. Cheng, L. Wang, P. Wang and L. Deng, *Chem. Rev.*, 2018, **118**, 9930–9987.
- 20 R. McKie, J. A. Murphy, S. R. Park, M. D. Spicer and S.-Z. Zhou, *Angew. Chem., Int. Ed.*, 2007, **46**, 6525–6528.
- 21 S. R. Park, N. J. Findlay, J. Garnier, S. Zhou, M. D. Spicer and J. A. Murphy, *Tetrahedron*, 2009, **65**, 10756–10761.
- 22 N. J. Findlay, S. R. Park, F. Schoenebeck, E. Cahard, S.-Z. Zhou, L. E. A. Berlouis, M. D. Spicer, T. Tuttle and J. A. Murphy, *J. Am. Chem. Soc.*, 2010, **132**, 15462–15464.
- 23 F. E. Hahn, V. Langenhahn, T. Lügger, T. Pape and D. Le Van, *Angew. Chem., Int. Ed.*, 2005, **44**, 3759–3763.
- 24 F. E. Hahn, C. Radloff, T. Pape and A. Hepp, *Chem. – Eur. J.*, 2008, **14**, 10900–10904.
- 25 R. A. Baglia, J. P. T. Zaragoza and D. P. Goldberg, *Chem. Rev.*, 2017, **117**, 13320–13352.
- 26 G. F. Manbeck and E. Fujita, *J. Porphyrins Phthalocyanines*, 2015, **19**, 45–64.

- 27 C. Costentin, H. Dridi and J.-M. Savéant, *J. Am. Chem. Soc.*, 2015, **137**, 13535–13544.
- 28 J. Hohenberger, K. Ray and K. Meyer, *Nat. Commun.*, 2012, **3**, 720.
- 29 M. J. Ingleson and R. A. Layfield, *Chem. Commun.*, 2012, **48**, 3579–3589.
- 30 K. Riener, S. Haslinger, A. Raba, M. P. Högerl, M. Cokoja, W. A. Herrmann and F. E. Kühn, *Chem. Rev.*, 2014, **114**, 5215–5272.
- 31 P. P. Chandrachud and D. M. Jenkins, *Tetrahedron Lett.*, 2015, **56**, 2369–2376.
- 32 A. Biffis, M. Baron and C. Tubaro, in *Adv. Organomet. Chem.*, ed. P. J. Pérez, Academic Press, 2015, vol. 63, pp. 203–288.
- 33 V. Charra, P. de Frémont and P. Braunstein, *Coord. Chem. Rev.*, 2017, **341**, 53–176.
- 34 J. W. Kück, R. M. Reich and F. E. Kühn, *Chem. Rec.*, 2016, **16**, 349–364.
- 35 A. C. Lindhorst, S. Haslinger and F. E. Kühn, *Chem. Commun.*, 2015, **51**, 17193–17212.
- 36 S. M. Hölzl, P. J. Altmann, J. W. Kück and F. E. Kühn, *Coord. Chem. Rev.*, 2017, **352**, 517–536.
- 37 A. H. Mageed, *J. Organomet. Chem.*, 2019, **902**, 120965.
- 38 R. Kumar, B. Pandey, A. Sen, M. Ansari, S. Sharma and G. Rajaraman, *Coord. Chem. Rev.*, 2020, **419**, 213397.
- 39 L. Roy, *ChemPlusChem*, 2019, **84**, 893–906.
- 40 Q. Liang and D. Song, *Chem. Soc. Rev.*, 2020, **49**, 1209–1232.
- 41 B. N. Jha, N. Singh and A. Raghuvanshi, *Organic Synthesis-A Nascent Relook*, IntechOpen, 2020.
- 42 G. G. Zámbo, J. F. Schlagintweit, R. M. Reich and F. E. Kühn, *Catal. Sci. Technol.*, 2022, **12**, 4940–4961.
- 43 W. W. H. Wong, M. S. Vickers, A. R. Cowley, R. L. Paul and P. D. Beer, *Org. Biomol. Chem.*, 2005, **3**, 4201–4208.
- 44 A. Weiss, H. Pritzkow and W. Siebert, *Angew. Chem., Int. Ed.*, 2000, **39**, 547–549.
- 45 A. Weiss, V. Barba, H. Pritzkow and W. Siebert, *J. Organomet. Chem.*, 2003, **680**, 294–300.
- 46 C. E. H. Bawn, *Biographical Memoirs of Fellows of the Royal Society*, 1975, **21**, 569–584.
- 47 V. V. Rostovtsev, L. G. Green, V. V. Fokin and K. B. Sharpless, *Angew. Chem., Int. Ed.*, 2002, **41**, 2596–2599.
- 48 C. W. Tornøe, C. Christensen and M. Meldal, *J. Org. Chem.*, 2002, **67**, 3057–3064.
- 49 M. Meldal and C. W. Tornøe, *Chem. Rev.*, 2008, **108**, 2952–3015.
- 50 L. Liang and D. Astruc, *Coord. Chem. Rev.*, 2011, **255**, 2933–2945.
- 51 I. Kim, K. C. Ko, W. R. Lee, J. Cho, J. H. Moon, D. Moon, A. Sharma, J. Y. Lee, J. S. Kim and S. Kim, *Org. Lett.*, 2017, **19**, 5509–5512.
- 52 J. Cho, J. Shin, M. Kang, P. Verwilt, C. Lim, H. Yoo, J. G. Kim, X. Zhang, C. S. Hong, J. S. Kim and S. Kim, *Chem. Commun.*, 2021, **57**, 12139–12142.
- 53 G. G. Zámbo, J. Mayr, M. J. Sauer, T. P. Schlachta, R. M. Reich and F. E. Kühn, *Dalton Trans.*, 2022, **51**, 13591–13595.
- 54 M. A. Bernd, F. Dyckhoff, B. J. Hofmann, A. D. Böth, J. F. Schlagintweit, J. Oberkofler, R. M. Reich and F. E. Kühn, *J. Catal.*, 2020, **391**, 548–561.
- 55 H. M. Bass, S. A. Cramer, A. S. McCullough, K. J. Bernstein, C. R. Murdock and D. M. Jenkins, *Organometallics*, 2013, **32**, 2160–2167.
- 56 K. Riener, S. Haslinger, A. Raba, M. P. Hogerl, M. Cokoja, W. A. Herrmann and F. E. Kühn, *Chem. Rev.*, 2014, **114**, 5215–5272.
- 57 A. A. Danopoulos, N. Tsoureas, J. A. Wright and M. E. Light, *Organometallics*, 2004, **23**, 166–168.
- 58 R. R. Fraser, T. S. Mansour and S. Savard, *J. Org. Chem.*, 1985, **50**, 3232–3234.
- 59 M. R. Anneser, S. Haslinger, A. Pöthig, M. Cokoja, J.-M. Basset and F. E. Kühn, *Inorg. Chem.*, 2015, **54**, 3797–3804.
- 60 S. Meyer, I. Klawitter, S. Demeshko, E. Bill and F. Meyer, *Angew. Chem., Int. Ed.*, 2013, **52**, 901–905.
- 61 C. Schremmer, C. Cordes, I. Klawitter, M. Bergner, C. E. Schiewer, S. Dechert, S. Demeshko, M. John and F. Meyer, *Chem. – Eur. J.*, 2019, **25**, 3918–3929.
- 62 Based on personal experience, already 100 ppm of oxygen under dry conditions are enough to decompose the iron precursor.
- 63 M. R. Anneser, G. R. Elpitiya, X. B. Powers and D. M. Jenkins, *Organometallics*, 2019, **38**, 981–987.
- 64 P. P. Chandrachud, H. M. Bass and D. M. Jenkins, *Organometallics*, 2016, **35**, 1652–1657.
- 65 S. A. Cramer and D. M. Jenkins, *J. Am. Chem. Soc.*, 2011, **133**, 19342–19345.
- 66 J. F. DeJesus and D. M. Jenkins, *Chem. – Eur. J.*, 2020, **26**, 1429–1435.
- 67 R. R. Fraser and T. S. Mansour, *J. Org. Chem.*, 1984, **49**, 3442–3443.
- 68 K. Daasbjerg, *Acta Chem. Scand.*, 1995, **49**, 878–887.
- 69 K. M. Blatchford, C. J. Mize, S. Roy and D. M. Jenkins, *Dalton Trans.*, 2022, **51**, 6153–6156.
- 70 Z. Lu, S. A. Cramer and D. M. Jenkins, *Chem. Sci.*, 2012, **3**, 3081–3087.
- 71 J. Donat, P. Dubourdeaux, M. Clémancey, J. Rendon, C. Gervasoni, M. Barbier, J. Barilone, J. Pécaut, S. Gambarelli, P. Maldivi and J.-M. Latour, *Chem. – Eur. J.*, 2022, **28**, e202201875.
- 72 F. Dyckhoff, J. F. Schlagintweit, M. A. Bernd, C. H. G. Jakob, T. P. Schlachta, B. J. Hofmann, R. M. Reich and F. E. Kühn, *Catal. Sci. Technol.*, 2021, **11**, 795–799.
- 73 J. W. Kück, M. R. Anneser, B. Hofmann, A. Pöthig, M. Cokoja and F. E. Kühn, *ChemSusChem*, 2015, **8**, 4056–4063.
- 74 M. R. Anneser, S. Haslinger, A. Pöthig, M. Cokoja, V. D'Elia, M. P. Högerl, J.-M. Basset and F. E. Kühn, *Dalton Trans.*, 2016, **45**, 6449–6455.
- 75 F. Dyckhoff, J. F. Schlagintweit, R. M. Reich and F. E. Kühn, *Catal. Sci. Technol.*, 2020, **10**, 3532–3536.
- 76 M. R. Anneser, G. R. Elpitiya, J. Townsend, E. J. Johnson, X. B. Powers, J. F. DeJesus, K. D. Vogiatzis and D. M. Jenkins, *Angew. Chem., Int. Ed.*, 2019, **58**, 8115–8118.

- 77 T. P. Schlachta, J. F. Schlagintweit, M. R. Anneser, E.-M. H. J. Esslinger, M. Muhr, S. Haslinger and F. E. Kühn, *Inorg. Chim. Acta*, 2021, **518**, 120228.
- 78 J. F. Schlagintweit, C. Hintermeier, M. R. Anneser, E.-M. H. J. Esslinger, S. Haslinger and F. E. Kühn, *Chem. – Asian J.*, 2020, **15**, 1896–1902.
- 79 A. A. Massie, C. Schremmer, I. Rüter, S. Dechert, I. Siewert and F. Meyer, *ACS Catal.*, 2021, **11**, 3257–3267.
- 80 C. Kupper, A. Schober, S. Demeshko, M. Bergner and F. Meyer, *Inorg. Chem.*, 2015, **54**, 3096–3098.
- 81 C. Kupper, J. A. Rees, S. Dechert, S. DeBeer and F. Meyer, *J. Am. Chem. Soc.*, 2016, **138**, 7888–7898.
- 82 M. Ghosh, H. H. Cramer, S. Dechert, S. Demeshko, M. John, M. M. Hansmann, S. Ye and F. Meyer, *Angew. Chem., Int. Ed.*, 2019, **58**, 14349–14356.
- 83 C. Cordes, I. Klawitter, I. Rüter, S. Dechert, S. Demeshko, S. Ye and F. Meyer, *Inorg. Chem.*, 2022, **61**, 7153–7164.
- 84 H. V. Huynh, Y. Han, R. Jothibasu and J. A. Yang, *Organometallics*, 2009, **28**, 5395–5404.
- 85 D. Tapu, D. A. Dixon and C. Roe, *Chem. Rev.*, 2009, **109**, 3385–3407.
- 86 H. V. Huynh, *Chem. Lett.*, 2021, **50**, 1831–1841.
- 87 H. V. Huynh, *Chem. Rev.*, 2018, **118**, 9457–9492.
- 88 O. Back, M. Henry-Ellinger, C. D. Martin, D. Martin and G. Bertrand, *Angew. Chem., Int. Ed.*, 2013, **52**, 2939–2943.
- 89 S. V. C. Vummaleti, D. J. Nelson, A. Poater, A. Gómez-Suárez, D. B. Cordes, A. M. Z. Slawin, S. P. Nolan and L. Cavallo, *Chem. Sci.*, 2015, **6**, 1895–1904.
- 90 J. W. Ogle and S. A. Miller, *Chem. Commun.*, 2009, 5728–5730, DOI: [10.1039/B914732B](https://doi.org/10.1039/B914732B).
- 91 X.-X. He, Y. Li, B.-B. Ma, Z. Ke and F.-S. Liu, *Organometallics*, 2016, **35**, 2655–2663.
- 92 C.-L. Do-Thanh, N. Khanal, Z. Lu, S. A. Cramer, D. M. Jenkins and M. D. Best, *Tetrahedron*, 2012, **68**, 1669–1673.
- 93 D. G. Gusev, *Organometallics*, 2009, **28**, 6458–6461.
- 94 N. U. D. Reshi and J. K. Bera, *Coord. Chem. Rev.*, 2020, **422**, 213334.
- 95 W. A. Herrmann, O. Runte and G. Artus, *J. Organomet. Chem.*, 1995, **501**, C1–C4.
- 96 C. Hirtenlehner, C. Krims, J. Hölbling, M. List, M. Zabel, M. Fleck, R. J. F. Berger, W. Schoefberger and U. Monkowius, *Dalton Trans.*, 2011, **40**, 9899–9910.
- 97 A. B. P. Lever, *Inorg. Chem.*, 1990, **29**, 1271–1285.
- 98 S. Haslinger, J. W. Kück, E. M. Hahn, M. Cokoja, A. Pöthig, J.-M. Basset and F. E. Kühn, *Inorg. Chem.*, 2014, **53**, 11573–11583.
- 99 A. F. Holleman and N. Wiberg, *Grundlagen und Hauptgruppen-elemente*, De Gruyter, Berlin, Boston, 2017.
- 100 J. England, C. R. Davies, M. Banaru, A. J. P. White and G. J. P. Britovsek, *Adv. Synth. Catal.*, 2008, **350**, 883–897.
- 101 M. S. Chen and M. C. White, *Science*, 2007, **318**, 783–787.
- 102 A. Company, L. Gómez and M. Costas, *Iron-Containing Enzymes: Versatile Catalysts of Hydroxylation Reactions in Nature*, The Royal Society of Chemistry, 2011, DOI: [10.1039/9781849732987-00148](https://doi.org/10.1039/9781849732987-00148), pp. 148–208.
- 103 S. B. Isbill, P. P. Chandrachud, J. L. Kern, D. M. Jenkins and S. Roy, *ACS Catal.*, 2019, **9**, 6223–6233.
- 104 M. C. MacInnis, J. C. DeMott, E. M. Zolnhofer, J. Zhou, K. Meyer, R. P. Hughes and O. V. Ozerov, *Chem*, 2016, **1**, 902–920.
- 105 L. Mercs, G. Labat, A. Neels, A. Ehlers and M. Albrecht, *Organometallics*, 2006, **25**, 5648–5656.
- 106 E. Bill, in *Practical Approaches to Biological Inorganic Chemistry*, ed. R. R. Crichton and R. O. Louro, Elsevier, Second edn, 2020, pp. 201–228, DOI: [10.1016/B978-0-444-64225-7.00006-7](https://doi.org/10.1016/B978-0-444-64225-7.00006-7).
- 107 P. Gütllich, *Chem. Unserer Zeit*, 1970, **4**, 133–144.
- 108 P. Gütllich, *Chem. Unserer Zeit*, 1971, **5**, 131–141.
- 109 D. F. Evans, *J. Chem. Soc.*, 1959, 2003–2005, DOI: [10.1039/JR9590002003](https://doi.org/10.1039/JR9590002003).
- 110 C. A. Grapperhaus, B. Mienert, E. Bill, T. Weyhermüller and K. Wieghardt, *Inorg. Chem.*, 2000, **39**, 5306–5317.
- 111 A. L. Speelman and N. Lehnert, *Acc. Chem. Res.*, 2014, **47**, 1106–1116.
- 112 R. G. Serres, C. A. Grapperhaus, E. Bothe, E. Bill, T. Weyhermüller, F. Neese and K. Wieghardt, *J. Am. Chem. Soc.*, 2004, **126**, 5138–5153.
- 113 R. V. Parish and R. H. Platt, *J. Chem. Soc. A*, 1969, 2145–2150, DOI: [10.1039/J19690002145](https://doi.org/10.1039/J19690002145).
- 114 A. Chanda, X. Shan, M. Chakrabarti, W. C. Ellis, D. L. Popescu, F. Tiago de Oliveira, D. Wang, L. Que, T. J. Collins, E. Münck and E. L. Bominaar, *Inorg. Chem.*, 2008, **47**, 3669–3678.
- 115 A. R. McDonald and L. Que, *Coord. Chem. Rev.*, 2013, **257**, 414–428.
- 116 S. Saito and A. Osuka, *Angew. Chem., Int. Ed.*, 2011, **50**, 4342–4373.
- 117 J. A. Shelnut, X.-Z. Song, J.-G. Ma, S.-L. Jia, W. Jentzen, C. J. Medforth and C. J. Medforth, *Chem. Soc. Rev.*, 1998, **27**, 31–42.
- 118 S. Muralidharan and E. M. Boon, *J. Am. Chem. Soc.*, 2012, **134**, 2044–2046.
- 119 W. Jentzen, J.-G. Ma and J. A. Shelnut, *Biophys. J.*, 1998, **74**, 753–763.
- 120 K. K. Anderson, J. D. Hobbs, L. Luo, K. D. Stanley, J. M. E. Quirke and J. A. Shelnut, *J. Am. Chem. Soc.*, 1993, **115**, 12346–12352.
- 121 G. G. v Dooren, A. T. Kennedy and G. I. McFadden, *Antioxid. Redox Signal.*, 2012, **17**, 634–656.
- 122 D. Shimizu and A. Osuka, *Chem. Sci.*, 2018, **9**, 1408–1423.
- 123 P. Hlavica, *J. Inorg. Biochem.*, 2011, **105**, 1354–1364.
- 124 X. Huang and J. T. Groves, *Chem. Rev.*, 2018, **118**, 2491–2553.
- 125 D. Dolphin, T. G. Traylor and L. Y. Xie, *Acc. Chem. Res.*, 1997, **30**, 251–259.
- 126 D. Harris, G. Loew and L. Waskell, *J. Inorg. Biochem.*, 2001, **83**, 309–318.
- 127 R. Reynolds, L. L. Line and R. F. Nelson, *J. Am. Chem. Soc.*, 1974, **96**, 1087–1092.
- 128 N. G. Connelly and W. E. Geiger, *Chem. Rev.*, 1996, **96**, 877–910.

- 129 L. Song and W. C. Trogler, *Angew. Chem., Int. Ed. Engl.*, 1992, **31**, 770–772.
- 130 J. K. Kochi, *Acc. Chem. Res.*, 1992, **25**, 39–47.
- 131 O. Hammerich and V. D. Parker, *Electrochim. Acta*, 1973, **18**, 537–541.
- 132 T. P. Schlachta, M. R. Anneser, J. F. Schlagintweit, C. H. G. Jakob, C. Hintermeier, A. D. Böth, S. Haslinger, R. M. Reich and F. E. Kühn, *Chem. Commun.*, 2021, **57**, 6644–6647.
- 133 W. E. Geiger, *J. Am. Chem. Soc.*, 1974, **96**, 2632–2634.
- 134 J. Balej, *Electrochim. Acta*, 1976, **21**, 953–956.
- 135 A. Raba, M. Cokoja, S. Ewald, K. Riener, E. Herdtweck, A. Pöthig, W. A. Herrmann and F. E. Kühn, *Organometallics*, 2012, **31**, 2793–2800.
- 136 B. B. Wayland, L. F. Mehne and J. Swartz, *J. Am. Chem. Soc.*, 1978, **100**, 2379–2383.
- 137 S. H. Strauss and R. H. Holm, *Inorg. Chem.*, 1982, **21**, 863–868.
- 138 N. J. Silvernail, B. C. Noll, C. E. Schulz and W. R. Scheidt, *Inorg. Chem.*, 2006, **45**, 7050–7052.
- 139 S. Haslinger, A. C. Lindhorst, J. W. Kück, M. Cokoja, A. Pöthig and F. E. Kühn, *RSC Adv.*, 2015, **5**, 85486–85493.
- 140 W. R. Scheidt and C. A. Reed, *Chem. Rev.*, 1981, **81**, 543–555.
- 141 I. Klawitter, M. R. Anneser, S. Dechert, S. Meyer, S. Demeshko, S. Haslinger, A. Pöthig, F. E. Kühn and F. Meyer, *Organometallics*, 2015, **34**, 2819–2825.
- 142 J. H. Enemark and R. D. Feltham, *Coord. Chem. Rev.*, 1974, **13**, 339–406.
- 143 D. J. Thomas and N. Lehnert, *Reference Module in Chemistry, Molecular Sciences and Chemical Engineering*, Elsevier, 2017, DOI: [10.1016/B978-0-12-409547-2.11678-6](https://doi.org/10.1016/B978-0-12-409547-2.11678-6).
- 144 W.-M. Ching, C.-H. Chuang, C.-W. Wu, C.-H. Peng and C.-H. Hung, *J. Am. Chem. Soc.*, 2009, **131**, 7952–7953.
- 145 J. Heinemann and H.-C. Böttcher, *Z. Anorg. Allg. Chem.*, 2022, **648**, e202100368.
- 146 F. Roncaroli, M. Videla, L. D. Slep and J. A. Olabe, *Coord. Chem. Rev.*, 2007, **251**, 1903–1930.
- 147 L. E. Goodrich, S. Roy, E. E. Alp, J. Zhao, M. Y. Hu and N. Lehnert, *Inorg. Chem.*, 2013, **52**, 7766–7780.
- 148 B. Weber, H. Görls, M. Rudolph and E. G. Jäger, *Inorg. Chim. Acta*, 2002, **337**, 247–265.
- 149 J. Li, A. Banerjee, P. L. Pawlak, W. W. Brennessel and F. A. Chavez, *Inorg. Chem.*, 2014, **53**, 5414–5416.
- 150 I. K. Choi, Y. Liu, D. Feng, K. J. Paeng and M. D. Ryan, *Inorg. Chem.*, 1991, **30**, 1832–1839.
- 151 Z. Wei and M. D. Ryan, *Inorg. Chem.*, 2010, **49**, 6948–6954.
- 152 J. Pellegrino, S. E. Bari, D. E. Bikiel and F. Doctorovich, *J. Am. Chem. Soc.*, 2010, **132**, 989–995.
- 153 A. J. Jasnowski and L. Que, *Chem. Rev.*, 2018, **118**, 2554–2592.
- 154 M. R. Anneser, G. R. Elpitiya, J. Townsend, E. J. Johnson, X. B. Powers, J. F. DeJesus, K. D. Vogiatzis and D. M. Jenkins, *Angew. Chem., Int. Ed.*, 2019, **58**, 8115–8118.
- 155 S. Meyer, O. Krahe, C. Kupper, I. Klawitter, S. Demeshko, E. Bill, F. Neese and F. Meyer, *Inorg. Chem.*, 2015, **54**, 9770–9776.
- 156 D. Macikenas, E. Skrzypczak-Jankun and J. D. Protasiewicz, *J. Am. Chem. Soc.*, 1999, **121**, 7164–7165.
- 157 R. Kumar, A. Ansari and G. Rajaraman, *Chem. – Eur. J.*, 2018, **24**, 6818–6827.
- 158 M. Nakamura, *Fundamentals of Porphyrin Chemistry*, 2022, 631–659, DOI: [10.1002/9781119129301.ch14](https://doi.org/10.1002/9781119129301.ch14).
- 159 C. Kupper, B. Mondal, J. Serrano-Plana, I. Klawitter, F. Neese, M. Costas, S. F. Ye and F. Meyer, *J. Am. Chem. Soc.*, 2017, **139**, 8939–8949.
- 160 S. A. Cramer, R. Hernández Sánchez, D. F. Brakhage and D. M. Jenkins, *Chem. Commun.*, 2014, **50**, 13967–13970.
- 161 J. Umbreit, *Am. J. Hematol.*, 2007, **82**, 134–144.
- 162 F. Odden, Y. Chiba, J. Nakazawa, T. Ohta, T. Ogura and S. Hikichi, *Angew. Chem., Int. Ed.*, 2015, **54**, 7336–7339.
- 163 J. P. Collman, C. J. Sunderland, K. E. Berg, M. A. Vance and E. I. Solomon, *J. Am. Chem. Soc.*, 2003, **125**, 6648–6649.
- 164 R. Li, H. Kobayashi, X. Yan and J. Fan, *Catal. Today*, 2014, **233**, 140–146.
- 165 J.-L. Clément, N. Ferré, D. Siri, H. Karoui, A. Rockenbauer and P. Tordo, *J. Org. Chem.*, 2005, **70**, 1198–1203.
- 166 G. R. Buettner, *Free Radical Res. Commun.*, 1993, **19**, 79–87.
- 167 S. Ye, C. Kupper, S. Meyer, E. Andris, R. Navrátil, O. Krahe, B. Mondal, M. Atanasov, E. Bill, J. Roithová, F. Meyer and F. Neese, *J. Am. Chem. Soc.*, 2016, **138**, 14312–14325.
- 168 O. Pestovsky, S. Stoian, E. L. Bominaar, X. Shan, E. Münck, L. Que Jr. and A. Bakac, *Angew. Chem., Int. Ed.*, 2005, **44**, 6871–6874.
- 169 A. N. Biswas, M. Puri, K. K. Meier, W. N. Oloo, G. T. Rohde, E. L. Bominaar, E. Münck and L. Que, *J. Am. Chem. Soc.*, 2015, **137**, 2428–2431.
- 170 M. Puri, A. N. Biswas, R. Fan, Y. Guo and L. Que, *J. Am. Chem. Soc.*, 2016, **138**, 2484–2487.
- 171 J.-U. Rohde, J.-H. In, M. H. Lim, W. W. Brennessel, M. R. Bukowski, A. Stubna, E. Münck, W. Nam and L. Que, *Science*, 2003, **299**, 1037–1039.
- 172 S. Ye, C.-Y. Geng, S. Shaik and F. Neese, *Phys. Chem. Chem. Phys.*, 2013, **15**, 8017–8030.
- 173 F. Neese, *J. Inorg. Biochem.*, 2006, **100**, 716–726.
- 174 S. Sinnecker, N. Svensen, E. W. Barr, S. Ye, J. M. Bollinger, F. Neese and C. Krebs, *J. Am. Chem. Soc.*, 2007, **129**, 6168–6179.
- 175 F. G. Cantú Reinhard and S. P. de Visser, *Chem. – Eur. J.*, 2017, **23**, 2935–2944.
- 176 W. Nam, Y.-M. Lee and S. Fukuzumi, *Acc. Chem. Res.*, 2014, **47**, 1146–1154.
- 177 O. Shoji and Y. Watanabe, in *Fifty Years of Cytochrome P450 Research*, ed. H. Yamazaki, Springer Japan, Tokyo, 2014, pp. 107–124, DOI: [10.1007/978-4-431-54992-5\\_6](https://doi.org/10.1007/978-4-431-54992-5_6).
- 178 C. Krebs, D. Galonić Fujimori, C. T. Walsh and J. M. Bollinger, *Acc. Chem. Res.*, 2007, **40**, 484–492.
- 179 S. Shaik, H. Hirao and D. Kumar, *Acc. Chem. Res.*, 2007, **40**, 532–542.
- 180 H. Hirao, L. Que Jr., W. Nam and S. Shaik, *Chem. – Eur. J.*, 2008, **14**, 1740–1756.
- 181 D. Janardanan, Y. Wang, P. Schyman, L. Que Jr. and S. Shaik, *Angew. Chem., Int. Ed.*, 2010, **49**, 3342–3345.

- 182 G. Xue, R. De Hont, E. Münck and L. Que, *Nat. Chem.*, 2010, **2**, 400–405.
- 183 S. Ye and F. Neese, *Proc. Natl. Acad. Sci. U. S. A.*, 2011, **108**, 1228–1233.
- 184 B. Pandey, M. Jaccob and G. Rajaraman, *Chem. Commun.*, 2017, **53**, 3193–3196.
- 185 C. Cordes, M. Morganti, I. Klawitter, C. Schremmer, S. Dechert and F. Meyer, *Angew. Chem., Int. Ed.*, 2019, **58**, 10855–10858.
- 186 J. Kaizer, E. J. Klinker, N. Y. Oh, J.-U. Rohde, W. J. Song, A. Stubna, J. Kim, E. Münck, W. Nam and L. Que, *J. Am. Chem. Soc.*, 2004, **126**, 472–473.
- 187 P. Comba, S. Fukuzumi, H. Kotani and S. Wunderlich, *Angew. Chem., Int. Ed.*, 2010, **49**, 2622–2625.
- 188 C. V. Sastri, J. Lee, K. Oh, Y. J. Lee, J. Lee, T. A. Jackson, K. Ray, H. Hirao, W. Shin, J. A. Halfen, J. Kim, L. Que, S. Shaik and W. Nam, *Proc. Natl. Acad. Sci. U. S. A.*, 2007, **104**, 19181–19186.
- 189 O. Planas, M. Clémancey, J.-M. Latour, A. Company and M. Costas, *Chem. Commun.*, 2014, **50**, 10887–10890.
- 190 X.-S. Xue, P. Ji, B. Zhou and J.-P. Cheng, *Chem. Rev.*, 2017, **117**, 8622–8648.
- 191 D. Mandal, R. Ramanan, D. Usharani, D. Janardanan, B. Wang and S. Shaik, *J. Am. Chem. Soc.*, 2015, **137**, 722–733.
- 192 D. Mandal and S. Shaik, *J. Am. Chem. Soc.*, 2016, **138**, 2094–2097.
- 193 S. T. Kleespies, W. N. Oloo, A. Mukherjee and L. Que, *Inorg. Chem.*, 2015, **54**, 5053–5064.
- 194 T. J. Collins and A. D. Ryabov, *Chem. Rev.*, 2017, **117**, 9140–9162.
- 195 E. P. Talsi and K. P. Bryliakov, *Coord. Chem. Rev.*, 2012, **256**, 1418–1434.
- 196 T. H. Yosca, J. Rittle, C. M. Krest, E. L. Onderko, A. Silakov, J. C. Calixto, R. K. Behan and M. T. Green, *Science*, 2013, **342**, 825–829.
- 197 S. Hong, H. So, H. Yoon, K.-B. Cho, Y.-M. Lee, S. Fukuzumi and W. Nam, *Dalton Trans.*, 2013, **42**, 7842–7845.
- 198 J. D. Franolic, M. Millar and S. A. Koch, *Inorg. Chem.*, 1995, **34**, 1981–1982.
- 199 X. Ji, P. Tong, D. Yang, B. Wang, J. Zhao, Y. Li and J. Qu, *Dalton Trans.*, 2017, **46**, 3820–3824.
- 200 H. Kämpf, D. Daunke, F. W. Heinemann and A. Grohmann, *Appl. Phys. A: Mater. Sci. Process.*, 2008, **93**, 303–311.
- 201 G. T. Kubas, T. G. Spiro and A. Terzis, *J. Am. Chem. Soc.*, 1973, **95**, 273–274.
- 202 G. Winnewisser, M. Winnewisser and W. Gordy, *J. Chem. Phys.*, 1968, **49**, 3465–3478.
- 203 A. Mueller and W. Jaegermann, *Inorg. Chem.*, 1979, **18**, 2631–2633.
- 204 J. M. Goicoechea and H. Grützmacher, *Angew. Chem., Int. Ed.*, 2018, **57**, 16968–16994.
- 205 F. F. Puschmann, D. Stein, D. Heift, C. Hendriksen, Z. A. Gal, H.-F. Grützmacher and H. Grützmacher, *Angew. Chem., Int. Ed.*, 2011, **50**, 8420–8423.
- 206 L. N. Grant, J. Krzystek, B. Pinter, J. Telser, H. Grützmacher and D. J. Mindiola, *Chem. Commun.*, 2019, **55**, 5966–5969.
- 207 L. L. Liu, D. A. Ruiz, F. Dahchek, G. Bertrand, R. Suter, A. M. Tondreau and H. Grützmacher, *Chem. Sci.*, 2016, **7**, 2335–2341.
- 208 R. E. Cowley, E. Bill, F. Neese, W. W. Brennessel and P. L. Holland, *Inorg. Chem.*, 2009, **48**, 4828–4836.
- 209 M. T. Mock, C. V. Popescu, G. P. A. Yap, W. G. Dougherty and C. G. Riordan, *Inorg. Chem.*, 2008, **47**, 1889–1891.
- 210 S. J. Bonyhady, D. E. DeRosha, J. Vela, D. J. Vinyard, R. E. Cowley, B. Q. Mercado, W. W. Brennessel and P. L. Holland, *Inorg. Chem.*, 2018, **57**, 5959–5972.
- 211 B. P. Jacobs, R. G. Agarwal, P. T. Wolczanski, T. R. Cundari and S. N. MacMillan, *Polyhedron*, 2016, **116**, 47–56.
- 212 J. R. Wolf, C. G. Hamaker, J.-P. Djukic, T. Kodadek and L. K. Woo, *J. Am. Chem. Soc.*, 1995, **117**, 9194–9199.
- 213 K. Gopalaiah, *Chem. Rev.*, 2013, **113**, 3248–3296.
- 214 T. Jikyo and G. Maas, *Chem. Commun.*, 2003, 2794–2795, DOI: [10.1039/B310256D](https://doi.org/10.1039/B310256D).
- 215 T. Shimizu, D. Miyasaka and N. Kamigata, *J. Org. Chem.*, 2001, **66**, 7202–7204.
- 216 A. Velian and C. C. Cummins, *J. Am. Chem. Soc.*, 2012, **134**, 13978–13981.
- 217 O. Fujimura and T. Honma, *Tetrahedron Lett.*, 1998, **39**, 625–626.
- 218 E. F. Kühn and M. A. Santos, *Mini-Rev. Org. Chem.*, 2004, **1**, 55–64.
- 219 Ö. Karaca, M. R. Anneser, J. W. Kück, A. C. Lindhorst, M. Cokoja and F. E. Kühn, *J. Catal.*, 2016, **344**, 213–220.
- 220 G. Cheng, G. A. Mirafzal and L. K. Woo, *Organometallics*, 2003, **22**, 1468–1474.
- 221 C. G. Hamaker, G. A. Mirafzal and L. K. Woo, *Organometallics*, 2001, **20**, 5171–5176.
- 222 G. A. Mirafzal, G. Cheng and L. K. Woo, *J. Am. Chem. Soc.*, 2002, **124**, 176–177.
- 223 E. Boutin, L. Merakeb, B. Ma, B. Boudy, M. Wang, J. Bonin, E. Anxolabéhère-Mallart and M. Robert, *Chem. Soc. Rev.*, 2020, **49**, 5772–5809.
- 224 T. K. Zimmermann and F. E. Kühn, *Chem. Unserer Zeit*, 2015, **49**, 248–259.
- 225 S. Gonell, J. Lloret-Fillol and A. J. M. Miller, *ACS Catal.*, 2021, **11**, 615–626.
- 226 I. Azcarate, C. Costentin, M. Robert and J.-M. Savéant, *J. Am. Chem. Soc.*, 2016, **138**, 16639–16644.
- 227 N. Saravanan, M. Balamurugan, K. S. Shalini Devi, K. T. Nam and A. Senthil Kumar, *ChemSusChem*, 2020, **13**, 5620–5624.
- 228 C. Römelt, J. Song, M. Tarrago, J. A. Rees, M. van Gastel, T. Weyhermüller, S. DeBeer, E. Bill, F. Neese and S. Ye, *Inorg. Chem.*, 2017, **56**, 4745–4750.
- 229 C. Römelt, S. Ye, E. Bill, T. Weyhermüller, M. van Gastel and F. Neese, *Inorg. Chem.*, 2018, **57**, 2141–2148.
- 230 C. Amatore and J. M. Saveant, *J. Am. Chem. Soc.*, 1981, **103**, 5021–5023.
- 231 M. Ju and J. M. Schomaker, *Nat. Rev. Chem.*, 2021, **5**, 580–594.

- 232 L. Degennaro, P. Trinchera and R. Luisi, *Chem. Rev.*, 2014, **114**, 7881–7929.
- 233 D. Intrieri, P. Zardi, A. Caselli and E. Gallo, *Chem. Commun.*, 2014, **50**, 11440–11453.
- 234 G. Coin, R. Patra, S. Rana, J. P. Biswas, P. Dubourdeaux, M. Clémancey, S. P. de Visser, D. Maiti, P. Maldivi and J.-M. Latour, *ACS Catal.*, 2020, **10**, 10010–10020.
- 235 P. Scheiner, *Tetrahedron*, 1968, **24**, 349–356.
- 236 J. B. Sweeney, *Chem. Soc. Rev.*, 2002, **31**, 247–258.
- 237 P. Zardi, A. Pozzoli, F. Ferretti, G. Manca, C. Mealli and E. Gallo, *Dalton Trans.*, 2015, **44**, 10479–10489.
- 238 K. H. Hopmann and A. Ghosh, *ACS Catal.*, 2011, **1**, 597–600.
- 239 E. J. Klinker, T. A. Jackson, M. P. Jensen, A. Stubna, G. Juhász, E. L. Bominaar, E. Münck and L. Que Jr., *Angew. Chem., Int. Ed.*, 2006, **45**, 7394–7397.
- 240 L. Que and W. B. Tolman, *Nature*, 2008, **455**, 333–340.
- 241 T. Omura and R. Sato, *J. Biol. Chem.*, 1962, **237**, PC1375–PC1376.
- 242 P. R. E. Ortiz De Montellano, *Cytochrome P-450 Structure, Mechanism and Biochemistry*, Plenum Press, New York, 1995.
- 243 M. Costas, K. Chen and L. Que, *Coord. Chem. Rev.*, 2000, **200–202**, 517–544.
- 244 K. A. Srinivas, A. Kumar and S. M. S. Chauhan, *Chem. Commun.*, 2002, 2456–2457, DOI: [10.1039/B207072N](https://doi.org/10.1039/B207072N).
- 245 W. Nam, Y. O. Ryu and W. J. Song, *J. Biol. Inorg. Chem.*, 2004, **9**, 654–660.
- 246 J. W. Kück, A. Raba, I. I. E. Markovits, M. Cokoja and F. E. Kühn, *ChemCatChem*, 2014, **6**, 1882–1886.
- 247 M. C. White, A. G. Doyle and E. N. Jacobsen, *J. Am. Chem. Soc.*, 2001, **123**, 7194–7195.
- 248 E. A. Mikhalyova, O. V. Makhlynets, T. D. Palluccio, A. S. Filatov and E. V. Rybak-Akimova, *Chem. Commun.*, 2012, **48**, 687–689.
- 249 R. Mas-Ballesté and L. Que, *J. Am. Chem. Soc.*, 2007, **129**, 15964–15972.
- 250 J. Y. Ryu, J. Kim, M. Costas, K. Chen, W. Nam and L. Que Jr, *Chem. Commun.*, 2002, 1288–1289, DOI: [10.1039/B203154J](https://doi.org/10.1039/B203154J).
- 251 M. Fujita and L. Que Jr., *Adv. Synth. Catal.*, 2004, **346**, 190–194.
- 252 K. Chen, M. Costas, J. Kim, A. K. Tipton and L. Que, *J. Am. Chem. Soc.*, 2002, **124**, 3026–3035.
- 253 R. Mas-Ballesté, M. Costas, T. van den Berg and L. Que Jr., *Chem. – Eur. J.*, 2006, **12**, 7489–7500.
- 254 K. Chen and L. Que Jr., *Angew. Chem., Int. Ed.*, 1999, **38**, 2227–2229.
- 255 S. A. Hauser, M. Cokoja and F. E. Kühn, *Catal. Sci. Technol.*, 2013, **3**, 552–561.
- 256 A. Schmidt, N. Grover, T. K. Zimmermann, L. Graser, M. Cokoja, A. Pöthig and F. E. Kühn, *J. Catal.*, 2014, **319**, 119–126.
- 257 M. K. Tse, K. Schröder and M. Beller, in *Modern Oxidation Methods*, ed. J.-E. Bäckvall, Wiley-VCH, Weinheim, 2010, vol. 2, pp. 1–36.
- 258 Y. Feng, J. England and L. Que, *ACS Catal.*, 2011, **1**, 1035–1042.
- 259 C. L. Hill, *Nature*, 1999, **401**, 436–437.
- 260 H. J. H. Fenton, *J. Chem. Soc., Trans.*, 1894, **65**, 899–910.
- 261 N. M. F. Carvalho, A. Horn, R. B. Faria, A. J. Bortoluzzi, V. Drago and O. A. C. Antunes, *Inorg. Chim. Acta*, 2006, **359**, 4250–4258.
- 262 F. Haber, J. Weiss and W. J. Pope, *Proc. R. Soc. London, Ser. A*, 1934, **147**, 332–351.
- 263 N. A. Vermeulen, M. S. Chen and M. Christina White, *Tetrahedron*, 2009, **65**, 3078–3084.
- 264 L. Gómez, I. Garcia-Bosch, A. Company, J. Benet-Buchholz, A. Polo, X. Sala, X. Ribas and M. Costas, *Angew. Chem., Int. Ed.*, 2009, **48**, 5720–5723.
- 265 E.-M. H. J. Esslinger, J. F. Schlagintweit, G. G. Zámbo, A. M. Imhof, R. M. Reich and F. E. Kühn, *Asian J. Org. Chem.*, 2021, **10**, 2654–2662.
- 266 V. Dantignana, A. Company and M. Costas, *Isr. J. Chem.*, 2020, **60**, 1004–1018.
- 267 J. Chen and R. J. M. Klein Gebbink, *ACS Catal.*, 2019, **9**, 3564–3575.
- 268 M. Costas, *Coord. Chem. Rev.*, 2011, **255**, 2912–2932.
- 269 B. Meunier, *Chem. Rev.*, 1992, **92**, 1411–1456.
- 270 M. R. Bukowski, S. Zhu, K. D. Koehntop, W. W. Brennessel and L. Que, *J. Biol. Inorg. Chem.*, 2004, **9**, 39–48.
- 271 N. Ségaud, C. Johnson, A. Farre and M. Albrecht, *Chem. Commun.*, 2021, **57**, 10600–10603.
- 272 A. Nandy, C. Duan, M. G. Taylor, F. Liu, A. H. Steeves and H. J. Kulik, *Chem. Rev.*, 2021, **121**, 9927–10000.
- 273 A. Nandy, C. Duan, C. Goffinet and H. J. Kulik, *JACS Au*, 2022, **2**, 1200–1213.



## Tailoring activity and stability: Effects of electronic variations on iron-NHC epoxidation catalysts

Tim P. Schlachta<sup>a</sup>, Greta G. Zámbo<sup>a</sup>, Michael J. Sauer<sup>a</sup>, Isabelle Rüter<sup>b</sup>, Carla A. Hofer<sup>a</sup>, Serhiy Demeshko<sup>b</sup>, Franc Meyer<sup>b</sup>, Fritz E. Kühn<sup>a,\*</sup>

<sup>a</sup> Technical University of Munich, School of Natural Sciences, Department of Chemistry and Catalysis Research Center, Molecular Catalysis, Lichtenbergstraße 4, 85748 Garching, Germany

<sup>b</sup> Georg-August-Universität Göttingen, Institut für Anorganische Chemie, Tammannstraße 4, 37077 Göttingen, Germany

### ARTICLE INFO

#### Keywords:

Non-heme iron complexes  
N-heterocyclic carbene  
Epoxidation catalysis  
Lewis acids  
Electronic properties  
Iron NHC complexes  
Electronic fine-tuning of catalyst  
Catalytic optimization  
Tailoring catalytic properties

### ABSTRACT

A comparative study of three iron(II) NHC epoxidation catalysts with different electronic properties is performed to gain more profound insight into the influence of electronic variations on catalytic performance. One iron complex contains a pyridyl-NHC ligand, the other two are prepared with a modified ligand counterpart. The complexes are comprehensively characterized by various methods including Mössbauer, SQUID and DFT. While a lower electron density at the iron atom can be associated with a decline in epoxidation activity, a more electron rich iron center does not necessarily correspond with higher activity, due to reduced catalyst stability. Addition of Lewis acids increases both activity and stability significantly and is more effective than temperature variations. All three epoxidation catalysts achieve high selectivity, with a maximum TOF of 24 500 h<sup>-1</sup> and TON of >700 for the unmodified complex. More nucleophilic alkenes promote higher activity and conversion.

### 1. Introduction

In nature, iron containing enzymes like cytochrome P450, facilitate the oxidation of various substrates under mild conditions with high activity and selectivity [1]. Aspired to mimic their reactivity, iron based complexes have been intensively studied in oxidation reactions. The relatively low price of iron in comparison to noble metals, as it is one of the most abundant elements in the Earth's crust, make iron complexes interesting candidates for applications in industrial catalysis, although the cost of the ligands may be considerable [2]. A potentially lower toxicity of iron is often also mentioned as another advantage of iron complexes. However, even though iron is an essential trace element, toxicity of catalysts depends on several factors, e.g. ligands and oxidation state, and cannot be assessed as generally as it is often attempted, particularly by laypersons or in popular science [2–4].

Previous research on bio-inspired iron catalysts featured N-donor ligands, like porphyrins or other non-heme ligands [5–12]. In catalytic epoxidations, the use of N-heterocyclic carbene (NHC) ligands has been shown to be superior to N-donor ligands [13–17], especially in terms of activity given in turnover frequency (TOF). A variety of NHC ligated Fe systems outperform one of the most active N-ligated iron catalysts (25

200 h<sup>-1</sup>) [18] as well as other organometallic transition metal benchmark catalysts, e.g. based on Re (up to ca. 40 000 h<sup>-1</sup>) [13] or Mo (up to > 50 000 h<sup>-1</sup>) [19]. A TOF of > 400 000 h<sup>-1</sup> and a turnover number (TON) of ca. 1200 were reached at room temperature in the presence of Lewis acid Sc(OTf)<sub>3</sub> as additive by the current benchmark system for homogeneous olefin epoxidation, an iron(II) tetracarbene complex (**a**, and its iron(III) homologue **b**, Fig. 1), published by our group [15]. Nevertheless, for a potential application in industry, particularly the stability has to be significantly increased, while maintaining high activity. Therefore, we have investigated various methods described in the following to improve the catalytic performance of our benchmark catalyst (**a/b**) or to synthesize a next-generation iron epoxidation catalyst. Application of Lewis acids like Sc(OTf)<sub>3</sub> already more than doubled the average number of catalytic cycles possible with one active center derived from **a** from ca. 500 to ca. 1200 by, among other reasons, suppressing a deactivation pathway, the formation of a diiron(III)-μ<sub>2</sub>-oxo species [14–15,20–21]. The impact of modification of the NHC backbone with electron donating (**c**, **d**) and accepting moieties (**e**, **f**, Fig. 1) on the catalytic performance was investigated next by our group. Complexes **c** and **d** are more active than **e** and **f**, but they all lack behind in activity compared to **a** and **b** [22]. The stability could also not be

\* Corresponding author.

E-mail address: [fritz.kuehn@ch.tum.de](mailto:fritz.kuehn@ch.tum.de) (F.E. Kühn).

<https://doi.org/10.1016/j.jcat.2023.07.018>

Received 22 May 2023; Received in revised form 16 July 2023; Accepted 20 July 2023

Available online 22 July 2023

0021-9517/© 2023 Elsevier Inc. All rights reserved.

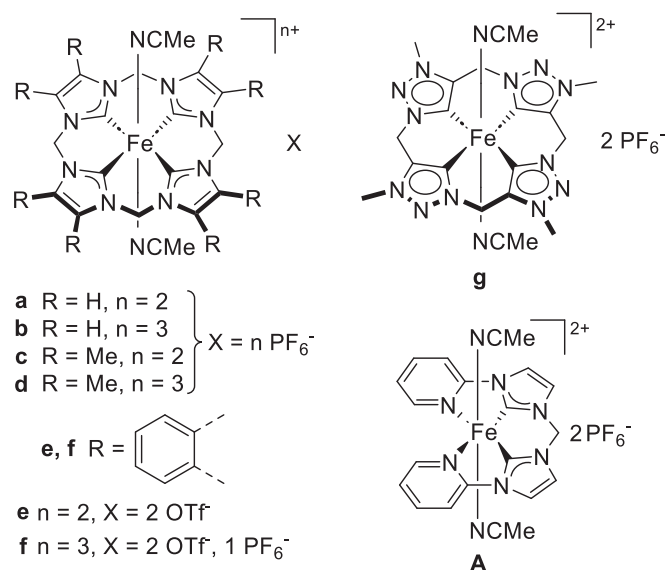


Fig. 1. (Pre-)Catalysts.

enhanced: while **f** has a similar TON of 1000, the catalytic performance of **c** and **d** is hampered by their low stability. A different strategy is the electronic fine-tuning of the iron center through axial ligand substitution, with which we could for example increase the stability of iron-NHC catalysts in C–H hydroxylation by up to 34% [23]. However, in epoxidation catalysis this method even decreased the catalytic performance [24–26]. The rate determining step in epoxidation catalysis is assumed to be the formation of an electrophilic iron(IV) or iron(V)-oxo intermediate and a more electron rich iron(III) center is presumed to facilitate its formation [22,27–28]. Hence, an iron(II) tetracarbenes (**g**, Fig. 1) containing the theoretically strongest electron donating ligand in this series and thus most electron rich iron center has been investigated by us. However, preliminary experiments did not indicate a beneficial effect as a comparably low TOF of 41 000 h<sup>-1</sup> is reached in presence of Sc(OTf)<sub>3</sub> [16].

In order to deepen the understanding of the influence of electronic changes on the catalytic performance, a different catalytic system from our group is used in this work (**A**, Fig. 1). The pyridine-NHC-based system [29], although less active, is structurally similar to the “flagship” iron tetracarbenes scaffold, while being sufficiently different and, most importantly, easy to modify to make it a suitable candidate. Iron(II) complex **A** specifically has been extensively studied in C–H hydroxylation [23,30–33] and a preliminary study on the epoxidation of olefins has been conducted by us [34]. The latter was largely done using <sup>1</sup>H NMR spectroscopy. In this work, the results are reevaluated using GC analysis as a more precise method and compared to two novel iron(II)

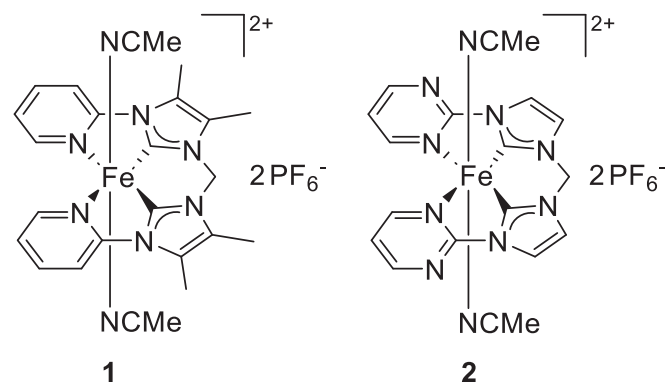


Fig. 2. Novel complexes.

complexes, **1** and **2** (Fig. 2), in the epoxidation of *cis*-cyclooctene as model substrate. In addition, a series of more challenging olefin substrates is screened with all three complexes and the impact of Lewis acidic additives is investigated. **1** and **2** are designed to have a more electron rich (**1**) and less electron rich iron center (**2**) than **A**, by having a ligand with supposedly donating (**1**) or accepting properties (**2**), respectively. The impact of these modifications of the catalytic system on its catalytic performance allows to gain valuable information for the epoxidation reaction in general, such as whether these effects are universal or limited to the tetracarbenes framework, in order to advance research related to the benchmark catalytic system. Furthermore, the synthesis of the two novel complexes **1**, bearing two methyl groups at the 4 and 5 position of the imidazole backbone, and **2**, having the pyridine moiety formally substituted by pyrimidine, is reported. The new compounds **1** and **2**, and if applicable, **A**, are elaborately characterized using NMR spectroscopy, electrospray mass spectrometry (ESI-MS), single crystal X-ray diffraction (SC-XRD), UV/Vis spectroscopy, cyclic voltammetry (CV), Mössbauer spectroscopy, buried volume and steric map calculations, SQUID magnetometry (for **A**), DTF calculations, and elemental analysis.

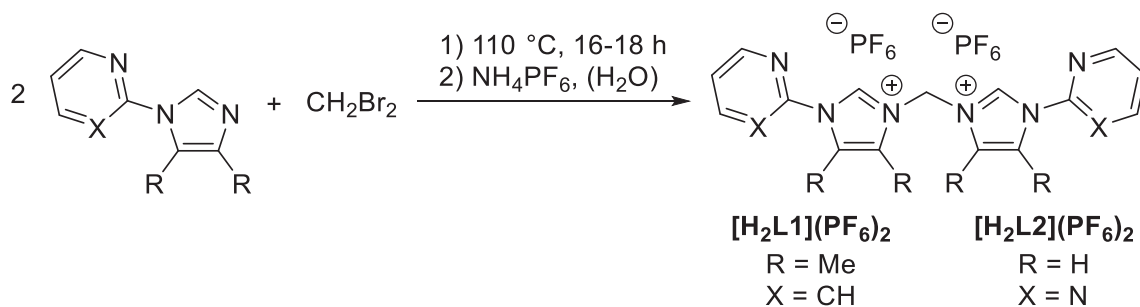
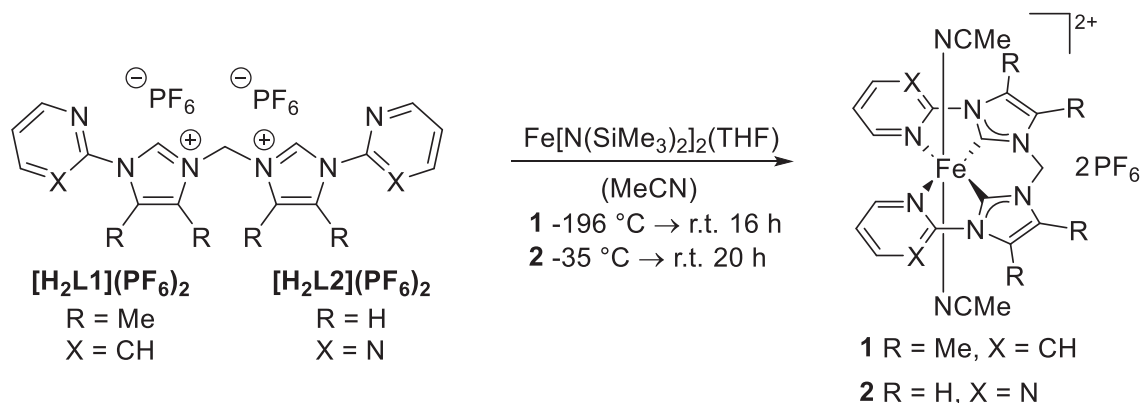
## 2. Results and discussion

### 2.1. Synthesis and characterization of the iron(II) complexes **1** and **2**

The synthesis of the ligand precursor of **1** starts with the coupling of two 2-(4,5-dimethyl-1*H*-imidazol-1-yl)pyridine [35] moieties with excess dibromomethane without additional solvent to give the dibromide salt [H<sub>2</sub>L1](Br)<sub>2</sub>. In a next step, the bromide anions are exchanged with weakly coordinating hexafluorophosphate anions in order to increase the solubility towards organic solvents and as additional purification step [28], to obtain [H<sub>2</sub>L1](PF<sub>6</sub>)<sub>2</sub> (Scheme 1). The synthesis of the ligand precursor of **2**, [H<sub>2</sub>L2](PF<sub>6</sub>)<sub>2</sub>, follows the same pathway with 2-(1*H*-imidazol-1-yl)pyrimidine [35–36] as starting material (Scheme 1).

Direct metalation of the ligand precursors with the iron(II) precursor and internal base Fe[N(SiMe<sub>3</sub>)<sub>2</sub>]<sub>2</sub>(THF) affords the complexes **1** and **2** (Scheme 2) [28,37]. The amide as strong, non-nucleophilic base is often used for the synthesis of iron(II) NHC complexes. It deprotonates the imidazolium salts and iron immediately coordinates to the *in-situ* generated carbenes. The thereby formed amine HN(SiMe<sub>3</sub>)<sub>2</sub> is readily removed under vacuum [28].

Similar to **A**, both **1** and **2** are diamagnetic low-spin iron(II) (*S* = 0) complexes, as indicated in <sup>1</sup>H NMR and as evidenced in the following. Successful complexation is confirmed by the absence of the C2 imidazolium proton resonance signals in the <sup>1</sup>H NMR spectra. The two labile axial MeCN ligands are quickly exchanged in solution with deuterated MeCN, resulting in two equivalents of free MeCN being visible in the <sup>1</sup>H NMR spectrum. The signals of the methylene bridges are singlets, verifying the equatorial coordination of the ligand, like in complex **A**. The carbene signals in <sup>13</sup>C NMR are sensitive to the electronic properties of the metal center and allow evaluation of the σ-donor strength of the NHC ligand [28,38]. The NHC moieties of **1** should be stronger σ-donors than the unmodified imidazolylidenes of **A** due to the +1 effect of the methyl groups at the backbone. This expectation is supported by Tolman electronic parameters [39]. The <sup>13</sup>C<sub>NHC</sub> signal of **1** (215.49 ppm) is shifted upfield 0.66 ppm compared to **A** (216.15 ppm [29]), confirming the stronger electron donation in **1**. This change appears to be rather small but any difference exceeding 0.4 ppm in NMR is significant by means of statistic uncertainty [28,38]. The upfield shift can be explained by an increased diamagnetic shielding term of the carbene carbon atom in **1** due to its higher electron density donated by the methyl groups. For **2**, the <sup>13</sup>C<sub>NHC</sub> signal (216.24 ppm) does not show any significant shift change compared to **A** because both NHC units have the same chemical structure. Nevertheless, the electron density of the iron center in **2** should be lower than in **A**, mainly because of pyrimidine being a weaker

Scheme 1. Synthesis of ligand precursors  $[\text{H}_2\text{L1}](\text{PF}_6)_2$  and  $[\text{H}_2\text{L2}](\text{PF}_6)_2$ .Scheme 2. Synthesis of iron(II) complexes **1** and **2**.

$\sigma$ -donor than pyridine due to the -I effect of adding a second nitrogen atom to the aromatic ring, while the amount of  $\pi$ -backdonation is expected to stay the same [40]. The successful synthesis of **1** and **2** is further shown with ESI-MS where three characteristic fragments are detected of the iron center with equatorial ligand and without, with one, or with both axial MeCN ligands, demonstrating again the lability of the axial ligands. The chemical composition of the new complexes is confirmed by elemental analysis. Like **A**, **1** and **2** can be stored as solid under ambient conditions for a few weeks without degradation. Furthermore, all three complexes are stable in solution in untreated HPLC-grade MeCN (*i.e.* not dried or degassed) under ambient conditions for at least one day.

The redox potential of a complex can provide further insight into the electronic properties of its metal center, which is influenced by the surrounding ligands. Actually, for the iron tetracarbenes system of **a-f**, a linear correlation between chemical shift of the  $^{13}\text{C}_{\text{NHC}}$  signal and redox potential has been found, allowing to predict one parameter once the respective other parameter is known [28]. Similarly, for a series of complexes derived by axial ligand substitution of **A**, a linear relationship could be established between the redox potentials and the highest occupied molecular orbital (HOMO) energy determined by DFT [41]. The redox potential of **1** is  $E_{1/2} = 0.337 \text{ V}$  (see SI), which is 86 mV lower than that of **A** ( $E_{1/2} = 0.423 \text{ V}$ ) [29,41–43], indicating a more electron rich iron center in **1**, as had been intended. In contrast, **2** has a 136 mV more positive half-cell potential of  $E_{1/2} = 0.559 \text{ V}$  compared to **A**, implying a lower electron density at the iron center due to a weaker equatorial  $\sigma$ -donor [28]. While **1** shows a reversible redox process ( $\Delta E = 106 \text{ mV}$ ), complex **2** has a quasi-reversible redox process ( $\Delta E = 259 \text{ mV}$ ). Possible explanations of the latter could be a conformational change upon oxidation to iron(III), like a  $180^\circ$  ring-flip of one pyrimidine unit or the coordination of a third MeCN molecule, leading to decoordination of one pyrimidine from the iron atom. Such a behavior has been observed with similar complexes [42–44].

The UV/Vis spectrum of **1** shows similar absorption characteristics

like **A**, but slightly red-shifted (see SI). The bathochromic effect of around 8 nm can be explained by a higher electron donation in **1** due to the methyl substituents, decreasing the energy of the HOMO/LUMO gap [45–47]. The characteristic two absorption maxima around 340 nm and 400 nm (**A**: 329 and 400 nm, **1**: 340 and 408 nm, **2**: 355 and 403 nm) can be assigned to charge-transfer bands based on similar complexes [41].

Solid material of all three Fe(II) complexes was studied using  $^{57}\text{Fe}$  Mössbauer spectroscopy at 80 K to gain further information about their electronic properties. They all exhibit isomer shifts in the range of octahedral iron(II) low-spin species [28,48] (**A**:  $\delta = 0.26 \text{ mm s}^{-1}$ ; **1**:  $\delta = 0.23 \text{ mm s}^{-1}$ ; **2**:  $\delta = 0.24 \text{ mm s}^{-1}$ ) but are more positive compared to **a** ( $\delta = 0.08 \text{ mm s}^{-1}$ ) [28,49], attributed to the weaker  $\sigma$ -donation of the equatorial ligand compared to the tetracarbenes ligand. However, they are on the same scale as the 18-membered iron tetracarbenes Fe(II) complexes ( $\delta = 0.23 \text{ mm s}^{-1}$ ) [28,50–51]. A small influence of the donating properties of the methyl substitution in the backbone of **1** is visible, moving the isomer shift as expected to smaller values for a more electron rich iron center. The length of the Fe–ligand bonds can have a considerable impact on the isomer shift through compression of the *s*-orbitals resulting in a higher electron density [48]. However, all three complexes show similar bond lengths (Table 1) resulting in similar  $\delta$  values. The quadrupole splittings are rather large for iron(II) low-spin

**Table 1**  
Comparison of selected structural parameters of **A** [29], **1** and **2**.

Bond lengths (Å)	Fe–C <sub>NHC</sub>	Fe–N	Fe–NCMe
<b>A</b>	1.837(2)	2.096(2)	1.915(2)
<b>1</b>	1.8429(18)	2.0801(16)	1.9283(18)
<b>2</b>	1.8359(14)	2.1028(12)	1.9146(12)
Bond angles (°)	C <sub>NHC</sub> –Fe–C <sub>NHC</sub>	C <sub>NHC</sub> –Fe–N'	MeCN–Fe–NCMe
<b>A</b>	85.85(9)	165.12(6)	172.23(7)
<b>1</b>	86.59(11)	165.84(7)	167.99(8)
<b>2</b>	86.01(9)	165.12(6)	170.73(7)

complexes. No valence contribution is expected for them, but the results are in line with a heteroleptic ligand coordination sphere (different equatorial donor atoms and axial ligands) and strongly anisotropic covalent bonds (*vide infra*) as already seen in the case of the 18-membered tetracarbenes complexes [28,50–53]. Especially the strong  $\sigma$ -donation of the NHC moieties in an equatorial plane deforms the charge distribution surrounding the iron nucleus leading to the observed high quadrupole splitting. The quadrupole splitting increases in the order **2** ( $\Delta E_Q = 1.80 \text{ mm s}^{-1}$ ) < **A** ( $\Delta E_Q = 2.07 \text{ mm s}^{-1}$ ) < **1** ( $\Delta E_Q = 2.22 \text{ mm s}^{-1}$ ) due to the increasing electron donor strength of the equatorial ligands and the resulting higher amount of deformation of the electric field (Fig. 3).

All three complexes **A**, **1** and **2** are low-spin diamagnetic complexes at 293 K. The magnetic susceptibility of complex **A** was analyzed exemplarily using a SQUID magnetometer from 2 K up to 400 K (see SI). No thermally induced spin crossover [54] from low-spin to high-spin is observed at elevated temperatures. **A** is diamagnetic up to 400 K reflecting the strong ligand field induced by the NHC ligand.

Single crystals suitable for SC-XRD were obtained by slow evaporation of a solution of **1** in MeCN and by slow vapor diffusion of 1,4-dioxane into a solution of **2** in MeCN (see SI). Both **1** (Fig. 4) and **2** (Fig. 5) show a distorted-octahedral geometry around the Fe center, as had been observed for **A**. The tetradentate ligand is coordinating equatorial and the labile MeCN ligands axial to the iron(II) center. In all three complexes, the Fe–C<sub>NHC</sub> bond (~1.839 Å) is significantly shorter than the Fe–N bond (~2.101 Å, see Table 1). In **1**, the Fe–N bond is significantly shorter and the Fe–NCMe bond significantly longer in terms of statistic uncertainty (*i.e.* three times the weighted standard deviation) [28] compared to the other two complexes. Apart from that, the structures are similar. The vertical axis passing through the two axial MeCN ligands and the iron center is more curved compared to iron tetracarbenes complexes [28], probably because of the steric influence of the open NCCN ligand.

The ligand modifications should only change one variable, the electronic properties of the complexes, to ensure a good comparability of the catalytic experiments. The catalytic pocket is intended to remain constant. This is proposed to be the case, as derived by the structural parameters shown in Table 1 of the iron(II) pre-catalysts, and confirmed by calculations regarding the percentage of buried volume %V<sub>Bur</sub> of the iron center, being around 86%V<sub>Bur</sub> for all three (see SI). The topographic steric maps of the buried volume of **A** are exemplarily shown in Fig. 6 (for **1** and **2** see SI).

Finally, DTF calculations were performed to gain more insights of the electronic properties of **A**, **1** and **2**. In the case of **c/d**, the worse catalytic performance compared to **a/b** was explained by computational methods, which indicated – contrary to the experimental methods – that the  $\sigma$ -donation of the methyl groups in fact is counterbalanced with an increased  $\pi$ -backbonding character [22]. This results in a less electron rich iron center compared to **a/b**, and, as a more electron-rich iron(III) center is expected to be beneficial for catalysis (*vide supra*), worse catalytic performance. The electronic influence of the ligand in **A**, **1** and **2** is investigated by calculation of the electronic charge of the respective low-spin iron(III) center. Löwdin population analysis [55] was applied for that reason. The iron(III) Löwdin charge is most negative for **1**, followed by **A** and **2** (Table 2). This trend is in accordance to the experimentally determined electronic properties of the three complexes, with **1** having the most electron rich iron center, **A** in between and **2** with the lowest electron density at the nucleus. Contrary to **c/d** [22], the methyl groups in **1** appear to only increase the  $\sigma$ -donation towards the iron atom without enhanced  $\pi$ -backbonding character.

The strong equatorial electron donation of the tetracarbenes ligand in iron tetracarbenes like **a/b** (Fig. 1) rises the  $3d_{x^2-y^2}$  above the  $3d_{z^2}$  orbital, opposite to most *N*-ligated iron complexes, leading to exclusive triplet reactivity in epoxidation catalysis [28]. This is also the case for **A** [41], **1** and **2**, based on the calculation of the LUMO and LUMO + 1 orbitals (see SI). Despite having only two NHCs, the  $x^2-y^2$  orbital is also elevated above the  $z^2$  orbital (see SI), justifying again the suitability of

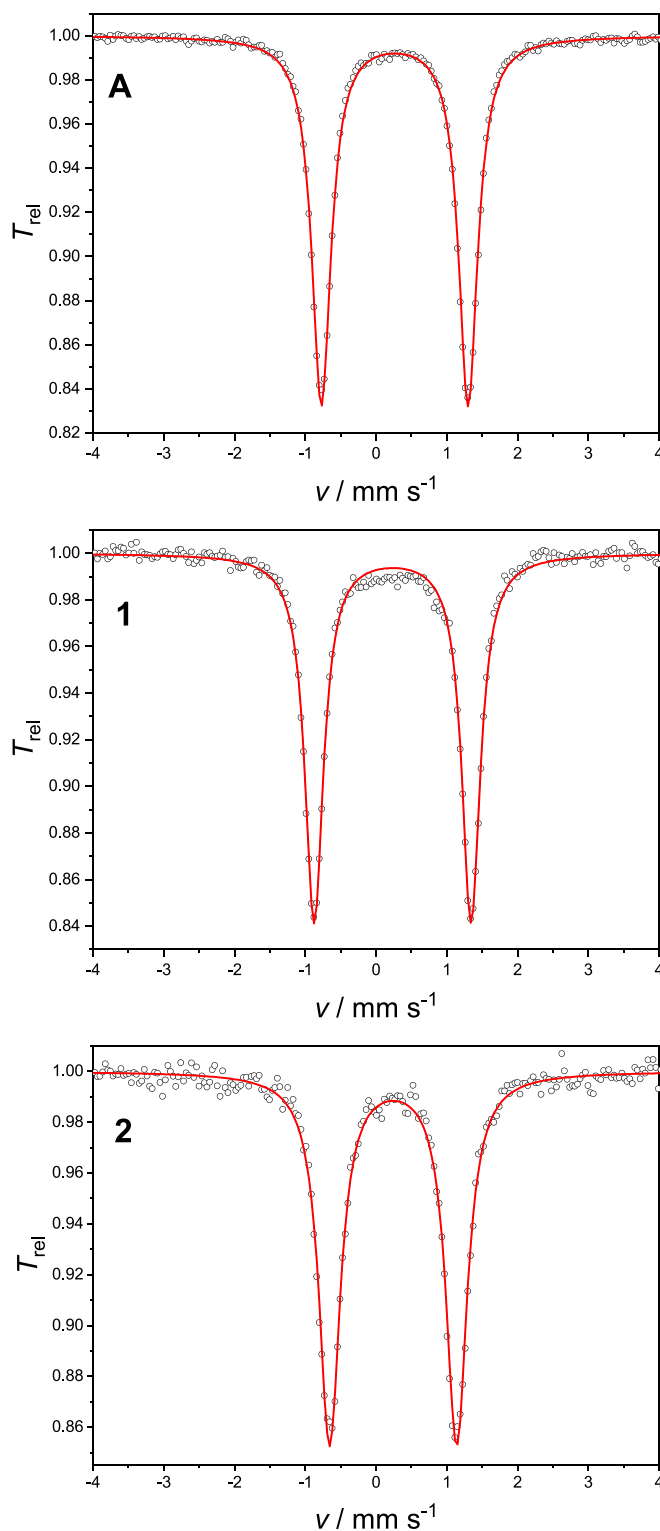
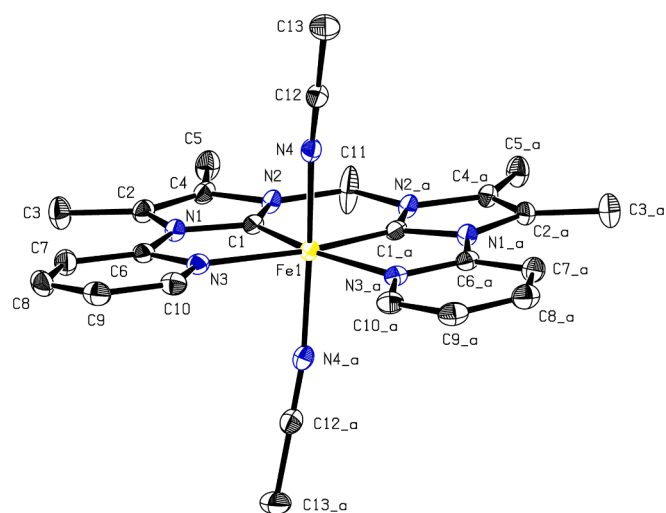
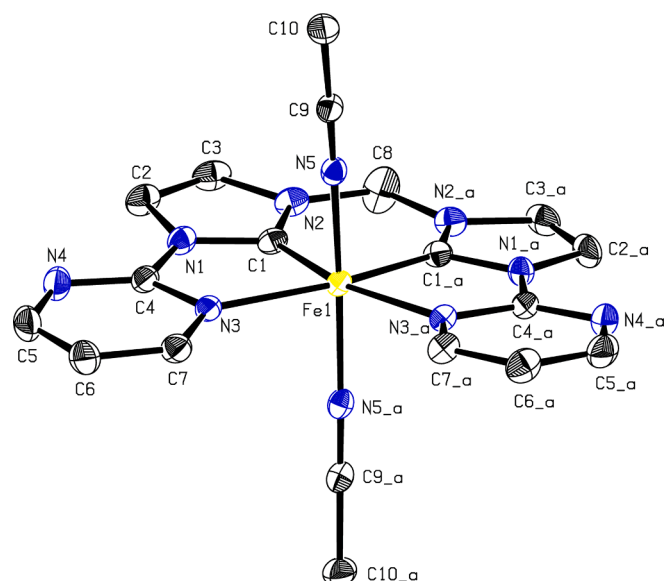


Fig. 3. Zero-field  $^{57}\text{Fe}$  Mössbauer spectrum of solid **A**, **1** and **2** at 80 K. The red line represents a simulation with  $\delta = 0.26 \text{ mm s}^{-1}$  and  $\Delta E_Q = 2.07 \text{ mm s}^{-1}$  (**A**, top);  $\delta = 0.23 \text{ mm s}^{-1}$  and  $\Delta E_Q = 2.22 \text{ mm s}^{-1}$  (**1**, middle);  $\delta = 0.24 \text{ mm s}^{-1}$  and  $\Delta E_Q = 1.80 \text{ mm s}^{-1}$  (**2**, bottom).



**Fig. 4.** ORTEP-style representation of the cationic fragment of complex **1**. Hydrogen atoms and hexafluorophosphate anions are omitted for clarity. Thermal ellipsoids are shown at a 50% probability level.



**Fig. 5.** ORTEP-style representation of the cationic fragment of complex **2**. Hydrogen atoms and hexafluorophosphate anions are omitted for clarity. Thermal ellipsoids are shown at a 50% probability level.

the catalytic system of **A/1/2** for comparison with **a/b** in epoxidation catalysis in the following, due to an expected similar reactivity.

## 2.2. Catalytic olefin epoxidation reactions

The impact of the ligand modifications of **1** and **2** on the catalytic performance is investigated in the following. All three complexes **A**, **1** and **2** are employed as catalysts in olefin epoxidation reactions. Standard conditions are defined as 20 °C using H<sub>2</sub>O<sub>2</sub> (1.50 eq.) as oxidant, MeCN as solvent, *cis*-cyclooctene (1.00 eq.) as model substrate in the presence of one of the three complexes as catalyst (0.02 eq.). Hydrogen peroxide was used as oxidant, as it has been found to be superior in comparison to other common peroxides such as *tert*-butyl hydroperoxide or the urea hydrogen peroxide adduct in iron-NHC epoxidation catalysis [14,34]. In addition, being atom-efficient and environmentally friendly are two further advantages [56–57]. Excess of H<sub>2</sub>O<sub>2</sub> was used for best results based on previous optimizing studies with different loadings

[14,34]. For the quantification of the formed epoxide, GC-FID and <sup>1</sup>H NMR spectroscopy were applied.

In a first experiment, all three complexes have been employed in the olefin epoxidation of *cis*-cyclooctene under standard conditions for 60 min (Fig. 7). Complex **A** achieves a conversion of 84% after 10 min that afterwards only marginally increases to 87% at 60 min. Surprisingly, **1** shows a slightly lower activity than **A**, reaching 16% conversion after 30 s versus 20% for **A**. In contrast to **A**, however, **1** only reaches a conversion of 20% after 1 min (**A**: 32%), which does not increase during the remaining time. This indicates a relatively short lifetime of the catalyst. Possible degradation (*vide infra*) might involve the dissociation of the NCCN ligand, C–C bond formation resulting in a highly-strained annulated 2,2'-biimidazole and subsequent cleavage of the methylene bridge, as observed under oxidative conditions for **A** [44,58]. **2** in turn shows a remarkably longer lifetime albeit being the least active catalyst, as expected, and stays active for 4 h, reaching a conversion of 45% (see SI). As demonstrated by its higher redox potential, the initial required pre-oxidation from Fe<sup>II</sup> to Fe<sup>III</sup> might be slower in the case of **2**, restraining the activity. These different catalytic performances are mainly attributed to the different electronic properties of the complexes due to the equatorial ligand modifications. All complexes achieve a selectivity of > 99% under the applied conditions, placing them among the most selective Fe-NHC catalytic systems, on par with **a/b** [28].

A stable diiron(III)- $\mu_2$ -oxo complex is formed in iron tetracarbene epoxidation catalysis of **a** and **b**, possessing a low activity [15,20–21]. This dead-end species can be reactivated through the addition of Lewis acids like Sc(OTf)<sub>3</sub>. Interestingly, in the presence of Lewis acids, **a**, **b** and the diiron(III)- $\mu_2$ -oxo complex all show the same activity (TOF of ~410 000 h<sup>-1</sup>), which can be explained by the suppression of this deactivation pathway, the formation of the bridged oxo-species [15,24]. In addition, the observed activity (TOF) is several times higher compared to systems without additive (**a**: 50 000 h<sup>-1</sup>; **b**: 183 000 h<sup>-1</sup>) and the stability is significantly enhanced (TON: 1200 vs. without additive **a**: 390; **b**: 740) [15,28].

Although no  $\mu_2$ -oxo bridged complex of **A** has been reported, the analogy of these two catalytic systems suggests similar mechanisms. The impact of Lewis acids on **A** has not been studied yet. Therefore, in a next experiment, the olefin epoxidation of *cis*-cyclooctene under standard conditions for 60 min is repeated but in the presence of Sc(OTf)<sub>3</sub>, the most efficient Lewis acid found for **a/b** [15]. Under these conditions, all three catalysts achieve relatively high conversions (**A**: 100%; **1**: 92%; **2**: 97%, Fig. 8), implying a similar deactivation pathway being present in the first experiment in Fig. 7, which is now suppressed. Furthermore, both stability (measured as TON, e.g. 10 vs. 46 for **1**, entry 14 and 15) and activity (determined as TOF, e.g. 1 700 h<sup>-1</sup> vs. 18 000 h<sup>-1</sup> for **A**, entry 2 and 3) are significantly enhanced (Table 3). Another reason for the beneficial effect of Lewis acids on the catalytic activity is their ability to facilitate crucial proposed mechanistic steps like the initial oxidation of Fe<sup>II</sup> to Fe<sup>III</sup>, and the OH<sup>•/•-</sup> cleavage of the Fe<sup>III</sup>-OOH intermediate shifting the rate determining step towards olefin oxidation [15,28,59]. Selectivity is not influenced by the Lewis acid and remains unchanged high (Table 3). In fact, for **a**, the selectivity is even improved from 94% to 99% upon addition of Sc(OTf)<sub>3</sub> [14–15].

Different catalyst concentrations have been screened in the epoxidation of *cis*-cyclooctene under standard conditions using the three complexes with and without Sc(OTf)<sub>3</sub> as additive. They all show a nearly linear relationship between catalyst loading and conversion (Table 3, visualized in the SI). **A** reaches an initial TOF of up to 3 400 h<sup>-1</sup> (entry 7) and TON of up to 65 (entry 9) without any additive. In the presence of Sc(OTf)<sub>3</sub>, **A** achieves a highest TOF of 24 500 h<sup>-1</sup> (entry 10), which albeit being an order of magnitude lower than the benchmark iron tetracarbene system **a/b** (~410 000 h<sup>-1</sup>), still is on par with the most active *N*-donor based iron catalysts (25 200 h<sup>-1</sup>). This emphasizes once more the beneficial effect of employing NHC ligands in epoxidation catalysis [28]. Most *N*-ligated iron complexes have TONs of less than 100 [9], and one of the highest reported TONs are 180 [18], 715 [60] and 252 [61],

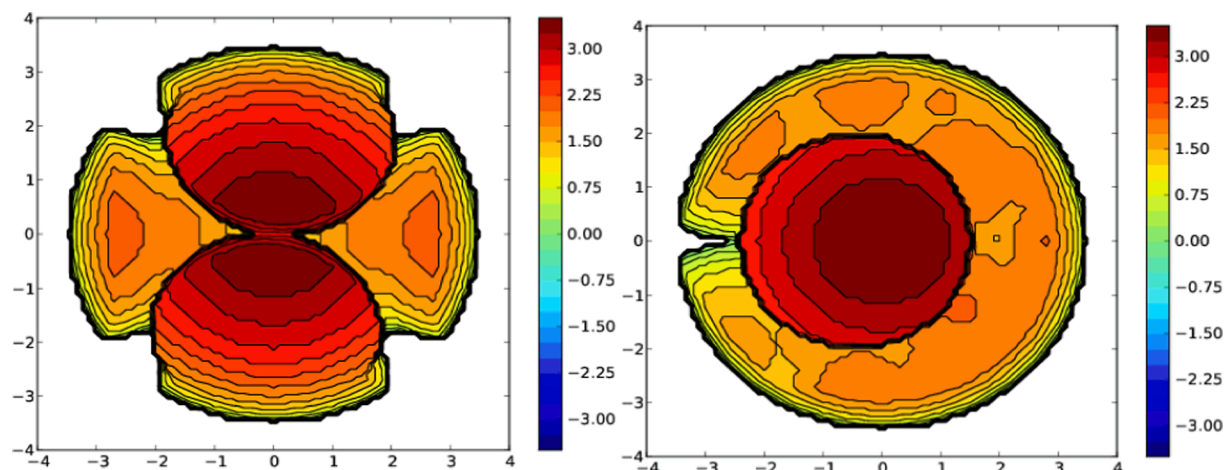


**Fig. 6.** Topographic steric maps of the buried volume of **A**. The red and blue colors show the more- and less-hindered zones in the catalytic center, respectively. Left: View towards the opening of the NCCN ligand of **A** with the axial ligands horizontal and the NCCN ligand vertical. Right: View on top of **A**, with the red circle marking the axial ligands and the broader orange area representing the NCCN ligand underneath with its opening to the left.

**Table 2**

Calculated charges at the iron(III) center of **A**, **1** and **2** using the Löwdin charge model. Values are given in atomic units and were rounded to the third decimal digit.

Complex	<b>A</b>	<b>1</b>	<b>2</b>
Löwdin	-1.249	-1.263	-1.236

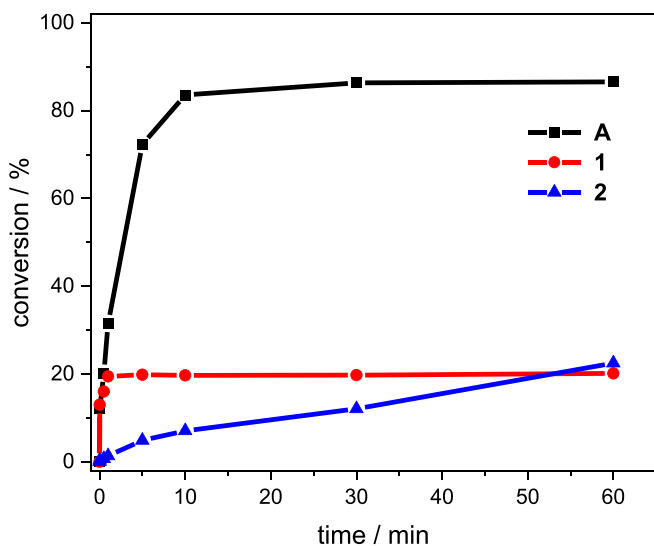


**Fig. 7.** Time-dependent epoxidation of *cis*-cyclooctene (67.3  $\mu\text{mol/mL}$ , 1.00 eq.) in MeCN using **A**, **1** or **2** (1.35  $\mu\text{mol/mL}$ , 0.02 eq.) as catalyst, and  $\text{H}_2\text{O}_2$  (50% aq., 101  $\mu\text{mol/mL}$ , 1.50 eq.) as oxidizing agent at 20 °C. Conversions are determined by GC-FID.

but the latter with low selectivity towards the epoxide. Using 0.1 mol% of **A**, a remarkable TON of 711 is attained at 20 °C, which is, to the best of our knowledge, the second highest reported one for a Fe-NHC catalytic system, with the highest TON of 1200 at 20 °C for **a/b** [28]. **1** with the supposedly more electron rich center has at least the second highest TOF of the three complexes with 7 600  $\text{h}^{-1}$ , and a TON of 46 in the presence of  $\text{Sc}(\text{OTf})_3$  (entry 15). **2** has no measurable TOF after 10 s due to its slow nature without additive, but a TON of 23 can be determined after 4 h and complete reaction (entry 19). However, despite having the least electron rich center, **2** achieves nearly full conversion after 10 min

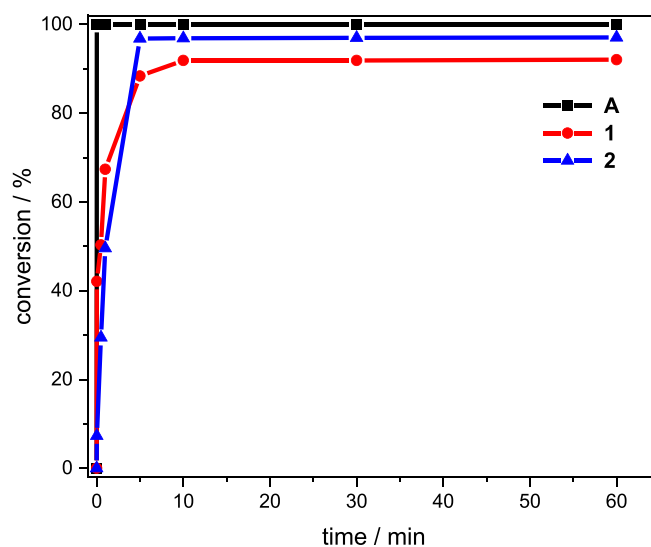


**Fig. 8.** Time-dependent epoxidation of *cis*-cyclooctene (67.3  $\mu\text{mol/mL}$ , 1.00 eq.) in MeCN using **A**, **1** or **2** (1.35  $\mu\text{mol/mL}$ , 0.02 eq.) as catalyst,  $\text{Sc}(\text{OTf})_3$  (6.73  $\mu\text{mol/mL}$ , 0.10 eq.), and  $\text{H}_2\text{O}_2$  (50% aq., 101  $\mu\text{mol/mL}$ , 1.50 eq.) as oxidizing agent at 20 °C. Conversions are determined by GC-FID.

with  $\text{Sc}(\text{OTf})_3$ , a maximum TOF of 1 300  $\text{h}^{-1}$  and a TON of 49 (entry 20). The TON is even slightly higher than **1** and as high as for **A** (50, entry 3).

Variable temperature studies of all three complexes were performed next (Table 3, Fig. 9). Decreasing the temperature below 20 °C has been shown to be beneficial for the stability of Fe-NHC catalysts and thus leading to an enhanced catalyst lifetime [14,17,34]. On the other side, **e/f** (Fig. 1) with an electron pulling tetracarbene ligand similar to **2** have been found to be remarkable temperature-tolerant, albeit also requiring these higher temperatures for an enhanced activity [22]. **A** has a lower activity at 0 °C (400  $\text{h}^{-1}$ , entry 1) but achieves an effectively full conversion (98%) in 60 min reaction time in comparison to the 20 °C run (87%), which is attributable to the 14% higher stability with a TON of 49 vs. 43 at 20 °C (entry 2). Based on the slope, a lower catalyst loading would still have been sufficient for complete conversion with a longer reaction time. Increasing the temperature to 40 °C enhances the activity and an initial TOF of 2 200  $\text{h}^{-1}$  is determined (entry 4). However, deactivation of **A** also occurs faster, reducing the total conversion to 42% at a TON of 21. For **2**, a rise of the temperature to 40 °C also is beneficial for the activity (200  $\text{h}^{-1}$ , entry 21) and at 60 °C the highest

**Table 3**Epoxidation of *cis*-cyclooctene by **A**, **1** and **2** at different catalyst concentrations, temperature, and with or without additive.

entry	catalyst	T [°C]	loading [mol%]	additive	X [%] <sup>[a]</sup> (10 min)	S [%]	TOF [h <sup>-1</sup> ] <sup>[b]</sup>	TON (60 min)
1	A	0	2	–	33	> 99	400	49
2	A	20	2	–	80	> 99	1 700	43
3	A	20	2	Sc(OTf) <sub>3</sub>	100	99	18 000	50
4	A	40	2	–	38	> 99	2 200	21
5	A	20	1	–	43	> 99	2 700	43
6	A	20	1	Sc(OTf) <sub>3</sub>	100	99	20 800	100
7	A	20	0.5	–	24	> 99	3 400	48
8	A	20	0.5	Sc(OTf) <sub>3</sub>	96	99	22 600	194
9	A	20	0.1	–	7	> 99	2 900	65
10	A	20	0.1	Sc(OTf) <sub>3</sub>	26	99	24 500	711
11	1	-10	2	–	2	> 99	0	4
12	1	0	2	–	27	> 99	1 000	19
13	1	0	2	Sc(OTf) <sub>3</sub>	74	> 99	6 500	44
14	1	20	2	–	19	> 99	900	10
15	1	20	2	Sc(OTf) <sub>3</sub>	91	99	7 600	46
16	1	20	1	–	10	> 99	900	11
17	1	20	0.5	–	5	> 99	1 400	12
18	1	20	0.1	–	1	> 99	1 300	12
19	2	20	2	–	6	> 99	0	23
20	2	20	2	Sc(OTf) <sub>3</sub>	97	99	1 300	49
21	2	40	2	–	22	> 99	200	15
22	2	60	2	–	20	> 99	700	13
23	2	20	1	–	3	> 99	0	3
24	2	20	0.5	–	1	> 99	0	2
25	2	20	0.1	–	0	–	0	0

Reaction conditions: *cis*-cyclooctene (67.3 μmol/mL, 1.00 eq.) in MeCN, Fe-catalyst, if stated Sc(OTf)<sub>3</sub> (6.73 μmol/mL, 0.10 eq.), and H<sub>2</sub>O<sub>2</sub> (50% aq., 101 μmol/mL, 1.50 eq.). Selectivity is related to the epoxide. [a] Conversions are determined by GC-FID. [b] TOFs are determined after 10 s. [c] TON determined after 10 min. [d] TON determined after 240 min. T = temperature. X = conversion. S = selectivity.

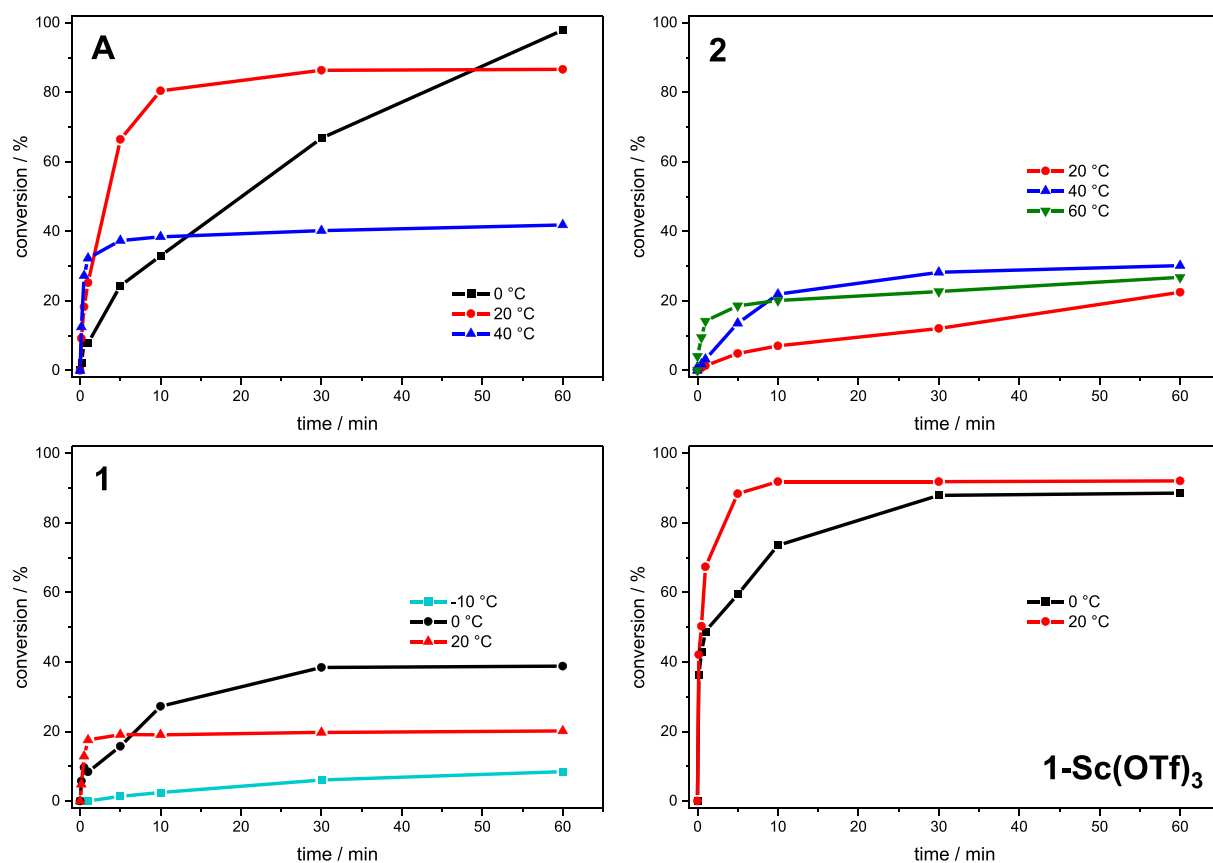


**Fig. 9.** Time-dependent epoxidation of *cis*-cyclooctene (67.3 μmol/mL, 1.00 eq.) in MeCN, Fe-catalyst (1.35 μmol/mL, 0.02 eq.), and H<sub>2</sub>O<sub>2</sub> (50% aq., 101 μmol/mL, 1.50 eq.) as oxidizing agent at different temperatures. Conversions are determined by GC-FID. Top left: **A** as catalyst. Top right: **2** as catalyst. Bottom left: **1** as catalyst. Bottom right: **1** as catalyst with Sc(OTf)<sub>3</sub> (6.73 μmol/mL, 0.10 eq.).

initial TOF of 700 h<sup>-1</sup> (entry 22) without additive is attained. But even at higher temperatures, **2** still requires longer reaction times for a complete reaction. On the other side, this is evidence of the high temperature-tolerance of **2**. Based on the rather low stability of **1** in comparison to **A** and **2** (Fig. 7) the temperature was lowered for **1**. At 0 °C a significant increase of the stability can be observed for **1**, as the TON is almost doubled (0 °C: 19 vs. 20 °C: 10, entries 12 and 14). Hence, the total conversion is also twice as high (39% vs. 20%, Fig. 9) and the activity is even slightly higher (1000 h<sup>-1</sup> vs. 900 h<sup>-1</sup>). Lowering the temperature to -10 °C does not benefit the stability further, as the activity is reduced drastically giving a total conversion of only 8% after 60 min with a TON of 4. In all cases, and in contrast to other Fe-NHC catalysts [17,22], the high selectivity of >99% remains constant even at elevated temperatures.

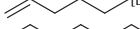
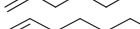
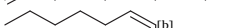
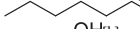
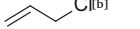
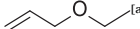
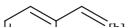
Reducing the temperature to 0 °C could enhance the stability for **A** and **1**, which can be explained by potentially decelerated catalyst deactivation, e.g. slower formation of an assumed  $\mu_2$ -oxo species or NCCN ligand dissociation (*vide supra*). However, lowering the temperature to 0 °C in the presence of Sc(OTf)<sub>3</sub> does not further increase the stability for **1** (entry 13, Fig. 9) but in this case reduces the activity (entry 13 vs 15). Therefore, using a Lewis acid as additive is superior to varying the temperature in the present case and achieves the best catalytic performance. Furthermore, the significant beneficial effect for the stability by addition of Sc(OTf)<sub>3</sub> gives the following indications: a) The formation of a deactivation species without Lewis acid as dead-end in the catalytic cycle. However, this species can either be reactivated or its formation suppressed by Lewis acids such as Sc(OTf)<sub>3</sub>. It is likely, that this species is a diiron- $\mu_2$ -oxo complex, as it was demonstrated for the tetracarbene system **a/b**, and both **a/b** and **A/1/2** are structurally similar and show analog reactivity in epoxidation catalysis. For **a/b**, this diiron(III)- $\mu_2$ -oxo complex could be reactivated with Lewis acids and had the same activity like **a/b**. b) The presence of an additional degradation pathway. If the formation of a diiron- $\mu_2$ -oxo complex was the only decomposition mechanism, addition of Sc(OTf)<sub>3</sub> should give complete conversions for all three complexes. This is, however, not the case. In contrast to the formation of the deactivation species, this degradation

is terminal and results in a permanently decomposed catalyst. As mentioned above, possible degradation might involve the dissociation of the NCCN ligand, C–C bond formation resulting in a highly-strained annulated 2,2'-biimidazole and subsequent cleavage of the methylene bridge, as observed under oxidative conditions for **A** [44,58]. But also carbene oxidation, as observed for **a/b**, methylene bridge oxidation or carbene protonation are plausible [24]. c) The formation of the deactivated species is faster than the terminal degradation. In the case of faster permanent decomposition, the addition of Lewis acids would not have a significant effect on the stability and lifetime of the catalyst.

Epoxides do not only act as final products in industry, but are also building blocks in synthetic organic chemistry [62–65]. In the following, various relevant olefin substrates are screened with **A**, **1** and **2** in the epoxidation catalysis for 5 min with Sc(OTf)<sub>3</sub>, as their epoxides are valuable intermediates in industry (Table 4). Here, the functional group tolerance is tested as well. The respective epoxides are for example used as monomers in polymerization (entry 27) [66], as stabilizers for halogen hydrocarbons or oil-soluble bases in cosmetics (entries 28–32) [67], epoxy resins (entry 34) and reactive diluent for epoxy resins (entry 36) [63].

The overall best catalytic performance is achieved by **A**, followed by **2** while **1** has the lowest substrate adaptability. **A** converts the smaller ring *cis*-cyclohexene completely with high selectivity (>99%, entry 27), whereas **1** and **2** show rather low reactivity to this substrate with 27% and 22% conversion, respectively, albeit retaining the high selectivity of >99%. The terminal alkenes (entries 28–30) are again completely converted by **A** (selectivity > 90%) but for **1** and **2** the conversion drops with a longer hydrocarbon chain from 71% to 28% for **1** and 92% to 54% for **2**. **1** shows the lowest selectivity for 1-hexene (68%) and 1-octene (71%), and it drastically drops to 20% for 1-decene, in contrast to the other catalysts (**A**: 90%; **2**: 82%), because of diol formation. Interestingly, **2** reaches a new maximum TOF of 6 400 h<sup>-1</sup> in the epoxidation of 1-decene. The iron(III) tetracarbene **b** favors the *cis*-2-octene over the *trans* isomer, a behavior also common for other iron epoxidation catalysts [14,68]. **A** follows this trend with an epoxide yield of 86% (*cis*) against 80% (*trans*). However, especially for **1**, this trend is reversed

**Table 4**  
Epoxidation of various olefin substrates using **A**, **1** and **2** as catalyst with 5 min reaction time and Sc(OTf)<sub>3</sub>.

Entry	Substrate	<b>A</b>			<b>1</b>			<b>2</b>		
		X [%]	S [%]	TOF [h <sup>-1</sup> ] [c]	X [%]	S [%]	TOF [h <sup>-1</sup> ] [c]	X [%]	S [%]	TOF [h <sup>-1</sup> ] [c]
26		100	> 99	18 000	88	> 99	7 600	97	99	1 300
27		100	> 99	18 000	27	> 99	4 900	22	> 99	0
28		100	93	–	71	68	–	92	87	–
29		100	95	17 400	34	71	3 800	61	82	1 500
30		100	90	17 500	28	20	2 800	54	82	6 400
31		100	86	–	53	76	–	70	84	–
32		100	80	–	64	87	–	66	93	–
33		100	37	–	41	0	–	78	33	–
34		76	> 99	–	11	78	–	38	> 99	–
35		100	> 99	18 000	100	> 99	18 000	47	> 99	1 200
36		34	0	–	15	0	–	18	0	–
37		85	86	–	22	76	–	17	67	–

Reaction conditions: substrate (67.3  $\mu\text{mol/mL}$ , 1.00 eq.) in MeCN, Fe-catalyst (1.35  $\mu\text{mol/mL}$ , 0.02 eq.), Sc(OTf)<sub>3</sub> (6.73  $\mu\text{mol/mL}$ , 0.10 eq.) and H<sub>2</sub>O<sub>2</sub> (50% aq., 101  $\mu\text{mol/mL}$ , 1.50 eq.), 20 °C, 5 min. Selectivity is related to the epoxide. [a] Conversions are determined by GC-FID. [b] Conversions are determined by <sup>1</sup>H NMR spectroscopy, applying benzene as external standard. [c] TOFs are determined after 10 s. X = conversion. S = selectivity.

with an epoxide yield of 40% for *cis*-2-octene compared to 56% for the *trans* isomer. **2** effectively has the same epoxide yields for both isomers (*cis*: 58% vs. *trans*: 61%). Allyl alcohol (entry 33) and allyl chloride (entry 34) are more challenging to epoxidize resulting in either a low selectivity for the former due to diol and aldehyde formation or low conversion for the latter. Interestingly, in the epoxidation of the allyl ethyl ether (entry 35) **1** is on par with **A**, reaching the highest TOF of 18 000 h<sup>-1</sup> for **1** in this study at complete conversion and >99% selectivity. In this case, **2** is left behind and achieves only 47% conversion. No epoxide formation is observed for all catalysts using styrene as substrate, opposite to **A** without Sc(OTf)<sub>3</sub> and **a** with or **b** without Sc(OTf)<sub>3</sub> [14–15,34]; instead formation of a variety of side products is observed (see SI). Chalcone is also rather difficult to epoxidize, especially by **1** and **2**. In general, a more nucleophilic character of the alkene through inductive effects results in a higher reactivity towards the epoxide, which is in line with an electrophilic active species [14,60]. For example, a highly substituted alkene is more reactive compared to its terminal alkene due to the +I effect of the substituents and the –M effect of the carbonyl in chalcone reduces the reactivity of the alkene.

### 3. Conclusions and outlook

Two novel complexes **1** and **2** were synthesized, characterized and, together with **A**, applied as catalysts in the epoxidation of olefins. The methyl backbone modifications in **1** result in a more electron rich iron center than in **A**. A less electron rich iron center is achieved by substitution of pyridine with pyrimidine in **2**. The impact of the different electronic properties of the complexes on the catalysis has been investigated. Surprisingly, the activity is the highest for **A**, followed by **1** and, as expected, lowest for **2**. Although **2** is the least active, it has the longest lifetime. Hence, **2** eventually achieves a higher conversion than **1**. The catalysts enable an overall high selectivity, placing them among the most selective Fe-NHC catalytic systems, on par with **a/b**. Addition of Sc(OTf)<sub>3</sub> as Lewis acid increases the activity and stability of all catalysts significantly, while their selectivity remains high, in contrast to the benchmark system **a/b**. The enhancement of the activity and stability with Sc(OTf)<sub>3</sub> indicates the presence of two degradation pathways; one can be suppressed by Sc(OTf)<sub>3</sub>, while the slower pathway is terminal. In the epoxidation of *cis*-cyclooctene with Sc(OTf)<sub>3</sub> as additive, a TOF of 24 500 h<sup>-1</sup> is achieved for **A**, followed by 7 600 h<sup>-1</sup> for **1** and 1 300 h<sup>-1</sup> for **2**. **A** reaches a remarkable TON of 711, **1** a TON of 46 and **2** a TON of 49. Lower temperatures can increase the stability for **A** and **1**, and higher temperatures lead to enhanced activity for **2**. Various other substrates have been screened in the epoxidation reaction. **A** has the best overall catalytic performance, followed by **2** and **1**. In general, more nucleophilic alkenes lead to a higher activity and conversion toward the epoxide.

This work demonstrates ligand modification as easy and effective tool to steer the electronic properties of transition metal catalysts and how they can influence the catalytic performance. The impact of electronic variations on the epoxidation catalysis was studied on the iron NHC catalytic system **A/1/2** as potential tool for optimization of the benchmark system **a/b**. **A/1/2** was chosen as candidate due to its structural and electronic similarities to **a/b**. Electronic changes of **A/1/2** result in the same catalytic trends as for **a/b** in epoxidation. This confirms the universal underlying mechanistic functionality for both systems. Further evidence for that is the similar effect of Lewis additives on catalysis and the inferred presumed alike degradation of the catalysts.

Interestingly, the overall lower activity of the **A/1/2** system compared to the flagship iron tetracarbene system **a/b** is likely a result of the lower electron density at the iron center of the first compared to the latter with its significantly stronger electron donating tetracarbene ligand. Furthermore, decreasing the electron density at the iron atom in **2** is again reducing the activity vs. **A** – however, this is not true for the opposite: increasing the electron density in **1** does not lead to a higher activity vs. **A**. In other words, modifications within the catalytic system

of **A** towards a more electron rich iron center in **1** are not accompanied by improved activity, analog to the tetracarbene system (**c/d** vs. **a/b**). While the  $\sigma$ -donation of the dimethylimidazole is counterbalanced with enhanced  $\pi$ -backbonding in **c/d** [22] – which has been proposed as explanation for the missing catalytic benefit of the tetracarbene modification in **c/d** vs. **a/b** – this is not the case for **1**, which contains the same ligand modification like **c/d**, namely two methyl groups at the 4 and 5 position of the imidazole backbone. Here, all analytical methods support the higher electron density in **1** compared to **A**. In theory, a higher electron density is expected to increase the activity due to acceleration of the formation of the Fe<sup>IV/V</sup> = O active species as the rate determining step [22,28], but a ligand modification might have a larger impact on other factors, which in turn suppress the activity gain, such as catalyst stability. Indeed, complex **1** has a reduced stability compared to **A**. Based on the overall best catalytic performance out of all three complexes, **A** seems to have the most balanced set of properties like electron density and ligand/catalyst stability, analog to the unmodified benchmark system **a/b**. In the case of the tetracarbene system **a/b**, the increase of electron density, like in **c/d** or more pronounced in **g**, also does not result in an improved activity in epoxidation of *cis*-cyclooctene vs. **a/b**. While more catalytic experiments of **g** are necessary for a comprehensive discussion, this raises doubts to the simple relation of the electron density at the iron atom and catalytic activity. A crucial factor to be considered is the stability of a new or modified ligand under oxidative conditions. Other parameters might be the ligand rigidity or overall geometry. In any case, more knowledge about the catalytic mechanism and structure activity relationships in epoxidation catalysis are required in order to tailor the next generation of catalysts with the desired features.

### 4. Experimental

#### 4.1. General procedures and analytical methods

The syntheses of complexes **1** and **2** were performed under argon atmosphere using standard Schlenk and glovebox techniques as well as dry and degassed solvents. 4,5-Dimethyl-1*H*-imidazole [22], 2-(4,5-dimethyl-1*H*-imidazol-1-yl)pyridine [35], 2-(1*H*-imidazol-1-yl)pyrimidine (ACE pressure tube under Ar atmosphere) [35–36] were synthesized according to literature procedures. Fe[N(SiMe<sub>3</sub>)<sub>2</sub>]<sub>2</sub>(THF) has been synthesized according to a modified literature procedure (see SI) [69–73]. Solvents were purified, dried and degassed using standard methods [74] or received from a solvent purification system by M. Braun. All other chemicals were obtained from commercial suppliers and were used without further purification. NMR spectra were recorded on a Bruker Advanced Ultrashield AV400 (<sup>1</sup>H NMR, 400.13 MHz; <sup>13</sup>C NMR, 100.53 MHz). The chemical shifts are given in  $\delta$  values in ppm (parts per million) relative to TMS (tetramethylsilane) and are reported relative to the residual deuterated solvent signal [75]. Elemental analyses (C/H/N/S) were obtained by the microanalytical laboratory at Technical University Munich. Electrospray ionization mass spectrometry (ESI-MS) data were measured on a Thermo Fisher Ultimate 3000. Electrochemical measurements were carried out using an EmStat3 + potentiostat using a three-electrode cell equipped with glassy carbon electrodes as counter and working electrodes and Ag/AgNO<sub>3</sub> (0.1 mM) as the reference electrode. Potentials are measured with a scan rate of 100 mV/s and reported with reference to an internal standard of ferrocenium/ferrocene (Fc<sup>+/0</sup>). Tetrabutylammonium hexafluorophosphate (100 mM in MeCN) was used as electrolyte. The concentration of the complexes was about 2 mM. UV/Vis spectra were recorded on an Agilent Cary 60 UV-Vis spectrophotometer with a concentration of 0.2 mM complex in acetonitrile. Solid material of all Fe(II) complexes (30 to 40 mg) was studied using <sup>57</sup>Fe Mössbauer spectroscopy at 80 K. <sup>57</sup>Fe Mössbauer spectra were measured using a <sup>57</sup>Co source in a Rh matrix using an alternating constant acceleration Wissel Mössbauer spectrometer equipped with a Janis closed-cycle helium cryostat.

Transmission data were collected, and isomer shifts are reported relative to iron metal at ambient temperature. Experimental data were simulated with *mf2.SL* software.[76] A temperature-dependent magnetic susceptibility measurement of **A** (19.4 mg) was carried out with a *Quantum-Design* MPMS3 SQUID magnetometer equipped with a 7 Tesla magnet in the range from 400 to 2.0 K at a magnetic field of 0.5 T. The powdered sample was contained in a polycarbonate capsule (29.4 mg) and fixed in a non-magnetic sample holder. Each raw data file for the measured magnetic moment was corrected for the diamagnetic contribution of the sample holder and the polycarbonate capsule. The molar susceptibility data was corrected for the diamagnetic contribution. Temperature-independent paramagnetism ( $TIP = 1980 \cdot 10^{-6} \text{ cm}^3 \text{ mol}^{-1}$ ) and paramagnetic impurities ( $PI = 1.3\%$  with  $S = 5/2$ ) were included according to  $\chi_{\text{calc}} = (1 - PI) \cdot \chi + PI \cdot \chi_{\text{mono}} + TIP$ . Simulation of the experimental magnetic data was performed with the *julX* program.[77].

#### 4.2. Catalytic procedures

**Experimental remarks.** GC analysis was performed with an Agilent Technologies 7890B GC-FID system with a 7693A Automatic Liquid Sampler for 150 samples with G4513A Autoinjector using a HP-5 column (30 m  $\times$  320  $\mu\text{m}$   $\times$  0.25  $\mu\text{m}$ ). NMR spectra were recorded on a Bruker Advanced Ultrashield AV400 (400 MHz) or AV500 (500 MHz) spectrometer at a temperature of 297 K. Chemical shifts ( $\delta$ ) are reported in ppm and referenced to the residual signal of the deuterated solvent [75].

**Catalytic procedure.** All catalytic reactions were conducted in a cryostat (JulaboFP-50). Acetonitrile (HPLC-grade) as solvent was applied for all experiments, which are screened *via* GC (substrates: *cis*-cyclooctene, *cis*-cyclohexene, 1-octene, 1-decene and allyl ethyl ether). The screening of other substrates (*cis*-cyclohexene, 1-hexene, allyl alcohol, allyl chloride, styrene, chalcone, *cis*-2-octene and *trans*-2-octene) was performed using  $^1\text{H}$  NMR spectroscopy and deuterated acetonitrile as solvent. The catalyst was added from a preformed stock solution in acetonitrile corresponding to the appropriate stoichiometry to a solution of the respective substrate (1.00 eq., 67.3  $\mu\text{mol/mL}$ ). Hydrogen peroxide (50% aq., 1.50 eq., 101  $\mu\text{mol/mL}$ ) was used as oxidizing agent and, if required,  $\text{Sc}(\text{OTf})_3$  as additive (0.10 eq., 8.41  $\mu\text{mol/mL}$ ). The reaction was started upon addition of the catalyst stock solution, by adding the catalyst solution all at once. The reaction was terminated by adding electrolytically precipitated activated  $\text{MnO}_2$  in order to decompose the excess of  $\text{H}_2\text{O}_2$  in the reaction solution. After filtration over activated neutral alumina (separation of the catalyst), GC samples were prepared for each experiment and time point using 200  $\mu\text{L}$  filtrate, diluted with 1300  $\mu\text{L}$  MeCN, in which *p*-xylene (0.9  $\mu\text{L/mL}$ ) is dissolved as an external standard. For the screening *via*  $^1\text{H}$  NMR spectroscopy, 500  $\mu\text{L}$  filtrate was added to 1  $\mu\text{L}$  benzene as external standard. Control experiments without catalyst were performed for all reactions and did not show catalytic activity. An additional blank experiment with a simple iron salt, iron(II) chloride, in the presence of  $\text{H}_2\text{O}_2$  was conducted to highlight the importance of iron complexes associated with NHCs due to minimal product and unselective side-product formation. Analogous, the additive  $\text{Sc}(\text{OTf})_3$  itself shows minimal unselective catalytic activity [15].

#### 4.3. Synthetic procedures

##### [**H<sub>2</sub>L1**](Br)<sub>2</sub>

The synthesis follows a similar procedure with regard to literature methods [78]. 2-(4,5-Dimethyl-1*H*-imidazol-1-yl)pyridine (0.49 g, 2.83 mmol, 2.00 eq.) is dissolved in excess dibromomethane (4.00 mL, 57.3 mmol, 40.5 eq.) and heated to 110 °C for 16 h while stirring. The brown oil is dried *in vacuo*, leaving a brown solid, which is washed with MeCN (~27 mL) to yield a white precipitate. The brown supernatant is removed, the white solid is washed with cold MeCN and dried *in vacuo* to obtain [**H<sub>2</sub>L1**](Br)<sub>2</sub> as white powder (0.35 g, 0.74 mmol, 48%).

$^1\text{H}$  NMR (400.13 MHz,  $\text{CDCl}_3$ ):  $\delta$  10.92 (s, 2H, NCHN), 8.59 (dd,  $^3J = 4.8$ ,  $^4J = 1.8$  Hz, 2H,  $H_{\text{py}}$ ), 8.24 (d,  $^3J = 7.9$  Hz, 2H,  $H_{\text{py}}$ ), 8.04 (td,  $^3J = 7.9$ ,  $^4J = 1.8$  Hz, 2H,  $H_{\text{py}}$ ), 7.74 (s, 2H,  $\text{CH}_2$ ), 7.52 (dd,  $^3J = 7.6$ ,  $^3J = 4.8$  Hz, 2H,  $H_{\text{py}}$ ), 2.67 (s, 6H,  $\text{CH}_3$ ), 2.41 (s, 6H,  $\text{CH}_3$ ).

MS-ESI (*m/z*): [**H<sub>2</sub>L1** - H<sup>+</sup>]<sup>+</sup> calcd., 359.20; found, 359 (100); [**H<sub>2</sub>L1** + H<sup>+</sup> - CH<sub>2</sub>ImPy]<sup>+</sup> calcd., 174.10; found, 174 (35).

##### [**H<sub>2</sub>L1**](PF<sub>6</sub>)<sub>2</sub>

The synthesis follows a similar procedure with regard to literature methods [78]. [**H<sub>2</sub>L1**](Br)<sub>2</sub> (202 mg, 388  $\mu\text{mol}$ , 1.00 eq.) is dissolved in 2 mL  $\text{H}_2\text{O}$  and slowly added to a vigorously stirred solution of  $\text{NH}_4\text{PF}_6$  (316 mg, 1.94 mmol, 5.00 eq.) in 25 mL  $\text{H}_2\text{O}$ . After stirring for 45 min, the white precipitate is filtered off and washed with cold  $\text{H}_2\text{O}$ . The white solid is redissolved in 1.5 mL acetone and precipitated by adding 7 mL  $\text{Et}_2\text{O}$ . The precipitate is filtered, washed with  $\text{Et}_2\text{O}$  and dried under vacuum to obtain [**H<sub>2</sub>L1**](PF<sub>6</sub>)<sub>2</sub> as white powder (118 mg, 181  $\mu\text{mol}$ , 47%). The product is dried overnight at 60 °C at  $10^{-3}$  mbar and stored under argon.

$^1\text{H}$  NMR (400.13 MHz,  $\text{CD}_3\text{CN}$ ):  $\delta$  9.01 (s, 2H, NCHN), 8.68 (ddd,  $^3J = 4.8$  Hz,  $^4J = 1.9$  Hz,  $^4J = 0.9$  Hz, 2H,  $H_{\text{py}}$ ), 8.14 (td,  $^3J = 7.9$  Hz,  $^4J = 1.9$  Hz, 2H,  $H_{\text{py}}$ ), 7.68 (ddd,  $^3J = 7.6$  Hz,  $^3J = 4.8$  Hz,  $^4J = 0.9$  Hz, 2H,  $H_{\text{py}}$ ), 7.63 (dd,  $^3J = 8.0$ ,  $^4J = 0.9$  Hz, 2H,  $H_{\text{py}}$ ), 6.45 (s, 2H,  $\text{CH}_2$ ), 2.40 (s, 6H,  $\text{CH}_3$ ), 2.34 (s, 6H,  $\text{CH}_3$ ).

$^{13}\text{C}$  NMR (100.53 MHz,  $\text{CD}_3\text{CN}$ ):  $\delta$  151.06 (2C, CH), 147.31 (2C, CH), 141.36 (2C, CH), 136.36 (2C, CH), 130.01 (2C, CH), 129.36 (2C, CH), 127.34 (2C, CH), 120.74 (2C, CH), 57.33 (1C,  $\text{CH}_2$ ), 9.86 (2C,  $\text{CH}_3$ ), 8.96 (2C,  $\text{CH}_3$ ).

MS-ESI (*m/z*): [**H<sub>2</sub>L1**](PF<sub>6</sub>)<sub>2</sub><sup>+</sup> calcd., 505.17; found, 505 (10); [**H<sub>2</sub>L1** - H<sup>+</sup>]<sup>+</sup> calcd., 359.20; found, 359 (100); [**H<sub>2</sub>L1** + H<sup>+</sup> - CH<sub>2</sub>ImPy]<sup>+</sup> calcd., 174.10; found, 174 (12).

Anal. calcd. for  $\text{C}_{21}\text{H}_{24}\text{F}_{12}\text{N}_6\text{P}_2$ : C 38.78; H 3.72; N 12.92. Found: C 38.87; H 3.56; N 12.71.

##### [**FeL1**(MeCN)<sub>2</sub>](PF<sub>6</sub>)<sub>2</sub> (1)

The synthesis follows a similar procedure with regard to literature methods [78].  $\text{Fe}[\text{N}(\text{SiMe}_3)_2](\text{THF})$  (302 mg, 673  $\mu\text{mol}$ , 1.00 eq.) is dissolved in ~5 mL MeCN giving a green solution, which becomes yellow and light brown after 15 min and is frozen in liquid  $\text{N}_2$ . A solution of [**H<sub>2</sub>L1**](PF<sub>6</sub>)<sub>2</sub> (492 mg, 756  $\mu\text{mol}$ , 1.12 eq.) in 10 mL MeCN is added over 1 min to the frozen solution, which changes its color to red and is slowly warmed to r.t. while stirring overnight. The following red suspension is dried *in vacuo* and suspended in 20 mL MeCN. The solvent is removed under vacuum and the red solid is suspended in 20 mL MeCN again. This is repeated once more to remove residual amine. The red suspension (in 20 mL MeCN) is filtrated, and the yellow residue is washed twice with 20 mL MeCN in order to dissolve all solid. The three filtrates are collected in one batch (60 mL MeCN) and 60 mL  $\text{Et}_2\text{O}$  are added to precipitate an orange solid. The orange solid is filtered off, washed with  $\text{Et}_2\text{O}$  (3  $\times$  4 mL), dried at 60 °C at  $10^{-3}$  mbar overnight to yield 370 mg of the iron complex. The orange filtrate (60 mL MeCN + 60 mL  $\text{Et}_2\text{O}$ ) is concentrated under vacuum until ~10 mL of dark-red solution are remaining. 40 mL of  $\text{Et}_2\text{O}$  are added to give an orange precipitate, which is filtrated, washed with  $\text{Et}_2\text{O}$  (3  $\times$  5 mL), dried at 60 °C at  $10^{-3}$  mbar overnight to yield additional 15 mg of iron complex. [**FeL1**(MeCN)<sub>2</sub>](PF<sub>6</sub>)<sub>2</sub> can be obtained as orange powder in total yield of 73% (385 mg, 490  $\mu\text{mol}$ ). Single crystals suitable for X-ray diffraction were obtained by slow evaporation of a solution of [**FeL1**(MeCN)<sub>2</sub>](PF<sub>6</sub>)<sub>2</sub> in MeCN over 3 weeks at r.t. under ambient conditions (see SI for details).

$^1\text{H}$  NMR (400.13 MHz,  $\text{CD}_3\text{CN}$ ):  $\delta$  9.60 (ddd,  $^3J = 5.4$  Hz,  $^4J = 1.7$  Hz,  $^4J = 0.9$  Hz, 2H,  $H_{\text{py}}$ ), 8.29 (ddd,  $^3J = 8.5$  Hz,  $^3J = 7.5$  Hz,  $^4J = 1.7$  Hz,

$^2\text{H}$ ,  $H_{\text{py}}$ , 8.17 (dt,  $^3J = 8.5$  Hz,  $^4J = 0.9$  Hz, 2H,  $H_{\text{py}}$ ), 7.72 (ddd,  $^3J = 7.5$  Hz,  $^3J = 5.4$  Hz,  $^4J = 0.9$  Hz, 2H,  $H_{\text{py}}$ ), 6.77 (s, 2H,  $\text{CH}_2$ ), 2.77 (d,  $^5J = 1.2$  Hz, 6H,  $\text{CH}_3$ ), 2.50 (d,  $^5J = 1.2$  Hz, 6H,  $\text{CH}_3$ ), 1.96 (s, 6H,  $\text{CH}_3\text{CN}$ ).

$^{13}\text{C}$  NMR (100.53 MHz,  $\text{CD}_3\text{CN}$ ):  $\delta$  215.49 (2C,  $C_{\text{carbene}}$ ), 156.93 (2C, CH), 153.56 (2C, CH), 141.95 (2C, CH), 131.08 (2C, CH), 127.51 (2C, CH), 123.71 (2C, CH), 114.03 (2C, CH), 62.30 (1C,  $\text{CH}_2$ ), 11.70 (2C,  $\text{CH}_3$ ), 9.00 (2C,  $\text{CH}_3$ ).

MS-ESI ( $m/z$ ):  $[\text{FeL1} + \text{HCOO}]^+$  calcd., 459.12; found, 458.89 (69);  $[\text{FeL1}(\text{MeCN})_2]^{2+}$  calcd., 248.09; found, 247.63 (50);  $[\text{FeL1}(\text{MeCN})]^{2+}$  calcd., 227.57; found, 227.26 (82);  $[\text{FeL1}]^{2+}$  calcd., 207.06; found, 207.21 (100).

Anal. calcd. for  $\text{C}_{25}\text{H}_{28}\text{F}_{12}\text{FeN}_8\text{P}_2$ : C 38.19; H 3.59; N 14.25. Found: C 38.41; H 3.68; N 14.23.

#### $[\text{H}_2\text{L2}](\text{Br})_2$

The synthesis follows a similar procedure with regard to literature methods [78]. 2-(1H-imidazol-1-yl)pyrimidine (323 mg, 1.65 mmol, 2.00 eq.) is dissolved in excess dibromomethane (25 mL, 358 mmol, 433 eq.) and heated to 110 °C for 16 h while stirring. The brown suspension is dried *in vacuo*. The crude product is dissolved in MeOH (~20 mL), precipitated with approximately 30 mL of EtOAc, filtered and washed with EtOAc to yield  $[\text{H}_2\text{L2}](\text{Br})_2$  as off-white powder (291 mg). To increase the yield, the yellow filtrate was dried *in vacuo*. The brown solid was suspended in little MeOH,  $\text{Et}_2\text{O}$  was added and the resulting light-brown precipitate was filtered, washed with MeCN and  $\text{Et}_2\text{O}$  to give additional  $[\text{H}_2\text{L2}](\text{Br})_2$  as off-white powder (55 mg). 74% yield in total (346 mg, 0.61 mmol).

$^1\text{H}$  NMR (400.13 MHz,  $\text{DMSO}-d_6$ ):  $\delta$  10.59 (ps. t,  $^4J = 1.7$  Hz, 2H, NCHN), 9.11 (d,  $^3J = 4.9$  Hz, 4H,  $H_{\text{pym}}$ ), 8.59 (ps. t,  $^4J = 2.0$  Hz, 2H,  $\text{CH}_{\text{im}}$ ), 8.39 (ps. t,  $^4J = 2.0$  Hz, 2H,  $\text{CH}_{\text{im}}$ ), 7.84 (t,  $^3J = 4.9$  Hz, 2H,  $H_{\text{pym}}$ ), 6.99 (s, 2H,  $\text{CH}_2$ ).

MS-ESI ( $m/z$ ):  $[\text{H}_2\text{L2} - \text{H}^+]^+$  calcd., 305.13; found, 305.10 (43);  $[\text{H}_2\text{L2}]^{2+}$  calcd., 153.06; found, 153.10 (100);  $[\text{H}_2\text{L2} + \text{H}^+ - \text{CH}_2\text{ImC}_4\text{H}_3\text{N}_2]^+$  calcd., 147.07; found, 147.03 (72).

#### $[\text{H}_2\text{L2}](\text{PF}_6)_2$

The synthesis follows a similar procedure with regard to literature methods [78].  $[\text{H}_2\text{L2}](\text{Br})_2$  (614 mg, 1.32 mmol, 1.00 eq.) is dissolved in around 14 mL  $\text{H}_2\text{O}$  and slowly added to a vigorously stirred solution of  $\text{NH}_4\text{PF}_6$  (1.02 g, 6.25 mmol, 5.00 eq.) in 25 mL  $\text{H}_2\text{O}$ . After stirring for 15 min, the off-white precipitate is filtered off, washed with  $\text{H}_2\text{O}$  and  $\text{Et}_2\text{O}$ . The product is dried at 60 °C at  $10^{-3}$  mbar and stored under argon.  $[\text{H}_2\text{L2}](\text{PF}_6)_2$  is obtained as off-white solid in 69% yield (542 mg, 909  $\mu\text{mol}$ ).

$^1\text{H}$  NMR (400.13 MHz,  $\text{DMSO}-d_6$ ):  $\delta$  10.51 (ps. t,  $^4J = 1.4$  Hz, 2H, NCHN), 9.11 (d,  $^3J = 4.9$  Hz, 4H,  $H_{\text{pym}}$ ), 8.59 (ps. t,  $^4J = 1.9$  Hz, 2H,  $\text{CH}_{\text{im}}$ ), 8.25 (ps. t,  $^4J = 1.9$  Hz, 2H,  $\text{CH}_{\text{im}}$ ), 7.83 (t,  $^3J = 4.9$  Hz, 2H,  $H_{\text{pym}}$ ), 6.86 (s, 2H,  $\text{CH}_2$ ).

$^1\text{H}$  NMR (400.13 MHz,  $\text{CD}_3\text{CN}$ ):  $\delta$  9.89 (m, 2H, NCHN), 8.95 (d,  $^3J = 4.9$  Hz, 4H,  $H_{\text{pym}}$ ), 8.38 (m, 2H,  $\text{CH}_{\text{im}}$ ), 7.88 (m, 2H,  $\text{CH}_{\text{im}}$ ), 7.70 (t,  $^3J = 4.9$  Hz, 2H,  $H_{\text{pym}}$ ), 6.68 (s, 2H,  $\text{CH}_2$ ).

$^{13}\text{C}$  NMR (100.53 MHz,  $\text{DMSO}-d_6$ ):  $\delta$  160.32 (4C, CH), 151.81 (2C, CH), 138.38 (2C, CH), 123.56 (2C, CH), 122.97 (2C, CH), 119.66 (2C, CH), 59.30 (1C,  $\text{CH}_2$ ).

$^{13}\text{C}$  NMR (100.53 MHz,  $\text{CD}_3\text{CN}$ ):  $\delta$  161.13 (4C, CH), 152.86 (2C, CH), 137.77 (2C, CH), 124.51 (2C, CH), 124.17 (2C, CH), 121.43 (2C, CH), 60.89 (1C,  $\text{CH}_2$ ).

MS-ESI ( $m/z$ ):  $[\text{H}_2\text{L2} + \text{PF}_6]^+$  calcd., 451.10; found, 450.77 (77);  $[\text{H}_2\text{L2} - \text{H}^+]^+$  calcd., 305.13; found, 305.11 (37);  $[\text{H}_2\text{L2}]^{2+}$  calcd., 153.06; found, 153.09 (100).

Anal. calcd. for  $\text{C}_{15}\text{H}_{14}\text{F}_{12}\text{N}_8\text{P}_2$ : C 30.22; H 2.37; N 18.79. Found: C 30.19; H 2.14; N 18.56.

#### $[\text{FeL2}(\text{MeCN})_2](\text{PF}_6)_2$ (2)

The synthesis follows a similar procedure with regard to literature methods [78]. A  $-35$  °C cold solution of  $\text{Fe}[\text{N}(\text{SiMe}_3)_2](\text{THF})$  (178 mg, 396  $\mu\text{mol}$ , 1.05 eq.) in 5 mL MeCN is added to a  $-35$  °C cold solution of  $[\text{H}_2\text{L2}](\text{PF}_6)_2$  (225 mg, 377  $\mu\text{mol}$ , 1.00 eq.) in 5 mL MeCN. The red solution becomes a red suspension after 10 min and is stirred at r.t. for 20 h. The formed dark brown solution is dried *in vacuo* and suspended in 10 mL MeCN. 10 mL  $\text{Et}_2\text{O}$  are added to precipitate an orange solid. The brown supernatant is removed and the solid washed twice with 3 mL  $\text{Et}_2\text{O}$ , once dropwise with around 0.5 to 1 mL MeCN and finally 3 mL  $\text{Et}_2\text{O}$  again.  $[\text{FeL2}(\text{MeCN})_2](\text{PF}_6)_2$  can be obtained as orange solid in 68% yield (189 mg, 258  $\mu\text{mol}$ ). Single crystals suitable for X-ray diffraction were obtained by slow vapor diffusion of 1,4-dioxane into a solution of  $[\text{FeL2}(\text{MeCN})_2](\text{PF}_6)_2$  in MeCN after 1 to 2 weeks (see SI for details).

$^1\text{H}$  NMR (400.13 MHz,  $\text{CD}_3\text{CN}$ ):  $\delta$  9.77 (dd,  $^3J = 5.4$ ,  $^4J = 2.2$  Hz, 2H,  $H_{\text{pym}}$ ), 9.13 (dd,  $^3J = 4.9$ ,  $^4J = 2.2$  Hz, 2H,  $H_{\text{pym}}$ ), 8.33 (d,  $^4J = 2.3$  Hz, 2H,  $\text{CH}_{\text{im}}$ ), 7.87 (d,  $^4J = 2.4$  Hz, 2H,  $\text{CH}_{\text{im}}$ ), 7.79 (ps. t,  $^3J = 5.2$  Hz, 2H,  $H_{\text{pym}}$ ), 7.02 (s, 2H,  $\text{CH}_2$ ), 1.96 (s, 6H,  $\text{CH}_3\text{CN}$ ).

$^{13}\text{C}$  NMR (100.53 MHz,  $\text{CD}_3\text{CN}$ ):  $\delta$  216.24 (2C,  $C_{\text{carbene}}$ ), 164.28 (2C, CH), 161.34 (2C, CH), 160.68 (2C, CH), 126.69 (2C, CH), 120.99 (2C, CH), 120.55 (2C, CH), 64.86 (1C,  $\text{CH}_2$ ).

MS-ESI ( $m/z$ ):  $[\text{FeL2} + \text{HCOO}]^+$  calcd., 405.05; found, 404.91 (96);  $[\text{FeL2}(\text{MeCN})_2]^{2+}$  calcd., 221.05; found, 220.61 (67);  $[\text{FeL2}(\text{MeCN})]^{2+}$  calcd., 200.54; found, 200.27 (94);  $[\text{FeL2}]^{2+}$  calcd., 180.02; found, 180.03 (100).

Anal. calcd. for  $\text{C}_{19}\text{H}_{18}\text{F}_{12}\text{FeN}_{10}\text{P}_2$ : C 31.17; H 2.48; N 19.13. Found: C 31.20; H 2.29; N 18.84.

#### Declaration of Competing Interest

The authors declare that they have no known competing financial interests or personal relationships that could have appeared to influence the work reported in this paper.

#### Data availability

No data was used for the research described in the article.

#### Acknowledgements

Dr. Irina Znakovskaya is thanked for preliminary SQUID measurements. I.R. acknowledges support from the Fonds der Chemischen Industrie (Kekulé fellowship). Part of this work has been supported by the Deutsche Forschungsgemeinschaft (DFG), project no. 445916766 (to F.M.), in the framework of the Research Unit “Bioinspired Oxidation Catalysis with Iron Complexes” (FOR 5215).

#### Appendix A. Supplementary material

Supplementary data to this article can be found online at <https://doi.org/10.1016/j.jcat.2023.07.018>.

#### References

- [1] O. Shoji, Y. Watanabe, in: Fifty Years of Cytochrome P450 Research (Ed.: H. Yamazaki), Springer Japan: Tokyo, 2014, pp. 107–124, DOI: 10.1007/978-4-431-54992-5\_6.
- [2] K.S. Smith, H.L.O. Huyck, G.S. Plumlee, M.J. Logsdon, L.F. Filipek, in: The Environmental Geochemistry of Mineral Deposits: Part A: Processes, Techniques,

- and Health Issues Part B: Case Studies and Research Topics, Vol. 6, Society of Economic Geologists, 1997, pp. 29–70, DOI: 10.5382/Rev.06.02.
- [3] K.S. Egorova, V.P. Ananikov, *Organometallics* 36 (2017) 4071–4090, <https://doi.org/10.1021/acs.organomet.7b00605>.
- [4] K.S. Egorova, V.P. Ananikov, *Angew. Chem. Int. Ed.* 55 (2016) 12150–12162, <https://doi.org/10.1002/anie.201603777>.
- [5] D. Dolphin, T.G. Traylor, L.Y. Xie, *Acc. Chem. Res.* 30 (1997) 251–259, <https://doi.org/10.1021/ar960126u>.
- [6] I.D. Cunningham, T.N. Danks, J.N. Hay, I. Hamerton, S. Gunathilagan, C. Janczak, *J. Mol. Catal. A: Chem.* 185 (2002) 25–31, [https://doi.org/10.1016/S1381-1169\(02\)00057-2](https://doi.org/10.1016/S1381-1169(02)00057-2).
- [7] M.A. Sainna, S. Kumar, D. Kumar, S. Fornarini, M.E. Crestoni, S.P. de Visser, *Chem. Sci.* 6 (2015) 1516–1529, <https://doi.org/10.1039/C4SC02717E>.
- [8] K.P. Bryliakov, E.P. Talsi, *Coord. Chem. Rev.* 276 (2014) 73–96, <https://doi.org/10.1016/j.ccr.2014.06.009>.
- [9] S.M. Hölzl, P.J. Altmann, J.W. Kück, F.E. Kühn, *Coord. Chem. Rev.* 352 (2017) 517–536, <https://doi.org/10.1016/j.ccr.2017.09.015>.
- [10] C.-L. Sun, B.-J. Li, Z.-J. Shi, *Chem. Rev.* 111 (2011) 1293–1314, <https://doi.org/10.1021/cr100198w>.
- [11] W.N. Oloo, L. Que, *Acc. Chem. Res.* 48 (2015) 2612–2621, <https://doi.org/10.1021/acs.accounts.5b00053>.
- [12] L. Que, W.B. Tolman, *Nature* 455 (2008) 333–340, <https://doi.org/10.1038/nature07371>.
- [13] S.A. Hauser, M. Cokoja, F.E. Kühn, *Catal. Sci. Technol.* 3 (2013) 552–561, <https://doi.org/10.1039/C2CY20595E>.
- [14] J.W. Kück, M.R. Anneser, B. Hofmann, A. Pöthig, M. Cokoja, F.E. Kühn, *ChemSusChem* 8 (2015) 4056–4063, <https://doi.org/10.1002/cssc.201500930>.
- [15] F. Dyckhoff, J.F. Schlagintweit, R.M. Reich, F.E. Kühn, *Catal. Sci. Technol.* 10 (2020) 3532–3536, <https://doi.org/10.1039/D0CY00631A>.
- [16] G.G. Zámbo, J. Mayr, M.J. Sauer, T.P. Schlachta, R.M. Reich, F.E. Kühn, *Dalton Trans.* 51 (2022) 13591–13595, <https://doi.org/10.1039/D2DT02561B>.
- [17] J.F. Schlagintweit, F. Dyckhoff, L. Nguyen, C.H.G. Jakob, R.M. Reich, F.E. Kühn, *J. Catal.* 383 (2020) 144–152, <https://doi.org/10.1016/j.jcat.2020.01.011>.
- [18] R. Mas-Ballesté, L. Que, *J. Am. Chem. Soc.* 129 (2007) 15964–15972, <https://doi.org/10.1021/ja075115i>.
- [19] A. Schmidt, N. Grover, T.K. Zimmermann, L. Graser, M. Cokoja, A. Pöthig, F.E. Kühn, *J. Catal.* 319 (2014) 119–126, <https://doi.org/10.1016/j.jcat.2014.08.013>.
- [20] M.R. Anneser, S. Haslinger, A. Pöthig, M. Cokoja, V. D'Elia, M.P. Högerl, J.-M. Basset, F.E. Kühn, *Dalton Trans.* 45 (2016) 6449–6455, <https://doi.org/10.1039/C6DT00538A>.
- [21] T.P. Schlachta, M.R. Anneser, J.F. Schlagintweit, C.H.G. Jakob, C. Hintermeier, A. D. Böth, S. Haslinger, R.M. Reich, F.E. Kühn, *Chem. Commun.* 57 (2021) 6644–6647, <https://doi.org/10.1039/D1CC02027G>.
- [22] M.A. Bernd, F. Dyckhoff, B.J. Hofmann, A.D. Böth, J.F. Schlagintweit, J. Oberkofler, R.M. Reich, F.E. Kühn, *J. Catal.* 391 (2020) 548–561, <https://doi.org/10.1016/j.jcat.2020.08.037>.
- [23] S. Haslinger, A. Raba, M. Cokoja, A. Pöthig, F.E. Kühn, *J. Catal.* 331 (2015) 147–153, <https://doi.org/10.1016/j.jcat.2015.08.026>.
- [24] F. Dyckhoff, J.F. Schlagintweit, M.A. Bernd, C.H.G. Jakob, T.P. Schlachta, B. J. Hofmann, R.M. Reich, F.E. Kühn, *Catal. Sci. Technol.* 11 (2021) 795–799, <https://doi.org/10.1039/D0CY02433C>.
- [25] E.-M.-H.-J. Esslinger, J.F. Schlagintweit, G.G. Zámbo, A.M. Imhof, R.M. Reich, F.E. Kühn, *Asian J. Org. Chem.* 10 (2021) 2654–2662, <https://doi.org/10.1002/ajoc.202100487>.
- [26] T.P. Schlachta, J.F. Schlagintweit, M.R. Anneser, E.-M.-H.-J. Esslinger, M. Muhr, S. Haslinger, F.E. Kühn, *Inorg. Chim. Acta* 518 (2021), 120228, <https://doi.org/10.1016/j.ica.2020.120228>.
- [27] M. Guo, Y.-M. Lee, S. Fukuzumi, W. Nam, *Coord. Chem. Rev.* 435 (2021), 213807, <https://doi.org/10.1016/j.ccr.2021.213807>.
- [28] T.P. Schlachta, F.E. Kühn, *Chem. Soc. Rev.* 52 (2023) 2238–2277, <https://doi.org/10.1039/D2CS01064J>.
- [29] A. Raba, M. Cokoja, S. Ewald, K. Riener, E. Herdtweck, A. Pöthig, W.A. Herrmann, F.E. Kühn, *Organometallics* 31 (2012) 2793–2800, <https://doi.org/10.1021/om2010673>.
- [30] A.C. Lindhorst, J. Schütz, T. Netscher, W. Bonrath, F.E. Kühn, *Catal. Sci. Technol.* 7 (2017) 1902–1911, <https://doi.org/10.1039/C7CY00557A>.
- [31] A. Raba, M. Cokoja, W.A. Herrmann, F.E. Kühn, *Chem. Commun.* 50 (2014) 11454–11457, <https://doi.org/10.1039/C4CC02178A>.
- [32] A.C. Lindhorst, M. Drees, W. Bonrath, J. Schütz, T. Netscher, F.E. Kühn, *J. Catal.* 352 (2017) 599–605, <https://doi.org/10.1016/j.jcat.2017.06.018>.
- [33] G.G. Zámbo, J.F. Schlagintweit, R.M. Reich, F.E. Kühn, *Catal. Sci. Technol.* 12 (2022) 4940–4961, <https://doi.org/10.1039/D2CY00127F>.
- [34] J.W. Kück, A. Raba, I.I.E. Markovits, M. Cokoja, F.E. Kühn, *ChemCatChem* 6 (2014) 1882–1886, <https://doi.org/10.1002/cctc.201402063>.
- [35] A. Raba, M.R. Anneser, D. Jantke, M. Cokoja, W.A. Herrmann, F.E. Kühn, *Tetrahedron Lett.* 54 (2013) 3384–3387, <https://doi.org/10.1016/j.tetlet.2013.04.060>.
- [36] L. Zhu, L. Cheng, Y. Zhang, R. Xie, J. You, *J. Org. Chem.* 72 (2007) 2737–2743, <https://doi.org/10.1021/jo062059f>.
- [37] A.A. Danopoulos, N. Tsoureas, J.A. Wright, M.E. Light, *Organometallics* 23 (2004) 166–168, <https://doi.org/10.1021/om0341911>.
- [38] H.V. Huynh, Y. Han, R. Jothibasu, J.A. Yang, *Organometallics* 28 (2009) 5395–5404, <https://doi.org/10.1021/om900667d>.
- [39] D.G. Gusev, *Organometallics* 28 (2009) 6458–6461, <https://doi.org/10.1021/om900654g>.
- [40] W. Yao, K. Kavallieratos, S. de Gala, R.H. Crabtree, *Inorg. Chim. Acta* 311 (2000) 45–49, [https://doi.org/10.1016/S0020-1693\(00\)00308-X](https://doi.org/10.1016/S0020-1693(00)00308-X).
- [41] S. Haslinger, J.W. Kück, E.M. Hahn, M. Cokoja, A. Pöthig, J.-M. Basset, F.E. Kühn, *Inorg. Chem.* 53 (2014) 11573–11583, <https://doi.org/10.1021/ic501613a>.
- [42] S. Haslinger, A.C. Lindhorst, J.W. Kück, M. Cokoja, A. Pöthig, F.E. Kühn, *RSC Adv.* 5 (2015) 85486–85493, <https://doi.org/10.1039/C5RA18270K>.
- [43] D.T. Weiss, M.R. Anneser, S. Haslinger, A. Pöthig, M. Cokoja, J.-M. Basset, F.E. Kühn, *Organometallics* 34 (2015) 5155–5166, <https://doi.org/10.1021/acs.organomet.5b00732>.
- [44] S. Haslinger, J.W. Kück, M.R. Anneser, M. Cokoja, A. Pöthig, F.E. Kühn, *Chem. Eur. J.* 21 (2015) 17860–17869, <https://doi.org/10.1002/chem.201503282>.
- [45] D.A. Kurtz, K.R. Brereton, K.P. Ruoff, H.M. Tang, G.A.N. Felton, A.J.M. Miller, J. L. Dempsey, *Inorg. Chem.* 57 (2018) 5389–5399, <https://doi.org/10.1021/acs.inorgchem.8b00360>.
- [46] C. Kupper, J.A. Rees, S. Dechert, S. DeBeer, F. Meyer, *J. Am. Chem. Soc.* 138 (2016) 7888–7898, <https://doi.org/10.1021/jacs.6b00584>.
- [47] E.U. Mughal, M. Mirzaei, A. Sadiq, S. Fatima, A. Naseem, N. Naem, N. Fatima, S. Kausar, A.A. Altaf, M.N. Zafar, B.A. Khan, *Royal Society Open Science* 7 (2020), 201208, <https://doi.org/10.1098/rsos.201208>.
- [48] P. Gütllich, E. Bill, A. X. Trautwein, *Mössbauer Spectroscopy and Transition Metal Chemistry: Fundamentals and Applications*, Springer Berlin Heidelberg: Berlin, Heidelberg, 2011, DOI: 10.1007/978-3-540-88428-6.
- [49] J. Donat, P. Dubourdeaux, M. Clémancey, J. Rendon, C. Gervasoni, M. Barbier, J. Barilone, J. Pécaut, S. Gambarelli, P. Maldivi, J.-M. Latour, *Chem. Eur. J.* 28 (2022) e202201875.
- [50] S. Meyer, I. Klawitter, S. Demeshko, E. Bill, F. Meyer, *Angew. Chem. Int. Ed.* 52 (2013) 901–905, <https://doi.org/10.1002/anie.201208044>.
- [51] C. Schremmer, C. Cordes, I. Klawitter, M. Bergner, C.E. Schiewer, S. Dechert, S. Demeshko, M. John, F. Meyer, *Chem. Eur. J.* 25 (2019) 3918–3929, <https://doi.org/10.1002/chem.201805855>.
- [52] P. Gütllich, *Chem. unserer Zeit* 4 (1970) 133–144, <https://doi.org/10.1002/ciuz.19700040502>.
- [53] P. Gütllich, *Chem. unserer Zeit* 5 (1971) 131–141, <https://doi.org/10.1002/ciuz.19710050502>.
- [54] P. Gütllich, *Eur. J. Inorg. Chem.* 2013 (2013) 581–591, <https://doi.org/10.1002/ejic.201300092>.
- [55] P.O. Löwdin, *J. Chem. Phys.* 18 (1950) 365–375, <https://doi.org/10.1063/1.1747632>.
- [56] C.L. Hill, *Nature* 401 (1999) 436–437, <https://doi.org/10.1038/46704>.
- [57] R. Noyori, M. Aoki, K. Sato, *Chem. Commun.* (2003) 1977–1986, <https://doi.org/10.1039/B303160H>.
- [58] S. Haslinger, A. Pöthig, M. Cokoja, F.E. Kühn, *Acta Cryst. C* 71 (2015) 1096–1099, <https://doi.org/10.1107/S2053229615021968>.
- [59] F.G. Cantú Reinhard, S.P. de Visser, *Chem. Eur. J.* 23 (2017) 2935–2944, <https://doi.org/10.1002/chem.201605505>.
- [60] E.A. Mikhalyova, O.V. Makhlynets, T.D. Palluccio, A.S. Filatov, E.V. Rybak-Akimova, *Chem. Commun.* 48 (2012) 687–689, <https://doi.org/10.1039/C1CC15935F>.
- [61] A. Company, L. Gómez, X. Fontrodona, X. Ribas, M. Costas, *Chem. Eur. J.* 14 (2008) 5727–5731, <https://doi.org/10.1002/chem.200800724>.
- [62] H.C. Kolb, M.G. Finn, K.B. Sharpless, *Angew. Chem. Int. Ed.* 40 (2001) 2004–2021, [https://doi.org/10.1002/1521-3773\(20010601\)40:11<2004::AID-ANIE2004>3.0.CO;2-5](https://doi.org/10.1002/1521-3773(20010601)40:11<2004::AID-ANIE2004>3.0.CO;2-5).
- [63] S.T. Oyama, in: *Mechanisms in Homogeneous and Heterogeneous Epoxidation Catalysis* (Ed.: S. T. Oyama), Elsevier: Amsterdam, 2008, pp. 3–99, DOI: 10.1016/B978-0-444-53188-9.00001-8.
- [64] H.H. Szmant, *Organic Building Blocks of the Chemical Industry*, Wiley, New York, 1989.
- [65] C. Anaya de Parrodi, E. Juaristi, *Synlett* 2006 (2006) 2699–2715, <https://doi.org/10.1055/s-2006-950259>.
- [66] I. Kim, S.M. Kim, C.-S. Ha, D.-W. Park, *Macromol. Rapid Commun.* 25 (2004) 888–893, <https://doi.org/10.1002/marc.200300287>.
- [67] A. Ansmann, R. Kawa, M. Neuss, *Patent* US7083780B2, 2006.
- [68] R. Mas-Ballesté, M. Costas, T. van den Berg, L. Que Jr., *Chem. Eur. J.* 12 (2006) 7489–7500, <https://doi.org/10.1002/chem.200600453>.
- [69] M.M. Olmstead, P.P. Power, S.C. Shoner, *Inorg. Chem.* 30 (1991) 2547–2551, <https://doi.org/10.1021/ic00011a017>.
- [70] R.A. Andersen, K. Faegri Jr., J.C. Green, A. Haaland, M.F. Lappert, W.P. Leung, K. Rypdal, *Inorg. Chem.* 27 (1988) 1782–1786, <https://doi.org/10.1021/ic00283a022>.
- [71] D.L.J. Broere, I. Čorić, A. Brosnahan, P.L. Holland, *Inorg. Chem.* 56 (2017) 3140–3143, <https://doi.org/10.1021/acs.inorgchem.7b00056>.
- [72] A. Fedulin, A.J. von Wangelin, in: *Encyclopedia of Reagents for Organic Synthesis*, pp. 1–4, DOI: 10.1002/047084289X.rm02274.
- [73] A. Eichhöfer, Y. Lan, V. Mereacre, T. Bodenstern, F. Weigend, *Inorg. Chem.* 53 (2014) 1962–1974, <https://doi.org/10.1021/ic401677j>.
- [74] W. L. Armarego, *Purification of laboratory chemicals*, Butterworth-Heinemann: 2017, <https://www.sciencedirect.com/book/9780128054574/purification-of-laboratory-chemicals#book-description>.
- [75] G.R. Fulmer, A.J.M. Miller, N.H. Sherden, H.E. Gottlieb, A. Nudelman, B.M. Stoltz, J.E. Bercau, K.I. Goldberg, *Organometallics* 29 (2010) 2176–2179, <https://doi.org/10.1021/om100106e>.

- [76] E. Bill, mf2.SL, Max-Planck Institute for Chemical Energy Conversion: Mülheim/Ruhr, Germany, 2021.
- [77] E. Bill, julX, Max-Planck Institute for Chemical Energy Conversion: Mülheim/Ruhr, Germany, 2008.
- [78] A. D. Raba, Synthesis of Iron N-Heterocyclic Carbene Complexes and Their Application in the Oxidation Catalysis of Hydrocarbons, PhD thesis, Verlag Dr.Hut: München, 2014, <https://www.dr.hut-verlag.de/978-3-8439-1788-9.html>.



# Chiral imidazolium and triazolium salts as NHC and aNHC ligand precursors: A promising framework for asymmetric epoxidation catalysis

Tim P. Schlachta, Leon F. Richter, Fritz E. Kühn\*

Technical University of Munich, School of Natural Sciences, Department of Chemistry and Catalysis Research Center, Molecular Catalysis, Lichtenbergstraße 4, 85748 Garching, Germany

## ARTICLE INFO

**Keywords:**  
NHC ligands  
aNHC ligands  
Chiral ligands  
Asymmetric catalysis

## ABSTRACT

Two chiral imidazolium salts and one chiral triazolium salt were synthesized containing a chiral cyclohexane bridge based on the salen ligand framework of the *Jacobsen-Katsuki* epoxidation catalysts. They are promising NHC and aNHC ligand precursors for asymmetric epoxidation or C–H oxidation catalyzed by organometallic compounds. The ligand framework offers plenty of opportunities for modification.

## 1. Introduction

Olefin epoxidation is important for the synthesis of bulk chemicals, fine chemicals, and pharmaceuticals [1–4]. In the latter two areas many of the most interesting olefins are prochiral. To obtain enantiopure epoxides, chiral-directing catalysts are required. The *Jacobsen-Katsuki* epoxidation is a classical method to convert unfunctionalized alkenes containing alkyl and aryl substituents at high enantioselectivity [5,6]. As catalyst, a Mn(III) complex with a chiral salen ligand framework is employed [5,6]. Chirality is achieved by substitution of the ethylenediamine backbone, for example with *trans*-1,2-diaminocyclohexane.

Our group has developed a series of highly active and stable iron *N*-heterocyclic carbene (NHC) epoxidation catalysts [7–18]. Among them is the current benchmark system for homogeneous olefin epoxidation, an iron(II) tetracarbene [14,15,19]. An activity given in turnover frequency (TOF) of over 400 000 h<sup>-1</sup> and a turnover number (TON) of around 1 200 are reached in the conversion of *cis*-cyclooctene as model substrate at room temperature with Sc(OTf)<sub>3</sub> as additive [19]. The use of NHC ligands as strong  $\sigma$ -donors has been shown to be superior to *N*-ligated Fe complexes in epoxidation, especially in terms of activity and stability [10,13,15,17,19,20].

The motivation for this work is to combine the asymmetric catalytic properties induced by the chiral salen framework with the benefits of NHC ligands. Therefore, three ligand precursors containing a chiral cyclohexane bridge for potential application in asymmetric epoxidation NHC catalysts are reported.

## 2. Results and discussion

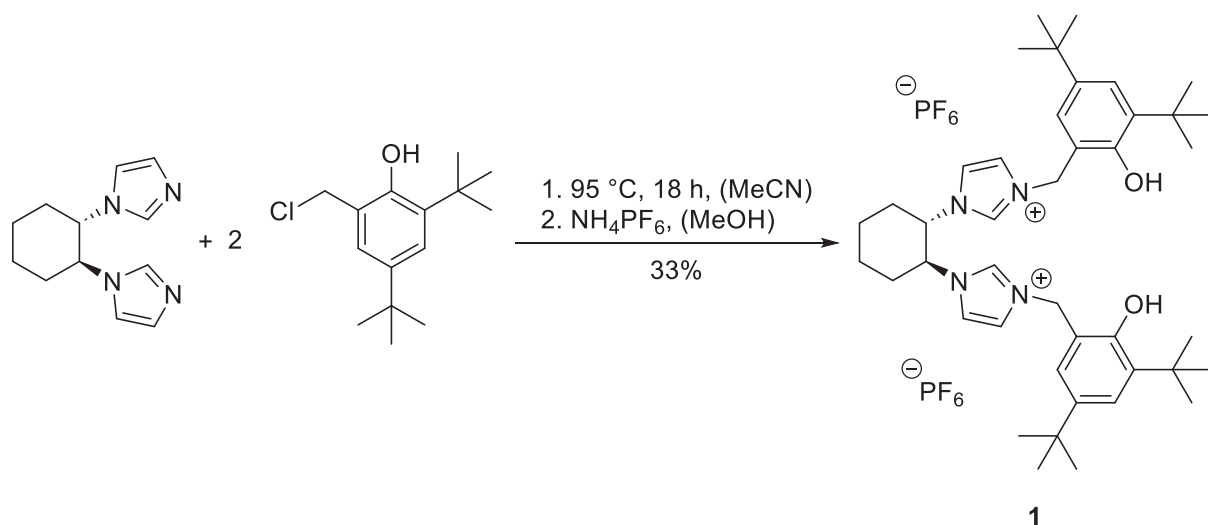
Some NHC ligands containing a chiral cyclohexane bridge are already established in literature [21–24]. In the first ligand precursor (**1**, *Scheme 1*) the imine functionality of the salen ligand is formally substituted with imidazole containing phenol groups with bulky *tert*-butyl wings, as also seen in the *Jacobsen* catalyst [25]. The steric demand prevents dimerization of the complex and possibly influences the trajectory of the alkene, important for the enantioselectivity of the catalyst [26]. The imidazolium chloride salt can be obtained by reaction of (1*S*,2*S*)-1,2-di(1*H*-imidazol-1-yl)cyclohexane [24,27,28] with two equivalents of 2,4-di-*tert*-butyl-6-(chloromethyl)phenol [29–32]. An anion exchange with NH<sub>4</sub>PF<sub>6</sub> is conducted as further purification step and to enhance the solubility of the ligand precursor in organic solvents for future complexation reactions to give **1** (see SI).

In a similar fashion, the chiral ligand precursor **2** can be obtained by reaction of (1*S*,2*S*)-1,2-di(1*H*-imidazol-1-yl)cyclohexane [24,27,28] with two equivalents of 2-(chloromethyl)pyridine hydrochloride (*Scheme 2*). In **2**, the phenol groups are replaced with pyridine. The structure of ligand precursor **2** resembles open-chain iron bis(pyridine)-bis(NHC) complexes, which have been extensively studied in epoxidation reactions but also C–H hydroxylation reactions, among others [8,12,33–35]. Thus, iron NHC complexes with **2** as ligand would be interesting to test in asymmetric C–H oxidation reactions and compare their catalytic performance with the achiral iron NHC catalysts.

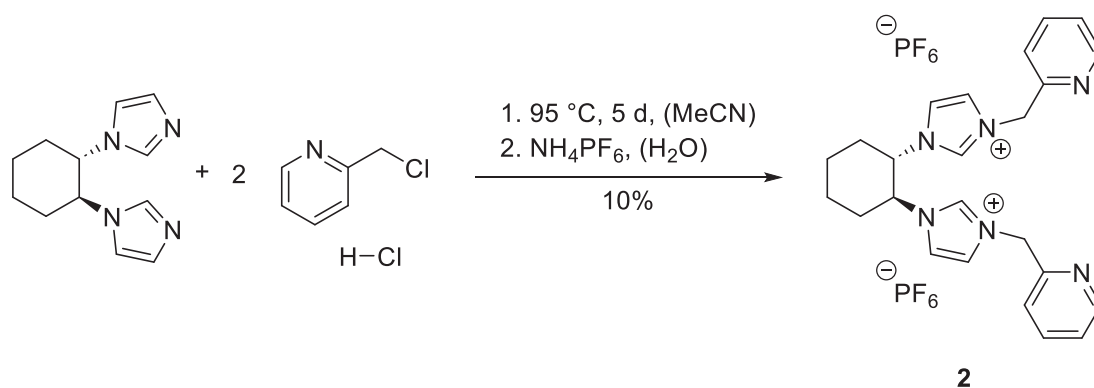
The third chiral ligand precursor (**9**, *Scheme 6*) has been designed based on a framework similar to **1** but having triazole moieties instead of

\* Corresponding author.

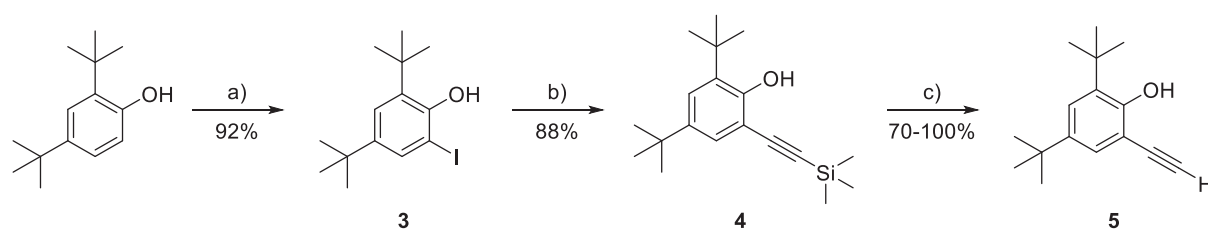
E-mail address: [fritz.kuehn@ch.tum.de](mailto:fritz.kuehn@ch.tum.de) (F.E. Kühn).



Scheme 1. Synthesis of the chiral ligand precursor 1.

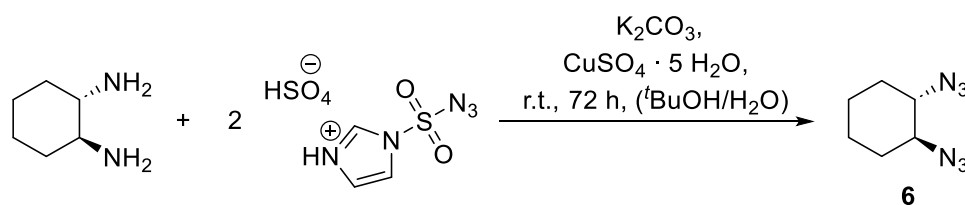


Scheme 2. Synthesis of the chiral ligand precursor 2.

Scheme 3. Synthesis of the alkyne building block 5. a) *p*TsOH (0.10 eq.), NIS (1.21 eq.), (DCM), r.t., 3 d. b) TMSA (1.30 eq.), Pd(PPh<sub>3</sub>)Cl<sub>2</sub> (0.05 eq.), CuI (0.05 eq.), (NEt<sub>3</sub>) 55 °C, 18 h. c) K<sub>2</sub>CO<sub>3</sub> (3.00 eq.), KF (2.00 eq.), (MeOH), r.t., 3.5 h.

imidazole. The triazole units are intended to be methylated in order to act as abnormally coordinating NHCs (aNHC). aNHCs are even stronger  $\sigma$ -donors than normal NHCs and their bonds to the metal center possess a highly covalent character [36]. However, during the epoxidation reaction, the iron catalysts are expected to reach high oxidation states (+4

or + 5) [10]. First row transition metals prefer ionic interactions particularly at these high valence states [36]. Therefore, the phenol wings are designed to synergistically enhance the bonding of the aNHCs for a more robust catalyst, while the strong electron donation especially from the aNHC units is expected to increase the activity.

Scheme 4. Synthesis of the diazide 6. K<sub>2</sub>CO<sub>3</sub> (31.6 eq.), CuSO<sub>4</sub> • 5 H<sub>2</sub>O (0.05 eq.), (tBuOH/H<sub>2</sub>O), r.t., 72 h.



compounds are promising NHC (1–2) and aNHC ligand precursors (9) for organometallic complexes. An application as ligands in iron catalysts for the asymmetric epoxidation or C–H oxidation is intended. The ligand framework offers plenty of opportunities for further modification, e.g. at the chiral bridge, the imidazole/triazole units and at the pyridine/phenol wings. The use of chiral anions can also be investigated in future catalytic studies [42,43].

### CRedit authorship contribution statement

**Tim P. Schlachta:** Conceptualization, Data curation, Formal analysis, Investigation, Methodology, Project administration, Visualization, Writing – original draft, Writing – review & editing. **Leon F. Richter:** Visualization. **Fritz E. Kühn:** Resources, Writing – review & editing, Supervision.

### Declaration of competing interest

The authors declare that they have no known competing financial interests or personal relationships that could have appeared to influence the work reported in this paper.

### Data availability

No data was used for the research described in the article.

### Acknowledgements

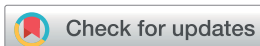
Maximilian Schick, Marina Speckbacher and Johannes Herbert Voigtland are acknowledged for their valuable synthetic support. We are grateful to Dr. J. F. Schlagintweit for inspiration for this work. Florian R. Neururer and Prof. Dr. Stephan Hohloch provided helpful synthetic advice.

### Appendix A. Supplementary data

Supplementary data to this article can be found online at <https://doi.org/10.1016/j.rechem.2024.101421>.

### References

- H.C. Kolb, M.G. Finn, K.B. Sharpless, *Angew. Chem. Int. Ed.* 40 (2001) 2004–2021, [https://doi.org/10.1002/1521-3773\(20010601\)40:11<2004::AID-ANIE2004>3.0.CO;2-5](https://doi.org/10.1002/1521-3773(20010601)40:11<2004::AID-ANIE2004>3.0.CO;2-5).
- S. T. Oyama, in *Mechanisms in Homogeneous and Heterogeneous Epoxidation Catalysis* (Ed.: S. T. Oyama), Elsevier: Amsterdam, 2008, pp. 3–99, DOI: 10.1016/B978-0-444-53188-9.00001-8.
- H.H. Szmant, *Organic building blocks of the chemical industry*, Wiley, New York, 1989.
- C. Anaya de Parrodi, E. Juaristi, *Synlett* 2006 (2006) 2699–2715, <https://doi.org/10.1055/s-2006-950259>.
- Q.H. Xia, H.Q. Ge, C.P. Ye, Z.M. Liu, K.X. Su, *Chem. Rev.* 105 (2005) 1603–1662, <https://doi.org/10.1021/cr0406458>.
- T. Katsuki, *Synlett* 2003 (2003) 0281–0297, <https://doi.org/10.1055/s-2003-37101>.
- F. Dyckhoff, J.F. Schlagintweit, M.A. Bernd, C.H.G. Jakob, T.P. Schlachta, B. J. Hofmann, R.M. Reich, F.E. Kühn, *Catal. Sci. Technol.* 11 (2021) 795–799, <https://doi.org/10.1039/D0CY02433C>.
- C.A. Hoefler, N.K. Dietl, G.G. Zámbo, T.P. Schlachta, R.M. Reich, F.E. Kühn, *J. Organomet. Chem.* (2024) 123018, <https://doi.org/10.1016/j.jorganchem.2024.123018>.
- T.P. Schlachta, M.R. Anneser, J.F. Schlagintweit, C.H.G. Jakob, C. Hintermeier, A. D. Böth, S. Haslinger, R.M. Reich, F.E. Kühn, *Chem. Commun.* 57 (2021) 6644–6647, <https://doi.org/10.1039/D1CC02027G>.
- T.P. Schlachta, F.E. Kühn, *Chem. Soc. Rev.* 52 (2023) 2238–2277, <https://doi.org/10.1039/D2CS01064J>.
- T.P. Schlachta, J.F. Schlagintweit, M.R. Anneser, E.-M.-H.-J. Esslinger, M. Muhr, S. Haslinger, F.E. Kühn, *Inorg. Chim. Acta* 518 (2021) 120228, <https://doi.org/10.1016/j.ica.2020.120228>.
- T.P. Schlachta, G.G. Zámbo, M.J. Sauer, I. Rüter, C.A. Hoefler, S. Demeshko, F. Meyer, F.E. Kühn, *J. Catal.* 426 (2023) 234–246, <https://doi.org/10.1016/j.jcat.2023.07.018>.
- G.G. Zámbo, J. Mayr, M.J. Sauer, T.P. Schlachta, R.M. Reich, F.E. Kühn, *Dalton Trans.* 51 (2022) 13591–13595, <https://doi.org/10.1039/D2DT02561B>.
- M.R. Anneser, S. Haslinger, A. Pöthig, M. Cokoja, J.-M. Basset, F.E. Kühn, *Inorg. Chem.* 54 (2015) 3797–3804, <https://doi.org/10.1021/ic503043h>.
- J.W. Kück, M.R. Anneser, B. Hofmann, A. Pöthig, M. Cokoja, F.E. Kühn, *ChemSusChem* 8 (2015) 4056–4063, <https://doi.org/10.1002/cssc.201500930>.
- M.A. Bernd, F. Dyckhoff, B.J. Hofmann, A.D. Böth, J.F. Schlagintweit, F. Oberkofler, R.M. Reich, F.E. Kühn, *J. Catal.* 391 (2020) 548–561, <https://doi.org/10.1016/j.jcat.2020.08.037>.
- J.F. Schlagintweit, F. Dyckhoff, L. Nguyen, C.H.G. Jakob, R.M. Reich, F.E. Kühn, *J. Catal.* 383 (2020) 144–152, <https://doi.org/10.1016/j.jcat.2020.01.011>.
- M. Wu, C.-X. Miao, S. Wang, X. Hu, C. Xia, F.E. Kühn, W. Sun, *Adv. Synth. Catal.* 353 (2011) 3014–3022, <https://doi.org/10.1002/adsc.201100267>.
- F. Dyckhoff, J.F. Schlagintweit, R.M. Reich, F.E. Kühn, *Catal. Sci. Technol.* 10 (2020) 3532–3536, <https://doi.org/10.1039/D0CY00631A>.
- S.A. Hauser, M. Cokoja, F.E. Kühn, *Catal. Sci. Technol.* 3 (2013) 552–561, <https://doi.org/10.1039/C2CY20595E>.
- Y. Li, J. Tang, J. Gu, Q. Wang, P. Sun, D. Zhang, *Organometallics* 33 (2014) 876–884, <https://doi.org/10.1021/om400825e>.
- L.G. Bonnet, R.E. Douthwaite, R. Hodgson, *Organometallics* 22 (2003) 4384–4386, <https://doi.org/10.1021/om030527v>.
- P. Gigler, B. Bechlers, W.A. Herrmann, F.E. Kühn, *J. Am. Chem. Soc.* 133 (2011) 1589–1596, <https://doi.org/10.1021/ja110017c>.
- J.F. DeJesus, D.M. Jenkins, *Chem.-Eur. J.* 26 (2020) 1429–1435, <https://doi.org/10.1002/chem.201905360>.
- E.M. McGarrigle, D.G. Gilheany, *Chem. Rev.* 105 (2005) 1563–1602, <https://doi.org/10.1021/cr0306945>.
- H. Jacobsen, L. Cavallo, *Chem. Eur. J.* 7 (2001) 800–807, [https://doi.org/10.1002/1521-3765\(20010216\)7:4<800::AID-CHEM800>3.0.CO;2-1](https://doi.org/10.1002/1521-3765(20010216)7:4<800::AID-CHEM800>3.0.CO;2-1).
- M. Mechler, W. Frey, R. Peters, *Organometallics* 33 (2014) 5492–5508, <https://doi.org/10.1021/om500762r>.
- M. Mechler, R. Peters, *Angew. Chem. Int. Ed.* 54 (2015) 10303–10307, <https://doi.org/10.1002/anie.201502930>.
- C.-T. Chen, C.-C. Hung, Y.-J. Chang, K.-F. Peng, M.-T. Chen, *J. Organomet. Chem.* 738 (2013) 1–9, <https://doi.org/10.1016/j.jorganchem.2013.04.004>.
- M. Lanznaster, H.P. Hratchian, M.J. Heeg, L.M. Hryhorczuk, B.R. McGarvey, H. B. Schlegel, C.N. Verani, *Inorg. Chem.* 45 (2006) 955–957, <https://doi.org/10.1021/ic050809i>.
- H. Bao, Z. Wang, T. You, K. Ding, *Chin. J. Chem.* 31 (2013) 67–71, <https://doi.org/10.1002/cjoc.201201008>.
- N. Maudoux, E. Tan, Y. Hu, T. Roisnel, V. Dorcet, J.-F. Carpentier, Y. Sarazin, *Main Group Met. Chem.* 39 (2016) 131–143, <https://doi.org/10.1515/mgmc-2016-0036>.
- A. Raba, M. Cokoja, W.A. Herrmann, F.E. Kühn, *Chem. Commun.* 50 (2014) 11454–11457, <https://doi.org/10.1039/C4CC02178A>.
- A.C. Lindhorst, M. Drees, W. Bonrath, J. Schütz, T. Netscher, F.E. Kühn, *J. Catal.* 352 (2017) 599–605, <https://doi.org/10.1016/j.jcat.2017.06.018>.
- S. Haslinger, A. Raba, M. Cokoja, A. Pöthig, F.E. Kühn, *J. Catal.* 331 (2015) 147–153, <https://doi.org/10.1016/j.jcat.2015.08.026>.
- W. Stroek, M. Keilwerth, D.M. Pividori, K. Meyer, M. Albrecht, *J. Am. Chem. Soc.* 143 (2021) 20157–20165, <https://doi.org/10.1021/jacs.1c07378>.
- M. Schilz, L. Plenio, *J. Org. Chem.* 77 (2012) 2798–2807, <https://doi.org/10.1021/jo202644g>.
- M. Baltrun, F.A. Watt, R. Schoch, C. Wölper, A.G. Neuba, S. Hohloch, *Dalton Trans.* 48 (2019) 14611–14625, <https://doi.org/10.1039/C9DT03099A>.
- M.T. Tautz, Juan, Grijalvo, Santiago; Eritja, Ramon; Saldias, Cesar; Aleman, Carlos; Diaz Diaz, David, *RSC Adv.* 2019, 9, 20841–20851, DOI: 10.1039/c9ra03316e.
- G.T. Potter, G.C. Jayson, G.J. Miller, J.M. Gardiner, *J. Org. Chem.* 81 (2016) 3443–3446, <https://doi.org/10.1021/acs.joc.6b00177>.
- F. Friscourt, G.-J. Boons, *Org. Lett.* 12 (2010) 4936–4939, <https://doi.org/10.1021/ol1022036>.
- S. Liao, B. List, *Angew. Chem. Int. Ed.* 49 (2010) 628–631, <https://doi.org/10.1002/anie.200905332>.
- M. Mahlau, B. List, *Angew. Chem. Int. Ed.* 52 (2013) 518–533, <https://doi.org/10.1002/anie.201205343>.


 Cite this: *RSC Adv.*, 2024, **14**, 10244

# Synthesis, characterization, and biomedical evaluation of ethylene-bridged tetra-NHC Pd(II), Pt(II) and Au(III) complexes, with apoptosis-inducing properties in cisplatin-resistant neuroblastoma cells†

 Wolfgang R. E. Büchele,<sup>‡a</sup> Tim P. Schlachta,<sup>‡a</sup> Andreas L. Gebendorfer,<sup>a</sup> Jenny Pamperin,<sup>cd</sup> Leon F. Richter,<sup>de</sup> Michael J. Sauer,<sup>a</sup> Aram Prokop<sup>\*bcd</sup> and Fritz E. Kühn<sup>id\*ab</sup>

Synthesis and characterization of the first two cyclic ethylene-bridged tetradentate NHC ligands, with an unsaturated (imidazole) and saturated backbone (2-imidazoline), are described. Complexes of both ligands containing palladium(II) have been obtained. For platinum(II) and gold(III), only the unsaturated tetracarbene complexes could be isolated. The attempts to synthesize a methylene-bridged 2-imidazoline macrocycle are also described. Furthermore, a novel bisimidazolium ligand precursor and its open-chain Pd<sup>II</sup> and Pt<sup>II</sup> tetracarbene complexes are obtained. Finally, it is shown that the unsaturated gold(III) tetracarbene is able to induce apoptosis in malignant SK-N-AS neuroblastoma cells *via* the mitochondrial and ROS pathway and overcomes resistance to cisplatin *in vitro*.

 Received 16th February 2024  
 Accepted 14th March 2024

DOI: 10.1039/d4ra01195c

[rsc.li/rsc-advances](https://rsc.li/rsc-advances)

## Introduction

N-heterocyclic carbenes (NHCs), first described in 1991,<sup>1</sup> have found many applications.<sup>2</sup> There are several structural features that allow the tuning of their electronic properties. Ring size, the adjacent heteroatoms, *N*-substituents, and the backbone can be modified. Changing one or more structural properties of a NHC ligand can lead to significantly different reactivities and stabilities of the resulting complexes.<sup>3</sup> Often several NHC units are combined in multidentate ligands, making use of the chelating effect, and a plethora of multidentate NHC metal complexes has been reported.<sup>4,5</sup>

Our group has developed several bidentate and cyclic tetradentate NHC ligands. The respective transition metal complexes have been applied *e.g.* in medicinal chemistry<sup>6,7</sup> and epoxidation catalysis.<sup>3</sup> While the bidentate ligands can form open-chain tetracarbene complexes,<sup>8,9</sup> the tetradentate ligands give cyclic tetracarbene compounds. Most commonly applied in our recent examinations is the calix[4]imidazolium ligand precursor (**a**, Fig. 1).<sup>10</sup> Its iron complex (**c**) can be used as olefin epoxidation catalyst achieving unprecedented activity.<sup>3</sup> Coinage metal tetracarbene complexes (and metal NHC complexes in general<sup>11–17</sup>) have been investigated regarding their anti-proliferative activity and selectivity against cancer cells (**b**, **d–f**, Fig. 1).<sup>6,7</sup>

<sup>a</sup>Technical University of Munich, School of Natural Sciences, Department of Chemistry and Catalysis Research Center, Molecular Catalysis, Lichtenbergstraße 4, 85748 Garching, Germany. E-mail: fritz.kuehn@ch.tum.de; Tel: +49 89 289 13477

<sup>b</sup>Department of Pediatric Hematology/Oncology, Children's Hospital Cologne, Amsterdamer Straße 59, 50735 Cologne, Germany

<sup>c</sup>Department of Pediatric Oncology/Hematology, Helios Clinics Schwerin, Wismarsche Straße 393-397, 19055 Schwerin, Germany. E-mail: aram.prokop@helios-gesundheit.de

<sup>d</sup>Department of Human Medicine, MSH Medical School Hamburg, Am Kaiserkaai 1, 20457 Hamburg, Germany

† Electronic supplementary information (ESI) available: Synthetic details, biological studies, analytical data and crystallographic data. CCDC 2299372–2299374. For ESI and crystallographic data in CIF or other electronic format see DOI: <https://doi.org/10.1039/d4ra01195c>

‡ These authors contributed equally to this work.

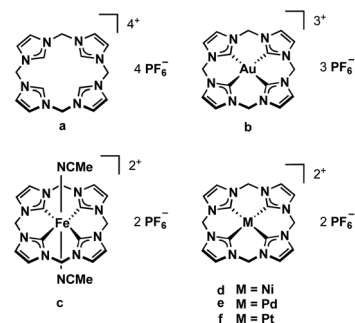


Fig. 1 Tetracarbene ligand precursor **a** and derived transition metal complexes **b–f**.



In this study, the scope of multidentate NHC ligands is extended with an ethylene-bridged bisimidazolium ligand precursor and two cyclic ethylene-bridged tetradentate NHC ligands, with an unsaturated (imidazole) and saturated backbone (2-imidazoline). Pd<sup>II</sup>, Pt<sup>II</sup> and Au<sup>III</sup> tetracarbene complexes containing the novel ligands are synthesized, characterized and applied in preliminary medicinal studies regarding their activity in inducing apoptosis in malignant cells. Finally, the synthetic attempts to a calix[4]imidazolium macrocycle (structurally analog to **c** but with a saturated backbone) are described, because there is an increasing demand for reliable training data, including data on negative outcomes, for machine learning systems in chemistry.<sup>18</sup>

Especially the two new macrocyclic ligand precursors are intended to lay the foundation for electronic comparisons induced by the different backbone in future studies. The unsaturated backbone of the imidazole moiety causes partial aromaticity, increasing NHC stability by *ca.* 100 kJ mol<sup>-1</sup>.<sup>19–21</sup> A saturated backbone, in turn, can lead to higher basicity because the electron density is more concentrated on the C2 carbene carbon atom due to the lack of  $\pi$ -interactions.<sup>22</sup>

## Results and discussion

The synthesis of a saturated macrocyclic ligand precursor similar to **c**, but containing 2-imidazoline moieties instead of imidazole, calix[4]imidazolium, was pursued parallel to the synthesis of the other ligand precursors. However, the synthesis was not successful with the chosen synthetic approaches as described in the ESI<sup>†</sup>.

### Synthesis and characterization of H<sub>2</sub>L3

H<sub>2</sub>L3 is based on the literature known ethylene-bridged imidazoline moiety (**1**).<sup>23</sup> Alkylation of **1** with MeI in MeCN at 82 °C, followed by an anion exchange with NH<sub>4</sub>PF<sub>6</sub> in water, gives H<sub>2</sub>L3 in 91% yield (Fig. 2).

### Synthesis and characterization of H<sub>4</sub>L5/6 and H<sub>4</sub>L8/L9

For the preparation of H<sub>4</sub>L5/6 and H<sub>4</sub>L8/9, a slightly modified literature procedure for similar macrocycles was used (Fig. 3).<sup>10</sup> Ring closure to form the macrocyclic imidazolium salt **a** is commonly achieved with CH<sub>2</sub>(OTf)<sub>2</sub>,<sup>3</sup> but also CH<sub>2</sub>Br<sub>2</sub> is reported.<sup>24</sup> Here the ethylene-bridged imidazoline **1** (ref. 23) and the ethylene-bridged imidazole **7** (ref. 25) are reacted with ethylene bistriflate (**4**) under dry conditions at -45 °C over a period of 5 h in dry MeCN for H<sub>4</sub>L5 and H<sub>4</sub>L8 (see ESI<sup>†</sup>).

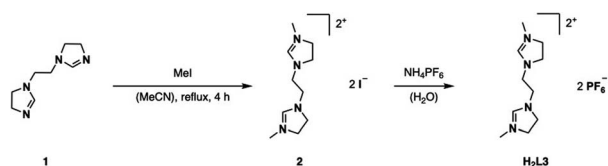


Fig. 2 Synthesis of ligand precursor H<sub>2</sub>L3 via alkylation and anion exchange.

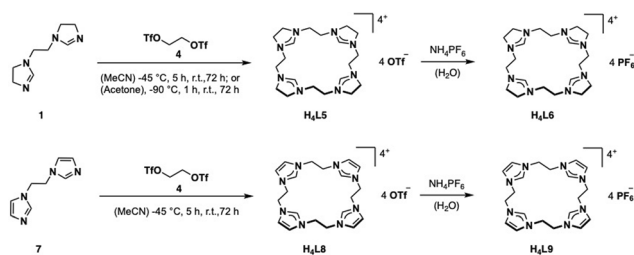


Fig. 3 Synthesis of ligand precursors H<sub>4</sub>L5/6 and H<sub>4</sub>L8/9 via ring closure with ethylene bistriflate and anion exchange.

The synthesis of H<sub>4</sub>L5 and H<sub>4</sub>L8 yields a mixture of a 20-membered macrocycle (87% H<sub>4</sub>L5 and 90% H<sub>4</sub>L8, as determined by NMR), consisting of four imidazole [C[4] units], and a 30-membered macrocycle (13% H<sub>4</sub>L5, 10% H<sub>4</sub>L8) consisting of six imidazole [C[6] units] (see ESI<sup>†</sup>). Separation attempts of C[4] and C[6] via column chromatography, precipitation or sublimation were not successful. However, by increasing the cooling period during the addition of the ethylene bistriflate at -45 °C to a total of 5 h, the purity of the kinetically preferred C[4] unit could be easily increased up to 98% C[4] for H<sub>4</sub>L5 and in case of H<sub>4</sub>L8 an increase up to 100% (ESI<sup>†</sup>). Due to the absence of similar macrocyclic imidazolium compounds, H<sub>4</sub>L5 is compared to **a** and H<sub>4</sub>L8 in the following.<sup>3</sup>

Relative to **a**, all signals of H<sub>4</sub>L5 and H<sub>4</sub>L8 are upfield shifted, indicating a higher electronic density due to the +I effect of the ethylene bridge leading to an increased shielding effect in the NMR.<sup>10,26</sup> The higher upfield shift of H<sub>4</sub>L5 compared to H<sub>4</sub>L8 can be explained by the electronic inducing effect of the saturated bond.<sup>20,26,27</sup>

Unlike in <sup>1</sup>H-NMR, each individual <sup>13</sup>C signal of H<sub>4</sub>L8 in DMSO-d<sub>6</sub> is in the same range as the signals obtained for the macrocyclic compound **a**.<sup>10</sup> However, in case of H<sub>4</sub>L5, opposite to the <sup>1</sup>H-NMR, the C2 carbon resonance at 159.16 ppm is downfield shifted compared to H<sub>4</sub>L8 and **a** (H<sub>4</sub>L8,  $\Delta\delta \leq 22.08$  ppm, **a**,  $\Delta\delta \leq 22.0$  ppm), thus contradicting expectations. According to literature and as described by H. V. Huynh, the hypothetical free carbene of the imidazoline ligand H<sub>4</sub>L5 should be a stronger  $\sigma$ -donor than H<sub>4</sub>L8, so an enhanced upfield shift of the C2 signal of H<sub>4</sub>L5 should have been detectable.<sup>20,28,29</sup> Interestingly this expectation is not met here, and apparently other factors play a role. Every other resonance in the <sup>13</sup>C-NMR is upfield shifted.<sup>10</sup>

Salt metathesis of the formed macrocyclic salts can be performed with NH<sub>4</sub>PF<sub>6</sub> to increase the solubility in organic solvents and as additional purification step.<sup>3,30</sup> Thus, an anion exchange in water towards PF<sub>6</sub><sup>-</sup> is conducted with H<sub>4</sub>L5 and H<sub>4</sub>L8, resulting in H<sub>4</sub>L6 (81%) and H<sub>4</sub>L9 (88%).

### Synthesis and characterization of complexes (Pd/PtL3, PdL5/6, Pd/PtL8, Pd/AuL9)

A well-established route to obtain NHC complexes is to convert the corresponding imidazolium salts with group 10 metal acetates. In this reaction, the acetate serves as an internal base capable of deprotonating imidazolium- and imidazolium



salts to form NHCs, which subsequently coordinate to the metal.<sup>6,31–33</sup> An alternative route is *via* a silver transmetalation.<sup>34</sup> In the first approaches, attempts were made to synthesize the respective Ag<sup>I</sup> complex with **H<sub>2</sub>L3** to obtain a dinuclear structure similar to already published open chain bis-NHC-complexes.<sup>9,25,35</sup> However, no product formation was observed in our case. Either no reaction took place or complex signals were observed in the aliphatic region of  $\delta = 1.9\text{--}4.4$  ppm in the <sup>1</sup>H-NMR after purification, indicating the decomposition of **H<sub>2</sub>L3**. Several other conditions with different Ag<sup>I</sup>-salts and addition of sodium acetate as internal base at different temperatures were tested without success. A possible problem might be the stability of the Ag<sup>I</sup>-complex. Another issue might be hydrolysis of imidazolines under acidic and basic conditions.<sup>36,37</sup> It has been proposed in literature that the moisture in the solvent can react with sodium acetate to generate hydroxide ions which can attack the electrophilic center of the C2 carbon and lead to ring-opening products, rather than nucleophilic attacking the acidic proton at the C2 carbon.<sup>38</sup> Therefore, the next attempts were conducted under moisture-free reaction conditions by using dried solvents. Even the direct metalation with palladium(II) acetate or palladium(II) chloride under dry reaction conditions did not lead to the desired product. The focus was then shifted to a combination of the transmetalation route using Ag<sub>2</sub>O *in situ* with the direct metalation, by applying the respective metal precursor and sodium acetate as a mild base in dry solvents (Fig. 4).

The absence of the acidic imidazolium proton signal and appearance of characteristic carbene carbon signals confirms the successful formation of **PdL3** and **PtL3**. Unfortunately, despite several attempts, a clean elemental analysis for **PtL3** could not be obtained. Also, the <sup>1</sup>H-NMR of **PtL3** shows some impurities, which could not be identified and no <sup>195</sup>Pt isotope coupling phenomena was observed in the <sup>13</sup>C-NMR.

The carbene carbon signal of **PdL3** at 194.29 ppm in DMSO-d<sub>6</sub> [**PtL3**; 188.38 ppm in CD<sub>3</sub>CN], is surprisingly downfield shifted compared to other Pd(II) bis-NHCs reported in literature.<sup>39,40</sup> Due to the theoretically stronger  $\sigma$ -donation of the imidazolynilidene ligand **H<sub>2</sub>L3** compared to its unsaturated analog, an upfield shift of the <sup>13</sup>C<sub>NHC</sub> signal was expected. Literature indicates that the significant downfield shift of the carbene carbon resonance from imidazolium to imidazolium compounds is a general phenomenon.<sup>38,41,42</sup> Another interesting fact is that the analytic data, including HR-ESI-MS and elemental analysis, are not supporting a dinuclear complex or a mono-carbene complex as expected, but indicate that **PdL3** has rather a [**Pd(L3)**]<sub>2</sub>(PF<sub>6</sub>)<sub>2</sub> structure similar to **e**. This is further

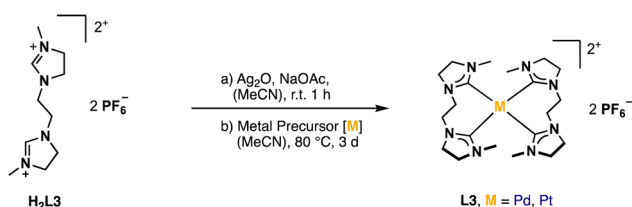


Fig. 4 General synthesis of Pd/PtL3.

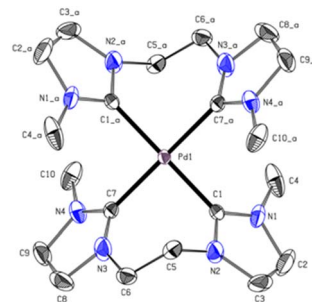


Fig. 5 ORTEP-style representation of the cationic fragment of complex **PdL3**. Hydrogen atoms and hexafluorophosphate anions are omitted for clarity. Thermal ellipsoids are shown at a 50% probability level. Selected bond lengths (Å) and angles (°): C1–Pd1 2.039(2); C7–Pd1 2.038(2); C7<sub>a</sub>–Pd1–C7 180.0; C7–Pd1–C1<sub>a</sub> 91.64(9); C7–Pd1–C1 88.36(9); C7<sub>a</sub>–Pd1–C1<sub>a</sub>–N2<sub>a</sub> 55.30.

confirmed by single-crystal X-ray diffraction (SC-XRD). The **PdL3** complex displays a distorted square planar structure. Two **L3** ligands coordinate to the Pd center, resulting in an open-chain tetracarbene complex of similar geometry like the cyclic complex **e**.<sup>34</sup> The Pd–C (2.039 Å, 2.038 Å) distances are in good accord with palladium(II) NHC complexes reported in literature.<sup>34,39</sup> The alkyl groups of the ligand **L3** adopt a *syn* conformation in the solid state, while the imidazole rings are tilted by 55.30° out of the palladium square plane (Fig. 5).

The **PtL3** complex exhibits a similarly distorted square planar structure compared to **PdL3**. The Pt–C (2.033 Å, 2.039 Å) distances are comparable to similar literature known group 10 NHC compounds.<sup>43–47</sup> The alkyl groups of **L3** also adopt a *syn* conformation, while the imidazole rings are tilted by 50.53° out of the palladium square plane as in **PdL3** (Fig. 6).

### Complex PdL5/6 and PdL8/9

Since **H<sub>4</sub>L5** and **H<sub>4</sub>L8** are quite similar to other macrocycles (**a**), it seemed suitable to synthesize **PdL5** and **PdL8** according to alike compounds *via* the direct metalation route.<sup>32</sup> Therefore, **H<sub>4</sub>L8** was first converted with Pd(OAc)<sub>2</sub> in a mixture of dry

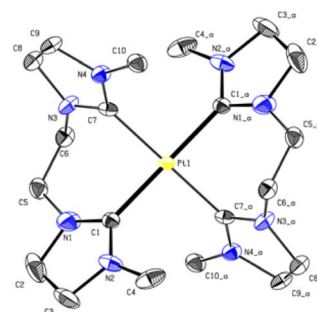


Fig. 6 ORTEP-style representation of the cationic fragment of complex **PtL3**. Hydrogen atoms and hexafluorophosphate anions are omitted for clarity. Thermal ellipsoids are shown at a 50% probability level. Selected bond lengths (Å) and angles (°): Pt1–C1 2.0337 (18); Pt1–C7 2.039 (6); C1<sub>a</sub>–Pt1–C1 180.00(7); C1–Pt1–C7<sub>a</sub> 91.2(5); C1–Pt1–C7 88.8(5); C7<sub>a</sub>–Pd1–C1<sub>a</sub>–N2<sub>a</sub> 50.53°.

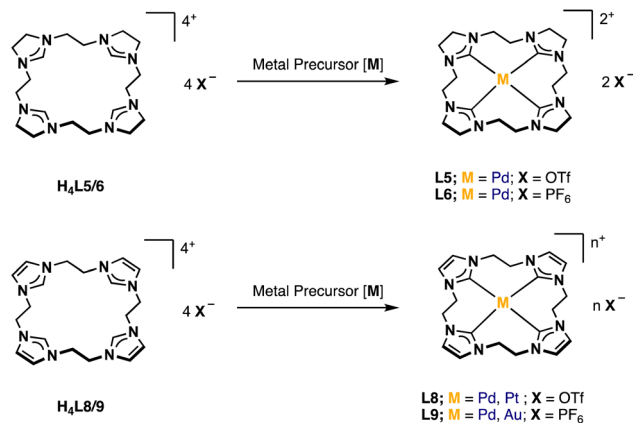


Fig. 7 General synthesis of PdL5/6, Pd/PtL8 and Pd/AuL9.

DMSO/MeCN (1 : 1) at 40 °C for 16 h.<sup>34</sup> However, no product formation was observed after work-up. Several other conditions such as increasing temperature and reaction time led to the absence of the imidazolium protons and the formation of new product signals in the <sup>1</sup>H-NMR after 4 d at 80 °C. Still these intensities were very low, and no product could be isolated. Another approach was tried *via* the transmetalation route with Ag<sup>+</sup> salts, but this also led to no product formation. Finally, both **PdL8** (50%, Fig. 7) and **PdL5** (3%) could be obtained by applying the same reaction conditions as for the already synthesized complexes **PdL3** and **PtL3**. The yield of the imidazolynilidene tetracarbenic complex could be increased to 46%, by using **H<sub>4</sub>L6** instead of **H<sub>4</sub>L5**, resulting in **PdL6**.

Again, the absence of the acidic position 2 proton signals in the <sup>1</sup>H-NMR and appearance of the carbene carbon peaks confirm the formation of Pd(II) carbene complexes. The observed chemical shift of **PdL8** is in the typical range of Pd(II) tetra-NHC compounds and indicates the formation of a complex with similar coordination sphere as **e**.<sup>6,34,45</sup> The <sup>1</sup>H-NMR of **PdL5** in CD<sub>3</sub>CN shows three signals, with two of them in a similar range to **PdL8** and one upfield shifted signal of the backbone protons. As already mentioned in the discussion of **H<sub>4</sub>L5**, the <sup>13</sup>C-NMR of **PdL5** is contrary to expectations. The carbene carbon of **PdL5** (191.30 ppm) is surprisingly strong downfield shifted compared to **PdL8** (165.84 ppm) and in a similar range to the carbene carbon of **PdL3** (195.6 ppm in CD<sub>3</sub>CN). Literature indicates that the significant downfield shift of the carbene carbon resonance from imidazole to imidazoline compounds is a general phenomenon.<sup>38,41,42</sup> The uncertainty of a <sup>13</sup>C-NMR measurement is expected to be below 0.1 ppm; by using three times the weighted standard deviation, a difference of >0.4 ppm is required for a significant difference that exceeds the statistic uncertainty.<sup>3,48</sup> Therefore, **PdL5** (191.30 ppm in CD<sub>3</sub>CN) and **PdL8** (165.84 ppm in CD<sub>3</sub>CN) show a sufficiently different chemical shift to allow its discussion. In general, the normal NHC unit (without any modification) of the tetracarbenic ligands is in a range of rather low to negligible π-backdonation, hence the changes in electronic properties are dominated by the σ-donation of the tetracarbenes.<sup>3,29</sup> According to literature, the imidazoline ligand **L5** should be in general

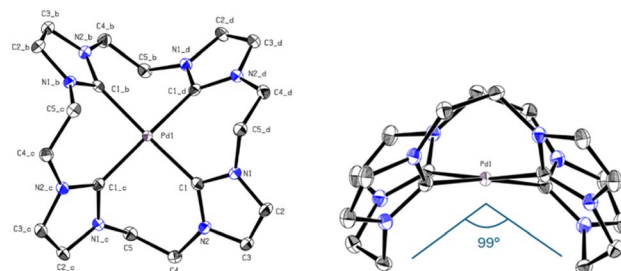


Fig. 8 ORTEP-style representation of the cationic fragment of complex PdL9. Hydrogen atoms and hexafluorophosphate anions are omitted for clarity. Thermal ellipsoids are shown at a 50% probability level. Selected bond lengths (Å) and angles (°): C1–Pd 2.019(2), C1–Pd1–C1\_b 172.03(12), C1–Pd1–C1\_d–N2\_d 53.62, C5–Pd1–C5\_b 98.97°.

a stronger σ-donor than **L8**, so an enhanced upfield shift of the carbene signal would have been detectable.<sup>3,20,28,29</sup> Interestingly, this expectation is also not met here, and apparently other factors may play a role, as already observed with **PdL3** and **PtL3**. Therefore, further investigations on this subject, *e.g.* by means of DFT calculations, have to be carried out, since only conjectures can be made with the present analytical data. The elemental analysis and HR-ESI-MS for **PdL8** are in accord with a composition [**Pd(L8)**](OTf)<sub>2</sub> similar to **e**. It needs to be noted that no clean elemental analysis of **PdL6** could be obtained. However, the elemental analysis and HR-ESI-MS of **PdL6** are in accordance with the composition [**PdL6**](PF<sub>6</sub>)<sub>2</sub>. Due to unsatisfying results in crystallization of **PdL8**, an anion exchange in water towards PF<sub>6</sub><sup>−</sup> was conducted, resulting in **PdL9** (41%). Single crystals suitable for SC-XRD were obtained by slow diffusion of Et<sub>2</sub>O into MeCN solution of **PdL9**. As expected, the Pd(II) ion is coordinated in a nearly square planar fashion with C–Pd–C angles deviating from 180° by ~8°, thus lifting the metal slightly above the carbene carbon atom plane (Fig. 8). However, due to the C<sub>2</sub>-bridge, the ligand is strongly bent (C5–Pd1–C5\_b = 98.97°) and adopts a crisp-shape, while tilting the imidazole rings 53.62° in an alternating pattern out of the palladium square plane.<sup>49</sup> The Pd–C distance (2.019 Å) is comparable to those of other cyclic Pd(II) tetracarbenic compounds reported in literature.<sup>6,34,43,45–47</sup>

In the following Table 1 the M–C<sub>carbene</sub> bond lengths [Å], the C<sub>carbene</sub>–M–C<sub>carbene</sub> angle [°], the tilt of the NCN unit [°] of the complexes **Pd/PtL3** and **PdL9** and additionally the C<sub>bridge</sub>–M–C<sub>bridge</sub> angle [°] for **PdL9** are summarized.

Table 1 Summary of the M–C<sub>carbene</sub> bond lengths [Å], the C<sub>carbene</sub>–M–C<sub>carbene</sub> angle [°], the tilt of the NCN unit [°] of the complexes Pd/PtL3 and PdL9 and the C<sub>bridge</sub>–M–C<sub>bridge</sub> angle [°] for PdL9

Compound	PdL3	PtL3	PdL9
M–C <sub>carbene</sub> [Å]	2.038 2.039	2.033 2.039	2.019
C <sub>carbene</sub> –M–C <sub>carbene</sub> [°]	180	180	172.03
Tilt NCN unit [°]	55.30	50.53	53.62
C <sub>bridge</sub> –M–C <sub>bridge</sub> [°]	—	—	98.97



### Complex PtL8

Applying the same reaction conditions and work-up methods to  $\text{Pt}(\text{MeCN})_2\text{Cl}_2$  instead of  $\text{Pd}(\text{OAc})_2$  results in the formation of **PtL8** (25%, Fig. 7). The absence of acidic proton signals in the  $^1\text{H-NMR}$  and the appearance of the carbene  $^{13}\text{C}$ -peak at 159.39 ppm in  $\text{CD}_3\text{CN}$  confirms the formation of the respective  $\text{Pt}(\text{II})$  complex. The chemical shift of the carbene carbon is in accordance with  $\text{Pt}(\text{II})$  tetra-NHC complexes previously reported in literature and is slightly shifted to the upfield compared to **PdL8** ( $^{13}\text{C}_{\text{NHC}}$  in  $\text{CD}_3\text{CN}$  at 165.84 ppm) by 6.45 ppm.<sup>43,46,50</sup> No  $^{195}\text{Pt}$  isotope coupling was observed. The  $^1\text{H-NMR}$  in  $\text{CD}_3\text{CN}$  shows similar signals compared to **PdL8**, where the bridge protons also split into two multiplets at 5.01 and 4.44 ppm. In addition, HR-ESI-MS is in accordance to a similar composition as **PdL8**. Despite multiple attempts, no single crystals suitable for SC-XRD were obtained. However, the discussed analytical data strongly support a similar structure compared to **PdL8** and similarly structured tetracarbene ligand.<sup>6,34</sup>

### Complex AuL9

For the synthesis of **AuL9** (Fig. 7), the same reaction conditions were applied as reported in the literature for similar complexes.<sup>51</sup> Therefore, **H<sub>4</sub>L8** was converted with  $\text{KAuCl}_4$  and  $\text{NaOAc}$  in dry DMSO under exclusion of light at 100 °C for 5 h. After the work-up, including an ion exchange to  $\text{PF}_6^-$  as a purification step, **AuL9** (47%) was obtained. The absence of acidic proton signals in the  $^1\text{H-NMR}$  and the appearance of a new  $^{13}\text{C}$ -peak at 146.03 ppm in  $\text{CD}_3\text{CN}$  confirm the formation of the respective  $\text{Au}(\text{III})$  complex. The chemical shift of the carbene carbon is in accord with  $\text{Au}(\text{III})$  tetracarbene complex (**e**) previously reported in literature and slightly downfield shifted by 1.79 ppm when compared to **e**.<sup>51</sup> Furthermore, the backbone carbons are also slightly downfield shifted by 0.68 ppm. The  $^1\text{H-NMR}$  in  $\text{CD}_3\text{CN}$  shows similar signals compared to complex **PdL8** and **PtL8** with the backbone protons at 7.47 ppm and the bridge protons as two multiplets in close proximity at 4.83 and 4.71 ppm. Both elemental analysis<sup>52</sup> and HR-ESI-MS are in agreement with the composition  $[\text{Au}(\text{L15})](\text{PF}_6)_3$ . Although no single crystals suitable for SC-XRD were obtained, the discussed analytical data strongly support the coordination of one tetracarbene ligand similar to **PdL9**.

## Biological evaluation

### Induction of apoptosis as cell death type

**PdL3**, **PdL8**, **AuL9** and their respective protonated ligand precursors were tested for their apoptotic effects on Nalm-6 cells (human B cell precursor leukemia cell line) and SK-N-AS cells (human neuroblastoma cell line) at different concentrations and quantified by the nuclear DNA fragmentation by flow cytometry analysis. **PdL3** and **PdL8** as well as the ligand precursors do not show any apoptosis inducing effects in Nalm-6 cells and SK-N-AS cells (see ESI<sup>†</sup>). **AuL9** shows no apoptotic effect in Nalm-6 cells, but significant apoptosis induction by **AuL9** is detected in SK-N-AS cells (Fig. 9A); therefore, the effect of **AuL9** in SK-N-AS cells was further characterized.

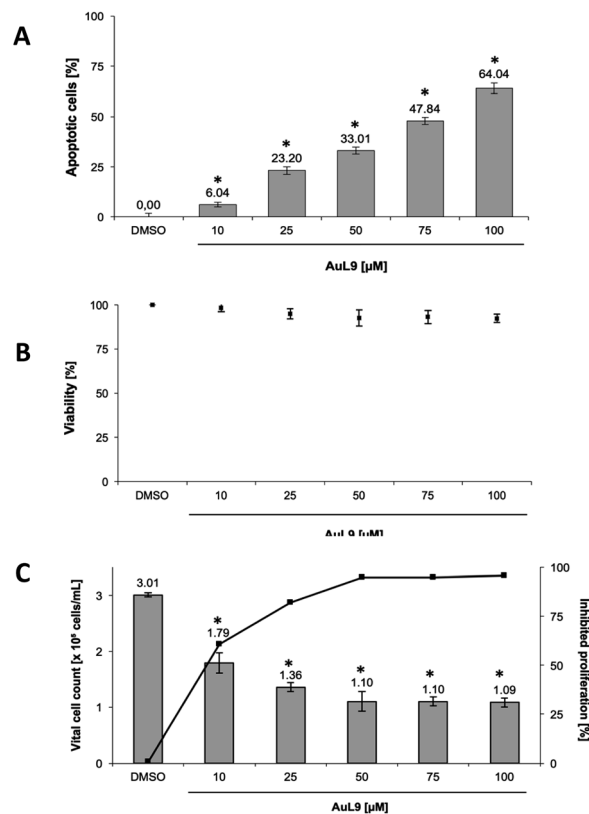


Fig. 9 (A) **AuL9** induces apoptosis in SK-N-AS cells. The cells were treated with different concentrations of **AuL9** and incubated for 96 h. Nuclear DNA fragmentation was analyzed. (B) To exclude unspecific cytotoxic effects, such as necrotic cell death, the viability of SK-N-AS cells was determined by measurement of LDH release into the medium after 2 h of incubation with different concentrations of **AuL9**. No significant LDH release could be detected in cells treated with **AuL9** up to a concentration of 100  $\mu\text{M}$ . Values are given as mean% of DMSO control  $\pm$  SD ( $n = 3$ ). (C) The inhibition of proliferation of **AuL9** treated SK-N-AS cells was measured after 48 h using the CASY Cell-Counter System. A significant inhibition of cell growth was observed at concentrations as low as 10  $\mu\text{M}$ . Inhibition of proliferation is given in mean% of control  $\pm$  SD ( $n = 3$ ); \*:  $p < 0.05$  vs. DMSO,  $t$ -test.

To exclude necrotic effects of **AuL9**, lactate dehydrogenase (LDH) leakage from SK-N-AS cells after 2 h incubation with **AuL9** was measured. LDH is released from the cell in case of necrosis and can be detected in the cell culture medium in case of loss of cell integrity and thus serves as a necrosis indicator.<sup>53</sup> **AuL9** shows no significant non-specific cytotoxic effects on SK-N-AS cells in the relevant concentration range up to 100  $\mu\text{M}$  (Fig. 9B).

In addition to apoptosis induction, it was tested whether **AuL9** can inhibit the proliferation of malignant cells. For this purpose, SK-N-AS cells were incubated with different concentrations of **AuL9** for 48 hours. The proliferation inhibition was determined by comparing the total cell number of vital cells of the DMSO control with the total cell number of vital cells of the treated cells. The results show that **AuL9** inhibits cell proliferation of SK-N-AS cells in a dose-dependent manner (Fig. 9C). A concentration of 50  $\mu\text{M}$  **AuL9** causes nearly 100% inhibition of proliferation, indicating G1 arrest.



For the investigation of the mechanism of action of **AuL9**, the mitochondrial membrane potential of SK-N-AS cells was measured after 48 h incubation with **AuL9**. It was shown that the mitochondrion and thus the intrinsic apoptosis pathway plays at least a partial role in the effect of **AuL9** (Fig. 10A).

To further characterize the role of mitochondria in **AuL9**-induced apoptosis, the apoptosis pathway mediated by reactive oxygen species (ROS) was investigated. Therefore, *N*-acetylcysteine (NAC) as a known ROS inhibitor and H<sub>2</sub>O<sub>2</sub>, which belongs to the ROS, as a positive control was investigated. It was shown that apoptosis induction could be significantly inhibited by NAC. It can therefore be concluded that the generation of ROS plays a role in the **AuL9**-induced apoptosis (Fig. 10B). However, it is not possible in the present state to be sure how the ROS are generated and whether **AuL9** directly leads to an increased ROS production or triggers pathways that result in the generation of ROS.

### Overcoming cisplatin resistance

Cisplatin is a well-known chemotherapeutic agent for the treatment of many different types of cancer.<sup>54</sup> The development of resistance in tumor cells is a major problem in therapy and is usually the limiting factor in the cure of cancer patients.<sup>55</sup>

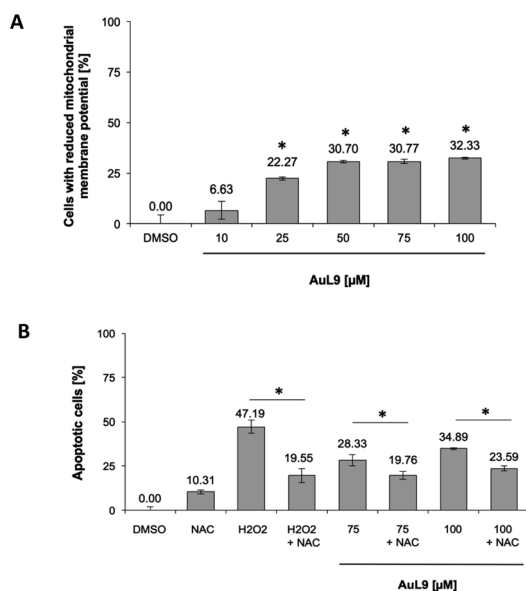


Fig. 10 (A) The mitochondrial membrane potential in SK-N-AS cells was impaired by **AuL15** treatment, which implicates mitochondrial pathway involvement in apoptosis induction. The mitochondrial membrane potential was measured by flow cytometric analysis in SK-N-AS cells after 48 h of incubation with different concentrations of **AuL15** and staining with the cationic dye JC-1. Values are mean% of cells with low mitochondrial membrane potential  $\pm$  SD ( $n = 3$ ); \* $p < 0.05$  vs. DMSO, *t*-test. B The induction of apoptosis in SK-N-AS cells in response to **AuL15** treatment was shown to be dependent on the ROS mediated pathway. The cells were incubated for 72 h with 50  $\mu$ M H<sub>2</sub>O<sub>2</sub> as a positive control or different concentrations of **AuL15** with or without pretreatment of the cells with the ROS inhibitor *N*-acetylcysteine (NAC, 5 mM) 1.5 h prior to substance addition. Nuclear DNA fragmentation was analyzed by flow cytometric analysis. Values are mean% of apoptotic cells  $\pm$  SD ( $n = 3$ ); \* $p < 0.05$  vs. DMSO, *t*-test.

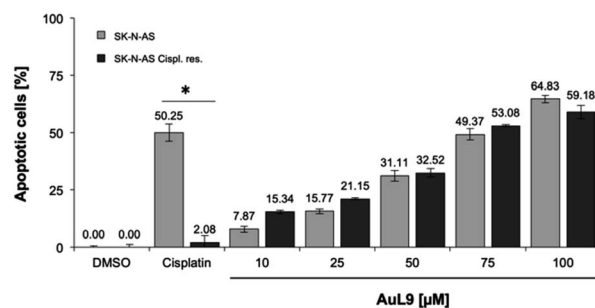


Fig. 11 SK-N-AS and SK-N-AS cisplatin resistant cells were treated with different concentrations of **AuL15** and incubated for 96 h. It is shown that **AuL9** was also effective in inducing apoptosis in cisplatin resistant cells, thus overcoming resistance. 8.25  $\mu$ M cisplatin has been used as a positive control to prove resistance. Nuclear DNA fragmentation was analyzed by flow cytometric analysis. Values are mean% of apoptotic cells  $\pm$  SD ( $n = 3$ ); \* $p < 0.05$  vs. DMSO, *t*-test.

Therefore, it is of great importance for drug development that new agents are able to overcome cytostatic drug resistance. In addition to SK-N-AS cells, **AuL9** was tested on cisplatin resistant SK-N-AS cells and cisplatin resistance overcoming could be demonstrated (Fig. 11). In a previous characterization of the cisplatin resistant SK-N-AS cells, procaspase-8 under expression was shown.<sup>56</sup> The cisplatin resistance overcoming of SK-N-AS cells indicates that procaspase-8 has a minor role in **AuL9**-induced apoptosis.

## Conclusion and outlook

A synthetic approach to a calix[4]imidazolium macrocycle as saturated analog to **a** is presented. The synthesis of two new macrocyclic ligand systems, being bridged by ethylene groups and containing imidazoline (**H<sub>4</sub>L5/6**) and imidazole moieties (**H<sub>4</sub>L8/9**) are discussed. In addition, a novel bisimidazolium ligand precursor (**H<sub>2</sub>L3**) is described. All complexes (**Pd/PtL3**, **PdL5/6**, **Pd/PtL8**, **Au/PdL9**) with their respective ligands synthesized in this work are not accessible *via* the direct metalation of the respective ligand, due to irreproducible or unreliable results, except for **AuL9**. Even the route *via* the silver salt transmetalation does not lead to reliable results. The silver complexes of the respective ligands could not be isolated, probably due to instability of the respective complexes. Therefore, a modified synthetic method has been established. Here, *in situ* transmetalation with silver oxide is used in combination with the metal precursor and an excess of sodium acetate as a mild base, resulting in the corresponding complexes. Furthermore, the complexes **PdL3**, **PdL8**, **AuL9** and their respective ligands were tested for their ability to induce apoptosis on Naml-6 and SK-N-AS cells. According to the experiments performed, the data suggest that **AuL9** is capable of inducing apoptosis in malignant cells *via* the mitochondrial and ROS pathway. However, so far, an effect could only be observed on SK-N-AS neuroblastoma cells. In addition, a relatively high dose of **AuL9** is required to induce apoptosis in neuroblastoma cells, which could be challenging for clinical applicability. **AuL9** is able to overcome resistance to cisplatin in



neuroblastoma cells (SK-N-AS) *in vitro*. Further characterization experiments would be required to determine the exact mechanism of action of **AuL9**, for example identification of molecular targets that are involved in the **AuL9** induced apoptosis, as well as the selectivity for cancer cells.

## Experimental section

### General procedures and analytical methods

Unless otherwise stated, all manipulations were performed under normal atmosphere without dried and degassed chemicals. All syntheses regarding the complexes were conducted under the exclusion of light. Every work-up was performed under normal atmosphere without dried and degassed chemicals; the complexes' work-ups were conducted in addition under the exclusion of light unless otherwise stated. Purification, in case of the Pt and Pd complexes, is achieved by dissolving the crude product in MeCN and filtering it through basic aluminum oxide to remove impurities. Acidic aluminum oxide promotes the decomposition of the complexes while pH-neutral aluminum oxide leads in smaller yields.<sup>6</sup> All obtained complexes are air- and water stable; however, **PtL3**, **PtL8** and **AuL9** decompose after extensive exposition to light. Solvents were obtained water-free from a MBraun solvent purification system and stored over molecular sieves (3 Å). The procedures for novel compounds obtained during the synthetic approaches to the saturated macrocyclic ligand precursor, containing 2-imidazoline moieties instead of imidazole, calix[4]imidazolium, (2-imidazoline, *N*-benzyl-2-imidazoline, 3,3'-methylenebis(1-benzyl-2-imidazolium)dibromide, *N*<sup>1</sup>,*N*<sup>1</sup>,*N*<sup>2</sup>,*N*<sup>2</sup>-tetrabenzylethane-1,2-diamine, *tert*-butyl (2-aminoethyl)carbamate, *tert*-butyl 2-imidazoline-1-carboxylate) are stated in the ESI.† *N*-Benzylethylenediamine (**12**),<sup>57–59</sup> ethylenebis(trifluoromethanesulfonate) (**4**),<sup>60</sup> 1,1'-ethylene-di-2-imidazoline (**1**)<sup>23</sup> and 1,1'-ethylenebis-1*H*-imidazolyl (**7**)<sup>25,61</sup> were synthesized according to literature procedures. All other reagents were purchased from commercial suppliers and used without further purification. NMR spectra were recorded on a Bruker Avance DPX 400 (<sup>1</sup>H-NMR, 400 MHz; <sup>13</sup>C-NMR, 100 MHz; <sup>19</sup>F-NMR, 376 MHz) and chemical shifts are given in  $\delta$  values in ppm (parts per million) relative to TMS (tetramethylsilane) and reported relative to the residual signal of the deuterated solvent.<sup>62</sup> Elemental analysis (C/H/N) were obtained by the Microanalytical Laboratory at Technische Universität München. Electrospray ionization mass spectrometry (ESI-MS) data were acquired on a Thermo Fisher Ultimate 3000 and with higher resolution (HR-ESI-MS) on Exactive Plus Orbitrap from Thermo Fisher.

### Synthetic procedures

**Alkylbisimidazoline diiodide (2)**. **1** (5.00 g, 30.0 mmol, 1.00 eq.) is dissolved in MeCN (300 mL) and MeI (213 g, 1.50 mol, 50.0 eq.) is added. The resulting reaction mixture is heated to reflux for 4 h. After cooling to ambient temperature, all volatile compounds are removed *in vacuo*. The resulting crude material is redissolved in a small amount of MeCN (5 mL) and an off-

white solid is precipitated after the addition of Et<sub>2</sub>O (40 mL). The crude material is collected *via* centrifugation and washed with (3 × 5 mL) Et<sub>2</sub>O. After removal of all volatile compounds *in vacuo*, **2** is obtained as an off-white solid (11.1 g, 24.7 mmol, 82%). <sup>1</sup>H-NMR (400 MHz, DMSO-*d*<sub>6</sub>)  $\delta$  (ppm) = 8.54 (s, 2H, *N*-*CH*-*N*), 3.91 (s, 8H, CH<sub>3</sub>-*N*-CH<sub>2</sub>-CH<sub>2</sub>), 3.70 (s, 4H, CH<sub>2</sub>-CH<sub>2</sub>), 3.12 (s, 6H, CH<sub>3</sub>). <sup>13</sup>C-NMR (101 MHz, DMSO-*d*<sub>6</sub>)  $\delta$  (ppm) = 159.12 (*N*-*CH*-*N*), 50.96 (*C*<sub>(backbone)</sub>), 48.70 (*C*<sub>(backbone)</sub>), 45.02 (CH<sub>2</sub>-CH<sub>2</sub>), 35.08 (CH<sub>3</sub>). Elemental analysis: for C<sub>10</sub>H<sub>20</sub>I<sub>2</sub>N<sub>4</sub> (%) anal. calc.: C: 26.68, H: 4.48, N: 12.45, found: C: 26.66, H: 4.48, N: 12.39.

**Alkylbisimidazolium hexafluorophosphate (H<sub>2</sub>L3)**. **2** (100 mg, 222  $\mu$ mol, 1.00 eq.) is dissolved in H<sub>2</sub>O (1 mL) and added to a solution of NH<sub>4</sub>PF<sub>6</sub> (217 mg, 1.33 mmol, 6.00 eq.) in H<sub>2</sub>O (1 mL). The resulting white precipitate is collected, washed three times with H<sub>2</sub>O (2 mL, 2 mL, 1 mL) and dried subsequently *in vacuo*. Without further purification, the titled compound **H<sub>2</sub>L3** is obtained as a white solid (98 mg, 202  $\mu$ mol, 91%). <sup>1</sup>H-NMR (400 MHz, DMSO-*d*<sub>6</sub>)  $\delta$  (ppm) = 8.39 (s, 2H, *N*-*CH*-*N*), 3.88 (s, 8H, CH<sub>3</sub>-*N*-CH<sub>2</sub>-CH<sub>2</sub>), 3.67 (s, 4H, CH<sub>2</sub>-CH<sub>2</sub>), 3.11 (s, 6H, CH<sub>3</sub>). <sup>13</sup>C-NMR (101 MHz, DMSO-*d*<sub>6</sub>)  $\delta$  (ppm) = 158.77 (*N*-*CH*-*N*), 50.36 (*C*<sub>(backbone)</sub>), 48.12 (*C*<sub>(backbone)</sub>), 44.55 (CH<sub>2</sub>-CH<sub>2</sub>), 34.43 (CH<sub>3</sub>). <sup>19</sup>F-NMR (376 MHz, DMSO-*d*<sub>6</sub>)  $\delta$  (ppm) = -70.15 (d, <sup>1</sup>J<sub>P-F</sub> = 713 Hz, PF<sub>6</sub><sup>-</sup>). Elemental analysis: for C<sub>10</sub>H<sub>20</sub>F<sub>12</sub>N<sub>4</sub>P<sub>2</sub> (%) anal. calc.: C: 24.70, H: 4.15, N: 11.52, found: C: 24.28, H: 4.01, N: 11.17.

**Calix[4](-Et-Et)-imidazoliumtrifluoromethanesulfonate (H<sub>4</sub>L5)**. **1** (1.00 g, 6.17 mmol, 2.00 eq.) is dissolved in dry MeCN (1.5 L), cooled to -45 °C and a solution of **4** (2.02 g, 6.20 mmol, 2.01 eq.) in dry MeCN (50 mL) is added dropwise over 6 h. After the addition, the reaction mixture is stirred for 72 h at ambient temperature. All volatile compounds are removed *in vacuo* and the resulting crude material is dried subsequently *in vacuo*. Without further purification the titled compound **H<sub>4</sub>L5** is obtained as an off-white solid (1.50 g, 1.54 mmol, 50%). Note: everything is conducted under inert conditions. <sup>1</sup>H-NMR (400 MHz, DMSO-*d*<sub>6</sub>)  $\delta$  (ppm) = 8.46 (s, 4H, *N*-*CH*-*N*), 3.95 (s, 16H, CH<sub>2</sub>(bridge/backbone)), 3.74 (s, 16H, CH<sub>2</sub>(bridge/backbone)). <sup>13</sup>C-NMR (101 MHz, DMSO-*d*<sub>6</sub>)  $\delta$  (ppm) = 159.16 (*N*-*CH*-*N*), 120.80 (q, <sup>1</sup>J<sub>19F-13C</sub> = 320 Hz, OTf<sup>-</sup>), 48.15 (CH<sub>2</sub>(bridge/backbone)), 44.54 (CH<sub>2</sub>-CH<sub>2</sub>(bridge/backbone)). <sup>19</sup>F-NMR (376 MHz, DMSO-*d*<sub>6</sub>)  $\delta$  (ppm) = -77.74 (CF<sub>3</sub>). Elemental analysis for C<sub>24</sub>H<sub>36</sub>N<sub>8</sub>O<sub>12</sub>F<sub>12</sub>S<sub>4</sub> (%) anal. calc.: C 29.27; H 3.68; N 11.38; S 13.02 found: C 29.37; H 3.67; N 11.01; S 13.12.

**Calix[4](-Et-Et)-imidazoliumhexafluorophosphate (H<sub>4</sub>L6)**. **H<sub>4</sub>L5** (300 mg, 304  $\mu$ mol, 1.00 eq.) is dissolved in H<sub>2</sub>O (50 mL) and added to a solution of NH<sub>4</sub>PF<sub>6</sub> (223 mg, 1.37 mmol, 4.50 eq.) in H<sub>2</sub>O (50 mL). The resulting white precipitate is collected, washed three times with H<sub>2</sub>O (10 mL, 7 mL, 5 mL), Et<sub>2</sub>O (3 mL, 2 mL) and dried subsequently *in vacuo*. Without further purification, the titled compound **H<sub>4</sub>L6** is obtained as a white solid (240 mg, 248  $\mu$ mol, 81%). However, a small amount of OTf<sup>-</sup> is still detectable in the <sup>19</sup>F-NMR. <sup>1</sup>H-NMR (400 MHz, DMSO-*d*<sub>6</sub>):  $\delta$  (ppm) = 8.44 (s, 4H, *N*-*CH*-*N*), 3.93 (s, 16H, CH<sub>2</sub>(backbone)/CH<sub>2</sub>(bridge)), 3.72 (s, 16H, CH<sub>2</sub>(bridge)/CH<sub>2</sub>(backbone)). <sup>1</sup>H-NMR (400 MHz, CD<sub>3</sub>CN):  $\delta$  (ppm) = 7.98–7.82 (m, 4H, *N*-*CH*-*N*), 4.00–3.82 (m, 16H, CH<sub>2</sub>(backbone)/CH<sub>2</sub>(bridge)), 3.73–3.65



(m, 16H,  $CH_{2(\text{bridge})}/CH_{2(\text{backbone})}$ ).  $^{19}\text{F}$ -NMR (376 MHz,  $\text{CD}_3\text{CN}$ ):  $\delta$  (ppm) =  $-72.45$  (d,  $^1J_{\text{P-F}} = 713$  Hz,  $\text{PF}_6^-$ ). ESI-MS:  $m/z$  = calc. for  $[\text{H}_4\text{L6-PF}_6^-]^{+}$ : 823.20 ( $[\text{M-PF}_6^-]^{+}$ ); found: 822.94; calc. for  $[\text{H}_4\text{L6-2PF}_6^-]^{+}$ : 339.11 ( $[\text{H}_4\text{L6-2PF}_6^-]^{+}$ ); found: 339.12.

#### Calix[4](-Et-Et)-imidazoliumtrifluoromethanesulfonate

**(H<sub>4</sub>L8)**. 7 (1.00 g, 6.17 mmol, 2.00 eq.) is dissolved in dry MeCN (1.5 L), cooled to  $-30$  °C and a solution of 4 (2.02 g, 6.20 mmol, 2.01 eq.) in dry MeCN (100 mL) is added dropwise over 5 h. After the addition, the reaction mixture is stirred for 72 h at ambient temperature. All volatile compounds are removed *in vacuo* and the resulting crude material is washed eight times with cold acetone (10 mL, 5 mL, 5 mL, 3 mL, 3 mL, 2 mL, 2 mL, 1 mL) and dried subsequently *in vacuo*. Without further purification, the titled compound **H<sub>4</sub>L8** is obtained as a white solid (1.50 g, 1.54 mmol, 50%).  $^1\text{H}$ -NMR (400 MHz,  $\text{CD}_3\text{CN}$ )  $\delta$  (ppm) = 8.57 (t,  $^4J = 1.6$  Hz, 4H, N-CH-N), 7.39 (d,  $^4J = 1.7$  Hz, 8H, CH), 4.71 (s, 16H,  $CH_2$ ).  $^{13}\text{C}$ -NMR (101 MHz,  $\text{CD}_3\text{CN}$ )  $\delta$  (ppm) = 138.49 (N-CH-N), 124.49 (HC=CH), 121.80 (q,  $^1J_{19\text{F}-13\text{C}} = 320$  Hz, OTf<sup>-</sup>), 50.14 ( $CH_2-CH_2$ ).  $^{19}\text{F}$ -NMR (376 MHz,  $\text{CD}_3\text{CN}$ )  $\delta$  (ppm) =  $-79.32$  ( $\text{CF}_3$ ).  $^1\text{H}$ -NMR (400 MHz,  $\text{DMSO-d}_6$ )  $\delta$  (ppm) = 9.00 (t,  $^4J = 1.7$  Hz, 4H, N-CH-N), 7.57 (d,  $^4J = 1.6$  Hz, 8H, CH), 4.74 (s, 16H,  $CH_2$ ).  $^{13}\text{C}$ -NMR (101 MHz,  $\text{DMSO-d}_6$ )  $\delta$  (ppm) = 137.08 (N-CH-N), 123.28 (HC=CH), 120.66 (q,  $^1J_{19\text{F}-13\text{C}} = 320$  Hz, OTf<sup>-</sup>), 49.24 ( $CH_2-CH_2$ ). Elemental analysis for  $\text{C}_{24}\text{H}_{28}\text{N}_8\text{O}_{12}\text{F}_{12}\text{S}_4$  (%) anal. calc.: C 29.54; H 2.84; N 11.54; S 13.13 found: C 29.54; H 2.84; N 11.54; S 13.25. ESI-MS:  $m/z$   $[\text{H}_4\text{L8-4OTf}]^{4+}$  calc.: 95.06, found: 94.91,  $[\text{H}_4\text{L8-3OTf}]^{3+}$  calc.: 176.39, found 176.36,  $[\text{H}_4\text{L8-2OTf}]^{2+}$  calc.: 339.07, found: 339.22,  $[\text{H}_4\text{L8-1OTf}]^{1+}$  calc.: 827.03, found 826.93.

#### Calix[4](-Et-Et)-imidazoliumhexafluorophosphate (H<sub>4</sub>L9)

**H<sub>4</sub>L8** (3.20 g, 3.28 mmol, 1.00 eq.) is dissolved in  $\text{H}_2\text{O}$  (300 mL) and added to a solution of  $\text{NH}_4\text{PF}_6$  (3.20 g, 19.66 mmol, 6.00 eq.) in  $\text{H}_2\text{O}$  (50 mL). The resulting white precipitate is collected, washed three times with  $\text{H}_2\text{O}$  (10 mL, 7 mL, 5 mL) and dried subsequently *in vacuo*. Without further purification, the titled compound **H<sub>4</sub>L9** is obtained as a white solid (2.80 g, 2.85 mmol, 88%).  $^1\text{H}$ -NMR (400 MHz,  $\text{CD}_3\text{CN}$ )  $\delta$  (ppm) = 8.44 (t,  $^4J = 1.6$  Hz, 4H, N-CH-N), 7.33 (d,  $^4J = 1.7$  Hz, 8H, CH), 4.70 (s, 16H,  $CH_2$ ).  $^{19}\text{F}$ -NMR (376 MHz,  $\text{CD}_3\text{CN}$ )  $\delta$  (ppm) =  $-72.30$  (d,  $^1J_{\text{FP}} = 713$  Hz,  $\text{PF}_6^-$ ).  $^1\text{H}$ -NMR (400 MHz,  $\text{DMSO-d}_6$ )  $\delta$  (ppm) = 9.00 (s, 4H, N-CH-N), 7.55 (d,  $^4J = 1.6$  Hz, 8H, CH), 4.73 (s, 16H,  $CH_2$ ).  $^{13}\text{C}$ -NMR (101 MHz,  $\text{DMSO-d}_6$ )  $\delta$  (ppm) = 137.26 (N-CH-N), 123.49 (HC=CH), 49.44 ( $CH_2-CH_2$ ). Elemental analysis for  $\text{C}_{20}\text{H}_{28}\text{N}_8\text{F}_{24}\text{P}_4$  (%) anal. calc.: C 25.01; H 2.94; N 11.67; S 0.00 found: C 25.08; H 2.90; N 11.31; S 0.00.

#### Pd[C<sup>Et</sup>C<sub>imi</sub>(Me)<sub>2</sub>C<sup>Et</sup>C<sub>imi</sub>(Me)<sub>2</sub>]hexafluorophosphate (PdL3)

$\text{Ag}_2\text{O}$  (150 mg, 648  $\mu\text{mol}$ , 1.05 eq.) is added to a solution of **H<sub>2</sub>L3** (300 mg, 617  $\mu\text{mol}$ , 1.00 eq.) and NaOAc (202 mg, 2.47 mmol, 4.00 eq.) in dry MeCN (15 mL) and stirred for 1 h at ambient temperature, followed by the addition of  $\text{Pd}(\text{OAc})_2$  (145 mg, 648  $\mu\text{mol}$ , 1.05 eq.). The resulting reaction mixture is heated to 80 °C for 3 d. After cooling to ambient temperature, the reaction mixture is filtered over a short plug of basic aluminum oxide. The filter column is eluted with MeCN (20 mL) and all volatile compounds are removed *in vacuo*. The resulting crude material is resuspended in MeCN (5 mL) and centrifuged. Upon the addition of  $\text{Et}_2\text{O}$  (20 mL) to the supernatant, a white solid is

precipitated. The crude material is collected *via* centrifugation, washed with  $\text{Et}_2\text{O}$  ( $3 \times 5$  mL), redissolved in MeCN (5 mL) and precipitated with  $\text{Et}_2\text{O}$  (15 mL). After drying *in vacuo*, the titled compound **PdL3** is obtained as an off-white solid (140 mg, 178  $\mu\text{mol}$ , 29%). Single crystals suitable for SC-XRD were obtained by slow diffusion of  $\text{Et}_2\text{O}$  into MeCN solution of **PdL3**.  $^1\text{H}$ -NMR (400 MHz,  $\text{CD}_3\text{CN}$ )  $\delta$  (ppm) = 4.32–4.22 (m, 4H,  $CH_{2(\text{backbone})}$ ), 3.71–3.51 (m, 20H,  $CH_2-CH_2$ ,  $CH_{2(\text{backbone})}$ ), 2.97 (s, 12H,  $CH_3$ ).  $^{13}\text{C}$ -NMR (101 MHz,  $\text{CD}_3\text{CN}$ )  $\delta$  (ppm) = 195.6 (N-C-N), 51.72 ( $C_{(\text{bridge})}$ ,  $C_{(\text{backbone})}$ ), 51.26 ( $C_{(\text{bridge})}$ ,  $C_{(\text{backbone})}$ ), 46.5 ( $CH_2$ ), 37.62 ( $CH_3$ ).  $^{19}\text{F}$ -NMR (376 MHz,  $\text{CD}_3\text{CN}$ ):  $\delta$  (ppm) =  $-72.94$  (d,  $^1J_{\text{P-F}} = 706$  Hz,  $\text{PF}_6^-$ ).  $^1\text{H}$ -NMR (400 MHz,  $\text{DMSO-d}_6$ )  $\delta$  (ppm) = 4.35–4.13 (m, 4H,  $CH_{2(\text{backbone})}$ ), 3.82–3.57 (m, 20H,  $CH_2-CH_2$ ,  $CH_{2(\text{backbone})}$ ), 2.95 (s, 12H,  $CH_3$ ).  $^{13}\text{C}$ -NMR (101 MHz,  $\text{DMSO-d}_6$ )  $\delta$  (ppm) = 194.29 (N-C-N), 50.94 ( $C_{(\text{bridge})}$ ,  $C_{(\text{backbone})}$ ), 50.56 ( $C_{(\text{bridge})}$ ,  $C_{(\text{backbone})}$ ), 45.76 ( $CH_2$ ), 37.17 ( $CH_3$ ). Elemental analysis: for  $\text{C}_{20}\text{H}_{36}\text{F}_{24}\text{N}_8\text{P}_4\text{Pd}_1$  (%) anal. calc.: C 30.60, H: 4.62, N: 14.28, found: C: 30.93, H: 4.55, N: 14.14, S: 0.00. HR-ESI-MS:  $m/z$   $[\text{PdL3-2PF}_6^-]^{2+}$  calc.: 247.1044, found: 247.1039,  $[\text{PdL3-PF}_6^-]^{+}$  calc.: 639.1735, found: 639.1720.

#### Pt[C<sup>Et</sup>C<sub>imi</sub>(Me)<sub>2</sub>C<sup>Et</sup>C<sub>imi</sub>(Me)<sub>2</sub>]hexafluorophosphate (PtL3)

$\text{Ag}_2\text{O}$  (150 mg, 648  $\mu\text{mol}$ , 1.05 eq.) is added to a solution of **H<sub>2</sub>L3** (300 mg, 617  $\mu\text{mol}$ , 1.00 eq.) and NaOAc (202 mg, 2.47 mmol, 4.00 eq.) in dry MeCN (15 mL) and stirred for 1 h at ambient temperature, followed by the addition of  $\text{PtCl}_2$  (145 mg, 648  $\mu\text{mol}$ , 1.05 eq.). The resulting reaction mixture is heated to 80 °C for 3 d. After cooling to ambient temperature, the reaction mixture is filtered over a short plug of basic aluminum oxide. The filter column is eluted with MeCN (20 mL) and all volatile compounds are removed *in vacuo*. The resulting crude material is resuspended in MeCN (5 mL) and centrifuged. Upon the addition of  $\text{Et}_2\text{O}$  (20 mL) to the supernatant, a white solid is precipitated. The crude material is collected *via* centrifugation, washed with  $\text{Et}_2\text{O}$  ( $3 \times 5$  mL) and redissolved in MeCN (5 mL) and precipitated with  $\text{Et}_2\text{O}$  (15 mL). After drying *in vacuo*, the titled compound **PtL3** is obtained as an off-white solid (23 mg, 26  $\mu\text{mol}$ , 4%). Single crystals suitable for SC-XRD were obtained by slow diffusion of  $\text{Et}_2\text{O}$  into MeCN solution of **PtL3**. Note; a clean EA could not be obtained, and the NMR includes impurities.  $^1\text{H}$ -NMR (400 MHz,  $\text{CD}_3\text{CN}$ )  $\delta$  (ppm) = 4.35–4.26 (m, 4H,  $CH_{2(\text{backbone})}$ ), 3.72–3.51 (m, 20H,  $CH_2-CH_2$ ,  $CH_{2(\text{backbone})}$ ), 2.94 (s, 12H,  $CH_3$ ).  $^{13}\text{C}$ -NMR (101 MHz,  $\text{CD}_3\text{CN}$ )  $\delta$  (ppm) = 188.38 (N-C-N), 51.47 (d,  $C_{(\text{bridge})}$ ,  $C_{(\text{backbone})}$ ), 46.39 ( $CH_2$ ), 37.44 ( $CH_3$ ).

$\text{Pd}[\text{C}^{\text{Et}}\text{C}^{\text{Et}}\text{C}_{\text{imi}}\text{OTf}]$  (**PdL5**).  $\text{Ag}_2\text{O}$  (155 mg, 670  $\mu\text{mol}$ , 2.20 eq.) is added to a solution of **H<sub>4</sub>L5** (300 mg, 305  $\mu\text{mol}$ , 1.00 eq.) and NaOAc (200 mg, 2.42 mmol, 8.00 eq.) in dry MeCN/DMSO (12 mL 1 : 1) and stirred for 1 h at ambient temperature, followed by the addition of  $\text{Pd}(\text{OAc})_2$  (71.8 mg, 320  $\mu\text{mol}$ , 1.05 eq.). The resulting reaction mixture is heated to 80 °C for 3 d and is filtered, after cooling to ambient temperature, over a short plug of basic aluminum oxide. The filter column is eluted with MeCN (100 mL) and all volatile compounds are removed *in vacuo*. The resulting oily solution (still approx. 6 mL of DMSO remaining) is resuspended in MeCN (6 mL) and centrifuged. Upon the addition of  $\text{Et}_2\text{O}$  (25 mL) to the supernatant, a brown/black solid is precipitated. After another addition of  $\text{Et}_2\text{O}$  (120 mL) a white



solid is precipitated. The white crude material is collected *via* centrifugation, washed with Et<sub>2</sub>O (3 × 5 mL) and redissolved in MeCN (5 mL). After purification [3 times dissolving in MeCN (4 mL) and precipitating with Et<sub>2</sub>O (~15 mL)] and removing all volatile compounds *in vacuo*, the titled compound **PdL5** is obtained as an off-white solid (7.00 mg, 8.87 μmol, 3%). <sup>1</sup>H-NMR (400 MHz, CD<sub>3</sub>CN): δ (ppm) = 4.10–4.00 (m, 8H, CH<sub>2,(bridge)</sub>), 3.76–3.54 (m, 16H, CH<sub>2,(backbone)</sub>), 3.52–3.45 (m, 8H, CH<sub>2,(bridge)</sub>). <sup>13</sup>C-NMR (101 MHz, CD<sub>3</sub>CN): δ (ppm) = 191.3 (N–C–N), 51.0 (CH<sub>2,(bridge)</sub>/CH<sub>2,(backbone)</sub>), 47.4 (CH<sub>2,(backbone)</sub>/CH<sub>2,(bridge)</sub>). <sup>19</sup>F-NMR (376 MHz, CD<sub>3</sub>CN): δ (ppm) = –79.33 (CF<sub>3</sub>). ESI-MS: *m/z* = calc. for [PdL5–OTf]<sup>+</sup>: 639.13 ([PdL5–OTf]<sup>+</sup>); found: 639.44; calc. for [PdL5–2OTf]<sup>2+</sup>: 245.09 ([M–2OTf]<sup>2+</sup>); found: 245.20.

**Pd[(cC<sup>Et</sup>CC<sup>Et</sup>C<sub>imi</sub>)PF<sub>6</sub>] (PdL6).** PdL6 is synthesized analog to PdL5; by converting H<sub>4</sub>L6 (230 mg, 238 μmol, 1.00 eq.) with Ag<sub>2</sub>O (121 mg, 522 μmol, 2.20 eq.) in dry MeCN (4 mL) while stirring for 1 h at ambient temperature, followed by the addition of NaOAc (156 mg, 1.90 mmol, 8.00 eq.), Pd(OAc)<sub>2</sub> (56.0 mg, 249 μmol, 1.05 eq.) and is heated at 75 °C for 4 d. After purification [3 times dissolving in MeCN (4 mL) and precipitating with Et<sub>2</sub>O (~15 mL)] and removing all volatile compounds, PdL6 is obtained as a pale-yellow solid (85.0 mg, 109 μmol, 46%). <sup>1</sup>H-NMR (400 MHz, CD<sub>3</sub>CN): δ (ppm) = 4.13–4.02 (m, 8H, CH<sub>2,(bridge)</sub>), 3.78–3.60 (m, 16H, CH<sub>2,(backbone)</sub>), 3.52–3.46 (m, 8H, CH<sub>2,(bridge)</sub>). <sup>19</sup>F-NMR (376 MHz, CD<sub>3</sub>CN): δ (ppm) = –72.78 (d, <sup>1</sup>J<sub>P31–F19</sub> = 707 Hz, PF<sub>6</sub>) elemental analysis for C<sub>20</sub>H<sub>32</sub>F<sub>12</sub>N<sub>8</sub>P<sub>2</sub>Pd (%) anal. calc.: C 30.76; H 4.13; N 14.13; found: C 29.50; H 4.07; N 14.35. ESI-MS: *m/z* = calc. for [PdL6–PF<sub>6</sub>]<sup>+</sup>: 635.14 ([M–PF<sub>6</sub>]<sup>+</sup>); found: 635.21. HR-ESI-MS: *m/z* [PdL6–2PF<sub>6</sub>]<sup>2+</sup> calc.: 245.0887, found: 245.0890, [PdL6 + H<sub>2</sub>O–2PF<sub>6</sub>]<sup>2+</sup> calc.: 254.0940, found: 254.0944, [PdL6–PF<sub>6</sub>]<sup>+</sup> calc.: 635.1422, found: 635.1425, [PdL6 + H<sub>2</sub>O–PF<sub>6</sub>]<sup>+</sup> calc.: 653.1527, found: 653.1534.

**Pd[(cC<sup>Et</sup>CC<sup>Et</sup>C)OTf] (PdL8).** Ag<sub>2</sub>O (74.7 mg, 322 μmol, 1.05 eq.) is added to a solution of H<sub>4</sub>L8 (320 mg, 307 μmol, 1.00 eq.) and NaOAc (202 mg, 2.46 mmol, 4.00 eq.) in dry MeCN (15 mL) and stirred for 1 h at ambient temperature, followed by the addition of Pd(OAc)<sub>2</sub> (72.4 mg, 322 μmol, 1.05 eq.). The resulting reaction mixture is heated to 80 °C for 4 d. After cooling to ambient temperature, the reaction mixture is filtered over a short plug of basic aluminum oxide. The filter column is eluted with MeCN (50 mL) and all volatile compounds are removed *in vacuo*. The resulting crude material is resuspended in MeCN (5 mL) and centrifuged. Upon the addition of Et<sub>2</sub>O (20 mL) to the supernatant, a white solid is precipitated. The crude material is collected *via* centrifugation, washed with Et<sub>2</sub>O (3 × 5 mL) and redissolved in MeCN (5 mL). After the precipitation with Et<sub>2</sub>O (15 mL) and drying *in vacuo*, the titled compound PdL8 is obtained as an off-white solid (119 mg, 153 μmol, 50%). <sup>1</sup>H-NMR (400 MHz, CD<sub>3</sub>CN) δ (ppm) = 7.20 (s, 8H, CH), 5.02–4.93 (m, 8H, CH<sub>2</sub>), 4.47–4.39 (m, 8H, CH<sub>2</sub>). <sup>13</sup>C-NMR (101 MHz, CD<sub>3</sub>CN) δ (ppm) = 165.84 (N–C–N), 123.77 (CH), 49.11 (s, CH<sub>2</sub>–CH<sub>2</sub>). <sup>1</sup>H-NMR (400 MHz, DMSO-*d*<sub>6</sub>) δ (ppm) = 7.52 (s, 8H, CH), 5.05–4.95 (m, 8H, CH<sub>2</sub>), 4.52–4.42 (m, 8H, CH<sub>2</sub>). <sup>13</sup>C-NMR (101 MHz, DMSO-*d*<sub>6</sub>) δ (ppm) = 163.80 (N–C–N), 123.32 (CH), 48.14 (CH<sub>2</sub>–CH<sub>2</sub>). Elemental analysis for C<sub>20</sub>H<sub>28</sub>N<sub>8</sub>F<sub>24</sub>P<sub>4</sub> + 1 MeCN (%) anal. calc.: C 35.07; H 3.31; N 15.33; S 7.80 found: C 35.26; H 3.21; N 15.73; S 7.82. HR-ESI-MS: *m/z* [PdL8–2OTf]<sup>2+</sup> calc.:

241.0574, found: 241.0570, [PdL8–OTf]<sup>+</sup> calc.: 631.0674, found: 631.0658.

**Pd[(cC<sup>Et</sup>CC<sup>Et</sup>C)PF<sub>6</sub>] (PdL9).** PdL8 (95 mg, 122 μmol, 1.00 eq.) is dissolved in H<sub>2</sub>O (35 mL), after the addition of NH<sub>4</sub>PF<sub>6</sub> (50.0 mg, 305 μmol, 2.5 eq.) a white precipitate is collected *via* centrifuge and washed three times with H<sub>2</sub>O (5 mL, 3 mL, 3 mL) and Et<sub>2</sub>O (10 mL, 5 mL, 3 mL). After drying *in vacuo*, the titled compound PdL9 is obtained as an off-white solid (39 mg, 50 μmol, 41%). Single crystals suitable for SC-XRD were obtained by slow diffusion of Et<sub>2</sub>O into MeCN solution of PdL8. <sup>1</sup>H-NMR (400 MHz, CD<sub>3</sub>CN) δ (ppm) = 7.22 (s, 8H, CH), 4.97 (m, 8H, CH<sub>2</sub>), 4.43 (m, 8H, CH<sub>2</sub>). <sup>19</sup>F-NMR (376 MHz, CD<sub>3</sub>CN) δ (ppm) = –72.93 (d, <sup>1</sup>J<sub>FP</sub> = 713 Hz, PF<sub>6</sub><sup>–</sup>). HR-ESI-MS: *m/z* [PdL9–2PF<sub>6</sub>]<sup>2+</sup> calc.: 241.0574, found: 241.0570, [PdL9–PF<sub>6</sub>]<sup>+</sup> calc.: 627.0796, found: 627.0782.

**Pt[(cC<sup>Et</sup>CC<sup>Et</sup>C)OTf] (PtL8).** Ag<sub>2</sub>O (209 mg, 900 μmol, 2.20 eq.) is added to a solution of H<sub>4</sub>L8 (400 mg, 410 μmol, 1.00 eq.) and NaOAc (202 mg, 2.46 mmol, 4.00 eq.) in dry MeCN (30 mL) and stirred for 1 h at ambient temperature, followed by the addition of Pt(MeCN)<sub>2</sub>Cl<sub>2</sub> (156 mg, 450 μmol, 1.10 eq.). The resulting reaction mixture is heated to 80 °C for 3 d and is filtered, after cooling to ambient temperature, over a short plug of basic aluminum oxide. The filter column is eluted with MeCN (50 mL) and all volatile compounds are removed *in vacuo*. The resulting crude material is resuspended in MeCN (5 mL) and centrifuged. Upon the addition of Et<sub>2</sub>O (20 mL) to the supernatant, a white solid is precipitated. The crude material is collected *via* centrifugation, washed with Et<sub>2</sub>O (3 × 5 mL) and redissolved in MeCN (5 mL). After the precipitation with Et<sub>2</sub>O (15 mL) and drying *in vacuo*, the titled compound PtL8 is obtained as an off-white solid (90 mg, 103 μmol, 25%). <sup>1</sup>H-NMR (400 MHz, CD<sub>3</sub>CN) δ (ppm) = 7.19 (s, 8H, CH), 5.11–4.94 (m, 8H, CH<sub>2</sub>), 4.50–4.38 (m, 8H, CH<sub>2</sub>). <sup>1</sup>H-NMR (400 MHz, DMSO-*d*<sub>6</sub>) δ (ppm) = 7.49 (s, 8H, CH), 5.06–4.97 (m, 8H, CH<sub>2</sub>), 4.54–4.44 (m, 8H, CH<sub>2</sub>). <sup>13</sup>C-NMR (101 MHz, CD<sub>3</sub>CN) δ (ppm) = 159.39 (N–CH–N), 123.58 (HC=CH), 48.86 (CH<sub>2</sub>–CH<sub>2</sub>). <sup>19</sup>F-NMR (376 MHz, CD<sub>3</sub>CN) δ (ppm) = –79.27 (CF<sub>3</sub>). HR-ESI-MS: *m/z* [PtL8–2OTf]<sup>2+</sup> calc.: 285.5881, found: 285.5864, [PtL8–OTf]<sup>+</sup> calc.: 720.1287, found: 720.1264.

**Au[(cC<sup>Et</sup>CC<sup>Et</sup>C)PF<sub>6</sub>] (AuL9).** H<sub>4</sub>L8 (500 mg, 458 μmol, 1.00 eq.), KAuCl<sub>4</sub> × 2H<sub>2</sub>O (209 mg, 505 μmol, 1.05 eq.), and NaOAc (197 mg, 2.41 mmol, 5.00 eq.) are suspended in dry DMSO (5 mL). The resulting reaction mixture is stirred for 5 h at 100 °C and filtered at ambient temperature. MeCN (5 mL) is added to the filtrate. After the addition of Et<sub>2</sub>O (30 mL) to the solution, white solid precipitated. It is washed with MeCN (3 × 5 mL) and DCM (2 × 5 mL) and after the removal of all volatiles *in vacuo*, the solid is dissolved in H<sub>2</sub>O (2 mL) and added dropwise to a solution of NH<sub>4</sub>PF<sub>6</sub> (353 mg, 2.17 mmol, 4.00 eq.) in H<sub>2</sub>O (5 mL). The resulting white precipitate is collected and washed with H<sub>2</sub>O (3 × 5 mL) and after removal of all volatiles *in vacuo*, the titled compound AuL9 (230 mg, 228 μmol, 47%) is obtained as a white solid. <sup>1</sup>H-NMR (400 MHz, CD<sub>3</sub>CN) δ (ppm) = 7.47 (s, 8H, CH), 4.89–4.77 (m, 8H, CH<sub>2</sub>), 4.76–4.66 (m, 8H, CH<sub>2</sub>). <sup>13</sup>C-NMR (101 MHz, CD<sub>3</sub>CN) δ (ppm) = 146.03 (N–CH–N), 125.92 (HC=CH), 48.58 (CH<sub>2</sub>–CH<sub>2</sub>). Elemental analysis for C<sub>20</sub>H<sub>24</sub>F<sub>24</sub>AuF<sub>18</sub>N<sub>8</sub>P<sub>3</sub> × 0.1 MeCN (%) anal. calc.: C 24.62; H 2.70; N 11.11;



S 0.00 found: C 24.82; H 2.78; N 11.15; S 0.57. HR-ESI-MS:  $m/z$  [AuL9-3PF<sub>6</sub><sup>-</sup>]<sup>3+</sup> calc.: 191.0591, found: 191.0587, [AuL9-PF<sub>6</sub><sup>-</sup>]<sup>+</sup> calc.: 863.1068, found: 863.1038.

## Conflicts of interest

There are no conflicts to declare.

## Acknowledgements

All authors thank Prof. Dr T. Simon (University Cologne) for providing the SK-N-AS cell line, Dr Seeger for providing the Nalm-6 cell line. A. Prokop thanks the Dr. Kleist Foundation (Berlin), Foundation David (Cologne), Koch Foundation (Berlin) and Blankenheimerdorf e.V. (Eifel) for the financial support in the biological studies. Further thanks go to A. Gradenegger, F. Tschernuth from Prof. Dr S. Inoue, and C. Hofer for synthetic support of the compound **H<sub>4</sub>L8** and Patrick Mollik for HR-ESI-MS measurements. Thanks also go to Rea Sangiovanni for the graphical abstract.

## Notes and references

- 1 A. J. Arduengo, R. L. Harlow and M. Kline, *J. Am. Chem. Soc.*, 1991, **113**, 361–363, DOI: [10.1021/ja00001a054](#).
- 2 P. Bellotti, M. Koy, M. N. Hopkinson and F. Glorius, *Nat. Rev. Chem.*, 2021, **5**, 711–725, DOI: [10.1038/s41570-021-00321-1](#).
- 3 T. P. Schlachta and F. E. Kühn, *Chem. Soc. Rev.*, 2023, **52**, 2238–2277, DOI: [10.1039/D2CS01064J](#).
- 4 A. Biffis, M. Baron and C. Tubaro, in *Adv. Organomet. Chem.*, ed. P. J. Pérez, Academic Press, 2015, vol. 63, pp. 203–288, DOI: [10.1016/bs.adomc.2015.02.002](#).
- 5 V. Charra, P. de Frémont and P. Braunstein, *Coord. Chem. Rev.*, 2017, **341**, 53–176, DOI: [10.1016/j.ccr.2017.03.007](#).
- 6 M. A. Bernd, E. B. Bauer, J. Oberkofler, A. Bauer, R. M. Reich and F. E. Kühn, *Dalton Trans.*, 2020, **49**, 14106–14114, DOI: [10.1039/D0DT02598D](#).
- 7 E. B. Bauer, M. A. Bernd, M. Schütz, J. Oberkofler, A. Pöthig, R. M. Reich and F. E. Kühn, *Dalton Trans.*, 2019, **48**, 16615–16625, DOI: [10.1039/C9DT03183A](#).
- 8 J. F. Schlagintweit, C. H. G. Jakob, K. Meighen-Berger, T. F. Gronauer, A. Weigert Muñoz, V. Weiß, M. J. Feige, S. A. Sieber, J. D. G. Correia and F. E. Kühn, *Dalton Trans.*, 2021, **50**, 2158–2166, DOI: [10.1039/D0DT04114A](#).
- 9 C. H. G. Jakob, B. Dominelli, J. F. Schlagintweit, P. J. Fischer, F. Schuderer, R. M. Reich, F. Marques, J. D. G. Correia and F. E. Kühn, *Chem.-Asian J.*, 2020, **15**, 4275–4279, DOI: [10.1002/asia.202001104](#).
- 10 M. R. Anneser, S. Haslinger, A. Pöthig, M. Cokoja, J.-M. Basset and F. E. Kühn, *Inorg. Chem.*, 2015, **54**, 3797–3804, DOI: [10.1021/ic503043h](#).
- 11 G. Moreno-Alcántar, P. Picchetti and A. Casini, *Angew. Chem., Int. Ed.*, 2023, **62**, e202218000, DOI: [10.1002/anie.202218000](#).
- 12 M. Mora, M. C. Gimeno and R. Visbal, *Chem. Soc. Rev.*, 2019, **48**, 447–462, DOI: [10.1039/C8CS00570B](#).
- 13 M. G. Karaaslan, A. Aktaş, C. Gürses, Y. Gök and B. Ateş, *Bioorg. Chem.*, 2020, **95**, 103552, DOI: [10.1016/j.bioorg.2019.103552](#).
- 14 L. Oehninger, R. Rubbiani and I. Ott, *Dalton Trans.*, 2013, **42**, 3269–3284, DOI: [10.1039/C2DT32617E](#).
- 15 I. Ott, in *Inorganic and Organometallic Transition Metal Complexes with Biological Molecules and Living Cells*, ed. K. K.-W. Lo, Academic Press, 2017, pp. 147–179, DOI: [10.1016/B978-0-12-803814-7.00005-8](#).
- 16 I. Ott, in *Adv. Inorg. Chem.*, ed. P. J. Sadler and R. van Eldik, Academic Press, 2020, vol. 75, pp. 121–148, DOI: [10.1016/bs.adioch.2019.10.008](#).
- 17 S. Nayak and S. L. Gaonkar, *ChemMedChem*, 2021, **16**, 1360–1390, DOI: [10.1002/cmdc.202000836](#).
- 18 Nature Editorial, *Nature*, 2023, **617**, 438, DOI: [10.1038/d41586-023-01612-x](#).
- 19 C. Heinemann, T. Müller, Y. Apeloig and H. Schwarz, *J. Am. Chem. Soc.*, 1996, **118**, 2023–2038, DOI: [10.1021/ja9523294](#).
- 20 M. N. Hopkinson, C. Richter, M. Schedler and F. Glorius, *Nature*, 2014, **510**, 485–496, DOI: [10.1038/nature13384](#).
- 21 T. P. Schlachta, Master's thesis, Technical University of Munich, Garching, Germany, 2020.
- 22 M. Scholl, S. Ding, C. W. Lee and R. H. Grubbs, *Org. Lett.*, 1999, **1**, 953–956, DOI: [10.1021/ol990909q](#).
- 23 P. S. Athey and G. E. Kiefer, *J. Org. Chem.*, 2002, **67**, 4081–4085, DOI: [10.1021/jo016111d](#).
- 24 Y. Chun, N. J. Singh, I. C. Hwang, J. W. Lee, S. U. Yu and K. S. Kim, *Nat. Commun.*, 2013, **4**, 1797, DOI: [10.1038/ncomms2758](#).
- 25 Z. Li, E. R. R. Mackie, P. Ramkisson, J. C. Mather, N. Wiratpruk, T. P. Soares da Costa and P. J. Barnard, *Dalton Trans.*, 2020, **49**, 12820–12834, DOI: [10.1039/D0DT02225J](#).
- 26 J. W. Emsley, J. Feeney and L. H. Sutcliffe, *High Resolution Nuclear Magnetic Resonance Spectroscopy*, Elsevier, 2013, vol. 2.
- 27 R. J. Abraham, M. Canton and L. Griffiths, *Magn. Reson. Chem.*, 2001, **39**, 421–431.
- 28 P. de Frémont, N. Marion and S. P. Nolan, *Coord. Chem. Rev.*, 2009, **253**, 862–892, DOI: [10.1016/j.ccr.2008.05.018](#).
- 29 H. V. Huynh, *Chem. Rev.*, 2018, **118**, 9457–9492, DOI: [10.1021/acs.chemrev.8b00067](#).
- 30 T. P. Schlachta, G. G. Zámbo, M. J. Sauer, I. Rüter, C. A. Hofer, S. Demeshko, F. Meyer and F. E. Kühn, *J. Catal.*, 2023, **426**, 234–246, DOI: [10.1016/j.jcat.2023.07.018](#).
- 31 W. A. Herrmann, G. Gerstberger and M. Spiegler, *Organometallics*, 1997, **16**, 2209–2212.
- 32 P. De Fremont, N. Marion and S. P. Nolan, *Coord. Chem. Rev.*, 2009, **253**, 862–892.
- 33 J. F. Schlagintweit, L. Nguyen, F. Dyckhoff, F. Kaiser, R. M. Reich and F. E. Kühn, *Dalton Trans.*, 2019, **48**, 14820–14828.
- 34 P. J. Altmann, D. T. Weiss, C. Jandl and F. E. Kühn, *Chem.-Asian J.*, 2016, **11**, 1597–1605, DOI: [10.1002/asia.201600198](#).
- 35 B. Dominelli, G. M. Roberts, C. Jandl, P. J. Fischer, R. M. Reich, A. Pöthig, J. D. G. Correia and F. E. Kühn, *Dalton Trans.*, 2019, **48**, 14036–14043, DOI: [10.1039/C9DT03035B](#).
- 36 M. M. Watts, *J. Am. Oil Chem. Soc.*, 1990, **67**, 993–995.



- 37 M. A. Kalam, K. Haraguchi, S. Chandani, E. L. Loechler, M. Moriya, M. M. Greenberg and A. K. Basu, *Nucleic Acids Res.*, 2006, **34**, 2305–2315, DOI: [10.1093/nar/gkl099](https://doi.org/10.1093/nar/gkl099).
- 38 C.-Y. Liao, K.-T. Chan, C.-Y. Tu, Y.-W. Chang, C.-H. Hu and H. M. Lee, *Chem.–Eur. J.*, 2009, **15**, 405–417, DOI: [10.1002/chem.200801296](https://doi.org/10.1002/chem.200801296).
- 39 W. A. Herrmann, M. Elison, J. Fischer, C. Köcher and G. R. J. Artus, *Angew Chem. Int. Ed. Engl.*, 1995, **34**, 2371–2374, DOI: [10.1002/anie.199523711](https://doi.org/10.1002/anie.199523711).
- 40 D. T. Weiss, P. J. Altmann, S. Haslinger, C. Jandl, A. Pöthig, M. Cokoja and F. E. Kühn, *Dalton Trans.*, 2015, **44**, 18329–18339, DOI: [10.1039/C5DT02386F](https://doi.org/10.1039/C5DT02386F).
- 41 R. Dorta, E. D. Stevens, N. M. Scott, C. Costabile, L. Cavallo, C. D. Hoff and S. P. Nolan, *J. Am. Chem. Soc.*, 2005, **127**, 2485–2495, DOI: [10.1021/ja0438821](https://doi.org/10.1021/ja0438821).
- 42 M. Süßner and H. Plenio, *Chem. Commun.*, 2005, 5417–5419, DOI: [10.1039/B512008J](https://doi.org/10.1039/B512008J).
- 43 F. E. Hahn, V. Langenhahn, T. Lügger, T. Pape and D. Le Van, *Angew. Chem., Int. Ed.*, 2005, **44**, 3759–3763, DOI: [10.1002/anie.200462690](https://doi.org/10.1002/anie.200462690).
- 44 R. McKie, J. A. Murphy, S. R. Park, M. D. Spicer and S.-z. Zhou, *Angew. Chem., Int. Ed.*, 2007, **46**, 6525–6528, DOI: [10.1002/anie.200702138](https://doi.org/10.1002/anie.200702138).
- 45 Z. Lu, S. A. Cramer and D. M. Jenkins, *Chem. Sci.*, 2012, **3**, 3081–3087, DOI: [10.1039/C2SC20628E](https://doi.org/10.1039/C2SC20628E).
- 46 C. S. t. Brinke and F. Ekkehardt Hahn, *Dalton Trans.*, 2015, **44**, 14315–14322, DOI: [10.1039/C5DT02115D](https://doi.org/10.1039/C5DT02115D).
- 47 H. M. Bass, S. A. Cramer, A. S. McCullough, K. J. Bernstein, C. R. Murdock and D. M. Jenkins, *Organometallics*, 2013, **32**, 2160–2167, DOI: [10.1021/om400043z](https://doi.org/10.1021/om400043z).
- 48 H. V. Huynh, Y. Han, R. Jothibasur and J. A. Yang, *Organometallics*, 2009, **28**, 5395–5404, DOI: [10.1021/om900667d](https://doi.org/10.1021/om900667d).
- 49 P. J. Altmann and A. Pöthig, *Chem. Commun.*, 2016, **52**, 9089–9092, DOI: [10.1039/C6CC00507A](https://doi.org/10.1039/C6CC00507A).
- 50 H. M. Bass, S. A. Cramer, J. L. Price and D. M. Jenkins, *Organometallics*, 2010, **29**, 3235–3238, DOI: [10.1021/om100625g](https://doi.org/10.1021/om100625g).
- 51 E. B. Bauer, M. A. Bernd, M. Schütz, J. Oberkofler, A. Pöthig, R. M. Reich and F. E. Kühn, *Dalton Trans.*, 2019, **48**, 16615–16625.
- 52 It needs to be noted that the elemental analysis still includes MeCN as an impurity.
- 53 F. K.-M. Chan, K. Moriwaki and M. J. De Rosa, in *Immune Homeostasis: Methods and Protocols*, ed. A. L. Snow and M. J. Lenardo, Humana Press, Totowa, NJ, 2013, pp. 65–70, DOI: [10.1007/978-1-62703-290-2\\_7](https://doi.org/10.1007/978-1-62703-290-2_7).
- 54 S. Dasari and P. B. Tchounwou, *Eur. J. Pharmacol.*, 2014, **740**, 364–378, DOI: [10.1016/j.ejphar.2014.07.025](https://doi.org/10.1016/j.ejphar.2014.07.025).
- 55 N. Vasani, J. Baselga and D. M. Hyman, *Nature*, 2019, **575**, 299–309, DOI: [10.1038/s41586-019-1730-1](https://doi.org/10.1038/s41586-019-1730-1).
- 56 J. F. Schlagintweit, C. H. G. Jakob, N. L. Wilke, M. Ahrweiler, C. Frias, J. Frias, M. König, E.-M. H. J. Esslinger, F. Marques, J. F. Machado, R. M. Reich, T. S. Morais, J. D. G. Correia, A. Prokop and F. E. Kühn, *J. Med. Chem.*, 2021, **64**, 15747–15757, DOI: [10.1021/acs.jmedchem.1c01021](https://doi.org/10.1021/acs.jmedchem.1c01021).
- 57 A. Frost and A. Carlson, *J. Org. Chem.*, 1959, **24**, 1581–1582, DOI: [10.1021/jo01092a614](https://doi.org/10.1021/jo01092a614).
- 58 D. E. Goldberg and K. C. Patel, *J. Inorg. Nucl. Chem.*, 1972, **34**, 3583–3584, DOI: [10.1016/0022-1902\(72\)80260-4](https://doi.org/10.1016/0022-1902(72)80260-4).
- 59 L. W. Jenneskens, J. Mahy, E. M. M. de Brabander-van den Berg, I. van der Hoef and J. Lugtenburg, *Recl. Trav. Chim. Pays-Bas*, 1995, **114**, 97–102, DOI: [10.1002/recl.19951140305](https://doi.org/10.1002/recl.19951140305).
- 60 E. Lindner, G. von Au and H. J. Eberle, *Chem. Ber.*, 1981, **114**, 810–813.
- 61 Z. Li, E. R. Mackie, P. Ramkissoon, J. C. Mather, N. Wiratpruk, T. P. S. da Costa and P. J. Barnard, *Dalton Trans.*, 2020, **49**, 12820–12834.
- 62 G. R. Fulmer, A. J. M. Miller, N. H. Sherden, H. E. Gottlieb, A. Nudelman, B. M. Stoltz, J. E. Bercaw and K. I. Goldberg, *Organometallics*, 2010, **29**, 2176–2179, DOI: [10.1021/om100106e](https://doi.org/10.1021/om100106e).

